Zbigniew K. Walczak

Processes of Fiber Formation

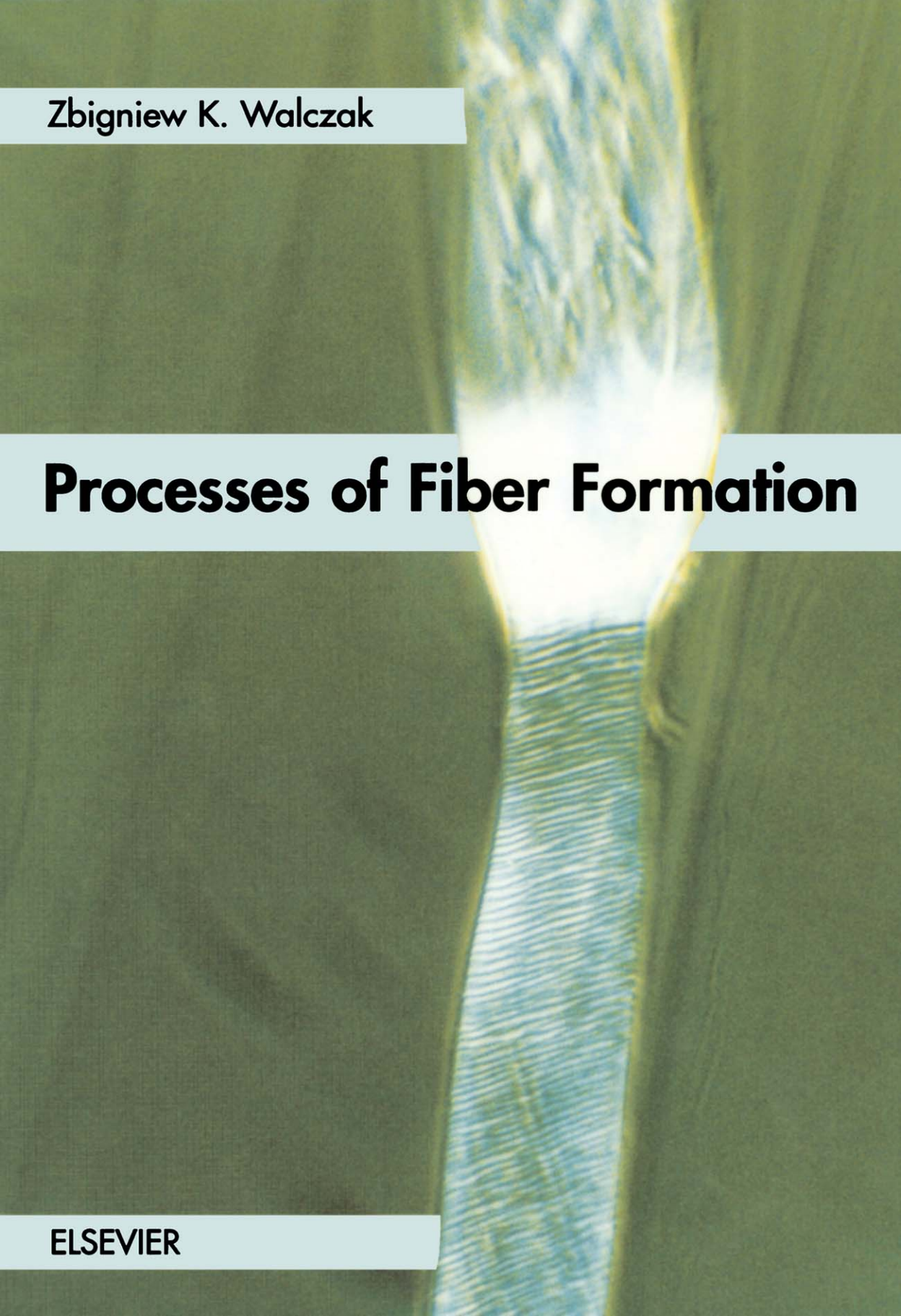

ELSEVIER

Processes of Fiber Formation

This Page Intentionally Left Blank

Processes of Fiber Formation

Zbigniew K. Walczak

2002
ELSEVIER
AMSTERDAM – LONDON – NEW YORK – OXFORD – PARIS – SHANNON - TOKYO

ELSEVIER SCIENCE Ltd
The Boulevard, Langford Lane
Kidlington, Oxford OX5 1GB, UK

First edition 2002

Library of Congress Cataloging in Publication Data
A catalog record from the Library of Congress has been applied for.

British Library Cataloguing in Publication Data
A catalogue record from the British Library has been applied for.

You can contact the author at:
Zbigniew K. Walczak
Paseo de San Gervasio 56, 5°, 4ª
E-08022 Barcelona
Spain - España
E-mail: zwalczak@fiberformation.com

ISBN: 0 08 044040 1

♾ The paper used in this publication meets the requirements of ANSI/NISO Z39.48-1992 (Permanence of Paper).
Printed in The Netherlands.

PREFACE

More than twenty years have passed since the publication of my first book on the subject of fiber formation. Nonetheless, time has its own right. Though throughout the last twenty-five years the fundamental research activity in the field was low worldwide, some progress was made, and thus a presentation of the current status appears to be necessary.

It is almost a paradox that on the one hand, the fiber formation process has passed its centennial birthday, while on the other hand, in some circles, it continues to be considered a craft. In this book I intend to show that fiber formation is a multidisciplinary, complex, often difficult to comprehend **science**. The fiber formation presented here is based on the systematics published in my first book, on numerous important publications concerning different unit processes involved, as well as on my own research conducted over some thirty years. By taking the broadest possible view, a sort of a "frontal attack", it was possible to develop the ways of full description of the fiber formation process. The outcome of the process has been made also predictable *in principle*. The reservation *in principle* means that the outcome of a process may be predicted on the basis of laboratory analytical data and process parameters within a relatively narrow range of conditions. Obtaining full predictability requires additional fundamental research on the behavior of viscoelastic spectra, and on development of new, solid fundamentals of polymer crystallization kinetics, especially of the kinetics of crystal growth.

It can not be neglected to underscore that fiber formation is treated here as one process with three different variants: formation from melt and formation from solution either by the wet or by the dry method. In essence, the difference between the formation from melt and solution differs only by one additional aspect: the presence of a solvent, and this is insufficient to treat it as a separate process. The plural form, processes, relates to the many "unit processes" involved in the formation of a fiber. For this reason, the subject of fiber formation is treated generally as formation from the melt. The additional unit processes pertinent to the formation from solution are treated in a separate chapter which describes the additional complications.

Fiber formation consists of a number of physical processes with nonlinear behaviors occurring and influencing each other simultaneously. In some cases, still another chemical process may be involved. Several disciplines are involved, many different experimental techniques. For these reasons, some of the introductory chapters on raw material properties, rheology, or certain parts of the engineering aspects may appear to some readers as unnecessary, too elementary, or outright boring. Nonetheless, people educated in various disciplines enter into this field, and to facilitate access to the subject, such a broad range of background subjects had to be covered.

Many of my own findings and solutions concerning some of the most vital aspects of fiber formation are presented here for the first time. A book form gives

a better stage to present a complex, systemic approach and a mutual confirmation of the different techniques, results, and conclusions. Since, in my view, a theory without corroboration is useless, every original solution presented here has been confirmed experimentally numerous times and under various conditions. And here is the need and place to express my greatest appreciation and gratitude to those with whom I was lucky to work during different periods on the experimental parts of the endeavors: Ms. Janet B. Fryzel, Mr. Nolan Smith, and Mr. Alan C. Smith. Some of the experimental tasks were very demanding for accuracy, some, like program debugging, were trying to the patience — nonetheless, execution of every task was really admirable.

All the parts involving aerodynamics could not have been written without the generous consultations, or rather teachings, of Professor Juliusz Łukasiewicz, Jr. chief of von Karmàn Gas Dynamics Facility, Arnold Engineering Development Center, Tullahoma, Tennessee and later of Carlton University, Ottawa, Ontario.

I owe special gratitude to Mr. Rainer Typke for his learned and generous help at the time when my computer broke down and needed the hardware to be replaced, the new operating systems introduced. His help saved many of my older programs, and much time and frustration.

An expression of deep appreciation and thanks I direct to my daughter Agatha C. Walczak-Typke for the editing and proof reading of this book, despite the heavy load of her own work; a Dixie style: *Thank you. Thank you. Thank you.*

And last, though not least, I would like to express my long standing and great appreciation to my wife Krystyna for her patience over the time of our togetherness lost to this book. Instead of a display of dissatisfaction, she was generous enough to apply her artistry to design the cover for this book.

I owe a special *thank you* to all of the publishers who granted me their permission for copying material from other publications. Also, some of the illustrations have been made available by the authors and my gratitude is extended to them, though, sorry to say, many of them are already deceased.

Zbigniew K. Walczak

Barcelona, 2001.

CONTENTS

I INTRODUCTION

I.1 Historical Background

The first *artificial fibers* were made toward the end of nineteenth century on the basis of natural polymers: cellulose and casein. The knowledge of fully synthetic polymers was at that time still highly inadequate.[1–5]

These natural polymers do not melt – they decompose at elevated temperature. This simple fact dictated the first methods of fiber formation. The polymers, or their modifications, could, however, be dissolved. In solution form the shape of the materials could be changed, and by subsequent solvent removal the shape could be fixed. On these principles were based the first patents protecting fiber formation.[6–9]

Cellulose does not dissolve easily in any of the commonly used solvents of that time. Later, the choice of solvents for cellulose was extended by the addition of cuprammonium – a substance not very pleasant to work with. The realities of difficult solubility led to the development of another way to prepare solutions: namely through formation of cellulose derivatives: nitrocellulose and cellulose xanthate – a product of reaction between cellulose and carbon disulfide. In the case of xanthates, immediately after shaping the solution into fibers xanthate was regenerated back to cellulose. This became known as the rayon process, which, with many refinements, is still in commercial use.

There are two applicable ways to remove the solvent: evaporation or extraction. Thus the processes which today are referred to as dry spinning and wet spinning , or more correctly as dry or wet fiber formation, were born. In the former, the solvent is removed through evaporation, while in the latter the solvent is removed through extraction, with or without a chemical reaction taking place simultaneously. In both of the methods diffusion plays the key role. The rayon process involved a chemical reaction to regenerate the cellulose, thus it was limited to a wet treatment for the sake of the reaction, as well as for an extraction of the byproducts.

With continuing progress in the area of synthetic polymers, thermoplastic polymers eventually came under consideration for fiber formation. The thermoplastic nature of the polymers allowed the omitance of solvents as a processing aide, but extrusion and further processing of the highly viscous melt brought new problems. These were reflected primarily in new demands on hardware. The higher viscosity of polymer melts and larger emphasis on the attenuation of the fiber diameters necessitated the involvement of the science of rheology; problems connected with fiber formation became for rheology an important field of research.

In the past the three methods of fiber formation – dry, wet, and melt spinning – were treated as entirely different processes having very little in common. From an operational point of view, this opinion may be justified to some extent. Indeed, from theoretical and technological points of view, these processes are very similar.

Schematic representation of fiber formation by all three main variants of the

process is given in Figure I-1. To begin with, the dry polymer is either melted or dissolved, possibly after a modifying reaction. While the polymer melting is continuous in screw melters or extruders, or fed directly from continuous polymerization units, dissolution is performed in batches. In the old days melting was accomplished on grill heaters located closely to the spinning blocks. In any of the cases, the polymer solution or melt is transported to spinning blocks. The necessary pressure is delivered either by extruder, as in contemporary melt spinning, or by compressed gas (nitrogen), as in spinning from solution or grill heater melted polymer.

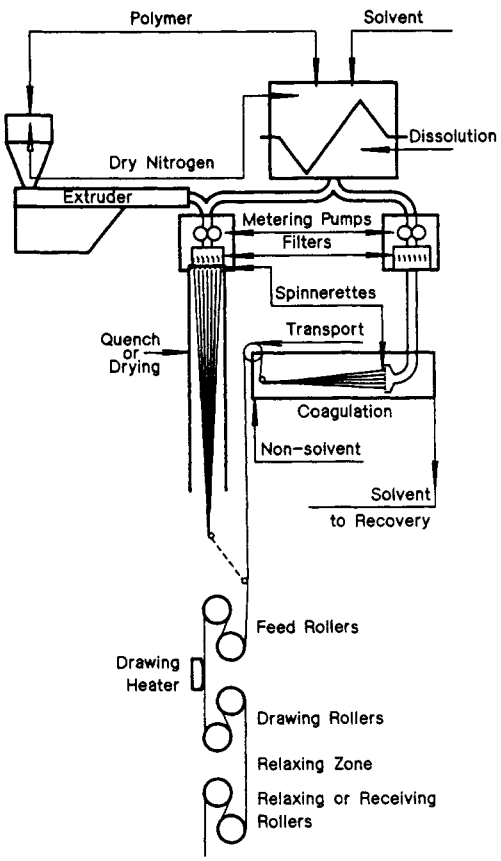

Figure I.1: *Schematic representation of the fiber formation process.*

The spinning block is equipped with a cavity for a fluid metering pump, and channels which lead the polymer melt or solution to another cavity, where the filter and spinnerette are located. The spinnerette is a metal plate, sufficiently thick to withstand the pressure gradient and equipped with a multitude of capillaries through which the polymer or its solution are extruded. The block must be

equipped with means for rigid control of temperature.

In the case of wet formation processes, spinnerettes are not mounted in the spinning block but on transfer tubes which allow the spinnerettes to be submerged in the coagulation bath or located few millimeters above the fluid surface.

So far, for all three formation methods, processing is quite similar. Some differences begin from this point on. The purpose of the treatment of the extruded stream is the same in each method: to solidify the polymer. The means of accomplishing this goal vary with each method and constitute the main point of differentiation.

When a molten polymer is extruded through a capillary it will solidify on cooling. The cooling medium may be gas or liquid. If a stream of polymer solution is extruded into a gas atmosphere the solvent may be removed only by evaporation, the heat of evaporation must be delivered by the gas. In the wet methods the polymer stream is extruded from spinnerettes submerged, or almost submerged, directly into a fluid which extracts the solvent from the filaments. If a chemical reaction accompanies the process, the course of events is more complicated. In regenerative processes the polymer is regenerated, it becomes insoluble – it coagulates – and phase separation occurs. Polymer may also be synthesized from precursors, or may be cross linked by the coagulating baths which render it insoluble. The diffusion processes are temperature dependent, so the coagulating bath must be well thermostated. In case of chemical reactions taking place in the coagulation bath, temperature control may become more complex due to the heat of reaction. Extraction by itself does not involve significant thermal effects.

In the case of formation from solution, the solvents and nonsolvents used must be recovered for economical, as well as safety and ecological reasons. The prevalent method of solvent recovery from the gas is by adsorption on activated carbon, with subsequent steam regeneration of the carbon bed, and separation of water and solvent (distillation). This method of regeneration is quite expensive. In cases of wet method, usually only distillation suffices; this method may be more economical, particularly if the solvent is more volatile than water.

Many industrial operations are interrupted at this point. Fibers obtained in wet processes at this point may require washing, and certainly drying. If dry formation is done using relatively high boiling solvents, the formed fibers may also need additional washing to remove residual traces of solvent. Another reason to interrupt the operation here may be crimping and/or heat treatment processes, which may proceed at a different rate than the formation itself. Besides, crimping is usually done on dry fibers, or with steam, under controlled moisture level. There are, however, many operations where the fibers are subjected to plastic deformation (neck drawing) in one line with the formation process.

The process of polymer solidification is quite complex. The majority of the polymers used for fiber formation do form a crystalline structure. The crystallization process usually takes place simultaneously with the solvent removal or due to decrease of temperature of the melt. Slower crystallizing polymers have only large viscosity increase due to the cooling of polymer melts, crystallization process takes

place in further steps. It is quite understandable that the crystallization process proceeds differently, depending on the temperature change, presence or absence of a solvent. Besides the phase and temperature changes, the filament diameter is attenuated by stretching . And all that at the same time! The stretching is necessary as it is essentially impossible to extrude the filaments at their final thickness. For this reason one extrudes as small a diameter as practical for all possible reasons, and then the filaments are extended while still molten or still containing enough solvent. The large number of processes and events taking place simultaneously in the relatively small space and very short time contribute to the immense complexity of the whole problem of fiber formation. This complexity of quench, drying, and coagulation zone creates the greatest obstacle in unraveling the different phenomena, in developing a complete and sufficiently accurate theoretical description of the whole process, as well as difficulties with the understanding of the nature and the essence of the process.

The formed, undrawn fibers ("spun fibers" in the industrial slang), which have been washed and dried if necessary, do not have good physical, and particularly tensile, properties. Very early in the history of fiber making it was discovered that the fibers as formed may be permanently deformed by a relatively low stretching force. Such stretching results in an increase of the tensile strength. Therefore, almost all fibers, irrespectively of the method of their formation, are subjected to such a deformation. The stretching operation is usually carried out by transporting the fibers through rollers driven at different surface speeds. In Figure I-1 the rollers are identified as feed (or take up) rollers and drawing rollers. From the point of view of crystalline morphology of fibers, the stretching corresponds to plastic deformation; it is often called "neck drawing" due to the characteristic abrupt diameter change, which resembles a bottle neck, or simply the drawing. The plastic deformation is usually performed at elevated temperature, though below the onset of melting of the crystalline structure. After the stretching operation, the fibers may show a tendency for some recovery. It is advisable to let them recover under controlled conditions: to add a pair of relaxing rollers rotating at appropriately lower velocity than the drawing rollers.

Depending on the polymer and process used, and on the type and quality of product intended, the drawn fibers may be subjected to various finishing operations: washing, heat setting, winding on bobbins, or cutting for staple.

There is another finishing operation, which is not necessarily performed at the end of the manufacturing line. These are finishes applied for different purposes: to facilitate drawing and/or crimping, to prevent electrostatic charging, and almost always to improve textile processing . Depending on the type and the purpose of the treatment, the finish may be applied at different stages of the manufacturing line.

The above description of fiber making is brief and highly simplified. It is to serve as a starting point for detailed discussion of all the essential phases and the phenomena taking place during the process, and as the initial vocabulary or bridge for communication with the reader. The scheme given above concerns only

the manufacturing of the classical fibers and disregards some newer methods and products. Some of the newer processes, raw materials, and products, such as polymer blends, bicomponent fibers, spunbonded materials, are treated in an abbreviated fashion, because the majority of the technological problems they involve represents only modifications of the basic principles of fiber formation. However, some of these problems will be given some attention since they represent either interesting solutions to problems, or a good example for the principles working in different processes, or because they have experienced commercial success

I.2 Nonconventional Formation Methods

As mentioned above, the fiber formation process is complex. This simple fact represents a strong driving force to attempt to simplify the technology. The always present need for the reduction of manufacturing costs reinforces the drive toward new and simpler formation methods. The initial efforts have been concentrated on attempts to eliminate the roller type transport of fibers and spinnerettes as expensive pieces of high precision hardware.

The first known attempts to eliminate fiber transport rollers in fiber formation from polymer solution date back to 1934. In place of rollers between the capillary and collecting device, an electrostatic field of 50 to 300 kV was applied.[11–14] Such a process usually bears the name of *electrostatic spinning.*

Spraying of a polymer solution, or melt, by means of high pressure and high velocity air[15–17] represents another technique leading to similar results. Extrusion of polymer melt through a long slit type die was still another method leading to the same general goal. The extruded filaments may then be extended in a Venturi type jet with high velocity gas. Such jets are able to provide the necessary extensional force. This group of methods is normally referred to as *spray spinning.*

In another attempt to eliminate the spinnerette, a process has been developed where a polymer solution or melt is introduced axially to the center of a rotating cone or bell. The centrifugal force distributes the fluid over the internal surface of the bell into a film of progressively decreasing thickness. When the film leaves the edge of the cone, the film splits into fibers. Solidification takes place by the way of drying or cooling. The centrifugal force is sufficient to extend the fibers to as fine diameter as fractions of denier*.[19] Such a process bears the name of *centrifugal spinning.*

There exists a process which combines centrifugal and electrostatic forces. The centrifugal - electrostatic processes find an application mainly to manufacturing of spunbond fabrics.[20,21]

Another group of nonconventional processes concentrates on facilitating melt processing of high molecular mass polymers. All of these methods invariably "dilute" the polymer with solvent what lowers the viscosity to various degree. The

*Denier, den or dpf, is a measure of mass, or weight, titer; it is the weight of a filament of the length of 9000 meters. A "metric" mass titer is tex, Tx, the weight of a 1000 m long filament. The "decitex", dTx, is most often used.

solvent selection represents a crucial point in those processes. In some cases solvents are selected so that they become non - solvents at lower temperature and/or pressure. In some cases the solvent violently evaporates when the extrusion pressure ceases upon leaving the spinnerette. Yet another processes, aimed at obtaining very high strength and high modulus fibers, extrude the polymer only swollen by the solvent to a state of gel.

All of the nonconventional processes are governed by the same laws and principles as the conventional fiber formation methods. On the other hand, all of the nonconventional processes seem to have some deficiency, none of them is ideal. The most common fallacies are: nonuniform fiber diameter, both fiber-to-fiber, and/or along the fiber. For the majority of the processes without spinnerettes it is virtually impossible to subject the spun fibers to cold drawing (plastic deformation). Generally, only certain products or raw materials, which do not require plastic deformation at all, or only to a modest extent, are suited for such processes, e. g. elastomers. Some spunbonded processes, mainly for disposable products, where dimensional stability of the fibers and higher tensile strength are not required, utilize the nonconventional methods. The inherent deficiencies of the nonconventional methods are serious enough to prevent, or seriously limit, application of the products as traditional textile fibers for apparels. Some of the semimelt processes yield high class fibers, but the high price limits their application to very special purposes.

I.3 Traditional Understanding of the Process

Development of new technologies is often done by *trial and error*. The technology of fiber formation went through a similar period. Moreover, that period lasted longer, relatively speaking, due to the complexity of the physics of the unit processes involved and the extraordinary many simultaneous and interrelated unit processes involved. It is well known that trial and error approaches usually result in an abundance of errors, but every new inductive science must go through such a difficult childhood. By now, the technology is over hundred years old. During all that time, a great wealth of observations and experience has been accrued. Alas, the majority of this knowledge has not been published. The commercial significance of fiber manufacturing explains the hesitation in the publication of anything that may prove important. This was particularly true of the initial trial and error period. Nevertheless, as fiber formation has gradually obtained the rank of science, more and more information has found its way into scientific journals; though sometimes with substantial delay. [22–30] As a result of the specific spirit of secrecy in which the fiber industry has placed itself, the fiber makers and the fiber making procedures have became surrounded with a peculiar aura of an art, if not a black magic.

During the long studies of the raw material - process - product relation, it was established quite early that despite the most scrupulously held constant polymer properties, small changes in processing may cause "unduly" severe changes in the

product properties. Similar sensitivity of process - product relations were known in metallurgy, but never to such a significant extent. In metallurgy, the majority of such changes could be ultimately related to some minute variations of chemical composition or to the crystalline polymorphism, or both. Gradually, with time it became evident that, by their nature, macromolecules usually do not attain thermodynamic equilibrium.[31] The large chain-like molecules assume a multitude of different conformations depending on their thermal history and history of their mechanical perturbations. Because of the lack of more accurate knowledge, the thermal history was held responsible for everything, particularly for everything bad, that could happen. The lack of a sufficient explanation and of a well grounded understanding did not allow to lay a firm theoretical basis for fiber production. Empirical formulations and "the rule of thumb" became the last resort. On the basis of mainly qualitative observations of different processes, a number of *"iron rules"* for fiber formation have been gathered.[32] They are:

- Narrow molecular mass distribution in a polymer facilitates the processing and generally improves the product properties.
- Increase of shear rate in the spinnerette increases the fiber tenacity.
- Increase of the spin stretch usually increases the crystallinity of the formed fibers.
- Tension in neck drawing, at a given draw ratio, is proportional to the crystallinity in the undrawn fiber.
- Maximum crystallinity that is obtainable in the drawn fibers depends in inverse proportion on the degree of crystallinity present immediately before the neck drawing operation.

Aside from the simplistic form, these rules represent an immensely significant basis for the past development work, and they may still be helpful to understanding of the many results published under the headings of "surprising". But it must be also realized that the experimental verification of some of the points, although performed many times over, represents a difficult task. Proper separation of different variables is of utmost importance. In every formation process not all of the variables are individually and independently adjustable. Modern testing equipment allows the measurement of the spinline conditions,[33,34] thus it has simplified the verification of those qualitative rules. More importantly the equipment provided a firm basis for the modern quantitative description of the process. In view of the quantitative information, some of the *"iron rules"* were found to need qualifying footnotes.

Aside from their historic significance and practical importance, *"the iron rules"* describe the process neither completely, nor even adequately. Fiber formation is one of the most complex processes the chemical industry has ever dealt with. Therefore, one cannot expect it to be described sufficiently by only a few "rules". Despite the unquestionable progress, at this moment there are still no full and

complete quantitative solutions available. The fully quantitative scientific predictability is still limited since several of the fundamental problems in polymer physics have not been solved yet.[31]

I.4 Newer Theoretical Approaches

In the early 1950s, work began on a more scientific approach to fiber formation. Earlier, products and processes were invented, studied, and developed only by chemists and engineers. The newer approach in fiber research involved many physicists.[35–37] One may distinguish two different methods characteristic to those efforts.

In one of the approaches, the exploratory work was carried out on certain aspects of product or process. Usually the studied problems were selected so to cover a very narrow area of specialization, often limited to using only one experimental technique. Some of the investigations of this kind produced much valuable data. Some of these studies of the *unit processes* were deep indeed. However, the isolated conditions sometimes put limitations on the general validity of the interpretations. The experiments were simply too much out of context in relation to the entire process. In studying literature of that period, it is often necessary to reevaluate and reinterpret the published conclusions. Taking into account the principles of the methodology of sciences,[38] such studies of isolated aspects may be justified, provided that the potential dangers of premature generalizations are heeded, so that misleading conclusions are avoided.

As the first approach was predominant in more "descriptive" areas, e.g. fiber structure, the second one involved attempts of quantifying the process. With sufficient fairness one may credit E. H. Andrews[35] as its originator. Many quantitative descriptions of great value have been obtained, though unfortunately, not always were they immediately applicable in practice. As an example one may quote the Andrew's solution of heat transfer equation,[35] which gives good results in case of non-crystallizing polymers. Since the process of polymer crystallization under strain had not been solved at that time, it was a scientific distortion to put the large heat of crystallization at an arbitrarily chosen point of the spinline. A certain dose of impatience and underestimation of the process complexity can be detected in some of the interpretations and conclusions assigned to these otherwise substantial achievements.

The quantitative descriptions of the unit processes involved in fiber formation pose calculational difficulties, only a small fraction of them may be solved analytically. In recent years the application of widely available, potent, and fast computers to cope with the difficulties of the purely computational nature have placed the fiber formation technology where it is today. Computers allow a wide use of numerical methods and simultaneous solution of systems of equations. In this way, today the fiber formation process may be fully quantitatively defined only with the necessity of experimental analytical support.

The full development of fiber formation technology, that is, to the point of total

quantitative predictability on the basis of laboratory analyses, is still incomplete. The full predictability of the process appears to depend mainly on the filling of the gaps in polymer physics. It is also imperative that the future research endeavors be undertaken so that the complexity of the whole process be considered and respected both in its theoretical and experimental aspects.

On the other hand, we must be grateful to past researchers for the development of the starting points. After the thorny beginning, compilation of the available methods, proper reinterpretation of them, provided a strong base for the current state of knowledge in the field.

In the following chapters, all theoretical treatment of the unitary processes and phenomena involved in fiber formation and available today will be given separate accounts. Simultaneously, the theories will be confronted with the wealth of the available experimental evidence. The analysis of the mutual relationships and influences between the unit processes involved in fiber formation plays a crucial part. The available quantitative descriptions and their agreement with experiments – *ergo* their applicability will be ascertained. The different aspects of the process will be brought into one entity: into a logical system of fiber formation science, as it stands today. Though some areas of polymer physics still require solutions, the amount of confirmed information already gathered, when logically assembled, permits the fiber formation technology to be rightfully called the **fiber formation science**.

I.5 References

1. J. Blyth and W. A. Hofmann, *Ann.*, **53 (1845)**, 283, 311.
2. M. Berthelot, *Bull. Soc. Chim. France*, **6 (1866)**, 294.
3. G. Gustavson, *Ber.*, **7 (1874)**,731.
4. H. Staudinger, *Helv. Chim. Acta*, **5 (1922)**, 785.
5. W. H. Carothers: *Collected Papers*, Vol. 1 of the *High Polymers series*, Interscience Publ., New York, 1940.
6. *German Pat.* **No. 38,368 (1885)**.
7. *French Pat.* **No. 203,741 (1890)**.
8. *German Pat.* **No. 108,511 (1898)**.
9. *German Pat.* **No. 170,051 (1904)**.
10. *Brit. Pat.* **No. 609,796** to Imperial Chemical Ind., Ltd.
11. *U.S. Pat.* **No. 1 975 504, (1934)** to A. Formahls and R. Schreiber - Gastell.
12. *U.S. Pat.* **No. 2 116 942, (1938)** to A. Formahls and R. Schreiber - Gastell.
13. *U.S. Pat.* **No. 2 048 651, (1936)** to Massachusetts Institute of Technology.
14. *Can. Pat.* **No. 937 827, (1973)** to Farbenfabriken Bayer A. G.
15. *U.S. Pat.* **No. 2 988 469, (1961)** to American Viscose.
16. *U.S. Pat.* **No. 3 689 342, (1973)** to Celanese.
17. D. E. Till, *Mod Textile Mag.*, **(1959)**, 36.

18. R. R. Bentin, D. T. Lohkamp, *TAPPI*, **56 (1973)**, 74.

19. *Brit. Pat.* **No. 1 132 135 (1968)** to Monsanto.

20. J. Fine and S. A. De Tora, *U. S. Pat.*, **No. 4,223,101 (1980)**, to Inmont Corp.

21. *U.S. Pat. Appl.* No. 486 567, to Inmont Corp.

22. R. Hill (Ed.): *Fibers from Synthetic Polymers*, Elsevier Polymer Series, Vol. 6, Amsterdam - New York - London, 1953; *Fasern aus synthetischen Polymeren*, Berliner Union, Stuttgart, 1956.

23. H. Hopf, F. Wenger, and A, Müller: *Die Polyamide*, Springer Verlag, Berlin - Götingen - Heidelberg, 1954.

24. H. Klare, E. Fritsche, and V. Grőbe, *Synthetische Fasern aus Polyamiden*, Akademie Verlag, Berlin, 1963.

25. H. Ludewig (Ed.): *Polyesterfasern*, Akademie Verlag, Berlin, 1965.

26. S. A. Rogovin: *Chemiefasern, Grundlagen der Chemie und Technologie*, Fachbuchhandlung, Leipzig, 1960.

27. F. Fourne: *Synthetische Fasern*, Wissenschaftliche Verlagsgesel-lschaft, Stuttgart, 1965.

28. T. Rosner, H. Wójcikiewicz: *Włókna syntetyczne*, Wydawnictwo Naukowo - Techniczne, Warszawa, 1969.

29. T. Rosner: *Włókna sztuczne*, Wydawnictwo Naukowo - Techniczne, Warszawa, 1966

30. H. Mark, A. Atlas, and S. Cernia: *Man - Made Fibers*, Vol. 1-3, Interscience Publ., New York, 1967-68.

31. H. A. Stuart (Ed.): *Die Physik der Hochpolymeren*, Springer Verlag, Berlin - Wien - Heidelberg, 1956, Vol. 3, pp. 414 ff, 550 ff., 557 ff.

32. A. Nowakowski: *Technology of Plastics and Synthetic Fibers*, lectures at Polytechnic of Łódz, 1953.

33. K. L. Reifsnider: *A New Device for Time-Resolved Study of X-Ray Diffraction Events*, Ph.D. Dissertation, Dept. of Mechanics, The John Hopkins Univ., University Press, 1968.

34. K. L. Reifsnider, *private communication.*

35. E. H. Andrews, *Brit. J. Appl. Phys.*, **10 (1959)**, 39.

36. H. Berg, *Kolloid-Z.*, **210 (1966)**, 64.

37. A. Ziabicki and K. Kedzierska, *Kolloid-Z.*, **171 (1960)**, 51; A. Ziabicki: *Fizyka procesów formowania włókien*, Wydawnictwo Nau-kowo - Techniczne, Warszawa, 1970; *Fundamentals of Fibre Formation*, J. Wiley Publ., New York, 1976.

38. K. Ajdukiewicz: *Logika pragmatyczna* (Pragmatic logics), Panstwowe Wydawnictwo Naukowe, Warszawa, 1965, Part III.

II POLYMER AS RAW MATERIAL

II.1 Structure and Character

The majority of polymers used for the manufacture of fibers are of organic nature. The physical behavior of polymers differs from the behavior of the *ordinary*, low molecular mass, substances. The differences are caused principally by the large and nonuniform size of the polymer molecules. In organic chemistry, this is known as the notion of *homolog series*. Polymers, however, may be considered rather as mixtures of homologs.

In the case of ordinary compounds, we speak of molecular mass, while in the case of polymers, we may speak only about an average molecular mass, since the molecules are of uneven size. The molecular mass may have various distributions, and here one needs the help of statistics to describe them. The commonly used averages, presented in a mathematical form, are:

$$\langle M_n \rangle = \frac{\sum_i n_i M_i}{\sum_i n_i} \tag{II.1}$$

$$\langle M_w \rangle = \frac{\sum_i n_i M_i^2}{\sum_i n_i M_i} \tag{II.2}$$

$$\langle M_z \rangle = \frac{\sum_i n_i M_i^3}{\sum_i n_i M_i^2} \tag{II.3}$$

$$\langle M_{z+1} \rangle = \frac{\sum_i n_i M_i^4}{\sum_i n_i M_i^3} \tag{II.4}$$

In equations II.1 through II.4 n_i denotes the number of molecules of mass M, $\langle M \rangle$ is average molecular mass (colloquially molecular weight). The subscripts mean:

- n represents *number average* molecular mass, where species of each molecular mass are represented by their number or mole fraction.
- w represents *mass average* (or weight average) molecular mass. Here, molecular mass of each of the species is represented by its weight.
- z represents the so called *z-average molecular mass*. This average has primarily mathematical meaning, while physically, it is related to some volume dependence, *e.g.* like radius of gyration in light scattering experiments.
- $z+1$ is called $z+1$ - *average*; it has only mathematical significance.

There is one more – perhaps the most commonly used average: the *viscosity average* molecular mass. Particularly until the advent of newer instrumental methods, like the gel permeation (or size exclusion) chromatography this has been the

most commonly used average, since the viscosity measurements are easier than other techniques for molecular mass determination.. The unquestionable problem connected with viscosity average is that it is not really constant: its relation to other averages depends on the solvent used. In limiting cases it may equal the weight average. Otherwise it is smaller, down to a minimum reaching about half the difference between the weight and number averages. Mathematically the viscosity average molecular mass may be presented as

$$\langle M_\eta \rangle = \left(\sum_{i=0}^{n} w_i M_i^a \right)^{1/a} \tag{II.5}$$

Here, w_i is weight fraction of species of molecular mass M_i, a is the Mark-Houwink exponent in the intrinsic viscosity equation $[\eta] = KM^a$, which may vary from 0.5 for *theta solvent* to 1.0 for a very good solvent. As the a coefficient approaches unity, the viscosity average approaches the weight average molecular mass, though this occurs rarely. [3,4]

The Gauss distribution is, perhaps, the most fundamental and common in statistics. Its mathematical formulation in relation to molecular mass is:

$$W(M) = \frac{1}{\sigma\sqrt{2\pi}} \exp\left[\frac{(M - M_m)^2}{2\sigma^2}\right] \tag{II.6}$$

where M_m is the median value of molecular mass, around which the curve is symmetric, and at the same time it represents the number average molecular mass; σ describes the breadth of the distribution, it corresponds to the standard deviation in statistics. The value of standard deviation, σ_n, may be expressed in terms of the average of molecular masses of different type:

$$\sigma_n = \sqrt{\langle M_w \rangle \langle M_n \rangle - \langle M_n \rangle^2} \tag{II.7}$$

The molar fraction of 0.6826 lies within the limits of $\pm\sigma$. Figure II.1 shows a Gaussian distribution of molecular mass. Unfortunately, there are few polymers which have Gaussian distribution. The normal logarithmic distribution seems to be more common. The mathematical form of the *"log-normal"* distribution, as it is called for short, is the Gaussian distribution, where the molecular mass fraction in the exponent is substituted by its natural logarithm. The standard deviation, σ_w*, for the distribution where the number of molecules is substituted with a weight fraction, is

$$\exp(\sigma_w^*)^2 = \frac{\langle M_w \rangle}{\langle M_n \rangle} = \frac{\langle M_z \rangle}{\langle M_w \rangle} \tag{II.8}$$

An example of the *log-normal* distribution curve is presented in Figure II.2. In the normal distribution the maximum of the curve coincides with the number average molecular mass. In log-normal distribution this is not the case: log-normal distribution is characterized by a larger fraction of smaller molecules. The distribution curves encountered experimentally often resemble log-normal distribution,

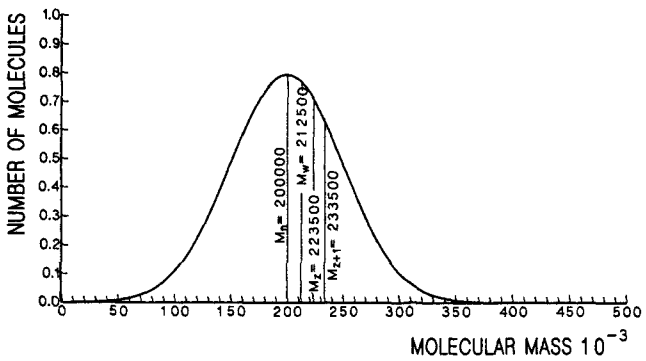

Figure II.1: *Gaussian distribution of molecular masses.*

though they do not fit exactly into its mathematical form. Therefore, a number of modifications to the log-normal distribution equation have been suggested to accommodate the discrepancies. For details on these distributions the reader is referred to the polymer textbooks.[1,2]

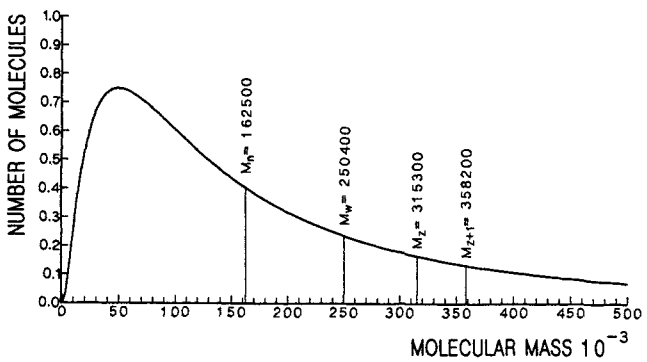

Figure II.2: *Example of a normal logarithmic type of molecular mass distribution.*

Experimentally, molecular mass distribution and all the averages are commonly determined by the size exclusion chromatography. Other methods are used less frequently as they are experimentally more difficult. These methods usually yield molecular mass averages of different type. Particularly troublesome are other methods for determination of mass distributions. However, from the direct specialized methods like osmometry for number average, light scattering for weight average, and ultra centrifuge for weight and z-average, more accurate data may be obtained. The size exclusion chromatography requires calibration, which is based on the direct methods.

Polydispersity of polymers, as expressed by the weight average over number average ratio, rarely is less then 2 and in some cases may reach as high as ten or twelve. This is true both for commercial and for experimental polymers. The lower

values are more typical for condensation type polymers, the higher values occur primarily with some vinyl-type polymers. Polymers of higher average molecular mass have a tendency toward having a somewhat broader mass distribution.[5]

Polydispersity may be high also due to the blending of different polymer batches, or as a result of not very stable continuous polymerization processes. In such cases one may encounter bimodal, or even multimodal distributions which do not have any general mathematical representations given *a priori*.

Practically, all the fiber forming polymers known currently have linear chain structure. The molecular formulas predict such linearity quite clearly.

The group of polyamides **polyamides**, is based either on $\alpha - \omega$ difunctional acids and $\alpha - \omega$ iamines or on $\alpha - \omega$ aminoacids. Aromatic diacids or diamines make the melting point very high and may increase the strength substantially. Examples of structural formula of an $\alpha - \omega$ diacid and $\alpha - \omega$ diamine, as well as Stuart-Briegleb models of single mer of nylon 6 and a segment of nylon 66 with amid bonds and with one CH2 group on each side, respectively, are:

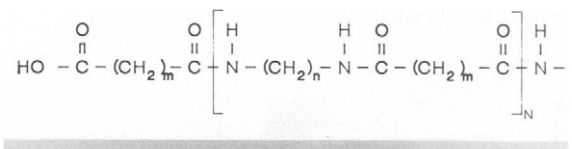

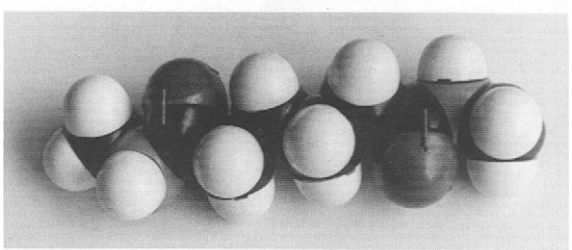

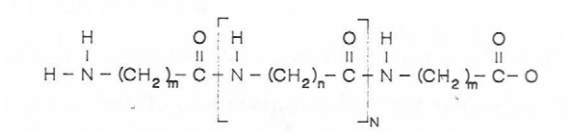

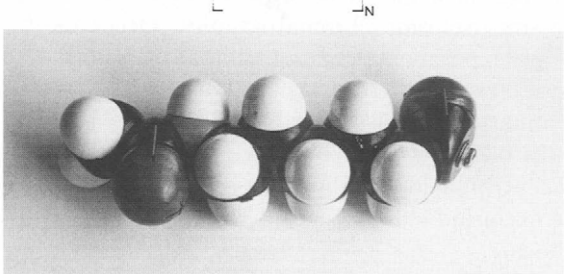

Poly(acrylonitrile) (usually called *acrylic fiber*) has an irregular stereo con-

figuration, often containing small amounts of comonomers, does not melt and is processed from solution:

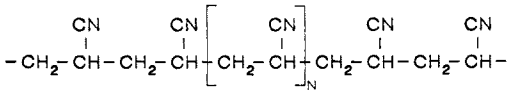

Polyesters in their most common version are based on terephthalic acid and glycols of different length, most often ethylene glycol. Structural formula and Stuart-Briegleb model of one mer of poly(ethylene terephthalate) are:

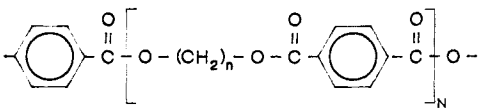

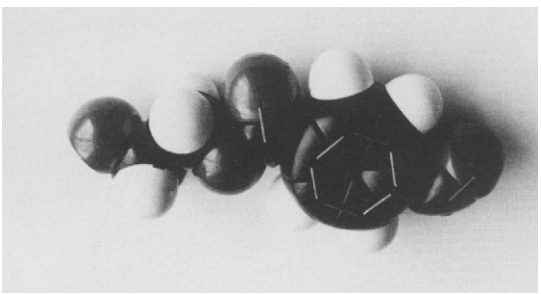

Polyethylene (or *polymethylene*, if it has a most regular structure), is a polymer of high theoretical interest due to the structure simplicity, commercially it is less attractive due to low melting. Structural formula and Stuart - Briegleb model of three mer segment are:

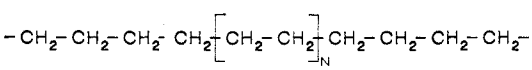

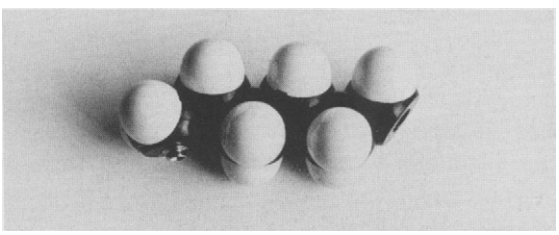

Isotactic **polypropylene**, which cannot assume a planar *zig - zag* but instead has a helical conformation as found in crystals. Structural formula and Stuart-Briegleb model of a two mer segment are:

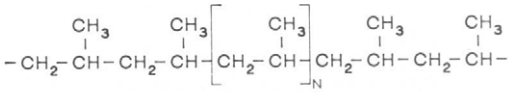

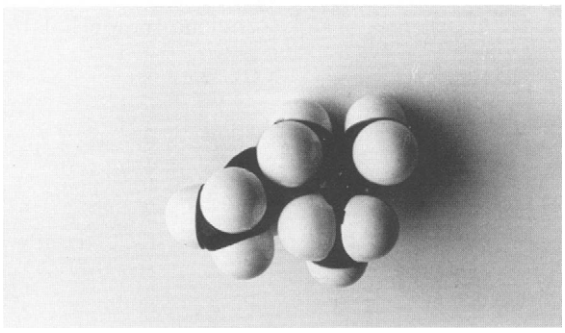

Syndiotactic-**polypropylene**, has planar conformation but usually melts lower than its isotactic counterpart:

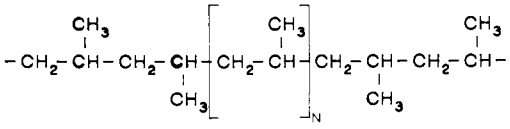

Naturally, the list of polymers used for manufacturing of fibers is substantially longer, especially when one takes into consideration the so-called high performance fibers and modifications of naturally occurring polymers. If any of the useful polymers, from the fiber formation point of view, have chain branching synthesized intentionally, then the side chains are rather short. Unfortunately, almost all polymers contain some fraction of chains with long branches built in unintentionally, as imperfections, as a result of side reactions. In the case of low molecular mass compounds, products of side reactions are removed during purification processes; in the case of polymers, such purification is impossible, particularly if the

side products are built into the chains. It must be stressed that long chain branching, particularly when it is severe enough to form cross linked, gel molecules, is most detrimental to the polymer quality, to the ease of processing, and potentially to the polymer usefulness.[6,8] Doubtlessly, in commercial operations such chain imperfections often represent a strong economic factor.

In melts and in solutions, the polymer molecules are coiled into what looks like a little balls. How tightly a polymer coils depends on the flexibility of chain, and in the case of solutions, the quality of the solvent.[9,10] It is indeed difficult to imagine a rod with length to diameter ratio of several thousands staying fully extended, or close to it, especially when one considers interaction with other molecules. Conditions like this may be met only in cases of very rigid molecule structure (e.g. liquid crystal polymers).

In concentrated solutions and in the melts, the coiled polymer molecules are not entirely independent. To some degree, the coils are interpenetrated and the chains entangled. A fully quantitative description of the chain morphology in concentrated solutions and in the melts is currently impossible. The problem of chain conformation in solid state is also not less important; it will be discussed in the next sections.

As the molecules lack full freedom of motion, they cannot always assume such spatial positions as would correspond to a minimum of free energy in the system. Thus, polymers belong to the systems which are not in thermodynamic equilibrium.[11] This fact is of great theoretical and practical importance:[12] it is the basis for the phenomenon that the very same polymer can have different properties in solid state. The same specimen may be crystallized to different degrees, and many of the crystalline forms will be in a *meta*-stable state for practically an indefinite time under normal service conditions. The same specimen may also be crystallized to the same degree, but if the crystalline morphology is different, the properties will be different also. Mostly the physical properties will differ to a larger degree, e.g. tensile strength, Young's modulus, creep, etc. The non-equilibrium character of polymers is responsible for the influence of processing on the product properties. Full knowledge of the appropriate relationships is necessary to fully utilize all the possibilities that any type of processing offers.

Molecular structure, regardless of whether it is more or less ideal, has an obviously quite dominant role in determining fiber properties. So, the presence or absence of polar forces, as well as their strength, determine many properties. Poly(acrylonitrile), which has very strong polar groups, is able to form good and strong fibers even at low levels of crystallinity; the polar forces hold the supermolecular structure together. Polyolefines, with no polar forces to speak of, need much higher levels of crystallinity and higher molecular mass to form sufficiently stable, low creeping fibers.[13] If well crystallizing polymers have, in addition, strong polar forces or hydrogen bonds, or both,[14,15] like poly(ethylene terephthalate), the resulting fibers have excellent mechanical properties. On the other hand, the dense crystalline morphology of the fibers may create problems with diffusion related properties such as dyeability and water absorption. The last two properties

are important, particularly in fibers aimed at applications in garments, sanitary materials, or insulating materials. Nonpolar polymers, like polyethylene or polypropylene, are used for such applications where dyeing is not important or may be substituted with pigmenting the polymer in bulk.

The chemical structure of polymers also accounts for such properties as stability against heat, oxidation, microorganisms, and different kinds of radiation, as well as resistance to hydrolysis, to attacks of different solvents, etc.[16–18]

In essence, the polymer presents a certain potential range of obtainable fiber properties. Exactly which properties are utilized depends on the processing. The degree of development and the level of sophistication of the process are reflected in the utilized fraction of the potential a polymer offers.

II.2 Polymer Crystals

II.2.a Crystal Structure

Some polymers have been found to be able to crystallize. Those polymers which are able to crystallize give X-ray diffractograms typical of crystalline structure superposed on a halo obtained normally from amorphous materials. The "crystalline part" of polymer diffractograms is similar to powder diffractograms of low molecular mass crystalline compounds. Fibers give usually diffractograms similar to single crystal, indicating presence of orientation.

The duality of x-ray diffraction patterns suggests the notion of semicrystallinity in polymers. Although the first x-ray observations were made in the late twenties or early thirties, the crystallography of polymers is still open for a development effort.

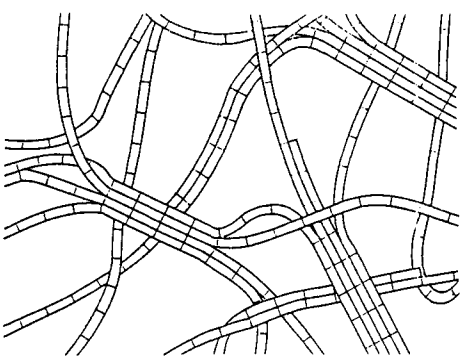

Figure II.3: *First depiction of crystalline structure in polymers after Hermann, Gerngross, and Abitz.*[19–21]

The first attempts to describe the structure of polymer crystals were published

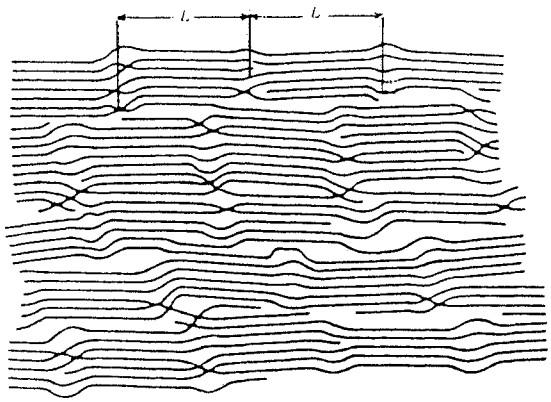

Figure II.4: *Model of polymer crystallinity by Hess and Kiessig.*[24,25] *Reproduced by permission of the copyrights owner, Dietrich Steinkopf Verlag.*

by Hermann and Gerngross[19–21] in 1932. Their model is presented schematically in Figure II.3. With only minor modifications, Statton reactivated the model in 1959.[22] This interpretation of polymer crystals is usually referred to as the *fringed micelle model.* Based on the low angle X-ray scattering obtained from fibers, Hess and Kiessig[23,24] developed in 1942 another model, which was characterized by substantially more order and alternating arrangement of areas of crystalline - non-crystalline material (see Figure II.4). None of the models, though, was able to provide explanation of the material properties, particularly, the properties of fibers.

In 1957, three different laboratories reported the discovery of polymer single crystals.[25–27] Electron microscopic investigations of single crystals revealed that the crystal dimensions were incompatible with dimensions of fully extended polymer chains - *ergo* - the chains in the crystal must be folded. The folds were found to be around 100 Å in size. The large surfaces of the single crystals, though they physically belong to the crystal, contain the molecule folds. The folds do not have the packing regularity of a crystal, hence they may then be considered noncrystalline. The thickness of single crystal was found to be variable and dependent on the growth conditions: temperature and medium, e.g. solvent or melt. Thickness of the crystal lamellae, as they have been named, has been found to coincide with the long periodicity, as determined by low angle X-ray scattering. Table II.1 presents, as an example, the relationship between the growth conditions of polyethylene crystals and corresponding long periods.[28] Later investigations indicated that at large supercoolings, the long periods reach a constant value independent of the crystallization temperature.[29–31] Further, it has been found that the long period grows also during isothermal crystallization beginning from some minimum. This minimum value of long period corresponds also to the long period obtained in crystallization from solution.[38] The most recent investigations[39] show that during crystallization of monodisperse polyethylene, the long period grows in steps, doubling, tripling, and quadrupling the minimum long period, l^*. Figure II.5 presents a proposed mechanism of the jump changes of chain folding,[39] which

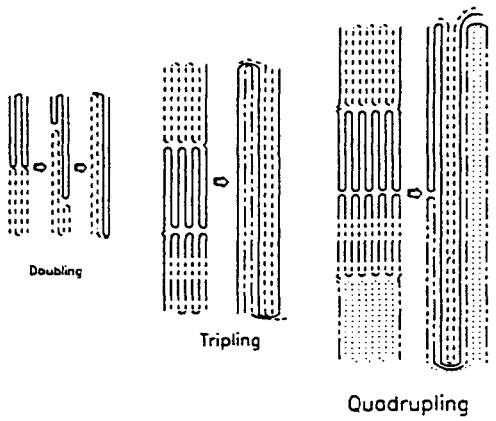

Figure II.5: *Sketch illustrating a scheme for refolding which leads to multiplication of the minimum fold size. Reproduced from P. J. Barham and A. Keller*[39] *by permission of the copyrights holder, John Wiley & Sons, Inc.*

is observable irrespectively of the crystallization medium, but in the melt it proceeds at substantially higher rates.

Table II.1.
Long Period of Polyethylene Crystals
in Relation to Growth Conditions.

Medium	Temperature, ^oC	Long Period, Å
o-Xylene	50	92.5
o-Xylene	60	102.0
o-Xylene	70	111.5
o-Xylene	80	120.5
o-Xylene	90	150.0
Polyethylene melt	120	190.0
Polyethylene melt	125	223.0
Polyethylene melt	130	355.0

A number of investigators[40–42] have suggested that one molecule may be involved in more than one lamella, creating *tie molecules*. The tie molecules connect different lamellae with stronger bonds than might be provided by the poorly ordered fold planes. E. W. Fischer and co-workers[43] have shown that in general, one molecule, $l*$,[32–37] crystallizes in more than one lamella. In the same paper Fischer describes an X-ray based method of detailed quantitative analysis of the molecule involvement in lamellae.

Based on thermodynamic considerations,[44–48] it was predicted that stability of polymer crystal has two maxima: one at a limited thickness – which depends on crystallization temperature and is realized in folded chain crystals, the other maximum of stability corresponds to fully extended chain conformation. Crystals with fully extended chains have been obtained experimentally. Namely, polyethy-

lene crystallizes with extended chains when the crystallization process is carried out at pressures in excess of 2300 *atm.*[49] Also, polymers with very rigid chains are unable to coil. Therefore, their normal mode of crystallization is with extended chains. Some of the so-called *high performance* fibers are based on such, or similar, polymers.

What makes polymers crystallize? This is an important question. The answer may be: the tendency to give up an excess of energy which may be achieved by entering into proper positions in relation to other chains. Why is it then that some polymers crystallize and other do not? Regularity of crystalline lattices requires some minimum of regularity in polymer chain. At some point it was believed that the regularity needed is very high,[50] so high that the chains would need to be nearly perfectly stereoregular. Such rigid requirements may be correct if "perfect" crystals are to be obtained. Commonly, however, crystals are not so "perfect" and are able to accommodate chain imperfections. Polypropylene with four to five chlorine atoms per hundred carbon chain atoms shows only relatively minor deformation of crystalline lattice.[51] The degree of crystallinity of polyethylene decreases gradually with the increasing number of "foreign" substituents, like chlorine, methyl, isopropyl.[52] Copolymers with three or five percent of a comonomer are quite well able to form crystalline materials. Different stereoisomers, in comparison to copolymers, represent only a minor disturbance of the chain regularity.[53,54] The feature most detrimental to crystallization is chain branching, particularly long chain and frequent branching. There is evidence that, despite the imperfections, polymers do crystallize, but the imperfections influence the resulting crystal morphology, as well as the crystallization rate.[140]

Great progress in evaluation of X-ray diffraction data made by Hosemann and collaborators[55,56] in the early 1950's led to the formulation of the notion of *paracrystallinity*. Crystalline structure ceased to be treated in terms of "black and white", it moved into the "grey" area. Crystal structure may range from perfection down, through *paracrystals* distinguishing *smectic* and *nematic* morphologies, all the way to an amorphous state. The nematic form describes some degree of lateral order between the molecules, though distances are not fully regular. The smectic form is somewhat more ordered, the chain elements or groups become ordered laterally, though still not in the constraints of a regular crystalline lattice. Methods to analyze the imperfections became known, though the reasons for the imperfections would not be determined equally precisely. Generally, the causes of imperfections are believed to belong to two categories:

primo – those resulting from the irregularities in chain conformation, and

secundo – imperfections of the geometry of the polymer chain itself.

The first category includes improper alignment of the chain in the lattice, unusual configuration of folds, incorporation of chain ends in the lattice, inversion of helix turns, etc. The second category includes steric imperfections, chain branches, comonomer units, chemical imperfections built into the chains, end groups of different chemical nature, etc.[53,57]

It has been shown that even well developed polymer crystals, including single

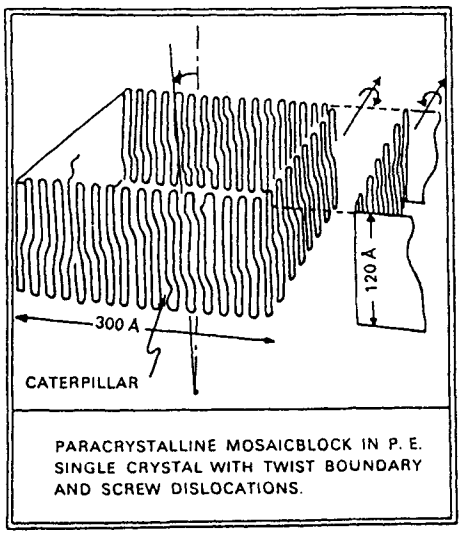

Figure II.6: *Schematic drawing of a mosaic block boundaries, according to R. Hosemann et al.*[58] *Reproduced by permission of the copyright owner, International Union of Crystallography.*

crystals, do not have a completely homogeneous structure. If a single polymer crystal is analyzed by X-ray diffraction, one obtains values for the size of the crystal substantially smaller than the whole crystal mat, usually only around 100 Å. The same is true with any other polymer crystals. Crystals, including single crystals, are built of small blocks which have been given the name *paracrystalline mosaic blocks*.[58,59] The size of the small blocks is strongly related to the paracrystalline lattice distortions:

$$\bar{D} = \frac{\alpha^2 \bar{a}}{g^2} \tag{II.9}$$

Here, a is distance between the lattice planes, $\bar{D}$ represents the average size of the paracrystalline particle in a direction perpendicular to the considered lattice plane, g is the paracrystalline lattice distortion factor, and α characterizes the forces binding the network planes. For many polymers, including polyethylene, the value of α is around 0.15. This relationship indicates that the distortions in crystalline lattice are additive, they superimpose in some way. Therefore the distortions are effectively growing with the growth of the crystal. Depending on the magnitude of the distortions, what is reflected by the g-factor, depends the number of crystalline unit cells grown to the point where the distortion becomes large enough to create a discontinuity of the total structure. The local distortion of the order becomes so large that the area appears to X-ray diffraction as noncrystalline (Figure II.6). The question of lattice distortions has been further refined and related to particular lattices by Blöchl and Bonart.[139] Under the influence of relatively small forces, a single crystal mat or lamella breaks down along the distorted and weak boundaries between mosaic blocks.[60,61]

It has been suggested[89,90,130] that the process of crystallization is preceded by precipitation of the molecules in their coiled form. Subsequently, the molecules crystallize to a large extent within the coils. It has been suggested even that at the conditions close to crystallization, the chain segments within a coil are already largely parallel to obtain the maximum packing.[58] The connections between the lamellae are suggested to originate in the chain entanglements. From a mechanistic point of view these suggestions appear quite plausible.

At the current state of knowledge it is easy to realize that the notion of crystallinity is quite ill-defined. Should the fold planes be considered as crystalline or not? They belong, though, to a single crystal. Even a single crystal is not viewed as hundred per cent crystalline by X-ray. Density and heat of fusion must vary with the degree of crystal perfection. The only solution to the problem appears to be adherence to the concept of paracrystallinity and observation of the necessity to indicate the method of analysis by which the degree of crystallinity has been deduced. Naturally, closer description of the structural features, like the g-factor, type of distortions,[62] long period, etc., additionally clarifies the meaning, but the analyses may be time consuming and expensive. Thus, very often we must remain satisfied with the more or less approximate description of the order in the polymer solid state.[63,64]

II.2.b Melting of Crystals

If a thermodynamic equilibrium would exist in a partially crystalline system, then the change in free energy during the melting of a small crystal layer would equal:

$$\Delta G^0 = \Delta H^0 - T\Delta S^0 = 0 \tag{II.10}$$

Here ΔG^0 is change in free energy, and ΔH^0, ΔS^0 are changes of melting enthalpy and melting entropy, respectively. All the values are calculated per mole. From equation II.10 one may find the equilibrium temperature:

$$T' = \Delta H^0/\Delta S^0 \tag{II.11}$$

If the actual temperature of a specimen would become greater than T', then ΔG^0 would become negative and the crystal would melt. If, on the other hand, the specimen temperature would decrease below T', then ΔG^0 would become positive and further crystallization would proceed.

In case of low molecular mass compounds, when the crystals are sufficiently large, ΔG^0 and ΔS^0 are material constants which do not change. In such cases, equation II.11 defines the melting point. For high molecular mass compounds, both enthalpy and entropy change during melting. The enthalpy of melting depends quite strongly on the crystallization temperature and on the molecular mass of the polymer. The value of enthalpy increases with increasing crystallization temperature and decreases with increasing molecular mass to reach an equilibrium point for infinitely long polymer chains at the melting temperature.[104]

The total entropy, S, of a polymeric system consists of:

1. Transition entropy, S_t, which is connected with vibrations of the center of gravity of the entire molecule.
2. Entropy of internal vibrations, S_w, which is related to the vibrations of different segments of a molecule, while the center of gravity does not shift.
3. Configurational entropy, S_c, which arises from changes of form and spatial arrangement of the molecule.

In effect one may write:

$$S = S_t + S_\nu + S_c$$

During the melting of polymers, the configurational entropy, S_c, undergoes changes and because of this the equilibrium temperature, T' changes also. This complicates an adequate description of the melting phenomena in polymers. In addition, the degree of crystallinity may also be affected by the crystallization temperature.[64] Polymer melting may be described adequately only in the form of a relationship between the crystallization temperature and the corresponding melting temperature, as it is shown in Figure II.7. The slope of melting temperature, T_m, against crystallization temperature, T_c, is usually around 0.5.[1] In practice, however, the values range from 0.3 to 0.8. The large deviations from the expected value of 0.5 may be partially due to the fact that experimental determination of the relationship is rather difficult. Also, at larger supercoolings the melting temperature becomes constant and independent of the crystallization temperature.[29–31] If the point is not well defined, the experimental points may become confused, leading to an incorrect slope. The slope, on the other hand, is of utmost importance, as it determines the point where the temperature of melting equals the temperature of crystallization, $T_m = T_c$, that is the *equilibrium melting point*, T_m^0. Practically, this point is determined by the point of intersection of the line of T_m *versus* T_c with the line of slope equal one. The thermodynamic equilibrium melting pint is defined as the temperature at which the free energy of an infinite crystal, consisting of fully extended chains, is equal to that of a liquid polymer.[28] Equilibrium melting point is a material constant, barring any alterations resulting from polymer chain imperfections. However, such cases are rather common. Polyethylene crystallized under high pressure does melt at the equilibrium melting temperature, or close to it.

Molecular mass has an influence on melting point.[1,66,104]

$$T_m = T_m^0 \cdot \frac{2RT_mT_m^0}{(\Delta H_m)_u} \cdot \frac{lnX}{X} + f(x) \qquad \text{(II.12)}$$

Here $(\Delta H_m)_u$ is the melting enthalpy of a monomer unit, R is, as usual, the gas constant, and X is degree of polymerization. $f(X)$ represents a long expression, but its numerical value is normally negligibly small. This influence is primarily a reflection of different chain end groups acting as impurities. Consequently, the

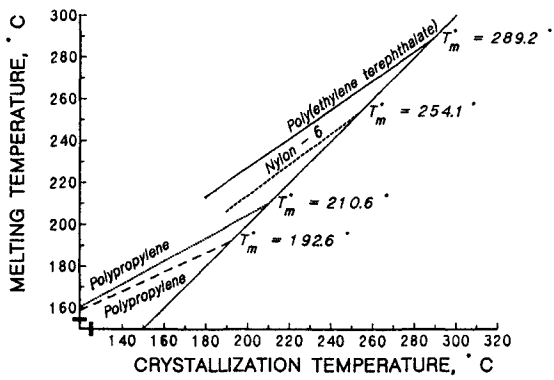

Figure II.7: *Relationship between crystallization and melting temperatures: poly(ethylene terephthalate):*[95] $T_m = 0.694\,T_c + 88.43$; *nylon-6:*[132] $T_m = 0.7445\,T_c + 64.91$; *polypropylene:*[131] $T_m = 0.4644\,T_c + 103.13$ *and* $T_m = 0.5501\,T_c + 97.74$.

influence decreases strongly with increasing molecular mass, so for the majority of common cases it may be neglected. Recently, it has been also reported[67] that molecular mass has some effect on the lamella growth, and this would, naturally, influence melting temperature. However, the influence becomes negligible already above degree of polymerization of 500, and its influence decreases further with increasing degree of polymerization.

As has been mentioned above, the crystalline long period depends on crystallization temperature. Now we see that melting point depends on the size of long period; thus, melting temperature depends on crystallization temperature. The logic of structure and behavior is complete. However, one needs to take into account the medium in which crystallization proceeds, and whether refolding is possible or not. This may modify the melting point.

Polymers do not usually have sharp melting points. It is still not entirely clear what are the thermodynamic reasons underlying this fact. The ratio of the fold surface area to the crystal size depends on long period:[68]

$$T_m = T_m^0 \left[\frac{1 - 2\sigma}{(L\Delta H_f)} \right] \tag{II.13}$$

where σ is surface free energy of the fold surfaces, ΔH_f heat of fusion, and L is long period. It is claimed[69,70] that heat of fusion decreases with molecular mass. On the other hand, melting temperature is sensitive to molecular mass only at low molecular masses (*e.g.* for polyethylene below $2 \cdot 10^4$)[71]

The theory of partial melting[42,72,94] treats the fold sites differently. It assumes that a polymer below its melting point reaches its absolute minimum of free energy when it is almost completely crystalline. The steric hindrances do not allow the minimum of free energy to be reached. Only a relative, metastable equilibrium between the crystalline and unordered layers may be achieved. The length of the unordered chains reflects a temperature dependent equilibrium, and this explains the broad melting of polymers, as well as some decrease in crystallinity. The

latter is accompanied by an increase of the thickness of interlamellar layers as temperature increases. In addition, surface melting results in an increase of specific heat. Taking these into account, the great influence of long periodicity on the thermal behavior of polymers becomes obvious. The dependence of the degree of crystallinity on temperature is:[42]

$$\alpha(T) = \left(1 + dT \cdot \frac{\rho_a}{L\rho_\alpha \pi}\right)^{-1} \tag{II.14}$$

Here ρ_a is density of the unordered layer, ρ_α is density of the crystalline layer, L is thickness of the crystalline layer, and d stands for the thickness of the unordered layer.

Partial melting may take place only when the unordered molecules have both ends tied to the crystal surface. Figure II.8 shows such situations as cases A and B. Case D, with only one end tied in the crystal, does not aid the surface melting. In cases of typical tie molecules, like case C, partial melting should not be expected, since the distance between the tied points is affected by melting. Cases like E are not very likely to occur, but should they happen, melting may be affected. Significant experimental support, based on X-ray analyses, for the partial melting theory has been reported by Kavesh and Schultz.[73]

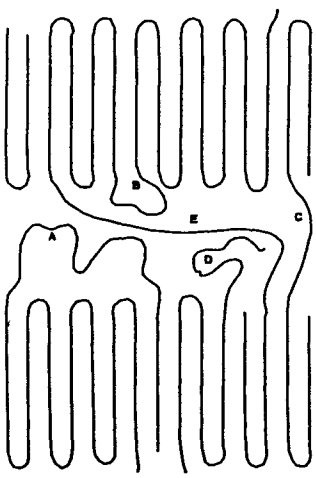

Figure II.8: *Possible chain arrangements, other than adjacent reentry, between crystalline lamellae. After Fischer.*[42]

Newer investigations[137] show that partial melting is due also to the "wandering" of paracrystalline portions between crystalline $\leftrightarrow$ paracrystalline (*intermediate*) $\leftrightarrow$ amorphous. Partial melting involves not only the chain folds; a large role is played by the distribution of long period sizes.[138]

Besides surface melting, there are several other reasons why melting may be broadened:

- Small temperature gradients during crystallization may cause small differences in the size of long period, and furthermore in melting temperature.
- Imperfections in the crystalline lattice.[12,28]
- Impurities lower the melting points of crystals, as in the case of low molecular mass compounds.
- Chain branching has a very complex influence on melting point, much more complex than formulated by Flory.[74,75]

The great number of possible combinations of length, frequency, and distribution of branches along the chains give a basis for the complexity.[71] The true reasons for melting point broadening are, most likely, of very complex nature and attributable to many factors,[76] including the broadening effect of the instruments used.

If a polymer crystal is subjected to elevated temperature, though still substantially below its actual melting temperature, the melting temperature may increase. This process is called *annealing*. The annealing effect is observable above a certain temperature, T_α, which coincides with a transition in the viscoelastic spectrum, the so called α_c transition. In terms of structure, long period grows exponentially with time to an asymptotic value.[28,77–82] Macroscopic density of the crystal also increases. There is no linearity in the relationship between the long period growth and temperature. Density increases show a linear relationship with the reciprocal value of the long period for a given constant temperature. When the annealing temperature exceeds a certain maximum that is close to the melting point of the specimen, the long period does not reach an equilibrium.[82]

Newer investigations[141 & *ref*] show that not all crystals have equally strong α_c relaxation, which is related to the translational chain motions. The translation may proceed through various mechanisms, like chain rotation, helical jumps, "crankshaft" jumps. The translation is obviously more difficult, if possible, for polymers with large side groups, rigid chains, and extensive chain entanglements. Some polymers do not have the α_c transition; they form *nonductile crystals* , or according to other terminology, are *crystal fixed.* The rate of growth of long period is considered dependent on molecular mass,[83] which is usually connected with higher degree of chain entanglement. The growth of long period during annealing is accomplished by a mechanism similar to refolding during crystallization: by longitudinal translation of the chains within the crystalline lattice after the lattice has been softened sufficiently for such a process to take place. The softening is possible within the temperature interval beginning with T_α and upwards to some temperature close, but not reaching, the actual melting point of the specimen.[80,81] It is also possible that partial melting is involved in the process.[76,78] There are conflicting views regarding the influence of annealing on the crystal perfection: some authors believe that the perfection increases,[82] others claim the opposite effect to be true.[28]

Annealing processes are accompanied by macroscopic changes of the sample shape, *e.g.* shrinking when a sample was previously oriented, or formation of holes

during annealing of single crystal mats. These changes of shape may occur only when a sample is annealed without a restraint imposed on its dimensions. All of the description given above concerns only such cases. During isometric annealing, polymers behave differently. Such cases will be discussed in other sections.

It is not without significance whether a sample is annealed in air or in a liquid. Annealing in liquids is much more effective, the new equilibrium is reached faster even when using liquids which do not interact physicochemically with the polymer. A more intense heat transfer must be responsible for the accelerating effect.[84]

In experimental practice, the measured melting temperature often depends on the heating rate during the experiment. This effect may be related to the partial annealing.[85]

Heat treatment, sometimes even at relatively low temperature, can have an influence on the entropy of some noncrystalline elements of the structure. Stresses on noncrystalline molecules imposed by crystallization of other molecule segments may gain a chance of relaxation. Such a relaxation would result in a change of configurational entropy. Even without noticeable change in long periodicity, melting point may be affected,[86] but certainly the macroscopic shape of the specimen will be altered.

There are known cases when annealing caused changes of the crystallographic form.[87,88] Such change, if it takes place, is responsible for the most serious changes of melting behavior. Other properties may be affected also, and quite strongly at that.

II.2.c Crystallization Kinetics

It is generally accepted that the kinetics of polymer crystallization follows the Avrami equation originally developed for low molecular mass compounds and for metals in particular:[91–95]

$$1 - \alpha = \exp(-Kt^n) \tag{II.15}$$

In this equation α represents the degree of crystallinity, t is time, n is constant, depending on the process of nucleation and assuming values $1 \leq n \leq 4$, which according to the original development must be integers. K is here a rate constant. The majority of polymers seem to follow the equation fairly well, but n is almost always fractional. The equation reflects neither the influence of molecular mass on the kinetics, nor the temperature dependence of the process.

Another approach to crystallization kinetics is also based on thermodynamic considerations. The earliest notions go as far back as Gibbs.[96] R. Becker[97] formulated the nucleation rate in a condensed phase, $n*$, as:

$$n^* = n_0 \exp\left(-\frac{\Delta F^* + \Delta\phi^*}{kT}\right) \tag{II.16}$$

Here n_0 is an unspecified constant, ΔF^* is the free energy of activation for the transport of a molecule across the phase boundary, k is Boltzmann's constant, and

T is temperature. $\Delta\phi^*$ is the greatest contributor in the equation and represents a "barrier" which is inversely proportional to temperature. Fisher and Turnbull[98] reformulated the equation:

$$\Delta\phi^* = \frac{4\ b_0\ \sigma_1\ \sigma_2}{\Delta f} \tag{II.17}$$

where b_0 is thickness of the crystallizing entity, and is assumed constant; σ_1 and σ_2 are the interfacial free energies per unit area for the nucleus faces $a\,b_0$ and $c\,b_0$; Δf represents the free energy of fusion per unit of volume of the macroscopic crystal:

$$\Delta f = \frac{[\Delta h_f(T_m^0 - T)]}{T_m^0} \tag{II.18}$$

In equation II.18 Δh_f is the heat of fusion per unit volume of the crystal, T_m^0 is the equilibrium melting point, T is crystallization temperature. Thus, equation II.16 in the Fisher and Turnbull version may assume the following form:

$$n^* = \left(\frac{NkT}{h}\right) \exp\left(-\frac{\Delta F^*}{kT}\right) \exp\left[-\frac{4\ c_0\ \sigma_1\sigma_2\ T_m^0}{\Delta h_f \times \Delta T \times kT}\right] \tag{II.19}$$

The additional notation in equation II.19 has the usual meaning: N is Avogadro's number, h is Planck constant, $\Delta T = T_m^0 - T$.

Hoffman and co-workers[99] have modified the Fisher-Turnbull equation and for three dimensional homogeneous nucleation of polymer crystal they suggest:

$$I^* = \left(\frac{NkT}{hV_m}\right) \exp\left(-\frac{\Delta F^*}{RT}\right) \exp\left\{-\frac{32\ \sigma^2\ \sigma_e(T_m^0)^2}{[\ \Delta h_f \times \Delta T \times kT]^2}\right\} \tag{II.20}$$

Here V_m represents *" molar volume of the order of magnitude of that associated with a chain length of the fold period"*; as the free energy of activation for transport. WLF equation for activation energy of flow (see chapter on rheology) is used to describe the transport,[12] $\Delta F^* = \Delta F^*_{WLF} = 4120T/(51.6 + T - T_g)$, where T_g is the glass transition temperature. To improve the agreement between the results calculated from equation II.20 and those obtained from experiment, the authors[99] add to the denominator of the last segment of the equation a correcting factor y^2, with the value of y close to unity.

There were attempts made to improve the agreement between equation II.20 and experimental data by dividing the problem into three "regimes". Definition of the "regimes" is based approximately on the degree of supercooling.[113–117] These attempts appear to be somewhat artificial however, and the entire Hoffman-Lauritzen theory has been subjected to very severe criticism.[118–123] Improvements of the equation, as well as new solutions of the problem have been suggested by many authors,[118–130] many of the solutions are based on extension of the Avrami equation to nonisothermal conditions. These efforts offer some small improvements, but none of them is significant, so far. A detailed review of the efforts may be found in a paper by Di Lorenzo and Silvestre.[142]

Confrontations of experimental results with equation II.20 show some agreement, though it is not complete. Figure II.9 presents a superposition of the experimental crystallization rate against temperature with the least square fit of the data into equation II.20. This happens to be one of the closest results obtainable. Least square fits give a coefficient for the nucleation term very close to the values

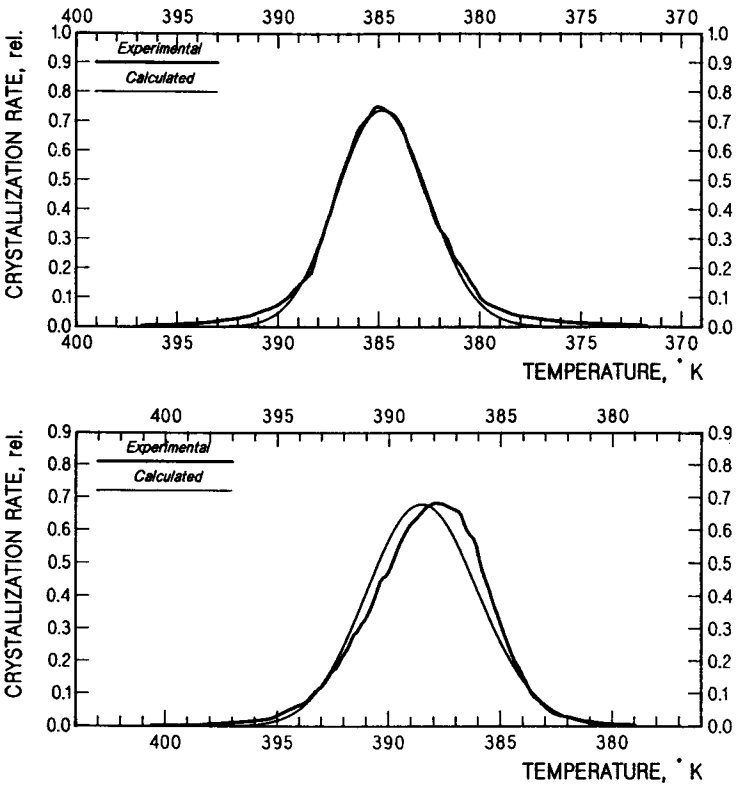

Figure II.9: *Experimental crystallization rate (heavy line) in comparison with a least square fit into Equation II.20. Experimentally determined activation energy of flow was used in the calculation. Two different polypropylenes.*

expected from the theory. However, the "flow" term with the WLF activation energy calls for coefficients ranging between 50 and 60. Thus the model of this segment must be deemed incorrect. The WLF equation is valid for temperature close to glass transition, and by no means higher than 40 or 50 ° K. Crystallization, on the other hand takes place usually at much more than 100 ° K above glass transition temperature. Similar reservations have been voiced earlier by Mandelkern. The shape of the rate curve with the WLF energy indicates that the crystal

growth tends to lag behind the nucleation, but for quiescent crystallization the discrepancies are not large and are usually taken as experimental error. If, instead of the WLF activation energy, activation energy determined experimentally from polymer melt flow is used, (see section III.8) the agreement between the equation II.20 and experiment improves only marginally. There is still a coefficient substantially different from unity. Use of the rheologic shift factor, instead of activation energy, also improves the fit a little, though not enough. These observations lead to the suspicion that the assumption that the overall rate of crystallization is solely governed by the nucleation rate may be incorrect, at least as far as polymers are involved. The subject is discussed somewhat further in section IV.5. As imperfect as it may be, equation II.20 by Hoffman and co-workers remains for the time being the most convenient way to describe crystallization kinetics.[120]

A very significant finding, based on atomic force microscopic studies, has been reported lately:[131] growth of lamellae does not proceed at a constant rate. Authors of the paper suggest that besides the primary nucleation rate, I_0, there is a secondary nucleation on the growth surfaces. The combined nucleation rate is described as follows.

$$I = I_0 \exp\left[-\frac{4l_0\sigma_a\sigma_b}{(\Delta H)kT}\right] \times \left[-\frac{8\sigma_e\sigma_a\sigma_b}{(\Delta H)kT}\right] \times \left[-\frac{\Delta E_{act}}{R(T-T_g)}\right] \qquad \text{(II.21)}$$

where I_0 is the rate of formation of the initial nucleation, l_0 is the fold period of the initial nucleus, which may or may not be identical with the lamellae fold length, depending on the growth conditions, E_{act} actvation energy for molecular motion. The remaining notation is as in equation II.20.

The authors[131] present an excellent agreement of their experimental data with the equation. The work seems to represent a movement in a good direction, however, it is somewhat too early to estimate generality of the solution; probably, it is still incomplete.

It is well known that the rate of crystallization is affected by molecular mass. An example of experimental demonstration of such a dependence is presented in Figure II.10.[100]

In the case of polydisperse systems (in industrial practice we have always to deal with such polymers) the crystallization rate is proportional to the number average molecular mass.[101,104] It has been also reported[105,106] that the relationship between crystallization half-time and number average molecular mass goes through a minimum, tion of which varies with the temperature of crystallization.

For a lower crystallization temperature, the minimum in the rate of crytallization shifts toward lower molecular masses. These reports, however, did not find any additional confirmations. On the other hand, it has been found[35,40] that fractionation according to molecular mass may take place during crystallization of polydisperse polymers. This indicates that the molecular mass influence is strong indeed. In equation II.20 the molecular mass is reflected only indirectly through its influence on the surface energy, which increases with increasing molecular mass. For polyethylene this relationship is given in table II.2.[122]

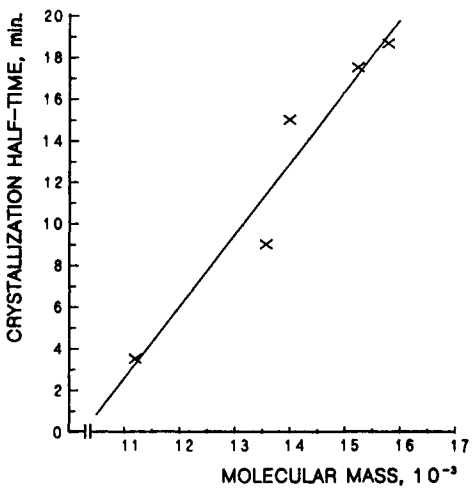

Figure II.10: *Half-time of crystallization of poly(ethylene terephthalate) in relation to the number average molecular mass.*[100]

For the sake of illustration, crystallization half-time for several polymers, as obtained from isothermal crystallization interpreted according to the Avrami equation (II.15), is quoted in Figure II.11.

Table II.2
Relationship Between Surface Free Energy
and Molecular Mass[122]

M_w	$\frac{M_w}{M_n}$	σ, $\frac{erg}{cm^2}$
15,700	1.10	13.1
17,000	1.11	16.0
25,200	1.08	15.3
61,600	1.09	16.3
83,900	1.10	17.4
115,000	1.15	19.4
195,000	1.11	17.9

The descriptions of crystallization kinetics do not take into account the new developments in the area of crystal structure. All the solutions suggested so far assume that polymers crystallize with the chains folded, the fold size depending on the temperature — at equilibrium melting temperature the fold size equals the size of the extended chain (it is infinite). Newer suggestions of the relationship between molecule coils in the melt, or solution, and crystallization into mosaic blocks have many logical connections with other facts, but it would be very difficult to interpret

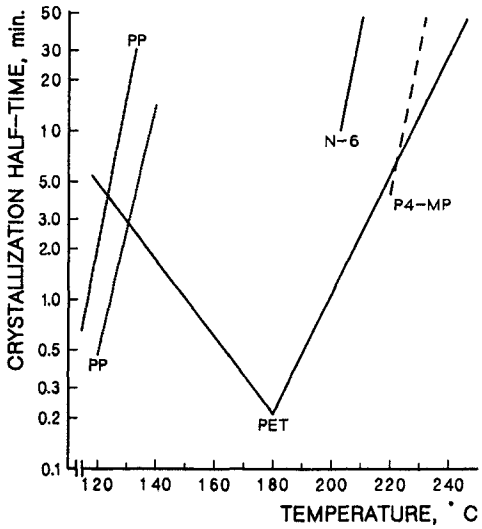

Figure II.11: *Influence of crystallization temperature on crystallization half-time.*[95,132,133] *PET - Poly(ethylene terephthalate), PP – polypropylene, N-6 – poly(aminocaprolacam) (nylon-6), P4-MP – poly(4-methylopentene).*

these in any quantitative terms. Also, the suggestion of parallelization of chains already in the coils[130] connects well with the mosaic blocks, but it also has the flavor of predetermined nucleation, and this may be difficult to reconcile with the available evidence on kinetics.

Another aspect that might have substantially larger influence than admitted so far in kinetics is rheology, especially chain entanglements and relaxation processes.

II.3 Polymer Solutions

Even though macromolecules dissolve more slowly, with more difficulty, and usually solutions of relatively low concentration are obtained, there are similarities between them and the solutions of low molecular mass compounds. If a polymer has cross linked structure, which usually forms a tridimensional grid, the molecules cannot be fully separated and a solution cannot be formed. If under such circumstances a solvent penetrates into the network, it swells it: a *polymer gel* is formed.

The similarity between solutions of polymers and of low molecular mass compounds permits that the classic general thermodynamics of solutions may be applied also for polymer solutions, though with qualified success.[134–136] In agreement with the second law of thermodynamics, the Gibbs' free energy G is related to enthalpy, H, entropy, S, and temperature by the following equation:

$$G = H - T\,S = U + p\,V - T\,S \tag{II.22}$$

where U is internal energy, p represents pressure, and V stands for volume.

The change of Gibbs' energy resulting from the addition of one mole of a component i to an infinite volume of a solution is named partial molar Gibbs' energy, or *chemical potential*, μ_1:

$$\left(\frac{\partial G}{\partial n_i}\right)_{T,p,n_i} = \bar{G}_i = \mu_i \tag{II.23}$$

After some mathematical manipulations which are described in the textbooks of polymer physics or thermodynamics one may arrive at the relationship:

$$G = H - T\,S = U + p\,V - T\,S \tag{II.24}$$

where U is internal energy, p represents pressure, and V stands for volume.

Mathematical manipulations lead further to the relationship:

$$\mu_i = \mu_i^o + R\,T\,lna_i = \mu_i^o + R\,T\,ln(x_i\gamma_i) \tag{II.25}$$

where μ_i^o is the chemical potential of a pure substance. The relative activity, a, may be separated into the mole fraction, x_i, and the coefficient of activity, γ_i. While the contribution of the mole fraction is called the ideal component, the contribution resulting from the coefficient of activity is called the *excess function*:

$$\Delta\mu_1 = \mu_i - \mu_i^o = R\,T\;\; x_i + R\,T\,lnc_i = \Delta\mu_i^i + \Delta\mu_i^e \tag{II.26}$$

According to the magnitude and sign of the excess function the solutions may be classified into four types: ideal, athermal, regular, and real (irregular). If a solution is ideal then the contribution to Gibbs' energy results from the ideal entropy of mixing, the enthalpy is zero. In athermal solutions the enthalpy of mixing is equal zero but the entropy of mixing is different than the ideal. In regular solutions, enthalpy of mixing is not zero, and there is no excess of entropy of mixing. For irregular solutions the enthalpy of mixing and the excess entropy of mixing are different from zero.

In macromolecular science we have the notion of θ-solutions. These are pseudoideal solutions where the enthalpy of mixing and the excess of entropy of mixing compensate each other. The exact compensations usually take place at some temperature, specific for the system, which is called the *theta temperature*. The θ-solutions behave like ideal solutions, though by definition they are not ideal, as the enthalpy of mixing and excess entropy of mixing are different from zero. Also, ideal solutions are independent from temperature, while the behavior of θ-solutions is temperature dependent.

An amount of energy equal to $N\,z\,\epsilon/2$ per one mole is needed to separate molecules at an infinite distance; here z is the number of neighbors, and ϵ is the energy per bond, N is Avogadro's number. This energy equals the internal molar energy of evaporation, ΔE_{vap}, and in relation to the molar volume, V , one may write:

$$e_j = \frac{\Delta\,E_{vap}}{V_j} = -0.5\frac{N\,\epsilon\,z}{V_j} \tag{II.27}$$

The quantity e is called *cohesive energy density* and the square root of the cohesive energy density is called *solubility parameter*: δ:

$$\delta_j \equiv e_j^{\frac{1}{2}} \tag{II.28}$$

Mixing of solvent, s, and polymer, p, produces two polymer - solvent bonds at the expense of one solvent - solvent bond and one polymer - polymer bond. The energy change is then:

$$2\ \Delta\ \epsilon = 2\ \epsilon_{ps} - (\epsilon_{ss} + \epsilon_{pp}) \tag{II.29}$$

In accordance with quantum mechanics considerations, the interaction of two different spherical molecules on the basis of dispersion forces is equal to the geometric mean of the interaction energies of the involved molecules between themselves. One may write then:

$$\epsilon_{ps} = -(\epsilon_{ss} \cdot \epsilon_{pp}) \tag{II.30}$$

Equation II.29 may be rewritten as:

$$-2\ \Delta\epsilon = (\epsilon_{ss}^{\frac{1}{2}})^2 - 2\ \epsilon_{ps} + \epsilon_{pp}^{\frac{1}{2}})^2 \tag{$II.29\,a$}$$

And from equations II.29a and II.30 in relation to the molar volume

$$\Delta\ \epsilon = -\frac{1}{2}\ \left(|e_s s|^{\frac{1}{2}} - |e_{pp}|^{\frac{1}{2}}\right)^2 \tag{II.31}$$

By the definition of the solubility parameter and in relation to the molar volume one may write :

$$\Delta\epsilon = -\frac{1}{2}\,(\delta_s - \delta_p)^2 \tag{II.32}$$

Equation II.32 represents the basis of the frequently used practical system of predicting expected solubility. If there is a large difference in the absolute value of the cohesive energy densities, then there will be essentially no interaction, and no dissolution will take place. The same is true in relation to the solubility parameters. If, on the other hand, the difference between the two solubility parameters (or cohesive energy densities) is zero, then the polymer will be well soluble. The question arises: How large a range around zero still allows for dissolution to take place? The empirically found answer is: between ± 0.8 and ± 3.4. The uncertainty of the answer lies in the fact that the solubility parameter is considered to consist of three components: $\delta^2 = \delta_d^2 + \delta_p^2 + \delta_h^2$, related to dispersion, dipole, and hydrogen bonding forces, respectively. Dispersion forces do not vary appreciably, but the other components do. Consequently, the solubility parameters are classified for polarity and hydrogen bonding. Even with this differentiation, the system is not fool-proof, it gives only orientational predictions. The old rule that "like dissolves like" is not to be forgotten in practical considerations of solubility.

The solubility parameters may be calculated from equation II.27, and the necessary data for solvents are tabulated in literature. Since polymers cannot be

brought into vapor state, the solubility parameters may be determined only indirectly. It is important to stress that polymer solubility is very "sensitive", it may be affected by differences seemingly as small as distribution of substituents along the chain, not to speak of stereoregularity of the chain, and the like.

With the help of statistical thermodynamics; the equation for molar enthalpy of mixing has been derived as:[1]

$$\Delta H = R\,T\,x_s\,\phi_p\,(\chi_0 + \sigma\,\phi_p) \tag{II.33}$$

where

$$\chi = \frac{z\,X_s\,\Delta\epsilon}{k\,T} \tag{II.34}$$

and

$$\chi = \chi_0 + \sigma\phi_p \tag{II.35}$$

The designations in equations II.32 to II.34 are: x is mole fraction, ϕ is volume fraction, X is number of segment units, z stands for the number of neighbors, N is the number of molecules, χ represents the Flory - Huggins polymer solvent interaction parameter k, T, R, have the conventional meaning. The Flory - Huggins interaction parameter, χ , is assumed to have a linear dependence on the volume fraction of polymer with the slope of σ. This is correct for some polymers, and with some approximation for the others; for lower concentration the assumption is mostly correct. The reduced molar Gibbs energy of mixing, in view of the above, may be given as

$$\frac{\Delta\bar{G}}{RT} = \frac{\phi_s\phi_p\chi_0 + \phi_s\vartheta_p^2\sigma + \phi_s\ln\phi_s + X_sX_p^{-1}\phi_p\ln\phi_p}{X_s} \tag{II.36}$$

Figure II.12 represents the reduced molar energy of mixing as a function of the volume fraction of a polymer. The different curves are calculated for the degree of polymerization of 100 and solvent of $X_s = 1$. The interaction parameter is as given on the graph. The temperature slope, σ, is taken as zero. For the sake of comparison, an additional curve for the degree of polymerization of one (it is for the monomer) is given with $\chi = 0.5$. From the graph one may easily appreciate what an increase in the degree of polymerization does to solubility, not to speak of the influence of the interaction parameter.

Along similar lines of statistical thermodynamic reasoning, one may give formulations for the chemical potential of solvent:

$$\Delta\mu_s = RT\left[(\chi_0 - \sigma + 2\sigma\chi_p)\,\phi_p^2 + ln\,(1-\phi_p) + (1 - X_s/X_p)\,\phi_p\right] \tag{II.37}$$

and chemical potential for polymer:

$$\Delta\mu_p = RT\left[(\chi_0\phi_s + 2\sigma\phi_p\phi_s - 1) \times \times\phi_s X_p/X_s + \phi_s + \ln\phi_p\right] \tag{II.38}$$

Figure II.13 presents the chemical potential of a solvent with degree of polymerization of one ($X_s = 1$) as a function of volume fraction of polymer, ϕ_p, of

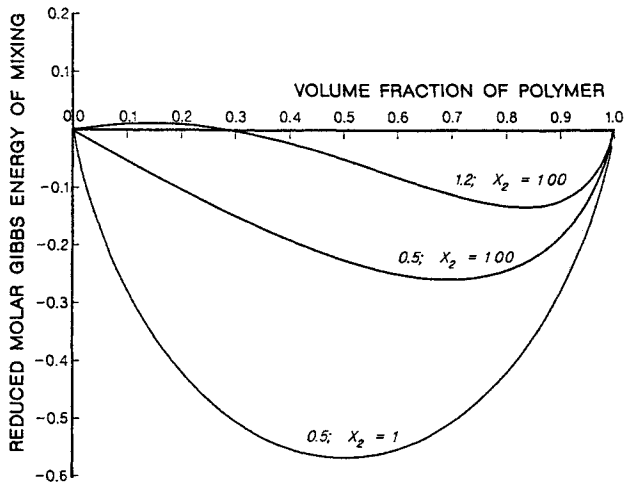

Figure II.12: *Reduced molar Gibbs energy of mixing as a function of volume fraction of a polymer. Data for the degree of polymerization of 100 and various values of the interaction parameter.*

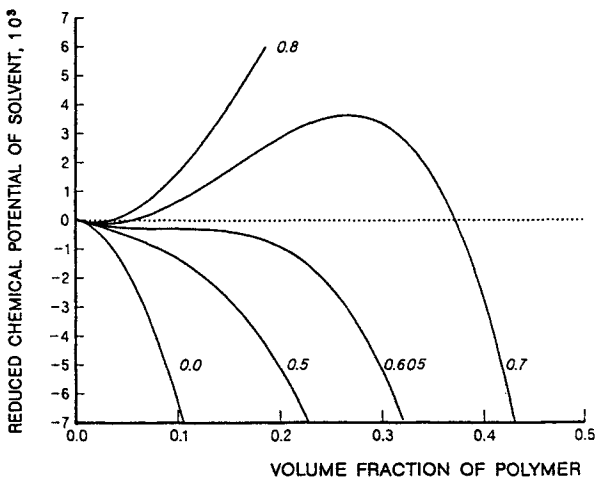

Figure II.13: *Reduced chemical potential of solvent ($X_s = 1$) as a function of the volume fraction of a polymer of degree of polymerization (X_p) of 100. Parameter: polymer - solvent interaction, χ.*

degree of polymerization of $100 \cdot (X_p = 100)$. The calculations for different polymer - solvent interaction parameters have been performed using equation II.36 with slope $\sigma = 0$. With the increasing value of the interaction parameter, the initial portion of the curve becomes more extended and seemingly flatter, though a minimum, initially insignificant, forms. At higher values than some critical χ, a small minimum and a large maximum form.

The chemical potentials, $\Delta\ \mu_s$ and $\Delta\ \mu_p$, may be obtained by extrapolation of the line tangent to the function $\Delta G / RT = f|;(\phi_p)$. The equation of the tangent line is

$$Y = A + B\phi_p \tag{II.39}$$

where

$$B = N_p\ X_p\ \left[\left(\frac{\Delta\ \mu_p}{X_p}\right) - \left(\frac{\Delta\ \mu_s}{X_s}\right)\right] \phi_p^{-1} \tag{II.39 a}$$

and

$$A = \frac{N_p\ X_p\ \Delta\ \mu_s}{\phi_p\ X_s} \tag{II.39 b}$$

The final relationships are then

$$\lim_{\phi \to 0} Y = \frac{N_p\ X_p\ \Delta\ \mu_s}{X_s\ \phi_p} \tag{II.40}$$

$$\lim_{\phi \to 1} Y = \frac{N_p\ \Delta\ \mu_p}{\phi_p} \tag{II.40 a}$$

There is no theory which would describe solubility adequately, completely, and with few exceptions. For this reason, development of a good solution system requires a great deal of experimental work; detailed thermodynamic measurements are to be highly recommended, despite the fact that they are so laborious. However, it is still good to remember the old rule that *"like dissolves like"*.

Some polymers are capable of association in solution. The association is usually due to some specific groups, often end groups. Hydrogen bonding is one of the strongest and most common, but other types of associating forces may be involved. Some stereoregular polymers are capable of the formation of mutually complementary stereo structures – stereo complexes. The associated solutions behave, naturally, like solutions of polymers of appropriately higher molecular mass.

One of the more important and characteristic properties of polymer solutions is viscosity. This topic is treated briefly in section III.7.

II.4 References

1. H.-G. Elias: *Makromoleküle*, Hüttig & Wepf Verlag, Basel – Heidelberg – New York, 4th Edn., 1981; *Macromolecules*, Plenum Press, New York - London, 1984.
2. P. C. Hiemenz: *Polymer Chemistry*, Marcel Dekker Publ., New York – Basel, 1984.
3. F. W. Billmayer, Jr., *A. C. S. Polymer Preprints*,**3, (1961)**, 627.

4. G. Meyerhoff, *Fortschr. Hochpol. Forsch.*,**3 (1961)**, 59.
5. H. A. Stuart (Ed.): *Die Physik der Hochpolymeren*, Springer Verlag, Berlin - Heidelberg, 1954, Vol. 2, 366.
6. N. A. Plate, T. Kheu, and V. P. Shibayev, *J. Polymer Sci., Pt. C*, **16 (1967)**, 1; N. A. Plate, *Pure Appl. Chem.*, **30 (1972)**, 217.
7. P. Ceflin, E. Sittler, and O, Wichterle, *Coll. Czech. Chem. Commun.*, **25 (1960)**, 2522.
8. H. Hopf, A. Mller, and F. Wenger: *Die Polyamide*, Springer Verlag, Berlin – Göttingen-Heidelberg, 1954.
9. H. A. Stuart (Ed.): *Die Physik der Hochpolymeren*, Springer Verlag, Berlin – Heidelberg, 1953, Vol. 1.
10. P. Flory: *Statistical Mechanics of Chain Molecules*, Interscience Publ., New York, 1969.
11. S. Wisniewski, B. Staniszewski, and R. Szymanik: *Thermodynamics of Nonequjilibrium Processes*, D. Reidel Publ., Dordrecht, Holland - Boston, U.S.A. and Polish Scientific Publishers, Warszawa, 1976.
12. H. A. Stuart (Ed.): *Die Physik der Hochpolymeren*, Springer Verlag, Berlin – Heidelberg, 1955, Vol. 3.
13. G. Natta, *S.P.E. Trans.*,**1963**, 99.
14. O. B. Edgar and R. Hill, *J. Polymer Sci.*,**8 (1952)**, 1.
15. H. Mark, *Ind. Eng. Chem.*,**44 (1952)**, 2110; 2124.
16. W. H. Sharkey and W. E. Mochel, *J. Am. Chem. Soc.*,**81 (1959)**, 3000.
17. G. Valk, H. Krussmann, and P. Diehl, *Makromol. Chem.*,**107 (1967)**, 158.
18. E. A. Trippetts and V. Zimmermann, *J. Appl. Polymer Sci.*,**8 (1964)**,2465.
19. K. Hermann, O. Gerngross, and W. Abitz, *Z. Phys. Chem.*,**B10 (1930)**, 371; *Biochem. Z.*,**228 (1930)**, 409.
20. K. Hermann and O. Gerngross, *Kautschuk*, **8 (1932)**, 181.
21. O. Gerngross, K. Hermann, and H. Lindermann, *Kolloid Z.*, **60 (1932)**, 276.
22. W. O. Statton, *J. Polymer Sci.*, **41 (1959)**, 143.
23. K, Hess and H. Kiessig, *Naturwiss.*, **31(1943)**, 171;*Z. phys. Chemie.*, **A193 (1944)**, 196.
24. K. Hess, H. Mahl, and E. Gutter, *Kolloid-Z.*,**155 (1957)**, 1.
25. E. W. Fischer, *Z. Naturforsch.*, **12a (1957)**, 753.
26. P. H. Till, *J. Polymer Sci.*, 24 (1957), 301.
27. A. Keller, *Phil. Mag.*, **2 (1957)**, 1171.
28. P. H. Geil: *Polymer Single Crystals*, Interscience Publ., New York, 1963.
29. Z. K. Walczak, *unpublished results*, 1969.
30. P. Dreyfuss and A. Keller, *J. Polymer Sci., Polymer Phys.*, **11 (1973)**, 193.
31. P. Dreyfuss, *J. Polymer Sci., Polymer Phys.*, **11 (1973)**, 201.
32. J. D. Hoffman and J. J. Weeks, *J. Chem. Phys.*, **37 (1962)**, 1723.
33. J. J. Weeks, *J. Res. Nat. Bur. Stand.*, **A67 (1963)**, 441.
34. J. Dlugosz, G. V. Fraser, D. T. Grubb, A. Keller, J. A. Odell, and P. L. Goggin, *Polymer*, **17 (1981)**, 471.

35. P. J. Barham, R. A. Chivers, D. A. Jarvis, J. Martinez – Salazar, and A. Keller, *J. Polymer Sci., Polymer Letters*, **19 (1981)**, 539.

36. R. A. Chivers, J. Martinez – Salazar, P. J. Barham, and A. Keller, *J. Polymer Sci., Polymer Phys.*, **20 (1982)**, 1717.

37. P. J. Barham, D. A. Jarvis, and A. Keller, *J. Polymer Sci., Polymer Phys.*, **20 (1982)**, 1733.

38. J. Martnez – Salazar, P. J. Barham, and A. Keller, *J. Mater. Sci.*, 20 (1985), 1616.

39. P. J. Barham and A. Keller, *J. Polymer Sci., Polymer Phys.*, **27 (1989)**, 1029.

40. F. J. Padden and H. D. Keith, *J. Appl. Phys.*, **37 (1966)**, 51.

41. H. D. Keith, F. J. Padden, and R. G. Vadimsky, *Science.* **150 (1965)**, 1026; *J. Polymer Sci., Pt. A*, **4 (1966)**, 267; *J. Appl. Phys.*, **37 (1966)**, 4027.

42. E. W. Fischer, *Kolloid Z.*, **218 (1967)**, 97.

43. E. W. Fischer, K. Hahn, J. Kugler, U. Struth, R. Born, and M. Stamm, *J. Polymer Sci., Polymer Phys.*, **22 (1984)**, 1491.

44. E. W. Fischer, *Z. Naturforsch.*, **14a (1959)**, 584.

45. A. Peterlin and E. W. Fischer, *Z. Phys.*, **159 (1960)**, 272.

46. A. Peterlin, *J. Appl. Phys.*, **31 (1960)**, 1934.

47. A. Peterlin, E. W. Fischer, and Chr. Reinhold, *J. Polymer Sci.*, **62 (1962)**, 12; *J. Chem. Phys.*, **37 (1962)**, 1403.

48. A. Peterlin and Chr. Reinhold, *J. Polymer Sci., Pt. A*, **37 (1962)**, 2801.

49. T. Arakawa and B. Wunderlich, *J. Polymer Sci., Pt. C.*, **1967(No. 16)**, 653.

50. G. Natta, P. Pino, and G. Mazzanti, *Gazz. Chim. Ital.*, **87 (1957)**, 528.

51. N. A. Plate, T. Kheu, and V. P. Shibayev, *J. Polymer Sci., Pt. C.*, **1967(No. 16)**, 1133.

52. W. Glenz, H. Kilian, and F. H. Müller, *Kolloid Z.*, **206 (1966)**, 104.

53. T. Amano, *Kolloid Z.*, **206 (1966)**, 97.

54. R. L. McCullough and R. L. Miller, *J. Polymer Sci., Pt. B.*, **1 (1963)**, 77.

55. R. Hosemann and S. N. Bagchi: *Direct Analysis of Diffraction by Matter*, North Holland Publ., Amsterdam, 1962.

56. W. Ruland, *Acta Cryst.*, **14 (1961)**, 1180.

57. E. Martuscelli, *J. Polymer Sci., Polymer Phys.*, **11 (1975)**, 1.

58. R. Hosemann, W. Wilke, and F. J. Balta – Calleja, *Acta Cryst.*, **21 (1966)**, 118.

59. R. Hosemann, K. Lemm, A. Schöhnfeld, and W. Wilke, *Kolloid Z.*, **216-217 (1967)**, 103.

60. I. L. Hay and A. Keller, *Kolloid Z.*, **204 (1965)**, 43.

61. A. Peterlin, *J. Polymer Sci., Pt. C.*, **1965(No. 9)**, 61.

62. D. H. Reneker and J. Mazur, *Polymer*, **29 (1988)**, 3,

63. S. Kavesh and J. M. Schultz, *Polymer Eng. Sci.*, **9 (1969)**, 452.

64. S. Kavesh and J. M. Schultz, *J. Polymer Sci., Pt. A-2*, **8 (1970)**, 243.

65. B. von Falkai, *Makromol. Chem.*, **41 (1960)**, 86.

66. P. J. Flory: *Principles of Polymer Chemistry*, Cornell Univ. Press, Ithaca, New York, 1953, p. 568.

67. Y. Tanzawa, H. Miyaji, Y. Miyamoto, and H. Kiho, *Polymer*, **29 (1988)**, 904.
68. A. Peterlin and G. Meinel, *J. Polymer Sci., Pt. C.*, **1966 (No 2)**, 85.
69. L. Mandelkern, A. L. Allon, and M. Gopalan, *J. Phys. Chem.*, **72 (1968)**, 309.
70. H. E. Bair and R. Salovey, *J. Macromol. Sci., Phys.*, **B3 (1969)**, 3.
71. E. P. Otocka, R. J. Roe, and H. E. Bair, *J. Polymer Sci., Phys.*, **10 (1972)**, 2069.
72. E. W. Fischer, Y. Nukushina, and Y. Itoh, *J. Polymer Sci., Polymer Letters*, **3 (1965)**, 383.
73. S. Kavesh and J. M. Schulz, *J. Polymer Sci., Pt. A-2*, **9 (1971)**, 85.
74. P. J. Flory, *Trans. Faraday Soc.*, **51 (1955)**, 848.
75. M. J. Richardson, P. J. Flory, and J. B. Jackson, *Polymer*, **4 (1963)**, 221.
76. A. Nakajima, S. Hayashi, and H. Nashimura, *Kolloid Z.*, **229 (1969)**, 107.
77. A. Peterlin: *The Role of Chain Folding in Fibers* in *Man Made Fibers*, Ed. by Mark, Atlas, and Cernia, Interscience Publ., New York, 1968, Vol. 1.
78. E. W. Fischer and G. F. Schmidt, *Angew. Chem.*, **74 (1962)**, 551.
79. N. Hirai, Y. Yamashita, T. Mishuhala, and Y, Tamura, *Labor. Surf. Sci., Fac. Sci., Okajima Univ.*, **2 (1961)**, 1.
80. A. Peterlin, *J. Polymer Sci., Pt. B*, **2 (1963)**, 279.
81. J. D. Hoffman, *S. P. E. Trans.*, **4 (1964)**, 315.
82. J. Laboda – Čačković, R. Hosemann, and W, Wilke, *Kolloid Z.*, **235 (1969)**, 1162.
83. A. Peterlin, *Polymer*, **6 (1965)**, 25.
84. D. R. Buchanan and J. D. Dumbleton, *J. Polymer Sci., Pt. A-2*, **7 (1969)**, 17.
85. F. Rybnikař, *Makromol. Chem.*, **110 (1967)**, 268.
86. G. Meinel and A. Peterlin, *J. Polymer Sci., Polymer Letters*, **5 (1967)**, 613.
87. A. T. Jones, J. M. Aizlewood, and D. R. Beckett, *Makromol. Chem.*, **75 (1964)**, 134.
88. H. Awaya, *Nippon Kagaku Zasshi*, **83 (1962)**, 865; cit. in *C. A.*, **58 (1963)**, 14120c.
89. D. M. Sadler and A. Keller, *Macromolecules*, **10 (1977)**, 1128.
90. E. W. Fischer, *cit. in ref. 130.*
91. M. Avrami *J. Chem. Phys.*, **7 (1939)**, 1103; **8 (1940)**, 212.
92. R. B. Williamson: *The Solidification of Polymers*, Massachusetts Institgute of Technology, Res. Rep. **No. R-66-51**, Cambridge, Mass., 1966.
93. P. Parrini and G. Corrieri, *Makromol. Chem.*, **62 (1963)**, 83.
94. H. G. Zachmann and H. A. Stuart, *Makromol. Chem.*, **41 (1960)**, 131.
95. J. H. Griffith and B. G. Rånby, *J. Polymer Sci.*, **44 (1960)**, 44.
96. J. W. Gibbs: *The Collected Works*, Vol. I., *Thermodynamics*, Yale University Press, 1906.
97. R. Becker, *Ann. Physik*, **32 (1938)**, 128.
98. J. Fisher and D. Turnbull, *J. Chem. Phys.*, **17 (1949)**, 71.
99. J. D. Hoffman and F. Gornick: *Nucleation in Polymers* in *The Nucleation Phenomena*, Am. Che. Soc. Publ., 1966; and references cited.
100. W. H. Cobbs and R. L. Burton, *J. Polymer Sci.*, **10 (1953)**, 275.

101. K. Űberreiter, G. Kanig, and A. Brenner, *J. Polymer Sci.*, **16 (1955)**, 53.

102. F. Bueche: *Physical Properties of Polymers*, Interscience Pubs., New York, 1962.

103. P. H. Lindenmeyer and V. F. Holland, *J. Appl. Phys.*, **35 (1964)**, 55.

104. K. Űberreiter and K.- J. Lucas, *Makromol. Chem.*, **140 (1970)**, 65.

105. L. Mandelkern, J. G. Fatou, and K. Ohno, *J. Polymer Sci, Polymer Letters*, **6 (1968)**, 615.

106. P. H. Geil, F. R. Anderson, B. Wunderlich, and T. Arakawa, *J. Polymer Sci., Pt. A*, **2 (1964)**, 3707.

107. A. J. Pennings, *J. Polymer Sci., Pt. C*, **16 (1967)**, 1799.

108. D. M. Sadler, *J. Polymer Sci., Pt. A*, **9 (1971)**, 9.

109. A. Mehta and B. Wunderlich, *Makromol. Chem.*, **153 (1972)**, 327; *Colloid. Polymer Sci.*, **253 (1975)**, 193.

110. B. Wunderlich, *J. Polymer Sci., Pt. C*, **43 (1973)**, 29.

111. E. Ergoz and L. Mandelkern, *J. Polymer Sci., Polymer Letters*, **11)1973)**, 73.

112. D. H. Jones, A. J. Latham, A. Keller, and J. Girolame, *J. Polymer Sci., Polymer Phys. Ed.*, **11(1973)**, 1759.

113. J. D. Hoffman, L. J. Frolen, G. S. Ross, and J. I. Lauritzen, Jr., *J. Res. Nat. Bur. Stand.*, **79A (1975)**, 671.

114. J. D. Hoffman, G. T. Davis, and J. I. Lauritzen, Jr., in *Treatise on Solid State Chemistry*, N. B. Hannay (Ed.), Plenum Press, New York, 1976, Vol. 3.

115. J. D. Hoffman, *Polymer*, **23 (1982)**, 656.

116. J. D. Hoffman, *Polymer*, **24 (1983)**, 3.

117. J. D. Hoffman and R. L. Miller, *Macromolecules*, **210 (1988)**, 3028.

118. F. C. Frank and M. Tossi, *Proc. Roy. Soc.*, **263 (1961)**, 323.

119. F. C. Frank, *J. Cryst. Growth*, **22 (1974)**, 233.

120. J.- J. Point, *Disc. Faraday Soc.*, **68 (1979)**, 167.

121. J.- J. Point, *Macromolecules*, **12 (1979)**, 770.

122. J.- J. Point, M. Ch. Colet, and M. Dosière, *J. Polymer Sci., Polymer Phys.*, 24 (1986), 357.

123. J.- J. Point and M. Dosière, *Polymer*, **30 (1989)**, 2292.

124. M. Hikosaka, *Polymer*, **28 (1987)**, 1257.

125. M. Hikosaka, *IUPAC Conference*, Montreal, Canada, 1990.

126. M. Hikosaka, *Polymer*, **31 (1990)**, 458.

127. D. M. Sadler, *Polymer*, **28 (1987)**, 1440.

128. M. L. Mansfield, *Polymer*, **29 (1988)**, 1755.

129. J. I. Scheinbeim, L. Petrone, and B. A. Newman, *Macromolecules*, **26 (1993)**, 933.

130. T. A. Kavassalis and P. Sundararajan, *Macromolecules*, **26 (1993)**, 4144.

131. J. K. Hobbs, T. J. McMaster, M. J. Miles and P. J. Barham, *Polymer*, **39 (1998)**, 2437.

132. Z. K. Walczak, *unpublished results*, 1968.

133. M. Inoue, *J. Polymer Sci.*, **55 (1961)**, 753.

134. H. Mark and A. Tobolsky: *Physical Chemistry of Polymers*, (Polish transl., Warszawa, 1957, pp. 242–271.

135. G. J. van Amerongen in *Elastomers and Plastomers*, Ed. R. Houwunk, (Polish transl.), Warszawa, 1953, pp. 388 ff.

136. E. E. Walker in *Fasern aus Synthetischen Polymeren*, Ed. R. Hill, Stuttgart, 1956, pp. 336 ff.

137. W. Chen, Y. Fu, B. Wunderlich, and J. Cheng, *J. Polymer Sci., Pt. B, Polymer Phys.*, **32 (1994)**, 2661.

138. G. R. Strobl, M. J. Schneider, and I. G. Voigt-Martin, *J. Polymer Sci., Polymer Phys. Ed.*, **18 (1980)**, 1361.

139. G. Blöchl and R. Bonart, *Makromol. Chem.*, **187 (1986)**, 1525.

140. J. J. Janimak and D. C. Basset, *Polymer*, **40 (1999)**, 459.

141. W. G. Hu and K. Schmidt - Rohr, *Acta Polym.*, **50 (1999)**, 271.

142. M. L. Di Lorenzo and C. Silvestre, *Prog. Polymer Sci.*, **24 (1999)**, 917.

III RHEOLOGY

III.1 Introductory Definitions

In the course of fiber formation from fluids such as polymer melts or polymer solutions, it is necessary to push the fluids through openings, holes, or capillaries under pressure, as well as to extend, to draw the fluids under tensional forces. Therefore, we must pay attention to the behavior of polymeric fluids under such conditions. It is necessary to know how the polymeric fluids behave when subjected to various strains and stresses.[1,2] Rheology is a very large field, so in this little introduction the subject is abbreviated "to bare bones" only. The description is limited to the theory of viscoelasticity, particularly as presented by N. W. Tschoegl[1] and A. J. Staverman and F. Schwartzl.[64] Other important aspects are treated in a sketchy way, with the exception of the slightly more detailed description of capillary flow.

If we have a cylindrical rod, and if we stretch the rod by pulling by its two ends, we supply the force, F, in the direction of the material axis. The applied force causes a deformation, elongation or extension, ΔL, of the initial length, L_0. If the extension is not excessive the deformation will be proportional to the applied force by some proportionality constant: $F = k\Delta L$, where $\Delta L = L - L_0$. If we relate the force to the cross sectional area of the specimen and the increase of length to the initial length, we obtain stress, σ, and strain, ε.

$$\sigma = E \cdot \varepsilon \tag{III.1}$$

Equation III.1 represents the formulation of the Hooke's law, where E represents the proportionality constant, known as the *modulus of elasticity.*

Another deformation type of concern is shearing, or laminar shear flow. Let us assume that we have two surfaces, A, and, B separated by the distance, Y. The space between the two surfaces is filled with a fluid, as in Figure III.1. If the bottom surface, B, is moving in relation to the surface A in the direction x, then the fluid contained between the surfaces will be subjected to a shearing force. The fluid velocity at any distance between the plates will be $v(Y)$, while the fluid velocity at each of the surfaces will remain zero. The force needed to move the surfaces, in analogy to Hooke's law, depends on the surface area and on the gradient of velocity dv/dY. The proportionality constant, η, is called *viscosity.*

$$\tau = \eta\dot{\gamma} \tag{III.2}$$

Here we designate *shearing stress*, $\tau = F/a$, and *rate of shearing*, $\dot{\gamma} = dv/dY$

Both equations, III.1 and III.2, are *constitutive equations*, equations that depend only on the nature of the material and are independent of the geometry of the body. The form of these equations was introduced by Isaac Newton, and materials which obey equation III.2 are often referred to as *Newtonian fluids.*

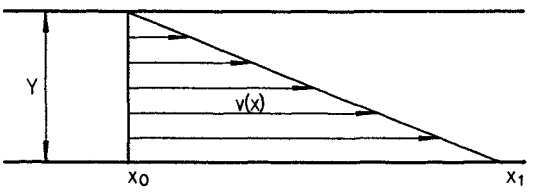

Figure III.1: *Shear flow of a fluid between surfaces.*

In the case of a cylindrical surface, like the interior of a capillary, shear stress at the wall surface, τ_w, may be calculated as

$$\tau_w = Pr/(2l) \tag{III.3}$$

where P stands for the pressure drop in the capillary of length l and of radius r. In reality, certain velocity gradients develop at the entry to the capillary, and these gradients cause some pressure losses. These losses, named after their discoverer, Couette, depend on the radius of the capillary, so equation III.3 is often given in the form which corrects for those losses:

$$\tau_w = Pr/[2(l + nr)] \tag{III.4}$$

The value of n must be determined experimentally.

The rate of shear for the flow in a capillary may be calculated as

$$\dot{\gamma} = \frac{4Q}{\pi r^3} \tag{III.5}$$

where Q is the volume of polymer flowing through the capillary in a unit of time, usually in a second.

Equation III.1 relates to materials which are purely elastic, and equation III.2 describes behavior of materials which are purely viscous. Real materials that are purely elastic or purely viscous are extremely rare; combinations of both behaviors are most common. We shall look into some of the reasons for this.

Usually, when a material is under the action of forces, the forces do not act only in one direction. Hence, it is important to examine the forces active in a body under stress. If we imagine a body in space, the forces and moments acting on this body may be characterized by resultant force elements, moment element, and a unitary vector normal to the surface being acted upon. In a Cartesian coordinate system, the state of stress in a body may be characterized by nine components resulting from three coordinates, one on each plane, and three vectors for each plane (Figure III.2). The state of stress may be represented by a second order *stress tensor*:

$$|\sigma_{ij}| = \begin{vmatrix} \sigma_{11} & \sigma_{12} & \sigma_{13} \\ \sigma_{21} & \sigma_{22} & \sigma_{23} \\ \sigma_{31} & \sigma_{32} & \sigma_{33} \end{vmatrix} \tag{III.6}$$

The components which are perpendicular to the coordinate planes are called *normal stresses* , and are on the diagonal of the tensor $(\sigma_{11}, \sigma_{22}, \sigma_{33})$. The components with "mixed" indices are called *shear stresses*. Analogously, one may derive

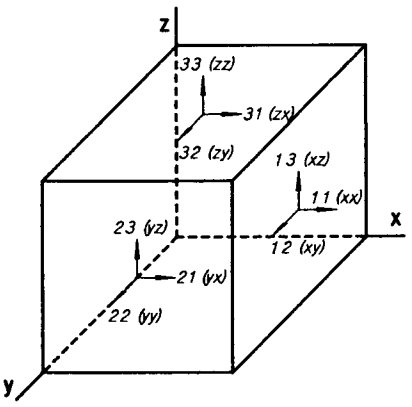

Figure III.2: *Components of the stress tensor.*

a *strain tensor* where

$$\gamma_{ij} = \frac{\frac{\partial u_i}{\partial_j} + \frac{\partial u_j}{\partial x_i}}{2} \tag{III.7}$$

$$|\gamma_{ij}| = \begin{vmatrix} \gamma_{11} & \gamma_{12} & \gamma_{13} \\ \gamma_{21} & \gamma_{22} & \gamma_{23} \\ \gamma_{31} & \gamma_{32} & \gamma_{33} \end{vmatrix} \tag{III.8}$$

Here too, the components on the diagonal are called *normal strains* and the components with "mixed" indices are called *shearing strains.*

According to the definition of deformation in simple shear $\varepsilon_{12} = \partial u_1/\partial u_2$ the corresponding strain component in simple shear is $\gamma_{12} = \partial u_1/2\partial u_2$. Thus ε_{12} may be named the *amount of shear* and γ will be the *shear strain.* In analogy to this the shear rate is twice the corresponding tensor component.

Equation III.2 may be given in terms of the tensor components:

$$\tau = G\gamma \tag{III.9}$$

where G is the *shear modulus*, $\tau = \sigma_{12}$ and $\gamma = 2\lambda_{12}$.

If a material is subjected to isotropic forces (pressure), then in agreement with equation III.7 we have:

$$p = -K(\gamma_{11} + \gamma_{22} + \gamma_{33}) \tag{III.10}$$

where K is the *bulk modulus*

Lateral contraction of a body subjected to uniaxial extension may be expressed as

$$-\gamma_{22}/\gamma_{11} = \mu \tag{III.11}$$

Here μ represents *Poisson's ratio.*

Different moduli and Poisson's ratio may be expressed by each other in a number of different ways:

$$E = \frac{9KG}{3K + G} = 3K(1 - 2) = 2G(1+) \tag{III.12}$$

$$G = \frac{3KE}{9K - E} = \frac{E}{2(1+\mu)} = \frac{3K(1-2\mu)}{2(1+\mu)} \tag{III.13}$$

$$K = \frac{GE}{9G - 3E} = \frac{2G(1+\mu)}{3(1-2\mu)} = \frac{E}{3(1-2\mu)} \tag{III.14}$$

$$\mu = \frac{E}{2G} - 1 = 0.5 - \frac{E}{6K} = \frac{3K - 2G}{6K + 2G} \tag{III.15}$$

Behavior of an elastic material may be expressed also through the *elastic compliance*:

$$\gamma = J\tau \tag{III.16}$$

where J is the *shear compliance*, and $J = 1/G$. In further analogy we have

$$\varepsilon = D\sigma \tag{III.17}$$

Here D is the *tensile compliance* or *stretch*, $D = 1/E$. Bulk modulus, K has corresponding *bulk compliance*, $B = 1/K$. Likewise one may quote the mutual interrelationships:

$$J = 2\ D\ (1+\mu) = \frac{3\,D - B}{3} = \frac{2\ B(1+\mu)}{3\,(1-2\mu)} \tag{III.18}$$

$$D = \frac{J}{2\,(1+\mu)} = \frac{B}{3\,(1-2\,\mu)} = \frac{B}{9} + \frac{J}{3} \tag{III.19}$$

$$B = 9\,D - 3\ J = \frac{3\ J\,(1-2\ \mu)}{2\,(1+\mu)} = 3\ D(1-2\ \mu) \tag{III.20}$$

$$\mu = \frac{J}{2\ D} - 1 = 0.5 - \frac{B}{6\ D} = \frac{3\ J\ 2\ B}{6\ J + 2\ B} \tag{III.21}$$

For purely linear viscous flow, in conjunction with equation III.2 we have:

$$\tau = \sigma_{12} \qquad \text{and} \qquad \dot{\gamma} = \dot{\lambda}/2 \tag{III.22}$$

The viscous analog of *tensile* or *elongational* or *Trauton's viscosity* for extension acting in the 1 - direction:

$$\zeta = \frac{\sigma_{11}}{\dot{\lambda}_{11}} \tag{III.23}$$

For zero extension rate, extensional viscosity reduces to $\zeta = 3\eta$.

For an incompressible, isotropic fluid, *normal stress difference* in the directions transverse to the flow direction may be defined as:

$$\sigma_{11} - \sigma_{22} = 2\,\eta\,(\dot{\gamma}_{11} - \dot{\gamma}_{22})$$

The stresses, strains, and rates of strain are identical in both transverse directions. Further,

$$\zeta = \frac{(\sigma_{11} - \sigma_{22})}{\lambda_{11}} \tag{III.24}$$

Equation III.24 is valid for extensional viscosity of an incompressible fluid, while for a solid there is a difference caused by the fact that $\sigma_{22} = 0$.

Under influence of stress or strain, some rearrangements on the molecular scale take place inside the material. These changes do require some finite time to occur. The time may be very short, almost infinitely short, or it may be long. If the rearrangements take infinitely much, or closely so, time we have purely elastic material; the energy invested in the material is stored. If the time for the molecular relocation is infinitely short we have purely viscous material; all the energy input is spent on overcoming the internal friction. Practically all real materials are viscoelastic as there are neither infinitely long nor infinitely short rearrangement times to be encountered. The relation between the time needed for the rearrangements and the time scale of the experiment may be described by the *Deborah number*:

$$N_D = \theta_{mat}/\theta_{exp} \tag{III.25}$$

Linear viscoelastic material is not characterized by a simple summation of the viscous and elastic behavior. Instead, the simplest constitutive equation for a viscoelastic body has the form of a linear differential equation of the form:

$$\sigma + a\, d\sigma/dt = b\gamma + c\, d\gamma/dt \tag{III.26}$$

III.2 Excitations and Responses

A more adequate representation of real materials requires differential equations containing higher derivatives of stress and strain. Behavior of some materials may be impossible to describe by linear equations, and the coefficients may not be constant. However, every material may be treated as linear if one considers it in terms of infinitesimal deformations. In practice, many materials show linear behavior over a fairly large interval of deformations; the strain, however, must remain below a certain limit, the value of which is a material property. If the response to a stimulus is to be linear, two conditions must be satisfied: 1^o – the increase in a stimulus must increase the response by the same factor, and 2^o – a sequence of stimuli must result in a response which is the sum of responses to the individual stimuli in the sequence. The general relation between the time dependent stress and strain is

$$\sum_{n=0}^{\infty} u_n \frac{d^n\sigma(t)}{dt_n} = \sum_{m=0}^{\infty} q_m \frac{d^m\varepsilon(t)}{dt_m} \tag{III.27}$$

u_n and q_m are constant coefficients. Equation III.27 may be put in the form of an linear differential operator equation, which is being used in the form of its Laplace transform

$$\bar{f}(s) = \int_0^{\infty} f(t)e^{-st}\, dt \tag{III.28}$$

where s is the transform variable.

If the strain at $t = 0$ is taken as the reference strain, then the one sided Laplace transformation may be used. In this way, the differential equation with constant coefficients in the *time domain* becomes an algebraic equation in the *complex domain*. Transformation of the operator equation gives

$$\bar{u}(s)\ \bar{\sigma}(s) = \bar{q}(s)\ \bar{\varepsilon}(s) \tag{III.29}$$

where $\bar{\sigma}(s)$ and $\bar{\varepsilon}(s)$ are transforms of stress and strain, respectively. Also,

$$\bar{u}(s) = \sum_n u_n s^n \qquad \text{and} \qquad \bar{q}(s) = \sum_m q_m s^m \tag{III.30}$$

represent polynomials of the variable of transforms. From equations III.29 and III.30 one obtains

$$\bar{\sigma}(s) = \bar{Q}(s)\bar{\varepsilon}(s) \qquad \text{and} \qquad \bar{\varepsilon}(s) = \bar{U}(s)\bar{\sigma}(s) \tag{III.31}$$

where

$$\bar{Q}(s) = \frac{\bar{q}(s)}{\bar{u}(s)} \qquad \text{and} \qquad \bar{U}(s) = \frac{\bar{u}(s)}{\bar{q}(s)} \tag{III.32}$$

Applying the nomenclature proposed by Tschoegl,[68] $\bar{Q}(s)$ and $\bar{U}(s)$ are called *operational relaxance* and *retardance*, respectively, in shear. The corresponding relations between stress and rate of strain are the *operational impedance* and *admittance*, respectively.

The operator equation (III.27) and its transform (equation III.28) represent one of the possible forms of the general constitutive equation for viscoelastic bodies. It describes the superposition of response to any chain of excitations. The additivity is essential to the linear behavior. In the time domain, these characteristics may be expressed in the form of *Boltzmann superposition integrals*:

$$\sigma(t) = \int_0^\infty Q(t-u)\ \varepsilon(u)\ du \tag{III.33}$$

$$\varepsilon(t) = \int_0^\infty U(t-u)\ \sigma(u)\ du \tag{III.33 a}$$

Due to commutativity of the convolution operation, equations III.33 may be also written as

$$\sigma(t) = \int_0^\infty Q(u)\ \varepsilon(t-u)\ du \tag{III.34}$$

$$\varepsilon(t) = \int_0^\infty U(u)\ \sigma(t-u)\ du \tag{III.34 a}$$

In equations III.33 u denotes the *historic time* and in III.34 it denotes the *elapsed time*. It is, however, immaterial whether stress is taken as excitation and strain as response, or *vice versa*. Equations III.31 represent Hooke's law for shear flow in the complex plane. In equation III.31, $\bar{\epsilon}(s)$ is the *excitation transform* and $\bar{\sigma}(s)$ is the *response transform*; in equation III.31a, the roles are reversed. "The response and excitation transforms are connected through the *respondances*, $Q(s)$ and $U(s)$, which may also be called *material transforms* because they embody the properties of the material."[1] Viscoelastic behavior is time dependent: it is governed by the role of time in the excitation function. Therefore, it is important to examine the material behavior under influence of different types of excitation functions. Figure III.3 presents four of the more important excitation functions:

1. impulse applied at the time zero with a very short time of duration;
2. step excitation, where the impulse remains constant from the time zero on;
3. slope excitation, with the impulse increasing at a constant rate;
4. harmonic excitation. The harmonic excitation is of particularly great importance for experimental purposes.

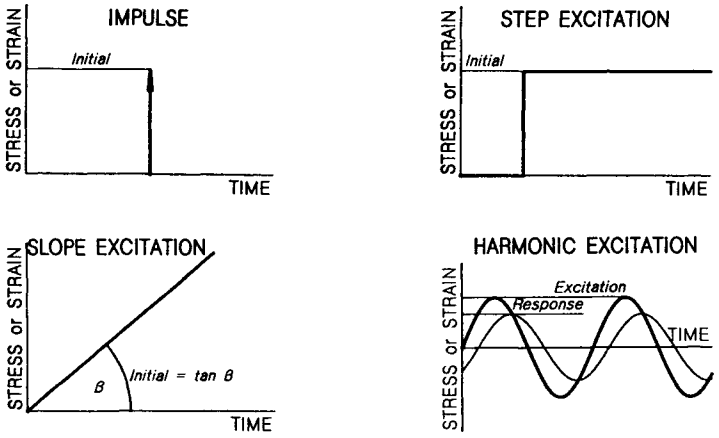

Figure III.3: *Different types of excitation functions.*

Strain impulse excitation may be presented as

$$\varepsilon(t) = \hat{\varepsilon}_0 \, \delta(t) \tag{III.35}$$

where $\delta(t)$ is the impulse or *delta function*:

$$\delta(t;\varepsilon) = (1/\pi) \int_0^\infty e^{-\varepsilon\omega} \cos(\omega t) \, d\omega = \frac{\varepsilon}{\pi(\varepsilon^2 + t^2)} \tag{III.36}$$

where ε may take any positive values. The function is bell shaped, with an increasing value of ε it becomes broader, but the integral of the function always

equals unity. If ε approaches zero, the bell shaped curve vanishes, and the height increases indefinitely:

$$\delta(t) = \frac{1}{\pi} \lim_{\varepsilon \to 0} \frac{\varepsilon}{(\varepsilon^2 + t^2)} \tag{III.37}$$

As described by equation III.37, the function $\delta(t) = \infty$ for $t = 0$, and $\delta(t) = 0$ for $t \neq 0$.

Laplace transformation gives

$$\bar{\varepsilon}(s) = \hat{e}_0 \tag{III.38}$$

After substitution into equation III.31, one obtains operational relaxance, and similarly operational retardance, respectively:

$$\bar{Q}(s) = \frac{\bar{\sigma}(s)}{\hat{\varepsilon}_0} \qquad \text{or} \qquad \bar{U}(s) = \frac{\bar{\varepsilon}(s)}{\hat{\sigma}_0} \tag{III.39}$$

where $\bar{\varepsilon}_0$ and $\bar{\sigma}_0$ are impulse strength, strain and stress, respectively. Retransformation of the equations gives

$$Q(t) = \frac{\sigma(t)}{\hat{\varepsilon}_0} \qquad \text{or} \qquad U(s) = \frac{\varepsilon(i)}{\hat{\sigma}_0} \tag{III.40}$$

The relaxance represents the response of the material to a unit impulse of strain, and retardance represents the response to a unit impulse of stress. The strain and stress, as functions of time, become respectively:

$$\sigma(t) = \int_0^t Q(t-u)\ \varepsilon(u)\ du = \int_0^t Q(u)\ \varepsilon(t-u) du \tag{III.41}$$

$$\varepsilon(t) = \int_0^t U(t-u)\ \sigma(u)\ du = \int_0^t U(u)\ \sigma(t-u)\ du \tag{III.42}$$

Step excitation is very widely used for experimental purposes. A mathematical description of it may be obtained from the integral of the delta function as ε tends to zero. The equation is

$$\begin{aligned} h(t) &= 0.5 + \frac{1}{\pi} \lim_{\varepsilon \to 0} \arctan(t/\varepsilon) = \\ &= 0.5 + \frac{1}{\pi} \lim_{\varepsilon \to 0} \int_0^\infty \exp(-\varepsilon\omega)\ \frac{\sin(\omega t)}{\omega}\ d\omega \end{aligned} \tag{III.43}$$

The delta function may be considered a derivative of the step function: $\delta(t) = dh(t)/dt$. The step function is $h(t) = 0$ for $t < 0$ and $h(t) = 1$ for $t > 0$.
The excitation function may be taken as

$$\varepsilon(t) = \varepsilon_0 \, h(t) \tag{III.44}$$

The Laplace transform of III.44, $\bar{\varepsilon}(s) = \varepsilon_0/s$ together with the Hooke's law, gives

$$\bar{\sigma}(s) = \frac{\bar{Q}(s)}{s} \, \varepsilon_0 \tag{III.45}$$

$\bar{Q}(s)/s$ is the transform of the modulus connecting time dependent stress with a unit step of strain. Consequently, after combining with equation III.45 and retransformation, one obtains:

$$G(t) = \frac{\sigma(t)}{\varepsilon_0} = \int_0^t Q(u) \, du \tag{III.46}$$

where $G(t)$ is the *shear relaxation modulus.*

Analogously, we may write the relationships for the shear strain response to a unit step stress, σ_0.

$$J(t) = \frac{\varepsilon(t)}{\sigma_0} = \int_0^t U(u) \, du \tag{III.47}$$

where $J(t)$ is *creep compliance* in shear. $G(0)$ and $J(0)$ represent the *instantaneous modulus* and *instantaneous compliance*, respectively.

Inversion of the Laplace transform of equation III.46 leads to four different forms of the relationship, in which $G(0)$ has been substituted with G_g - glassy modulus, respectively *glassy compliance* .

$$\sigma(t) = G_g \, \varepsilon(t) - \int_0^t \frac{dG(t-u)}{du} \, \varepsilon(u) \, du \tag{III.48}$$

$$\sigma(t) = G_g \, \varepsilon(t) - \int_0^t \frac{dG(u)}{du} \, \varepsilon(t-u) \, du \tag{$III.48\,a$}$$

$$\sigma(t) = \int_0^t G(t-u) \, d\varepsilon(u) \tag{$III.48\,b$}$$

$$\sigma(t) = \int_0^t G(t) \, \frac{d\varepsilon(t-u)}{du} \, du \tag{$III.48\,c$}$$

$$\varepsilon(t) = J_g\ \sigma(t) - \int_0^t \frac{dJ(t-u)}{du}\ \sigma(u)\ du \tag{III.49}$$

$$\varepsilon(t) = G_g\ \sigma(t) - \int_0^t \frac{dJ(u)}{du}\ \sigma(t-u)\ du \tag{III.49 a}$$

$$\varepsilon(t) = \int_0^t J(t-u)\ d\sigma(u) \tag{III.49 b}$$

$$\varepsilon(t) = \int_0^t J(t)\ \frac{d\sigma(t-u)}{du} du \tag{III.49 c}$$

The *slope excitation* (see Figure III.3) means application of excitation which is growing at a constant rate, hence the other name *constant rate of stress (or strain) excitation.* In this type of excitation the limit of linear behavior of the material may be easily exceeded; the given solutions would, naturally, loose their validity.

If one denotes constant rate of strain as $\dot{\varepsilon}_0$ and constant rate of stress as $\dot{\sigma}_0$, then for a constant rate of strain is

$$\varepsilon(t) = \dot{\varepsilon}_0\ p(t) = \dot{\varepsilon}_0\ t \tag{III.50}$$

where $p(t)$ is the slope function, which is derived from the step function (equation III.43):

$$p(t) = t\ h(t) \tag{III.51}$$

For $t < 0$ $p(t) = 0$ and for $t > 0$ $p(t) = t$.
Laplace transformation of equation III.50 gives

$$\bar{\varepsilon}(s) = \dot{\varepsilon}_0/s^2 \tag{III.52}$$

and substitution into equation III.31 results in

$$\bar{\sigma}(s) = \frac{\bar{Q}(s)}{s^2}\ \dot{\varepsilon}_0 \tag{III.53}$$

$\bar{\sigma}(s)/\dot{\varepsilon}_9 = \bar{\eta}(s)$ represents the transform of time dependent *shear viscosity.* In effect, one obtains

$$\bar{\eta}(s) = \frac{\bar{Q}(s)}{s^2} = \frac{\bar{G}(s)}{s} = \eta(t) = \frac{\sigma(t)}{\dot{\varepsilon}_0} \tag{III.54}$$

The further relationships are:

$$\eta(t) = \frac{\sigma(t)}{\dot{\varepsilon}_0} = \int_0^t G(u)\ du = \int_0^t \int_0^v Q(u)\ \ du\ dv \tag{III.55}$$

$$\bar{Q}(s) = s\bar{G}(s) = s^2\ \bar{\eta}(s) \tag{III.56}$$

And from retransformation:

$$Q(t) = \frac{dG(t)}{dt} + G(0)\ \delta(t) = \frac{d^2\eta(t)}{dt^2} + \eta'(0)\ \delta(t) + \eta(0)\ \delta'(t) \tag{III.57}$$

$$G(t) = \frac{d\eta(t)}{dt} + \eta(0)\ \delta(y) \tag{III.58}$$

Equations for the response to constant rate of stress are analogous to those given for the response to the constant rate of strain.

Steady state *harmonic* or *sinusoidal* excitation (Figure III.4) is often used in testing. The sequence of reasoning is similar as for previous cases.[1] Harmonic strain excitation may be expressed mathematically as

$$\varepsilon(t) = \varepsilon_0\ [\sin(\omega t) + i\cos(\omega t)] = \varepsilon_0\ \exp(i\omega t) \tag{III.59}$$

In this case, ε_0 means strain amplitude and ω is frequency in radians. This is the general equation for sinusoidal curves, and in this case describes the *generalized harmonic strain* (or *stress*).

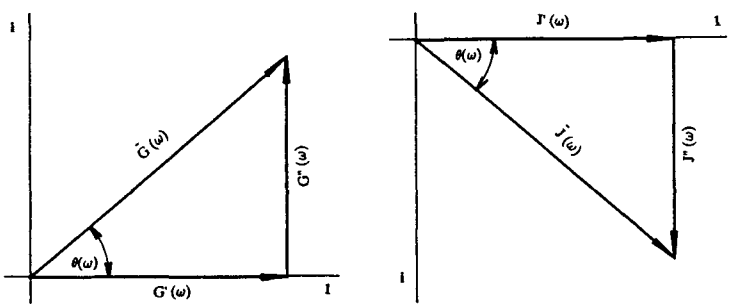

Figure III.4: *Vector resolution of complex modulus and complex compliance; modulus or storage compliance.*

Again, the process of deriving the equations is similar. The Laplace transform of the response to $\varepsilon(t)$ is

$$\bar{\varepsilon}(s) = \frac{\varepsilon_0}{s - i\,\omega} \tag{III.60}$$

After substitution to equation III.31 one obtains

$$\bar{\sigma}(s) = \frac{\varepsilon_0\ \bar{Q}(s)}{s - i\,\omega} \tag{III.61}$$

After retransformation to the real time axis, the total response obtained consists of two parts: 1^o – a steady state response in the form of a periodic function resulting from the poles of excitation, and 2^o – a nonperiodic transient response arising from the poles of the material transforms, $Q(s)$ and $U(s)$. For steady state, it is then

$$\frac{\bar{\sigma}_{ss}(s)}{\varepsilon_0} = \frac{\bar{Q}(i\,\omega)}{s - i\,\omega} \tag{III.62}$$

$$\sigma_{ss} = \bar{Q}(i\omega)\varepsilon_0 \, e^{i\omega t} \tag{III.63}$$

In this case, the response varies with frequency ω, which for steady state is of primary interest, rather than time. Consequently, one may denote $\varepsilon(\omega) = \varepsilon_0 \exp(i\omega t)$ and change the equations accordingly.

The quantity $\bar{Q}(i\omega)$ has the dimensions of modulus, and in polymer rheology is usually denoted $G^*(\omega)$ and called *complex shear modulus*, but it may also be called *harmonic relaxance.*

In analogy to the above, one may derive the *harmonic retardance* or *complex shear compliance*, $J^*(\omega)$.

$$\varepsilon_{ss}(t) = \bar{U}(i\omega)\sigma_0 e^{i\omega t} \tag{III.64}$$

$$J^*(\omega) = \bar{U}(s)|_{s=i\omega} \tag{III.65}$$

The complex nature of the modulus in compliance permits each of them to be decomposed into either Cartesian or polar coordinates:

$$G^*(\omega) = G'(\omega) + iG''(\omega) = \bar{G}(\omega) \, e^{i\theta(\omega)} \tag{III.66}$$

$$J^*(\omega) = J'(\omega) - iJ''(\omega) = \bar{J}(\omega) \, e^{-i\theta(\omega)} \tag{III.67}$$

$G'(\omega)$ and $J'(\omega)$ are proportional to the energy stored during a cycle of deformation in a unit of volume of a material and are called *storage modulus* and *storage compliance*, respectively. $G''(\omega)$ and $J''(\omega)$ are proportional to the energy dissipated per unit of volume of the material and are called *loss modulus* or *loss compliance*; $\theta(\omega)$ is *loss angle.* As may be seen from Figure III.4 the following relationships are self understood:

$$\bar{G}(\omega) = \{[G']^2 + [G''(\omega)]^2\}^{\frac{1}{2}} \tag{III.68}$$

$$\bar{J}(\omega) = \{[J']^2 + [J''(\omega)]^2\}^{\frac{1}{2}} \tag{III.68 a}$$

$$\tan\theta(\omega) = \frac{G''(\omega)}{G'(\omega)} = \frac{J''(\omega)}{J'(\omega)} \tag{III.69}$$

$$G'(\omega) = \bar{G}(\omega) \, \cos\theta(\omega) \tag{III.70}$$

$$G''(\omega) = \bar{G}(\omega) \, \sin\theta(\omega) \tag{III.70 a}$$

$$J'(\omega) = J(\omega) \, \cos\theta(\omega) \tag{III.71}$$

$$J''(\omega) = \bar{J}(\omega) \, \sin\theta(\omega) \tag{III.71 a}$$

$$\bar{G}(\omega) = \frac{\sigma_0(\omega)}{\varepsilon_0} \qquad \text{and} \qquad \bar{J}(\omega) = \frac{\varepsilon_0(\omega)}{\sigma_0} \tag{III.72}$$

Absolute modulus and compliance represent the ratio of the response amplitude to the excitation amplitude. The loss angle represents the phase difference of the response and excitation, the stress always reaches its peak before strain does.

The further relationships of interest are:

$$\dot{\varepsilon}(t) = d\varepsilon(t)/dt = -\varepsilon_0 \, \omega[\sin(\omega t) - i\cos(\omega t)] \tag{III.73}$$

$$\varepsilon(\omega) = \varepsilon_0(\omega)\ \exp\{i[\omega t - \theta(\omega)]\} \tag{III.74}$$

$$\varepsilon_0(\omega)\ \cos\theta(\omega) = \sigma_0\ J'(\omega) \tag{III.75}$$

$$\varepsilon_0(\omega)\ \sin\theta(\omega) = \sigma_0\ J''(\omega) \tag{III.75 a}$$

$$\dot{\varepsilon}(\omega) = d\varepsilon(\omega)/dt = i\omega\varepsilon(\omega) \tag{III.76}$$

$$\eta^*\ \omega = \frac{\sigma(\omega)}{i\omega\varepsilon(\omega)} = \frac{G^*(\omega}{i\omega} \tag{III.77}$$

$$G(t)\ \frac{\sigma(t)}{\varepsilon_0} = \mathcal{L}^{-1}\frac{\bar{\mathrm{Q}}(\mathrm{s})}{\mathrm{s}} = \int_0^{\mathrm{t}} \mathrm{Q(u)\ du} \tag{III.78}$$

$$\eta(t)\ \frac{\sigma(t)}{\varepsilon_0} = \mathcal{L}^{-1}\frac{\bar{\mathrm{Q}}(\mathrm{s})}{\mathrm{s}^2} = \int_0^{\mathrm{t}} \mathrm{G(u)\ du} \tag{III.79}$$

$$G^*(t) = \frac{\sigma(\omega)}{\varepsilon(\omega)} = [\bar{Q}(s)]_{s=i\omega} \tag{III.80}$$

$$J(t) = \frac{\varepsilon(t)}{\sigma_0} = \mathcal{L}^{-1}\frac{\bar{\mathrm{U}}(\mathrm{s})}{\mathrm{s}} \tag{III.81}$$

$$\chi(t) = \frac{\varepsilon(t)}{\dot{\sigma}_0} = \mathcal{L}^{-1}\frac{\bar{\mathrm{U}}(\mathrm{s})}{\mathrm{s}^2} \tag{III.82}$$

$$J^*(t) = \frac{\varepsilon(\omega)}{\sigma(\omega)}\ [\bar{U}(s)]_{s=i\omega} \tag{III.83}$$

III.3 Mechanical Models

It has been found convenient to represent material properties by mechanical models. The common symbols used for this purpose are presented in Figure III.5. The *spring* represents idealized storage of elasticity, without any losses to friction; E represents operational *elastance*, which is the proportionality coefficient for the relation between force, f, and displacement, x, or velocity, v. The *dashpot* represents idealized energy dissipation as heat, with no energy storage involved. *Frictance*, F, is the proportionality constant for the relation between force and constant velocity at which the two ends of the dashpot are moving. Kinetic energy may be represented by *mass*, which responds to applied force with pure inertia, with no energy storage or dissipation. The coefficient of proportionality between force and the resulting acceleration is called *inertance*. These relationships may be put in a mathematical form as follows:

Potential energy storage:

$$\bar{f}(s) = E\ \bar{x}(s) \tag{III.84}$$

Dissipation of energy:

$$\bar{f}(s) = F\ s\ \bar{x}(s) \tag{III.84 a}$$

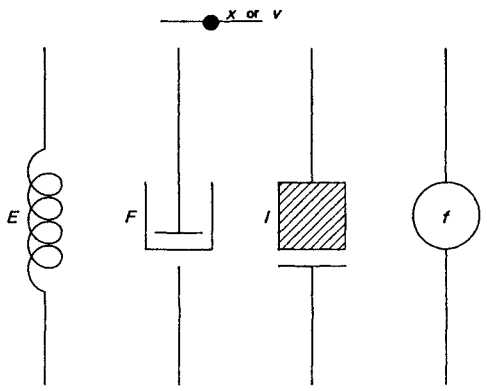

Figure III.5: *Symbols used in mechanical rheological models: E - for elastance of the spring, F - for frictance of the dashpot, I - for inertance of the mass, f - applied force, x - displacement, v - velocity.*

Storage of kinetic energy:

$$\bar{f}(s) = I\ s^2\ \bar{x}(s) \qquad (III.84\,b)$$

If the system is at rest, then:

$$x(0) = \dot{x}(0) = \ddot{x}(0) \equiv 0 \qquad (III.84\,c)$$

where the dots denote differentiation *versus* time.

The relaxances are additive, so

$$\bar{f}(s) = (I\,s^2 + Fs + E)\ \bar{x}(s) = Q_t(s)\ \bar{s} \qquad \text{(III.85)}$$

After retransformation of equation III.85 one obtains

$$f(t) = I\ \frac{d^2x(t)}{dt^2} + F\ \frac{dx(t)}{dt} + E\ s(t) \qquad \text{(III.86)}$$

The rules to be observed in the model analysis are:

- *relaxances add in parallel*
- *retardances add in series.*

These rules result from the fact that forces add in parallel and displacements add in series. In a parallel combination of the passive elements, all elements are displaced equally, then the forces in the elements are additive. In a series combination, the same force acts through all the elements, therefore the displacements are additive.

In cases of rotational motion, the transform of force is replaced by the transform of torque, $\bar{M}(s)$; the transform of the linear displacement is replaced by the transform of angular displacement, $\bar{\theta}(s)$. Consequently, the respondances change correspondingly: inertance to the moment of inertia, frictance to the moment of mechanical resistance, elastance to the moment of stiffness. The reciprocal of elastance is mechanical compliance, the reciprocal of frictance is called, μ, glidance.

In modeling rheological behavior the rheological respondances are translated to mechanical respondances by use of a *shape factor*, b. In this way, force and displacement (or torque and angular displacement) are converted to stress and strain.

$$\frac{\sigma}{\varepsilon} = b_t \frac{f}{x} = b_r \frac{M}{\theta} \tag{III.87}$$

Here b_t has the dimension of reciprocal length and b_r has the dimension of reciprocal volume. Thus, instead of force, displacement (or velocity), elastance and frictance we use stress, strain (or rate of strain), modulus, viscosity, respectively. Inertivity is usually omitted since it has negligible effect, except for cases involving high frequencies or impact, and then it is represented by the density of the material.

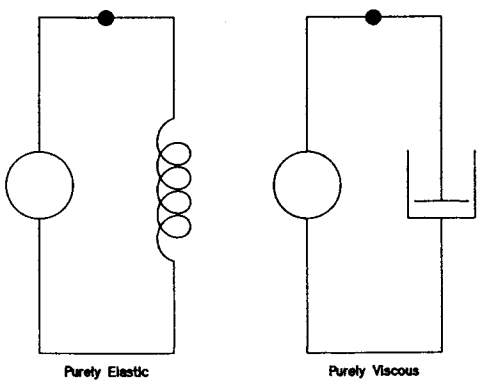

Figure III.6: *Models of purely elastic and purely viscous behavior.*

Figure III.6 exemplifies how purely elastic and purely viscous materials may be modeled using simple elements. One may write

$$\bar{\sigma}(s) = G\ \bar{\varepsilon}(s) \tag{III.88}$$

for the model of purely elastic, and

$$\bar{\sigma}(s) = \eta\ \bar{s}\ \varepsilon(s) = \eta\dot{\bar{\varepsilon}}\ (s) \tag{III.89}$$

for the model of purely viscous behavior. The models and equations III.88 and III.89 represent the equations III.1 and III.2. If one considers equation III.31, then it becomes evident that the relaxance, $Q(s)$, is G - the shear modulus. From equation III.89 and III.31 one may see that $\bar{Q}(s)$ is ηs. Both G and η are the model parameters. Per analogy, J and ϕ/s are operational retardances. For better visualization, all the quantities are gathered in table III.1.

Viscoelastic behavior may be represented in the simplest way by the Voigt or by the Maxwell model (Figure III.7). In the parallel Voigt model, all of the elements have the same strain and the stresses are additive.

$$\bar{Q}(s) = G + \eta\ s \tag{III.90}$$

Table III.1
Overview of Respondances.

Model Parameter	Operational Respondance	Harmonic Respondance
G	G	G
J	J	J
η	ηs	$i\omega\eta$
(ϕ)	ϕ/s	$\phi/i\omega$

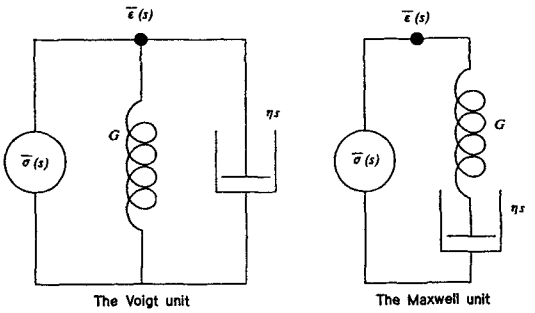

Figure III.7: *The simplest models of viscoelastic behavior: the Voigt unit and the Maxwell unit.*

and further

$$\bar{\sigma}(s) = (G + \sigma s)\ \bar{\varepsilon}(s) \tag{III.91}$$

which is a Laplace transform of the equation

$$\sigma = G\ \varepsilon + \eta\ \frac{d\varepsilon}{dt} \tag{III.92}$$

Equation III.92 is a simple combination of equations for purely elastic and purely viscous response. The retardance of the Voigt model is

$$\bar{U}_v(s) = \frac{J}{1 + \tau_v s} \tag{III.93}$$

where τ is *retardation time*, $\tau = J/\phi$, and $\phi = 1/\eta$.

The Maxwell arrangement of dash-pot and spring in a series may be described as

$$\bar{U}(s) = J + \frac{\phi}{s} \tag{III.94}$$

where $J = 1/G$ and $\phi = 1/\eta$. Furthermore

$$\bar{E}(s) = \left(J + \frac{\phi}{s}\right) \bar{\sigma}(s) \tag{III.95}$$

The differential equation which corresponds to III.95 is

$$\frac{d\varepsilon}{dt} = \frac{1}{\eta}\,\sigma + \frac{1}{G}\,\frac{d\sigma}{dt} \tag{III.96}$$

The relaxance of the Maxwell model is

$$\bar{Q}_M(s) = \frac{G\,\theta_M\,s}{1+\theta_M\,s} \tag{III.97}$$

where θ_M is *relaxation time*, $\theta_M = \eta/G$. With the help of relaxation and retardation times, one may write the equation for operational retardance of the Maxwell model

$$\bar{U}_M(s) = J + \left(\frac{\phi}{s}\right) = J\left(1 + \frac{1}{\theta_M\,s}\right) \tag{III.98}$$

and for the operational relaxance of the Voigt model

$$\bar{Q}_v(s) = G + \eta s = G\,(1+\theta_v s) \tag{III.99}$$

Real viscoelastic materials behave neither like the Maxwell nor like the Voigt model: they behave rather like some kind of combination of both models. A real viscoelastic material shows relaxation of stress, as well as a retardation of strain, depending on the kind of excitation. The delay in behavior reflects the time needed for the material to adjust to the changes forced upon it – it is easy to imagine this fact on the molecular level.

The meaning of the relaxation time becomes quite clear if one substitutes equation III.97 into equation III.45 and inverts the transform, which leads to

$$\sigma(t) = \varepsilon_0\,G\,\exp\left(\frac{-t}{\theta_m}\right) \tag{III.100}$$

Equation III.100 describes stress in a Maxwell unit when subjected to a constant strain of ε_0. Since $G\varepsilon_0 = \sigma_0$, the initial magnitude of stress, one therefore obtains

$$\sigma(t) = \sigma_0\,\exp\left(\frac{-t}{\theta_m}\right) \tag{III.101}$$

The initial stress relaxes exponentially with time. For a perfectly elastic material, the initial stress ought to remain constant for an indefinite time. For a perfectly viscous material the relaxation time ought to be zero.

From equation III.101 results that

$$t(\theta_M) = \sigma_0/e = 0.369\,\sigma_0. \tag{III.102}$$

In a similar way, one may substitute equation III.93 into $\bar{\varepsilon}(s) = \bar{U}(s)\sigma_0/s$ and retransform it to obtain

$$\varepsilon(t) = \sigma_0\,J\,\left[1 - \exp\left(\frac{-t}{\theta_v}\right)\right] \tag{III.103}$$

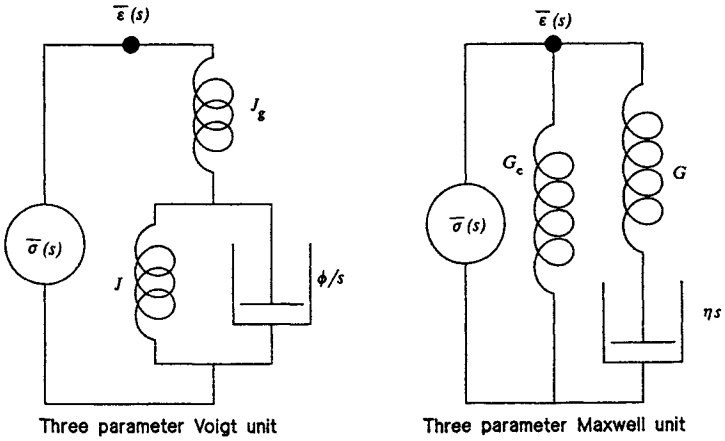

Figure III.8: *Three-parameter Voigt and Maxwell models.*

Equation III.103 describes strain as a function of the time that has elapsed since the stress σ_0 was applied. $J\sigma_\infty = \varepsilon_\infty$, the final strain at $t = \infty$. For $t = \theta_v$ $\varepsilon(\theta_v) = 0.631\ \varepsilon_\infty$.

In order to better describe the actual properties of a viscoelastic material, many units of both Maxwell and Voigt variety may be joined in different combinations. In fact, any of the constitutive equations derived in the past in different ways may be described by such combinations. In this highly abridged description of the rheological problems are quoted only simple examples: three parameter models of Voigt and of Maxwell.

Combinations of the different units make sense only when units of different kind are joined in the system. Figure III.8 shows such "expansions" of the unitary models previously considered. The Voigt model has been obtained by addition of a spring in series with a basic Voigt unit. The retardance of the model may be obtained using equation III.93 and the combination principle:

$$\bar{U}_v(s) = J_g + \frac{J}{1+\theta s} \tag{III.104}$$

$J/\phi = \theta$ is the retardation time of the model. For the step input one may obtain

$$\bar{\varepsilon}(s) = \sigma_0 + \left[\frac{J_g}{s} \times \frac{J}{s\ (1+\theta s)}\right] \tag{III.105}$$

and after retransformation

$$\varepsilon(t) = \sigma_0 \left\{J_g + J \left[1 - \exp\left(\frac{-t}{\theta}\right)\right]\right\} = \varepsilon_0 + \varepsilon \left[1 - \exp\left(\frac{-t}{\theta}\right)\right] \tag{III.106}$$

If a constant stress is applied, according to this model, there is an instantaneous strain, $\varepsilon_0 = J_g\sigma_0$, after which follows a delayed strain to reach an equilibrium value, $\varepsilon_e = \varepsilon_0 + \varepsilon = J_e\sigma_0$ at $t = \infty$. This kind of behavior is called *creep*, and

$J(t) = \varepsilon(t)/\sigma_0$ is called *creep compliance.* J_g is the instantaneous compliance (at $t = 0$), and J_e is the equilibrium compliance (at $t = \infty$), $J_e = J_g + J$. J is delayed (retarded) compliance.

Considering the three-element Voigt model under step strain, one may take advantage of the relation $Q(s)U(s) = 1$ and the defining relationship of equilibrium compliance to obtain

$$\bar{Q}_v(s) = \frac{1 + \theta s}{J_e + J_g \theta s} \tag{III.107}$$

and for a constant strain the stress transform is

$$\bar{\sigma}(s) = \varepsilon_0 \frac{1 + \theta s}{s\ (J_e + J_g \theta s)} \tag{III.108}$$

After inversion of the transform one obtains

$$\sigma(t) = \varepsilon_0 \left[\frac{1}{J_e} + \frac{J_e - J_g}{JeJg}\right] = \sigma_e + \sigma \exp\left(\frac{-t}{\theta'}\right) \tag{III.109}$$

where

$$\tau' = \frac{J_g\ \theta}{J_e} \tag{III.110}$$

The initial stress in response to a step strain is

$$\bar{\sigma}(0) = \sigma\ \varepsilon_e + \sigma = \varepsilon_0 \left[\frac{1}{J_e} + \frac{J_e - J_g}{J_e J_g}\right] = \frac{\varepsilon_0}{J_g} \tag{III.111}$$

If $t = \infty$, according to this model, the material relaxes to an equilibrium value of $\sigma_e = \varepsilon_0/J_e$.

If one considers the Maxwell model with an added parallel spring (Figure III.8), then the relaxance is

$$\bar{Q}_M(s) = G_e + \frac{G\ \theta\ s}{1 + \theta\ s} \tag{III.112}$$

Relaxances add in parallel, so for a step strain of magnitude ε_0 the Laplace transform is

$$\bar{\sigma}(s) = \varepsilon_0 \left(\frac{G_e}{s} + \frac{G\ \theta}{1 + \theta\ s}\right) \tag{III.113}$$

After inversion of the transform, one obtains

$$\sigma(t) = \varepsilon_0\ \left[G + G \exp\left(\frac{-t}{\theta}\right)\right] = \sigma_e + \sigma\ \exp\left(\frac{-t}{\theta}\right) \tag{III.114}$$

At $t = 0$, the stress is $\sigma_0 = \sigma_e + \sigma = G_g \varepsilon_0$, and the instantaneous modulus is

$$G_g = G_e + G \tag{III.115}$$

In the last equation G_e is *equilibrium modulus* and G is *relaxing modulus.* If $t = \infty$ then $\sigma_e = G_e \varepsilon_0$. The behavior is identical with the three-element Voigt model.

The three-parameter Maxwell model responds to a step stress as the Voigt model does, and the mathematical formalism is completely analogous. The three element models describe properties of solids (*arrheodictic*, cross linked polymers with equilibrium strain), while properties of liquids (*rheodictic*, where strain increases linearly with time, and there is no equilibrium value) are described better by four- parameter models.

Respondances are rational algebraic functions (polynomials) of complex transform variables. These functions have poles

$$\bar{U}_v(s) = \frac{\bar{u}_v(s)}{\bar{q}_v(s)} \quad \bar{Q}_M(s) = \frac{\bar{q}_M(s)}{\bar{u}_M(s)} \tag{III.116}$$

which are the roots of the polynomials in the denominators, $\bar{q}_v(s)$ and $\bar{u}_M(s)$. The roots of the numerators are equal zero. In this way the zeros of retardances are the poles of the relaxances and *vice versa*. This results from the fact that $U(s)Q(s) = 1$. The Voigt and Maxwell units have no zeros, therefore they are not real models.

For the rheodictic materials, and those include practically all fiber forming polymers, retardance must have a pole in the origin of the axes, while relaxances have a zero at the same point. For arrheodictic materials the situation is reversed. When the pole and zero locations are known, the respondances are fully determined.

Real polymers only in rare cases may be approximately described by three or four-element models. Generalized models (Figures III.9 and III.10) have been developed to fit the real polymers. Nevertheless, detailed description of the real polymers are better. However, a detailed description of the mathematical derivations would greatly exceed the boundaries of this book; hence, the reader is referred to the specialistic, original source.[1] Only some of the final equations will be quoted here.

Summation of a number of Maxwell units results in the generalized Maxwell - Wiechert model, the relaxance of which is

$$\bar{Q}(s) = \sum_{n=0}^{N-1} \frac{G_n \, \theta_n \, s}{1 + \theta_n \, s} \tag{III.117}$$

The corresponding relaxation modulus is:

$$G(t) = \sum_{n=0}^{N-1} G_n \exp\left(\frac{-t}{\theta_n}\right) \tag{III.118}$$

The relaxance may be interpreted as a superposition of exponentials representing some unitary processes. This model represents rheodictic materials; to obtain a description of arrheodictic materials, it is necessary to replace the spring and dashpot unit in the zero position of the Maxwell model with a spring of G_e. This

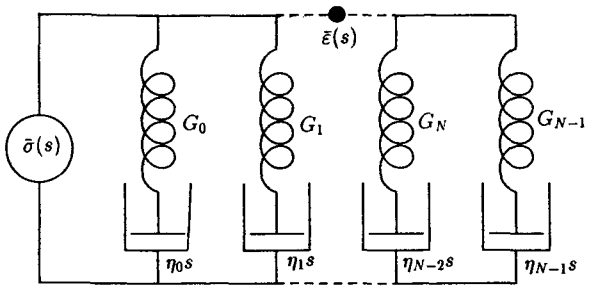

Figure III.9: *Generalized Maxwell - Wiechert model for the description of rheodictic material behavior.*

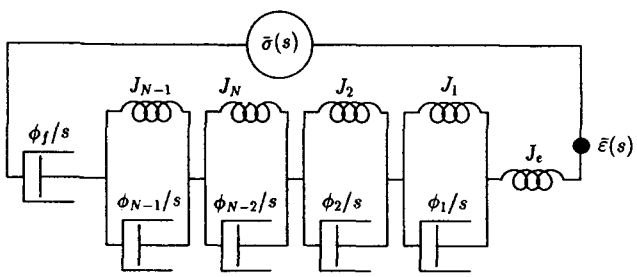

Figure III.10: *Generalized Voigt-Kelvin model for the description of rheodictic material behavior.*

new model would have the relaxance

$$\bar{Q}(s) = G_e + \sum_{n=1}^{N-1} \frac{G_n\ \theta_n\ s}{1 + \theta_n\ s} \tag{III.119}$$

It is important to stress that for the rheodictic materials, the summation in equations III.117 and III.118, as well as in others to follow, is carried out from zero to $N-1$ (consult also Figure III.9). In the case of arrheodictic descriptions, the summation needs to be carried from 1 to $N-1$, as the spring of G_e occupies the zero position.

The complex modulus of a rheodictic material is

$$G^*(\omega) = \sum_{n=0}^{N-1} \frac{G_n\ i\ \omega\ \theta_n}{1 + i\ \omega\ \theta_n} \tag{III.120}$$

The storage modulus equation is

$$G'(\omega) = \sum_{n=0}^{N-1} \frac{G_n\ \omega^2\ \theta_n^2}{1 + \omega^2\ \theta_n^2}. \tag{III.121}$$

For the loss modulus the equation is

$$G''(\omega) = \sum_{n=0}^{N-1} \frac{G_n\ \omega\ \theta_n}{1 + \omega\ \theta_n}. \tag{III.122}$$

It is necessary to stress that for the cases involving arrheodictic materials, the summations in equations III.120 through III.122 must be carried from $n = 1$ to $N - 1$. On integration of equation III.120 one obtains:

$$\eta(t) = \{G_e\}t + \sum_n G_n\ \theta_n\ \left[1 - \exp\left(\frac{-t}{\theta_n}\right)\right] =$$

$$= \{G_e\}\ t + \eta_{\{f\}} - \sum_n \eta_n\ \exp\left(\frac{-t}{\theta_n}\right) \tag{III.123}$$

The values in braces, for example $\{G_e\}$, concern arrheodictic behavior and for rheodictic behavior are to be omitted. Further,

$$\eta_{\{f\}} = \sum_n \eta_n = \sum_n G_n\ \theta_n \tag{$III.123\,a$}$$

is the sum of the viscosities of all dashpots, and is usually written simply as η. For rheodictic cases the sum represents the steady flow viscosity, η_f.

The generalized Wiechert model is often named the Kelvin model or Wiechert - Kelvin model, and for rheodictic behavior it is presented in Figure III.10. For arrheodictic behavior the dashpot, ϕ_f/s, is omitted. To avoid presentation of the equations separately for rheodictic and for arrheodictic materials, braces will be used for those terms which are to be omitted in the case of rheodictic behavior, e.g. $\{\phi_f/s\}$. This is opposite to the case of the generalized Maxwell model, where arrheodictic terms are put in braces. The retardance of such models may be presented in two different forms III.124 and III.124a:

$$\bar{U}(s) = J_g + \sum_{n=1}^{N-1} \frac{J_n}{1 + \theta_n\ s} + \left\{\frac{\phi_f}{s}\right\} \tag{III.124}$$

$$\bar{U}_\bullet(s) = J_e^{\{o\}} - \sum_{n=1}^{N-1} \frac{J_n\ \theta_n\ s}{1 + \theta_n\ s} + \left\{\frac{\phi_f}{s}\right\} \tag{$III.124\,a$}$$

It is necessary to note that the two forms of retardances are equivalent, $U(s) = U_\bullet(s)$, the notation is to indicate the origin of the different forms.

The creep compliance of the generalized Voigt model is

$$J(t) = J_g + \sum_n J_n\ \left[1 - \exp\left(\frac{-t}{\theta_n}\right)\right] + \{\phi_f\ t\} \tag{III.125}$$

or

$$J_\bullet(t) = J_e^{\{o\}} - \sum_n J_n\ \exp\left(\frac{-t}{\theta_n}\right) + \{\phi_f\ t\} \tag{$III.125\,a$}$$

The complex compliance is

$$\bar{J}^*(\omega) = J_g + \sum_{n=1}^{N-1} \frac{J_n}{1 + i\,\omega\,\theta_n} + \left\{ \frac{\phi_f}{i\,\omega} \right\} \tag{III.126}$$

or

$$\bar{J}^*_\bullet(\omega) = J_e^{\{o\}} - \sum_n \frac{J_n\, i\,\omega\,\theta_n}{1 + i\,\omega\,\theta_n} + \left\{ \frac{\phi_f}{i\,\omega} \right\} \tag{III.126 a}$$

The real and imaginary compliances are, respectively

$$\bar{J}'(\omega) = J_g + \sum_{n=1}^{N-1} \frac{J_n}{1 + [\omega^2\,\theta_n^2]} \tag{III.127}$$

or

$$\bar{J}_\bullet(\omega) = J_e^{\{o\}} - \sum_n \frac{J_n\,\omega^2\,\theta_n^2}{1 + \omega^2\,\theta_n^{*2}} \tag{III.127 a}$$

$$\bar{J}''(\omega) = \sum_{n=1}^{N-1} \frac{J_n\,\omega\,\theta_n}{1 + \omega^2\,\theta_n^2} + \left\{ \frac{\phi_f}{\omega} \right\} \tag{III.128}$$

The loss modulus has only one form, equation III.128.

The properties described by the equations III.117 through III.128 imply that a material has more than one relaxation or retardation time. The set of relaxation or retardation times may consist of several points, it may have many points to form a *discrete* spectrum, or it may also be taken as a *continuous spectrum.* The summation present in equations III.117 through III.128 suggest also than each time, θ_n, is associated with a modulus, G_n. One may then speak about a spectrum of moduli *versus* time, and, consequently, one may take modulus as *strength of a spectrum.* In a similar way, compliance may be taken as the strength of retardation spectrum. The pairs of G_n and n may be grouped and the groups treated as single relaxation time.

Experimental data may be fit into the model equations; there are several methods of doing so described in the literature on rheology.[1,2]

The fundamental equations of viscoelastic behavior (equations III.30 and III.31) may be described in a more generalized way: *response transform equals material transform multiplied by excitation transform.*[1] Since the excitation and response are clearly connected to time (or frequency), the material functions are also time dependent. However, for every imaginable driving function, there exists a different material function. To avoid the inconvenience of multiplicity of material functions a material response function has been introduced under the name *spectral distribution function* or just *relaxation spectrum.* There are relaxation spectra derived from response to strain, retardation spectra derived from response to stress. There may be line (or discrete) spectra or continuous, spectra *versus* time or *versus* frequency. Due to its fundamental importance, representation of the response function in the form of spectra is termed the *canonical representation.*

The generalized equation III.119 describing a discrete spectrum may be changed to describe a continuous relationship:

$$\bar{Q}(s) = \{G_e\} + \int_0^\infty \hat{Q}(\theta) \frac{\theta s}{1 + \theta\, s}\, d\theta \tag{III.129}$$

where $\hat{Q}(\theta)$ is a continuous function of the relaxation time, θ, and its integral replaces the sum of the discrete points G_n. The $Q(\theta)$ function is also called the *distribution of relaxation times.* The function has dimensions of modulus divided in time; it is the density of modulus per time. The *relaxation spectrum* – with the dimensions of modulus, in a common notation, may be given as

$$\hat{G}(\theta) = H(\theta) = \theta\, \hat{Q}(\theta) \tag{III.130}$$

If the new function (equation III.130) is introduced into equation III.129 one obtains:

$$\bar{Q}(s) = \{G_e\} + \int_{-\infty}^\infty H(\theta) \frac{\theta s}{1 + \theta\, s}\, d\ln\theta \tag{III.131}$$

The term $d\ln$ represents a conventional term which strictly formally ought to be written as $d\theta/\theta$; should this correct term be used, then the lower integration limit must be *zero.*

Other important relationships may be given as follows:

$$G(t) = \{G_e\} + \int_{-\infty}^\infty H(\theta)\, \exp\left(\frac{-t}{\theta}\right)\, d\ \ln\ \theta \tag{III.132}$$

$$G^*(\omega) = \{G_e\} + \int_{-\infty}^\infty H(\theta) \frac{i\,\omega\,\theta}{1 + i\,\omega\,\theta}\, d\ \ln\ \theta \tag{III.133}$$

$$G'(\omega) = \{G_e\} + \int_{-\infty}^\infty H(\theta) \frac{\omega^2\,\theta^2}{1 + \omega^2\,\theta^2}\, d\ln\theta \tag{III.134}$$

$$G''(\omega) = \int_{-\infty}^\infty H(\theta) \frac{\omega\,\theta}{1 + \omega^2\,\theta^2}\, d\ln\theta \tag{III.135}$$

$$\eta(t) = \{G_e t\} + \int_{-\infty}^\infty \theta\, H(\theta) \left[1 - \exp\left(\frac{-t}{\theta}\right)\right]\, d\ln\theta \tag{III.136}$$

As far as corresponding equations for the *retardation time spectrum* from the creep behavior are concerned, there is a full analogy to all the above.

$$\bar{U}(s) = J_g + \int_0^\infty \hat{U}(\theta) \frac{1}{1 + \theta\, s}\, d\theta\ + \left\{\frac{\phi_f}{s}\right\} \tag{III.137}$$

We introduce $\hat{J}(\theta)$, a continuous function of the retardation time, θ, and when its integral replaces the sum of the discrete points, the resulting $J(\theta)$ function is called the *distribution of retardation times.* Other remarks are analogous to those for the relaxation function. Common notation gives

$$\hat{J}(\theta) = L(\theta) = \theta\, \hat{U}(\theta) \tag{III.138}$$

If the function (equation III.138) is introduced into equation III.137 one obtains:

$$\bar{J}(s) = \frac{J_g}{s} + \int_{-\infty}^{\infty} L(\theta)\, \frac{1}{s\,(1+\theta\, s)}\, d\, \ln\theta + \left\{\frac{\phi_f}{s^2}\right\} \tag{III.139}$$

The term $d\ln\theta$ represents a conventional term which strictly formally ought to be written as $d\theta/\theta$; should this correct term be used, then the lower integration limit must be zero.

Other important relationships may be given as follows:

$$J(t) = J_g + \int_{-\infty}^{\infty} L(\theta)\, \left[1 - \exp\left(\frac{-t}{\theta}\right)\right]\, d\, \ln\theta + \{\phi_f\, t\} \tag{III.140}$$

$$J^*(\omega) = J_g + \int_{-\infty}^{\infty} L(\theta)\, \frac{1}{1+i\,\omega\,\theta}\, d\ln\theta + \left\{\frac{\phi_f}{i\,\omega}\right\} \tag{III.141}$$

$$J'(\omega) = J_g + \int_{-\infty}^{\infty} L(\theta)\, \frac{1}{1+\omega^2\,\theta^2}\, d\ln\theta \tag{III.142}$$

$$J''(\omega) = \int_{-\infty}^{\infty} L(\theta)\, \frac{\omega\,\theta}{1+i\,\omega\,\theta}\, d\ln\theta + \left\{\frac{\phi_f}{i\,\omega}\right\} \tag{III.143}$$

$$\chi(t) = \{J_e t\} - \int_{-\infty}^{\infty} \theta\, L(\theta)\, \left[1 - \exp\left(\frac{-t}{\theta}\right)\right]\, d\ln\theta + \frac{\{\phi_f\}\, t^2}{2} \tag{III.144}$$

In effect, experimental response functions are integrals over the continuous spectral distribution functions multiplied by the kernel functions specific to the time regime of the stimulus. Every given value of a response function depends on all the values of the spectral function from $\theta = 0$ to $\theta = \infty$. The experimental response functions are called *functionales.*

The relaxation and retardation spectra may also be expressed as functions of *relaxation (retardation) frequencies*, which are reciprocals of the corresponding times. The frequency functions form the basis for computation of the time spectra from the experimental response functions. Exact solutions of mathematical problems involved in the spectra calculation are known, however, they are rarely used,

not only due to their complexity, but also because of their sensitivity to input data inaccuracies. Approximate methods are most often used instead. Many different computational procedures to obtain both continuous and discrete point spectra are known. Description of all these methods greatly exceeds the main topic of this book, so the reader must be referred to the specific literature on the subject.[1–6], though, to some extent, we shall return to this subject in chapter IV.

For a long time it has been suspected[34,64] that relaxation functions may be affected by stress and/or strain to which the material is subjected. As the time progresses, there is more and more evidence, both theoretical and experimental, published[72&ref.] that it is indeed the case.

As it is evident from the above given canonical equations of the experimental response functions, a number of time independent material constants are included in the equations. Here, the constants, and their interrelations, are summarized. Equilibrium shear modulus

$$G_e = \lim_{s\to 0} \bar{Q}(s) = \lim_{t\to\infty} G(t) = \lim_{\omega\to 0} G'(\omega) \tag{III.145}$$

Glassy shear modulus

$$G_g = \lim_{s\to\infty} \bar{Q}(s) = \lim_{t\to 0} G(t) = \lim_{\omega\to\infty} G'(\omega) \tag{III.146}$$

Steady state (rheodictic) or equilibrium shear compliance

$$\begin{aligned} J_e^{\{o\}} &= \lim_{s\to 0} \left[\bar{U}(s) - \{\phi_f/s\}\right] = \\ &= \lim_{t\to\infty} \left[J(t) - \{\phi_f\ t\}\right] = \\ &= \lim_{\omega\to\infty} J'(\omega) \end{aligned} \tag{III.147}$$

Glassy shear compliance

$$J_g = \lim_{s\to\infty} \bar{U}(s) = \lim_{t\to 0} J(t) = \lim_{\omega\to\infty} J'(\omega) \tag{III.148}$$

Steady state shear fluidity

$$\phi_f = \lim_{s\to 0} s\ \bar{\phi}(s) = \lim_{t\to\infty} \phi(t) = \lim_{\omega\to\infty} \phi'(\omega) \tag{III.149}$$

Steady state shear viscosity

$$\eta_f = \lim_{s\to 0} s\ \bar{\eta}(s) = \lim_{t\to\infty} \eta(t) = \lim_{\omega\to\infty} \eta'(\omega) \tag{III.150}$$

III.4 Energy Considerations

It is important to note the energy questions connected to material deformation. In line with the brevity of this overview, only those relationships are quoted which

are most relevant to fiber formation processes. And so, for strain excitation – stress relaxation in step excitation cases the energy stored, $W_s(t)$, due to imposition of an initial strain, ε_0, is

$$W_s(t) = \left(\frac{\varepsilon_0^2}{2}\right)\left[\{G_e\} + \int_{-\infty}^{\infty} H(\theta)\ \exp\left(\frac{-2\ t}{\theta}\right)\ d\ln\theta\right] \tag{III.151}$$

The rate of energy storage, $\dot{W}_s(t)$, is

$$\dot{W}_s(t) = \varepsilon_0^2\left[G_g\ \delta\ (2\ t) - \int_{-\infty}^{\infty} \theta^{-1}\ H(\theta)\ \exp\left(\frac{-2\ t}{\theta}\right)\ d\ln\theta\right] \tag{III.152}$$

The energy dissipated, $W_d(t)$, under the same conditions may be described as

$$W_d(t) = \left(\frac{\varepsilon_0^2}{2}\right)\int_{-\infty}^{\infty} H(\theta)\ \left[1 - \exp\left(\frac{-2\ t}{\theta}\right)\right]\ d\ln\theta \tag{III.153}$$

The rate of energy dissipation, $\dot{W}_d(t)$, is

$$\dot{W}_d(t) = \varepsilon_0^2 \int_{-\infty}^{\infty} \theta^{-1}\ H(\theta)\ \exp\left(\frac{-2\ t}{\theta}\right)\ d\ln\theta \tag{III.154}$$

For creep behavior, stress excitation - strain retardation with step excitation, for a continuous retardation spectrum (continuous distribution of retardances) the stored energy, $W_s(t)$, is

$$W_s(t) = \left(\frac{\sigma_0^2}{2}\right)\left\{J_g + \int_{-\infty}^{\infty} L(\theta)\ \left[1 - \exp\left(\frac{-2\ t}{\theta}\right)\right]\ d\ln\theta\right\} \tag{III.155}$$

The corresponding rate of energy storage, $\dot{W}_s$, is

$$\dot{W}_s(t) = \frac{\sigma_0^2}{2}\left\{J_g(t) + 2\int_{-\infty}^{\infty} \theta^{-1}\ L(\theta)\left[1 - \exp\left(\frac{-2t}{\theta}\right)\right]\exp\left(\frac{-t}{\theta}\right) d\ln\theta\right\} \tag{III.156}$$

The dissipated energy, $W_d(t)$, under the same conditions is

$$W_d(t) = \left(\frac{\sigma_0^2}{2}\right)\left\{\int_{-\infty}^{\infty} L(\theta)\ \left[1 - \exp\left(\frac{-2\ t}{\theta}\right)\right]\ d\ln\theta + 2\ t\{\phi_f\}\right\} \tag{III.157}$$

The rate of energy dissipation, $\dot{W}_d(t)$, in accordance with the above, is formulated as

$$\dot{W}_d(t) = \sigma_0^2 \times \left[\int_{-\infty}^{\infty} \theta^{-1} \, L(\theta) \, \exp\left(\frac{-2\,t}{\theta}\right) \, d\ln\theta + \{\phi_f\} \right] \tag{III.158}$$

The total energy is, of course, the sum of the stored and dissipated energies.

III.5 Uniaxial Extension

The majority of the rheology issues covered above concerns shear stresses. Uniaxial extension (or compression) is at least as important, or even more so, in fiber formation and other areas (e.g. testing). The matrices of the transforms of stress and strain tensors for this case are:

$$|\bar{\sigma}_{ij}| = \begin{vmatrix} \bar{\sigma}_{11} & 0 & 0 \\ 0 & 0 & 0 \\ 0 & 0 & 0 \end{vmatrix} \tag{III.159}$$

$$|\bar{\gamma}_{ij}| = \begin{vmatrix} \bar{\gamma}_{11} & 0 & 0 \\ 0 & \bar{\gamma}_{22} & 0 \\ 0 & 0 & \bar{\gamma}_{33} \end{vmatrix} \tag{III.160}$$

From these tensors one can derive the following relationships:

$$\bar{\sigma}_{11}(s) = 2\,\bar{Q}(s)\,[\bar{\gamma}_{11}(s) - \bar{\gamma}_{22}(s)] \tag{III.161}$$

or

$$\bar{\sigma}_{11}(s) = 2\,s\,\bar{G}(s)\,[\bar{\gamma}_{11}(s) - \bar{\gamma}_{22}(s)] \tag{III.162}$$

From the last equations it follows that the shear modulus is known if the stress in transverse direction is known. Experimentally, however, it is very difficult to determine the transverse stress and to overcome this, the ratio of stress to strain is used instead. In the transform plane, the *stretch relaxance*, $\bar{Y}$, and *elongational (stretch) relaxation modulus*, $\bar{E}$, become

$$\frac{\bar{\sigma}_{11}(s)}{\bar{\gamma}_{11}(s)} = \bar{Y}(s) = s\,\bar{E}(s) \tag{III.163}$$

The canonical representations of the relaxance are

$$\bar{Y}(s) = \{E_e\} + \int_{-\infty}^{\infty} H_E(\theta) \, \frac{\theta\,s}{1+\theta\,s} \, d\ln\theta \tag{III.164}$$

$$\bar{Y}_\bullet(s) = E_g - \int_{-\infty}^{\infty} H_E(\theta) \, \frac{1}{1+\theta\,s} \, d\ln\theta \tag{III.165}$$

Here $H_E(\theta)$ is *elongational (or tensile, or stretch) modulus*, E_e and E_g are correspondingly *equilibrium* and *glassy elongational modulus* .

It is very important to stress that $H_E(\theta)$ is similar to the shear relaxation spectrum, but that there are fundamental differences in the relaxation behavior between the two.

The transform of the canonical equation of elongational viscosity may be presented as

$$\bar{Y}(s) = \frac{\bar{E}(s)}{s} = \frac{\{E_e\}}{s^2} + \int_{-\infty}^{\infty} H_E(\theta) \frac{\theta\, s}{1+\theta\, s}\, d\ln\,\theta \tag{III.166}$$

This leads to the expression for extensional viscosity analogous to equation III.136

$$\zeta(t) = \{E_e\ t\} + \int_{-\infty}^{\infty} \theta H_E(\theta) \left[1 - \exp\left(\frac{-t}{\theta}\right)\right] d\ln\theta \tag{III.167}$$

In considering compliance, by definition the *elongational retardance* is $\bar{L}(s) = 1/\bar{Y}(s)$ and the *elongational compliance* is $sD(s) = 1/E(s)$ and, by analogy with equation III.155, they may be presented as

$$\frac{\bar{\gamma}_{11}(s)}{\bar{\sigma}_{11}(s)} = \bar{L}(s) = s\,\bar{D}(s) \tag{III.168}$$

And further

$$\bar{L}(s) = E_g + \int_{-\infty}^{\infty} L_D(\theta) \frac{1}{1+\theta s}\, d\ln\ \theta + \left\{\frac{1}{\zeta_f\, s}\right\} \tag{III.169}$$

$$\bar{L}_{\bullet}(s) = D_e^{\{o\}} - \int_{-\infty}^{\infty} L_D(\theta) \frac{\theta\, s}{1+\theta\, s}\, d\ln\theta + \left\{\frac{1}{\zeta_f\, s}\right\} \tag{III.170}$$

$L_D(\theta)$ is the *elongational retardation spectrum*, D_g, and $D_e^{\{o\}}$ are the glassy and *pseudo-equilibrium compliance*, and ζ_f is the *steady state elongational viscosity.*

As mentioned above

$$H_E(\theta) \neq H(\theta) \neq H_K(\theta) \qquad \text{and} \qquad L_D(\theta) \neq L(\theta) \neq L_K(\theta) \tag{III.171}$$

The constants in equations III.169 and III.170 may be defined as

$$\int_{\infty}^{\infty} H_E(\theta)\, d\ln\theta = E_g - \{E_e\} \tag{III.172}$$

$$\int_{-\infty}^{\infty} L_D(\theta)\, d\ln\theta = D_e^{\{o\}} - D_g \tag{III.173}$$

If a material is subjected to uniaxial strain in any direction, the two remaining directions also display certain strain. The ratio of the lateral strain to the excitation strain is known as *Poisson's ratio.* While for purely elastic materials Poisson's ratio is a material constant, for viscoelastic materials Poisson's ratio is a time dependant function. If the undeformed material is isotropic, then the contraction in the two lateral directions is identical. Poisson's ratio is the same, irrespective of the type of excitation (stress or strain). A stretched material experiences stress relaxation in the strain direction but the transverse strain is delayed; it reaches its final value after infinite time. The strain retardation makes the problem analogous to compliance, so we have

$$\bar{\nu}s = \mu_g + \sum_{n=1}^{N-1} \mu_n \frac{1}{1+\theta_n\, s} = \mu_e - \sum_{n=1}^{N-1} \mu_n \frac{\theta_n\, s}{1+\theta_n\, s} \tag{III.174}$$

$$\bar{\mu}s = \frac{\mu_g}{s} + \sum_{n=1}^{N-1} \mu_n \frac{1}{s\,(1+\theta_n\, s)} = \frac{\mu_e}{s} - \sum_{n=1}^{N-1} \mu_n \frac{\theta_n}{1+\theta_n\, s} \tag{III.175}$$

In equations III.174 and III.175 $\bar{\nu}$ and $\bar{\mu}$ are analogous to $\bar{U}$ and $\bar{J}$. In this case θ is called *delay time*, as it is not identical with retardation time in tension. The glassy and equilibrium Poisson's ratios are designated respectively as μ_g and μ_e, and $\sum_n \mu_n = \mu_e - \mu_g$.

By its nature, Poisson's ratio is arrheodictic and it may have maximum value of -0.5 for ideally incompressible material at equilibrium. The glassy Poisson's ratio is normally smaller than 0.5, mostly closer to $\frac{1}{3}$.

The canonical representation of Poisson's ratio function may be derived by obtaining a spectrum of delay times, $m(\theta)$, analogously to the above given cases for Voigt model.

The final equations are:

$$\mu(t) = \mu_g + \int_{-\infty}^{\infty} m(\theta)\,[1 - \exp(-t/\theta)]\, d\ln\theta \tag{III.176}$$

$$\mu(t) = \mu_e + \int_{-\infty}^{\infty} m(\theta)\, \exp(-t/\theta)\, d\ln\theta \tag{III.177}$$

III.6 Extrudate Swelling

There is a phenomenon of particular importance to fiber formation: *die swell* or Barus effect or extrudate swelling. Namely, if a material is extruded from a capillary of a given diameter, the diameter of the extrudate almost always is larger than the diameter of the capillary used. This phenomenon is somewhat elusive; the available explanation appears incomplete, and the problem is certainly

very complex. Empirical observations indicate that die swell depends strongly on the capillary length (or aspect ratio) and on the rate of shear in the capillary.[7,8] Influence of these parameters on die swell may be appreciated from figures III.11, III.14. and III.15. These types of influences led to the belief that die swell is related to the melt elasticity,[9] to the relaxational processes. Further, it has been proved that die swell depends also on the extensional flow component developed at the entry to the capillary.[10,13]

V.Cogswell[11] relates die swell, B, to the recoverable strain, ε_R, as follows:

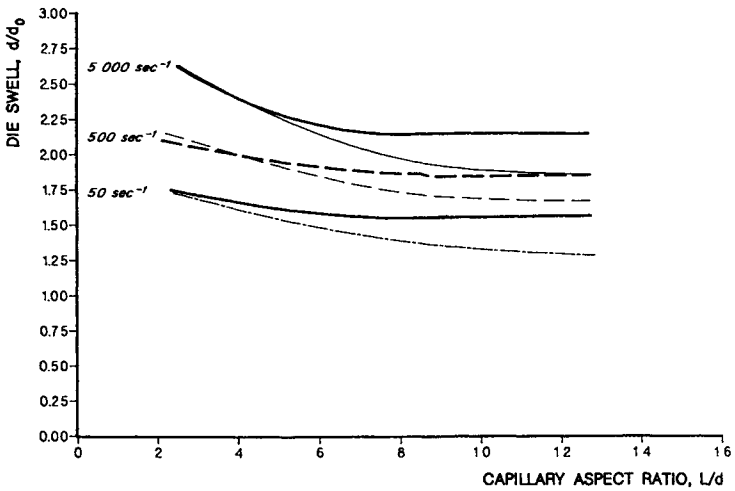

Figure III.11: *The relationship between die swell, defined as the ratio of the extrudate diameter over capillary diameter, and the angle of the capillary entrance cone: heavy lines* 60°, *fine lines* 20°. *After Walczak*[12]

$$\varepsilon_R = \ln B^2 \tag{III.178}$$

For the case of free convergence at the die entry, the extensional stress, σ_E, may be calculated from the relationship:

$$\sigma_E = \sigma_s / \tan\varphi \tag{III.179}$$

where φ is one half of the entry cone angle, σ_s is shear stress corresponding to the shear rate $\dot{\gamma} = 4Q/\pi r^3$ for the cone location, if the shear stress - shear rate relationship is known. Otherwise, there are approximate formulae for the extension rate:[14]

$$\dot{\varepsilon} = \left(\frac{\dot{\gamma}}{4}\right)\left[\frac{\sin^3\varphi}{(1-\cos\varphi)}\right] = \left(\frac{\dot{\gamma}}{2}\right)\sin\varphi\ \left[\frac{(1-\cos\varphi)}{2}\right] \tag{III.180}$$

and another:[11,13]

$$\dot{\varepsilon} = \left(\frac{\dot{\gamma}}{2}\right)\ \tan\varphi \tag{III.181}$$

Both of the above equations have been developed for Newtonian flow. The equation for non-Newtonian fluids developed by Cogswell[11] requires the knowledge of the local pressure drop, P_0, during extrusion, as well as the exponent in the power law equation, n, on which the derivation is based:

$$\dot{\varepsilon} = \frac{4\ \sigma_s}{[3\ (n+1)P_0]} \tag{III.182}$$

For the flow in conical ducts (entry to a capillary), the fluid velocity at the wall is zero, maximum velocity is in the center. In effect the flow velocity profile includes telescopic shear and elongation. Again, there is a disagreement as to the final formulation of extension rate in the Newtonian flow. Similarly as for the free convergence, all the suggested solutions become identical for the cone angle approaching zero. The only non-Newtonian solution is given by Cogswell:[11]

$$\dot{\varepsilon} = \left[\frac{3n+1}{n+1}\right] \times \left(\frac{\dot{\gamma}}{2}\right) \times \tan\varphi \tag{III.183}$$

Here n is the exponent in the power law equation $\sigma_s \propto \dot{\gamma}^n$. For Newtonian fluids, when $n = 1$, equation III.183 becomes

$$\dot{\varepsilon}_{max} = \dot{\gamma}\ \tan\varphi \tag{$III.183\,a$}$$

Die swell is the result of the superposition of the recoverable part of the extensional strain and of the expansion created by the normal shearing force facing cessation of the capillary wall restraint. The second reason was demonstrated by Zidan[15], in full agreement with the experimental work published by Goren and Wronski[16,17] and by Gavis and Madon[18], that even Newtonian fluids show extrudate expansion at Reynolds numbers below 16, while at higher Reynolds numbers the extrudate diameter is smaller than the capillary radius. Figures III.12 and III.13 present calculated flow patterns and velocity distribution in the vicinity of the capillary exit for Newtonian fluid with different ratios of wall friction coefficient, f, over viscosity, $\omega = f/2\eta$.

The die swell descriptions given above do not unite all the aspects of the phenomenon. The problem is even further complicated by the fact that die swell depends quite strongly on the shearing history of the polymer. This may be seen from the comparison given in Figure III.14, which represents the same polymer as obtained from polymerization in a powder form (top of figure) and after pelletization in a screw extruder with no degradation detectable analytically (bottom of figure). The only speculative explanation for this dependence, as nebulous as it may be, may be the change in the molecular entanglements leading to changes in the elastic response. The polymer history cannot be quantified yet. Die swell, as important as it is in fiber formation processes, still remains elusive and not fully defined.

It has been found that extensional viscosity (Trouton viscosity) may be best described in relation to tensile stress. It initially is equal to $3\eta_0$ (where η_0 is zero shear

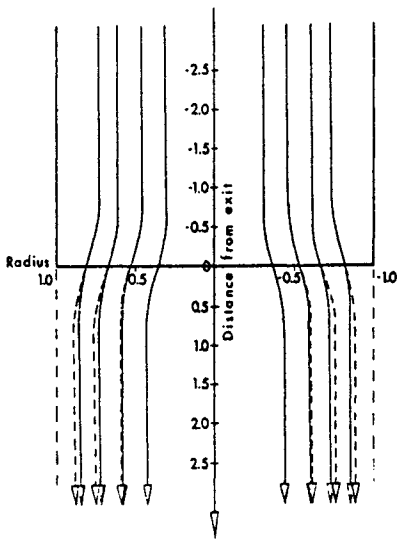

Figure III.12: *Streamlines in flow of Newtonian fluid in the vicinity of the capillary exit; negative values in the capillary, positive values outside the capillary. Parameter:* $\omega = 0.5$ *full drawn lines,* $\omega = 0.05$ *dashed lines. After Zidan.*[15]

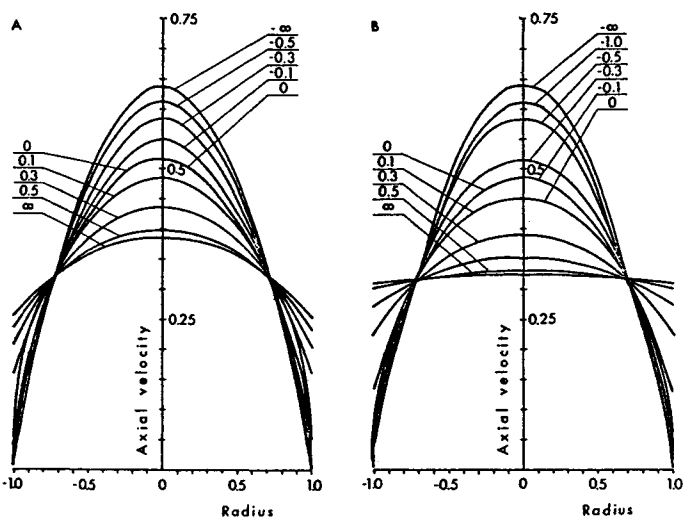

Figure III.13: *Velocity profiles in the vicinity of capillary exit, as calculated for Newtonian fluid. Parameter: distance from capillary (negative inside the capillary). A for* $\omega = 0.5$, *B for* $\omega = 0.05$. *After Zidan.*[15]

viscosity), and increases with increasing stress,[15,19,20] contrary to shear viscosity which decreases with increasing stress. The increase of extensional viscosity with stress continues to about $10^5 Pa$,[20] (ranging from $6.68 \cdot 10^5 Pa$ to $2.15 \cdot 10^5 Pa$[21]), thereafter the viscosity may become constant, and later decreases. The decrease

of viscosity with stress is responsible for flow instabilities, both in the capillary flow due to the extensional flow component, and in extensional flow as such.

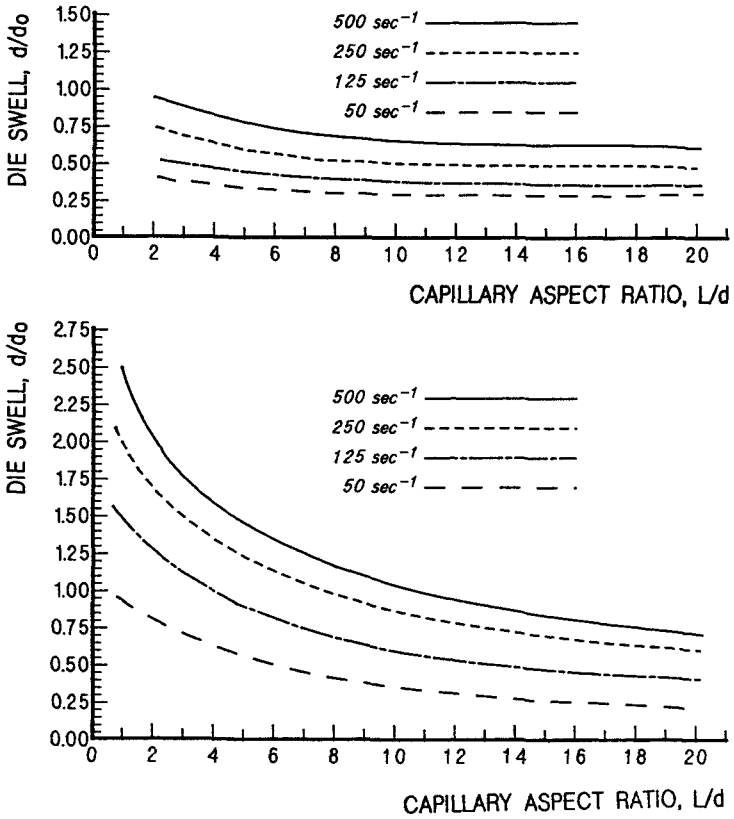

Figure III.14: *Die swell, $B = r/r_0$, in relation to the capillary aspect ratio, l/d; parameter shear rate. Top: polypropylene in powder form, "as polymerized", bottom: the same polymer as above but pelletized in a screw extruder.*[12]

In general, any rheological function in one mode may be obtained from data acquired in another mode if the two functions are available. For example, one may obtain the bulk relaxance in isotropic compression from data obtained in shear experiments. One may obtain information on shear flow from data obtained in uniaxial extension. Nevertheless, as an exception, information on extensional flow cannot be extracted from data obtained in other modes of deformation. It is unfortunate, as experimentally analyses of extensional flow are very difficult and are usually burdened with a larger error.

It appears important to mention, however, the simplified method of obtaining information on extensional flow from experiments with converging flow. Cogswell[28] postulated that the flow from a reservoir into a zero-length capillary represents a sum of a shear and extensional component. The suggested solutions were based on the power law constitutive equation. Bersted[29] substituted the power law

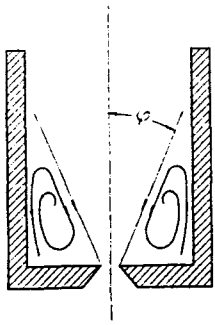

Figure III.15: *Schematic representation of the flow pattern at the entry to a capillary.*

equation, $\tau \propto \dot{\gamma}^n$, with a more "flexible" formula:

$$\eta = \frac{\eta_0}{1 + A\ \dot{\gamma}^{\frac{2}{3}}} \tag{III.184}$$

and the exponent, n, is

$$n = \frac{1 + \left(\frac{A\ \dot{\gamma}^{2/3}}{3}\right)}{(1 + A\ \dot{\gamma}^{\frac{2}{3}})} \tag{III.185}$$

where η_0 is zero-shear viscosity and $\dot{\gamma}$ is shear rate. In effect, the original Cogswell and the modified equations form the following set which describes the process: Pressure drop due to extension at any point of the cone:

$$P_E(h) = \left[\frac{\zeta \tan\varphi(h)}{3}\right] \quad [\dot{\gamma}(h-1) - \dot{\gamma}(h)] \tag{III.186}$$

Here, ζ is extensional viscosity, φ is one half of the angle of the entrance cone and $\tan\varphi = (2\eta/\zeta)^{1/2}$, h is the location in relation to the conical duct exit. Figure III.15 shows schematically the polymer flow in the vicinity of capillary entry. The vortices formed around the more or less conical flow pattern are the reason for the pattern development, unless the entry has conical walls to serve the same purpose. Pressure drop due to shear at any point of the cone:

$$P_S(h) = \frac{2\ \eta_0\ \dot{\gamma}(h-1)\ [1 - \Gamma^{n(h)}]}{3\ \tan\varphi(h)\ \left\{1 + \frac{[A\dot{\gamma}^{2/3}(h-1)]}{3}\right\}} \tag{III.187}$$

where $\Gamma = \dot{\gamma}(h)/\dot{\gamma}(h-1)$. The summaric pressure drop at any point is

$$P(h) = 2\ \sqrt{P_S(h)\ P_E(h)} \tag{III.188}$$

Total pressure drop is

$$P = \sqrt{\frac{8\ \eta_0\ \zeta}{9}} \times\ \Xi \tag{III.189}$$

where

$$\Xi = \left\{ \sum_{h=2}^{m} \frac{\dot{\gamma}(h-1)\,[\dot{\gamma}(h-1) - \dot{\gamma}(h)]\,(1-\Gamma)^{n(h)}}{\left(1 + \frac{[A\ \dot{\gamma}(h-1)^{2/3}]}{3}\right)} \right\}^{\frac{1}{2}} \tag{III.190}$$

Average extension rate is

$$\langle \dot{\varepsilon} \rangle = \frac{\dot{\gamma}_1}{2} \left\{ \frac{2\ \eta_0}{\zeta_1\,[1 + A\ \dot{\gamma}(1)^{2/3}]} \right\}^{\frac{1}{2}} \tag{III.191}$$

After rearranging equation III.189, extensional viscosity becomes

$$\zeta = \left(\frac{9}{8}\right) \left(\frac{P}{\Xi}\right)^2 \times\ \eta_0^{-1} \tag{III.192}$$

Change of the constitutive equation improves the agreement between the data calculated from conical capillary experiments and those obtained by direct measurements of extensional viscosity only insignificantly. As a next step improvement, Bersted[29] uses extensional viscosity as a function of extension rate instead of Cogswell's constant "average extensional viscosity" in equation III.186. Cogswell's equation for extension rate function in a conical capillary is

$$\varepsilon(h) = \tan\varphi(h)\ \left[\frac{2\ Q}{\pi r(h)^3}\right] \tag{III.193}$$

Further, it is assumed that

$$\begin{aligned} \zeta(h) \quad &= \zeta(h-1) \left[\tfrac{\dot{\varepsilon}(h)}{\dot{\varepsilon}(h-1)}\right]^{k(h)} \quad = \\ &= \zeta(h-1) \left[\tfrac{r(h)^3}{r(h-1)^3}\right]^{3k(h)} \quad = \\ &= \zeta(h-1) \left[\tfrac{\dot{\gamma}(h)}{\dot{\gamma}(h-1)}\right]^{k(h)} \end{aligned} \tag{III.194}$$

Finally, the pressure drop function due to extension is

$$\begin{aligned} P_E(h) \quad &= \quad \frac{\zeta(1)\tan\varphi(h)}{3[1+k(h)]} \times \left\{ \dot{\gamma}(h-1)\left[1 - \Gamma^{1-k(h)}\right] \times \right. \\ &\times \quad \left. \left[\frac{\dot{\gamma}(h-1)}{\dot{\gamma}(h-2)}\right]^{k(h-1)} \cdots \left[\frac{\dot{\gamma}(2)}{\dot{\gamma}(1)}\right]^{k(1)} \right\} \end{aligned} \tag{III.195}$$

The summaric pressure drop function of height h is

$$\begin{aligned} P(h) = \Bigg\{ &\left[\frac{8Q(h)}{3}\right] \left[\frac{\zeta(h)\dot{\gamma}(h-1)}{3+3k(h)}\right] \times \left[1 - \Gamma^{n(h-1)}\right] \times \\ &\times \left[1 - \Gamma^{1+k(h)}\right] \left[\frac{\dot{\gamma}(h-1)}{\dot{\gamma}(h-2)}\right]^{k(h-1)} \cdots \left[\frac{\dot{\gamma}(2)}{\dot{\gamma}(1)}\right]^{k(2)} \Bigg\}^{\frac{1}{2}} \end{aligned} \tag{III.196}$$

where

$$Q(h) = \frac{\eta_0 \, \dot{\gamma}(h-1)}{[1 + A \, \dot{\gamma}(h-1)^{2/3}]} \qquad (III.196\,a)$$

At the capillary exit ($h = 1$) the extensional viscosity is

$$\zeta = (P/\Xi)^2 \qquad (III.197)$$

In this case Ξ becomes

$$\Xi = \sum_{h=1}^{m} \left\{ \left(\frac{8 \, \eta_0 \, \dot{\gamma}(h-1)^2}{[9(1 + A \, \dot{\gamma}(h-1)^{2/3}]/3} \right) \times \right.$$

$$\left. \times \left[1 - \Gamma^{n(h-1)}\right] \left[1 - \Gamma^{1+k(h)}\right] \right\}^{\frac{1}{2}} \times Z(h) \qquad (III.197\,a)$$

where

$$Z(h) = \left\{ \frac{1}{[1 + k(h)]} \right\} \times \left[\frac{\dot{\gamma}(h-1)}{\dot{\gamma}(h-2)} \right]^{k(h-1)} \cdots \left[\frac{\dot{\gamma}(2)}{\dot{\gamma}(1)} \right]^{k(2)} \qquad (III.197\,b)$$

The above given calculations are rather involved, so it is obvious a computer has to be employed for their execution. Further, the value of $k(h)$ is not known *a priori*, and it probably varies with the extension rate. Consequently, the entire problem must be solved iteratively by employing equations III.184 through III.191 as the first approximation, and subsequently the extensional viscosity as a function of the extension rate is improved by fitting the data into equations III.196.[29] The agreement between the data so calculated and the results obtained from experimental determination of extensional viscosity is quite good for several polymers, however, for narrow molecular weight polystyrenes, the agreement is disappointing. In summary, experimental determination of extensional flow is to be recommended over the above given method of calculation. Nevertheless, the Cogswell and Bersted work seems important as it points to rather interesting phenomena taking place during extrusion through capillaries with conical entrance.

The work of Cogswell and Bersted has been extended further by J. R. Collier and co-workers.[66,67] These authors find that extensional flow data may be obtained from extrusion through hyperboloidal - conical dies ("capillaries"). The experiments may be conducted either by an axial coextrusion of two polymers with largely different viscosities (by a factor of 30 to 100)[66] or even without the "lubricating" polymer.[67]

Interesting investigations of die swell were reported by Tanner and co-workers.[60,61] Some of their key findings may be summarized as follows:

- For Newtonian fluids the maximum diameter of the extrudate is attained only 0.5 diameters below the exit of the capillary. This is true for non-Newtonian fluids at Weissenberg number of 1 ($Wi = \theta v/R$ where θ - relaxation time, $\bar{v}$ - average axial velocity, R - capillary diameter).

- Extrudate swelling is strongly dependent on both elasticity and cooling.
- Presence of a yield stress in a material strongly reduces the swelling.

In the end, one must conclude that the swelling problem is extremely complex and despite all the interesting work done thus far, a firm understanding and prediction ability still seem to lie in the future.

III.7 Flow Instability in Extrusion

Flow instabilities had been observed for a long time,[22–24] and many different theories have been put forth to explain it. It has been noticed that the onset of flow instabilities coincides with the Deborah number approaching one,[25,26] and this is understood as an indication that the instability is related to the viscoelastic nature of the fluid. Also, an interesting thermodynamic explanation of the flow instabilities has been offered,[27] and this is in agreement with the understanding that the flow instability is a phenomenon resulting from the viscoelastic nature of the polymer.

The recent two decades have brought more convincing interpretations of the phenomenon. During extrusion through a capillary, the necessary pressure requirement to drive the extrusion increases with the increasing flow rate. Nevertheless, the relationship is not as simple as it might result from the basic equations for flow in tubular ducts (capillaries). Figure III.16 shows the general relationship between pressure in the barrel of a capillary rheometer and polymer flow rate.[57–59] The graph is divided into five regions:

I – where extrudate is smooth and at constant flow, pressure is constant with time,

II – where extrudate has a more or less rough surface ("shark skin"), though pressure is constant with time,

III – where flow is unstable, uneven, spurting exit of polymer while pressure has a "saw tooth" relation with time,

IV – large deformations of extrudate: uneven diameter, spiral, "porous surface" and pressure mostly constant with time.

V – behavior very similar to that in region IV.

Hatzikiriakos[57] believes that the critical factor in formation of the "shark skin" is acceleration of the melt in the region of the capillary exit. The acceleration subjects the polymer stream to extensional forces with increasing extension rate, reaching around 1 to $3s^{-1}$. The large extensional flow causes slip at the wall of the capillary. The situation may be aggravated by large stresses at the entry to the capillary. As discussed above, the entry stresses are smaller in conical entries, particularly with small cone angles. This point agrees with the quite generally

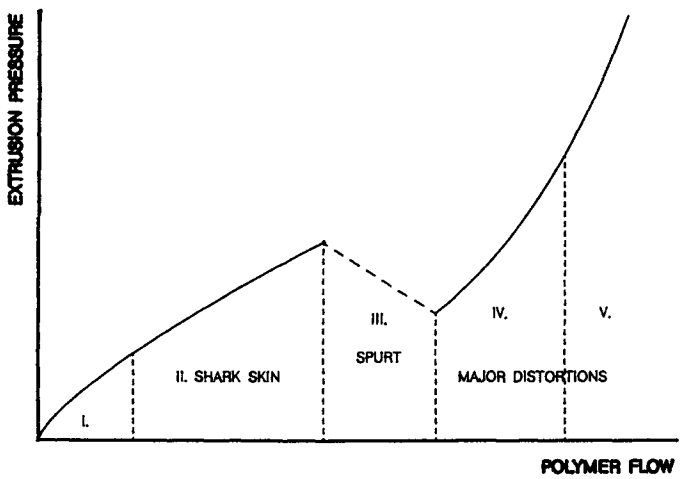

Figure III.16: *A general representation of the relationship between extrusion pressure and flow rate in a capillary extrusion. Section I - extrudate with smooth surface. Section II - extrudate with surface distortions ("shark skin"). Section III - unsteady (oscillatory) or surt flow. Section IV and V - extrudate with major distortions. After Molenaar and Koopman*[58]

known experience (see figure III.16). However, long standing common knowledge is that the geometry of the capillary entrance affects the instabilities (see figure III.17), and in the entry region, the polymer is subjected to extensional forces. Here Hatzikiriakos and Dealy's theory agrees with the facts, however the suggested formalization does not reflect it.

Hatzikiriakos and Dealy[56] have developed a model which describes the fracture phenomena, as represented in figure III.16, quite well. The model has been developed under the following assumptions:

- Viscosity is independent of pressure.
- In the low flow branches, the flow is isothermal.
- Elasticity of the fluid is not taken into account.
- Lubrication approximation is used as creeping flow is assumed.
- For the high flow branch, flat velocity profile (plug flow) is assumed.
- Empirical slip models are used, so slip velocity is taken as being dependant on actual stress (the stress history is neglected).
- Flow above the capillary entry is neglected.
- Normal stresses are calculated from empirical relationships.

The authors[57] conclude that the two most important factors contributing to the melt fracture are compressibility of the melt and slip on the capillary walls.

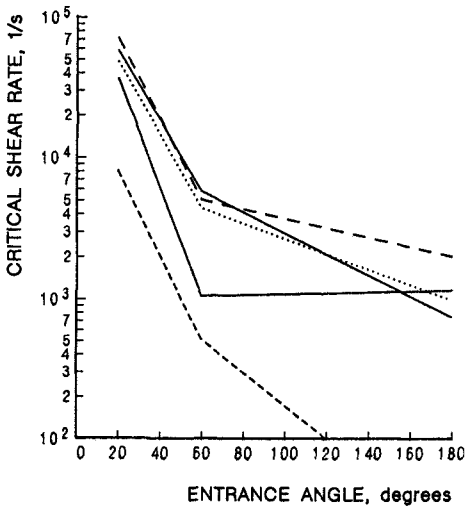

Figure III.17: *Onset of capillary flow instability (critical shear rate) in relation to the angle of capillary entrance cone.*[12]

The authors also suggest that melt elasticity, if accounted for, might improve the agreement between the calculated and experimental results.

Molenaar and Koopmans[58] base their model on the mechanism of relaxation oscillation, according to the earlier suggestion by Weill.[59] To describe the fracture phenomenon , the authors arrive at two coupled differential equations with one parameter:

$$\frac{dQ^*}{dt^*} = \frac{P^* - F^*(\Delta Q^*)}{\varepsilon} \tag{III.198}$$

$$\frac{dP^*}{dt^*} = -\Delta Q^* \tag{III.199}$$

where

$$\varepsilon \equiv \frac{K\ Q_i^2}{C\ P_0^2} \tag{III.200}$$

is a parameter. The notation here is P_0 means a characteristic pressure (taken as equal to $10^7\ Pa$), t is time, t^* is dimensionless time given by

$$t^* \equiv \left(\frac{C\ P_0}{Q_i}\right)^{-1} \cdot t \tag{III.201}$$

$$C \equiv A\ \chi\ h \tag{III.202}$$

A is cross sectional area of the barrel, h is the hight between the plunger and the capillary entry, χ is melt compressibility, Q_i is the inlet flow rate (constant), $Q_e(t)$ is extrudate flow rate. The flow rates are scaled with Q_i so that in the dimensionless form one has

$$Q_e^*(t) \equiv \frac{Q_e(t)}{Q_i} \tag{III.203}$$

and

$$\Delta Q^*(t^*) \equiv \frac{\Delta Q(t)}{Q_i} \tag{III.204}$$

while

$$\Delta Q \equiv Q_e(t) - Q_i \tag{III.205}$$

Naturally, $Q_i \equiv 1$. $P(t)$ is pressure in the barrel as a function of time. In its dimensionless form it is

$$P^*(t^*) \equiv \frac{P(t)}{P_0} \tag{III.206}$$

F is the characteristic material function which may be taken from a constitutive equation of the polymer and of the appropriate boundary conditions. One may write the following relationship between the change of pressure with time to the change of the total mass in the barrel:

$$P(t) = F[\Delta Q(t)] = \int_0^t \frac{Q_i - Q_e(t')}{C(t')}\, dt' \tag{III.207}$$

where $\Delta Q \equiv Q_e(t) - Q_i$.

Further, one may write

$$\frac{d\,[Q_e(t) - Q_i]}{dt} = \frac{d\,Q_e}{dt}\frac{[P - F(\Delta Q)]}{K} \tag{III.208}$$

The dimensionless material function is then

$$F^*(\Delta Q^*) \equiv \frac{[F(\Delta Q)]}{P_0} \tag{III.209}$$

Equation III.198 has only one parameter

$$\varepsilon \equiv \frac{K\,Q_i^2}{C\,P_0^2} \tag{III.210}$$

As results from the above considerations, the onset of "shark skin" (region II in figure III.16) depends only on the constitutive equation. The spurting portion of the curve (region III) is described by self excited oscillation of relaxation of a material which is able to dissipate energy, though energized in a constant way. The shape of the curve depicting the pressure function, $Q_e(t)$, depends on the material properties described by the function F^*. Therefore the behavior in region III depends on the elasticity. Similarly as in region II, in region IV two different stress values correspond to every shear rate. The high shear rate is in the center, the low shear rate, at the wall. This may result in a relatively smooth surface, but major distortions of the extrudate are also likely. The nature of the distortions may depend on a large number of factors related to the material and to the geometry of the hardware.

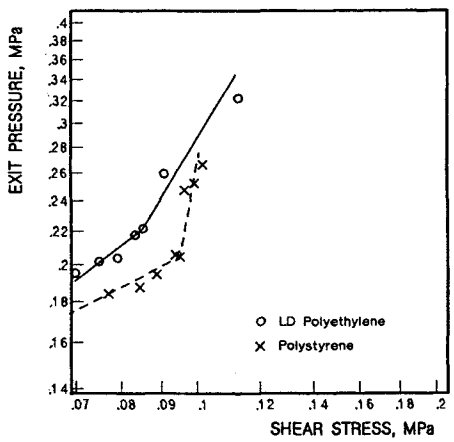

Figure III.18: *Exit pressure in relationship to shear stress. The transition point coincides with the onset of flow instability. After Han and Lamonte.*[62]

It has been noticed that if the angle of the capillary entrance cone is small (figure III.17 and III.18),[12,24] the flow instability starts at higher shear rates (critical shear rate, $\dot{\gamma}_{cr}$). This is consistent with equation III.179. The solution suggested by Molenaar and Koopman[59], in its principle, seems to be more suited to explain the effect of entry geometry. The formalization of the geometric factor still needs additional investigations.

Figure III.18 shows the results of very interesting investigations by Han and Lamonte.[62] The results seem to show convincingly that the elastic properties of a material are quite essential in considerations of flow instabilities.

Vinogradov[63] has determined that flow instabilities appear when stress reaches a critical value, that lies between 0.1 and 0.5 MPa. This value is valid for both shear and extensional deformation, provided that in extension this is the true stress. Vinogradov finds that the value holds for all the polymers known and is little dependent on molecular mass and temperature.

If one translates this to deformation rate, then, obviously, the molecular mass and temperature dependence will appear. The critical stress value is, in physical terms, dictated by the fact that the polymer is unable to accommodate more of reversible deformation. The critical stress value coincides with the exhaustion of the possibilities to further extend the entangled chain segments connecting different molecules. This is equivalent to the inability to accumulate much more of reversible deformation. In effect, at the critical stress, the polymer is forced to a glassy state where it becomes brittle. At this stage, polymers loose adhesion to their boundary surfaces, like capillary walls or plates of rotational rheometers. The last phenomenon causes the spurts from the capillary, the jumpy stress on rotational instruments. In this authors opinion the Vinogradov's suggestion seems to be correct in principle, though the limits for critical behavior appear to vary in a wider range, depending on the viscoelastic character of the polymer and on actual processing conditions.

In the last ten years or so, the attention of researchers has been turned toward the direction which may be termed as the questioning of the notion of zero velocity in a capillary flow. Besides the work quoted above, more evidence of slip on capillary walls has been published. J. Barone and co-workers[69] described a mechanism of local reversible molecular *coil* $\longleftrightarrow$ *stretch* mechanism taking place in the boundary layer at the capillary wall. This mechanism is responsible, on a molecular scale, for an oscillation of stress at the wall and wall slip at the exit of the capillary. This mechanism is considered to be responsible for the formation of *"shark skin"*. The coefficient of friction between the polymer and capillary wall has an influence on the magnitude of the effect. A low friction, *e.g.* achieved through a fluorocarbon coating, at the wall in the exit section of the capillary reduces the shark skin effect. Such a coating also reduces die swell.

M. E. Machay and D. J. Henson[70] found that polystyrene slips at stainless steel walls at all shear rates. The authors were unable to find a theory which would fit the data. They believe that the number of molecules adsorbed at the stainless surface is in a dynamic equilibrium, and this determines the slip behavior.

A. D. Yaring and M. D. Graham[71] have developed a model of the slip at polymer - solid interface. The model shows a fair agreement with published experimental data.

III.8 Molecular Rheology

The abbreviated discussion of rheology given above treats materials as a continuum. This, however, does not exhaust the problem. It is important to realize that ultimately it is the molecular structure of the material that rules over the properties, and certain questions may be answered only through considerations of the molecular structure.

The large size and large length to diameter ratio of polymer chains are the reason for the tendency of molecules to coil into more or less tight bundles. The shape of the coils undergoes constant changes due to natural molecular motions. Therefore, only the average size of the molecule may be calculated or determined (e.g. via light scattering). The molecule size is given usually as the *root mean square end-to-end distance*, $\langle L^2 \rangle^{1/2}$, or as the *root mean square radius of gyration*, $\langle f^2 \rangle^{1/2}$. The two values of unperturbed coils, without any solvent penetration, are related to each other as follows: $\langle L^2 \rangle_0 = 6\langle r^2 \rangle_0$. The average shape of the molecule coil is somewhat elongated, kidney-like, rather than spherical. Increase in chain branching results in the coil shape changing to more spherical. With the increasing rigidity of the chains, the chain dimensions increase, eventually approaching the shape of a rod, e.g. polymers forming liquid crystals.

In the unperturbed state, the radius of gyration of a polymer of given architecture is a function of molecular mass: $\langle r^2 \rangle_0 = KM$. For rod shape molecules, however, the relationship is $\langle r^2 \rangle_0 = KM^2$.

Based on Zimm's theory, the relaxation time of a polymer, θ, may be calculated

from the following relationship:

$$\theta = \frac{M(\eta_0 - \eta_s)}{(2.369\ c\ R\ T)} \tag{III.211}$$

where η_0 is zero-shear viscosity, η_s is viscosity of solvent, c represents solution concentration, and M, R, T have the usual meaning. For undiluted polymers, solvent viscosity becomes zero and polymer concentration is to be substituted with polymer density. The constant of 2.369 has been found by Tschoegl[30] to vary from $\pi^2/6$ to 2.369 as the shielding parameter varies from zero (for vanishing hydrodynamic interaction in the free draining coil) to infinity (for dominant hydrodynamic interaction). Temperature dependence of relaxation time is formulated as

$$\theta = \theta_0\ \frac{T_0\ \eta(T)}{T\ \eta(T_0)} \tag{III.212}$$

where the subscript zero designates the data at the reference temperature of T_0.

For polymers of low molecular mass (oligomers), up to a certain critical value of molecular mass, M_c, zero-shear melt viscosity is directly proportional to weight average molecular mass, M_w. In a double logarithmic plot, this gives a straight line of slope equaling one. Above the critical molecular mass, however, the relationship is

$$eta_0 = KM_w^{3.4} \tag{III.213}$$

How viscosity at non-zero shear rates deviates from equation III.213 may be seen from figure III.19. The shear rate related deviations have not been quantified yet.

The intersections of the line representing low molecular mass polymers (slope one) with the lines for non-zero shear rates indicate the points beyond which the polymer will be degraded due to the shear action. Based on this principle, another graph for polymer degradation may be constructed; an example is given in figure III.20.[31]

Temperature dependence of zero-shear viscosity may be described by the Arrhenius type equation:

$$\eta_0 = A_m \exp(E/R\ T) \tag{III.214}$$

where A_m a constant and E is activation energy of flow. However, both the activation energy and the pre-exponential factor depend on temperature and time, and therefore the equation is not general. Another solution has been proposed by H. Leaderman and furthered by Ferry, Tobolsky, Staverman, Schwartl: the so called shift factor, usually represented by a. The equation represents indeed a time-temperature equivalence shift factor. The shift factor represents a means by which such curves as shear modulus *versus* temperature, or stress relaxation modulus *versus* time and temperature, or viscosity *versus* temperature may be represented by a single *master curve* for each of the dependent variables. The effect of temperature change may be calculated by multiplying all values by a

common factor, $a(T)$, which is a function of temperature and which represents the equivalence of time and temperature.

$$\ln a = f(T) - f(T_0) \tag{III.215}$$

where T_0 is a reference temperature, a target temperature to which one attempts

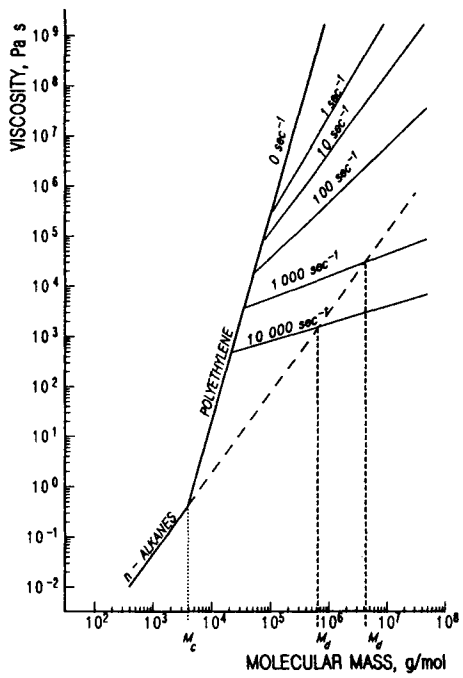

Figure III.19: *Relationship between melt viscosity and molecular mass of polyethylene, parameter: shear rate. M_D is the molecular mass beyond which the polymer will be degraded by respective shear rate. Data after H. P. Schreiber, E. B. Bagley, and D. C. West.*[31]

to recalculate the data.

Interpretation of rheology through chain entanglements[65] gives the following interpretation of the shift factor.

$$a = \ln\left(\frac{\theta}{\theta_g}\right) = \ln\left(\frac{\theta_0}{\theta_{0g}}\right) + 2\ln\left(\frac{E}{E_g}\right) \tag{III.216}$$

where θ is relaxation time, E is modulus of elasticity, the subscripts stand for: 0 related to the unit segment between entanglements, g at glass transition. From this equation one may also derive the WLF equation.[65]

The most frequently used equation for the shift factor is:

$$a = \frac{\rho_0 T_0}{\eta_0}\frac{\eta}{\rho T} \tag{III.217}$$

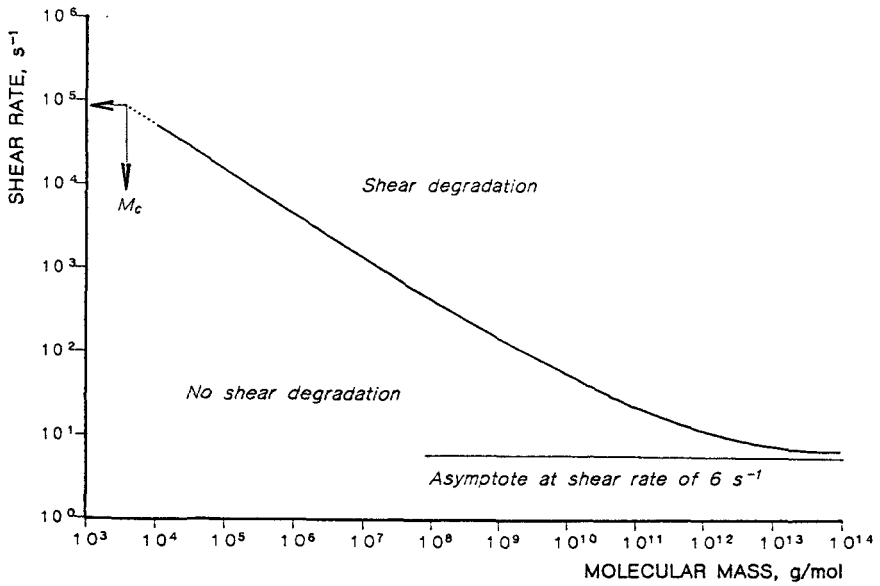

Figure III.20: *Degrading shear rate for polymer of a given molecular mass. Graph constructed on the basis of Figure III.19 for polyethylene.*[31]

where the symbols have their customary meaning, and subscript 0 represents values at the reference temperature. Other equations of frequent use are:

$$\frac{\rho_0 T_0}{\rho T} G(t \cdot a, T) = G(T_0, t) \tag{III.218}$$

$$\frac{\rho_0 T_0}{\rho T} G'(\omega/a, T) = G'(T_0, \omega) \tag{III.218 a}$$

$$\frac{\rho_0 T_0}{\rho T} G''(\omega/a, T) = G''(T_0, \omega) \tag{III.218 b}$$

$$\frac{\rho T}{\rho_0 T_0} J(t \cdot a, T) = J(T_0, t) \tag{III.219}$$

$$\frac{\rho T}{\rho_0 T_0} J'(\omega/a, T) = J'(T_0, \omega) \tag{III.219 a}$$

$$\frac{\rho T}{\rho_0 T_0} J''(\omega/a, T) = J''(T_0, \omega) \tag{III.219 b}$$

In equations III.215 and III.217, the meaning of the symbols is as throughout this chapter.

Considering equation III.215,[63] a simpler, though not so general, way of determining the a-factor has been devised specifically for some polymers. For polypropylene, equation III.220 has been found to be quite satisfactory. It, like other equations of similar type, is based on experimental results. Such equations are

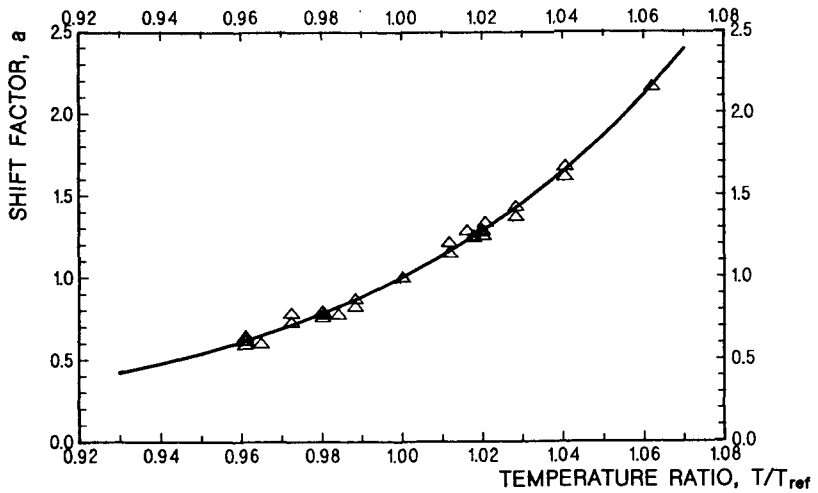

Figure III.21: *Dependence of the shift factor, a, on the ratio of temperatures. The relation has been devised for polypropylene on the basis of experimental data.*

convenient, especially when interpolations or extrapolations are needed. The extrapolated data are particularly convenient for considerations of crystallization, since rheological determinations below equilibrium melting point are rarely reliable, or even possible.

$$a = 4.129 \cdot 10^{-6} \cdot \exp\left[12,4260\left(\frac{T}{T_0}\right)\right] \tag{III.220}$$

Figure III.21 presents the original data for various propylene polymers and their agreement with equation III.220.

Williams, Landell, and Ferry have developed an equation, usually called the *WLF equation*[32], to calculate activation energy. This equation has been developed on the basis of considerations of the segmental motions in molecules. One of the many forms of the equation is

$$\log \eta(T) = \log \eta(T_s) - \frac{8.86\ (T - T_s)}{101.6 + (T - T_s)} \tag{III.221}$$

where the reference temperature is $T_s = T_g + 43$. For the majority of crystallizing polymers, this equation is inapplicable as at forty three degrees above glass transition the polymers are solids. Another form of the WLF equation that may be used is:

$$E(T) = \frac{4120\ T}{(51.6 + T - Tg)} \tag{III.222}$$

The activation energy so calculated is of acceptable accuracy for a temperature that is by no means higher than fifty degrees above glass transition, and preferably by no more than twenty degrees above glass transition. The activation energy so calculated may be used in equation III.214. An empirically determined activation energy of flow gives a straight line which has one point in common with the WLF

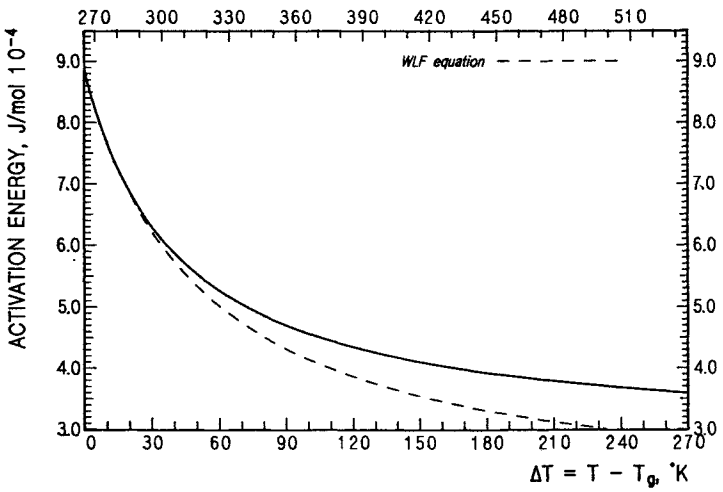

Figure III.22: *Activation energy of flow as calculated from WLF equation (dashed line) as compared to the activation energy calculated using equation III.223.*

hyperbolic equation: it is the point at glass transition temperature. The new equation has been found to hold well for polypropylene over the entire range of temperature, though its validity for other polymers needs to be established.[33] Possibly, the equation coefficients may be different for other polymers. The difference between the original WLF equation and the proposed modification may be seen in Figure III.22.

$$E(T) = T_g \ [334.29488 - 0.56625 \ (T - Tg)] \tag{III.223}$$

The equation yields the energy in J/mol. The activation energy may be used either with Arrhenius equation (III.214) or with another empirical equation, III.224 - III.225, relating both temperature and shear rate. Again, equation III.224 - III.225 has been corroborated with the experimental data on polypropylenes of a wide range of molecular masses; its validity for other polymers remains to be determined. .

$$\eta_0 = A_m \ \exp\left(\frac{E \ A_{\dot{\gamma}}}{R \ T}\right) \tag{III.224}$$

where

$$A_{\dot{\gamma}} = \frac{1 + l \ \dot{\gamma}^{1/2}}{1 + m \ \dot{\gamma}^{1/2}} \tag{III.225}$$

Here l and m are empirical constants which may be calculated by fitting experimental data into equations III.214 and III.223; correlation coefficients on the order of 0.999 or even 0.9999 are obtainable over six or eight decades of shear rates.[33] The coefficients in equation III.223 have no general validity, since every polymer batch needs a separate determination. Nevertheless, these kinds of empirical correlations serve as exceptionally convenient algorithms for various interpolations, *e. g.* such as are often needed in computerized data evaluation or predictions where

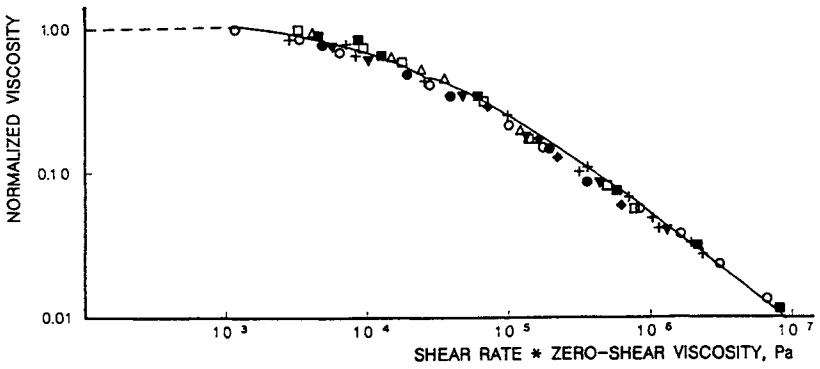

Figure III.23: *Relationship between reduced viscosity and product of shear rate and zero-shear rate viscosity, a temperature independent function. After Vinogradov and Mal'kin.*[34]

the points must be generated very densely. On many occasions, the solutions backed by full theoretical justification are not broad enough to serve the purpose.

Still another way of relating viscosity and temperature and shear rate is suggested by Vinogradov and Mal'kin,[34] who find that the reduced viscosity (ratio of viscosity at any shear rate over zero-shear rate viscosity) is a temperature independent function of the product of zero-shear rate viscosity and shear rate, $(\eta_0\dot{\gamma})$ as indicated in figure III.23.[34]

The solution suggested by Vinogradov and Mal'kin must be treated as an empirical one, similarly to other proposals which lack sufficient theoretical backing.

III.9 Viscosity of Solutions

Staudinger derived the following equations to describe the relationship between molecular mass of a polymer, solvent viscosity, and solution concentration, on one side, and viscosity of solution, on the other side:

$$[\eta] = K_m \; M \tag{III.226}$$

where $[\eta]$ is intrinsic viscosity defined as

$$\lim_{c \to 0} \frac{\eta - \eta_s}{c_s} = [\eta] \tag{III.227}$$

η is viscosity of polymer solution at concentration c, s is the viscosity of pure solvent, K_m represents a polymer characteristic constant, and M stands for the molecular mass. Staudinger's equation has been modified to improve its agreement in confrontation with experiment. In its present form, often called the Mark-Houwink equation, it has the following form:[35,36]

$$[\eta] = K \; M^{\alpha} \tag{III.228}$$

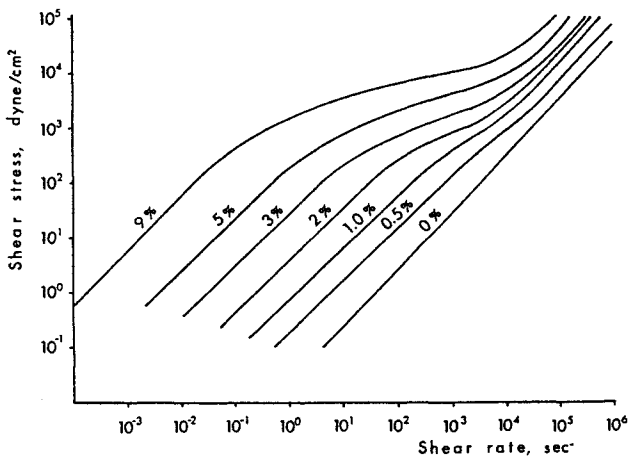

Figure III.24: *Shear stress as a function of shear rate for low to moderate concentrations of polyisobutylene in decalin.*[38]

Here α is a constant assuming values between 0.5 and 1.0, depending on solvent - polymer interaction. A value of $\alpha = 0.5$ corresponds to a system very close to precipitation (so called *theta solvent*, and $\alpha = 1$ means very good solubility. Extensive tabulations of the values of K and α may be found in literature.[37]

The Mark-Houwink equation is valid for diluted solutions only, where there is practically no interaction between the solute molecules. If one considers moderately or highly concentrated solutions as continuum systems, then all that has been said on rheology applies also to solutions. The difference may be that the general level of stresses is probably lower. In molecular terms, however, there are somewhat different problems involved. Unfortunately, the problems have not been fully solved yet. On the other hand, since polymer concentrations used in fiber formation range from under ten per cent to some sixty per cent, the behavior of concentrated solutions is technologically more interesting.

Brodnyan, Gaskins and Philipoff[38] have studied solutions of polyisobutylene in decalin. The quintessence of this work is presented in figure III.24. Qualitatively similar results have been obtained for other polymer solvent systems. As it is evident from figure III.24, the shape of the shear stress-shear rate function changes with concentration. In order to predict viscosities of concentrated polymer solutions, one may use equation III.211. However, knowledge of the relaxation time would be required, and usually this is not readily on hand. The attempts, which have been crowned with some success, to explain these variabilities have been based on the theory of free volume.

Free volume may be loosely described as the empty space between molecules resulting from the irregular structure of the molecules filling a volume, or shortly, a molecule packing effect.[39] The internal friction in liquids is related to the free volume, v_f.[40] Doolittle,[41] based on empirical grounds, has proposed the following

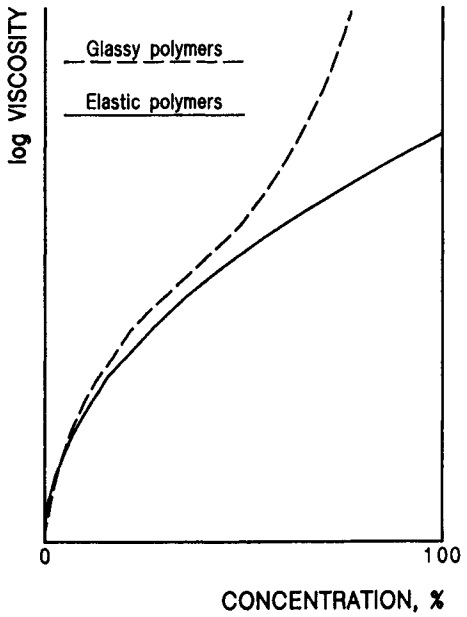

Figure III.25: *Generalized dependence of solution viscosity on the concentration of elastic and glassy polymers.*[39]

description of the relationship between free volume and viscosity:

$$\eta = A \ \exp(B \ v_0/v_f) \tag{III.229}$$

Here η is viscosity of solution, v_0 is the occupied volume, v_f is free volume, A and B are coefficients. The general dependence of solution viscosity on concentration has been given in graphic form by Tager and Dreval.[39] This curve is presented in figure III.25. It is worth stressing the relatively small increase of viscosity with increasing concentration once somewhat higher concentration levels are reached. For elastic polymers the slope is particularly low.

It is believed that solvents have larger free volume. Also, free volume is believed to be an additive property. Fujita and Kishimoto[42] assume the free volume of a solution to increase with increasing volume of solvent. Free volume depends also on the polymer concentration and on temperature of solution. Based on such considerations, these authors derived the following equation.

$$-\frac{1}{\ln a_c} = f(T\phi_*) + \frac{f(T\phi^*)}{\beta'(T)} \times \frac{1}{\phi - \phi^*} \tag{III.230}$$

in which

$$a_c = \frac{\eta(T\phi)(1-\phi^*)}{\eta(T\phi^*)(1-\phi)} \tag{III.230 a}$$

where $\eta(T\phi)$ is viscosity at temperature T and volume fraction of solvent ϕ, $\eta(T\phi*)$ is viscosity at the same temperature and another volume fraction of solvent ϕ^*,

considered as a comparative standard, $f(T\phi^*)$ is free volume of solution at standard concentration, $\beta'(T) = \gamma(T) - f(T_0), \gamma(T)$ is a function specific for given polymer-solvent system, and $f(T_0)$ is free volume of solvent at temperature T_0.

Equation III.230 may be simplified to a rectilinear form so the values of $\beta'(T)$ and $f(T\phi^*)$ may be obtained more easily:

$$-\frac{1}{\ln a_c} = F \frac{1}{(1-\phi^*)} \qquad (III.230\,b)$$

Validity of equation III.230b has been confirmed for many polymer-solvent systems. The rectilinearity appears to falter at ϕ larger than 0.5.[39,42–45]

Another approach to the problem has been offered by Kelly and Bueche,[46] who assume the free volume of a polymer to be

$$v_{fp} = 0.025 + 4.8 \cdot 10^{-4}(T - T_g) \qquad (III.231)$$

and the free volume of solvent as

$$v_{fs} = 0.025 + \alpha_S(T - T_{gs}) \qquad (III.232)$$

The notation here is: v_{fp} stands for free volume of polymer, v_{fs} stands for free volume of solvent, the coefficient of 0.025 represents the relative free volume of the polymer at glass transition, the value of $4.8 \cdot 10^{-4}(^oK)^{-1}$ is the temperature coefficient of changes of the free volume, S is a temperature coefficient of the order of $10^{-3}(^oK)^{-1}$. Further, under the assumption of the additivity of free volumes, Kelly and Bueche obtain

$$\begin{aligned} \frac{\ln \eta}{B} = \; & 4 \ln \rho \, \{\phi_p \, [0.025 + 4.8 \cdot 10^{-4}(T - T_g)] + \\ + \; & (1 - \phi_p) \, [0.025 + \alpha_S(T - T_{gs})]\}^{-1} \end{aligned} \qquad (III.233)$$

where ρ is density of the solution, ϕ_s and ϕ_p volume fractions of solvent and polymer, respectively, and B is a parameter which also includes molecular mass. Equation III.233 is in good agreement with experiment at temperatures above glass transition temperature of the polymer.

Several other equations for the dependence of viscosity on solution concentration may be found in the literature.[47,48]

Molecular mass has an influence on the solution viscosity similar to that on the melt viscosity. An equation entirely analogous to that for melts (equation III.213) may be written as

$$\eta = C \, P^{3.4} = K \, c^m \, M^{3.4} \qquad (III.234)$$

where P is degree of polymerization, and C and K are constants, c is the solution concentration. The exponent m varies between 4 and 5.6; the higher values are more likely to be valid at higher concentrations. For polymer below the

critical molecular mass, the slope is not constant and increases with increasing concentration.[39,49]

The influence of molecular mass on viscosity may also be obtained from equation III.211.

Another important function is the viscosity as a function of temperature. The activation energy of flow has a nonlinear dependence on concentration[39] and on molecular mass.[49–53] Consequently, the WLF equation is inapplicable here. Teramoto, Okada, and Fujita[49] have proposed a somewhat different relationship:

$$\frac{T - T_0}{\lg a_T} = \frac{[f(\phi T_0)]^2}{a_f(\phi)} + (T - T_0)\, f(\phi\, T_0) \qquad \text{(III.235)}$$

$$a_T = \frac{\eta(\phi\, T)}{\eta(\phi\, T_0)} \qquad (III.235\, a)$$

where T and T_0 are experiment and reference temperature, respectively, $f(\phi T_0)$ is free volume of solution at polymer volume fraction ϕ and at reference temperature T_0. The equation may be easily linearized by substituting $(T - T_0)/\lg a_T = f(T)$, and in this way all of the important parameters may be estimated.

There have been many different attempts to solve the relationship between viscosity, solution concentration, temperature, and molecular mass. Some of the theories agree with experiment only within limited ranges. The selection given here does not imply any particular preference.

The character of the solvent used has an influence on the solution viscosity. This influence becomes even stronger below the glass transition temperature of the polymer. The solvent quality also influences how strongly temperature influences viscosity. Also, the quality of solvent influences the activation energy of solution flow.[39] Viscosities of solutions do not necessarily depend on the viscosities of the solvents used. This is related to the changes of entropy upon dissolution. Viscosity is lower in those solvents which permit more flexibility of polymer chains. Naturally, the solvent viscosity will superimpose itself on the effect.

In concentrated polymer solutions, molecular interactions are appropriately high. Longer times are needed to reach thermodynamic equilibrium. The significance of these phenomena increases with increasing polarity of the polymer molecules. Increase of viscosity with time is one of the common properties of the concentrated solutions. It is usually called *aging* or *ripening* of the solution. The rate of such a process depends both on temperature and on agitation, and on the whole thermal and shear history of the solution. In this case, the concentration of polymer solutions is also important, the rate of viscosity increases is magnified by increasing concentration.[55,56] Different polymer-solvent systems may behave quite differently. This makes it exceedingly difficult to determine the exact mechanisms involved in the processes of solution aging. Since the viscosity of solutions increases on aging, it may be generally assumed that some kind of molecular association takes place. Depending on the type of association, molecular entanglements, molecular mobility, the rate of equilibration varies widely. There

are no quantitative theories related to this problem, every polymer-solvent system must be studied separately.

III.10 References

1. N. W. Tschoegl: *Phenomenological Theory of Linear Viscoeastic Behavior*, Springer Verlag, Berlin-Heidelberg-New York, 1989.
2. J. D. Ferry: *Viscoelestic Properties of Polymers*, John Wiley & Sons Publ., New York, 1980.
3. I. Emri, N. W. Tschoegl, *Rheol. Acta*, **32 (1993)**, 311, 327.
4. N. W. Tschoegl, *Seminar for Kimberly-Clark Corp.*, Roswell, Ga., Sept. 24, 1993.
5. V. M. Kamath, M. R. Mackley, *J. Non-Newtonian. Fluid Mech.*, **32 (1989)**, 119.
6. M. Baumgartel, H. H. Winter, *Rheol. Acta*, **28 (1989)**, 511.
7. V. Capuccio, A. Coen, F. Bertinotti, and W. Conti, *Chim. e Ind. (Milano)*, **44 (1962)**, 463.
8. E. B. Bagley, S. H. Storey, and D. C. West, *J. Appl. Polymer Sci.*, **7 (1963)**, 1661.
9. W. Philipoff and F. H. Gaskins, *Trans. Soc. Rheology*, **2, (1958)**, 263.
10. F. N. Cogswell, *Rheol. Acta*, **8 (1969)**, 187.
11. F. N. Cogswell, *Polymer Eng. Sci.*, **12 (1972)**, 64.
12. Z. K. Walczak: *Formation of Synthetic Fibers*, Gordon and Breach, London - New York, 1977, Chapter 2.
13. H. P. Hurlimann and W. Knappe, *Rheol. Acta*, **11 (1972)**, 292.
14. A. B. Metzner and A. P. Metzner, *Rheol. Acta*, **9 (1970)**, 174; **10 (1971)**, 434.
15. M. Zidan, *Rheol. Acta*, **8 (1969)**, 89.
16. S. L. Goren, *J. Fluid Mech.*, **25 (1966)**, 87.
17. S. L. Goren and S. Wronski, *J. Fluid Mech.*, **25 (1966)**, 185.
18. J. Gavis and M. Madon, *Phys. Fluids*, **10 (1967)**, 487. 18
19. J. L. White, *J. Appl, Polymer Sci.*, **8 (1964)**, 2339. 19
20. P. Lamb, *S.C.I. Monograph*, **26 (1967)**,296.
21. J. Vlachopoulos and M. Alam, *Polymer Eng. Sci.*, **12 (1972)**, 184.
22. E. B. Bagley, *Trans. Soc. Rheology*, **5 (1961)**, 355.
23. R. S. Spenser and R. E. Dillon, *J. Colloid Sci.*, **4 (1949)**, 251.
24. J. F. Tordella, *J. Appl. Phys.*, **27 (1956)**, 454.
25. R. T. Balmer and J. J. Kauzlarich, *A. I. Ch. E., J.*, **12, (1971)**, 1181.
26. J. R. A. Pearson, *Trans., J. Plast. Inst.*, **37 (1969)**, 285.
27. R. T. Balmer, *J. Appl. Polymer Sci.*, **18 (1974)**, 3127. 27
28. F. W. Cogswell, *Trans. Soc. Rheol.*, **16 (1972)**, 383. 28

29. B. H. Bersted, *Polymer Eng. Sci.*, **33 (1993)**, 1079.

30. N. W. Tschoegl, *J. Chem. Phys.*, **39 (1963)**, 149; **40 (1964)**, 473.

31. H. P. Schreiber, E. B. Bagley, and D. C. West, *Polymer*, **4, (1963)**, 355.

32. M. L. Williams, R. F. Landel, and J. D. Ferry, *J. Am. Chem. Soc.*, **77 (1955)**, 3701.

33. Z. K. Walczak, *previously unpublished results*, 1986.

34. G. V. Vinogradov, A. Ya. Mal'kin: *Reologiya polimerov (Rheology of polymers)*, Izdatelstvo Chimija, Moskva, 1977, p. 227-228; *Rheology of Polymers*, Springer Verlag, Berlin -Heidelberg - New York, 1980.

35. W. Kuhn, *Kolloid-Z.*, **62 (1933)**, 269; **68 (1934)**, 2.

36. R. Houwink, *J. prakt. Chem.*, **157 (1940)**, 15.

37. J. Brandrup and E. H. Immergut (Eds.), *Polymer Handbook*, Interscience Publ., New York, 1966, Chapter 4.

38. J. D. Brodnyan, F. H. Gaskins, and W. Philipoff, *Trans. Soc. Rheol.*, **1 (1957)**, 109.

39. A. A. Tager and V. E. Dreval, *Uspyekhy Khim.*, **36,(1967)**, 888.

40. A. I. Batschinskij, *Z. physik. Chem.*, **84 (1913)**, 6 , 143.

41. A. K. Doolittle, *J. Appl. Phys.*, **22 (1951)**, 1471; **23 (1952)**, 236.

42. H. Fujita and A. Kishimoto, *J. Chem. Phys.*, **34 (1961)**, 393.

43. J. Ferry, L. D. Grandine, Jr., and D. C. Udy, *J. Colloid Sci.*, **8 (1953)**, 529.

44. F. Bueche, *J. Appl. Phys.*, **24 (1953)**, 423; **30 (1959)**, 1114.

45. H. Fujita and E. Maekawa, *J. Phys. Chem.*, **66 (1962)**, 1053.

46. F. N. Kelly and F. Bueche, *J. Polymer Sci.*, **50 (1961)**, 549.

47. L. J. Zapas, *ACS, Polymer Preprints*, **15(No. 2)(1974)**, 131.

48. J. W. Van Krevelen: *Properties of Polymers*, Elsevier Publ., Amsterdam - London - New York, 1990, Chapter 19.

49. A. A. Tager, V. E. Dreval, and N. G. Trayanova, *Dokl. Akad. Nauk USSR*, **151 (1963)**, 140.

50. J. Oyanagi and M. Matsumoto, *J. Colloid Sci.*, **17 (1962)**, 426.

51. S. Yugushi, *Chem. High. Polymers (Japan)*, **19 (1962)**, 113.

52. R. F. Landel, J. W. Berge, and J. D. Ferry, *J. Colloid Sci.*, **12 (1957)**, 400.

53. R. S. Porter and J. F. Johnson, *J. Polymer Sci.*, **3 (1962)**, 11.

54. A. Teramoto, R. Okada, and H. Fujita, *J. Phys. Chem.*, **66, (1962)**, 1228.

55. S. Zahorski, *Arch. Mech.*, **23 (1971)**, 1433; **24 (1972)**, 681.

56. S. G. Hatzikiriakos and J. M. Dealy, *J. Rheol.*, **36 (1992)**, 845.

57. S. G. Hatzikiriakos, *Polymer Eng. Sci.*, **34 (1994)**, 1441.

58. J. Molenaar and R. J. Koopmans, *J. Rheol.*, **38 (1994)**, 99.

59. A. Weill, *Rheol. Acta*, **19 (1980)**, 623.

60. F. Sugeng, N. Phan - Thien, R. I. Tanner, *J. Rheology*, **31 (1987)**, 37.

61. C. R. Beverly, R. I. Tanner, *J. Rheology*, **33 (1989)**, 989.

62. C. D. Han and R.R. Lamonte, *Polymer Eng. Sci.*, **11 (1971)**, 385.

63. V. A. Vinogradov, *Rheol. Acta*, **14 (1975)**, 942.

64. A. J. Staverman and F. Schwartzl: *Linear Deformation Behaviour of High Polymers* in *Die Physik der Hochpolymeren*, Ed. H. A. Stuart, Springer Verlag, 1954, Vol. 4, p 56 ff.

65. J. Furukawa, *J. Appl. Polymer Sci.*, **57 (1995)**, 1085; 1095.

66. A. V. Pendse and J. R. Collier, *J. Appl. Polymer Sci.*, **59 (1996)**, 1305.

67. J. R. Collier, O. Romanoschi, and S. Petrovan, *J. Appl. Polymer Sci.*, **69 (1998)**, 2357.

68. N. W. Tschoegl, *Kolloid-Z.*, **174 (1961)**, 113.

69. J. R. Barone, N. Plucktavaesak, and S. Q. Wang, *J. Rheol.*, **42 (1998)**, 813.

70. M. E. Mackay and D. J. Henson, *J. Rhoel.*, **42 (1998)**, 1505.

71. A. L. Yarin and M. D. Graham, *J. Rheol.*, **42 (1998)**, 1491.

72. Y. Termonia, *J. Polymer Sci., Pt. B, Polymer Phys.*, **38 (2000)**, 2422.

IV POLYMER IN FIBER FORMATION

Polymer properties have been discussed in the preceeding chapters. The description was given from the point of view of those properties which are accessible analytically, using more or less standard characterization techniques. The dynamics of the process require us to take another look at polymer properties, a look from a different angle. It is necessary to be able to understand how a polymer behaves within the complex maze of changes and transformations taking place either simultaneously or during a very short span of time. The specifics of the fiber formation process put more stringent demands on some polymer properties, which for other methods of processing may be less important or outright not essential. There is also a question whether the behavior of polymer in the fiber formation process can be predicted on the basis of analytically accessible characterization. Answers to such questions will be sought in the following considerations.

IV.1 Melting of polymer

The question to be posed initially regards the temperature at which the polymer ought to be processed. To answer this question, two aspects must be considered:

Primo — polymer viscosity must be within a range allowing processing: the polymer must be extruded through an appropriately sized capillary without the use of excessively high pressure to drive the extrusion.

Secundo — if the polymer is able to crystallize, or to form some kind of molecular aggregates, then the processing temperature must be higher than the equilibrium melting point (or an equivalent transition point). Otherwise, control of the development of crystallinity (or other structural units) in the fibers may become impossible.

Determination of the relationship between crystallization and melting temperatures, as described in chapter II, resolves this question, as does the determination of the relationship between melt viscosity, on one side, and shear rate and temperature, on the other side. If a polymer is heated to its equilibrium melting point, then all the crystals melt. However, the notoriously high viscosity of polymers does not allow for a very quick "randomization" of the molecular conformation. This "randomization" process may be helped by mechanical means, particularly by shearing forces. Additional elevation of temperature beyond equilibrium melting point by some twenty degrees centigrade may also be recommended. In the case that a polymer does not meet the above specified requirements for minimum of melting temperature, then methods of fiber formation other than from the melt, ought to be considered. Namely, one may escape to formation from solution. The upper limit of melting temperature depends on the thermal stability of the polymer under consideration. For the majority of industrial processes of fiber formation, the residence time of polymer at melt temperature ranges between some twenty and thirty minutes. Thus, polymer must be able to withstand the temperature for such a length of time. Again, if a polymer does not meet this requirement, fiber

formation from solution should be considered.

Polymer degradation rarely displays a strong transition point in the rate - temperature relationship. Therefore, the reader must be warned about many "grey areas" and difficult decisions as far as this aspect of processing is concerned.

At this point it is important to note that substantial differences in the behavior of polymers do exist. In practically all cases, exposure of the polymer to an elevated temperature ought to be in absence of oxygen (air). Almost all polymers are prone to some oxidation at elevated temperature. The oxygen molecules usually become randomly built-in along the molecule chains. An addition of atoms or groups changes the molecule symmetry, and thereby affects polymer crystallizability and crystallization kinetics. Often polymers are sensitive to moisture at elevated temperature; this concerns primarily polycondensation type polymers which may hydrolyze. Hydrolysis reduces the molecular mass, while in polycondensation reactions high molecular mass is difficult to obtain. Also, changes of molecular geometry may result from reactions with water molecules. Some polymers may show a tendency to increase their viscosity with increasing residence time at high temperature. Polymers obtained as a result of polycondensation reactions are more apt to such a behavior. A cross linking reaction is often responsible for the viscosity increase; increase of elastic flow component usually accompanies such an increase of viscosity.

Proper chemical stabilization of the polymer may prevent or reduce the changes, generally referred to as *degradation*, to some acceptable level. This is, however, a domain of polymer chemistry, and as such is outside of the scope of this book.

Practically all "virgin" polymers do contain some amount of cross linked material. The cross linked material is usually recognizable as gel inclusions, rather than an "impurity" homogeneously distributed throughout the polymer. The presence of cross links is often the result of side reactions typical of organic synthesis. The gel content in the polymer represents an important reason for breaks of polymer stream during fiber formation. Quantitatively, the process discontinuity is in direct proportion to the amount of cross linked material present in the polymer. It seems that both the increase of melt elasticity and the material inhomogeneity are responsible for the negative effects. The increased discontinuity of a process represents, naturally, a very strongly negative economic factor.

A somewhat "special problem" are the polyolefines. The nature of the stereospecific (Ziegler-Natta and similar) catalysts is such that it is more economic to obtain high, rather than low, molecular mass polymers. This fact led to the very common practice that polymers are polymerized to a high molecular mass (usually in the neighborhood of one million Daltons) and later degraded to smaller molecules. Since shear degradation in extrusion is expensive because of high energy consumption, the process is usually aided by the addition of peroxides.

The reactions between peroxides and polyolefines lead initially to formation of cross links. Only during the later stages do the cross link points decompose with the resulting chain scission. It may be easily established analytically that the reactions are usually incomplete: there are residual peroxides, as well as a number of

cross links. Such raw materials may pass for some low grade fibers. Processing of highly cross linked polymers may not be done under a positive control; melt elasticity increases very substantially, as may be seen from a comparison of calculated and experimental relaxation times.[70a]

Naturally, an increase of elasticity has its influence on the polymer processability. The cross links do not seem to be evenly distributed, but instead form gel aggregates which often may even be observed microscopically in polarized light. Analytically, the gel content is determined gravimetrically by pressure filtration of very diluted (0.25 to maximum 0.5 per cent) polymer solution through a filter of 0.24 to 0.5 μm pore diameter. Molecular mass and viscosity of the polymer at hand will determine the actual experimental conditions within the given ranges.

The molten polymer is usually transferred to a so called *spinning block* or *spinning beam* which, aside from the metering pump and spinnerette, also houses a filter for polymer melt. The filter is usually located as close to the spinnerette entry as possible and consists of a sintered metal plate supported on a perforated metal disc. The filters are to retain accidental mechanical contaminants, as well as insufficiently dispersed delustrants (usually titanium dioxide), pigments, stabilizers, etc.

Because the polymer must pass through the small and tortuous channels of the filter, it becomes subjected to large shearing forces. The shearing forces, if not excessive, are beneficial to fiber formation process. One of the characteristic properties of polymers is memory. The term memory means that different specimens originating from the same polymer may possess somewhat different properties, depending on the history of shearing and heat treatment to which they were subjected.[1,2] It is believed that the reason underlying the phenomenon of memory are frozen stresses.[3] However, a particularly strong influence are entanglements of the polymer chain. And, naturally, all these are highly dependent on relaxation time. It has been determined that entanglements of polymer chains determine physical and rheological properties of melts and solids.[3]

Recent years have brought an increase in research activity on polymer chain entanglements, and as a result, some quantitative solutions have become available.[4] One may quote as one of the more general formulations the finding by Elias[5] that the Hooke number,

$$He \equiv \frac{\sigma_b}{E\varepsilon_b} \tag{IV.1}$$

is proportional to the inverse square of the density of entanglements, μ_e. Here σ_b is tensile strength at break, ε_b is strain at break, and E is tensile modulus (initial). The entanglement density is:

$$\nu_e = \frac{N_A\ \rho}{M_e} = \left(\frac{9}{4}\right) \times \frac{N_A\ \rho}{M_c} \tag{IV.2}$$

where N_A is Avogadro's number, ρ is density of amorphous polymer, M_c is critical molar mass above which entanglements can form, and M_e is average molar mass between the points of entanglement. The value of M_e may be determined from the

plateau of the relationship between the shear modulus and molecular mass.[6] The values of entanglement density, along with the molecule conformation (characteristic ratio), may also be calculated from the chemical structure of a polymer.[7] The calculated values are in quite fair agreement with those determined experimentally, though the experimental results have relatively large uncertainty too.

It is also well known that flow can either cause transformations like crystallization, mixing, and demixing, which normally result from temperature change, or may shift the temperature at which the transformation takes place.[8]

Determination of the exact changes in the molecule conformation and entanglements due to polymer flow is very complex. Therefore, there is still disagreement between some of the results published. It is known, however, that besides the flow intensity, as described by strain or strain rate, entanglements depend strongly on the type of flow, and on the geometry of the duct.[8,9]

IV.2 The Spinnerette

The spinnerette (or spinning jet) is the element of fiber formation hardware which serves to shape the polymer melt, or solution, into "infinitely long" cylinders. Since the heart of the spinnerette is the capillary, everything that applies to flow in a capillary also applies to flow in spinnerettes. The side phenomena which result mainly from the shearing action on the extruded polymer, have a strong influence on certain engineering tasks and on the behavior of the polymer in the subsequent processing stages. Ultimately, the shearing applied influences the final fiber properties. Here we have a certain similarity between the influence of spinnerette and filter on the processing performance of the polymer and on the final result, on the fiber properties.

The shearing a polymer experiences in the spinnerette influences the morphology of polymer melt. Some light on these influences is shed by the work of Han and Kim.[8] Fig. IV.1 shows an essential result obtained by Han and Kim: the relationship between pressure exerted by the polymer on the wall of the reservoir and capillary *versus* distance from the entrance to the capillary. The plot shows clearly the pressure loss in the entry to the capillary and the normal pressure present in the polymer at the exit from the capillary.

The exit pressure for a given geometry of the extrusion arrangement and conditions is $P_{ex} = \alpha\dot{\gamma}^{\beta}$. In this case α and β are constants characteristic for the material. The true shear stress at the wall may be calculated from the slope of the straight portion of the axial pressure profile, e.g. like in figure IV.1.

$$\tau_w = \left(\frac{-\partial p}{\partial x}\right) \times \left(\frac{D}{4}\right) \tag{IV.3}$$

In view of the above, it is clear that evaluation of the capillary flow data with the use of the common equation (equation III.4) or in the version suggested by

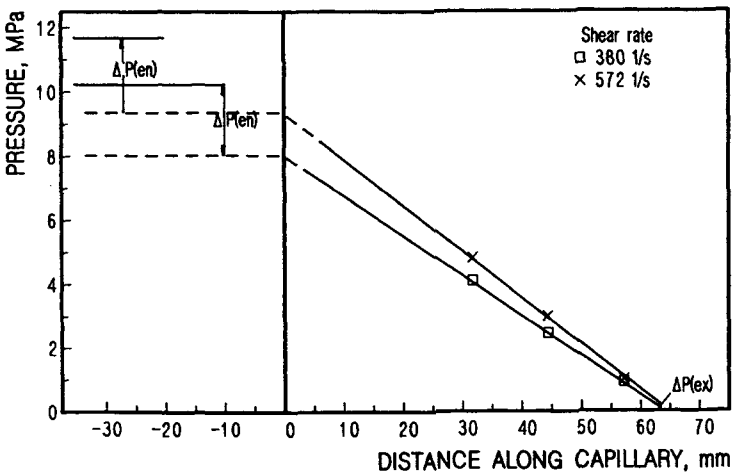

Figure IV.1: *Pressure profiles in reservoir and in capillary during extrusion of polyethylene at 180 C, capillary $L/D = 20$, the ratio of reservoir over capillary diameter is 9. After Han and Kim.*[8]

Bagley

$$\tau_w = \frac{\Delta P - \Delta P_{en}}{4\ (L\ /\ D)} = \frac{\Delta P}{4\ (L\ /\ D)\ +\ e} \tag{IV.4}$$

where ΔP is pressure difference necessary for extrusion, ΔP_{en} pressure drop in the entry to the capillary, D is diameter of the capillary, L is the length of the capillary, and e is the *"end correction"* according to Bagley.[10]

Han and Lamonte[11] have established that the pressure at the exit from the capillary equals the normal stress difference at this point:

$$P_{ex} = P_{11} - P_{22} \tag{IV.5}$$

From figure IV.1, one may see the magnitude of the pressure drop in the entry to the capillary for different shear rates. Figure IV.2 shows an influence of the ratio of reservoir over capillary diameters on the exit pressure. The repercussions of the flow pattern are far reaching indeed. Comparison of figure IV.2 with figures III.17 and III.18 is quite instructive.

Apparently the geometry has a strong influence on the vortices formed around the entry. The influence becomes insignificant above some value of reservoir to capillary ratio; for polyethylene investigated, this significant ratio is above 12, for other polymers may be somewhat different. The influence of conical entry to capillary, and of the magnitude of the cone angle on the process of extrusion was investigated, to some extent, by Han.[9] Direct measurements of pressure in the capillary, entry cone, and reservoir were conducted, similarly as in the earlier work by Han. It has been found that the magnitude of the pressure loss in the conical entry to the capillary depends on the cone angle. The minimum value seems to be reached in the entry of ninety degrees. However, the large scatter of the experimental data makes this minimum uncertain. The differences in the

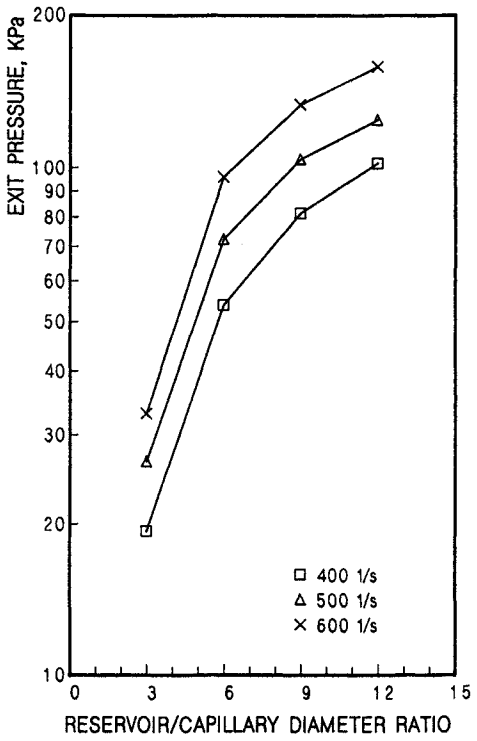

Figure IV.2: *Relationship between exit pressure drop and ratio of reservoir to capillary diameter ratio. After Han and Kim.*[8]

pressure loss for angles ranging from sixty to one hundred eighty degrees are small indeed. On the other hand, for angles of thirty degrees the pressure rises some twenty to thirty per cent, and for those of fifteen degrees, the pressure drop almost doubles.

The angle of the entry cone has significant influence on the exit pressure. In this case, the results for angles between sixty and one hundred and eighty degrees are similar, within large data scattering. For small angles, fifteen to thirty degrees, the exit pressure reaches values as low as one half of the results for large entrance angles. These results are in full agreement with those published elsewhere.[12] The data by Han[9] tend to indicate that the exit pressure for low cone angles and for high cone angles would be the same at shear rates of around 1500 s^{-1}. Other investigations[1,13] do not confirm such behavior, though carried out at shear rates as high as 7500 s^{-1}.

The results obtained by Han[9] show a difference in the behavior of high density and low density polyethylenes. Perhaps a different level of elastic flow component is responsible for this.

It must be added that the Poiseuille equations for flow in capillaries (equations III.3 to III.5) are valid for Newtonian fluids, characteristic of strictly parabolic velocity profile, or in other words for power law fluids with the exponent equal

unity. A generalization based on the power law leads to the velocity distribution along the capillary radius as[17]

$$V(r) = V(0)\left[1 - \left(\frac{r}{R}\right)^{(n+1)/n}\right] \tag{IV.6}$$

where $V(r)$ is velocity at radius r, r is position along the radius, R is capillary radius, and n represents the power law coefficient. Furthermore, the relationship between the polymer flow and the extrusion driving pressure may be presented in a general form as

$$Q = \left[\frac{n}{(n+1)}\right]\pi R\left[\frac{(\Delta P\ R^3}{(2\eta l)}\right]^{1/n} \tag{IV.7}$$

The velocity gradient then becomes

$$\dot{\gamma}\left(\frac{\partial V}{\partial r}\right)_{r=R} = -\left[\frac{(\Delta P\ R)}{(2\eta l)}\right]^{1/n} \tag{IV.8}$$

In the above equations l stands for the capillary length.

All of the equations for capillary flow as given above are valid for infinitely long capillaries. In the capillaries of finite length, and such we have in spinnerettes, the effective pressure, ΔP_e, is different from the pressure really applied, ΔP, and the difference may be given as

$$\Delta P_e = \frac{\Delta P - m\rho V_0^2}{1 + (r\ /l\ ))\,(k + (S_R\ /\ 2) + z\,(t\ /\tau)} \tag{IV.9}$$

where $V_0 = Q/\pi R^2$ is the average flow velocity, m is a coefficient dependant on the velocity profile, for Newtonian fluids $m = 1$, for polymer melts it may be taken as $m = 1.2$, ρ is polymer density, S_R is recoverable strain, t is transit time.

Viscoelastic fluids require also a longer time to develop stable flow. This translates naturally to an extended capillary length. Zahorski[28] has derived a correction for the capillary length in the form

$$\Delta l = \frac{l_v[(\Delta P_e - \Delta P) + (p_{11} - p_{22})]}{\Delta P_v} \tag{IV.10}$$

where Δl is the additional capillary length needed, l_v is the length of capillary needed to achieve stable flow of Newtonian (viscous) fluid, ΔP_v is the driving pressure for extrusion of viscous fluid, $p_{11} - p_{22}$ is normal stress difference. There is, however, a problem with the determination of the l_v value; the equation derived for the purpose by Goldstein[27] is inapplicable for viscoelastic fluids.

Thus, it may be seen that calculation of the capillaries for viscoelastic fluids may not be so simple, or so accurate. It may be necessary to apply special solutions involving constitutive equations for the specific case on hand.

A relatively large effort has been devoted to determining the influence of various modes of flow, as well as of the flow intensity, on the resulting polymer morphology, and ultimately on the corresponding polymer properties.[2,12–15] The results

obtained thus far and the conclusions offered by various authors are not entirely coherent. There are only few points to be stressed with some certainty. Namely:

- The effect a flow has on the polymer depends on the polymer type, *e. g.* noncrystallizable, block copolymer (thermoplastic elastomers), thermotropic liquid crystalline.[15]
- The effect of flow depends on its mode and geometry, *e. g.* shear, elongational, curvilinear.[8,15]
- Orientation caused by shear relaxes faster than it might be measured by any reliable technique.[13,15]
- In extensional flow, the polymers with flexible chains seem to be oriented to a degree too small to be measurable by any proper, currently available techniques.[13,15]
- Liquid crystalline polymers do not become oriented in a shear flow, while they become strongly oriented in extensional flow.[15,138]
- In melt shearing of A-B-A copolymers, the hard segments become little elongated.[15]
- Changes in entanglement density due to perturbations in flow, (*e. g.* tumbling of coiled molecules in shear flow) do not necessarily lead to orientation effects, but they certainly do lead to an increase in strength.[13]

Experience tells us that the quality of fibers and the ease of processing increase with increasing length of spinnerette capillary. But it also increases with increasing shear rate in the capillary.[13] The effect is most likely related to the increasing number of entanglements due to shear rate. The increased relaxation in long capillaries probably reduces the stresses to which the entangled chain segments are subjected, but without reducing the number of entangled chains. In effect, the die swell decreases, so the required attenuation of the fiber diameter is smaller. However, the mechanical strength of the fibers increases markedly with increasing shear rate in the capillary. Shear rates as high as $7500s^{-1}$ have been used with a substantial success. Nevertheless, in application of the high shear rates and large capillary length, one meets an overpowering challenge: the requirement of high extrusion pressures. Thus, technologically reasonable solutions will dictate where the right compromise lies. Besides, the critical shear rate, which is a complex result of polymer nature, geometry of equipment, and extrusion conditions, imposes another limitation on the intensification of the process. The phenomenon of extrudate fracture has been discussed in section III.8.

IV.3 Forces Acting in Quench Zone

An analysis of the forces acting on the filaments in the quench zone was conducted by Ziabicki and co-workers in the early sixties and later summarized in his

books.[16,17] The force balance has been determined to be

$$F_e + F_g = F_r + F_i + F_s + F_a \tag{IV.11}$$

where F stands for force, and the subscripts are: e – external (drawing), g – gravity, r – rheology, i – inertia, s – surface, and a – aerodynamic.

The external force is, naturally, the force applied by the take-up rollers or aerodynamic jet. The question is: how large a force needs to be applied for a given process? This is the answer expected from the examination of the entire force balance.

The gravity force may be presented as

$$F_g = g\frac{(1-\rho_0)}{\rho} \times \cos\chi \tag{IV.12}$$

In equation IV.12 the notation is: g – acceleration due to gravity, ρ_0 – density of the surrounding, ρ – density of filament, χ – angle between the filament and the horizontal. For the vertical formation, χ is 90°, provided that the path of the spinline is not altered, *e. g.* by a cross flow quench air. For horizontal spinning, wet processes included, χ equals 0. However, the line is normally deformed either by gravity or by buoyancy. The deformed line usually assumes a form of hyperbolic cosine (chain curve). Much more serious inaccuracy of equation IV.12 is connected with the change of filament density from that of a melt (or solution) all the way to a semicrystalline solid. As the changes of density are difficult to express in a form of a function, exact solutions need to involve numeric integration to take care both of the density changes and of the potential changes of the angle χ.

In case of vertical formation path, the gravity force acts in the same direction as drawing force. In horizontal configuration, some components of the gravity force may act in the same direction as gravity force, though on some sections of the spin line the force components may act in the opposite direction. All of the remaining forces act in the direction opposite to the drawing force.

The force needed for acceleration of the material (the force of inertia) has been described as

$$F_i(x) = \rho\, Q\, (\psi\, V - \psi_0\, V_0) \simeq \rho\, Q(V - \psi_0\, V_0) \tag{IV.13}$$

where x is distance from the spinnerette, ρ stands for polymer density at point x, while ρ_0 is initial polymer density, V is filament velocity at point x, and V_0 is initial polymer velocity, ψ represents a coefficient describing the velocity profile, the subscript 0 indicates a parabolic profile, for a flat velocity profile ψ equals unity. Since the overwhelming majority of the spinning path has a flat, or nearly flat, profile it is justified to simplify the equation to IV.13.$_2$ However, similarly as in the case of gravity, the changes of filament density are difficult to depict in the form of a function. Therefore, analytical solutions of equation IV.13 must be considered as quite inaccurate. The force of inertia is, naturally, acting in the direction opposite to the drawing force.

The surface force results from the interfacial tension between the filament surface and the surrounding medium, and from the change of filament curvature.

$$F_s = \pi \nu [R_0 - R \vartheta(x)] \tag{IV.14}$$

Here ν represents interfacial tension, R is fiber radius, while other notation is as above. Due to changes of temperature of the melt, surface tension may change by some ten per cent. For accurate results, temperature correction should be in place. In case of fiber formation from solution, changes of temperature may be not quite as large, but changes of polymer - solvent composition may have a much larger effect on surface tension and the appropriate corrections should by no means be neglected.

The forces of material deformation (the rheology force) have been treated by Ziabicki[16,17] in a very schematic and sketchy fashion. As may be seen from figure IV.3, the deformation forces are quite dominant in the process and must be considered much more seriously.

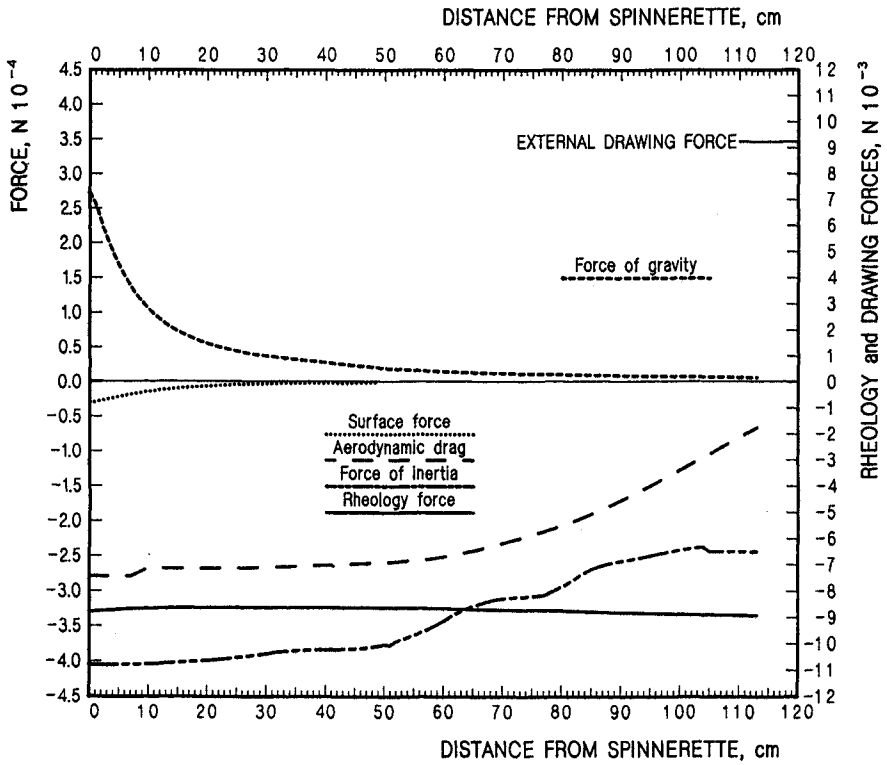

Figure IV.3: *Forces acting on a filament in quench zone. Medium fast process. Details in text. Note the different scales on the force axis.*

The next section on melt drawing reviews the status of that knowledge as of now.

The same may be said about the aerodynamic forces. The matter is considerably more complex than originally depicted by Ziabicki.[16,17] The magnitude of the forces present in industrial fiber formation, particularly at moderate and high velocities, brings them to a level comparable to the rheology forces. The flow of a large volume of air through the fiber paths, sometimes consisting of substantially more than a thousand filaments, makes things much more complex. These problems are discussed in the chapter on engineering physics. Figure IV.3 presents forces acting on a filament in an industrial process of fiber formation with final velocity in excess of 4000 m/min. The last point on the graph corresponds to 955 m/min. The polymer used was polypropylene of weight average molecular mass of 230 000. The data were collected during a detailed process analysis. Total external drawing force applied was 0.025 N per filament. The data for rheology forces result from the force balance, while all the other data result from calculations based on measured process parameters. For better visualization of the relative magnitude of the various forces, as well as for visualization of the shape of the curves, different scales have been put on the force axis.

IV.4 Diameter Attenuation

Upon leaving the spinnerette, the polymer stream is usually extended, which leads to a decrease of the filament diameter. It would be exceedingly difficult to extrude fibers of the final diameter, or the diameters would have to be very, very coarse indeed. The extension, as will be discussed below, has several more reasons and/or consequences than just diameter attenuation. The extension process brings, naturally, a question: will the filament break or not? Molten polymer, or polymer solution, intuitively are not expected to be able to withstand any significant stresses.

Nitschmann and Schrade[18] attempted to explain the extension- attenuation process in fiber formation by taking advantage of the Trouton studies[19] on extension of amorphous liquids. The work of Nitschmann and Schrade led to the construction of an interesting instrument, a kind of balance, for determination of extensional viscosity of polymer solutions. Determinations of extensional viscosity of casein fiber dope* and of solution of nitrocellulose, using Nitschmann and Schrade's "balance", gave interesting insight into the problems. It was found that elongational viscosity in its dependence on deformation rate, or on the stresses involved, shows quite different behavior than shear viscosity. This pioneering work, however interesting and important, brought more new questions than answers.

The important findings were that the extensional (Trouton) viscosity depends on the extension rate, similarly to shear viscosity. The similarity includes the fact that the relationship is not necessarily linear. In the nonlinear region, the shear and extension behavior are not necessarily parallel, or even similar. In both cases, though, when certain limiting value of deformation rate is exceeded, one observes

*solution for fiber formation

flow instability. It has been noticed also that as the filament diameter decreases (the extension increases), the filament is able to withstand higher force, extensional viscosity increases. The most striking observation was this: extensional viscosity showed a minimum in its dependence on stress (for casein fiber dope ranging from some 27 to 33 KPa, depending on the load, it is on rate of extension).

The first man-made fibers were obtained from polymer solutions; rupture of the filaments often led to break-up of the polymer stream into droplets. There were several attempts to devise a notion of *spinnability*[20–22], mostly involving viscosity and surface tension. In practice, however, the tests of spinnability were difficult to reproduce, impractical,[23] and therefore will not be elaborated on here.

The literature in the subject of elongational rheology and its application to fiber formation is sizeable. In 1979, C. J. S. Petrie[24] devoted to the subject a quite extensive and detailed monograph. Many of the suggestions appear under names that are notable in the field of rheology. Yet, the problems of elongational flow in fiber formation is deemed far from being solved. V. Tirtaatmadja and T. Sridhar[150] have tested experimentally application of various constitutive equations to extensional flow. Out of the models, Oldroyd - B, Gieskus, Perne, and White - Metzner with application of multiple retardation times, the best result obtained was extensional viscosity within the correct order of magnitude. This is by far not enough. To cope with the large number of proposals which often represent very interesting exercises in theory of rheology, we shall look at the phenomenological picture of fiber formation, and on this basis we shall present those solutions which seem to be in the best agreement with the science of rheology, as well as with the process realities. We shall try to propose those solutions which appear to carry the better promise. Figure IV.4 represents the events covered by the term "melt drawing". Section A of the figure gives a schematic pictorial representation, while section B presents a concretization of the scheme in the form of the pertinent analytical data collected in an commercial process of rather fast fiber formation (4070 m/min final fiber velocity) from polypropylene.

One may assume that after passing through filters, the polymer is "stripped of its memory". In reality, the history goes back to the moment of polymerization, but the intensive shearing may be able to reduce, or overpower, the remnants of the previous history to a negligible level. If so, than the meaningful history starts with the moment the polymer enters the spinnerette, the counter bores leading to the capillaries. As the introducing channels usually have a conical section leading to the capillary proper, the polymer is subjected to shearing and to extensional[25,26] deformation, which are superimposed on each other (see also sections III.6 and III.7). The elongational deformation imposed in the conical entry to the capillary relaxes to some extent in the cylindrical section of the capillary. Nevertheless, upon exit from the capillary the remaining elongation relaxes further, and together with the change of the parabolic velocity profile to a flat one, this causes the polymer stream to swell. There is a strain, or force, applied on the other end of the polymer stream.

In the example given in Figure IV.4 B, at the exit of the spinnerette, the stress

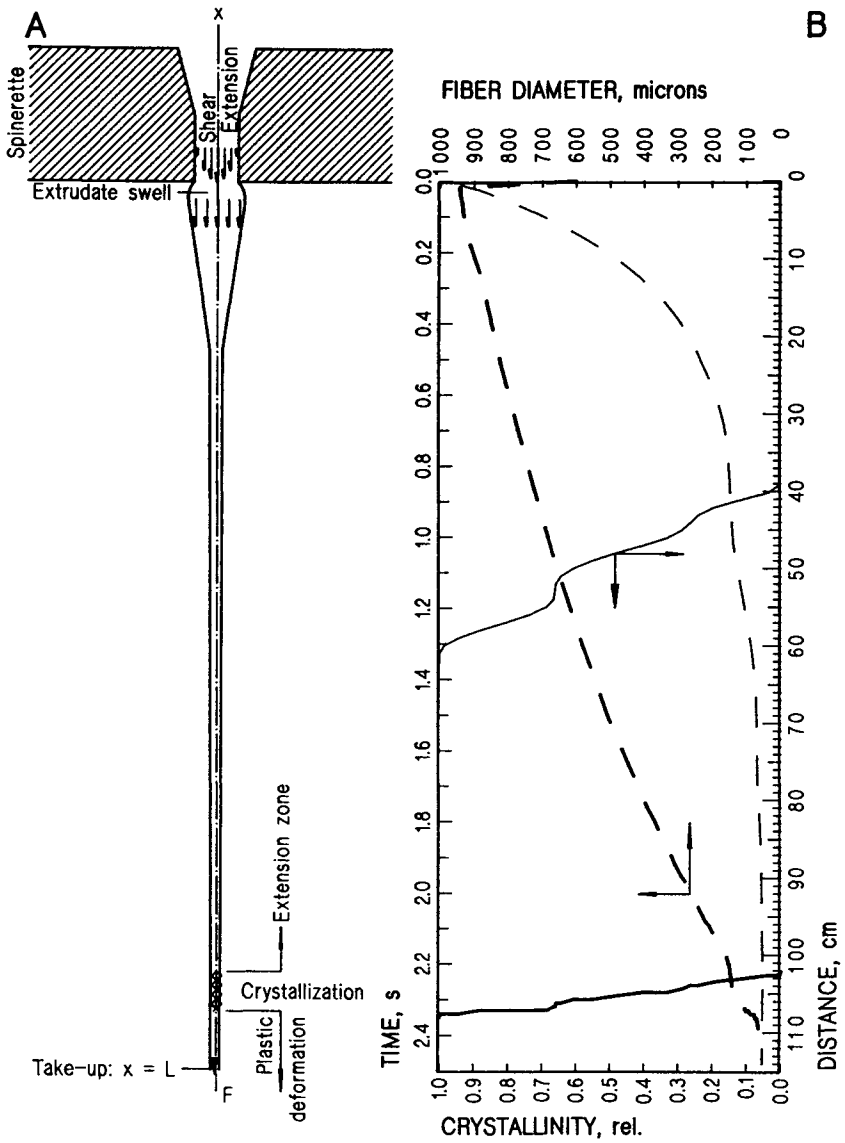

Figure IV.4: *A: Schematic representation of polymer flow in fiber formation. B: Diameter change (dashed lines) and crystallization (full drawn lines) against distance (fine lines) from spinnerette and against time (heavy lines). Analytical data from a commercial process.*

exerted by the drawing represents 14.5 per cent of the pressure needed to push the polymer through the cylindrical section of the capillary. It is true that the process

is quite fast, for slower processes the stress may fall down to 5, or even 3 per cent. However, for some processes, especially those faster ones, it may reach even 20 per cent. The range of stress cannot be considered negligible, and it should be taken into account in the capillary flow calculations as a negative pressure. The drawing stress, whatever its level, is insufficient to prevent the extrudate swelling completely, though it may diminish it. From the point of the maximum swell, begins the diameter attenuation. The attenuation process normally continues until final take-up of the ready fibers.

IV.4.a Basic Mechanics of Drawing

The initial portion of attenuation, by definition, proceeds according to the laws of elongation, extension, or stretching, depending on the preferred nomenclature. The initial segment of the process, where melt rheology ought to rule, ends when the polymer starts to crystallize. The initial stages of crystallization may also be possibly treated according to the melt rheology rules, but the material properties change quite dramatically and fast. Larger crystallization nuclei and small crystallites in the process of growing may act as points of cross linking. In the latter case the material would change from rheodictic into arrheodictic, and it would be subject to somewhat different rules of rheology; studies of these problems are in their infancy.[131]

When the crystallization process is completed, or nearly so, the material may be deformed according to the principles of plastic deformation. If one examines the course of crystallization in figure IV.4 B, then it is easy to find two "yield" segments, which may be read as a kind of change in the mechanism of diameter attenuation due to change of the material properties.

It is necessary to stress that the described process is accompanied by cooling, and in the depicted case, the cooling was rather intensive. And that is the way it is with almost all fiber formation processes, down to the start of crystallization, or other phase transition. The only exception may represent some wet process. However, the process of crystallization, as all other processes of phase transformation are, is exothermic. Exothermic is also plastic deformation. Thus, from the onset of crystallization, the processes are never isothermal.

It is necessary to point to the difference of interpretation of the process in terms of distance from spinnerette face and in terms of time. The curves plotted against time are usually smoother. The most striking may be a comparison between the crystallization process taking 35 cm distance (from 28 to 63 cm) but taking only 120 ms.

Among the more important efforts on a theoretical solution to the problem of material strength in extension, one must certainly quote that by M. Reiner and A. Freudenthal.[29] These authors extended the material strength theory on the basis of the maximum of distortional energy by M. T. Huber and H. Hencky. The static concept of distortional energy, E_0, has been substituted with the dynamic concept of the *power of distortion*, dE_0/dt. Further, the authors recall the representation

of the different forms of mechanical energy, as proposed by K. Weissenberg (figure IV.5). From the figure, it is evident that the sum of energies at any point of the triangular area, $E_K + E_P + E_D$, must equal the work of the external forces. The distortional energy is then, $E_0 = E_P + E_D$.

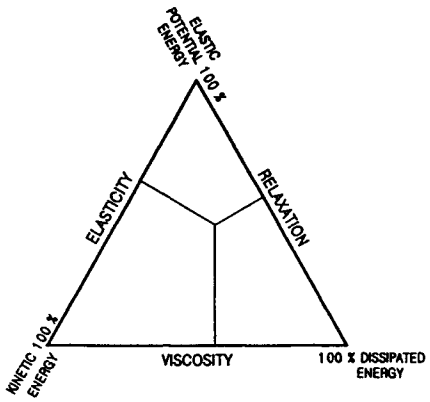

Figure IV.5: *Representation of the body conditions upon an input of energy, according to K. Weissenberg as cited in ref. 29.*

As the first condition, the Huber-Hencky theory states that *failure by distortion is governed by the maximum value of the elastic energy of distortion.* The modified formulation by Reiner and Freudenthal is given the following form

$$\int_{t=0}^{T} \frac{dE_P}{dt}\, dt = \int_{t=0}^{T} \frac{dE_0}{dt}\, dt - \int_{t=0}^{T} \frac{dE_D}{dt}\, dt \qquad \text{(IV.15)}$$

The kinetic energy influences the strength only in case of impact. In such cases, the kinetic energy becomes transformed into hydrostatic tension, which may lead to a failure. The second condition of the Huber-Hencky theory concerns cases when the rate at which the energy is transformed exceeds the ability of the material to be strained, *e. g.* if the magnitude of tensile stress caused exceeds the actual cohesion of the material.

Equation IV.15 implies that certain amount of the distortional energy may be dissipated during the time of the event. The dissipation is due to a viscous or/and plastic flow. In case the rate at which the distortional energy is delivered equals the rate at which the energy is dissipated,

$$\left(\frac{dE_0}{dt}\right) - \left(\frac{dE_D}{dt}\right) = 0 \qquad \text{(IV.16)}$$

then there is practically no limit to the amount of the distortional energy which might be supplied to the material without causing a failure. This is a case of *creep.*

By taking advantage of the Maxwell body, the authors[29] arrive at the following basic equations:

$$\left(\frac{1}{A}\right)\frac{dA}{dt} = -\left(\frac{1}{3\ E}\right)\frac{d}{dt}\left(\frac{P}{A}\right) - \left(\frac{1}{3\ \eta}\right) \times \left(\frac{P}{A}\right) \tag{IV.17}$$

The distortional energy is given as

$$E_0 = \frac{1}{6\ E}\int_{t=0}^{T} \frac{d}{dt}\left(\frac{P}{A}\right)^2 dt + \frac{1}{3\ \eta}\int_{t=0}^{T}\left(\frac{P}{A}\right)^2 dt =$$

$$= \frac{1}{6\ E}\left[\left(\frac{P}{A}\right)^2 - \left(\frac{P_0}{A_0}\right)^2\right] + \frac{1}{3\ \eta}\int_{t=0}^{T}\left(\frac{P}{A}\right)^2 dt \tag{IV.18}$$

In the above equations we have: P - force, A - area of cross section, E - modulus, η - viscosity, l - length, subscript 0 denotes initial value. Stress, $\sigma = P/A$, as a function of time needs to be determined by taking advantage of equation IV.17. Reiner and Freudenthal derive equations for several cases of deformation; for us, two of them may be interesting: constant velocity of strain and constant force.

For a case of constant velocity of strain the general equation has the form:

$$\frac{P}{A} = \exp(-t\ /\ \theta)\left[3\ E\frac{v_0}{l_0}\int \frac{\exp(t/\theta)}{1+(v_0\ t/l_0)}\ dt + \frac{P_0}{A_0}\right] \tag{IV.19}$$

The integral given in equation IV.19 has no finite solutions and cannot be solved by convergent series. The following approximate solution is suggested for cases with $0 \leq \Delta l \leq l_0$

$$\int \frac{\exp(t/\theta)}{1+v_0 t/l_0}dt = \int \frac{\exp(t/\theta)}{1+c_0 t/\theta}dt \simeq \exp\left[\frac{1}{1+2\ (c_0)^{3/2}} \times \frac{1}{\theta}\right] \tag{IV.20}$$

Here $c_0 = v_0\ \theta/l_0$ and represents the elongation at $t = \theta$. In this case velocity is constant: $v(t) = v_0 = const.$ The time-strain function is

$$\frac{\Delta l}{l_0} = \frac{c_0\ t}{\theta} \tag{IV.21}$$

The strain-stress function is given as

$$\frac{P}{A} = 3\ E\ c_0(1+2c_0^{3/2})\left[\exp\left(-\frac{2\ c_0^{3/2}}{1+2\ c_0^{3/2}} \times \frac{\varepsilon}{c_0}\right) - \exp\left(-\frac{\varepsilon}{c_0}\right)\right] \tag{IV.22}$$

where $\varepsilon = v\ t/l_0 = \Delta l/l_0$. The strain-load function has the form

$$P = \frac{3\ E\ A_0\ c_0(1+2c_0^{3/2})}{1+\varepsilon}\left[\exp\left(-\frac{2\ c_0^{3/2}}{1+2\ c_0^{3/2}} \times \frac{\varepsilon}{c_0}\right) - \exp\left(-\frac{\varepsilon}{c_0}\right)\right] \tag{IV.23}$$

The time-energy function is

$$E_0 = \frac{3\ E\ c_0^2(1+2c_0^{3/2})^2}{2}\left[\exp\left(-\frac{2\ c_0^{3/2}}{1+2\ c_0^{3/2}}\times\frac{t}{\theta}\right)-\exp\left(-\frac{t}{\theta}\right)\right]^2 +$$

$$+\ 3\ E\ c_0^2(1+2c_0^{3/2})^2\left\{-\frac{1+2\ c_0^{3/2}}{4\ c_0^{3/2}}\left[1-\exp\left(-\frac{4\ c_0^{3/2}}{1+2\ c_0^{3/2}}\times\frac{t}{\theta}\right)\right]-\right.$$

$$-\ 2\times\frac{1+2\ c_0^{3/2}}{1+4\ c_0^{3/2}}\left[1-\exp\left(-\frac{1+4\ c_0^{3/2}}{1+2\ c_0^{3/2}}\times\frac{t}{\theta}\right)\right]+$$

$$\left.+\ \frac{1}{2}\left[1-\exp\left(-\frac{2\ t}{\theta}\right)\right]\right\} \qquad \text{(IV.24)}$$

According to the above derivations, rupture occurs if

$$v_0\ [1-\exp(-t/\theta)] = \frac{[l_0\ (6\ E\ E_0)^{0.5}]}{(3\ \eta)} \qquad (IV.24\,a)$$

$$\frac{t}{\theta} = \ln\left[1-\frac{l_0\ (6\ E\ E_0)^{0.5}}{(3\ \eta\ v_0)}\right] \qquad (IV.24\,b)$$

As a consequence, if

$$v_0 < \frac{[l_0\ (6\ E\ E\ 0)^{0.5}]}{(3\ \theta)} \qquad \text{then} \qquad c_0 < \left[\frac{(2\ E_0)}{(3\ \eta)}\right]^{0.5} \qquad \text{(IV.25)}$$

All this means that the material can be strained indefinitely, so to say. Deformation under constant load, when $P = P_0 = const$, represents another possibility of interest in connection with fiber properties (creep), and in connection with diameter attenuation.

On integration of equation IV.17 one obtains

$$\frac{A}{A_0} = -\varepsilon_0 \ln\left(\frac{A}{A_0}\right) = 1-\frac{\varepsilon_0\ t}{\theta} \qquad \text{(IV.26)}$$

where $\varepsilon_0 = P_0/(3EA_0)$. Equation IV.26 may be simplified for commonly encountered cases when $A_0 \geq A \geq 0.5A_0$ as follows:

$$A = A_0\left(1-\frac{\varepsilon_0\ t}{\theta}\right) \qquad \text{(IV.27)}$$

When using this simplification one can obtain some important relationships. And so the time-velocity function is

$$v(t) = \frac{P_0\ l_0}{A_0\ 3\ \eta}\times\frac{1}{[1-(\varepsilon_0\ t)/\theta]^2} \qquad \text{(IV.28)}$$

Strain as function of time

$$\frac{\Delta l}{l_0} = \left[\frac{\varepsilon_0}{1-(\varepsilon_0\ t)/\theta)}\right]\left(\frac{t}{\theta}\right) \tag{IV.29}$$

Stress-strain relationship

$$\frac{\Delta l}{l_0} = \frac{\sigma}{\sigma_0} - 1 \tag{IV.30}$$

where $\sigma = P/A$ and $\sigma_0 = P_0/A_0$ and by assumption $P = P_0 = const.$

Energy as function of time is described by

$$E_0 = \frac{1}{6\ E}\left(\frac{P_0}{A_0}\right)^2 \frac{1}{[1-(\varepsilon_0\ t/\theta)]^2} + \frac{1}{3\ E}\left(\frac{P_0}{A_0}\right)^2 \frac{1}{1-(\varepsilon_0\ t/\theta)} \times \frac{t}{\theta} \tag{IV.31}$$

Failure takes place if

$$\sigma_0 = [1-(\varepsilon_0\ t/\theta)](6\ E\ E_0)^{0.5} \tag{IV.32}$$

at

$$\frac{t}{\theta} = \frac{3\ E\ A_0}{P_0} - \left(\frac{3\ E}{2\ E_0}\right)^{0.5} \tag{IV.33}$$

The main reservation to the above proposals of solution to the problem is the use of the shear viscosity and shear modulus. It is known that the extensional flow cannot be described on the basis of experiments in shear.[24,30,31]

IV.4.b Extensional Flow Problems

Development of extensional rheometry remains far behind shear analytical methods. Reliable instruments have been developed only relatively recently. Understanding of the basic nature, and consequently, interpretation of the experimental results still seem to be rather unsettled, at best.

A very substantial effort in the investigation of extensional flow has been invested by G. V. Vinogradov and the team of his co-workers. Significant and exciting results were presented in 1970.[32,33]

Vinogradov's team built its own rheometer and investigated high molecular mass noncrystallizable polymers to make the experimental work simpler, and to avoid complications due to crystallization. A very important element of these investigations was determination of relaxation for every point of extension collected. The completeness of the data collected allowed evaluation exceeding the customary procedures, and in some ways was nonconventional.

The extensional deformation has been formulated according to the method of Hencky, $\varepsilon = \ln(l/l_0)$. Here ε is total deformation, l_0 is initial length of the sample, l is length of the sample at some time t; ε_e is elastic (reversible) deformation, while ε_i is irreversible deformation, $\varepsilon_i = \ln(l_i/l_0)$, where l_i is length of the fully relaxed

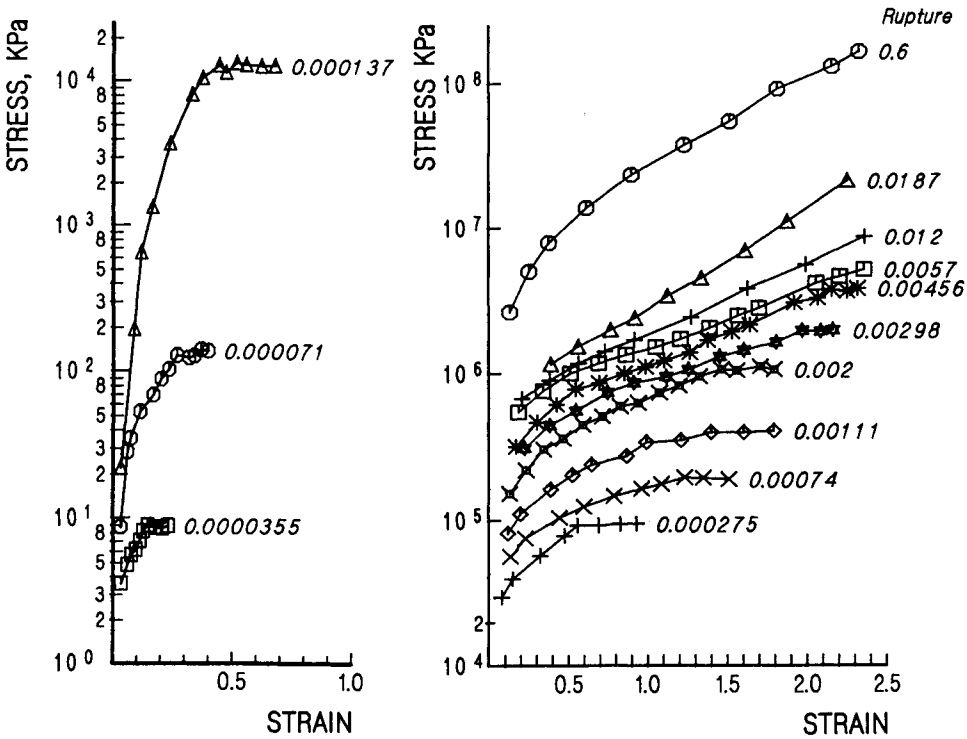

Figure IV.6: *True stress versus total strain for various strain rates (given as parameter). After G. V. Vinogradov et al.*[33].

sample, $\varepsilon_e = \varepsilon - \varepsilon_i$. Extensional viscosity is $\zeta = \sigma/\dot{\varepsilon}_i$, where σ represents true stress and $\dot{\varepsilon}_i$ stands for the rate of irreversible deformation. Modulus of elasticity is $E = \sigma/\varepsilon_e$.

From figure IV.6 - left, one may see that for low deformation rates, the true stress rises monotonically with strain to reach a plateau representing a constant value of stress at $\varepsilon = \dot{\varepsilon}_i = const$. With the increasing extension rate, the shape of the curves gradually change from convex toward stress axis, further to assume an S-shape, and further, at still higher extension rates, the plateau region disappears, up to the point of rupture. For those conditions where the constant stress is observable, the time, t_s, and deformation ε_s, where the constant stress begins, change rapidly with strain rates. This may be seen in figure IV.7. The onset of constant stress flow coincides with the maximum in the elastic deformation.

Figure IV.8 presents extensional viscosity on total (top) and on irreversible deformation, deformation rate is given as a parameter. One may notice that for some deformation rates, viscosity reaches a constant value independent of deformation. Before the region of constant value is reached, viscosity may pass through a maximum. Such a maximum is located in the vicinity of the point where the reversible and irreversible deformations are equal. Initially, viscosity grows with

increasing strain nearly linearly, especially if the irreversible strain is considered. The same is true independently of the rate of strain. The length of the nearly linear segment of the curve extends toward higher deformation as deformation rate increases. Eventually, a level of deformation rate is reached where the entire curve is linear, without a maximum, without a segment of constant viscosity.

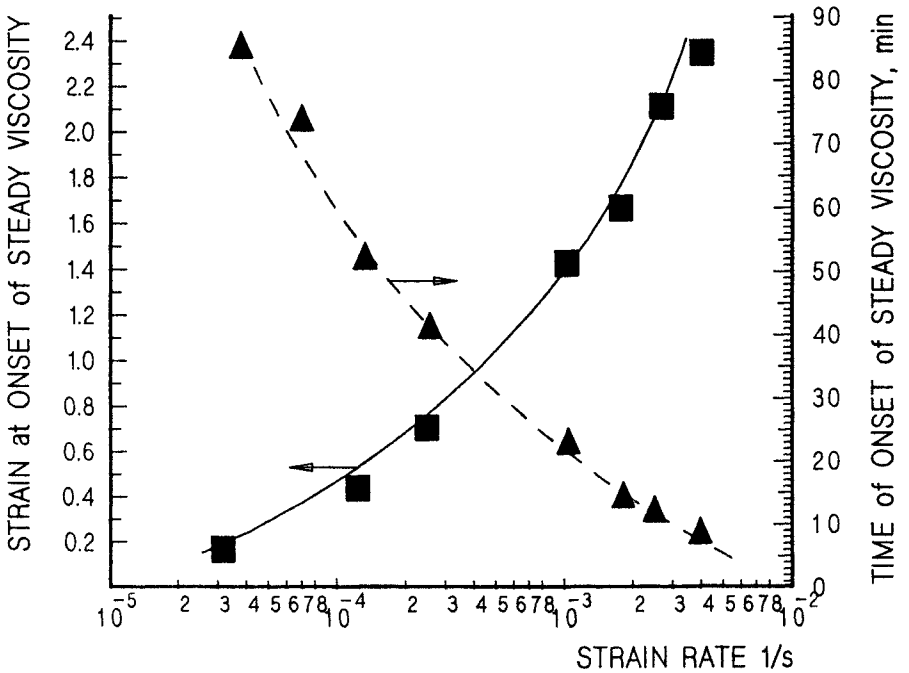

Figure IV.7: *Relationship between extensional viscosity and total strain (bottom), as well as irreversible strain (top). Deformation rates given as parameter. After G. V. Vinogradov and al.*[33]

Extrapolation of all the curves, irrespectively of the deformation rate, down to zero extension gives the Trouton viscosity, ζ_0, which is equal to three times the zero shear viscosity. The extrapolated Trouton viscosity agrees with the relationship proposed by Kargin and Sogol'owa[34]:

$$\zeta = \zeta_0(1 + \varepsilon_i) \tag{IV.34}$$

At low strain rates, viscosity of the constant, strain independent segment is equal to the Trouton viscosity; at higher deformation rates, however, this does not hold true.

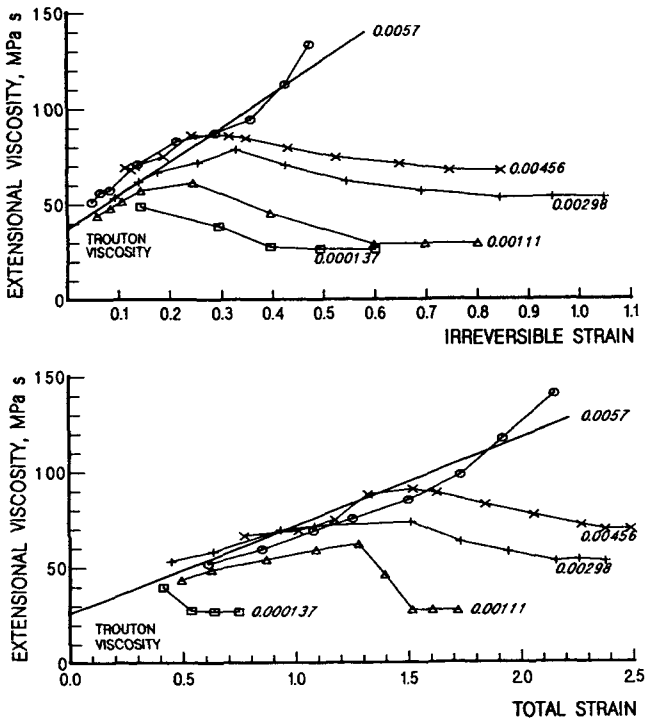

Figure IV.8: *Relationship between extensional viscosity and total strain (bottom), as well as irreversible strain (top). Deformation rates given as parameter. After G. V. Vinogradov et al.*[33]

Modulus of elasticity (figure IV.9) at low extension rates shows some similarity with the corresponding relationship for elongational viscosity. Namely, there is initially a maximum and a plateau, where the modulus does not change with extension. With increasing extension rate, the initial maximum disappears, but there is a segment of extension insensitive modulus. At high extension rates, no region of constant modulus appears before a rupture takes place.

Figure IV.10 and IV.11 show the influence of extension on the stress relaxation, given as $\ln(\sigma/\sigma_0)$ against time. Comparison of the two figures shows the difference in the relaxation behavior between the material stretched at the lowest and the highest deformation rates of those studied by Vinogradov et al.

At this point, a new way for assessment of the relaxation process is introduced: namely, the notion of the *initial time of relaxation*, which is defined as the initial slope of relaxation time versus natural logarithm of the stress decay:

$$\theta_0 = \lim_{t \to \infty} \left[\frac{dt}{d\ ln(\sigma/\sigma_0)} \right] \tag{IV.35}$$

In figure IV.12, the values of so obtained initial time of relaxation are plot-

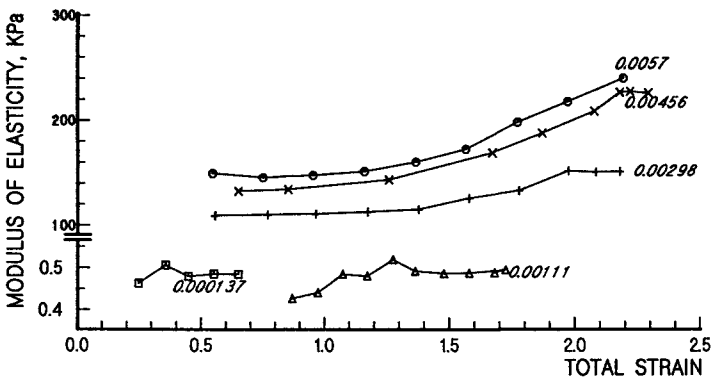

Figure IV.9: *Modulus of elasticity in relation to strain and strain rate (given as parameter). After G. V. Vinogradov et al.*[33]

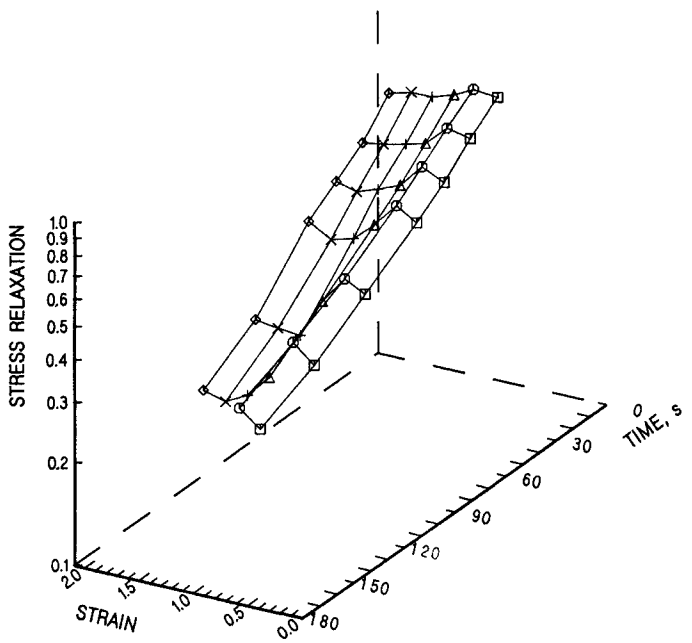

Figure IV.10: *Stress relaxation versus time and strain for extension rate of* $1.11 \cdot 10^{-3} s^{-1}$. *Data from G. V. Vinogradov et al.*[33]

ted against deformation for three deformation rates. It is noteworthy that some of the curves have maxima, and these maxima occur at values of deformation close to those encountered in the relationship between extensional viscosity and

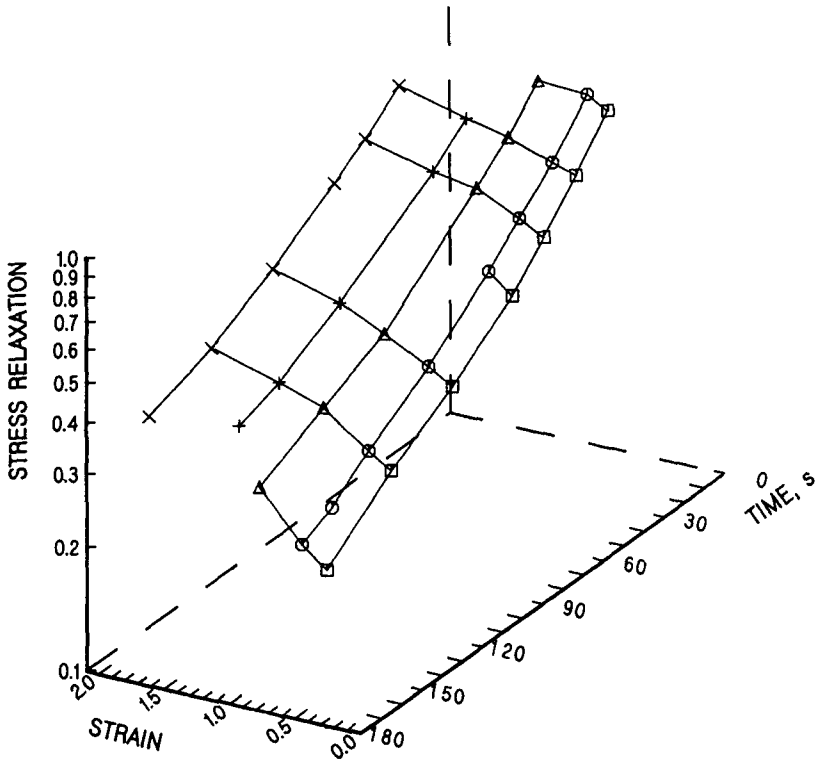

Figure IV.11: *Stress relaxation versus time and strain for extension rate of* $5.7 \cdot 10^{-3} s^{-1}$. *Data from G. V. Vinogradov et al.*[33]

deformation, which are indicated in the figure IV.12 by the arrows.

Although the extensional deformation, as evident from the above quoted results, cannot be treated in a simple Maxwellian fashion characterized by a single relaxation time, but rather with the entire spectrum, the authors use the linear formalism to describe the relation between the stress relaxation after the cessation of extension.

$$\sigma = \varepsilon \int_0^\infty \frac{N(s)}{s} \exp(-\ t\ s)\ \ ds \tag{IV.36}$$

The function $N(s)$, the *relaxation frequency distribution*, is calculated from $\sigma(t)$ using the first approximation method by Alfrey.[35]

$$N(s) = -\frac{dp}{\varepsilon\ d \ln t} \tag{IV.37}$$

where $s = 1/t$. If the calculations are conducted correctly, then it should result that

$$\int_0^\infty \frac{N\ (s)}{s}\ \ ds = \ \ \zeta \tag{IV.38}$$

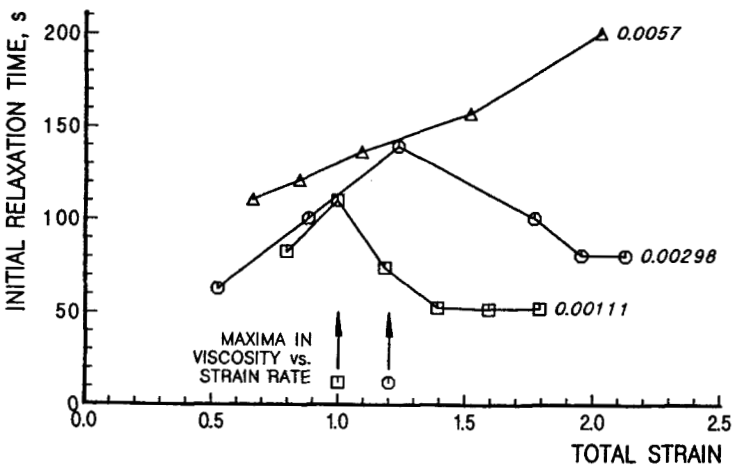

Figure IV.12: *Initial time of relaxation for different levels of strain. Strain rate given as parameter. After G. V. Vinogradov et al.*[33]

If the value of the integral is smaller than ζ, then the spectrum is incomplete.

Figure IV.13 presents the dependence of the relaxation frequency distribution function on frequency and strain in a three dimensional graph. Figure IV.14 gives in the similar form of the three dimensional graph the relationship between the relaxation frequency distribution functions on frequency for constant viscosity flow at different deformation rates.

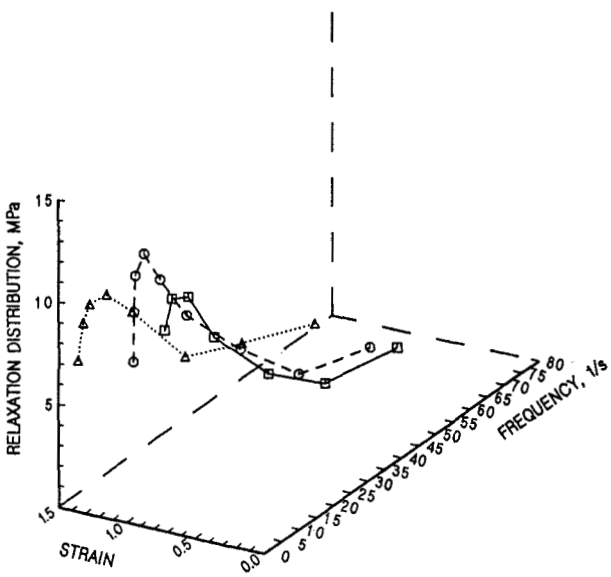

Figure IV.13: *Plot of relaxation frequency distribution in relation to the frequency and to strain. From the data by G. V. Vinogradov and al.*[33]

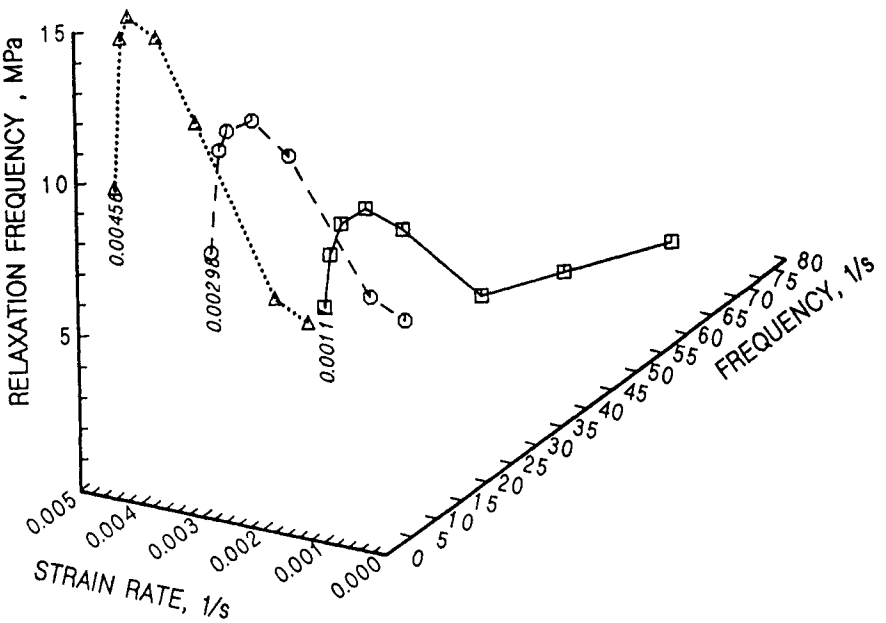

Figure IV.14: *Plot of the relationship between the relaxation frequency distribution and frequency for constant viscosity at different rates of deformation, From the data by G.V. Vinogradov et al..*[33]

Another important result of the investigations by Vinogradov *et al.*[33] is the indication of the strength of polymer in relation to the processing conditions. The molten samples of polystyrene investigated in the extensional rheometer were "instantly" vitrified upon extension and tested for strength. Results of these experiments are shown in figures IV.15 and IV.16, where the rupturing stress is plotted against the total strain (figure IV.15), and the rupturing stress against the irreversible strain (figure IV.16). The arrows in figure IV.15 indicate the values of the total deformation where the maxima of viscosity are reached before a steady state had been reached. Both of the figures witness to the fact that the rate of deformation has a significant effect on the strength of the vitrified samples. This permits also the inference that similar increase of strength regards the melt prior to the vitrification. Vinogradov *et al.* suggest that the increase of strength is primarily due to the increase of reversible, high elastic strain.

In a later publication, G. V. Vinogradov[36] elaborates on the flow instability in extension. According to his findings, a stable extensional flow may be realized as long as stress does not exceed the critical value of 0.1 to $0.5Pa$ – it is the same stress value as is for the shear experiments.

The authors[33] conclude that the total strain (or draw ratio, as it may be expressed) should not be regarded as the parameters determining orientation effect in the polymers. This is in full agreement with similar conclusions reached by other investigators at numerous other occasions. Vinogradov *et al.* emphasize that once the extension process reaches steady state, there is no strength increase any more.

This value is essentially independent from temperature and molecular mass for a given homologous series. It must be noticed, however, that critical shear rate depends on temperature and molecular mass.

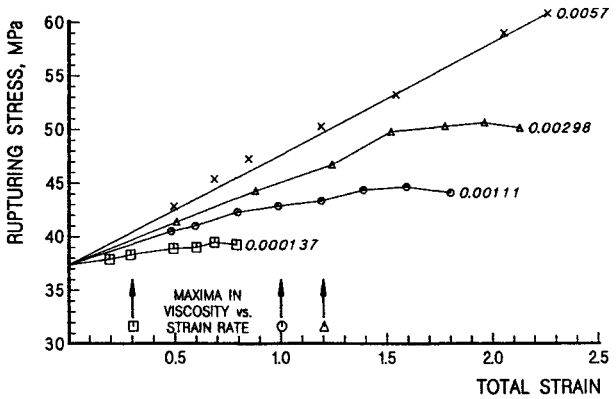

Figure IV.15: *Relationship between the rupturing stress and total strain. Extension rate as parameter. The arrows indicate the deformation at which the maximum of viscosity was attained. After G. V. Vinogradov.*[36]

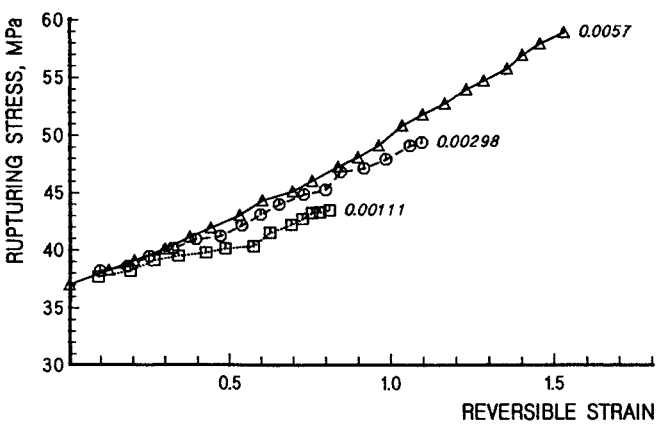

Figure IV.16: *Dependence of tensile strength on reversible strain. Extension rate as parameter. After G. V. Vinogradov.*[36]

At stresses and deformations below their critical values at isothermal conditions, the extensional viscosity remains constant within a reasonably narrow range. Conversely, if the critical values are exceeded, a flow instability may appear. The fact that when the critical stress (or strain) values are exceeded, the ability of polymer to accumulate additional irreversible deformation is reduced can be an explanation for the preceeding statement. On the other hand, the accumulation

of reversible deformation is limited to ultimately reach a level corresponding to its relaxation ability. Consequently, the polymer passes into a forced rubbery state and will start to fracture. In the forced rubbery state, the polymer behaves as a cured elastomer, where an increase of the deformation rate causes the reversible tensile deformation to pass through a maximum, which indicates passing into a glassy state – a state of brittleness.[37]

Other investigators[38–42] find, with substantial theoretical backing, that fractured flow of polymer melts shows significant dependence on extension rate and temperature. With increasing temperature, fracture starts at increasing extension rates. However, with significantly higher extension rates the fracturing disappears. The extension rate at which the fracture disappears increases with decreasing temperature.

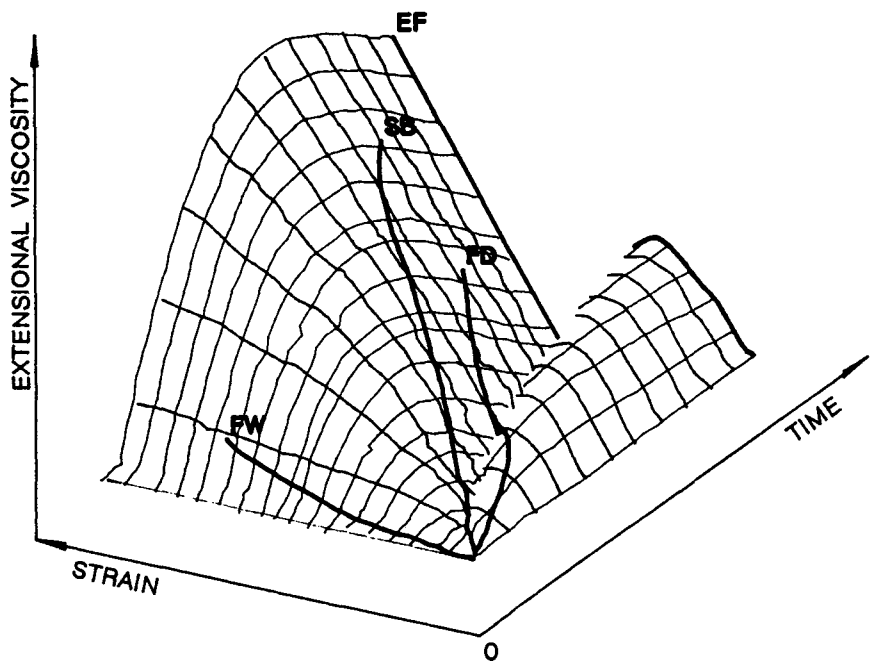

Figure IV.17: *Plot of the transient elongational viscosity as a function of the total strain and time calculated according to Marucci et al.*[43]*. The heavy lines indicate: SB - data calculated from spinning experiment, FD - determinations by the method of falling drop , FW - data calculated with falling weight method. EF - indicates beginning of the steady state (equilibrium) flow. Based on J. Ferguson and N. E. Hudson.*[47]

There is a substantial similarity between the observations by Vinogradov and the graph presented in figure IV.17 which gives a mapping of the transient elongational viscosity *versus* total strain and time.

Thanks to the work by J. Ferguson and N. E. Hudson[47], and naturally to the underlying constitutive equations,[43–46] we have a good visualization of the somewhat "strange" results of the exhaustive experimental studies by Vinogradov et. al.,[33,36] as well as an understanding of the reasons behind the differences in elongational viscosity when measured by different techniques. It would be interesting to determine how the results of the determinations of elongational flow in hyperboloid cone orifices[136,137] would compare with the other data of figure IV.17. The work of Ferguson and Hudson[47] also gives additional explanation of the transient shear flows discussed by Vinogradov.

It is important to realize that the majority of the experimental techniques for the determination of elongational viscosity, as well as the majority of industrial processes involve only the transient flow region. Undoubtedly, this creates a difficult situation if there is a necessity to relate laboratory analyses with the material behavior in any industrial process.

Phan-Thien and Tanner[48,49] have developed another linear model, with additional improvements over the model of Marucci *et al.*[43]. Additionally, the model does accommodate nonisothermal cases:

$$\mathcal{T} = \sum_{i=1} \mathcal{T}^{(i)}$$

$$\theta_i \frac{D}{Dt}\mathcal{T}^{(i)} - \mathcal{T}^{(i)} \frac{d}{dt}(\ln T) = \phi(T)\ K(tr\mathcal{T}^{(i)}\ \mathcal{T}^{(i)} = 2\ G_i\ \theta_i\ D \qquad \text{(IV.39)}$$

where

$$\phi(T) = \exp\left[\frac{c_1\ (T - T_r)}{c_2 + T - T_r}\right]$$

which represents the exponent of the inverse of WLF equation,

$$K(tr\mathcal{T}^{(i)} = \exp\left[\frac{\epsilon}{G_i}\ tr\ \mathcal{T}^{(i)}\right] \qquad \text{(IV.40)}$$

ϵ is a constant on the order of 0.01, D is stretching tensor, $\mathcal{T}$ is stress tensor, θ is relaxation time, G is modulus, and $G_1 = G\ H\ (1 - \xi)$, where H is relaxation function, and ξ is an adjustable parameter. Further,

$$\frac{D\ \mathcal{T}}{D\ t} = \frac{d\ \mathcal{T}}{d\ t} - \mathcal{L}\ \mathcal{T} - \mathcal{T}\ \mathcal{L}^{T}$$

with L, the macroscopic velocity gradient and $\mathcal{L} = L - \xi\ D$, and finally $tr\mathcal{T} = [3kT/(N\alpha^2)] \cdot \langle\lambda\rangle^2$, and $\langle\lambda\rangle^2$ is mean square extension of the molecular entanglement network strand.

The just given constitutive equation has been adapted for application to the fiber formation problem[49], giving the following set of equations:

$$K\mathbf{T}_i + \alpha_i \left\{ u \frac{d\ \mathbf{T}_i}{d\ m} - 2\ (1 - \xi) \frac{d\ u}{d\ m} \mathbf{T}_i \right\} = 2\ \alpha_i\ \frac{d\ u}{d\ m} \qquad \text{(IV.41)}$$

$$K\mathbf{P}_i + \alpha_i \left\{ u \frac{d\,\mathbf{P}_i}{d\,m} - (1-\xi)\frac{d\,u}{d\,m}\mathbf{P}_i \right\} = -\alpha_i \frac{d\,u}{d\,m} \tag{IV.42}$$

$$\sum_{i=1}^{N} \frac{\epsilon_i}{\alpha_i} \; (\mathbf{T}_i - \mathbf{P}_i) = u \tag{IV.43}$$

where $\alpha_i = \theta_i v_0 / L$ is Deborah number and $\epsilon_i = G_i\, \theta_i\, Q \;/\; F\, L$ but $\epsilon_i/\alpha_i = \phi_i$. The boundary conditions are given as:

$$z = 0, \qquad u = 1, \qquad \text{and} \qquad \sum_{i=1}^{N} \phi(bfT_i - \mathbf{P}_i) = 1$$

It is stipulated that the initial stress distribution does not affect the solution over the entire fiber path. This is the result of an assumption that at $z = 0$ $\mathbf{P}_i = 0$ and $\mathbf{T}_i = 1/N\phi_k$.

The final version of the equations for a fiber formation case is:

$$\sum_{k=1}^{N} \phi_k(\mathbf{T}_k - \mathbf{P}_k)\frac{d\,\mathbf{T}_i}{d\,m} = 2\,\Xi\,[1 + (1-\xi)\mathbf{T}_i] - \frac{K}{\alpha_i}\mathbf{T}_i \tag{IV.44}$$

$$\sum_{k=1}^{N} \phi_k(\mathbf{T}_k - \mathbf{P}_k)\frac{d\,\mathbf{P}_i}{d\,m} = -\Xi\,[1 + (1-\xi)\mathbf{P}_i] - \frac{K}{\alpha_i}\mathbf{P}_i \tag{IV.45}$$

where

$$\Xi = \frac{\sum\limits_{i=1}^{N} \phi_i/\alpha_i \; K(\mathbf{T}_i - \mathbf{P}_i)}{\sum\limits_{i=1}^{N} \phi_i \; [(1-2\,\xi)\mathbf{T}_i + \xi\;\mathbf{P}_i] + 3\sum\limits_{i=1}^{N} \phi_i} \tag{IV.46}$$

Equations IV.44 to IV.46 present a set of first order differential equations. The needed input is take-up force, initial velocity, and flow rate. In terms of analytical preparations, full rotational and oscillatory determinations are needed. Also, very crucial is the knowledge of the relaxation function, though the author does not specify what type of relaxation and this segment of the work raises some questions. Solution of this set of equations gives stress distribution along the spinline, velocity profile and draw ratio. The draw ratio, if known, cannot be specified independently.

Phan-Thien[49] presents a test of the validity of the equation on data obtained for formation of fibers from low density polyethylene[50] and polystyrene,[51] both noncrystallizable polymers. The formation processes were very slow, far from the industrial level of intensity. The agreement between the calculated results and the data measured from the experiment are much better than any of those published earlier. Nevertheless, the discrepancies grow with the growing distance from spinnerette, similarly like in many other publications, to reach some ten to fourteen per cent. One must admit that the calculations are quite involved, as is the analytical preparation.

Several authors concede that solution of the "spinning problem" by way of the constitutional equations developed thus far is essentially unsuccessful.[24,139–142]

IV.4.c Andigraphic Solution of Attenuation

Another way of resolving the "spinning problem" is offered by this author in the framework of a complex treatment of all the unit processes taking place in the quench zone.

When one considers a process with constant take-up force, then the force acting on any cross section along the spin line is constant, in the first approximation. The differences in force level are caused only by "the losses to the environment", etc. Additionally, as the polymer stream emerges from the exit of the spinnerette, it is subjected to a drawing force which may be understood as a case of step stress excitation. The force superimposes on the effects of the forces applied earlier in the extrusion process. The step application of force is a precondition for the qualification of a process as *creep*. After scrupulous examination of all kinds of analytical data collected on many different fiber formation processes, we find that they do not resemble extensional rheometric data or plots. With this in mind, in addition to the lack of real success in describing the process by all means tried thus far, it has been assumed that the process of diameter attenuation in fiber formation is a process of *creep*. As the additional justification for such an assumption, it may be given that in the course of attenuation, there is no qualitative difference between fiber formation with constant take-up velocity and constant take-up force. This is the matter of long recognized *"self regulation"* of the mutually interdependent quench zone processes. In a drawing process, *e.g.* during rheometer testing, the extension of the material is by definition under strain excitation, the diameter reduction is uniform over its entire length, while the extending force increases with the growing strain. In reality, in fiber formation this is not the case, despite the fact that in fiber makers' slang the operation is called *melt drawing*. K. Katayama, T. Amano, and K. Nakamura[63] quite long time ago observed during formation of fibers from polyethylene that diameter attenuation fits into the Kelvin-Voigt model, a model describing creep.

Figure IV.18 presents the apparent extensional viscosity and strain plotted against time. The data were taken from the detailed analyses of several medium fast industrial processes, and they span from the maximum of the die swell to the end of crystallization. All of the cases presented in figure IV.18 show very distinct similarity: the extensional viscosity (non-isothermal, as it is in the process) is practically constant at a very high level, possibly with a slight negative slope. According to Vinogradov, [33,36] this should be an indication of linearity of the system. Naturally, it is to be expected that shortly before the initiation of crystallization some kind of "havoc" takes place in the polymer morphology. One cannot expect to describe adequately this segment of polymer history by a linear relationship.

On the basis of the above assumptions, the empirical data may be used to calculate creep compliance as a function of time. From such a relationship one

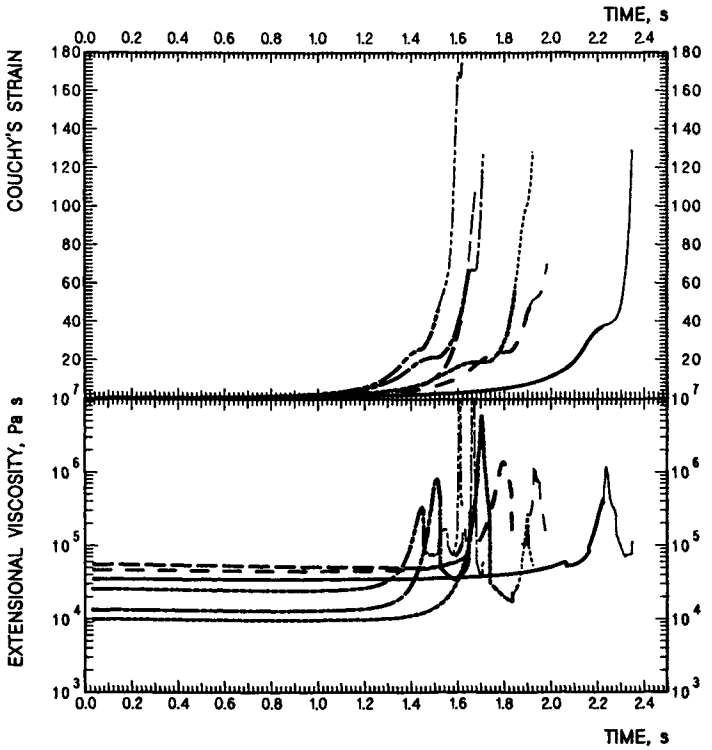

Figure IV.18: *Apparent extensional viscosity and strain obtained from analysis of several medium fast industrial processes of fiber formation. The time scale spans from the maximum of the die swell to the onset of crystallization. Polymer: polypropylene. Nonisothermal, "as is" data given.*

may calculate retardation distribution function which represents the essence of viscoelasticity and permits to depict all pertinent rheological functions: thus the title "andigraphic", from $\alpha\nu\tau\iota\gamma\rho\alpha\phi\phi\nu$ = depiction, image, reflection.

There are several methods available for calculations of the relaxation and retardation spectra.[31] The finite difference operator approximation method by Yasuda, Ninomiya, and Tschoegl[32] appears to be accurate and convenient, provided that the third order approximation equation is used. The needed equation is given as:

$$L(\theta/\beta^*) = \frac{J(h^3\ t) - (h^2 + h + 1)\ J(h^2\ t)}{(h^2 - 1)(h - 1)\ \ln\ h} + \\ + \frac{h(h^2 + h + 1)\ J(t) - h^3\ J(t)}{(h^2 - 1)(h - 1)\ \ln\ h}\Bigg|_{t=\theta} \qquad \text{(IV.47)}$$

The notation here is: L – creep retardation spectrum, t – time, θ – retardation time, h – finite difference time increment, β^* – spectral shift factor given for several $\log h$ values in table IV.1. Time is commonly used in a logarithmic scale and so

is the time increment. Following Tschoegl's[32] notation in equation IV.47 ht really means $\log t + \log\ h$ and $h^2 t$ corresponds to $\log t + 2\log h$ etc. The value of h is usually selected so that its logarithm equals between 0.1 and 0.5. With decreasing value of h, the accuracy of the spectra increases but with $h < 0.1$ the sensitivity to error in the input data greatly increases, and this may eventually lead to increased uncertainty of the obtained retardation function.

Table IV.1.
Spectral shift for various finite differences for third order approximation. After N. W. Tschoegl[31]

$\log h$	0.1	0.2	0.3	0.4	0.5
β^*	2.139	1.550	1.150	0.878	0.689

Once we have a retardation function, almost everything else may be calculated. The suggested way of process description is accurate. The retardation function is strongly affected by deviations in polymer chain structure and the suggested procedure provides data for the polymer one works with. There are, however, several points to be observed.

According to Stavermann and Schwartzl[52], the process of creep is inherently nonlinear. Following J. Marin[*cit.in* 52] creep is customarily interpreted as consisting of three parts:

1. Instantaneous creep, ε_0;
2. Transient creep, $[\varepsilon(t)]$, which increases with time from zero to some finite equilibrium value;
3. Steady state creep, $[\phi_f \cdot t]$, proportional to time (see Figures IV.19 and IV.20).

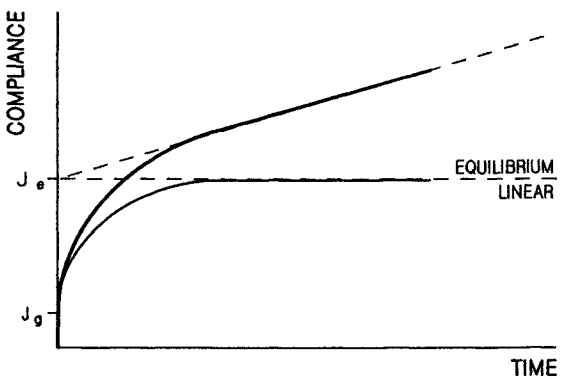

Figure IV.19: *Generalized schematic representation of compliance (or strain) versus time in response to step application of stress: creep behavior.*

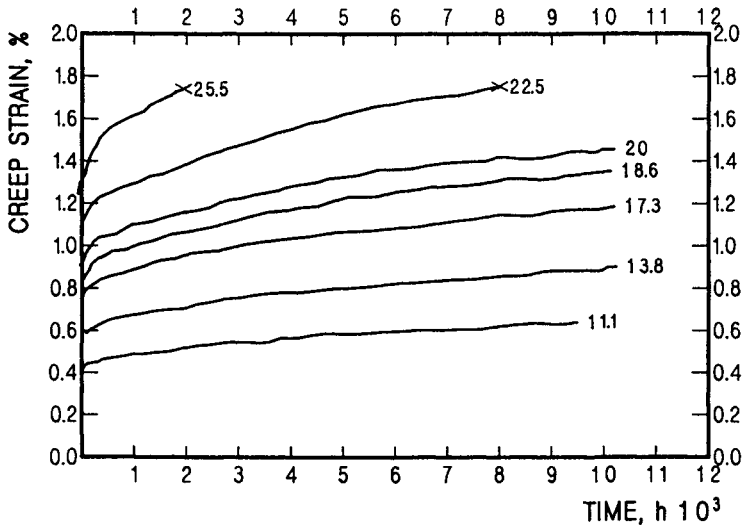

Figure IV.20: *Extensional creep of polymethyl methacrylate; parameter: initial stress in MPa. After J. Marin*[cit.in52]

The marks "linear" or "equilibrium" in figure IV.19 represent the strictly linear creep. The instant compliance (strain) is a nonlinear feature. The same is true of the steady state fluidity, $\phi_f \cdot t$, in figure IV.19 represented by the triangle contained between the lines tangent to the equilibrium compliance (dashed lines) and the full, measured compliance. The angle ϕ_f represents the rate of steady state fluidity increase.

If very large forces are applied, some "additional nonlinearities" in the creep behavior may be observed. In such cases one may escape to linearization of the data.[52] Linearization of rheological functions is easiest and correctly done by application of various definitions of strain.

According to K. Weissenberg[53], any function of the shape of the body which vanishes when the body is undeformed and which increases with increasing deformation may be used as a measure of strain. According to A. J. Stavermann and F. Schwartzl[52], the various commonly used definitions of strain are:

$$\varepsilon_C = \delta - 1 \qquad \textit{Cauchy} \qquad \text{(IV.48)}$$

$$\varepsilon_K = 0.5(\delta^2 - 1) \qquad \textit{Kirchhoff} \qquad \text{(IV.49)}$$

$$\varepsilon_H = \ln \delta \qquad \textit{Hencky} \qquad \text{(IV.50)}$$

$$\varepsilon_M = 0.5\left(1 - \frac{1}{\delta^2}\right) \qquad \textit{Murnaghan} \qquad \text{(IV.51)}$$

where $\delta = \frac{l}{l_0}$ which is equivalent to *draw ratio.*

Cauchy's strain is linear with the value of delta, Kirchhoff's strain in relation to Cauchy's increases with increasing delta. The remaining two functions, in relation

to Cauchy's, decrease with increasing delta, but Murnaghan's strain has a stronger decrease, its maximum limiting value is 0.5. Zero point, naturally, is common for all of the quoted definitions of strain.

When one calculates creep compliance, one uses, naturally, the initial stress and any of the given quoted strains. Murnaghan's strain needs to be used for industrial fiber formation processes at high speed and under high tension. For slower processes Hencky's strain may be sufficient. Cauchy's strain, possibly, may be applicable for very slow experimental ("academic") processes. Equation IV.47 may be used with any of the strains, but one must remember to recalculate the results into Cauchy's strain for use in generating other functions.

Generally, equation IV.47 ought to be applied to the experimental data with a correction for the transition from shear to extensional flow. The problem has been worked on by many different authors. The more interesting experimental work appears to be that by J. R. Clermont, J. M. Pierrad, and O. Scrivener,[56] and D. D. Goulden and W. C. MacSporran.[57] Attempts on a theoretical solution may be represented by work of R. Keunings, M. J. Crochet, and M. M. Denn.[58] The solutions offered do not seem to be quite yet ready for practical application.

Measurement of the maximum diameter of the die swell is somewhat elusive, as it also depends markedly on the deformation history. On industrial formation machines measurements of the die swell are very difficult due to deep recess in mounting of the spinnerettes, often the access in impossible. The diameter, or the related filament velocity, is needed for calculation of strain. If there is an error in the die swell size it will automatically propagate an error in the time scale. It seems that when the correct theoretical solution of the flow transition will be known, obtaining correct data on die swell may be easier.

The beginning of the attenuation process is usually considered to be at the maximum of the die swell diameter. For the representation of the creep curve, however, it is necessary to push the *zero time* back to the point where polymer enters the conical entrance to the capillary. This means that the *zero time* is where the extensional flow starts first. In this way the *zero time*, in comparison with the common notion of maximum of die swell, depends on the entire geometry of the capillary entry, on the length of the spinnerette capillary, as well as on the size and shape of the die swell.

The back calculation of compliance, J, or strain, with the retardation distribution function, L, on hand may be done with equation III.140. Nonetheless, there are also necessary the instantaneous compliance. J_0, and the steady state fluidity function, ϕ_f. In a classic way, one obtains those two values by the method shown in figure IV.19. This means that, J_0 - equals instantaneous compliance at time zero. The slope of the final section of the curve, ϕ_f, is usually taken as the steady state fluidity, $\phi_f(t)$.

The compliance back calculated from the retardation function represents only the transient flow portion, $J(t)$. The steady state fluidity in more intensive fiber formation processes for large strains deviates from linearity at longer times, t. Therefore, the procedure of calculating instantaneous compliance and steady state

fluidity must be modified. The transient flow compliance, as it is calculated from the retardation function, is subtracted from the experimental compliance over no more than a 50% of the time span of the process studied. One may also begin the calculations at some distance from the first point available. The obtained values *versus* time give a new function which represents a straight line, the slope of which determines the steady state fluidity, ϕ_f, and J_g is the intercept. In case of processes involving large strains the experimental curve at longer times invariably deviates from linearity, The process gradually changes from rheodictic to *pseudo-arrheodictic* behavior. The experimental compliance curve ceases to increase and reaches a more or less constant value which is typical for the arrheodictic behavior. The point where the steady state fluidity begins to deviate from linearity depends on the molecular mass of the polymer involved, as shown in figure IV.21. The molecular mass influence is likely to be rather indirect, caused really by the density and type of deep entanglements, or enchainments. One may want to fit the final segment of the curve into some nonlinear function, usually $\phi_f^*(t) = 1 - A \times \exp(ct)$. Such a treatment may improve the fit of the back calculated results to the point of virtual superposition of the experimental and back calculated curves. One may use one of the solutions suggested by Tschoegl[156], though some of them require data not easily available. The most suitable might seem the *prolongation method*, however, the method appears to be much more manipulative than the curve correction suggested above. It is true that the span of retardation times obtainable is very narrow but alteration of the spectrum seems objectionable. According to Tschoegl[156] the pseudo-arrheodictic behavior results from *pseudo-crosslinks* arising from strong and relatively durable entanglements, which are responsible for more than one viscoelastic mechanism reflected by multimodal distribution function. The data presented here may suggest that the observable effect of the pseudo-crosslinks is reflected by change of the steady state fluidity, rather than the transient flow reflected by the retardation spectrum. As it will be seen later in this chapter, the arrheodictic behavior is the "havoc in morphology" of the melt prior to the onset of crystallization. If long retardation times would be involved, they would be significantly longer than the times available in any fiber formation process.

Here we come to the temperature dependence: currently all of the formation processes from melt are nonisothermal, and so are many processes of formation from solution. There is a wide choice of recalculation possibilities according to temperature.[32,33,54,55] One may recalculate compliance according to (the same equation as III.219):

$$J(T_r, t_r) = J(T, a \cdot t_r) \times \left(\frac{\rho\, T}{\rho_r\, T_r} \right) \tag{IV.52}$$

where subscript r indicates reference temperature or at reference temperature, a is temperature-time shift factor, ρ is polymer density.† The retardation distribution

†Data on certain physical properties of some polymers are given in the Appendix.

function may be recalculated identically as compliance.

$$L(T_r, t_r) = L(T, a \cdot t_r) \times \left(\frac{\rho\, T}{\rho_r\, T_r} \right) \qquad (IV.52\,a)$$

The shift factor may be estimated either according to the equation III.217 or equation III.220 for polypropylene. For other polymers development of similar algorithms is highly advisable. Application of the recalculation procedures may be done in several different ways, or at several different stages. The two most obvious ways are:

1. Recalculation of compliance, and obtaining the retardation spectra for non-isothermal and for isothermal conditions separately.

2. Recalculation of the retardation function.

The first method of the two appears marginally more convenient. Nevertheless, the recalculation must be taken as an approximate procedure, as it has been developed for polymers of linear behavior. The extremely high viscosity immediately below the spinnerette is striking; one may simply presume that this is somehow connected with the transition from shear to extensional flow. We may recall one more time the comment by Stavermann and Schwartzl that creep is by its nature nonlinear; it may be that the degree of nonlinearity is *artificially increased by the process itself.* Even though the function of the shift factor *a versus* temperature, as suggested here, appears to give results sufficiently good for "technical applications", it might require a firm proof in a theoretical sense. Also, the recalculation is obviously only as good as reliable is the available shift factor – temperature function, and the whole function is needed for the purpose. Moreover, the regions where polymers crystallize always require an extrapolation.

All the isothermal compliance curves quoted here were recalculated to $240°C$. These curves show very rapid decrease of compliance at the end of the curve.
]

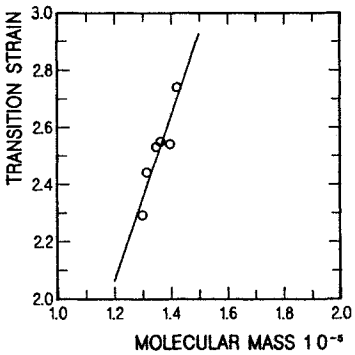

Figure IV.21: *Influence of molecular mass on the strain at which the behavior of polymer in creep changes to arrheodictic.*

One may pose a question whether this means that in an isothermal process such behavior would indicate an end of "spinnability".

Examples of practical application of the description of the rheology of fiber formation processes and confrontation of the calculated results with the experimental are given in the set of figures IV.22, IV.23, IV.24 and IV.25, pertaining to different industrial processes.

A comparison of the two processes represented in Figures IV.22 through IV.24 involves poly(propylenes) of zero shear viscosity 193.6 and 148.8 Pas at $240°C$. The second process was carried out with a substantially shorter quench zone, geometrically speaking, and with a greatly more intensive quench. The initial drawing stresses were 16.97 and 18.73 kPa, respectively.

It is important to stress that the magnitude of the force applied for drawing has a major influence on the creep process. The explanation of rheology through chain entanglements[135] does justify the influence of initial force on the creep process, but more development work seems to be needed before a practical application might be possible. As may be seen from Figures IV.23 and IV.24, primarily the instantaneous strain and steady state fluidity are affected. The steady state fluidity is influenced to a smaller degree, but at higher values of force the behavior is changing to arrheodictic, as mentioned above. From the work presented here one may see an influence of the initial stress on compliance and on the retardation function (figure IV.25). At lower initial stresses compliance is higher and it finds also a reflection in the retardation functions.

Vinogradov and co-workers,[33] as reported in section IV.4.b, figures IV.10 to IV.12, and particularly IV.13 and IV.14 suggest that the retardation function does not depend only on molecular mass or zero shear viscosity, but appears to depend also on the processing conditions. Both theoretical and experimental investigations[155&ref.] indicate with ever increasing strength that relaxation time, or relaxation spectrum, is not constant. In the case of solutions, irrespectively of solvent, it depends on the deformation rate. The influence of initial stress on compliance may be taken as a proven fact, though no quantitative description is yet available.

There is a number of formulas to calculate relaxation time, proposed by different authors.[32,152] All of the proposed equations are similar, the core of the equations is:

$$\theta = \frac{\eta_0}{RT} \tag{IV.53}$$

The retardation times, taken as the time corresponding to the maximum of the retardation spectrum determined for each of the processes studied and quoted here, range from about 0.35 s to about 0.52 s. These times differ substantially from the average relaxation and retardation times determined from the oscillatory shear experiments, where they range from 0.49 s to 0.73 s. The difference appears to be too large to be disregarded. The experimentally obtained retardation times agree well with the results of calculations according equation IV.53a. If a polymer contains cross linked material, the relaxation time increases. A similar effect may be expected in case of retardation time. Cross linking, often present in com-

mercial polymers elevates the relaxation time markedly. In fact, determination of relaxation time may serve, after a calibration, as an analytical procedure for the

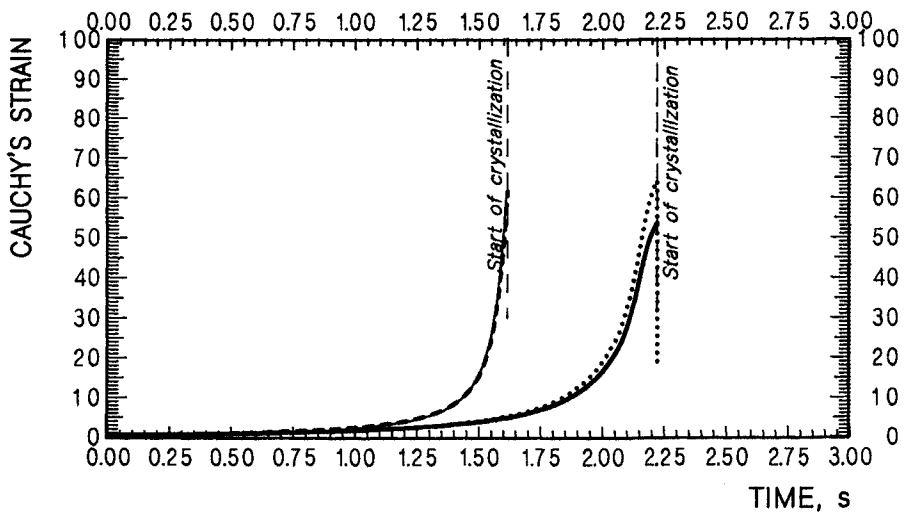

Figure IV.22: *Cauchy's strain in a fiber formation. The dotted line is back calculated. Heavy lines: nonisothermal data for a process with rapid quench, the pseudo-arrheodictic segment not corrected for. Finer lines: process at still more rapid quench, polymer of lower viscosity. Data corrected for the pseudo-arrheodictic flow segment.*

determination of cross linking. The creep retardation times for the polymers given in this chapter as examples are plotted in figure IV.26 against the corresponding

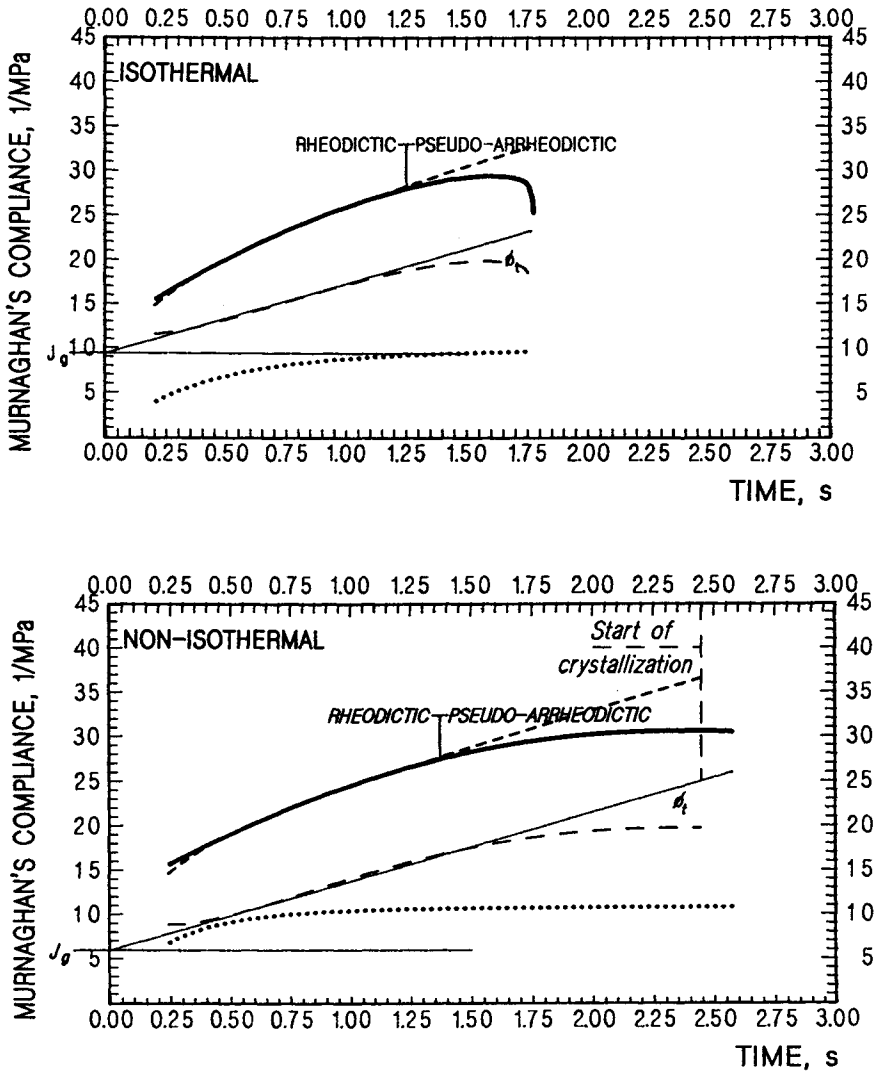

Figure IV.23: *Murnaghan compliance for the process given in Figure IV.22, heavy lines. Top: isothermal, bottom: non-isothermal. Heavy lines: full drawn – experimental curve, dotted – transient flow compliance, short dashed line – back calculated compliance (mostly superimposed with the experimental line). Fine lines: full drawn – linear steady state fluidity, ϕ_t, and glassy (instantaneous) compliance, J_g (intercept), long dashed – actual fluidity. Data not corrected for pseudo-arrheodictic behavior.*

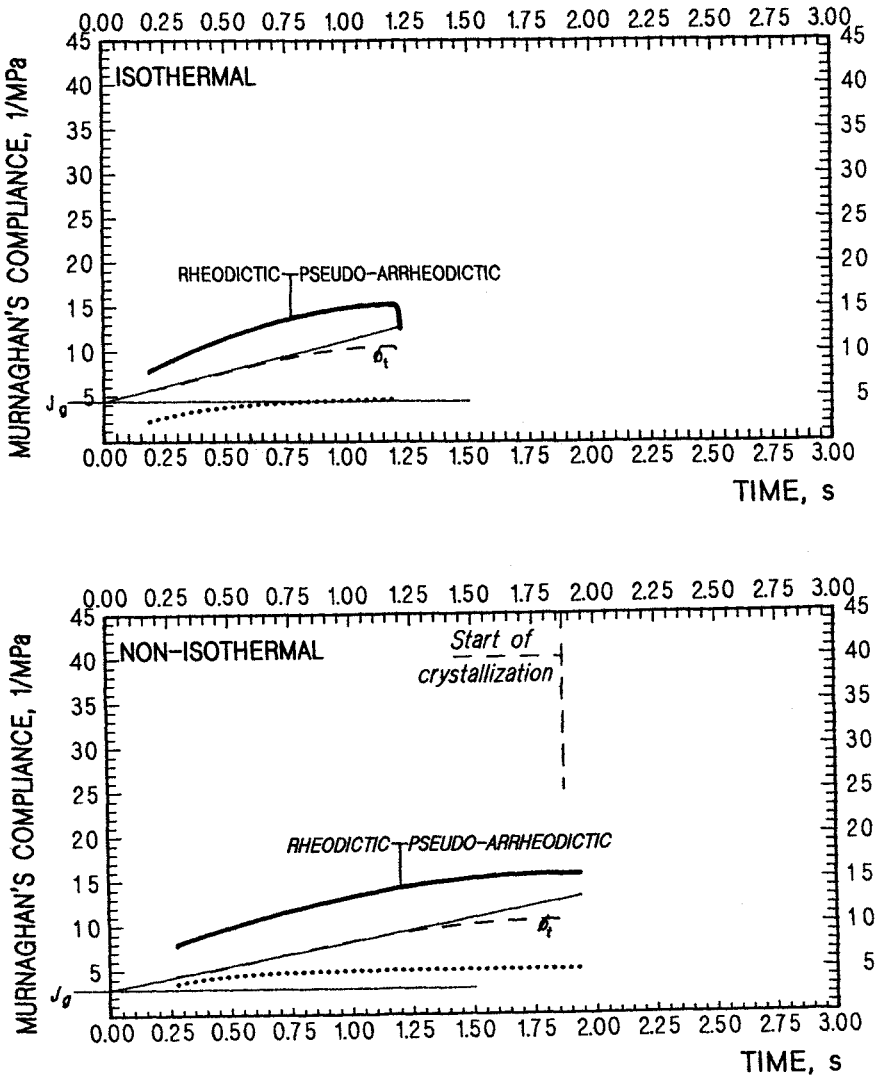

Figure IV.24: *Murnaghan compliance for the process given in Figure IV.22, finer lines. Top: isothermal, bottom: nonisothermal. Heavy lines: full drawn – experimental curve, dotted – transient flow compliance, short dashed line – back calculated compliance (fully superimposed with the experimental line). Fine lines: full drawn – linear steady state fluidity, ϕ_t, and glassy (instantaneous) compliance, J_g (intercept), long dashed – actual fluidity. Data corrected for pseudo-arrheodictic behavior.*

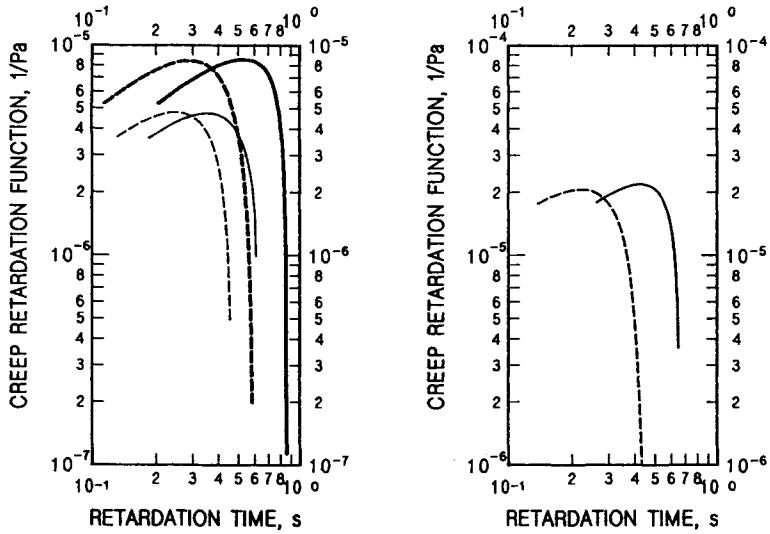

Figure IV.25: *Creep retardation functions: Left graph: for the process given in figure IV.23. Right graph: for the process given in figure IV.24. Full drawn lines – isothermal* $T_r = 240°C$, *dashed lines – nonisothermal.*

values calculated according to equation IV.53a. The deviations of the experimental results from the calculated line do not form any immediately apparent relationship to the initial extensional stress.

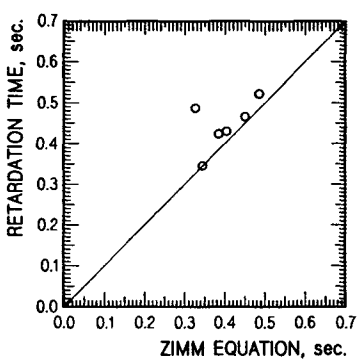

Figure IV.26: *Confrontation of the retardation times calculated from the Zimm equation (equation IV.53a is represented by the diagonal line) with the values determined experimentally. Data for* $240°C$.

$$\theta = \left(\frac{1}{1.8926}\right) \times \left(\frac{\eta_0 M_w}{\rho RT}\right) \qquad (IV.53\,a)$$

Based on the results of the creep calculations described above any relationship between the initial stress and retardation time may not be confirmed. Perhaps the high speed of the processes, and consequently the small range of retardation

times obtainable do not permit such a relationship to be observed.

It may also be necessary to assess the extent to which the data obtained in one process may be used to process manipulations. If the attempted changes in the conditions of formation are large, and if a correction accounting for the initial stress fails, at some point the retardation function may loose its validity even for approximate predictions; a new determination of the retardation function may be needed.

In general, from an analysis of the results, one may conclude that the treatment of the *fiber formation problem as a creep process* is correct. The agreement of the calculated data with the measurements conducted during actual experiments is excellent. The small span of time obtainable for the retardation spectra was initially of a serious concern. However, the results and their good agreement with experiments seem to dispel the fear. The pseudo-arrheodictic segment of the process appears to be related to the polymer fluidity, rather than to the retardation spectrum. The process takes only a very short time and the longer retardation time cannot play terribly significant role here. At some 0.5 s to 0.8 s the retardation functions drop quite precipitously off. If the retardation function were responsibly for the pseudo-arrheodictic behavior then a second peak would be necessary. Attempts to use the prolongation method indicated that to explain the pseudo-arrheodictic behavior observed experimentally would require retardation time unrealisticly long, compared to the time available in the process. The filaments are under tension during all the solidification process and beyond, and this may be the important factor to be considered here.

IV.4.d Spinline Stability

Stability of spinline represents an enormously important aspect of the economy of fiber manufacturing. It is not less interesting theoretically. It is of no surprise, then, that theoretical work on the subject started relatively early by J. R. A. Pearson and co-workers.[59–62] As a starting point, isothermal cases of Newtonian fluids were studied. It has been found that such fluids may be extended to a maximum draw ratio of 20.218. The effort appeared to be a good beginning for further studies. The isothermal spinning of Newtonian fluids *per se* has little practical meaning.

Unfortunately, the subsequent years have brought a score of publications repeating essentially the same work using slight modifications of the mathematical apparatus used. C. J. S. Petrie gives a quite extensive review of all those efforts.[24]

There appeared several attempts to describe stability of spinlines of Non-Newtonian polymers.[43] The theoretical considerations, using Maxwell fluid, lead to the conclusion that elasticity is beneficial to spinline stability. The results do not agree with the experimental determinations of fracture obtained during extension of strands of polyethylene: the samples fracture below the values of $\dot{\varepsilon}^*$ of some 40 to $50s^{-1}$ and cease to fracture again above values of $\dot{\varepsilon}^*$ of 65 to $70s^{-1}$. (Nondimensional extension rate $\dot{\varepsilon}^* = \theta\dot{\varepsilon}$ which is equivalent with the Weissenberg

number, Wi.) In the examples presented in this book, a spinline may be stable until the onset of crystallization when the Weissenberg number, calculated on the Henky's strain, reaches values close to seven, if advantage is taken of the maximum retardation time. If the retardation time corresponding to the maximum of the retardation function is taken, the corresponding values reach close to four. The beginning of change to arrheodictic behavior takes place at Weissenberg numbers 0.36 and 0.391. In this case the Weissenberg number, Wi, was calculated with the retardation times at the maximum of the spectrum and with Cauchy's strain. Clearly, it is difficult to see a relationship here.

Vinogradov[36,64] suggested that fracture, both in shear and in extension, occurs invariably between 0.1 and 0.5 MPa of true stress. The same author suggested that at the same values of stress crystallization may be starting. Analysis of the cases presented in this book as examples, as well as of many other processes, does not support this relationship to spinline instability. The build-up of recoverable work until onset of crystallization is presented in figure IV.29.

Jinan Cao[65] finds that there is a maximum in the filament velocity gradient, and flow instability starts in the area past the maximum value. In the processes presented here, there are several maxima of velocity gradient: the first one is usually close, mostly prior, to the onset of crystallization, and the others occur during crystallization and toward the end of it.

Malkin and Petrie[149], in an extensive paper, review all the efforts in solving the problem of spinline stability published through 1997. In their conclusion, the authors state that the only useful criteria are: Vinogradov's notion that failure would take place only for $Wi \geq 0.5$ (Wi = Weissenberg number), criteria resulting from the work by Reiner and Freudenthal[29] (see equations IV.33 and IV.34). Development of the ability to predict filament breaks is still found to require a considerable effort. Confusing shear and extensional properties, relaxation and retardation times, appears to be a serious flaw in the treatments published thus far – these parameters are not interchangeable.[31]

As important and as interesting as the topic is, we must still wait for a better solution to be able to take practical advantage of it. Perhaps the treatment of the fiber formation process as a case of creep experiment traveling with the velocity of polymer extrusion will allow for more definite solutions.

IV.5 Crystallization in Extensional Flow

The fact that polymers crystallize faster under influence of mechanical forces was noticed sometime in the forties.[67] The shortest crystallization half times determined dilatometrically amounted to some thirty seconds. On the other hand, total residence time of polymer in a quench zone was ranging from some fifteen down to three seconds. Despite the short residence time, it was not unusual to find that the crystallinity reached in the quench zone was equal to that found in the final fibers. A difference in the accelerating effect of forces on crystallization of different polymers was also noticed.

Probably the first attempt to study the phenomenon was published by P. Flory[151] in 1947. The work relates the temperature at which the crystallization begins to the relative extension of the molecules. In quantitative terms, the work gives the following equation:

$$\frac{h_f}{\kappa_b}\left(\frac{1}{T_m^0}-\frac{1}{T_{ci}}\right)=\frac{2\lambda l\beta N}{\pi^{1/2}}-\left(\frac{\lambda^2}{2}+\frac{1}{\lambda}\right)\frac{1}{N} \tag{IV.54}$$

where h_f is the enthalpy of fusion per chain segment, κ_b is Boltzmann's constant, T_m^0 is, as usually, the equilibrium melting/crystallization temperature, T_{ci} is initial (the highest) crystallization temperature, N is the number of segments per polymer chain, l stands for the length of a segment, $\beta=(3/1Nl^2)^{1/2}$, λ is the extension of polymer chain (equivalent to draw ratio as $\lambda=1$ means no extension).

Equation IV.54 is difficult to confront with experiments since the quantities obtainable experimentally are not easily translated into the parameters of the equation.

Van der Vegt and Smit[68] seem to have originated experimental studies of the influence of shear on the initiation of crystallization. The authors melted polypropylene in a capillary rheometer, cooled it somewhat and extruded at increasing shear stress. Initially, the polymers behaved normally, but after a certain value of stress had been exceeded, viscosity started to increase, sometimes rapidly. The increase of viscosity was attributed to the onset of crystallization. The shear stress and shear rate at which the crystallization began depended on the temperature of the experiment. At $160°C$, crystallization started at some 1.2 s^{-1} shear rate and about 45.7 kPa, while at $180°C$ the respective values were some 38 s^{-1} and 113.6 kPa.

In a follow-up of the van der Vegt-Smit experiments, it has been determined[134] from synchrotron X-ray diffraction that during extrusion, a "mobile mesophase" of hexagonal organization may form in capillaries, which under appropriate conditions, in terms of shear rate and/or temperature, may crystallize to freeze the capillary. Formation of such a mesophase does not take place in the entry to a capillary where the elongational flow predominates.

Similar semiquantitative experiments were performed during fiber formation experiments.[69] A flat plate X-ray camera had been installed on a fiber formation machine on which also temperature was measured with an infrared thermometer. It had been found, depending on the amount of draw, that the first sign of polypropylene crystallization could be noticed at filament temperature ranging from $160 to 180°C$. In polypropylene of molecular mass amounting to approximately 450000, thirty five per cent of crystallinity was reached within 102 ms.

The X-ray technique has been found very useful for the investigation of the onset of crystallization, and particularly for the development of orientation and other structural features.[69] It has been found essentially inapplicable for determination of the crystallization kinetics – an immensely important aspect of the entire process of fiber formation. Another technique for the purpose has been developed, which may be called determination of the *crystallization history*, or

CH for short.[70] The principle of the method is based on the relationship existing between the crystallization temperature and the melting point. (See also section II.2.b.) The principle of the method is simple, the instrument needed is the rather common differential scanning calorimeter (DSC), possibly of fast response. High quality, high precision experimental work is needed, as well as rather extensive calculations. The last problem is easily solved by computers, once the proper programs are available.

The following sequence of work is involved: initially one needs to perform as large as practical number of isothermal crystallizations, followed by immediate melting to determine the relationship between the crystallization temperature and the melting point. The equilibrium melting point is obtained at the same time. High accuracy data are needed, as the extrapolation to the equilibrium melting point is usually far reaching. As high as possible crystallization temperature is advisable, though caution is needed to avoid degradation of the polymer during a prolonged time at an elevated temperature. A simple graph, like that in figure IV.27, may be obtained together with an equation:

$$T_{melt} = a + bT_{crist} \tag{IV.55}$$

where

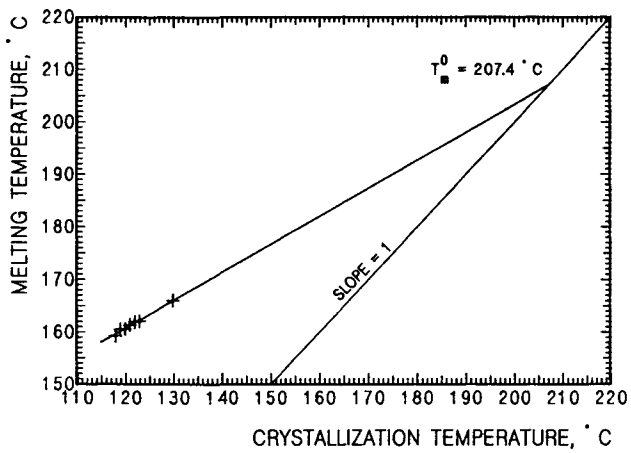

Figure IV.27: *The relationship between crystallization temperatures and melting points in a propylene polymer.*

$$T_m^0 = \frac{a}{1-b} \tag{IV.56}$$

In many instrumental analytical techniques, one has to deal with a problem generally referred to as *instrumental line broadening.* This means that what theoretically ought to be presented as a *mathematical line* in reality appears as a peak of some finite breadth. The most common reason for line broadening is the finite response time of the instrument and a finite rate of the investigated phenomenon. For example, if we melt a low molecular weight crystal in a DSC apparatus at

a given heating rate, the specimen requires some finite time to melt completely. Nevertheless, in that increment of time the instrument temperature climbs higher, and as a result we obtain a peak. The effect of process rate and of instrument response time superimpose to widen the broadening. In some processes, the polymer crystallization phenomena included, we have to deal with process/structure imperfections. A polymer chain with a slightly crippled structure, in comparison to its perfect half-brother, or just some more dense chain entanglements, may require a slightly larger degree of undercooling to crystallize and will also melt at lower temperature. This leads to an additional reason for peak broadening which is structure related and which may be specimen specific.

Correction for peak broadening was applied first to X-ray diffractograms in the early forties. The technique used for the purpose was deconvolution. If we denote the original function as $f(t)$ and its Fourier transform[71] as $\Im$, then

$$\Im = \int_{-\infty}^{\infty} f(t) \exp(-2\pi\nu it) dt \tag{IV.57}$$

If we then denote $f(t)$ the true melting function, $f_b(t)$ the peak we obtain from the instrument, and $f_e(t)$ the experimental melting function, and $\Im$, $\Im_b$, $\Im_e$ the respective Fourier transforms, then we may write a convolution equation:

$$\Im * \Im_b = \Im_e \tag{IV.58}$$

and further

$$\Im = \Im_e / \Im_b \tag{IV.59}$$

In practice, as a Fourier transform of a function we take the following representation:[71]

$$f(t) = \frac{A_0}{2} + \sum_{j=1}^{n} \left(A_j \cos j\frac{2\pi t}{T} + B_j \sin j\frac{2\pi t}{T} \right) \tag{IV.60}$$

and the coefficients of the transformed function are:

$$A_j = \frac{2}{m} \sum_{k=0}^{m-1} y_k \cos j\frac{2\pi k}{k} \tag{IV.60 a}$$

$$B_j = \frac{2}{m} \sum_{k=0}^{m-1} y_k \sin j\frac{2\pi k}{k} \tag{IV.60 b}$$

where m is the number of equally spaced discrete points representing the function, n is number of harmonic equations, preferably $n \leq m/2$.

The coefficients of the deconvoluted function are obtained according to the division of complex numbers:

$$A = \frac{(A_e A_b + B_e B_b)}{(A_b^2 + B_b^2)} \tag{IV.61}$$

$$A = \frac{(A_b B_e - A_e B_b)}{(A_b^2 + B_b^2)} \qquad (IV.61\,a)$$

It is common that deconvoluted functions may display "rumblings", that is, a series of maxima and minima located at the left and right peripheries of the investigated peak. The only remedy available to limit such "rumblings" to an acceptably low level, or to a range sufficiently distant to be unimportant, is to limit the number of the harmonic equations used to calculate the final deconvoluted function. Generally, good operator's judgment is necessary in such cases.

The question of the proper deconvoluting function is not completely closed. This author finds that the best results were obtained with functions generated from controlled crystallization at low rate of cooling (nonisothermal) and melting curve from the same controlled crystallization run. The critically important point is that the polymer must be the same as the sample investigated. The same is true of the determination of the $T_m = f(T_c)$ relationship. It must be the same polymer batch. Even small differences between different samples of polymer are sufficient to wreck the accuracy, or even the entire sense, of the determination. For example, if fibers are investigated - fibers are to be used, not the pellets or melt prior to the extrusion. One needs to observe some differences in long periodicity due to molecular mass, polymer perfection, etc.[129]

One may consider, and some special cases may require, the use of other functions for deconvolution. A combination of functions is possible. In the last case, e.g. two isothermal functions, a low and a high temperature, may be combined. The interpolated deconvolution function is simply a sum of the proper fractions, φ, of the Fourier coefficients:

$$A_{ja} = \varphi A_{j1} + (1 - \varphi) A_{j2} \qquad (IV.62)$$

$$B_{ja} = \varphi B_{j1} + (1 - \varphi) B_{j2} \qquad (IV.62\,a)$$

One must stress that there is some controversy regarding the crystallization - melting temperature relationship. It is true that at low crystallization temperature, the points do not follow a straight line. If the lowest range of temperature is of interest, a caution may be advisable. Some investigators suspect that the $T_m = f(T_c)$ function is not represented by an exactly straight line, but it curves somewhat upwards. However, if the procedures just described are followed exactly, some of the potential errors may cancel themselves out. On the other hand, for the time being there is no other method which would permit analysis of the extremely rapid process of crystallization. As will be seen below, the accuracy of the obtainable results is sufficiently high to satisfy even very demanding investigators.

The relationship between crystallization and melting temperatures may be affected by cold drawing (plastic deformation). Experience, in agreement with the theory, shows that small extent drawing may be well neglected, as the discrepancies would not exceed the experiment's error. More extensively drawn samples may present problems. The best choice, naturally, is utilization of specimens prior to any drawing operation.

The sequence of all the experimental DSC runs, aside from the determination of the crystallization - melting temperature relationship, is as follows:

- Melting of the polymer (fiber) specimen investigated (preferably at 10 to 20 $^{\circ}K/min$, depending on the response time of the instrument, up to a temperature of 20 to 40 $^{\circ}K$ above the equilibrium melting point and holding for some ten minutes to assure full melting. Higher molecular mass polymers may require more severe conditions.

- Crystallization at a low cooling rate (2 to max. 5 $^{\circ}K/min$), depending on the crystallization propensity of the investigated polymer. To shorten the run time, the initial forty to seventy degrees may be dropped at as fast a rate as the instrument may safely handle, without losing full temperature - time control.

- Upon completion of the crystallization run, immediate melting of the specimen at the same heating rate as during the first melting operation.

Naturally, all the baselines should be calculated to respect the baseline change due to the change of the heat capacity during the transition.[79]

The procedure described above yields three scans. From the third scan (melting curve) and the second scan (controlled crystallization curve), one obtains the deconvoluting function which is used to deconvolute the first melting curve (the first scan).

A word of caution is needed. When investigating polymers which crystallized under the influence of forces, one may find some unexpected shapes of the crystallization curves, which will become evident in figures IV.29 and IV.30, where crystallization history curves are reproduced.

Since the initial work of Flory[151], there have been several attempts to solve theoretically the problem of crystallization under influence of forces.[72–78] Unfortunately, none of the suggested solutions could accommodate the determinations obtained from a substantial number of experimental data. Intuitively, and in an agreement with the sense of the Flory's stipulations, the most promising appeared to be the suggestion by Cahn[72] and Hilliard[73] that the stored work input is responsible for the accelerating effect. Confrontation of this idea with the experimental data shows that the stipulated relationship indeed has merit.

As it was shown in section IV.4.c, from the retardation functions one may calculate the work input in creep. The work input, both the stored and the dissipated work, initially increases gently, then accelerates strongly at some point, very much in line with the changes of velocity to which it is connected. Figure IV.28 illustrates the stored and the dissipated work during fiber formation plotted against time. The results beyond the onset of crystallization are not necessarily "legitimate" due to the presence of crystalline phase in the fluid.

The word *initiation of crystallization*, similarly as the *end of crystallization* may sound somewhat nebulous as the crystallization rate function is vanishing to zero at both ends. For the sake of communication in real life, in this context we

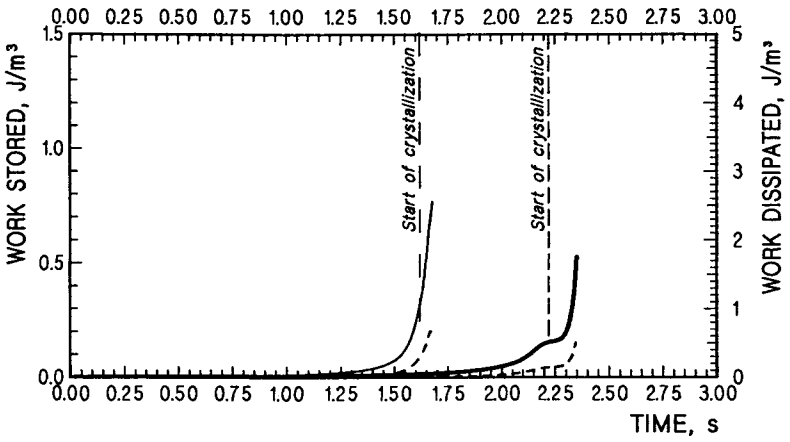

Figure IV.28: *Stored and dissipated (dashed lines) work in a process of fiber formation from polypropylene. Data to the beginning of crystallization versus time from die swell. Heavy lines : case from figure IV.23. Finer lines: case from figure IV.24.*

define the term as the point where the value of the rate function becomes larger that 0.001, or smaller than 0.001 for the beginning and the end of the process, respectively.

To quantify the crystallization processes, the Fisher-Turnbull, or otherwise called, Hoffman-Lauritzen, equation (equation II.20), as imperfect as it is, is used. An accelerating coefficient for the nucleation term was calculated using the equation coefficients as found from the least square fit of the quiescent, or "natural crystallization", curve obtained in a differential scanning calorimeter and a modified equation I.20 in the form given here as equation IV.63. An accelerating factor F_w for the heat of fusion was calculated to obtain the agreement with the experimental strain accelerated curves. Figures IV.29 through IV.32 show the results of such operations for two cases.

$$I^* = K_0 T \exp\left\{-\frac{32\ K_n (T_m^0)^2}{[\ \Delta H_f F_w T (T_m^0 - T)]^2}\right\} \exp\left(-\frac{K_f E_a}{RT}\right) \qquad \text{(IV.63)}$$

The factor correcting for the polymer flow, F_w, does not add to the heat of fusion, as expected by Hilliard[73], rather it multiplies it. The back calculated curves with an application of the experimentally, so to speak, determined factor superimpose exactly with the curve as obtained from the crystallization history determination. The accelerating factor at the point where crystallization starts may be presented according to the following relationship:

$$T_{ci} \times \left(\frac{T_m^0 - T_{ci}}{T_m^0}\right) = T_{ci}^* \times \left(\frac{T_m^0 - T_{ci}^*}{T_m^0}\right) \times \exp(W_{s,icr}) \qquad \text{(IV.64)}$$

In equation IV.64, $W_{s,ci}$ stands for the work stored up to the point of initiation of the accelerated crystallization, T_{ci} is the temperature at which the quiescent

crystallization is initiated, and T_{ci}^{*} is the initial temperature of crystallization under the influence of stored work. Other designations are as usual. When considering crystallization beyond the point of initiation, it is necessary to correct the stored work for the "freezing" of the nuclei or strains by the developing crystallinity. Finally, it leads to the following form for the correcting factor

$$F_w = \exp(W_s)(1 - \alpha) \tag{IV.65}$$

The equations IV.64 and IV.65 hold well only for the point of crystallization initiation. The segment of the curve describing crystal growth does not describe the experimentally obtained crystallization curve. If the amount of crystallinity developed up to a given time, α, is omitted in equation IV.65 then the correcting factor is strongly excessive and displaying some pulses coinciding with the beginnings of each crystallization peak. Introduction of the correction for freezing the work input by crystallization deepens the pulses. If a correcting factor calculated according to equations IV.64 and IV.65 is applied to the whole temperature range of a crystallization, somewhat surprising results are obtained. Very sharp, extremely large peaks are obtained at the beginning of each experimental peak. Equation IV.63, as originally developed by Fisher and Turnbull[143], and in all its different later versions, essentially describes only nucleation. That the nucleation is the slowest link of the crystal growth, and as such determines the overall rate of the crystal growth is taken as an axiom. Here we may see that the rate of nucleation is extremely fast, almost in explosive bursts reaching values of 10^{30} or higher, reaching numbers which are substantially higher than the physical possibilities. However, the growth of the crystals follows substantially slower. Figures IV.29, and IV.30 represent four different cases evaluated as just described. The correlation is excellent with the point of initiation of crystallization. The rest of the process remains largely unknown. Additional description of the processes given in figures IV.29 and IV.30 is given in Table IV.2.

Table IV.2.
Conditions of the processes presented in figures 4,29 and 4,30.

Figure	η_0 $Pa \cdot s$	σ_0 kPa	W_{ci} J/cm^3	$T_m^0 - T_{ci}$ $^\circ K$	t_{cr} ms
IV.29 top	193.6	16.973	0.2722	46.41	125,8
4,29 bottom	142.6	18.728	0.2855	48.81	101,9
IV.30 top	167.9	6.475	0.1485	62.79	74,1
IV.30 bottom	161.6	9.472	0.1888	56.59	61.6

The first important conclusion to be reached is that the rate of nucleation may be substantially higher than the rate of crystal growth. Similar conclusions may be drawn from fitting the experimental unaccelerated crystallization curves into the Hoffman-Lauritzen equation. In some cases, the experimental curve lags somewhat behind the calculated (figure II.9), but there the small differences may be often attributed to an experimental error, or to the imperfection of the equation. There

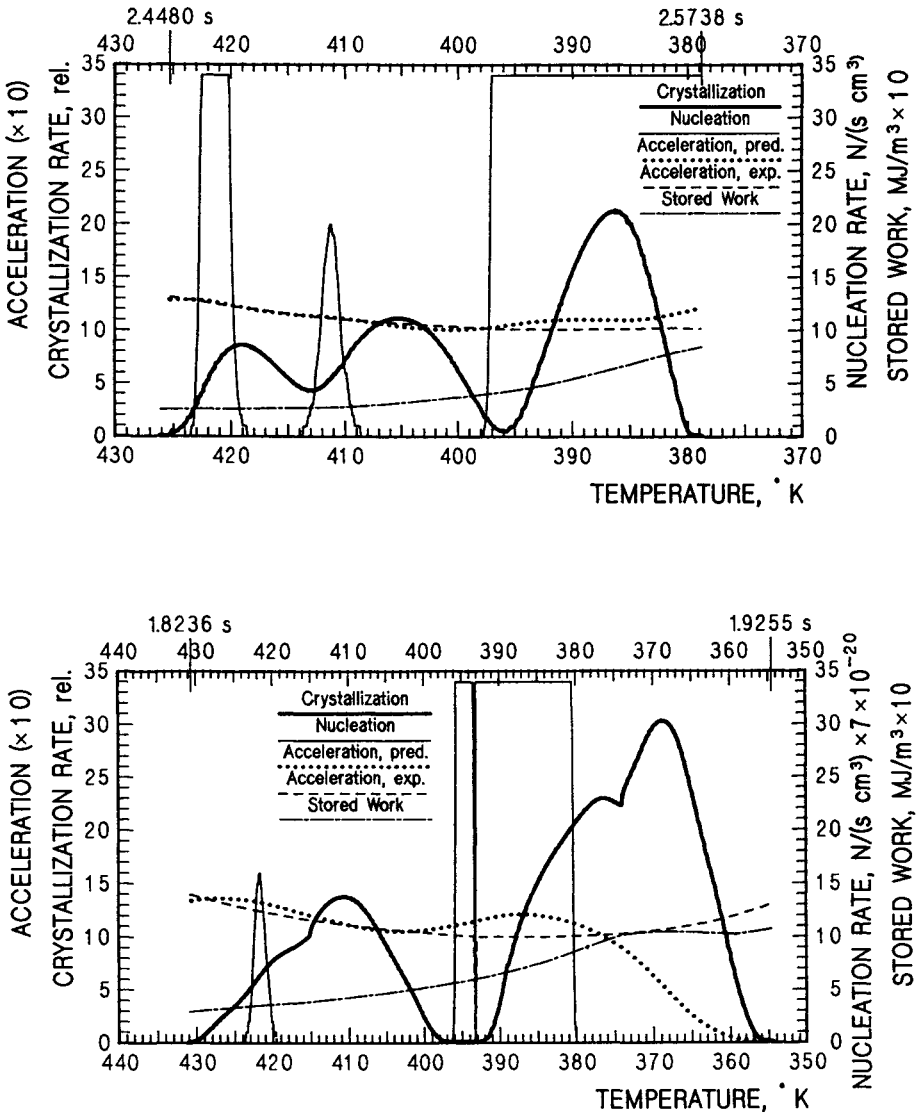

Figure IV.29: *Crystallization rates (heavy lines) and nucleation rate (finer line) during fiber formation versus temperature. Dashed line: accelerating factor from comparison with free crystallization curves. Dotted line: factor from equation IV.65. Dash-dotted line: stored work. Details in Table IV.2.*

is, however, no workable theory describing the rate of crystal growth, leave alone growth at strain accelerated conditions.

There is a number of unanswered observations concerning the interrelations

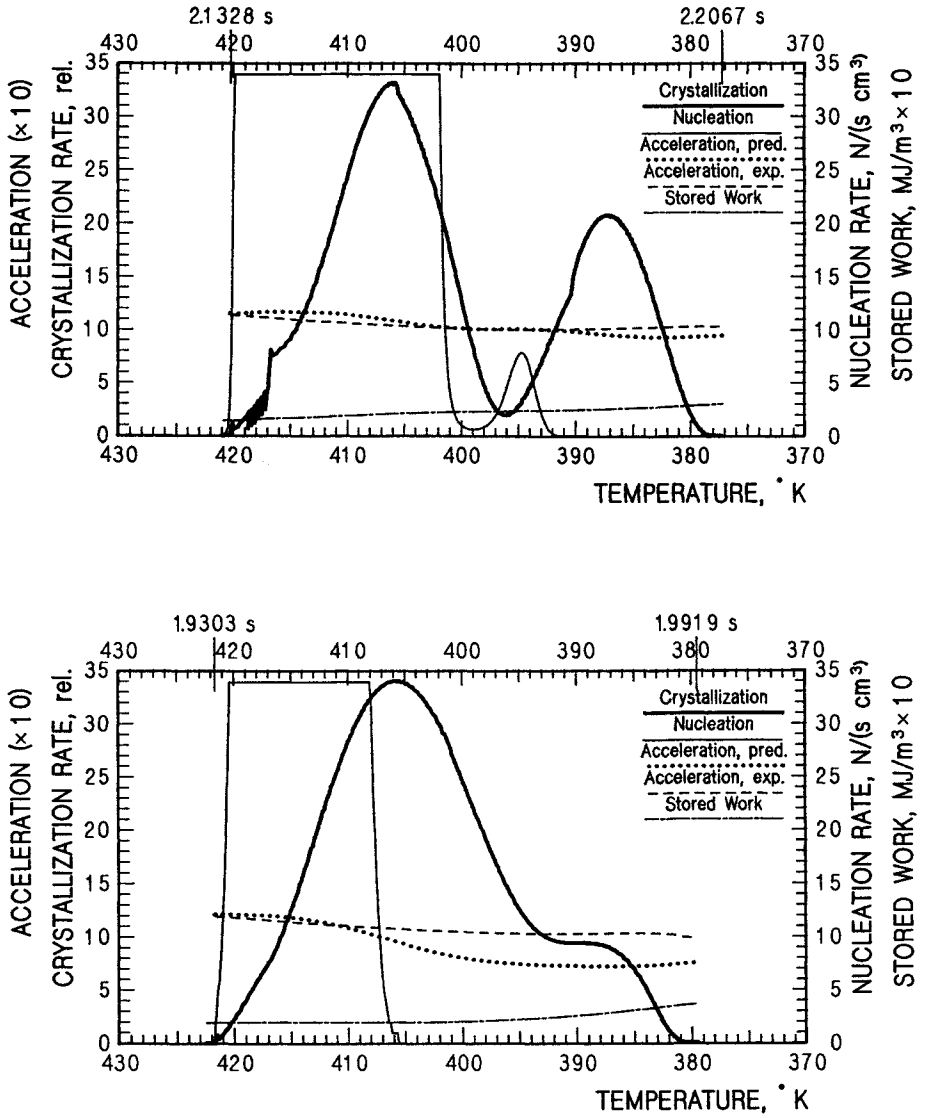

Figure IV.30: *Crystallization rates (heavy lines) and nucleation rate (finer line) during fiber formation versus temperature. Dashed line: accelerating factor from comparison with free crystallization curves. Dotted line: factor from equation IV.65. Dash-dotted line: stored work. Details in Table IV.2.*

between rheology and crystallization, they may be summarized as follows:

- One may notice that nucleation is invariably connected with a decrease of extension rate, and that this decrease is in some proportion to the size of

the nucleation peak.

- A large number of nuclei influences the rate of work storage, which seems to be connected to the point above.

- It may be admitted that the "excessive" nucleation in reality represents a nematic or smectic morphology, as described for the case of poly(ethylene terephthalate).[154] Nevertheless, direct comparison of crystallization of polypropylene and of PET calls for caution. Crystallization of PET is approached from temperatures lower than the glass transition, while crystallization of polypropylene is approached from the temperature of the melt. Polarity of PET may also be not without significance.

- Apparently great numbers of the formed nuclei must be either destroyed by the flow or "wasted" in some other way.

- Outside of the nucleation peaks, during crystal growth, the extension rate generally increases. One may suggest that the extensive nucleation forms a "homogeneous network", while crystal growth forms crystalline mats consisting of mosaic blocks which leads to some inhomogeneity. Points of stress concentration may lead to a partial break of the structure and to increase in strain. Similar changes in morphology may be responsible for the arrheodictic portion of the creep behavior.

- Interpretation of growth is only speculative. The stored work increases, in some cases very sharply, but crystal growth is by far not commensurate with it. One may even suppose that an increase of energy beyond some point slows the crystal growth. Analysis of the data of Table IV.2 indicates that total time of crystallization, t_{cr}, is shorter for those processes which employ lower initial stress, σ_0. At the same time one may notice, however, that the lower initial stress requires larger undercooling, $T_m^0 - T_{ci}$.

- The full crystallization times of the energy accelerated processes are shortened 550 times to well over one thousand times. From the cases presented here one may infer that the higher acceleration takes place when the stored work does not increase too rapidly.

- Very often the accelerated crystallization process proceeds down to the same low temperature as unaccelerated process does, or even markedly lower.

The development of a quantitative description of the growth kinetics, as difficult as it may be, is indispensable for any further progress in the field. It appears that for progress in this area, consideration of chain entanglements and their influence on the molecule mobility, transport, and extension of molecule segments might be essential.[135] Perhaps a flow equation would also give better agreement between the Fisher-Turnbull equation and quiescent experiments.

There is one more observation of utmost importance, which appears to agree well with the above given findings: a fast crystallization process results in larger

crystallites, a slow process gives smaller crystallites. It is exactly opposite to the cases of crystallization of low molecular mass compounds. One may suppose that the stored work factor which accelerates nucleation represents relatively permanent changes in the morphology of molecules. On the other hand, more intense flow of the molecules past one another disturbs the growth process. This finding also explains some of the old observations of various processes and relationships between processing conditions and fiber properties.

It is necessary to stress the good agreement between the results of such different analytical techniques utilizing many different instruments, both on various formation machines and in a characterization laboratory. All these results underwent extensive mathematical treatment and all agree within one or two per cent, or one or two degrees in temperature deviation. This agreement serves as an indication of a great coherence, and thereby a great reliability, of the interpretive system. As will be seen in the following chapters, this coherence extends still much further than so far described.

One may point to the disturbances in the beginning of the crystallization curve in figure IV.30 top. They might be taken as an artifact of determination of the crystallization history. In fact they are due to slight fluctuations in the stored work, which is only faintly visible in the figure due to large scaling factor. At any rate, even the disturbance has its justification.

A recently published paper[153] describes an investigation of the crystallization of amorphous poly(ethylene terephthatale) under influence of strain. The process was monitored by synchrotron X - ray analysis. Contrary to many other papers of such type, the experiments were well designed, without "mixed up" variables. The work confirms almost all the findings reported above. The strain induced process requires a critical degree of chain segment orientation which is dependent on temperature and draw ratio. The draw ratio represents a substitute for the stored energy. In the experiments reported[153] the process of crystal growth below $125°C$ started invariably after cessation of strain and ran to completion according to the first order transformation within one second. The rate of crystallization appears to be insensitive to temperature, indicating activation energy of $1kcal/(mole \times° K)$, or less, which is in a strong contrast to some 40 $kcal/(mole \times °K)$ for quiescent crystallization process. Above $125°C$ the process of relaxation is faster and the "oriented non-crystalline segments" formed during straining below $125°C$ are not formed above the critical temperature. One may inject here that polypropylene usually has higher molecular mass and much higher melt elasticity, consequently the degree of acceleration of nucleation ought to be correspondingly higher. Also, the critical temperature for no- nucleation may be expected to vary with molecular mass. Nonetheless, direct comparison of crystallization of polypropylene and of PET calls for a caution. Crystallization of PET is approached from temperatures lower than glass transition, while crystallization of polypropylene is approached from the temperature of the melt. Contrary to polypropylene, PET is polar, and this is not without a significance. The authors[153] also anticipate the possibility that a network of nuclei, or a mesophase, hinder the molecule, or segment, mobility

thereby restricting the crystallization.

One may conclude, as far as the smaller number of background data (rheology, crystallization history) permits, that the published work[153] presents a far reaching confirmation of the investigations of polypropylene crystallization described above.

In summary, one may conclude that the theoretical solution of crystallization process is far from satisfactory. The available equations may be used as a working tool but only as far as the initiation of crystallization is concerned. The nucleation segment of the equation may be close to being correct, but the rest of the factors influencing kinetics still need to be defined.

IV.6 Cold Drawing

In 1932 W. H. Carothers and J. W. Hill[80] have described a "peculiar" property of *as spun* polyester fibers. Namely, the fibers could be drawn at temperature ranging from room temperature to somewhat elevated temperatures, but less than the lowest melting point, and when the fiber was subjected to a sufficiently high force its diameter decreased abruptly forming a characteristic "neck", resembling

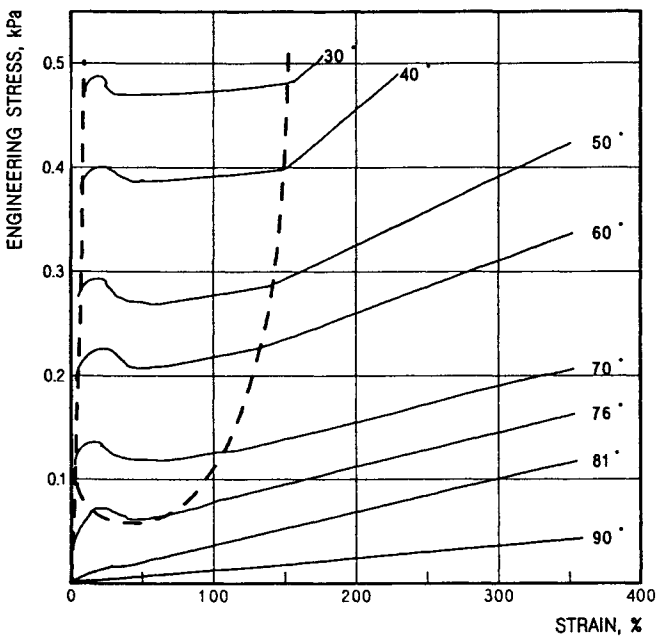

Figure IV.31: *Initial (engineering) stress - strain curves for cold drawing of chlorinated poly(vinyl chloride) at various temperatures. The dashed curve encompasses onset of the yield point and natural draw ratio until end of necking. Data from F. H. Müller*[81].

a bottle neck. A drawn specimen had a distinct boundary between the drawn, transparent, and undrawn, opaque sections of appropriately different diameters. This operation leads to fibers of uniform diameter possessing a structure orienta-

tion.

The diameter attenuation in cold drawing is not limited to the neck area. Only the initial portion of the total cold drawing extension takes place in the neck, the reminder takes place past the necking zone. It is generally assumed that the cold drawing temperature spans from some distance below the glass transition point up to the "lowest detectable" melting point. In reality the temperature range, as well as some other parameters of cold drawing depend very strongly on the amount of crystallinity and morphology of the *as spun* fibers and on the conditions of the drawing process. Stress strain curves of a cold drawing process for different temperatures are shown in figure IV.31 The thick dashed line encompasses the necking area, from the onset of yield to the *natural draw ratio.*

A few words need to be said about the semantics. The term *cold drawing* has been coined by the fathers of synthetic fibers and it may be a matter of needed courtesy to keep it, despite the fact that the drawing is not necessarily *cold.* Other terms may be found in the literature of the subject: *drawing with the neck formation* or simply *neck drawing*, or a term derived from structural and property considerations *plastic deformation.* There may be some confusion created by the fact that in some circles, particularly those of the fiber industry, the term cold drawing has been reserved to mean the drawing at a temperature below the glass transition for the polymer in question.

IV.6.a Mechanism of Drawing

The theoretical explanation of the discontinuous nature of cold drawing was the subject of numerous publications[82,94] over many years. All of these works were based on the same principles of so called *thin filament equations*, which represent a simplification of the theories of hydrodynamics and rheology. Also, it was believed that the necessary condition for a necking to take place is that the relation between strain and force must have an "S" shape, with a distinct minimum before the force goes up again, beyond the first maximum (figure IV.33 A).

This approach has been subjected to a convincing critique by S. Kase and M. Chang[95], who started from the same assumptions as in the previous work. Consideration of inertia in their solution led to the realization that the obtained equations are equivalent with the equations used in the area of *dynamic plasticity.* The basic equation in nondimensional form is:

$$\frac{\partial^2 \eta(X)}{\partial \lambda^2} = C_1 \frac{\partial^2 X}{\partial \tau^2} \tag{IV.66}$$

Here η is nondimensional tensile force, X is elongational deformation, λ is one dimensional space coordinate (Eulerian), and τ it time. Upon substitution of Hookean elasticity,

$$\eta(X) = X - 1 \tag{IV.67}$$

For $\eta(X)$, the authors[95] obtained the wave equation:

$$\frac{\partial^2 X}{\partial \lambda^2} = C_1 \frac{\partial^2 X}{\partial \tau^2} \tag{IV.68}$$

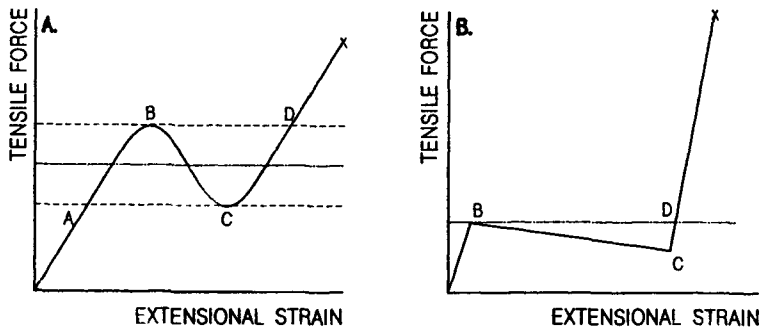

Figure IV.32: *Schematic representation of the type of relationship between tensile force and extensional strain necessary for a neck formation. A. for "rheological" theories*[82,94], *B. for the solution by S. Kase and M. Chang.*[95]

C_1 stands here for the inertia coefficient. Equation IV.68 is applicable to very fast plastic deformation problems, for example, determination of damage done by bullets. In the dynamic plasticity, the equation is used in somewhat different form:

$$V^2 \frac{\partial^2 u}{\partial \lambda^2} = \frac{\partial^2 u}{\partial \tau^2} \tag{IV.69}$$

$$V^2 = \frac{1}{\rho} \frac{d\eta(X)}{dX} \tag{IV.69 a}$$

where

$$X = \frac{\partial u}{\partial \lambda} \tag{IV.70}$$

where λ is one-dimensional Langrangean space coordinate, τ is time, u is displacement, ρ is material density, and η represents true compressive stress, X is infinitesimal deformation, V is wave velocity dependent on X. Equation IV.68 becomes equivalent to equations IV.69 – IV.70 when ρ in equation IV.69a is replaced with C_1. Then equation IV.69 represents the wave propagation at a velocity dependent on X:

$$V = \sqrt{\frac{1}{C_1} \frac{d\eta(X)}{dX}} \tag{IV.71}$$

At this point, Kase and Chang[95] draw the analogy to a very strong impact imposed on an aluminum rod, which produces two waves (see figure IV.33). The elastic wave A is propagating with the speed of sound in the material. The plastic wave B is moving with velocity V represented by equation IV.69, much slower than velocity of sound. In the form of wave A, the material is free of stress, between the waves A and B it is in an elastic compression, and it is in a plastic compression behind the yield form represented by wave B.

Kase and Chang[95] solved equation IV.69 numerically, the solution method is described in detail in the original paper. When for the solution was used a

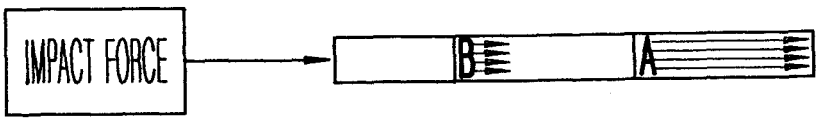

Figure IV.33: *Elastic wave A and plastic wave B propagating in an aluminum rod. Reproduced after Kase and Chang.*[95]

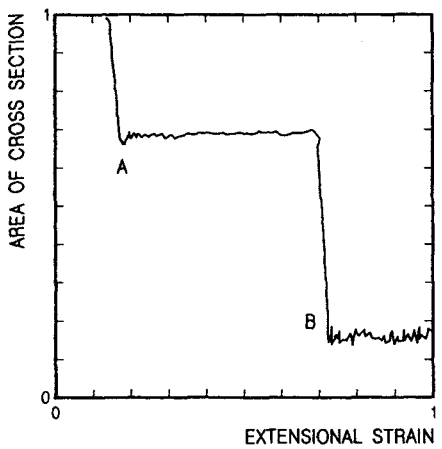

Figure IV.34: *Relationship between the extensional strain and the cross sectional area of a filament (both values nondimensional) resulting from equation IV.69 when constitutive function of figure IV.32B was used, including plasticity hysteresis. From Kase and Chang.*[95]

constitutive curve, like that in figure IV.33A the resulting description of necking represented a smoothly wavy curve. When a constitutive equation of the form given in figure IV.32 B was used, a representation of an abrupt, step change of the cross section area resulted. Such a curve is reproduced in figure IV.34 The calculations were done for the case of poly(ethylene terephthalate) with the sound velocity in the polymer of $v = \sqrt{E/\rho} = 1350\ m/s$.

The smoothness of the numerical calculation was greatly improved by the introduction of the plasticity hysteresis curve into the $\eta_{|}(X)$ function of figure IV.32 Without the consideration of the plasticity hysteresis, the obtained curves showed excessive noise.

The process of cold drawing still cannot be considered solved. Approximately at the same time when Kase and Chang published their paper, A. I. Leonov[96] published a derivation of the S-shape constitutive curve as resulting from surface tension. For now, there appears to be slightly too many theories that make sense and still lack of a definite one. Rather intensive work on the subject is being continued, new papers bring additional contributions, however, a definite solution

appears to be still a number of years away. Oleinik and co-workers[97,98] find that the initiation of drawing yield is governed by several different mechanisms, which may well explain the difficulties in finding a general solution. Also, the majority of the work published, understandably, is concerned with drawing at relatively low, or very low, velocities, which are closer to testing conditions than to industrial cold drawing processes.

Among the more interesting observations one is compelled to quote those by R. N. Howard[99,100], which offer a relatively simple solution. According to this proposal, cold drawing, particularly the post yield part of it may be described by a combination of the Gauss equation

$$\sigma_{true} = Y + G_p\left(\lambda^2 - \frac{1}{\lambda}\right) \tag{IV.72}$$

and the Eyring equation

$$\frac{1}{\lambda}\cdot\frac{d\lambda}{dt} \propto \exp\left[\left(\frac{E_0}{kT}\right) \times \sinh\left(\frac{\alpha\sigma}{kT}\right)\right] \tag{IV.73}$$

which has been simplified for isothermal cases to

$$\frac{1}{\lambda}\cdot\frac{d\lambda}{dt} = A\exp(B\sigma) \tag{IV.73 a}$$

where σ stands for true stress, Y is yield stress (extrapolated), G_p is the strain hardening modulus, $\lambda = l/l_0$ is extension ratio, α is a constant with dimension of volume, A and B are constants. The resulting new Gauss-Eyring equation is

$$\frac{d}{d\lambda}\left[\ln\left(\frac{1}{\lambda}\times\frac{d\lambda}{dt}\right)\right] = B\left[\sigma_0 - G_p\left(2\lambda + \frac{1}{\lambda^2}\right)\right] = I_n \tag{IV.74}$$

Here σ_0 is initial, "engineering" stress, and I_n has been named the *localization index*, as it determines if the rate of strain in a segment increases or decreases with the increasing strain under applied load or stress. At the beginning of the deformation at λ close to unity, equation IV.74 may be approximated by

$$I_{n(\lambda\approx 1)} = B(\sigma_0 - 3G_p) \tag{IV.75}$$

The constant B under isothermal conditions is equivalent to α, and B together with G_p and with the applied stress, σ_0, determine the mode of deformation. Also, at the beginning of a constant load or constant rate of extension, σ_0 may be identified with the yield stress. This is helpful in determining the ratio of Y/G_p. Necking has been determined by Considere[101] and Vincent[102] to occur when $Y/G_p = 3$.

The localization index initially rises, at the yield point it passes through zero and then turns negative above the critical value of λ, designated as λ_c. Such a course of events is characteristic for a stable necking. On the other hand, with the decreasing strain rate the yield strain increases.[110]

The rate of strain in the neck rises initially and later starts to fall. The point where the rate of strain reaches the value it has in the undeformed material determines the *natural draw ratio*, λ_D. This point coincides with the point where the engineering stress reaches again the value it has at the yield point. The value of λ_c may be calculated according to the equation:

$$Y/G_p = 2\lambda + 1/\lambda^2 \tag{IV.76}$$

The strain hardening modulus, G_p, depends on the molecular mass and it is independent on crystallinity. Several authors[103,107] have found that the materials with a higher molecular mass show a lower natural draw ratio and the molecular mass increases the strain hardening modulus.[109,100]

An approach similar to that by R. N. Howard has been taken later by other authors[132,133] with basically similar conclusions.

An interesting interrelation between the draw ratio, λ, and temperature has been reported by Butler *et al.*[111] The authors distinguish four drawing areas:

1. At very small final strains, smaller than the yield point, the drawing tension and the location of the draw zone fluctuate, a nonuniform cross section fiber is obtained.

2. At somewhat higher strains, one reaches a point "where the entire length of the fiber undergoes a drawing". If the final strain in this area is insufficiently high, the fiber may still show some diameter nonuniformities. The tension fluctuations are here less than in zone 1. The highest strain for this area produces the most uniform fibers, the necking is well defined, the tension fluctuations are at a minimum.

3. As the strain is further increased, the extension takes place in the neck and beyond, therefore, a second stage of drawing is formed, (*post yield draw*). A wide range of draw ratios is possible in this area.

4. With further increase of the draw ratio, the necking area becomes unstable. The obtained fibers may still be uniform and of a considerable strength. The drawing conditions here are poorly defined and the process is not under full control, as is the reproducibility.

The delineation of the different drawing zones depends on the temperature, at lower temperatures, the transition between zones two and three shift toward higher draw ratios. In the view of the authors,[111] if the draw ratio enters in the third area, the process should be conducted in two steps for optimum effects in the drawing operation: one strictly neck drawing to the natural draw ratio, and in a separate step the post yield drawing with a separate temperature and tension control.

The above quoted continuum theories represent a fair approximation of the described process. Whether substantial further progress will be made on this path may be debatable. Kasai and Kakudo[112] conducted a very detailed X-ray study of

the neck zone. A three millimeter thick rod was drawn to a ratio of 7.5. The neck area has been sectioned to 0.3 mm thick slices, and the so obtained specimens were investigated small segment by a small segment along the material stream lines with micro X-ray equipment. Naturally, only the fate of the crystalline portion of the material was studied.

The process, in the investigated specimen started with aligning the a-crystallographic axis nearly perpendicularly to the stream lines, and subsequently the c-crystallographic axis started to align along the stream lines. Similar conclusions had been reached earlier by Aggarval and co - workers[113] Initially, along the center line, the crystallite size remains unchanged, while in the side stream lines, the crystallite size increases. The degree of the increase becomes gradually larger when moving from the center to the specimen surface. In the later stages of the process, the crystallite size decreases, and when the orientation of the c- axis is almost exactly parallel, the crystallite size is about half of its original size. Similar work was performed later by Kuksyenko *et al.*[114] and the authors essentially reiterated the conclusions drawn by Kasai and Kakudo.

Whatever conclusions have been reached[113,114], they relate to the highly crystalline materials drawn under one set of conditions. The process for low crystalline materials is thus far not exactly known. Nonetheless, based on the above quoted studies one may doubt whether continuum theories may be the appropriate tool to describe the process. The structural aspects of cold drawing will be discussed in more detail in the chapter on fiber structure.

From the structural studies, it results that the drawing process affects primarily the noncrystalline portion of the polymer. According the the classical rubber elasticity theory[115], it is known that the drawing process decreases entropy; it is a decrease of the configurational entropy associated with the molecule orientation.

$$-\Delta S_c = \left(\frac{R}{2\alpha}\right)\left[\lambda^2 + \left(\frac{2}{\lambda}\right) - 3\right] \tag{IV.77}$$

where α is the number of monomer units between entanglements, and λ is the draw ratio.

One of the effects of the entropy change is an increase of melting point due to drawing.[116] *and ref.* Equation IV.75 has been combined[116] with the equations for the melting point of folded chain crystals to yield

$$\frac{1}{T_m} - \frac{1}{T_m^0} = \left(\frac{RT_m^0}{2x\alpha T_m \Delta H}\right)\left[\lambda^2 + \left(\frac{2}{\lambda}\right) - -3\right] \tag{IV.78}$$

where x is the degree of polymerization, and the remaining symbols have their traditional meaning. For polyethylene, the slope of the reciprocal melting point *versus* the drawing term, $\lambda^2 + 2/\lambda - 3$, has been found to be 4.9×10^{-8} deg K^{-1}. This influence is so small that for the majority of the commercially drawn fibers it may easily be neglected.

Very recent studies[144] & *ref.* relate the drawability, particularly the more extensive draw ratios, and the drawing performance to the α_c relaxation corresponding

to the Peterlin's T_α temperature (see section II.2.b). The α_c relaxation indicates the onset of translational motion of the polymer chains along the *c*- crystalline axis. It is quite obvious that it must strongly depend on the structure of the polymer chain. Large side groups are able to suppress the translational motions down to zero, which results in so called *crystal - fixed polymers*[144], or otherwise *nonductile crystals.* Strong hydrogen bonds have a similar effect, like in nylons. High molecular mass polymers theoretically permit more extensive drawing. Chain entanglements also suppress the α_c transition. Since long chains are more apt to high entanglements, the high molecular mass polymers not always may be drawn more intensively. Increase of temperature causes increase of the crystalline α_c relaxation. Hu and Schmidt - Rohr[144] stipulate that drawing involving chain translations is possible when the rate of α_c transition is larger than $10^3/s$. Nonetheless, extensive chain entanglement may suppress the drawability even at temperatures close to crystal melting. Strain rate has an effect similar to temperature,[107,144–148] activation energies of extensional flow and the activation energy of α_c relaxation are of a similar magnitude.

According to Hu and Schmidt - Rohr[144] drawing of polymers with nonductile or low ductile crystals is possible through deformation of amorphous areas, breakdown of crystalline lamellae, partial unwinding of some chains from the mosaic block surfaces, and sliding of the fibrils, that is, by the mechanisms considered for the classical fiber formation processes. Depending on the polymer and a particular morphology, the maximum of the achievable drawing without chain translational motion may be taken as no more than seven times.[144]

The extensive drawing is essential to the processes like solid state extrusion, gel - spun fibers or fibers formed from solution.

IV.6.b Results of Cold Drawing

As a result of cold drawing, the fiber density increases, and in connection with the changes of the entropy, the glass transition temperature also changes.[117] For poly(ethylene terephthalate), glass transition decreases with draw ratio to reach a minimum at $\lambda = 1.5$, later it increases to reach a maximum at $\lambda = 2$ to $2,5$, then further decreases monotonically. The density decreases with the draw ratio to a minimum at $\lambda = 1,5$, where the glass transition has a maximum, but later the density increases monotonically with increasing draw ratio. At very high draw ratios, the density may start to decrease again; if so, this is due to a micro void formation.

As the density increases with draw ratio, so increases the contents of the *trans* configuration of the polymer chains. The last fact indicates that initially the structure is less oriented than in the undrawn material, while at $\lambda > 2$ the amorphous molecules become more and more oriented along the fiber axis and also become more densely packed. These results appear to be in good accord with the X- ray investigations.

Glass transition is believed to be a phenomenon related to the relaxation,

a freezing/unfreezing of micro-Brownian motions, that is being explained either through the free volume theory or through changes in the configurational entropy. Recently the latter explanation seems to be gaining more acceptance.

G. Adam and J. H. Gibbs[118] give the following relationship between relaxation time, τ, and configurational entropy, S_c:

$$\tau = \frac{A}{T \cdot S_c} \tag{IV.79}$$

Configurational entropy is considered to consist of two parts[119]

$$S_c = S_{c1} + S_{c2} \tag{IV.80}$$

where S_{c1} is the entropy associated with the configuration of the molecular chain and S_{c2} is the entropy connected with the intermolecular interaction. Thus, S_{c1} is this portion of configurational entropy, which is sensitive to orientation.

A very significant effect of a cold drawing is the generation of heat. The amount of heat developed due to the mechanical work of drawing may be calculated from[120]

$$W_D = F_D v t_n \tag{IV.81}$$

Here W_D - mechanical work of drawing, F_D - drawing force, v - velocity of drawing, and t_n is the time the material spends in the neck.

Using the AGA Thermovision instrument, J. W. Maher *et al.*[120] have investigated the temperature distribution in a necking zone (figure IV.35). The filament temperature starts increasing at the same point where the filament starts necking, but the *hot spot*, the area where apparently the maximum of heat is developed, is close to the beginning of the necking. It is removed from the beginning of the onset of necking by about one half of the radius of undrawn fiber. The temperature decreases from this spot much faster toward the fiber surface and much slower along the fiber axis.

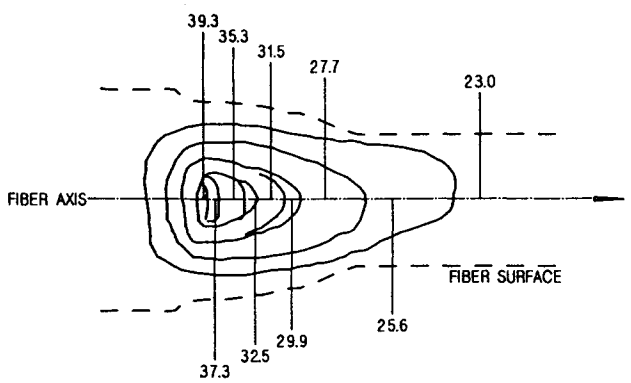

Figure IV.35: *Schematic representation of the temperature distribution in necking. Temperature given in* deg C. *Polymer: polycarbonate. After J. W. Maher et al.*[120]

As there is no reservation to the interesting experimental results, it is difficult to reconcile them with the X-ray investigations of the changes in the crystalline structure mentioned above. There is no doubt that a very large role is being played by the heat losses. Although the authors devote much space to the estimation of such losses, the considerations appear to be grossly incomplete, especially, as no heat conduction within the filament was considered. One may suspect that the heat develops uniformly along the fiber radius, or perhaps even more toward the surface (in agreement with the X-ray results). The net result in the form of a *hot spot* in the center of the fiber seems to be the effect of the heat losses to the filament surface. As usual, heat transfer along the fiber axis is negligible; the extension of the temperature map downstream is a probable result of the mass movement and of the radial heat transfer.

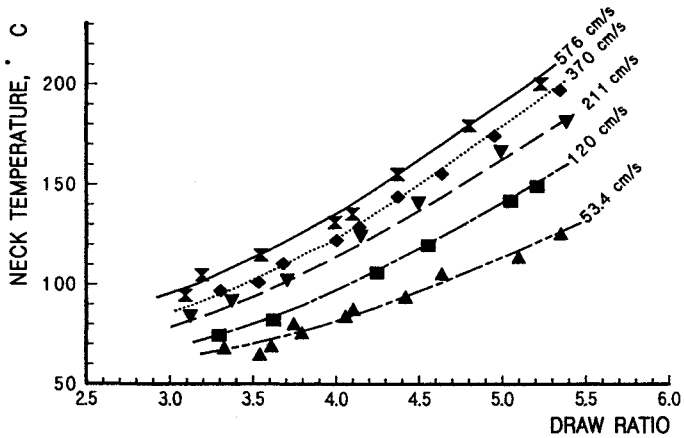

Figure IV.36: *Maximum temperature of necking zone during drawing of nylon 66 to various draw ratios. Drawing velocity in* $cm \cdot s^{-1}$ *given as parameter. Data quoted after Badami et al.*[127]

Exactly how large a role heat transfer plays in necking may be seen in an older work on a determination of the "wholesale" neck temperature in nylon 66.[127] Figure IV.36 presents neck temperature as it depends on the draw ratio and the drawing velocity which is given as a parameter. The figure speaks very loudly about the paramount role of heat exchange in the process. The rate of drawing — *ergo* the heat development, and of the drawing velocity – *ergo* time for the heat transport. Naturally, a balance of these two decides about the final effect.

Some portion of the drawing energy is spent on the bond rupturing. A study of bond rupture in polyethylene[121] shows that the total number of bonds broken in the polymer ranges from 5×10^{17} to $4 \times 10^{18} cm^{-3}$ in drawing at ambient temperature. Though, the values represent only 10^{-3} to 10^{-2} per cent of the total number of backbone bonds. The number is not large, but considering the associated decrease of molecular mass, it is not necessarily negligible. What is more important, in place of the broken bonds, various characteristic groups are formed, mostly carbonyl and vinyl, and it certainly does have an effect on the

fiber properties. It is necessary to take into account that the bond rupture process occurs mainly in the amorphous areas, that is, the tie and link molecules are broken — this weakens the fiber. Here the proportion of breaks to the total number of tie and link molecules is much larger.

The real purpose of this additional operation in fiber formation, of cold drawing, is improvement of physical properties of fibers. As a result of cold drawing, the tensile properties of fibers increase, and this at the expense of transverse properties; e.g., as the tensile strength goes up the abrasion resistance of fiber goes down. On the other hand, an undrawn fiber is mechanically fragile, its dimensions are unstable, it may be easily deformed. And this, from the utility stand point, is highly undesirable. The problem of effects of cold drawing on fiber properties will be discussed in more detail in chapter on fiber properties.

IV.6.c Orientation

The term *orientation* has already been mentioned above several times. Under this term we understand the description of the position of polymer crystals in relation to the fiber longitudinal axis. This is, however only a part of the notion, the *crystalline orientation.* The second part is *amorphous orientation.*

The notion of *amorphous orientation* is somewhat more difficult to define, one may even call it little nebulous. As polymer crystallizes in lammelar fashion, each lamella contains two fold surfaces. The fold surfaces consist of noncrystalline polymer chains looping back and forth, from a crystalline segment and back to a crystalline segment. If the folds were perfectly regular, they would form semicircles and the average orientation between the two fold surfaces would be perfectly circular, or random, without a preferred directionality.

In reality we have also tie molecules spanning from one lamella to another, as well as stretches of polymer chains which, for one reason or another, are not involved in a crystalline lattice. Thus, when we speak of the amorphous orientation, we refer to the irregularities of the fold sites and of the other chain segments, or of whole chains, which are not involved in the crystalline lattice. This type of orientation cannot be measured directly and unambiguously with the analytical techniques available thus far. Only indirect methods are available.

The crystalline orientation is relatively easy to define. It is the degree of alignment of the c - crystalline axis with the fiber axis. Why the c - axis? Because the polymer chains are always aligned parallel, as accurately as the bond angles permit, to the c - crystalline axis. In some cases, the molecules assume a regularly coiled conformation, then the axis of the coil is aligned parallel to the c - axis.

Direction of the crystalline axes may be determined from X-ray diffractograms, and is usually described by $\cos^2 \sigma$. Since we normally deal with a multiplicity of crystals, we must speak of an average orientation $\langle \cos^2 \sigma \rangle$. Here σ is the angle between the c-axis and the fiber axis z. This parameter is evaluated in terms of the orientation of the crystalline lattice plane normals, expressed also in terms of the cosine square. As the angles are used here the angles between the fiber axis

and the normal to a set of *hkl* crystallographic planes (see figure IV.37). The direction of the normal, P, is specified by the angles ϕ and ψ.

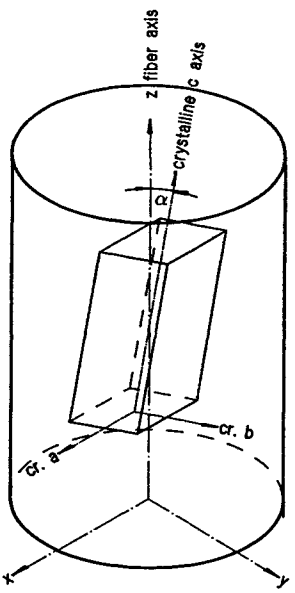

Figure IV.37: *Schematic representation of a crystalline c-axis orientation in relation to the fiber axis z as specified by the angle σ.*

Orientation may be determined from X-ray diffractograms by use of the following set of relations:[122,123]

$$\langle \cos^2 \phi \rangle = \frac{\int_0^{\pi/2} \int_0^{\pi/2} I(\phi, \psi) \cos^2 \phi \sin \phi d\psi d\phi}{\int_0^{\pi/2} \int_0^{\pi/2} I(\phi, \psi) \sin \phi d\psi d\phi} = \frac{\int_0^{\pi/2} I(\phi) \cos^2 \phi \sin \phi d\phi}{\int_0^{\pi/2} I(\phi) \sin \phi d\phi} \tag{IV.82}$$

$$I(\phi) = \int_0^{\pi/2} I(\phi, psi) d\psi \tag{IV.83}$$

$$\langle \cos^2 \sigma \rangle = 1 - \frac{(1 - 2\sin^2 \rho_2)\langle \cos^2 \phi_1 \rangle - (1 - \sin^2 \rho_1)\langle \cos^2 \phi_2 \rangle}{\sin^2 \rho_1 - \sin^2 \rho_2} \tag{IV.84}$$

Here the subscripts 1 and 2 refer to the two considered planes, and ρ is the angle between a plane normal and b-axis. The values of ρ are normally determined from the crystallographic analysis, and they are usually tabulated in literature on crystallographic data.

The determination of orientation by the $\langle \cos^2 \phi \rangle$ is limited, as for a perfectly parallel alignment it is unity and for c-axis normal (90 deg) to the fiber axis it

is zero. To move the description of the orientation closer to the physical reality, Hermans and Platzek[124] have developed the so called *orientation distribution function*, f:

$$f = 1 - \frac{3\sin^2\phi}{2} \equiv \frac{3\langle\cos^2\phi\rangle - 1}{2} \tag{IV.85}$$

According to this designation, a perfect alignment of c-axis with the fiber axis gives $f = 1$, an orientation of c-axis normal (90 deg) to the fiber axis gives $f = -0.5$, while a completely random distribution of the angles results if $f = 0$.

The orientation angle, as well as the distribution function, may be determined in relation to all three Cartesian axes. In such case $f_x + f_y + f_z = 0$.

Use of the orientation distribution function is particularly convenient for fibers with a low or moderate degree of orientation.

Besides wide angle X-ray diffraction and low angle X-ray scattering, there are several other methods of determining orientation in polymeric materials. Perhaps the simplest in execution and the most commonly used is determination of the optical birefringence. The method is based on the measurement of the refractive index difference in both the direction of fiber axis and perpendicular to it. Nevertheless, the birefringence is not a singular property determined by one factor only. In general, one may describe it as follows:

$$\Delta n = \sum \phi_i \Delta n_i^{phase} + \Delta n_f + \Delta n_\varepsilon \tag{IV.86}$$

where ϕ means volume fraction of different phase material. Birefringence may vary according to phase: crystalline, paracrystalline, amorphous, variable density, leave alone additives. Further, Δn_f represents birefringence of form: it is variations arising on the boundaries of phases or when the electric field, or dipole, is distorted by whatever cause. Δn_ε represents changes of the birefringence due to strain, a factor influencing the birefringence very strongly.

The orientation distribution function, f, (equation IV.85) is equal to the ratio of a specimen birefringe over the maximum obtainable birefringence for a given polymer. The last number represents a calculated quantity, which may be found tabulated in literature. Occasionally it happens, however, that highly drawn fibers show birefringence higher than the theoretical maximum. If this happens, it indicates invariably the presence of frozen internal stresses, and if so, the measured values must be deemed as quite useless.

Separation of the different reasons for change in birefringence is very difficult, often outright impossible. This, in combination with the relative simplicity of the determinations cause this method of orientation determination to be highly overused, which leads to many misinterpretations. A method of "micro determination" of birefringence, that is, variation of birefringence along fiber radius may offer some help in this respect. This method was proposed by Beier and Schollmeyer.[126]

Another way to determine orientation is by way of measurement of infrared (IR) dichroism. Certain bands in the IR spectrum, which are not affected by molecule conformation, may absorb polarized IR radiation selectively in a certain

plane. If such bands are present in a polymer, one may measure the ratio of intensity of polarized infrared light transmitted to the incident beam, when the measurements of the polarization direction are made in both perpendicular and parallel directions to the fiber axis. A dichroic ratio may be calculated as

$$R = \frac{\ln(I_0/I_{\|})}{\ln(I_0/I_{\perp})} \tag{IV.87}$$

where I_0 is the intensity of the incident beam, and $I_{\|}$ and $I_{\perp}$ are the intensities of the transmitted light parallel and perpendicular to the fiber axis. From the dichroic ratio, R, one may calculate the orientation function distribution:

$$f = \frac{(R-1)(R^{\infty}+2)}{(R^{\infty}-1)(R+2)} \tag{IV.88}$$

R^{∞}, the dichroic ratio for the perfect orientation may be calculated when the dipole connected to a specific group in oriented polymer oscillates at a right angle to the polymer chain axis.

Still another way of determining orientation is based on the fact that sound velocity in a material depends on the distances between atoms. Usually the distances in the main chain backbone differ from the distances between atoms of the neighbor polymer chains. For determination of orientation, it is necessary to know the sound velocity parallel and perpendicular to the fiber axis for the case of perfectly oriented polymer. Velocity parallel for polymers usually ranges between some 7 and $10 km/s$. The parallel velocity is usually either calculated theoretically or just estimated. The general relationship for the velocities is:[125]

$$\frac{1}{c^4} = \frac{1-\langle\cos^2\phi\rangle}{c_{\perp}^2} + \frac{\langle\cos^2\phi\rangle}{c_{\|}^2} \tag{IV.89}$$

In a completely random sample, when $f = 0$, according to equation IV.85 $\langle\cos^2\phi\rangle = 1/3$. Substituting this value into equation IV.89 gives

$$c_{\perp}^2 = \frac{2c_{\circ}^2 c_{\|}^2}{3c_{\|}^2 - c_{\circ}^2} \tag{IV.90}$$

In the above equations, c is velocity of sound, subscripts $\|$, $\perp$, and $\circ$ mean parallel, perpendicular, and randomly oriented, respectively. Since in all cases known so far $3c_{\|}^2 \gg c_{\circ}^2$ applies, then the value of perpendicular velocity calculated from an assumed value of parallel velocity and equation IV.90 is relatively little sensitive to the assumed value of parallel velocity, if it is the case. In view of this, equation IV.90 simplifies to:

$$c_{\perp}^2 = \frac{2c_{\circ}^2}{3} \tag{IV.91}$$

and equation IV.89 simplifies to

$$\frac{1}{c^2} = \frac{1-\langle\cos^2\sigma\rangle}{c_{\|}^2} \tag{IV.92}$$

In the end, the orientation distribution factor is:

$$f = 1 - \frac{c_\circ^2}{c^2} \tag{IV.93}$$

All the methods described, besides X-ray, give orientation of both crystalline and amorphous material. All of the methods are more or less sensitive to any residual stresses. To separate the crystalline and amorphous components, one must have X-ray determination plus analysis by any of the other techniques.

IV.7 Annealing

That crystals may be annealed, as well as what kind of changes the annealing process triggers, was mentioned in the section on polymer crystals. In fiber formation, advantage is taken of the annealing. Mostly it is done immediately after cold drawing, or sometimes it is considered even as an additional step of the cold drawing operation. The drawn fibers are crystalline structures which are oriented, and the orientation adds one more dimension to the annealing process.

Oriented structures may be annealed in two different ways: with or without a dimensional restrain. If the annealing process is conducted without the dimensional restrain, the fiber will shrink, and the shrinkage will increase with the increasing draw ratios and annealing temperature, but will decrease with increasing drawing temperature. If the shrinkage is prevented by mechanical restrain, there are still changes in the fiber structure that take place, though the changes will be somewhat different, and their influence on the material properties will also be different.

A fiber annealed with restrain will, obviously, not shrink, but crystalline orientation will decrease, and amorphous orientation usually decreases even more. Without restrain, all other conditions being equal, the *disorientations* are much larger, particularly the crystalline one.

The fiber's succeptibility, if one may call it so, to annealing depends strongly on the relationship of the temperature of original crystallization and temperature of cold drawing on one side, and on the temperature and time of annealing on the other side.

In some sense, annealing may be treated as a kind of "preshrinking", a way to prevent fiber shrinkage in its final use. Such treatment, however, is accompanied by change of another fiber properties, like tenacity, moduli, especially the initial modulus, orientation, density, dying characteristic, *etc.* A slight extension during annealing, sometimes treated as an additional drawing step, often prevents an excessive decrease of properties with a simultaneous gain in thermal stability of the fiber.

Every annealing process, irrespectively of restrain or lack of it, always leads to an increase in crystalline melting point of the polymer.

It may seem convenient to anneal fibers in a continuous operation with drawing, but this creates problems of its own. The annealing process is slow and therefore

it may be difficult to accommodate it in one line with the contemporary fast processes. A way to overcome such difficulties to some extent may be to apply a so called *heat shock*. This means application of high temperature, often above crystalline melting point, but over a short time. One may consider it as intensification of heat transfer to the fiber. In the same vein, a steam atmosphere may be applied in the annealing process.[128] Even liquids, like silicone oils and similar, have been applied for the same purpose.[129]

IV.8 References

1. Z. K. Walczak, *paper presented at the 70-th Annual A.I.Ch.E. Meeting*, Atlantic City, **Sept. 1, 1971**; *J. Appl. Polymer Sci.*, **17 (1973)**, 153. 1
2. R. Farber and J. Dealy, *Polymer Eng. Sci.*, **14 (1974)**, 435.
3. W. W. Grassley, *Adv. Polymer Sci.*, **16 (1974)**, 1.
4. S. F. Edwards, *J. Phys. A, Gen. Phys.*, **1 (1968)**, 15; P. G. de Gennes, *J. Chem. Phys.*, **55 (1971)**, 572; M. Doi, S. F. Edwards: *The Theory of Polymer Dynamics*, Oxford Univ. Press, Oxford, 1986.
5. H.-G. Elias, *Macromol. Chem., Phys.*, **195 (1994)**, 3117.
6. R. P. Wool, *Macromolecules*, **26 (1993)**, 1564.
7. S. Wu, *J. Polymer Sci.: B. Polymer Phys.*, **27 (1989)**, 723.
8. C. D. Han and K. U. Kim, *Polymer Eng. Sci.*, **11(1971)**, 395.
9. C. D. Han, *J. Appl. Polymer Sci.*, **17 (1973)**, 1403. 9
10. E. B. Bagley, *J. Appl. Phys.*, **28 (1957)**, 624.
11. C. D. Han and R. R. Lamonte, *Polymer Eng. Sci.*, **11 (1971)**, 385.
12. Z. K. Walczak: *Formation of Synthetic Fibers*, Gordon and Breach, London - New York, 1977, p. 55.
13. Z. K. Walczak, *J. Appl. Polymer Sci.*, **17 (1973)**, 169, 177.
14. P. J. Hendra, M. A. Taylor, H. A. Willis, *J. Polymer Sci.: Pt. C: Polymer Letters*, **24 (1986)**, 83.
15. P. Massa, A. Ten Bosch, P. Sixou, *J. Polymer Sci., Polymer Letters*, **21 (1983)**, 757.
16. A. Ziabicki: *Fizyka procesw formowania włókna*, Wydawnictwa Naukowo-Techniczne, Warszawa, 1970 (in Polish). (Physics of fiber formation processes)
17. A. Ziabicki: *Fundamentals of Fibre Formation*, John Wiley & Sons, New York - London - Sydney, 1976.
18. H. Nitschmann and J. Schrade, *Helv. Chim. Acta*, **31 (1948)**, 297.
19. F. T. Trouton, *Proc. Royal Soc. (London)*, **A77 (1906)**, 426.
20. N. Hirai, *J. Chem. Soc. Japan*, **75 (1954)**, 1021.
21. R. Gatoh, A. Aida, S. Hayashi, and N. Hirai, *Rheol. Acta*, **1 (1958)**, 213.
22. G. Fano, *Arch. fisiol.*, **5 (1908)**, 365.
23. M. Zidan, *Rheol. Acta*, **8 (1969)**, 89.
24. C. J. S. Petrie: *Elongational flows*, Pitman Publ., London, 1979.

25. F. N. Cogswell, *J. Non - Newtonian Fluid Mechanics*, **4 (1978)**, 23.

26. B. H. Bersted, *Polymer Eng. Sci.*, **33 (1993)**, 1079.

27. S. Goldstein: *Modern Developments in Fluid Mechanics*, Oxford University Press, London, 1952.

28. S. Zahorski in *Theoretical Rheology*, in J. F. Hutton, J. R. A. Pearson and K. Walters (Eds.), Appl. Science Publ., London, 1975, p. 40.

29. M. Reiner and A. Freudenthal, *Proc. of Fifth International Congress on Applied Mechanics*, 1938.

30. A. Kaye, D. G. Vale, *Rheol. Acta*, **8 (1969)**, 1.

31. N. V. Tschoegl, *Phenomenological Theory of Linear Viscoelastic Behavior*,Springer Verlag, Berlin - Heidelberg - New York, 1989.

32. G. V. Vinogradow, A. Ya. Mal'kin: *Reol'ogiya polimerov* (Rheology of Polymers), Izdatelstvo Chimiya, Moskva, 1977; *Rheology of Polymers*, Springer Verlag, Berlin - Heidelbeg - New York, 1980.

33. G. V. Vinogradov, V. D. Fikhman, B. V. Radushkevich, and A. Ya. Mal'kin, *J. Polymer Sci., Pt. A - 2*, **8 (1970)**, 657.

34. V. A. Kargin and T. I. Sogol'ova, *Zh. Phiz, Khim.*, **23 (1949)**, 540.

35. T. Alfrey: *Mechanical Behavior of High Polymers*, Interscience Publ., New York, 1948.

36. G. V. Vinogradov, *Rheol. Acta*,**12 (1975)**, 557; **14 (1975)**, 942.

37. T. L. Smith, *J. Polymer Sci*, **32 (1958)**, 99.

38. E. Orowan, *Rep. Prog. Phys.*, **12 (1949)**, 186.

39. H. Chung and A. S. Lodge, *Rheol. Acta*, **10 (1971)**, 448; **11 (1972)**, 127.

40. Y. Ide and J. L. White, *J. Appl, Polymer Sci.*, **20 (1976)**, 2511.

41. Y. Ide and J. L. White, *J. Non-Newtonian Fluid Mech.*, **2 (1977)**, 281.

42. D. Acierno, F. P. La Mantia, G. Iorio, G. Marucci, *J. Non- Newtonian Fluid Mech.*, **4 (1978)**, 99.

43. G. Marucci, G. Titomanlio, and G. C. Sarti, *Rheol. Acta*, **12 (1973**, 269.

44. D. Acierno, F. P. La Mantia, G. Marucci, and G. Titomanlio, *J. Non-Newtonian Fluid Mech.*, **1 (1976)**, 1.

45. D. Acierno, F. P. La Mantia, G. Marucci, and G. Titomanlio, *J. Non-Newtonian Fluid Mech.*, **1 (1976)**, 147.

46. D. Acierno, F. P. La Mantia, G. Marucci, and G. Titomanlio, *J. Non-Newtonian Fluid Mech.*, **2 (1977)**, 271.

47. J. Ferguson and N. E. Hudson, *Eur. Polymer J.*, **29 (1993)**, 141.

48. N. Phan - Thien and R. I. Tanner, *J. Non-Newtonian Fluid Mech.*, **2 (1977)**, 353.

49. N. Phan - Thien, *J. Rheology*, **22 (1978)**, 259.

50. J. A. Spearot, *PhD Dissertation*, University of Delaware, Newark, Delaware, **1972.**

51. G. R. Zeichner, *M. Ch. E. thesis*, University of Dalaware, Newark, Delaware, **1973.**

52. A. J. Stavermann and F. Schwartzl *Non Linear Deformation Behaviour of High Polymers*, in H. A. Stuart (Ed.):*Die Physik der Hochpolymeren*, Vol IV, chapter 2., Springer Verlag, Berlin - Heidelberg, New York, 1954.

53. K. Weissenberg, *cited in ref. 54, p.128.*

54. J. D. Ferry: *Viscoelestic Properties of Polymers*, John Wiley & Sons Publ., New York, 1980.

55. A. J. Stavermann and F. Schwartzl *Linear Behaviour of High Polymers*, in H. A. Stuart (Ed.):*Die Physik der Hochpolymeren*, Vol IV, chapter 1., pp. 59 ff., Springer Verlag, Berlin - Heidelberg, New York, 1954.

56. J. R. Clermont, J. M. Pierrad, and O. Scrivener, *J. Non- Newtonian Fluid Mech.*, **1 (1976)**, 175.

57. D. D. Goulden and W. C. MacSporran, *J. Non-Newtonian Fluid Mech.*, **1 (1976)**, 183.

58. R. Keunings, M. J. Crochet, and M. M. Denn, *Ind. Eng. Chem., Fundam.*, **22 (1983)**, 347.

59. M. A. Matovich and J. R. A. Pearson, *Ind. Eng. Chem., Fundam.*, **8 (1969)**, 512.

60. J. R. A. Pearson, and M. A. Matovich, *Ind. Eng. Chem., Fundam.*, **8 (1969)**, 605.

61. Y. T. Shah and J. R. A. Pearson, *Ind. Eng. Chem., Fundam.*, **11 (1972)**, 145.

62. J. R. A. Pearson and Y. T. Shah, *Ind. Eng. Chem., Fundam.*, **13 (1974)**, 134.

63. Ref. 25, pp. 199 ff.

64. G. V. Vinogradov, *Rheol. Acta*, **12 (1973)**, 273.

65. Jinan Cao, *J. Appl. Polymer Sci.*, **42 (1991)**, 143; **49 (1993)**, 1759.

66. K. Katayama, T. Amano, and K. Nakamura, *Appl. Polymer Symposia*, **20 (1973)**, 237.

67. A. Nowakowski, *Technology of Plastics and Synthetic Fibers*, Lectures at The Polytechnic of Łódź, 1953.

68. A. K. Van der Vegt and P. P. A. Smit, *Soc. Chem. Ind. (London), Monograph No. 26*, 1967, p. 313.

69. *ref. 12*, p. 100.

70. Z. K. Walczak, *unpublished results*, **(1976)**; *Thermal Bonding of Fibers*, Published by Kimberly-Clark Corp., 1992, p. 135.

71. G. A. Korn and T. M. Korn: *Mathematical Handbook for Scientists and Engineers*, McGraw Hill Publ., New York, 1961, Chapter 4.11-3, 8.7-1, 18.10-10, 20.3-6.

72. J. W. Cahn, *Acta Met.*, **10 (1962)**, 907.

73. J. E. Hilliard, in *Nucleation Phenomena*, ACS Publications, Washington, 1966, p. 77 ff.

74. K. Nakamura, T. Watanabe, K. Katayama, and T. Amano, *J. Appl. Polymer Sci.*, **16 (1972)**, 1077.

75. K. Nakamura, K. Katayama, and T, Amano, *J. Appl. Polymer Sci.*, **17 (1973)**, 1031.

76. A. Ziabicki, *Colloid Polym. Sci.*, **252 (1974)**, 207.

77. G. Eder and H. Janeschitz-Kriegl, *Colloid Polym. Sci.*, **266 (1988)**, 1087.

78. V. Brucato, S. Piccarolo, G. Titomanlio, *Makromol. Chem., Makromol. Symp.*, **68 (1993)**, 245.

79. A. Mehta, B. Wunderlich, *ACS Polymer Preprints*, **35 (1975)**, 393.

80. W. H. Carothers and J. W. Hill, *J. Am. Chem. Soc.*, **54 (1932)**, 1579.

81. F. H. Müller, *Kolloid Z.*, **114 (1949)**, 59; cit in *Die Physik der Hochpolymeren*, H. A. Stuart (Ed.), Springer Verlag, Berlin - Heidelberg - Wien, 1956, Vol. IV, p. 161.

82. E. Orowan, *Rep. Prog. Phys.*, **12 (1948)**, 185.

83. P. I. Vincent, *Polymer*, **1 (1960)**, 7.

84. A. Ziabicki, K. Kędzierska, *Kollid Z.*, **171 (1960)**, 51.

85. S. Kase, T. Matsuo, *J. Polym. Sci.*, **A3 (1965)**, 2541. 85

86. S. Kase, T. Matsuo, *J. Appl. Polymer Sci.*, **11 (1967)**, 251.

87. Y. Wada, A. Nakayama, *J. Appl. Polymer Sci.*, **15 (1971)**, 183.

88. J. L. Ericksen, *J. Elasticity*, **5 (1975)**, 191.

89. M. M. Denn, C. J. S. Petrie, P. Avenas, *AIChE J.*, **21 (1975)**, 791.

90. A. Considere, Ann. des pots des chausees, **ser. 6. No. 9**, 574.

91. B. Bernastein and L. J. Zapas, *J. Rheol.*, **25 (1981)**, 83.

92. B. Bernastein, E. A. Kearsley, and L. J. Zapas, *Trans. Soc. Rheol.*, **7 (1963)**, 391

93. B. D. Coleman and D. C. Newman, *J. Appl. Polymer Sci.*, **45 (1992)**, 997.

94. B. D. Coleman and D. C. Newman, *J. Polymer Sci., Pt. B, Polymer Physics*, **30 (1992)**, 25.

95. S. Kase, M. Chang, *Rheol. Acta*, **29 (1990)**, 46,

96. A. I. Leonov, *J. Rheol.*, **34 (1990)**, 155.

97. E. Oleinik, *Prog. Colloid Polym. Sci.*, **80 (1989)**, 140.

98. S. N. Rudnev, O. B. Salamantina, V. V. Vaenniy, and E. F. Oleinik, *Colloid Polym. Sci.*, **269 (1991)**, 460.

99. R. N. Howard, *Polymer*, **35 (1994)**, 3858.

100. R. N. Howard, *J. Polymer Sci, Pt B, Polymer Physics*, **3 (1995)**, 1481.

101. *cit in* A. Nadai, *The Theory of the Fracture and Flow of Solids*, McGraw - Hill, New York, 1950, p. 71.

102. P. I. Vincent, *Polymer*, **1 (1960)**, 7.

103. J. M. Andrews and I. M. Ward, *J. Mater. Sci.*, **5 (1970)**, 411.

104. J. S. Foot and I. M. Ward, *J. Mater. Sci.*, **10 (1975)**, 953.

105. F. Geleji, L. Koczy, I. Fulop, and G. Bodor, *J. Polymer Sci, Polymer Symp.*, **58 (1977)**, 253.

106. J. C. Engelaere, J. P. Cavrot, and F. Rietch, *Polymer*, **23 (1982)**, 766.

107. D. M. Sadler and P. J. Barham, *Polymer*, **31 (1990)**, 36.

108. P. I. Vincent, *Proc. Conf. Physical Basis of Yield and Fracture*, Oxford, 1966; Inst. of Physics and Phys. Soc., London, p. 155.

109. G. R. Williamson, B. Wright, and R. N. Haward, *J. Appl. Chem.*, **14 (1964)**, 131.

110. A. Marquez - Lucero, C. G'Sell, and K. W. Neale, *Polymer*, **30 (1989)**, 636.

111. R. H. Butler, D. C. Prevorsek, and Y. D. Kwon, *Polymer Eng. Sci.*, **2 (1982)**, 329.

112. N. Kasai and M. Kakudo, *J. Polymer Sci., Pt. A*, **2 (1964)**, 1955.

113. S. L. Aggarval, G. P. Tilley, and O. J. Sweeting, *J. Polymer Sci.*, **51 (1961)**, 551; *J. Appl. Polymer Sci.*, **1 (1959)**, 91.

114. V. S. Kuksyenko, S. Nizamidinov, and A. I. Slutsker, *Vysokomol. Soyed.*, **9 (1967)**, 91.
115. L. R. G. Treloar, *The Physics of Rubber Elasticity*, Oxford Univ. Press, London, 1975.
116. E. R. Story, J. N. Hay, *Polymer Communications*, **29 (1988)**, 9.
117. E. Ito and T. Hatakeyama, *J. Polymer Sci., Polymer Phys. Ed.*, **12 (1974)**, 1477.
118. G. Adam and J. H. Gibbs, *J. Chem. Phys.*, **43 (1965)**, 139.
119. T. Nose, *Polymer J.*, **2 (1971)**, 124; 427; 437.
120. J. W. Maher, R. N. Haward, and J. N. Hay, *J. Polymer Sci., Polymer Phys. Ed.*, **18 (1980)**, 2169.
121. C. L. Hammond, P. J. Hendra, B. G. Lator, W. F. Maddams, and H. A. Willis, *Polymer*, **29 (1988)**, 49.
122. O. Kratky, *Z. physik. Chem.*, **B50 (1941)**, 255.
123. Z. W. Wilchinsky, *J. Appl. Phys.*, **30 (1959)**, 792; **31 (1960)**, 1969; *Polymer*, **5 (1964)**, 271.
124. P. H. Hermans and P. Platzek, *Kolloid Z.*, **88 (1939)**, 68.
125. H.-G. Elias, *Macromolecules*, Plenum Press Publ., New York - London, 1984, p. 192 ff.
126. M. Beier and E. Schollmeyer, *Angew. Makromol. Chem.*, **128 (1984)**, 15.
127. D. V. Badami, F. P. Chappel, M. F. Culpin, D. Madoc Jones, and T. C. Tranter, *Rheol. Acta*, **1 (1961)**, 639.
128. P. H. Geil, *Polymer Single Crystals*, Interscience publ., New York, 1963, p. 424.
129. D. R. Buchanan and J. D. Dumbleton, *J. Polymer Sci., Pt. A-2*, **6 (1969)**, 113.
130. I. G. Voigt-Martin, *Adv. Polymer Sci.*, **67 (1985)**, 196.
131. M. Okamoto, H.Kubo, and T. Kataoka, *Polymer*, **39 (1998)**, 3135.
132. C. P. Buckley and D. P. Jones, *Polymer*, **36 (1998)**, 3301.
133. A. M. Adams, C. P. Buckley, and D. P. Jones, *Polymer*, **39 (1998)**, 5761.
134. J. W. H. Kolnaar, A. Keller, S. Seifert, C. Zschunke, and H. G. Zachmann, *Polymer*, **36 (1995)**, 3969.
135. J. Furukawa, *J. Appl. Polymer Sci.*, **57 (1995)**, 1085; 1095.
136. A. V. Pendse and J. R. Collier, *J. Appl. Polymer Sci.*, **59 (1996)**, 1305.
137. J. R. Collier, O. Romanoschi, and S, Petrovan, *J. Appl. Polymer Sci.*, **69 (1998)**, 2357.
138. W. A. Kernick III and N. J. Wagner, *Macromolecules*, **32 (1999)**, 1159.
139. M. M. Denn: *Process Modeling*, Longman – Wiley, London – New York, 1986.
140. B. M. Devereux, M. M. Denn, *Ind. Eng. Chem. Res.*, **33 (1994)**), 2384.
141. J.–F. Agassant, P. Avenas, J.–Ph. Sergent, P. J. Carreau: *Polymer Processing: Principles and Modelling*, Hanser Verlag, München, 1991.
142. G. Vassilatos, E. R. Schmelzer, and M. M. Denn, *Int. Polymer Process.*, **7 (1992)**, 144.
143. J. Fisher and D. Turnbull, *J. Chem. Phys.*, **17 (1949)**, 71.
144. W. G. Hu and K. Schmidt - Rohr, *Acta Polym.*, **50 (1999)**, 271.
145. I. F. Govaert and P. J. Lemstra, *Coll. Polymer Sci.*, **270 (1992)**, 455.

146. R. H. Boyd, *Polymer*, **26 (1988)**, 323.

147. S. Bensason, J. Minick, A. Moet, S. Chum, A. Hiltner, and E. Baer, *J. Polymer Sci., Part B, Polymer Phys.*, **34 (1996)**, 1301.

148. W. T. Mead and R. S. Porter, *J. Polymer Sci., Polymer Symp.*, **63 (1978)**, 289.

149. A. Ya. Malkin and C. J. S Petrie, *J. Rheol.*, **41 (1997)**, 1.

150. V. Tirtaamadja abd T. Sridhar, *J. Rheol.*, **39 (1995)**, 1133.

151. P. Flory, *Principles of Polymer Chemistry*, Cornell University Press, Ithaca, NY, 1953.

152. *ref. 54*, p. 262.

153. A. Mahendrasingam, C. Martin, F. Fuller, D. J. Blundell, R. J. Oldman, J. L. Harvie, D. H. MacKerron, C. Riekel, P. Engstrőm, *Polymer*, **40 (1999)**, 5553,

154. T. Asano, F. J. Baltá Calleja, A. Flores, M. Tanigaki, M. F. Mina, C. Sawatari, H. Itagaki, H. Takahashi, I, Hatta, *Polymer*,, **40 (1999)**, 6475.

155. Y. Termonia, *J. Polymer Sci., Pt. B, Polymer Phys.*, **38 (2000)**, 2422.

156. N. V. Tschoegl, *Phenomenological Theory of Linear Viscoelastic Behavior*,Springer Verlag, Berlin - Heidelberg - New York, 1989, Chapter 10.

V STRUCTURE OF FIBERS

A comparison of the physical properties of large, bulky objects with those of fibers made of the same polymer discloses surprisingly large differences: moduli, breaking stress, elongation at break. On the other hand, it has been said that the great majority of fiber formation processes is connected with some extent of cold drawing. It is known also that cold drawing introduces orientation into morphology of the drawn material. It results then that fibers must have an oriented structure.

Looking at the problem from still another point of view, we have to accept that though fibers are made so to develop certain properties, we may control the properties only indirectly. The process of fiber formation results in the creation of objects with a certain structure. The structure, in turn, is responsible for a set of properties. Consequently, the better an understanding of fiber structure and its formation we possess, the easier it will be to relate it to physical properties which we want to impart to the produced fibers.

V.1 Spun Fibers

One may rightfully expect that the process of cold drawing, and its effects, must depend on the state of polymer the process of cold drawing starts with. Nonetheless, the question goes further back to the question of the condition, or state, of the polymer which was extruded under the action of shear. Later, the material is extended with a tractional force, and crystallized to some extent. A question may then arise: What is the result of all these changes?

Polymer science has not given us the answers we would like to have. There is, however, a number of observations and different notions common in the circles of fiber makers. Many of these notions are correct and helpful, but there are also some which are outright wrong. And here we must overcome one very popular, more or less intuitive, but incorrect notion.

Often it is believed that the amorphous polymer has molecules oriented due to the action of shear and extension. Careful investigations of the problem were conducted over many years and some portion of them was published.[1] Similar investigations, though using different techniques, led to the same conclusions.[2,3] The result of these investigations is: the common fiber forming polymers consisting of flexible chain molecules are not oriented by the perturbations of extrusion, or the orientation does not survive the relaxation taking place in the die swell, and extension definitely does not introduce any measurable orientation of the melt. This is quite clearly visible in figure V.1. A meaningful orientation starts to develop at the end of crystallization, perhaps with a slight overlap, and is the result of the onset of the cold drawing.

The X-ray diffractograms presented in figure V.1 were obtained during fiber formation (on line) from polypropylene of molecular mass of 450,000. The polymer was extruded through a spinnerette of hole diameter 0.381 mm and aspect ratio of $l/d = 7$. In case A the polymer was extruded under shear rate of $\dot{\gamma} = 5000\ s^{-1}$.

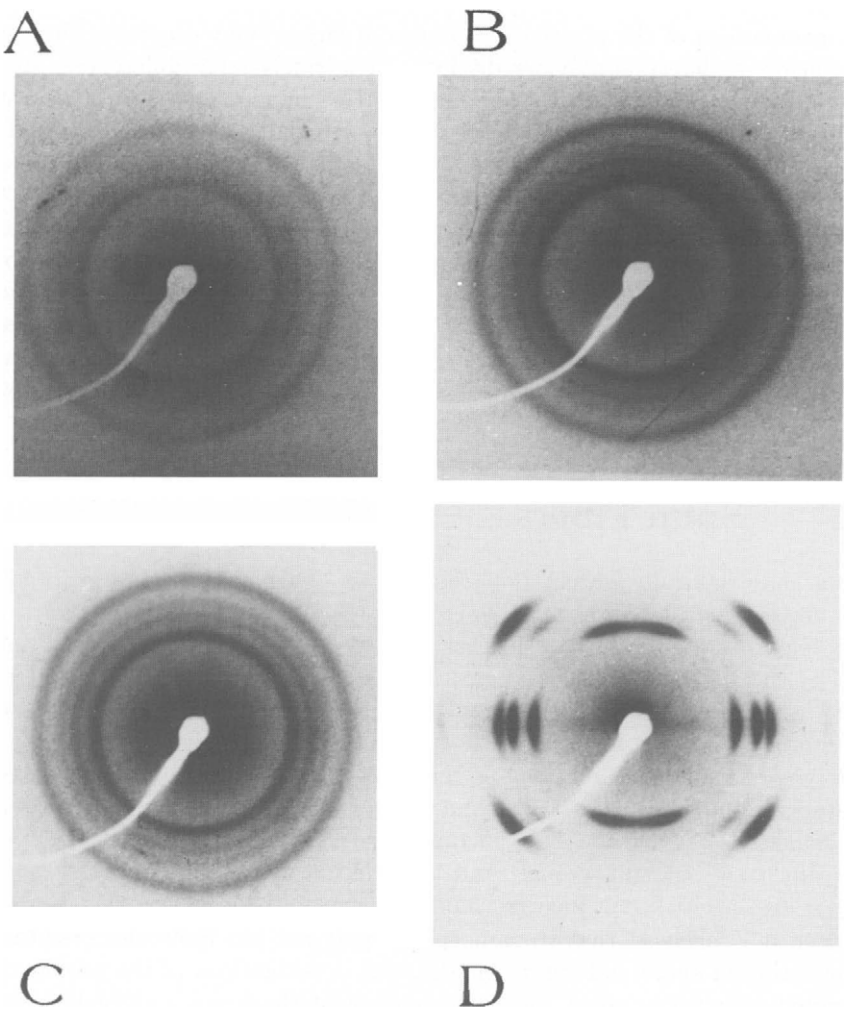

Figure V.1: *X-ray diffractograms obtained during fiber formation (on line) from polypropylene. Explanation in text. After Z. K. Walczak*[31]

Total melt extension (melt draw) between the spinnerette and the take-up roller amounted to $\lambda = 21\ \times$ at a modest take-up velocity of 50 m/min. Diffractogram A was obtained at the end of the crystallization range, and it represents 42 % of crystallinity and no signs of orientation. The quench intensity was adjusted so that the end of crystallization zone was within few centimeters from the take-up rollers. Diffractogram B was obtained also at the end of the crystallization zone, which, as a result of more intensive quench, was some distance upwards from the take-up rollers. Polymer, extrusion, melt extension, and take-up velocity were the same as in case A. The diffractogram B indicates $\alpha = 51$ % of crystallinity and crystalline

orientation is immeasurable. The diffractogram C represents another process, with the extrusion of the same polymer intensified to $\dot{\gamma} = 7500\ s^{-1}$ shear rate. The quench was as in case B, take-up velocity was 110 m/min, which amounted to the extension of $\lambda = 40\ \times$. The diffractogram was obtained at the end of crystallization zone, crystallinity was $\alpha = 52\ \%$ and orientation is immeasurable. Diffractogram D was obtained from the same process as diffractogram B, except very close to the take-up roller, far below the end of crystallization. During the travel from the end of crystallization (case B) to the take-up substantial orientation was developed, crystallinity determined by density was $\alpha = 52\ \%$.

What is affected, and particularly strongly, by shear, is the number of entanglements and their "strength".[4] This effect depends strongly also on molecular mass, or better, on the degree of polymerization, of the polymer involved.

As the investigations mentioned in section IV.4.c show, the creep retardation function and the retardation time depend to a quite marked degree on the magnitude of the drawing force. This means that something in the melt morphology is changing. A serious investigation, as difficult as it may be, of these phenomena and their relationships is needed. At present, details of the changes involved are not known, leave alone their quantification. With the currently available facts one may only speculate.

The strongest entanglements, the deepest reaching loops, seem to be responsible for formation of crystallization nuclei. The number of such long stems is normally so small that it escapes all applicable analytical techniques. By X-ray analysis of fibers collected at the point where the crystallization process just ends, one may sometimes detect traces of orientation, but the traces are so small that they cannot be quantified. Similarly, determination of birefringence on fibers collected from a moving spinline, with so called "cutting traps", showed only traces of orientation at the point where the crystallization process goes to its completion. For example, polypropylene spun at speeds close to 5000 m/min gave a birefringence of maximum 0.0010.

For the time being, we must leave the subject just with a short statement: depending on processing conditions, some important changes are introduced to the melt morphology. The changes are important to the future crystallization process. The nucleation rate may increase faster than the growth ability, and this has an impact on morphology of the crystals. However, the changes in the morphology of the melt prior to crystallization appear to be much stronger rather than numerous; they themselves escape the analytical techniques, only the effects are detectable.

Figure V.2 shows a transmission electron micrograph of polyethylene lamellar crystals growing epitaxially on the long "fibers" created through a baguette shearing of the solution to crystallize. Figure V.2A shows the general topography and interpenetration of the lamellae. Figure V.2B shows the same specimen at a higher magnification; here the interlamellar tie molecules along some longer range connections are clearly visible. .

The long "threads" are, most probably, the result of extention, due to flow, of

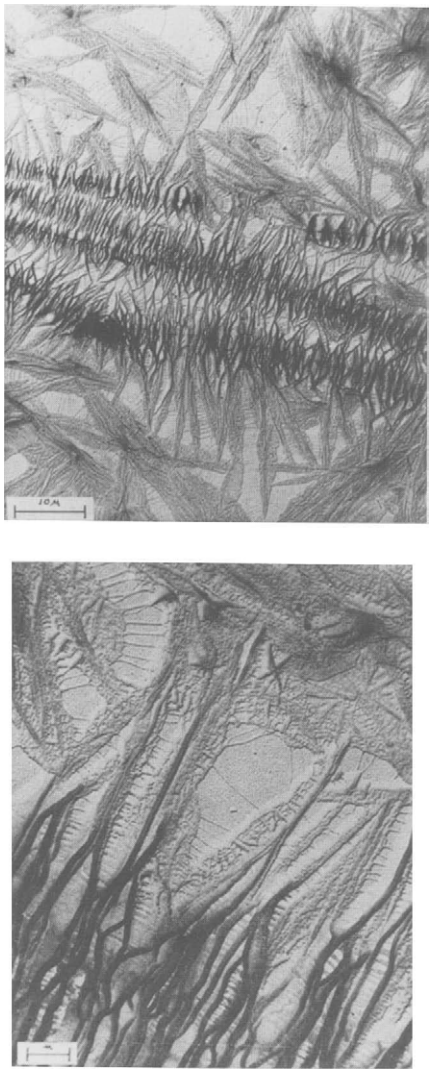

Figure V.2: *Transmission electron micrograph of row nucleated polyethylene crystals. Top: general view of morphology and interpenetration of various lamellae. Bottom: higher magnification than above showing interlamellar tie molecules and some longer range connections. Reproduced from R. C. Novak and R. B. Williamson*[5] *by permission of the copyrights owner, John Wiley & Sons, Inc.*

very strong, deeply nested entanglements. Most likely, these are loops formed at points far from molecule ends of both molecules involved. In a flow field, such long strands may also bundle together and in this way achieve the critical minimum size of a nucleus. Here it is easy to see that the size of the nucleus is rather the size

of its surface; length is then exchangeable with diameter. Once the process starts, normal, folded chain crystallization proceeds. It has been claimed lately[85] that the "shish" modus of crystallization is "autocatalytic". One shish initiated by strain may propagate further into unstrained areas. As the data presented in figures 4.29 through 4.31 of section IV.5 show, under influence of forces of fiber formation, the process of nucleation is substantially faster than the process of crystal growth. One may suppose also that it is faster than the possible propagation of shishes.

If the crystallization rate is high, large crystals are formed; if the process is slow, small crystallites along a and b-crystalline axes are formed. The true reason for this fact is unknown, though it may well be related to the discrepancy between the rates of nucleation and growth. Mainly the stored elastic energy seems to be responsible for the nucleation. What constitutes the limiting factor for the rate of crystal growth is yet unclear. The size of the crystallites (mosaic blocks) appears to be the result of competition between the velocity of flow and crystal growth. If the flow is faster, the growth may be disturbed, more imperfect alignments incorporated, larger g - factor results, and mosaic blocks formed are smaller. Nevertheless, though probable, this is a conjecture only

There are several theories claiming that certain preorder exists in polymer melts. Perhaps the furthest developed and most popular of these theories is the *meander model* developed by W. R. Pechhold and co-workers.[6–10] The model assumes the existence of more or less regular folds with dimensions similar to those present in crystals. The folds are less regular than in crystals. Besides them, there exist some *superfolds* which consist of parallel aligned chains spanning over a distance larger than one fold. Such superfolds may span from one meander cluster to another and, in effect, they may play a role similar to the entanglements, as assumed in the free coil theory, though they are anchored in the structure rather than in the conformation.

This author believes that in reality, noncrystalline melts consist of both elements, free coiled and clustered molecules. The ratio probably depends on the character of the polymer, on chain rigidity. The liquid crystals may serve as an extreme example where no, or almost no, coils exist.

Some of the entanglements, or the superfolds, due to their character or due to the flow forces, may not be able to develop into raw nuclei. Nevertheless, they form connections between different crystalline lamellae; they are responsible for the formation of *tie molecules.*

Barham and Keller[11] used synchrotron X-ray radiation to investigate *in situ* crystallization of polyethylene. The authors found that initially, polymer crystallized in very thin lamellae. Later, the lamellae thickened in steps to double, triple, or quadruple the length of the initial folds. Such a dramatic refolding was more frequent at a higher crystallization temperature. Later, after the dramatic refolding, the lamellae thickened logarithmically with time, similarly as they do in annealing. The stepwise refolding led to the formation of tie molecules between lamellae.

E. W. Fischer and co-workers,[12] using neutron scattering, confirmed the ex-

istence of the tie molecules and developed a method to determine the average number of clusters per one molecule, the radius of gyration of the centers of stems belonging to one cluster, and the radius of gyration of the centers of clusters in respect to the center of molecule. From these, one may calculate the average number of tie molecules.

It has been anticipated[13] that in a flow field, such long structures as the epitaxially growing lamellae cannot remain intact: they must bend back or break off, thereby disorienting themselves. Such effects have been shown quite convincingly by electron microscopic investigations conducted by G. Kanig.[14] Bending back and breaking of the long lamellae has been shown to take place in the initial stages of cold deformation. Similar events are equally, or even more likely, when some still noncrystalline polymer flows by the crystalline *kebabs*. One must accept that even in extensional flow, some structural elements pass by other elements and thus are subject to some shearing forces, which are strong to the point of possible chain scission, leave alone other deformations.

The crystalline lamellae of the majority of polymers do not form flat surfaces – they are mostly roof or hollow pyramid shaped.[15,16] This results from the fact that the majority of polymers crystallize in the lattices of low symmetry, where the c - crystallographic axis is not normal to the remaining axes, a and b.[17] This together with other kinds of irregularities and defects may contribute to the deformability of lamellae.

In the case of fiber formation from the melt, crystallization proceeds during more or less rapid cooling. This causes the lamellae to become gradually thinner as they are further removed from the nucleus; the long period depends on growth temperature. The interlamellar spaces become occupied by crystallizing amorphous material, or are penetrated by the thin lamellae originating from other nuclei.[18]

Although the long strands which form the *row nuclei* are undoubtedly oriented parallel to the flow direction, their number is far too small to be detectable as orientation. The epitaxially growing lamellae close to the row nucleus have probably chain folds parallel to the nucleus, the chain folds more remote from the nucleus change their alignment, sometimes drastically. If a crystal *shish-kebab* grows very large lamellae, then the dimensions normal to the c - crystallographic axis may be the largest. Flow of such "overgrown" lamellae may force an orientation of the c - crystallographic axis normal to the flow direction, to the fiber axis. It is not an exception that a certain amount of transversely oriented crystallites is found even in extensively drawn fibers; sometimes it is called "γ - orientation".

Investigation of a noncrystalline material is still difficult. The tools to do the investigation directly are few, quantification of the indirect results is difficult. This causes our knowledge of spun fibers prior to crystallization to be very sketchy, full of conjectures. One thing, however, is certain: the conditions of formation, temperature profile, shear in capillary, and extension profile play a very important role. It goes without special underlining that the polymer properties are also responsible for how the material reacts to the treatment.

V.2 Cold Drawing

The structure of undrawn fiber may be imagined to be similar to the *shish-kebab* shown in figure V.2. In reality, this should be taken as one of the main elements of the structure; nature gives here an almost infinite number of "mixed" situations. It is important how densely such *shish-kebabs* are packed together, the degree of the lamellae interpenetration, it is how deeply they intrude into their neighbors, how much of the still noncrystalline material is present and how is it distributed between the crystalline elements; all these are important. There are many researchers who agree to such a scheme.[19,20]

The structural changes taking place in neck drawing were studied in great detail by Kasai and Kakudo.[21] They found that starting from the yield point, or at the yield point according to a newer report,[74] all the way through the natural draw ratio, a process of destruction of the crystalline lamellae takes place. Kasai and Kakudo have confirmed that the lamellae break down into mosaic blocks, as earlier described by Hosemann and co-workers[22–25] and others.[26–28] The discontinuous break down of lamellae appears to be the reason for the formation of the neck. These authors also find that the deformation along the fiber axis changes gradually from the symmetric small angle X-ray scattering (SAXS) patterns to the four-point diagrams. While close to the specimen surface in the necking area, the diagrams become asymmetric, but past the necking area they assume the four-point pattern equal to that in the center of the specimen.[21]

There were quite conflicting reports by different authors regarding the degree of crystallinity and the magnitude of long period. Some authors claimed that crystallinity upon cold drawing goes up, some insisted that it goes down. Similar lack of agreement regarded long period.

From the perspective of time, it appears that all of the above cases may be true, depending on the structure of the undrawn fiber and on the process conditions. First of all, the drawing process is highly exothermal and temperature control may be difficult, particularly at high drawing rates and/or thick specimens. Whether total crystallinity goes up would obviously depend on the availability of a noncrystalline material.

If the temperature inside the neck increases a little, then the long period may grow due to some annealing effect. If the temperature increases significantly, then some portion of the crystals may melt and recrystallize. The necking area is very small, so the material will crystallize back after leaving the neck area, where cooling may be intensive, and in such a way the long period may decrease. Another mechanism for growth of long period may be similar to the mechanism of annealing: longitudinal translation along the chain axis.[50,51]

It has been published[74] recently that remelting, if at all possible, may take place only in the necking (at yield point), and it may be caused by stress, not necessarily by elevated temperature. In the remelting process, mainly imperfect crystals are involved.

The lamellae of a *shish-kebab* disintegrate into the mosaic blocks by forces

transmitted through the tie molecules. Some molecules are involved in two blocks, providing connections between the blocks originating from the same lamella. During the lamella break-down, these chains either unfold or break; they may also change their length due to translation motion along the chain axis, similarly as in annealing.[52] The last process seems to be slower and thereby less frequent. Several different mechanisms were suggested for the unfolding of chains from the crystal blocks.[26,29–30] The mechanism proposed by Kobayashi[29] seems to require significantly more force than might be available in an average drawing process. The mechanism proposed by Peterlin[26] requires far reaching recrystallization, or reorganization, of the block structure; it may take place to some extent, particularly when drawing is conducted at relatively high temperature.

The boundaries between the different blocks of one lamella represent a weak spot. X-rays do not see them as crystalline. It is entirely logical then that the destruction of the lamellae takes place along the weak spots. Based on the above, the principal scheme for change of lamellar morphology into fibrillar has been proposed as depicted in Figure V.3.[13,31]

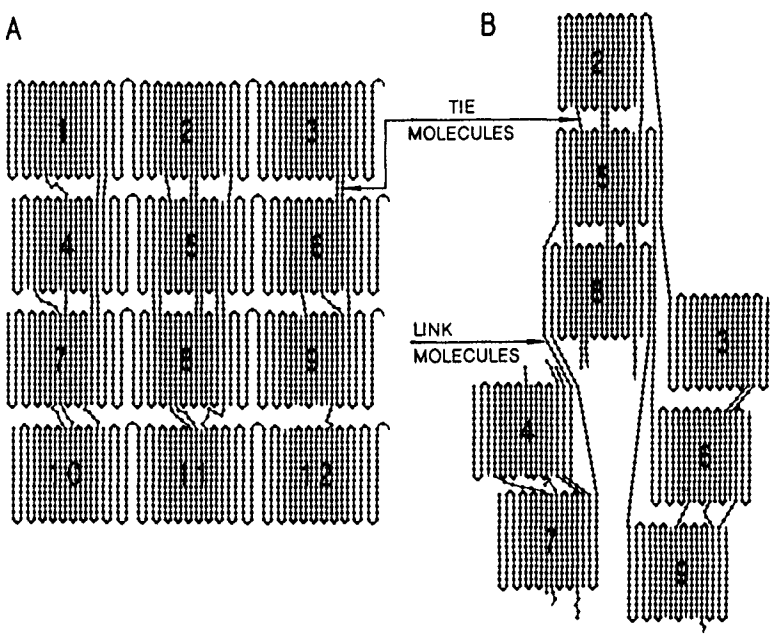

Figure V.3: *Schematic representation of the transformation from lamellar into fibrillar morphology as a result of cold drawing.*[13,31]

A strain imposed on a stack of crystal lamellae initially causes stretching of the tie molecules, which corresponds to the first, pre-yield part of the force-strain curve. Further stretching leads to tearing out of the mosaic blocks from their original places, leading to the initial abrupt discontinuous change in fiber diameter

(neck). The process of disintegration of a mat seems to start at the peak of the yield in the force-strain curve and proceeds throughout the entire natural draw ratio.

Since the tie molecules do not have equal length, the connected blocks cannot have exactly parallel fold planes. This causes a certain degree of unavoidable residual disorientation,[46] not to speak of various crystal defects – some of which may even assume the complexity of a knot.[47] The unequal length of the tie molecule may lead to occasional breaks of these ties.

When the drawing continues past the natural draw ratio, the slope of force-strain curve increases markedly. This increase is related to the further unfolding of the outer layers of the blocks. The unwound polymer, termed *link molecules*,[13,31] forms a kind of sheath around the core consisting of a "column" of blocks. The link molecules provide a long range connection both intrablocks and interblocks, simultaneously forming a layer defining the individual fibrils, a layer which thickens with increasing draw ratio.[32] The important difference between the tie and link molecules is that the tie molecules seem to have constant length, if recrystallization or translation are not involved, while link molecules have a length dependent on the draw ratio, and later thermal and strain history. Existence of the extended chain links in layers with some organization of hexagonal type has been confirmed by Z. Bartczak and co-workers.[75] The reported[76] peculiar longitudinal "voids" in etched polypropylene fiber cross sections may well be assumed to be the non-crystalline link molecules that have been etched away. The only problem with this interpretation may cause the high degree of axial dimensional regularity, as well as the lateral regular arrangement.

It is necessary to stress that the outer perimeter of a mosaic block has a larger concentration of lattice defects. Once it is removed from the mat, one should take into consideration an edge effect: the molecules are not held in place from all four sides. All this permits us to infer that it takes much less force to remove a polymer chain from the outside of a block rather than from the inside. The latter would more likely lead to a chain break. Existence of *destructible micro-paracrystals* has been proved[72] and will be discussed in section V.7.

It has been determined that neck drawing results in some chain breaks, but the number of ruptured bonds in high density polyethylene drawn at room temperature amounts only to 10^{-3} to 10^{-2} of one percent of the total number of chain carbon atoms. Increase of drawing temperature causes a decrease of bond ruptures, which may indicate also that some portion of the breaks is due to frictional forces involved in the drawing process.[52] In place of the ruptured bonds new chain ends are formed, from double bonds to various carbonyl groups, if the drawing is conducted in presence of oxygen, and this is usually the case.[45] Since the number of broken bonds is small, the effect on the average molecular mass is not very important and possibly correctable. The foreign characteristic groups are more detrimental to crystallization, and perhaps to certain chemical properties.

As the number of ruptured bonds is approximately steady over draw ratio up to seven, at higher strains the number of ruptures increases very sharply. As such

a high draw ratio is limited mainly to extension and formation of link molecules, one may easily infer that some of these molecules break.[45]

The breakdown of lamellae is not necessarily uniform, it may proceed in a staircase fashion[30] or along other not very regular patterns. With increasing draw ratio, the regularity of the formed fibrils increases to become quite regular, as may be seen in figures V.4 and V.5.[33,34] Figures V.6 and V.7[33,34] show the connections between the fibrils - particularly figure V.6 shows more details. Some of the connections may have a crystalline form themselves[36,37]. Figure V.8 shows that the fibrillar nature of a fiber extends over the entire cross section of a fiber.

The fibrils shown in figures V.4 to V.8 have diameters of the order of 2000 Å, and they may be composed of microfibrils of the type suggested in figure V.3. Such a bundling of fibrils has been reported by Bonart and Hosemann.[23] In fibers drawn to low draw ratios, *protofibrils* with diameters of the order of 6000 to 7000 Å have been found.[53] How the fibrils become gradually smaller is not clear; it appears that the division of protofibrils is similar to the breakdown of lamellae. Some tendency toward fibril splitting may be seen in figure V.6.

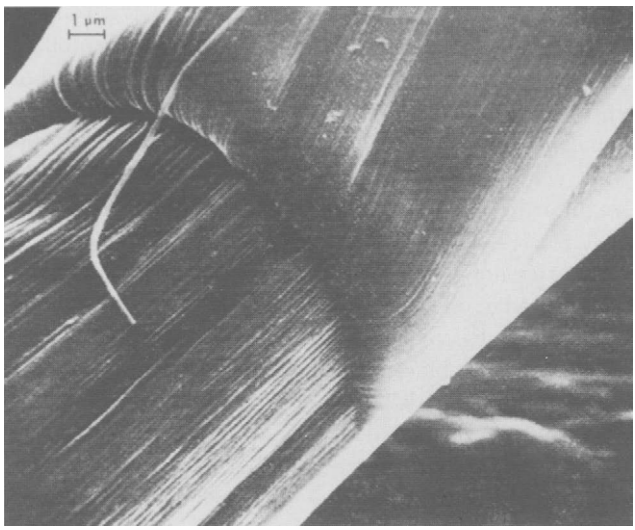

Figure V.4: *Scanning electron micrograph of skin peeled polyester fiber. Reproduced by courtesy of H. R. Billica.*[34]

Some of the interfibrillar connections may well assume intermediate phases. Hosemann's paracrystals cover the entire range from crystalline to noncrystalline, and the intermediate phases have been detected in fibers.[41]

The unfolding of molecules from the mosaic blocks may be seen as a decrease of the volume of crystalline material. Such a decrease of crystallinity was detected only at higher draw ratios.[32,44] This may be seen as an indication that the folds

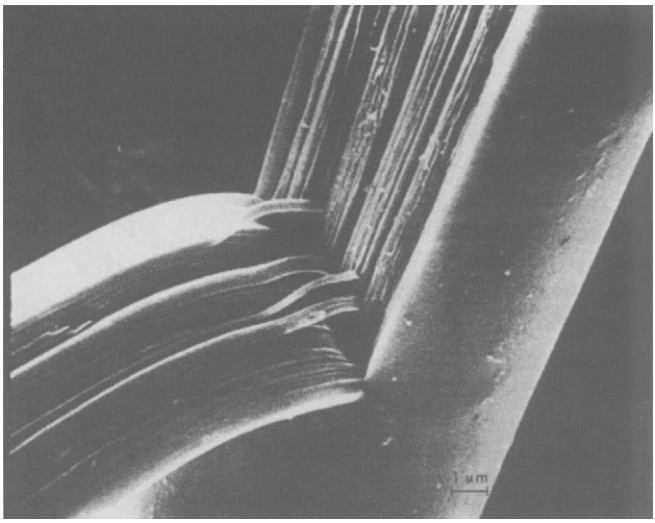

Figure V.5: *Scanning electron micrograph of a chord peeled polyester fiber. Reproduced by courtesy of H. R. Billica.*[34]

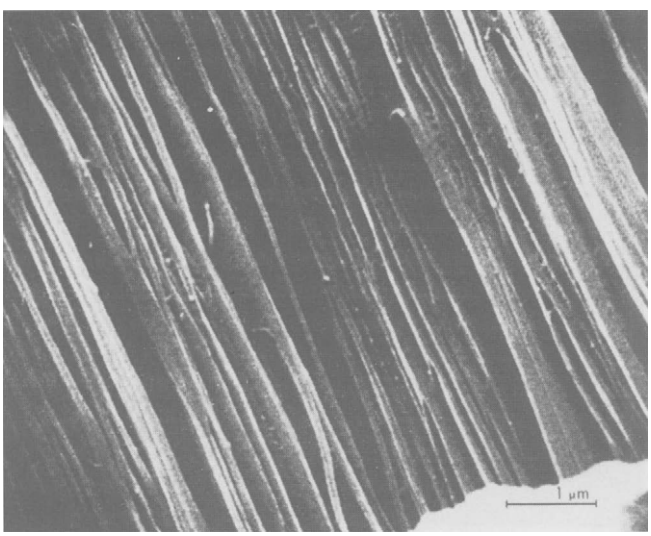

Figure V.6: *Stereoscan micrograph showing microfibrils and interconnections between them. Reproduced by courtesy of H. R. Billica.*[34]

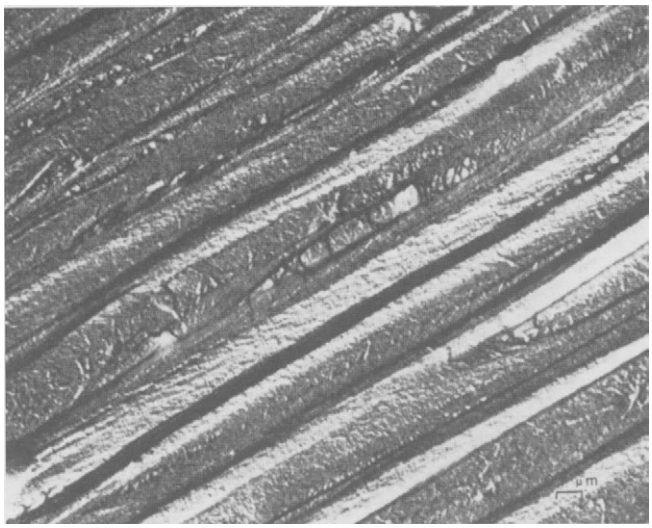

Figure V.7: *Micrograph of fibrils at higher magnification which shows more interfibrillar connections and voids. Reproduced by courtesy of H. R. Billica.*[34]

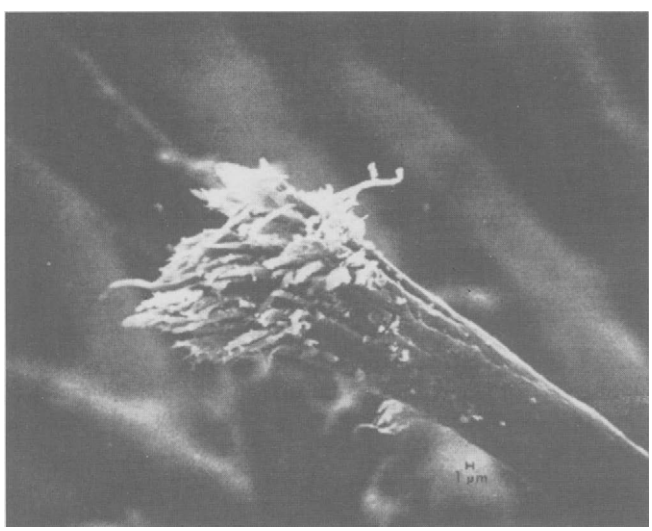

Figure V.8: *Micrograph of a fiber break which shows the fibrillar nature throughout the fiber cross section. Reproduced by courtesy of H. R. Billica.*[34]

unwound in drawing are not necessarily seen as crystalline by X-rays. More extensive drawing strips the block perimeter to a more perfect crystalline form,[41–43] but at the same time it produces more link molecules which are noncrystalline.

A structure similar to that proposed in figure V.3[13,31] has been suggested later by Prevorsek and co-workers.[35] Such a structure is strongly confirmed by the work of Billica and co-workers,[33,34] and others.[36,37]

Rolf Hosemann[38] has published a kind of "catalog" of different possibilities of structural arrangements in fiber; it is reproduced in figure V.9. These correspond primarily to the inner side of the fibrils – to their core.

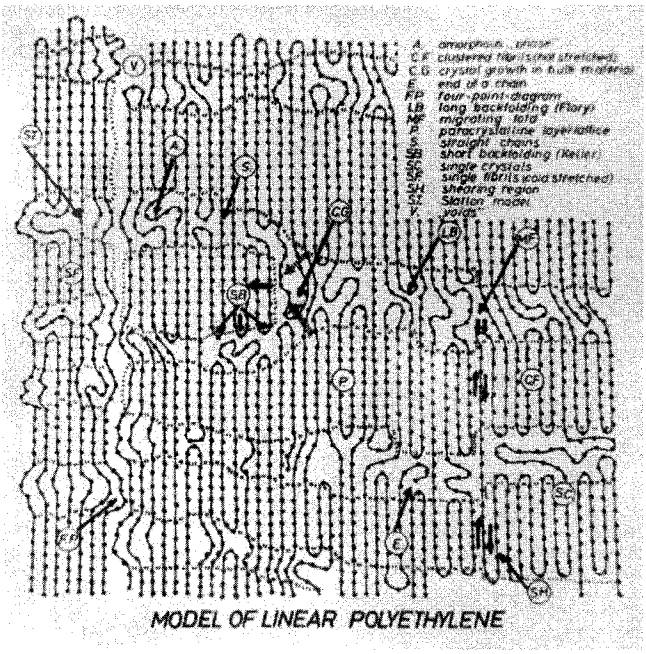

Figure V.9: *Schematic model of various crystalline structures which may be found in a drawn fiber as given by R. Hosemann.*[38] *Reproduced with permission of copyrights holder, Elsevier Science Publ.*

The investigations by Pinaud and co-workers[49] show that the orientation of amorphous material depends mainly on the crystalline orientation and morphology. This suggests that the amorphous chains are embedded in the crystalline elements. As it transpires from the presented picture of fiber structure, the crystalline forms serve as anchors for the amorphous chains, which are the main load bearing part of the structure.

As an additional argument for the above suggested fiber structure may serve the fact that if an undrawn fiber contains spherulites with radial arrangement, as it happens occasionally in slow formation processes, neck drawing is very difficult and no significant strength of fibers is obtainable.[40]

As every scheme is a simplification, one should remember not to vitrify it. The nature of various polymers and their crystallization habits, as well as the entire set of processing conditions have their say in the final outcome of a process in terms of a specific structure and further in terms of the properties. And this truism cannot be overemphasized, it is a matter of producing fibers with a desired set of properties, and it is a matter of process reproducibility.

When the drawing force is removed, a post-draw relaxation takes place. This is probably due to relaxation of the tie and link molecules. Considering the geometry, and particularly the length of the connections, the link molecules seem to bear more responsibility for the shrinkage. Being highly stretched, and thereby forced into "uncomfortable" positions, the ability of the links to crystallize in the new locations decreases with the increasing draw ratio and tension experienced by the link molecules. Upon removal of force, the link molecules relax and seek more "comfortable" positions.

It is well known that a fiber does stabilize. If drawing is divided into several stages, care must be taken that the fiber is not given the chance to relax.[48] If the fiber does relax, then only a limited amount of drawing will be possible in the next stage.

Considering the above presented fibrillar structure of drawn fibers one may conclude that the strength of fibers is dictated primarily by tie molecules and link molecules. As the number of the tie molecules in the drawing process is essentially constant, with the exception of occasional breaks or a major recrystallization, the number of link molecules increases with increasing draw ratio, especially above the natural draw ratio.

V.3 Drawing Performance

Some noncrystalline polymers may also be drawn with neck formation. It is assumed that in noncrystalline polymer, the molecular clusters play the role which the mosaic blocks play in crystalline polymers – knots of a net in which amorphous chains serve as the strings. This leads to the obvious conclusion that the neck drawing may be performed over the entire range of crystallinity starting from zero, or close to it, to as high as it may go. Nevertheless, the actual degree of crystallinity in the undrawn fibers has its significance.

Besides the total amount of crystallinity, one needs to consider the size of crystallites. As results from the studies of crystallization in polymer flow, the size of crystallites depends on the crystallization rate. Low rate of crystallization favors small crystallite size. The size of crystallites is also affected by the shear the polymer experienced during extrusion. High shear rates invariably lead to smaller size of crystallites. For example, increase of shear rate from 250 s^{-1} to 1250 s^{-1} causes a decrease of crystallite size from 90 $\mathring{A}$ down to 70 $\mathring{A}$. The influence of capillary length appears to be much more complicated.[1]

The significance of the crystallite size is rather obvious; drawing force requirement, number of link molecules, potential size of fibrils are related to the size

of mosaic blocks. The fiber properties are affected by the crystallite size more stronger than the drawing performance is influenced.

Capuccio and co-workers[54] studied extensively the fiber formation from polypropylene. The authors found a relationship between the degree of crystallinity in fiber before neck drawing and the maximum of tenacity obtainable, as presented in figure V.10. Though the range of crystallinity before drawing appears unusually wide, both on the high and on the low side of the bracket, the general trend and conclusion are very much in line with the findings of many researchers and regarding many polymers.

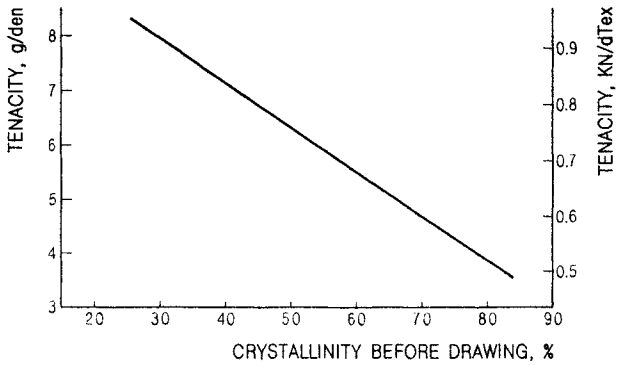

Figure V.10: *Maximum of obtainable fiber tenacity in relation to the degree of crystallinity existing in fiber before neck drawing. After V. Capuccio and co-workers.*[54]

Considering what was said above about the fiber structure, the results in figure V.10 are by no means surprising. It is certainly energetically easier to unwind molecular coils, rather than unfold long periods from a crystal block. Furthermore, larger number of the noncrystalline chains per fiber cross section may be obtained, and this means higher tenacity. Last, though not least, drawing of fibers with less crystallinity requires substantially less force. This makes the drawing process less vulnerable to fiber breaks, and in the end may lead to higher maximum draw ratio.

The amount of crystallinity alone does not mean everything. The degree of "preorientation" of the crystals before drawing is also important. Figure V.11[1] presents the influence of a small difference in crystalline orientation in undrawn fiber on drawing performance. Drawing force, for the same strain, increases substantially with increasing orientation. The resulting fiber tenacity is somewhat higher for more preoriented fibers, but only at low draw ratios; later the benefit disappears. Break elongation for fibers obtained from more preoriented filaments is lower, the modulus is higher. Closer analysis of these results, which are otherwise quite common, may indicate that the changes in the fiber are such that one may assume that the preorientation and the neck drawing are additive. To some extent this is true, but fiber properties loose on the additivity. The increase of the drawing force required is much larger than a simple additivity might justify, and in effect this may often limit the practical maximum draw ratio.

The experiments presented in figure V.11 indicate also the problem of structure

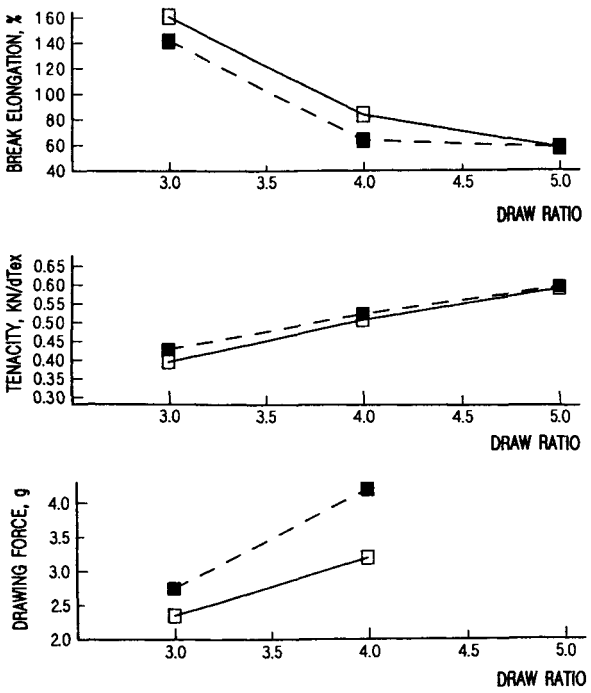

Figure V.11: *Comparison between the property build-up versus draw ratio for somewhat higher (filled squares) and somewhat lower (open squares) orientation in undrawn fibers. After Z. K. Walczak.*[1]

settling. The time span from the point where the neck drawing was initiated (end of the crystallization in the quench zone) to the drawing zone (for in-line drawing) was sufficient to start some structure settling, as is evident from the large increase in the drawing force requirement. True, the process was slow, maximum drawing speed 750 m/min, but still the time involved was short. Similar conclusions regarding structure setting (ageing) may be drawn from the work of L. C. E. Struik on ageing.[73]

Often multiple zone annealing is applied in order to increase fiber strength, especially for the so called "high strength" fibers. Such operations should be conducted so that the drawing temperature is gradually increased in subsequent zones. The temperature increase "softens" the structure, reducing the force requirement which normally increases with the draw ratio. Also, increasing the temperature helps to ease the problem of structure setting, as some finite time must pass between the drawing zones.

The influence of temperature on neck drawing has been discussed in section IV.6. Here, it is necessary to add that temperature also has an influence on crystallinity. The magnitude and direction of such an influence is also greatly dependent on the type and amount of crystallinity before drawing. Excessive drawing temperature may cause partial, or even more extensive, melting and subsequent recrystallization. It may determine whether crystallinity will increase or decrease,

and how much. High drawing temperature is also a matter of the thermal response and thermal stability of the fibers, as directed by the final size of crystalline long period and on the degree of relaxation of the link molecules. These matters are highly interrelated and it is impossible to describe them in very concrete terms. Every case must be separately analyzed and conducted accordingly.

V.4 Structure - Properties Relations

The discovery of fibrillar structure of fibers and the notion of link molecules, which hold a fibril together and at the same time separate it from its neighbors, led to the first model of fiber structure capable of explaining the majority of fiber properties. And so, one of the important questions, the loss of transverse properties accompanying every gain of tensional properties becomes easy to understand. With increasing stretch, the layer of principally noncrystalline chains surrounding a fibril grows in thickness and the individual polymer chains become more taut. Both of the states contribute to the lowering of the interfibrillar cohesion.

Another property which was impossible to explain with the earlier models of fiber structure was the large elongation to break in some fibers. It is highly improbable that tie molecules might accommodate fifty or sixty per cent of elongation. It is much more probable that upon application of force some of the periferal lamellae unfold further into the link molecules. It is thinkable that some of the folds on the mosaic blocks boundaries being poorly fit and subject to an edge effect may stay within the mosaic block with very little of energetic benefit. Such an unfolding may be energetically comparable to the uncoiling of rubber molecules. Such a hypothesis may explain the large strains, and the somewhat sluggish and incomplete recovery upon release of stress. It is thinkable that certain of the new environments acquired due to a strain may be energetically equivalent, or even better than at the starting point, before the extension.

High elongations may be encountered with fibers of a modest draw ratio. When a draw ratio is high, the periferal folds are stripped from the mosaic blocks to such an extent that there are no more imperfect, weakly held folds to succumb to the relatively low force available.

D. Hofmann and E. Schultz[55] conducted a very meticulous study of the crystalline and amorphous chain structure of high modulus polyethylene fibers. This work leaves essentially no doubt that *"The axial Young's modulus of smooth fibrillar samples is a function of the content of these taut tie molecule segments and the crystallinity of the samples. ... a high degree of crystalline orientation is the necessary but not a sufficient condition for obtaining high modulus specimen."*[55] The structure of some natural fibers, like silk or spider silk, is also of relatively low crystallinity, with very small and rather well oriented crystals. The strength depends on the amorphous chains which are anchored in the small crystals. High molecular mass ($> 300,000$) strongly contributes to the strength.[79 & *ref.*] Thus, there is no discrepancy in the principles of the fiber structure, be it natural or synthetic.

Some of the recently propagated theories suggest[52] that the forces involved in neck drawing are sufficient to pull out chains from a crystal; the shearing forces involved, particularly with non-polar polymers, are not prohibitively high. These theories may explain the elongation, though it would be much more difficult to explain eighty, or so, percent of the observable strain recovery. It seems highly unlikely for the chains to go back, to re-enter deep into the crystal. The size of the hysteresis loops does not agree with the notion that molecules are pulled out, and stay out of a crystal.

In a significant paper, N. S. Murthy and co-workers[78] present the results of small angle X-ray scattering (SAXS) with synchrotron radiation on a series of poly(ethylene terephthalate) fibers. An expanded data evaluation system, besides the standard long period, gave other quantities: diameter of lamella stack, interfibrillar spacing (including layers of link molecules and voids), length of lamellar stacks (few lamellae), length of fibrils, angle of the tilt of the lamella fold surface. The fibers investigated had various amounts of crystallinity and different degree of predraw orientation. The work confirms everything that was said above. The additional new information gained is that a small diameter of fibrils favors higher tensile strength. One might expect that a finer diameter of fibrils leads to a larger number of structural elements which must result in more uniform load distribution, and this gives higher strength. Also, the authors find that neck drawing results in the creation of voids, with numbers increasing with the increasing draw ratio; this has been observed before. However, significant elongated voids may be formed in the interfibrillar areas. Some of these voids may extend on distances comparable to the length of fibrils. Such voids may strongly affect the transverse strength of the fibers.

N. S. Murthy and co-workers[78] stress the difficulties with correlation of the fiber properties with fiber structure. In this multifaceted relationship, every element of the structure plays its role, none may be omitted, be it regarding the crystalline or the amorphous phase. Such a multivariable system is difficult from the experimental point of view, and equally so from the interpretation side.

The hypothesis of unfolding and refolding is very well compatible with the thermal response of fiber, with annealing. If the degree of shrinkage is small, it is mostly by way of shrinkage of the tie molecules connecting different blocks within a microfibril; they may participate in an improvement of the crystalline lattice, such shrinkage is irreversible. If shrinkage is more extensive, it is mostly through shrinkage of the intercrystalline link molecules, through a parallel shift of the fibrils.[35] Naturally, this is true in case of the fibers with the structure as already described. In case of fibers with predominantly extended chains, so called *high strength*, or *high modulus*, or *ultrahigh modulus and/or strength*, the mechanism of thermal shrinkage may be different.

V.5 High Strength Fibers

In the late sixties, so called *high performance fibers* came on the market. The intensive work on space exploration demanded new materials, new fibers for technical purposes and for some very specialized apparel were needed. As an answer to these challenges, *Nomex* and *Kevlar* were brought onto the world market.

High performance fibers are usually made of polymers with rigid chains. As a rule, the chain rigidity is obtained from monomers containing ring, or even condensed rings, structures. Most of these polymers have very high melting points, often higher than their thermal stability. Thus, fiber formation is mainly done from solutions, even though the only practical solvents may be as obnoxious as concentrated sulphuric acid. The more common of the polymers involved are: poly(p - phenylene-terephthalamide) (PPTA), poly(p - benzamide) (PBA), poly(aryl - ether - ether - ketone) (PEEK), poly(ethylene - naphthalene - 2,6 - dicarboxylate), poly(hydroxybenzoic acid - co - hydroxynaphthoic acid), and many others.

Shearing forces orient the polymers with rigid molecules only little, or not at all, but the rigid molecules are strongly oriented in extensional flow, even a weak one.[56,57,77] In effect, the fibers, even if the formation conditions prevent crystallization, possess a high degree of orientation. If such a noncrystalline fiber is heated above the glass transition temperature, the crystallization process starts and the developing structure is oriented and fibrillar.[58]

The highly fibrillar nature causes the fibers to easily defibrillate on action of normal forces, not to speak of fracture. The internal structure of the fibrils resembles the structure of "ordinary" fibers: lattice with paracrystalline lattice distortions of different degree (g-factor), and microparacrystals (mosaic blocks) of sizes comparable to those in the flexible chain polymers, except that the longitudinal size along the c-axis is substantially larger.[59] The fibrils have a diameter on the order of 600 *nm*. Naturally, the fibrils consist of paracrystalline blocks and are not, as some authors have implied, a result of the splitting of a fiber built of a single monocrystal. The fibrils really are the elements of the fiber structure. Some individual chains, or bundles of them, are built-in in two neighboring fibrils and provide interfibrillar links. They represent also the element of lower orientation.[36]

The individual fibrils, obtained from splitting a fiber, show a high degree of flexibility, quite contrary to the properties of the whole fiber. Some polymers produce *pleated* fibrils; that is, the fibrils have a *zig-zag* form, parallel to the fiber axis. The zig-zagging is inclined to the fiber axis by about 5°. One zig-zag extends for some five to six hundred nanometers. Such pleated structures are easily detectable by optical microscope due to periodic change of refractive index.[36] & *ref.*

Some of the high performance fibers show a skin-core effect which is due to the somewhat better orientation of the fibrils on the fiber surface and close to it. Inside the fiber, the parallelization of the fibrils with the fiber axis may be not quite so perfect.[36]

Generally, some of the lattice defects help the final fiber properties. Less perfect

structure may be less inclined to defibrillation. Often, to further improve the fiber properties along this line, small amounts of comonomers are polymerized. This is to reduce the perfection of the crystalline structure.

The chain rigidity of the many kinds of polymers varies significantly. Following this difference, the effect of processing on the structure and fiber properties also varies within very wide brackets.

Once the fibrillar structure of fibers was learned, and particularly after the fibrillar nature of the high performance polymers was explored, a great deal of effort was invested into obtaining strong fibers from ordinary flexible coil polymers. The great majority of the efforts originated in university research centers. This is understandable since the market for high performance fibers is small, prices are very high, competition is vigorous and profits rather low. The main goal of the research efforts was directed toward obtaining fibrillar structure with a minimum, or preferably with no chain folded crystals, or even something approaching extended chain crystals.

From a number of different techniques[60], the more successful seem to be only solid state extrusion and formation by gel-extrusion, and so called *ultra drawing.*

Research efforts on ultra drawing very recently have brought interesting results regarding the mechanism of extensive drawing[80] *& ref.* (see also section IV.6.a). It has been shown that the translational movement of polymer chain within the crystals is the crucial mechanism here. In terms of structure, the model, in principle, does not deviate much from the model given in figure V.3. Besides the unwinding of the noncrystalline chains and stripping of the less than perfect aligned chains on the perimeters of the mosaic blocks and formation of the link molecules, the tie molecules extend at the expense of the lateral dimensions of the mosaic blocks. Ultimately this may lead to bundles of extended molecules which are crystalline in some segments and with a lesser degree of order in the other segments. The fibrillar nature becomes less and less defined. The difference between the chain morphology in the interfibrillar areas and within the gradually thinning fibrils decreases. The ultradrawing, usually considered for $\lambda \geq 15$, is possible only for ductile crystals, it is for crystals showing $\alpha_c \geq 10^3/s$.[80]

V.6 Fibers from Block Copolymers

Commercially much more important are the fibers made from block copolymers, primarily from polyurethanes. Both the apparel and technical fibers industries have interest in the elastic materials.

The polymers in question here consist of alternating blocks of "hard" and "soft" nature. "Hard" means here a moiety either of high glass transition temperature, *e.g.* polystyrene, or strongly polar segment, particularly with hydrogen bonding capability, *e.g.* urethane groups, or segments capable of a crystalline lattice formation. The "soft" segment is usually a flexible chain of rubbery nature, like poly(butadiene), poly(isoprene), poly(oxymethylene), poly(adipic lactone), and other similar. The two segments are incompatible, and this is not difficult to

accomplish, as list of the compatible polymers is very short.

Incompatibility of the segments causes phase separation, and this is the *clue* of the matter. The material consists of two phases of different properties. The "hard" phase usually provides the strong anchors for the "soft" phase, which is responsible for the high rubbery stretch. In such a way we obtain highly elastic fibers, and so far this is about the only area of application for the block copolymers. The wealth of the different material properties this group of copolymers offers permits us to believe that a number of new, different fibers with marvelous properties will appear on the market.

The majority of the block copolymers is thermoplastic, though polyurethanes represent a borderline case. Despite the thermoplasticity, this group of polymers ought to be formed into fibers from solution; this is a matter of facilitating the phase separation. The morphology depends very strongly on the volume ratio of the two phases and on the sequence distribution along the copolymer chain. For example, the most "rubbery" materials are tri-blocks of H - S - H sequence, polyurethanes usually have alternating urethane (H) and soft segment. The elastic nature increases with the volume ratio of the soft segments, as well as with their length. Naturally, the degree of flexibility of the soft segment chains has a cardinal significance.

Separation of the phases proceeds according to the principle of achieving a maximum of separation at a minimum of the separating surface; this is just a matter of thermodynamics. The noncrystallizable blocks may agglomerate into spheres, or lamellae, or cylindrical forms. The crystallizable segments may form all kinds of crystalline morphological structures: spherulitic, lamellar.[61] Low temperature, high viscosity prevent the material from reaching the low energy goal. Processing of the materials from solution is the answer to the problem.

The proper selection of the solvent to use is not without great significance. The final selection of the most advantageous solvent is a matter of experimenting, and this is nothing new in the area of fiber formation from solution.

It is quite obvious that elastic fibers cannot be subject to cold drawing. For this reason it is even more important to provide for such process conditions which lead to the proper morphological organization at the moment of formation. There is little that can be done later. That "little" may be annealing which improves phase separation and perhaps coalesces some small, more dispersed areas.[61]

Extrusion of block copolymer melts is difficult. Even polymers of relatively low molecular mass, like elastomeric polyesters or polyamides, often show plug type flow in capillaries during melt extrusion.[62] Despite this, the flow through capillaries may have significant influence on the material properties, and the influence appears to be rather erratic.[63] In general, it is known that the large forces involved in extrusion through capillary brutalize the phase separation and it is a rule that comforting of a material gives better results.

V.7 Hard Elastic Fibers

In 1965, Celanese Corporation of America was granted a Belgian patent related to the invention of polyoxymethylene fibers of $2g/den$ tenacity and up to 250% of break elongation accompanied with a high recovery – 92% from 50% extension.[64] One year later a U.S. Patent was issued to DuPont De Nemours and Co. for similar fibers made of polypropylene and showing elongations at break up to 700%, but not quite as good a recovery as the previous work.[65] In both of the cases, the fibers were highly crystalline. Later it was shown that the so called *hard elastic fibers* may be obtained from practically any semicrystalline polymer, like nylon 6, poly(4-methyl pentene-1), poly(pivalolactone).

The initial publications, mostly patents, on the subject gave rather involved descriptions of the operational process variables leading to the hard elastic fibers. Work on the structure associated with such elastic fibers followed for some fifteen years, some of the highest caliber researchers became involved in it. From today's perspective, the results of all the investigations may be summarized as in figure V.12.

The elastic fiber structure consists primarily of crystalline mats which grow epitaxially on a small number of row nuclei. Besides being limited in number, most of the row nuclei are also limited in their length. The number of fibrils in an elastic fiber is very small, and preferably consisting of strongly distorted *destructible micro- paracrystals* of a small size along the a and b-crystalline axes.[66–70] There should be a rather small number of tie molecules involving an equally small fraction of the paracrystalline mosaic blocks of which the mats are built.

On extension, large segments of the lamellae bend and tilt, thereby increasing the interlamellar distance on portions of their surface. For this reason, the number of interlamellar connections needs to be small. The separation of the lamellae produces voids, which leads to an increase of the specimen volume on extension. Such volume increase has no place in the extension of rubbers or polyurethanes. During the investigation of the hard elastic fibers, the existence of the destructible micro-paracrystals has been determined. Up to twelve per cent of their volume could decrease on extension; this decrease means that the folds were transformed into link molecules. The unfolding is reversible, on cessation of strain the chains are folded back into their previous, or similar, positions.[70,72]

If in retrospect one analyzes the process conditions leading to the hard elastic fibers, particularly with the recent results obtained on crystallization in flowing polymer (section IV.5), it is easy to realize that all the precautions led toward the limiting of the rate of nucleation. If the process of nucleation is faster than the crystal growth, then increases the number of row nuclei which extend over larger distance and connect many lamellae in th *shish-kebob* fashion. Also, based on the work of Barham and Keller[11], one may suppose that under such process conditions the number of double or triple folds – *ergo* – tie molecules, would be drastically smaller.

In thermodynamic terms, the energy elasticity plays a role only below the yield

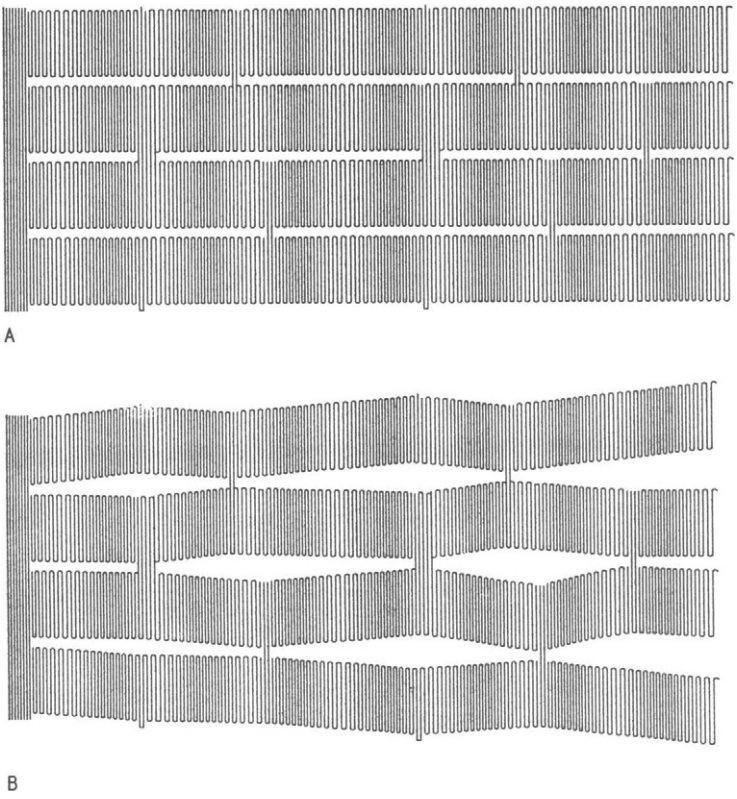

Figure V.12: *Schematic representation of the structure of hard elastic fibers: A - relaxed, B - strained.*

point, that is, below some five per cent of elongation. Above the yield point, the free energy increases with the increasing strain due to growth of inner surfaces. Entropy effects are classified as having a minor effect. The retractive force connected with generation of the link molecules on extension is mainly determined by the surface tension of the newly created surfaces.[70]

The hard elastic fibers did not make any great commercial career. The reason for this is simple: with the level of technical skills in the industry at the time of discovery of these fibers it was difficult to assure sufficient reproducibility of the processes. And last, though not least, the properties are insufficient to compete with polyurethane fibers. Recovery after extension in hard elastic fibers is relatively good, but that is relatively to the hard fibers, not to the elastic fibers.[71] And this is the key property of interest.

Why are we discussing here the hard elastic fibers? To show the wealth of possible structures obtainable from crystallizable polymers. If to connect the possibilities of development various structures with the sound ways of process manipulation, new sets of properties may be generated. Consequently, one may treat this

information merely as stepping stones to technology expansion to newer groups of polymers, perhaps to new formation methods. The work on the structure of hard elastic fibers brought many solutions to the problems concerning also the "regular", the "conventional" fibers, mass produced for the apparel industry, as well as for the more exotic applications.

V.8 References

1. Z. K. Walczak, *J. Appl. Polymer Sci.*, **17 (1973)**, 177. 1
2. H. Sasano, T. Kawai, *Makromol. Chem.*, **184 (1983)**, 217.
3. P. J. Hendra, M. A. Taylor, and H. A. Willis, *J. Polymer Sci, Pt. C., Polymer Letters*, **24 (1986)**, 83.
4. J. D. Tanzer, B. Crist, and W. W. Graessley, *J. Polymer Sci., Pt. B, Polymer Phys.*, **27 (1989)**, 859, 875.
5. R. B. Williamson and R. C. Novak, *J. Polymer Sci., Polymer Letters*, **5 (1967)**, 147.
6. W. R. Pechhold, *Colloid Polymer Sci.*, **258 (1980)**, 269.
7. W. R. Pechhold and H. P. Grossmann, *Faraday Discuss. Chem. Soc,*, **68 (1979)**, 58.
8. W. R. Pechhold, T. Gross, and H. P. Grossmann, *Colloid Polymer Sci.*, **260 (1982)**, 378.
9. W. R. Pechhold, *Polymer Bull.*, **7 (1982)**, 615.
10. W. R. Pechhold, *Makromol. Chem. Suppl.*, **6 (1984)**, 163.
11. P. J. Barham and A. Keller, *J. Polymer Sci., Pt. B, Polymer Phys.*, **27 (1989)**, 1029.
12. E. W. Fischer, K. Hahn, J. Kugler, U. Struth, R. Born, and A. Stamm, *J. Polymer Sci., Polymer Phys. Ed.*, **22 (1984)**, 1491.
13. Z. K. Walczak: *Formation of Synthetic Fibers*, Gordon and Breach, London - New York, 1977, p. 131.
14. G. Kanig, *Progr. Col. Polymer Sci.*, **57 (1975)**, 176. 14.
15. R. Bonart and R. Hosemann, *Makromol. Chem.*, **34 (1960)**, 105.
16. R. Bonart, *Kolloid - Z.*, **194 (1964)**, 97; **211 (1966)**, 14.
17. I. G. Voigt - Martin, E. W. Fischer, and L. Mandelkern, *J. Polymer Sci., Polymer Phus. Ed.*, **18 (1980)**, 2347.
18. G. R. Strobl, M. J. Schneider, and I. G. Voigt - Martin, *J. Polymer Sci., Polymer Phys. Ed.*, **18 (1980)**, 1361.
19. F. J. Padden and H. D. Keith, *J. Appl. Polymer Sci.*, **37 (1966)**, 51.
20. K. Katayama, T. Amano, and K. Nakamura, *Kolloid - Z.*, **226 (1968)**, 125.
21. N. Kasai and M. Kakudo, *J. Polymer Sci., Pt. A*, **2 (1964)**, 1955.
22. R. Hosemann, *Polymer*, **3 (1962)**, 349.
23. R. Bonart and R. Hosemann, *Kolloid - Z.*, **186 (1962)**, 16.
24. R. Hosemann, W. Wilke, and F. J. Balta - Calleja, *Acta Cryst.*, **21 (1966)**, 118.

25. R. Hosemann, K. Lemm, A. Schönfeld, and W. Wilke, *Kolloid - Z.*, **216-217 (1967)**, 103.
26. A. Peterlin, *J. Polymer Sci., Pt. C*, **No 9 (1965)**, 61. 26.
27. I. L. Hay and A. Keller, *Kolloid - Z.*, **204 (1965)**, 43.
28. A. Peterlin and K. Sakaoku, *J. Appl. Phys.*, **38 (1967)**, 4152.
29. K. Kobayashi *cit. in* P. H. Gail, *Polymer Single Crystals*, Interscience Publ., New York, 1963.
30. T. Matsumoto, T. Kawai, and H. Maeda, *Makromol. Chem.*, **107 (1967)**, 250.
31. Z. K. Walczak, *unpublished paper*, 1969.
32. K. Fujimoto, K. Iohara, S. Oswaki, and Y. Murase, *J. Appl, Polymer Sci.*, **42 (1991)**, 1509.
33. R. D. van Veld, G. Morris, H. R. Billica, *J. Appl. Polymer Sci.*, **12 (1968)**, 2709.
34. H. R. Billica, paper presented at *Meeting of The Society of Rheology*, Knoxville, Tennessee, October, 1971; *Private communications*, 1970 - 1972. 34.
35. D. C. Prevorsek, G. A. Tirpak, P. J. Harget, and A. C. Reimschuessel, *J. Macromol. Sci., - Phys.*, **B9 (1974)**, 733.
36. M. Panar, P. Avakian, R. C. Blumke, K. H. Gardner, T. D. Gierke, and H. H. Yang, *J. Polymer Sci., Polymer Phys. Ed.*, **21 (1983)**, 1955.
37. J. M. Brady and E. L. Thomas, *Polymer*, **30 (1989)**, 1615.
38. R. Hosemann, *Polymer*, **3 (1962)**, 349.
39. M. Aboulfaraj, C. G'Sell, B. Ulrich, and A. Dahoun, *Polymer*, **36 (1995)**, 731.
40. W. Chen, Y. Fu, B. Wunderlich, and J. Cheng, *J. Polymer Sci., Pt. B, Polymer Phys.*, **32 (1994)**, 2661.
41. W. Glenz, A. Peterlin, and W. Wilke, *J. Polymer Sci., Pt. A-2*, **9 (1971)**, 1243.
42. S. Nagaou, *J. Macromol. Sci. - Phys.*, **B10 (1974)**, 115.
43. J. Petermann and H. Gleiter, *J. Polymer Sci., Phys.*, **10 (1972)**, 2333; **1 (1973)**, 359.
44. T. Tagawa, T. Tabuchi, M. Kashima, and K. Kobayashi, *J, Macromo. Sci. - Phys.*, **B10 (1974)**, 331.
45. C. L. Hammond, P. J. Hendra, B. G. Lator, W. F. Maddams, and H. A. Willis, *Polymer*, **29 (1988)**, 49 *and ref. cited.*
46. K. Prasad, D. T. Grubb, *J. Polymer Sci., Pt. B, Polymer Phys.*, **28 (1990)**, 2199.
47. D. L. Tzou, K. Schmidt - Rohr, and H. W. Spiess, *Polymer*, **35 (1994)**, 4728.
48. A. O. Baranov and E. V. Prut, *J. Appl. Polymer Sci.*, P**44 (1992)**, 1557.
49. F. Pinaud, J. P. Jarry, Ph. Sergot, and L. Monnerie, *Polymer*, **23 (1982)**, 1575.
50. A. Peterlin, *J. Polymer Sci., Pt. B*, **2(1963)**, 279. 50
51. J. D. Hoffman, *S. P. E. Trans.*, **4 (1964)**, 315.
52. H. H. Kausch and C. J. G. Plummer, *Polymer*, **35 (1994)**, 3848.
53. Z. K. Walczak, *previously unpublished results*, 1992.
54. V. Capuccio, A. Coen, F. Bertinotti, and W. Conti, *Chim. e Ind. (Milano)*, **44 (1962)**, 463.
55. D. Hofmann and E. Schultz, *Polymer*, **30 (1989)**, 1964. 55.
56. D. E. Turek and G. P. Simon, *Polymer*, **34 (1993)**, 2750; 2763.

57. P. Maïssa, A. Ten Bosch, and P. Sixou, *J. Polymer Sci., Polymer Letters Ed.*, **21 (1983)**, 757.

58. D. J. Blundell, A. Mahendrasingam, D. McKerron, A. Turner, R. Rule, R. J. Oldman, and W. Fuller, *Polymer*, **35 (1994)**, 3875.

59. A. M. Hindeleh, R. Hosemann, G. Hinricksen, and H. Springer, *Polymer Comm.*, **31 (1990)**, 205.

60. T. Ohta, *Polymer Eng. Sci.*, **23 (1983)**, 697.

61. M. Dröscher, U. Bandara, and F. G. Schmidt, *Makromol. Chem., Suppl.*, **6 (1984)**, 107.

62. Z. K. Walczak, *previously unpublished results*, 1983.

63. J.-M. Charrier and R. J. P. Ranchoux, *Polymer Eng. Sci.*, **11 (1971)**, 381. 63.

64. *Belgian Pat.* **No 650,890 (Jan., 1965)** to Celanese Corporation of America.

65. A. J. Herrman, U. S. Pat. No 3,256,258 (June, 1966) to Du Pont De Nemours and Co., Inc.

66. R. Hosemann, J. Laboda-Čačković, and H. Čačković, *J. Polymer Sci., Polymer Symp.*, **42 (1973)**, 563.

67. E. Ferracini, A. Ferrero, J. Laboda-Čačković, R. Hosemann, and H. Čačković, *J. Macromol. Sci., Phys.*, **B10 (1974)**, 97. 67.

68. R. Hosemann, J. Laboda-Čačković, and H. Čačković, *Colloid Polymer Sci.*, **254 (1976)**, 782.

69. G. S. Y. Yeh, R. Hosemann, J. Laboda-Čačković, and H. Čačković, *Polymer*, **17 (1976)**, 309.

70. J. Laboda-Čačković, H. Čačković, and R. Hosemann, *J. Macromol. Sci., Phys.*, **b16 (1979)**, 127.

71. S. L. Cannon, G. B. McKenna, W. O. Statton, *J. Polymer Sci., Nacromol. Rev.*, **11 (1976)**, 209.

72. R. Hosemann, *Makromol. Chem. Suppl.*, **1 (1975)**, 559. 72.

73. L. C. E. Struik, *Polymer*, **30 (1989)**, 799, 815.

74. B. K. Annis, J. Strizak, G. D. Wignall, R. G. Alamo, and L. Mandelkern, *Polymer*, **37 (1996)**, 137.

75. Z. Bartczak, A. Gałęski, A. S. Argon, and R. E. Cohen, *Polymer*, **37 (1996)**, 2113.

76. M. I. Aabo El Maaty, D. C. Basset, R. H. Olley, M. G. Dobb, J. G. Tomkam and I. – C. Wang, *Polymer*, **37 (1996)**, 213.

77. W. A. Kernick III and N. J. Wagner, *Macromolecules*, **32 (1999)**, 1159.

78. N. S. Murthy, D. T. Grubb, K. Zero, C. J. Nelson, and G. Chen, *J. Appl. Polymer Sci.*, **70 (1998)**, 2527.

79. D. T. Grubb and L. W. Jelinski, *Macromolecules*, **30 (1997)**, 2860.

80. W. G. Hu and K. Schmidt - Rohr, *Acta Polym.*, **50 (1999)**, 271.

81. I. F. Govaert and P. J. Lemstra, *Coll. Polymer Sci.*, **270 (1992)**, 455.

82. R. H. Boyd, *Polymer*, **26 (1988)**, 323.

83. S. Bensason, J. Minick, A. Moet, S. Chum, A. Hiltner, and E. Baer, *J. Polymer Sci., Part B, Polymer Phys.*, **34 (1996)**, 1301.

84. W. T. Mead and R. S. Porter, *J. Polymer Sci., Polymer Symp.*, **63 (1978)**, 289.

85. I. Liberwirth, J. Loos, J. Petermann, A. Keller, *J. Polymer Sci., Pt. B, Polymer Phys.*, **38 (2000)**, 1183.

VI ENGINEERING PHYSICS

VI.1 Flow of Cooling Media

Fiber formation is always connected with handling of fluid flow of one sort or another. In the case of formation from melt, the filaments must be cooled. This is done mostly with the help of air, though on rare occasions a liquid (water) may be used. In cases of formation from solution, it is necessary to use either air for dry processes or liquids for wet processes. In every case, the questions of fluid dynamics is of major interest.

Occasionally, air is used as a means of transporting fibers. In some processes, aerodynamic drag is used as means to generate drawing force. Such processes are most often used in spunbonded processes. If a spunbonded process uses mechanical transport, air jets are applied for depositing the fibers on the conveying belts. The air flow in the equipment for fiber transport is somewhat more complex than in cooling problems.

VI.1.a Quench Systems

For fiber cooling, the air flow is applied either in *cross flow* or in *co-current flow*, which is some times called *radial flow*. In cases of dry formation from solution, the drying air (or neutral gas) is applied either in *co-current* or in *counter current*. The last system is used in formation from melt only exceptionally. In formation from melt, perhaps the most frequent is *cross flow* mode; this is the oldest system and still very popular.

An example of the realization of cross flow quench is given in figure VI.1. Previously conditioned to temperature and proper humidity, the air is introduced into a flow distribution chamber, A. The air stream is then directed perpendicularly to the filaments. Before the air reaches the fibers, however, it passes through a flow equalization honey comb layer, or layers, E, to force the air into a parallel flow. Sometimes honey comb is replaced with thick metal plates that have a plurality of holes. This is a less expensive method, but is "aerodynamically not recommended". Behind the honey comb, at least one layer of fine mesh screen should be placed to remove any vorticity from the air. More sophisticated, highly recommended equipment has the air introducing equipment segmented. The segments are provided with individual flow regulators, R, consisting of louvers or plates with mismatched holes. The last possibility appears aerodynamically more favorable. In the really elaborate systems, each segment may have individual temperature control. Plates, P, parallel to the axis of filament travel, are usually placed in order to guide the stream of flowing air to avoid unnecessary turbulence which may be caused by room drafts and by a pumping action of the moving filaments.

Figure VI.1 also shows a provision for the removal of fumes, D, emanating from the hot fibers and consisting of byproducts of polymer degradation and evaporat-

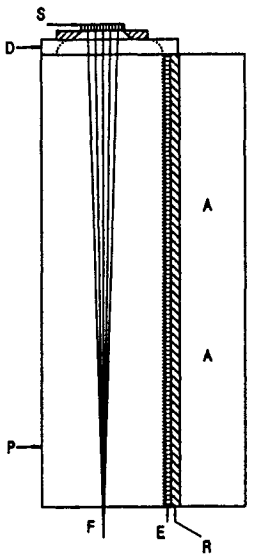

Figure VI.1: *Cross flow quench, with air flow perpendicular to the filaments. Explanation in text.*

ing or subliming additives, e.g. stabilizers. The fume removal arrangement is not a part of the quench system, but it usually does affect the work of the system. The majority of fumes is generated where the fibers are the hottest, close to the spinnerette, and therefore a "bar" or "ring" with applied suction is located as closely under the spinnerette as possible. The aspirated smoke must be led as early as possible through some condensing, dust retention, or absorbing equipment to remove the pollutants from the air before it is discharged back into the atmosphere. The suction may potentially influence the pattern of quench air flow. Good precautions should be taken that the cold air aspirated by the fume removal does not bounce off the spinnerette surface. With incompletely efficient fume removal, bouncing off spinnerette face included, some of the fume components may become deposited on the spinnerette surface. This requires cleaning, and this, in turn, diminishes the effective operating time.

The fume removing bar, square, or ring consists of a pipe with either a round or rectangular cross section, ranging from two to a maximum of ten centimeters in diameter and provided with a slot through which the air surrounding the fibers is aspirated. Only rarely is the fume removal supplied with air of its own; mostly it operates on "stolen" quench air.

In large commercial processes, all of the air used for quenching must be removed. The design of this is not very difficult, but care must be taken not to alter the intended quench pattern. The separate fume removal is necessary, as it is easier to purify a smaller volume of air. The importance of the fume removal to environmental protection is obvious. Design of this area should be treated care-

fully as air flow disturbances in this zone may very adversely affect the quality of fibers, especially their uniformity.

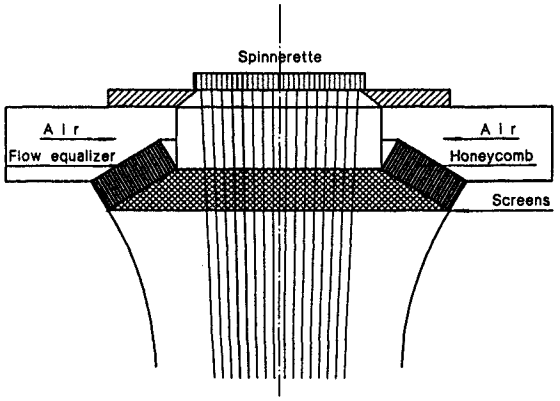

Figure VI.2: *Co-current quench, one of possible solutions for air introduction. Explanation in text.*

The parallel flow quench systems, sometimes called "radial systems", are usually preferred for processes utilizing round spinnerettes of 500 to 1500 filaments where there exists a concern about high fiber to fiber uniformity. The cooling air is introduced from a circumferential orifice inward, radially toward the center of the filament bundle. Naturally, non-circular spinnerettes do not prohibit the use of co-current quench. In the case of rectangular spinnerettes, the geometry would have to be changed to linear, most likely with two bars instead of a circular arrangement. In standard engineering terminology we are speaking about an axial - co-current system. The air should flow parallel to the axis of filament travel. The stream of air and fibers is usually contained within a pipe, often circular, the diameter of which, naturally, depends on the size of spinline and volume of air.

It proves to be difficult to design the orifice introducing the quench air for parallel flow. One of the possible solutions for circular spinnerettes is given in figure VI.2. The air is preferably introduced through at least two tangentially located inlet pipes to assure good air distribution in the circular main channel. The resulting circular motion of the air is broken by the equalizers, consisting of a bent honeycomb or a large number of capillary like holes drilled in a circular partition. Though the threadline comes in contact with the quenching air with some delay, the geometry of this solution allows the use of relatively high air velocities without causing appreciable disturbances of the threadline. Other possible solutions permit an earlier exposure of fibers to the quenching air, but they are more vulnerable to formation of air turbulence. On the other hand, delay of quench is a good technique applied often on purpose, and in such cases the delay may be many times larger than the necessary delay inherent to the design in figure VI.2.

An interesting solution for a co-current quench has been offered by Fuji-Filter Co. Cooling air is led between the walls of a double walled tube. The inner wall is made of slots inclined to direct the air stream radially. The initial angle of the air travel is around 75° in relation to the fiber path. The cooling air is introduced

from the bottom of the double walled tube which surrounds the fibers as they exit from the spinnerette.

There is no question, cross flow quench is more efficient and it offers relatively easy ways of *profiling* the flow intensity, as well as temperature along the filament path. As the negative points one must give the bellowing of the spinline, especially with higher intensity flow and with longer quench zones. In cases of large multi-filament spinlines, the air must pass through a large number of fiber rows, and as a result, the air flow intensity rapidly decreases and the temperature increases for each following row. This leads to a large gradient in quality of the fibers due to the unavoidable gradient in cooling intensity.

The co-current quench gives substantially better cooling uniformity, but overall quench efficiency is smaller, unfit for profiling. The low cooling efficiency may require intensive flow and this, in turn, on occasions may create excessive drag force on the fibers, thereby contributing to filament breaks.

Substantial increase in cooling intensity, as compared with co-current flow, may be obtained with a counter-current system. The air introduction is located at the level of exit of fibers. It does not require so careful a design since at this point the fibers have higher velocity and are not so fragile. Removal of the spent quench air close to the spinnerette is the critical point. Lacing up of a spinning position requires that the quench air be closed. Filament breaks create more unforgiving situations. Profiling of cooling intensity is also impossible. For dry formation from solution, in turn, this is the preferred solution.

VI.1.b Fluid Dynamics

In fiber formation from melt, in the quench zone the fibers exchange heat with the flowing air, hence air temperature is changing. As a matter of fact, in the dry formation from solution we have a similar situation, except that instead of air we have air with a changing concentration of solvent vapors in addition to changing temperature of air. All this means that there is a certain interaction between the moving filaments and the moving fluid.[1]

If we consider cross flow quench system, then the air is, in principle, perpendicular to the moving fibers. We say "in principle" because the fibers converge from a maximum of the diameter of the spinnerette hole pattern down to practically zero on the take up rollers or on a converging guide. In effect, we have a certain angle, usually not exceeding some 5°, perhaps 7°, between a fiber and the system axis, and the angle varies within the fiber tow. On occasions, the air may be guided under an angle somewhat different than 90°.

An object located in a stream of fluid is subject to drag forces. If we consider a fiber as a cylinder located in a stream of air then the drag exerted on the cylinder is proportional to the velocity component normal to the cylinder axis, which in figure VI.3 is designated v_n. In case that the air attacks the cylinder at an angle λ, the normal velocity component will be:

$$v_n = v \sin \lambda \tag{VI.1}$$

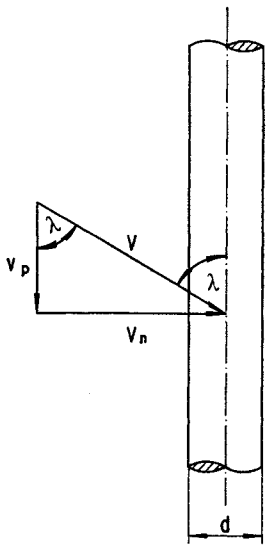

Figure VI.3: *Distribution of fluid velocities in cross flow.*

The flow of a fluid around the cylindrical obstacle depends on the magnitude of the Reynolds number calculated in relation to the cylinder diameter, d. The Reynolds number is given by

$$Re_d = \frac{v_n d}{\nu} \tag{VI.2}$$

where ν is kinematic viscosity of the fluid.*

Figure VI.4 shows schematically different patterns, depending on Reynolds number, of flow around a cylinder. In the figure, Case A corresponds to a laminar flow, case B is at the high limit of laminar flow, case C represents a turbulent flow which is considered[2] to take place above $Re_d > 10^5$. From figure VI.4 one may expect that the pressure around the cylinder should not be equal. Indeed, as shown in bottom of figure VI.4, the pressure, P, varies substantially. According to the potential theory, the pressure around the cylinder depends on the angle ϕ. At the point of incidence the angle is taken as $\phi = 0$.

$$P(\phi) = 1 - 4\sin^2\phi \tag{VI.3}$$

In practice, the pressure deviates rather strongly from that calculated from equation VI.3, and depends to a certain degree on the Reynolds number, as it is evident from figure VI.4. Above the critical value of Reynolds number, 10^5, the flow pattern changes markedly. The pressure differences are responsible, in part, for the drag, as well as for the bellowing. The magnitude of the pressure drag, D, per unit of cylinder length is given by equation VI.4.

$$D = C_D \frac{\rho v_n^2 d}{2} \tag{VI.4}$$

*Data on some physical properties of air are given in the Appendix.

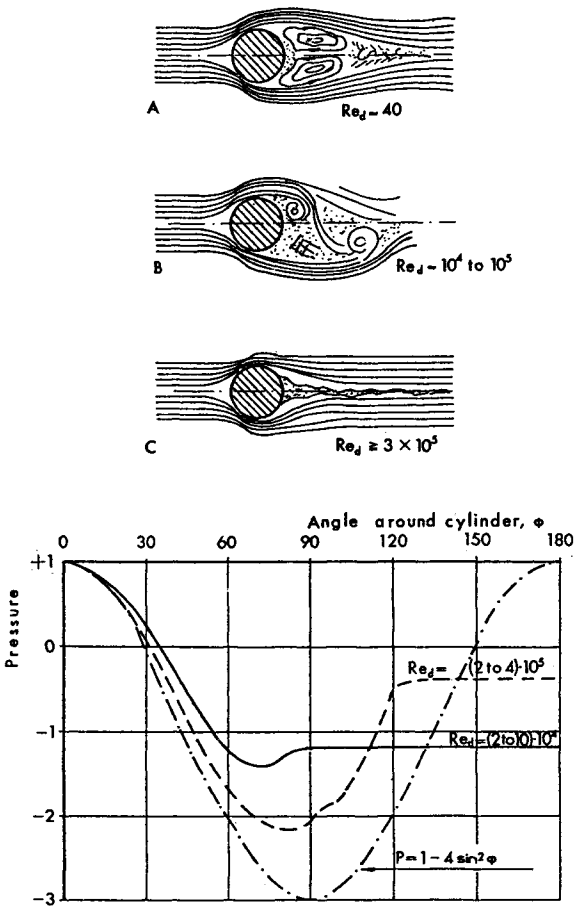

Figure VI.4: *Flow of fluid around a cylinder. Cases A and B laminar flow, case C turbulent flow. Bottom: pressure distribution around the circumference of a cylinder in a perpendicularly flowing stream of gas measured at indicated Reynolds numbers and calculated from equation VI.3. After S. F. Hoerner*[2]

where C_D is the coefficient of pressure drag dependent on the Reynolds number, d is cylinder (fiber) diameter, ρ is density of the fluid (air), and v_n normal component of the fluid velocity.

The magnitude of the coefficient of drag, C_D, in relation to the Reynolds number, Re_d, for a cylinder is shown in figure VI.5. The values may be also calculated with a very good approximation from the following equation, provided that $10^{-2} \leq Re_d \leq 7 \cdot 10^3$:

$$C_D = 9.9785 Re_d^{-0.7723} + 1.2482 Re_d^{-0.0355} \tag{VI.5}$$

The drag for cylinders with non-circular cross sections differs markedly from those with circular cross sections. While the drag coefficient for Reynolds numbers

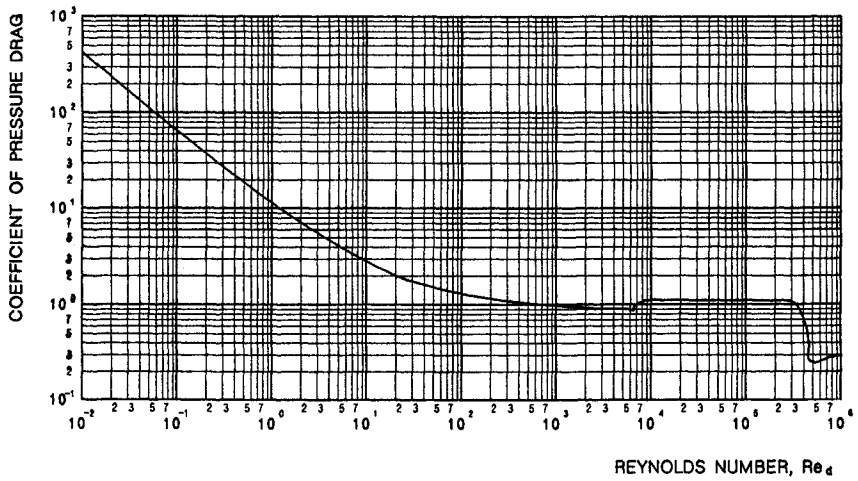

Figure VI.5: *Coefficient of pressure drag in relation to Reynolds number calculated on diameter of a cylinder. After S. F. Hoerner*[2]

10^4 to 10^5 for a circular cylinder is 1.2, for the same range of Reynolds numbers, cylinders with elliptical cross section of 2 : 1 axis ratio $C_D = 0.67$; for even sided triangular cross section with blunt edges $C_D = 1.4$, for a square cross section with blunt edges $C_D = 1.6$.[2]

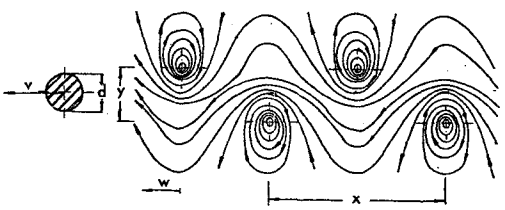

Figure VI.6: *Vortex street resulting from air flow around a long cylinder in transitional flow region. Explanation in text. After S. F. Hoerner*[2]

The perpendicular flow around cylinders may cause one more type of disturbance. The conditions of the transient flow, between laminar and turbulent, (case B in figure VI.4) may produce a so called *vortex street*, which is shown schematically in figure VI.6. The double row of vortices, alternating in their positions, is the reason for the acoustical phenomenon accompanying the vortex street that is called the *Aeolian harp*. The *vortex street* moves with a velocity w, it is some six times smaller than the air velocity, $w/v = 1/6$. The wavelength of the vortex street, x, depends on the diameter of the cylinder, a, and is equal $x = 4.5\ d$. The frequency of the vortices on one side of the street, f, is[3] given by:

$$f = v - w/x \tag{VI.6}$$

In the case when the effect of the "vortex street" would be strong enough to disturb the filaments, fiber nonuniformities might be caused with frequencies which

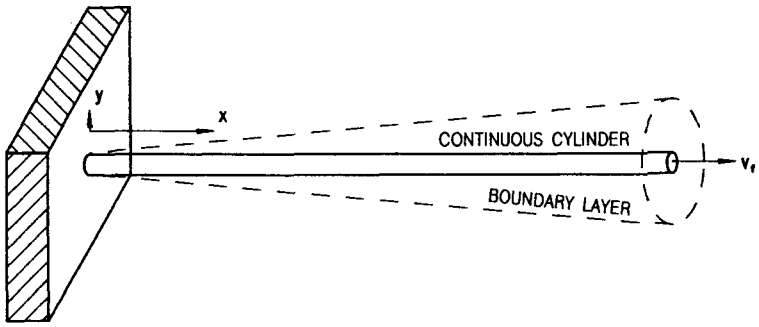

Figure VI.7: *Boundary layer around a moving continuous cylinder.*

could be of concern. If the vortex street is not strong enough to be detrimental to the fiber quality, it must be considered in every multifilament formation since the air flow after passing the first line of filaments is no longer laminar. No theoretical solution of these questions is available.

In the co-current quench system, the air flow is more or less parallel to the axis of the filament travel. The deviation from exactly parallel flow is by as much as is caused by the convergence of the filaments in the spinline. The parallel flow is the cause of frictional drag.

A theoretical solution for the frictional drag and for the boundary layer question for a continuous cylinder has been proposed by B. C. Sakiadis[3]. The boundary layer of a continuous cylinder emerging from a die or capillary, C, as presented in figure VI.7, is different from the boundary layer of a moving cylinder of finite length. In the first case, the boundary layer grows in the direction of motion, while in the latter case the direction of boundary layer growth is opposite.

As a starting point, Sakiadis takes the boundary layer equations for laminar, steady, and incompressible flow on a moving continuous cylindrical surface:

$$v\frac{\partial v}{\partial x} + v_n\frac{\partial v}{\partial r} = v\left(\frac{\partial^2 v}{\partial r} + \frac{1}{r}\frac{\partial v}{\partial r}\right), \tag{VI.7}$$

$$\frac{\partial v}{\partial x} + \frac{\partial v_n}{\partial r} + \frac{v_n}{r} = 0 \tag{VI.8}$$

where v is the fluid velocity component in the direction parallel to the cylinder axis x, v_n is the fluid velocity component parallel to the cylinder radius and directed along the y axis, which is normal to the cylinder axis x, r is the cylindrical coordinate from the axis of the cylindrical surface, a is cylinder diameter, and ν is kinematic viscosity of the fluid. The boundary conditions are set as follows: $v = v_f$; $v_n = 0$ at $r = a$; $v \to 0$ at $r \to \infty$. Additionally, it is assumed that

$$\left(\frac{\partial v}{\partial r}\right)_{r=\infty} = 0$$

The boundary conditions assumed for the continuous surface represent the difference in comparison with the solution for a cylinder of a finite length.

The major problem connected with the proposed solution of these equations is the selection of a velocity profile. Sakiadis[3] assumes the following velocity profile:

$$\frac{v}{v_f} = \left[1 - \frac{1}{\beta}\ln\left(1 + \frac{y}{a}\right)\right] \tag{VI.9}$$

where β is a function of x but is not a function of y.

Consequently, Sakiadis derived the following equations for the major parameters connected with the motion of a continuous cylindrical surface: Total dimensionless local coefficient of friction is:

$$C'_F = \frac{2\tau}{\rho v_f^2} = \frac{2\nu}{\beta a v_f} \tag{VI.10}$$

Total drag on the continuous surface is:

$$D_F = 2\pi a \int_{x=0}^{x=L} \tau_f dx = \rho v_f^2 \theta \tag{VI.11}$$

The dimensionless coefficient for total drag is:

$$C_F = \frac{D}{\rho \pi a L v_f^2} = \left(\frac{\theta}{\pi a^2}\right)\left(\frac{a}{L}\right) \tag{VI.12}$$

The pumping action or total volume of the fluid entrenched by the moving surface S is:

$$q = \Delta v_f \tag{VI.13}$$

The remaining notation in the equations VI.10 through VI.13 is: θ is the momentum area in dimensionless form and may be given as

$$\frac{\theta}{\pi a^2} = \frac{e^{2\beta} - 1}{2\beta^2} - \frac{1}{\beta} - 1 \tag{VI.14}$$

where β may be defined as

$$\frac{d\beta}{dx} = \frac{4v}{v_f a^2} \tag{VI.15}$$

or in its integral form

$$\frac{4vx}{v_f a^2} = 2\int_{\beta=0}^{\beta} \left(\frac{\beta e^{2\beta} - e^{2\beta}}{\beta^2} + \frac{1}{\beta} + \frac{1}{\beta^2}\right) d\beta \tag{VI.15 a}$$

The displacement area, Δ, may be given as dimensionless displacement area

$$\frac{\Delta}{\pi a^2} = \frac{e^{2\beta} - 2\beta - 1}{2\beta} \tag{VI.16}$$

and the dimensionless boundary layer thickness, δ, is

$$\frac{\delta}{a} = e^{\beta} - 1 \tag{VI.17}$$

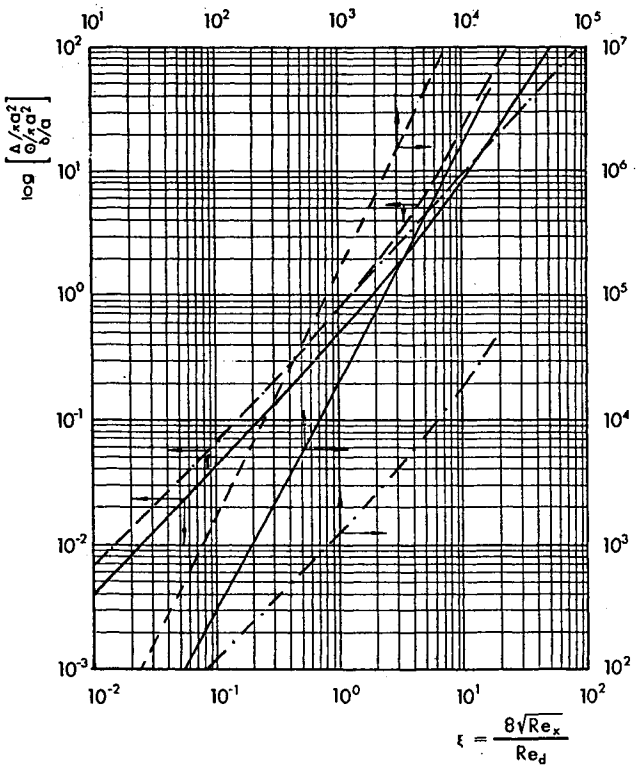

Figure VI.8: *Parameters of the moving continuous boundary layer which are dependent on ξ, a function of Reynolds numbers: δ/a – · – ; $\theta/\pi a^2$ —; $\Delta/\pi a^2$ - - -. After B. C. Sakiadis.*[3]

Figure VI.8 presents three parameters, $(\theta/\pi a^2), (\Delta/\pi a^2)$, and (δ/a) in relation to the parameter ξ, which is given by

$$\xi = 4\left(\frac{vx}{v_f a^2}\right)^{0.5} = \frac{8(Re_x)^{0.5}}{Re_d} \tag{VI.18}$$

The values of the momentum area given in the nomogram of figure VI.8 up to $\xi = 20$ may be calculated with a sufficient accuracy from the following algorithm:

$$\frac{\theta}{\pi a^2} = 1.2381\xi^{1.3428} \tag{VI.19}$$

The above quoted solution has been derived for the boundary layer problem for laminar flow, that is, for Reynolds numbers up to $Re = 10^5$. In the same series of publications, Sakiadis[3] also gives an approximate solution for turbulent flow conditions. The approach is supported by equations for continuous flat surface and determination of correcting ratios for curvature.

Total drag for turbulent flow is given as

$$D = \rho v_f^2 2\pi a\delta \left(\frac{1}{36} + \frac{1}{240}\frac{\delta}{a}\right) \tag{VI.20}$$

where δ represents the boundary layer thickness, and may be estimated from the following equation

$$\left(\frac{\delta}{a}\right)^{1.25} + 0.167\left(\frac{\delta}{a}\right)^{2.25} = 1.01\frac{x}{a}\left(\frac{v}{v_f a}\right)^{0.25} \tag{VI.21}$$

or from the formula

$$\frac{\delta}{a} = \kappa\lambda^{0.8} \tag{VI.22}$$

where

$$\lambda = \left[\frac{x}{a}\left(\frac{v}{v_f a}\right)^{0.25}\right] \tag{VI.22 a}$$

The relation between the coefficients κ and λ is given in table VI.1.

The ratio of the boundary layer thickness on a continuous cylindrical surface to the boundary layer thickness on an equivalent flat surface is

$$\frac{\delta}{\delta_p} = \kappa \tag{VI.23}$$

while the ratio of drag on the continuous cylindrical surface to the drag on an equivalent continuous flat surface is

Table VI.1
Relation between coefficients of equation for thickness of boundary layer in turbulent flow.[3]

$\lambda^{0.2}$	κ	$\lambda^{0.2}$	κ
0.0	1.000	3.0	0.281
0.5	0.987	3.5	0.220
1.0	0.891	4.0	0.177
1.5	0.682	5.0	0.122
2.0	0.500	6.0	0.088
2.5	0.671	7.0	0.068

$$\frac{D}{D_p} = \kappa\left[1 + 0.152\left(\frac{\delta}{a}\right)\right] \tag{VI.24}$$

The relationship between D/D_p and λ is given in table VI.2.

The boundary layer parameters for turbulent flow on a cylindrical surface are given also in figure VI.9. The momentum area may be calculated with good accuracy from the following simpler algorithm:

$$\log\left(\frac{\theta}{\pi a^2}\right) = -0.34256 + 1.0481\log\xi + 0.1824(\log\xi)^2 \qquad \text{(VI.25)}$$

Table VI.2
Relation between coefficients relating drag on continuous cylinder to continuous flat surface in turbulent flow.[3]

$\lambda^{0.2}$	D/D_p	$\lambda^{0.2}$	D/D_p
0.0	1.00	3.0	1.25
0.5	1.00	3.5	1.33
1.0	1.01	4.0	1.40
1.5	1.05	5.0	1.54
2.0	1.11	6.0	1.65
2.5	1.18	7.0	1.75

By Sakiadis's own admission and by later empirical investigations by many authors,[4–8] despite the apparent correctness of the theoretical solutions, the calculated coefficients of drag are much too small. Since the work by Sakiadis was published, several other attempts to solve the problems have appeared.[9–12] These works are not quoted here as the results deviate no more than 16% upwards of those of Sakiadis; it is simply not enough, by far. The general relationship used in the empirical solutions for the coefficient of drag is

$$C_f = BRe_d^a \qquad \text{(VI.26)}$$

The coefficients in equation VI.26, as quoted by different authors, are summarized in table VI.3. Measurements done by this author in a high velocity air drawing jet[15] fit fairly well with the coefficients given by Glicksman[5]; however, they fit much better with the re-evaluated results of Gould and Smith[8]. The equation coefficients for this fit are given in the last row of table VI.3. The differences quoted here amount to the calculations of Sakiadis multiplied by a factor of up to 3.5.

Gould and Smith[8] have investigated also the effect of proximity of fibers in a bundle. The authors have found that somewhere between the distance of 1200 μm and 670 μm and below, the filament boundary layers begin to affect each other to modify the drag force. For filaments spaced below that critical spacing, the coefficient of drag needs to be multiplied by a factor of approximately 0.83.

There were speculations about the reason for the deviations of the experimental coefficient of drag and the calculated values. The fluttering of the filaments, that is, vibrations of filaments along normal to the direction of motion was suggested as a potential reason. Such vibrations would change the flow pattern into

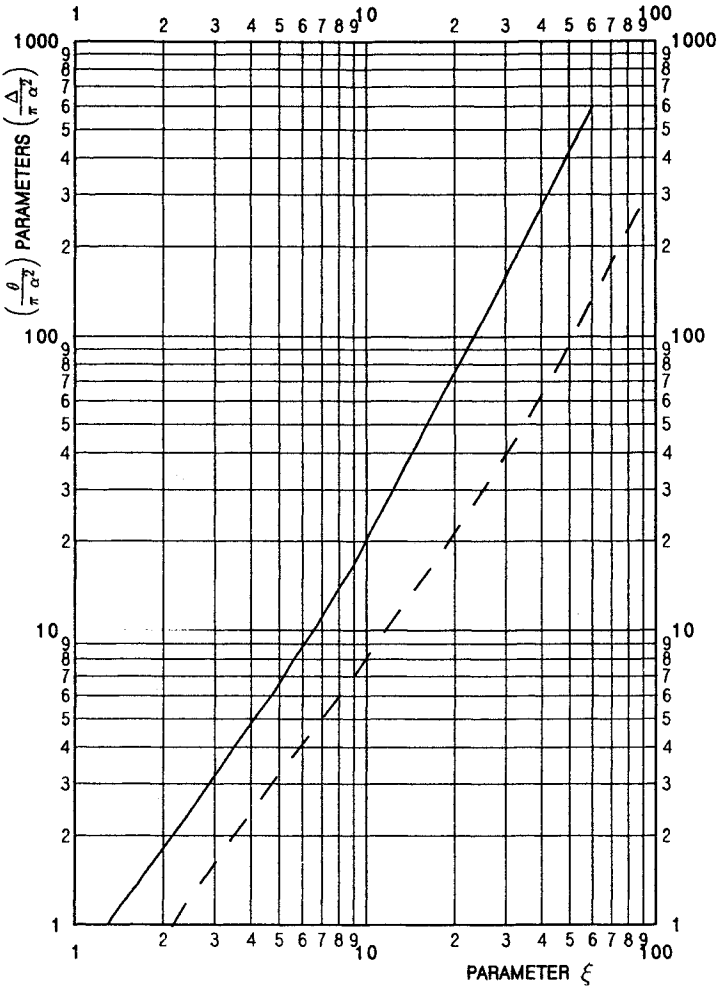

Figure VI.9: *Boundary layer parameters for cylindrical surfaces:* $\theta/(\pi a^2)$ *- continuous line,* $\Delta/(\pi a^2)$ *- dashed line. After B. C. Sakiadis*[3].

Table VI.3
Coefficients in equation VI.26 describing frictional drag.

From Re_d	To Re_d	B	a	ref
20	150	0.85	- 0.61	9
-	50	0.65	- 0.70	5
4	54	0.37	- 0.61	10
20	200	0.39	- 0.8	4
20	200	0.27	- 0.64	4, 8
20	200	0.24	- 0.61	6
50	300	0.36	- 0.50	15

a combination of axial and cross flow. Gould and Smith[8] have investigated the influence of tension applied to the filament on the drag force. They determined that freedom of movement indeed has an effect on the magnitude of drag force, and it is proportional to the fiber diameter: for filaments of 53 μm diameter, drag increased 10 %, while for 150 μm diameter, the increase amounted to 28 % at all tested velocities.

Also other interesting deviations from the boundary layer theory have been reported:[8] as the filament diameter increases above some 50 μm, the drag force decreases, eventually approaching the drag for flat plate. This area concerns filaments immediately after extrusion, close to the spinnerette, where the velocity is still small and the potential error in calculations more tolerable.

In practice, the co-current flow may be conducted close to its "pure form". Cross flow quench, the most frequently used system, always becomes a kind of "mixed flow" due to the axial flow component generated by the pumping action of the moving filaments. The flow pattern becomes even more complicated with the multifilament lines, as every row of filaments has contact with a somewhat different flow pattern of air. Solution of such problems is quoted in section VII.3.

A. Dutta[16,17] has proposed an approximate solution to estimate the magnitude of the pumping effect and its influence on uniformity of fibers in a bundle. Because of the high degree of approximation used in the solution, the work is not quoted here and the interested reader is directed to the original papers.

VI.1.c Fiber Jets

Jets[1] represent a convenient way of applying constant force drawing, provided that the fiber diameter is constant. Drawing jets are usually very forgiving for filament breaks, since a large portion of the breaks is *self threaded. Spunbond* processes use drawing jets almost as a standard of the industry. However, if substantial drawing forces are required, mechanical drawing units may be necessary, and in cases like that the jets are used to receive the fibers from the drawing rollers and to deposit them on a collecting device by simply blowing the fibers on. Naturally, there must be some kind of arrangement for an air removal on the other side of the receiving surface to prevent the fibers from being carried by the air all around.

The main body of the jets usually consists of a duct built of a sheet of metal in the form of a pipe with rectangular cross section. The smaller dimension in the circumference ranges from 10 to 25 millimeters. This "thickness" depends, obviously, on the the size of the spinline and on the questions of pressure drop, as will become clear below. The length of the main body ranges generally between 300 and 750 millimeters, only on rare occasions being longer. An example of such a jet is presented in figure VI.10.

In the design exemplified in figure VI.10, the air enters to the air tanks, which ought to be as large as a design would permit, located at both long sides of the jet. The large size of the tanks is needed to provide low velocity of air flow (assumed

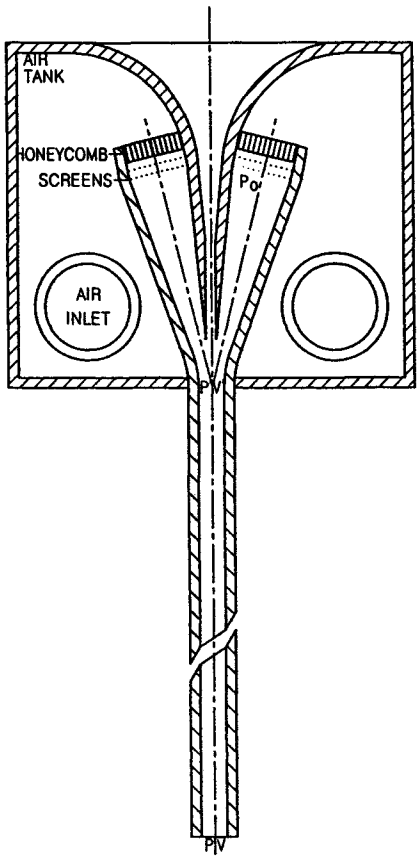

Figure VI.10: *An example of design of air jet for fiber drawing or deposition on surfaces. Explanation in text.*

zero) in this portion of the system. From the tank, the air enters through the honeycomb with a small size of cells and layer(s) of fine mesh screen(s) into a kind of short nozzle. The honeycomb and screens are to force the air into a parallel flow, to "clean" the air from possible vortices, and to create a small pressure difference between the air tank and the air entering the nozzle. Such a pressure difference helps to better equalize the air flow from the air tank to the nozzle, particularly, to equalize the air pressure along the long side of the jet.

The nozzle has a sharply decreasing cross section area to obtain highly accelerated flow. Again, this is a precaution against creation of vortices. Experience dictates that vorticity of flow is the strongest enemy of proper action of many jets, and in fact of many air machines.

At the beginning of the jet proper, the two streams of high velocity air from the two nozzles meet together with the "curtain" of fibers. From this point on the air and the fibers travel together through the length of the jet. During this travel, the air pressure becomes smaller and the air velocity increases. Since the maximum of the drag force exerted on the fibers is approximately at the beginning

of the jet, that is, at the point of junction, the velocity of fibers does not change appreciably during the travel through the jet.

Calculation of the air flow and of the jet performance must begin with a definition of the basic parameters regarding the considered number of fibers and their velocities, the force requirement, the jet design, and air flow. Here we have a number of relations to consider.

The hydraulic diameter of the jet:

$$D_h = \frac{4A}{S} \tag{VI.27}$$

where A is area of the duct cross section and S is the circumference of the duct.

The velocity of sound:

$$v_s = \sqrt{\frac{c_p}{c_v} RT} = 19.8252\sqrt{^\circ K} m/s \tag{VI.28}$$

where c_p and c_v is specific heat of air at constant pressure and constant volume, respectively; the ratio amounts to 1.4 (between $0^\circ C$ and $100^\circ C$ it changes only a fraction of one per cent). R and T have the usual meaning. The Mach number at the considered conditions is

$$M = \frac{v}{v_s} \tag{VI.29}$$

The Reynolds number for this case is defined as

$$Re = \frac{vD_h}{\mu} \tag{VI.30}$$

where μ is kinematic viscosity of air (at room temperature it is $1.4209 \cdot 10^{-2} m^2/s$).

With knowledge of the Reynolds number, one may obtain the friction factor, C_f, from the graph in figure VI.11. A more accurate value may be obtained from a numerical solution of the von Kármán - Nikuradse equation:

$$\frac{1}{\sqrt{C_f}} = -0.8 + 2log(Re\sqrt{C_f}) \tag{VI.31}$$

The other available equations of help are[18]:

$$C_f \frac{l}{D_h} = Y' - Y \tag{VI.32}$$

where

$$Y = \kappa \left\{ \frac{1}{M^2} - \left(\frac{\kappa + 1}{2} \right) \ln \left[\left(\frac{\kappa - 1}{2} \right) + \left(\frac{1}{M^2} \right) \right] \right\} \tag{VI.32 a}$$

Here Y' is Y at the entry to the jet, and $\kappa = c_p/c_v$. And another important equation is

$$\frac{p}{p'} = \frac{Z'}{Z} \tag{VI.33}$$

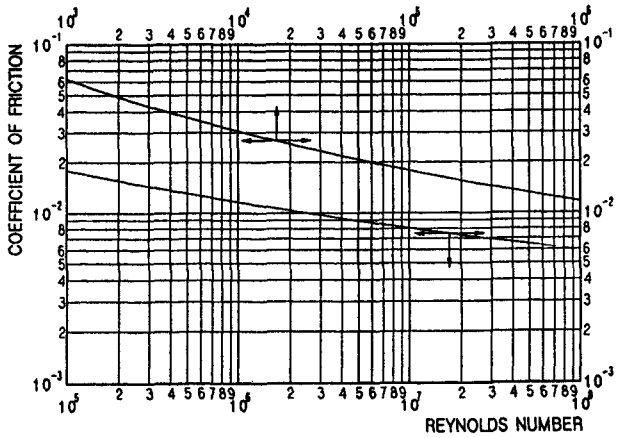

Figure VI.11: *The Kármán - Nikuradse function for friction coefficient in turbulent flow in smooth pipes. After Łukasiewicz*[18]

$$Z = M^2 \sqrt{\frac{\kappa - 1}{2} + \frac{1}{M^2}} \qquad (VI.33\,a)$$

As usually in design work, the main conceptual work is concentrated on working out the basic system in the form of a drawing. One of the biggest challenges here is a provision for the temporary widening of the fiber's entry to facilitate initial introduction of the fibers. The calculational part is rather straightforward, except it is time consuming, as all numerical solutions are.

Both, from the point of view of aerodynamics and economics, it is advantageous to design the jet so to utilize maximum of air velocity, without entering into supersonic flow. In this way, the relative velocity of air *versus* fiber will be at a maximum. The drawing force exerted on the fibers is, aside from the velocity difference, the result of fiber diameter and of the jet length. Such an approach permits the use of a minimum pressure loss due to an excessive length of the jet or large volume of air due to increase of the jet cross sectional area.

Reiterating the physical relationships one may summarize:

- The maximum of air velocity is at the exit of the jet.
- The minimum air velocity is at the beginning of the jet.
- The maximum of fiber velocity is also at the end of the jet.
- The velocity increase over the length of the jet is much larger for the air than for the fibers.
- The maximum of drawing force is located at the entry to the jet.

If the cross sectional area of the jet is small, then the friction factor is large and the air velocity gradient is very steep; the situation may arise that at the jet entry,

the fiber velocity is higher than the air velocity. Such a situation may be corrected by increasing the jet cross section, but this is connected with the requirement of larger air volume.

To impart some flexibility to the jet, and some safety margin, the velocity of air v' ought to be set higher than the fiber velocity at the entry. Based on the fiber diameter and velocity, as well as on the force requirement, one may estimate the air velocity and jet length. The equations needed for this are given in the preceeding section. It is necessary to remember that the drag force must be calculated on the velocity difference, $v_a - v_f$. The jet exit air velocity v translates into Mach number M, and its recommended value should be close to one. The pressure ratio p/p' may be read off of the table of flow parameters *versus* Mach number for subsonic flow[19] (see Appendix). The table gives also the ratio of temperature, which may be needed later to introduce corrections when working on a refinement of the initially crude calculations.

With the set velocity at the exit from the jet, it is necessary to calculate Reynolds number (equation VI.30). It is important to note that the Reynolds number so calculated is based on the maximum of air velocity, and this would lead to the largest coefficient of friction for the duct. To avoid this, the Reynolds number should be calculated on the average velocity, i.e. on the average of v' and $v = v_s$. The needed coefficient may be obtained either from figure VI.11 or from equation VI.31. However, it is better to calculate the group $C_f x/D_h$ with the help of equation VI.32. The value of Y may be treated as a constant since for $M = 1$ it amounts to $Y = 0.5580$. From the value of the group so obtained one may get the length of the duct. It often pays to prepare a graph of different lengths of jet for a range of Reynolds numbers with the "thickness" of the jet as a parameter. The width may be limited by other technological considerations.

As the next step, one may take advantage of equations VI.33. Since Z pertains to the exit conditions, $M = 1$, and furthermore Z is constant and amounts to $Z = 1.0954$. After obtaining a value for Z', one may obtain the value of p/p'. Earlier, the value of p'/p_0 was read off of the table in the Appendix. The value of p_0/p may be obtained from the relationship

$$\frac{\frac{p}{p'}}{\frac{p'}{p_0}} = \frac{p_0}{p}$$

Since $p = 1$ *ata*, p_0 is the absolute pressure needed to drive the system.

Some refinements may be introduced into the calculations after the initial results are available. Among others, it may be important to respect the temperature decrease during gas decompression. A temperature decrease of 10° to 20°C may easily take place, and this, in turn, may cause problems with room temperature or with water condensation on the equipment.

Jets like this may be operated also at lower air pressures. In such cases the performance may be obtained by somewhat different manipulation of the equations given above. Some of the solutions, particularly in cases when the sonic velocity at the exit is undesirable, may require numerical solutions of equations VI.32 and

VI.33.

A point of particular attention during such design work is that the coefficient of frictional drag decreases with increasing velocity. This is true both for the drag on fiber to be drawn, as well as for the loss of air pressure. On some occasions the decisions may be difficult to make.

It is a fair approximation that the air velocity along the jet changes linearly. Final calculation of the performance consists of the integration of the drag equation from the end of the jet where the maximum of relative velocity is found, upwards to the entry. Use of the final fiber diameter is a fair approximation.

The channel through which fibers are entering into the jet represents a point of potential air loss since there is a pressure differential on both ends. Normally the volume of lost air, Q, could be calculated as

$$Q = \frac{(p' - p)wb^3}{12\mu l} \tag{VI.34}$$

where w is the width of the channel (long dimension), b is the "thickness" of the channel, l its length, μ is, as usual, kinematic viscosity of air. However, the real situation is modified by the pumping action of the incoming fibers, and this depends on a number of factors: diameter of filaments, their number and velocity, geometry above the channel, etc. In effect, such calculations may give only orientational results.

For lay - down jets used for deposition of fibers on surfaces, the force requirement is quite low. As the removal of air underneath the collecting surface is always an unpleasant operation, minimizing the volume of air is in such cases highly recommended.

VI.2 Heat Exchange

VI.2.a Calculations

The numerous references to quench, cooling, filament temperature made throughout the preceeding chapters speak with a loud voice of the importance of temperature and heat exchange problems. The fact that the more serious work on theoretical solutions for the fiber formation have been started by E. H. Andrews[20] from calculations of temperature profile of poly(ethylene terephthalate) fibers in quench zone may be read as an additional indication of their very importance.

The heat flow equation, so familiar to engineers, is here the starting point:[20]

$$\frac{Q\rho c_p}{\pi\lambda_p}\frac{\partial T}{\partial l} = \frac{l}{u}\frac{\partial}{\partial t}\left(u\frac{\partial T}{\partial u}\right) + R^2\frac{\partial^2 T}{\partial l^2} + \frac{\partial H_F}{\partial l} \tag{VI.35}$$

The notation used here is: Q means volumetric polymer flow rate, ρ stands for polymer density, c_p is heat capacity of polymer at constant pressure, λ_p means thermal conductivity of polymer, T describes local filament temperature, l is distance from spinnerette, u is radial distance from the fiber axis, R determines the

filament radius at point l, and H_p stands for heat of phase change, which usually is crystallization.

The second term of the right hand side of equation VI.34 pertains to the conduction along the fiber axis. Since this type of heat conduction is generally considered very small in comparison with the other terms, it is therefore often omitted.

Solution of equation VI.34 is not the most easily executed task, as with all heat transfer problems. Usually a number of simplifications is introduced to make the solution more friendly. E. H. Andrews[20] separates the group

$$\frac{Q\rho c_p}{\pi\lambda_p} = Z \tag{VI.36}$$

and assumes it to be constant.† How large a variation may one assume as a constant? For example, for polypropylene from the spinnerette down to some 50° or 40°C value of Z changes by ten to fifteen per cent. In this author's opinion, for the solution of a differential equation, this is a non-negligible amount. Similar conclusions may be drawn from other publications.[21,22] Nevertheless, the same simplifications were made by many other authors.

Another source of obvious error is the generally practiced omission of heat of crystallization. Some authors apply it, but lack the information about the crystallization profile and its localization along the spinline, does falsify the results. Indeed it is difficult to say which is worse: the omission or such an incorrect application. The heat of crystallization is not a negligible quantity.

As a refinement of the work by E. H. Andrews[20], Wilhelm[23] suggests the following reasoning.

In a fiber element, at any place along the fiber traveling distance, the amount of heat delivered with the hot mass of polymer, h_1, is

$$h_1 = V dq \vartheta_{h1} \rho_p c_p \tag{VI.37}$$

and the amount of heat taken away by the mass of polymer, h_2, is

$$h_2 = V dq \vartheta_{h2} \rho_p c_p \tag{VI.38}$$

where h is the amount of heat, V is local filament velocity, q means filament cross section, ϑ stands for local filament temperature, ρ_p means density of polymer, and c_p describes specific heat of the polymer at constant pressure.

Besides the convective heat transfer, there also exists a heat transfer which, according to Fourier's equation, is

$$h_2 = \lambda_p \nabla^2 dQ \tag{VI.39}$$

where λ describes thermal conductivity of polymer, and Q represents volumetric polymer flow rate.

†Data on certain physical properties and their functions of temperature for some polymers are given in the Appendix.

The heat balance for a polymer segment is

$$h_1 - h_2 = h_3 \tag{VI.40}$$

and further

$$V dq(\vartheta_{q1} - \vartheta_{q2})\rho_p c_p = \lambda_p \nabla^2 \vartheta dQ \tag{VI.41}$$

Fiber velocity V may be represented as dl/dt, where l is distance along the fiber axis, and t is time. The change of temperature $(\vartheta_{q1} - \vartheta_{q2})$ may be written as $d\vartheta$. The physical properties of the polymer may be accumulated into a temperature conductivity number

$$a_p = \frac{\lambda_p}{c_p \rho_p} \tag{VI.42}$$

which permits us to rewrite equation VI.41 as

$$\frac{dl dq}{dt} d\vartheta = a_p \nabla^2 \vartheta dQ \tag{VI.43}$$

Since $dq \cdot dl = dQ$ equation VI.43 obtains a form

$$\frac{d\vartheta}{dt} = a_p \frac{\partial^2 \vartheta}{\partial u^2} + \frac{1}{u} \frac{\partial \vartheta}{\partial u} + \frac{\partial^2 \vartheta}{\partial l^2} \tag{VI.44}$$

where u continues to mean the radial distance from the fiber axis.

From the continuity equation we have

$$V = \frac{dl}{dt} = \frac{Q}{\pi R^2} \tag{VI.45}$$

so equation VI.45 may obtain the following form

$$\frac{\partial \vartheta}{\partial l} \frac{Q c_p \rho_p}{\pi \lambda_p} = R^2 \frac{\partial^2 \vartheta}{\partial u^2} + \frac{R^2}{r} \frac{\partial \vartheta}{\partial u} + R^2 \frac{\partial^2 \vartheta}{\partial l^2} \tag{VI.46}$$

The second group on the left hand side of equation VI.44 is equal to Z, as it was defined in equation VI.36.

In further steps Andrews makes somewhat strange assumptions and simplifications with a loss of accuracy. The equation was solved by E. L. Albasiny[24] numerically using nondimensional variables in a way which appears more satisfactory and accurate. And so, temperature ϑ is changed to nondimensional form by division with initial melt (spinnerette) temperature, T_0

$$\theta = \frac{\vartheta}{T_0} \tag{VI.47}$$

and by dividing the radial position, u, by the filament radius at a given distance from spinnerette

$$r = \frac{u}{R} \tag{VI.48}$$

Further, instead of distance, l, time, t is used. The last change is a matter of choice, it may depend on which form the function F, which describes the heat loss from the filament surface or the surface temperature, is available. Following Wilhelm[23], the change (loss) of heat may be defined as

$$dh = \alpha\theta dq \tag{VI.49}$$

where the surface segment $dq = 2\pi R dl$ and α is the heat transfer coefficient. From Fourier's formula

$$dh = -\lambda_p \frac{\partial\theta}{R\partial r} dq \Big|_{r=1} \tag{VI.50}$$

Equations VI.49 and VI.50 give the spatial boundary condition

$$\frac{\alpha R}{\lambda_p} = \frac{1}{\theta}\frac{\partial\theta}{\partial r}\Big|_{r=1} \tag{VI.51}$$

The heat transfer coefficient, α, may be substituted with an empirical function of heat loss from the filament surface, F, per unit length per time and degree of temperature.

$$-\frac{F(l)}{2\pi\lambda_p} = \frac{r}{\theta}\frac{\partial\theta}{\partial r}\Big|_{r=1} \tag{VI.51 a}$$

Further, boundary conditions are set as

$$\theta = 1 \quad \text{for all} \quad r \quad \text{at} \quad t = 0 \tag{VI.52}$$

$$\frac{\partial\theta}{\partial r} \quad \text{at} \quad r = 0 \tag{VI.53}$$

$$\frac{1}{\theta}\frac{\partial\theta}{\partial r} = -F(t) \quad \text{at} \quad r = 1 \tag{VI.54}$$

Now equation VI.46 becomes

$$Z\frac{\partial\theta}{\partial t} = \frac{\partial^2\theta}{\partial r^2} + \frac{1}{r}\frac{\partial\theta}{\partial r} \tag{VI.55}$$

for $0 < r < 1$. As it was mentioned above, the term describing heat conduction in the axial direction is omitted as insignificantly small.

Albasiny[24] applies the Crank-Nicolson[25] method for the finite difference approximation because of its good stability within the wide range of intervals used. Denoting as θ_i, Φ_1, and ϕ the values of $\theta(t)$, $\theta(t+\delta t/2)$, and $\theta(t+\delta t)$, respectively at the points $r_i = i\delta r$, where $i = 0, 1, 2, 3, ..., n$ and $\delta r = 1/n$, the finite difference representation of equation VI.54 becomes

$$Z\frac{\phi_1 - \theta_1}{\delta t} = \frac{1}{2(\delta r)^2}\left\{\phi_{i+1} - 2\phi_i + \frac{\phi_{i+1} - \phi_{i-1}}{2i} + \theta_{i+1} - 2\theta_i + \theta_{i-1} + \right.$$
$$\left. + \frac{\theta_{i+1} - \theta_{i-1}}{2i} - C_i(\phi_i) - C_i(\theta_i)\right\} + \frac{Z}{\delta t}C_t(\Phi_t) \tag{VI.56}$$

Here all the values C represent "difference corrections". For approximate calculations they may be neglected, but for accurate calculations they ought to be respected. $C_i(\phi_i)$ and $C_i(\theta_i)$ may be expressed in terms of differences in the r-direction. The correction $C_t(\Phi_t)$, however is connected to the differences in the time (or distance, as the case may be) direction. This term may be calculated, but the task is hard even for a computer; it may be made negligible if the interval δt is very small. This way is usually selected. According to the standard central difference notation, as given by Crank and Nicolson[25], the initial terms for the corrections are

$$C_i(\theta_t) = \frac{1}{6i}\mu\delta_r^3\theta_i + \frac{1}{12}\delta_r^4\theta_i + \doteq \tag{VI.57}$$

$$C_t(\Phi_i) = -\frac{1}{12}\delta_t^3\Phi_i + \frac{1}{120}\delta_t^5\Phi_i + \doteq \tag{VI.57 a}$$

The subscripts r and t indicate the difference operation in the r- or t-direction, respectively. μ represents the eigenvalue of the matrix representing the set of equations.

When starting the calculations from $t = 0$ (or $l = 0$), all the values from $\theta_0, \theta_1, ..., \theta_n$ are known. In such a case, equation VI.56 with $i = 1, 2, ..., n-1$ gives a set of $n-1$ simultaneous equations for $n+1$ unknowns $\phi_0, \phi_1, ..., \phi_n$. The two additional equations may be obtained when using VI.56 with $i = 0$ and $i = n$, but this way we introduce two additional unknowns ϕ_{-1} and ϕ_{n+1}. However, the boundary conditions VI.52 and VI.53 permit the elimination of those two additional unknowns, as at $i = 0$ the condition $\partial\theta/\partial r = 0$, which results from the symmetry condition

$$\theta_{-1} = \theta_{+1} \qquad \phi_{-1} = \phi_{+1} \tag{VI.58}$$

The term $(1\theta)\partial\theta/\partial r$ is replaced by its limiting value $\partial^2\theta/\partial r^2$. The condition $(1\theta)\partial\theta/\partial r = -F(t)$ at $i = n$ may be represented by the following

$$\frac{\theta_{n+1} - \theta_{n-1}}{2\delta r} - \frac{1}{6\delta r}\mu\delta^3\theta_n + ... = -\theta_n F(t) \tag{VI.59}$$

$$\frac{\phi_{n+1} - \phi_{n-1}}{2\delta r} - \frac{1}{6\delta r}\mu\delta^3\phi_n + ... = -\phi_n F(t+\delta t) \tag{VI.59 a}$$

Equations VI.56 and VI.59 may be combined and written in the following, operationally useful, way

$$p_i\phi_{i+1} - s\phi_i + (2-p_i)\phi_{i-1} = -p_i\theta_{i+1} + m_i\theta_i - (2-p_i)\theta_{i-1} + C_i(\phi_i) + C_i(\Theta_i) \tag{VI.60}$$

for $i = 0, 1, 2, ..., n$ where

$$p_0 = 2 \tag{VI.61}$$

$$s_0 = 2 + Z\frac{(\delta r)^2}{\delta t} \tag{VI.61 a}$$

$$m_0 = 2 - Z\frac{(\delta r)^2}{\delta t} \tag{VI.61 b}$$

$$C_0(\theta_0) = \frac{1}{12}\delta^4\theta_0 + ... \qquad (VI.61\,c)$$

$$p_i = 1 + \frac{1}{2i} \qquad (VI.62)$$

$$s_i = 2\left[1 + Z\frac{(\delta r)^2}{\delta t}\right] \qquad (VI.62\,a)$$

$$m_i = 2\left[1 - Z\frac{(\delta r)^2}{\delta t}\right] \qquad (VI.62\,b)$$

$$C_i(\theta_i) = \frac{1}{6i}\mu\delta^3\theta_i + \frac{1}{12}\delta^4\theta_i + ... \qquad (VI.62\,c)$$

$$p_n = 0 \qquad (VI.63)$$

$$s_n = 2\left[1 + Z\frac{(\delta r)^2}{\delta t}\right]2\left(1 + \frac{\delta r}{2}\right)\delta r F(t + \delta t) \qquad (VI.63\,a)$$

$$m_n = 2\left[1 - Z\frac{(\delta r)^2}{\delta t}\right]2\left(1 + \frac{\delta r}{2}\right)\delta r F(t) \qquad (VI.63\,b)$$

$$C_n(\theta_n) = \frac{1}{3}\mu\delta^3\theta_n + \frac{1}{12}\delta^4\theta_n + ... \qquad (VI.63\,c)$$

Solution of equation VI.59 requires solution of a set of $n+1$ equations at each step of the unknown ϕ_i. In matrix notation the problem may be given as

$$\mathbf{A}\theta(t + \delta t) = \mathbf{B}\theta(t) \qquad (VI.64)$$

where $\mathbf{A}$ and $\mathbf{B}$ are square matrices of order $n+1$ independent of t (or l). $\theta(t)$. $\theta(t)$ and $\theta(t + \delta t)$ are column vectors with components θ_i and ϕ_i, respectively. At time $j\delta t$ is

$$\theta(j\delta t) = (\mathbf{A}^{-1}\mathbf{B})^j\theta(0) \qquad (VI.65)$$

If the matrix $\mathbf{A}^{-1}\mathbf{B}$ has eigenvalues λ_i and eigenvectors $\mathbf{v}_i$, one may write

$$\theta(0) = \sum_{i=0}^{n} c_i\mathbf{v}_i \qquad (VI.66)$$

where c_i are constants. In effect, equation VI.65 may be rewritten as

$$\theta(j\delta t) = \sum_{i=0}^{n} c_i\lambda_i^j v_i \qquad (VI.67)$$

If we denote $Z(\delta r)^2/\delta t = b$ then

$$\mathbf{A} = -(\mathbf{C} + 2b\mathbf{I}) \qquad (VI.68)$$

$$\mathbf{A} = \mathbf{C} - 2b\mathbf{I} \qquad (VI.68\,a)$$

where $\mathbf{I}$ is the identity matrix of order $n+1$ and $\mathbf{C}$ is the square matrix of order $n+1$ given as

$$\mathbf{C} = \begin{vmatrix} 4 & -4 & . & . & . & . & . \\ -.5 & 2 & -1.5 & . & . & . & . \\ . & . & . & . & . & . & . \\ . & . & -(1-\frac{1}{2i}) & 2 & -(1+\frac{1}{2i}) & . & . \\ . & . & . & . & . & . & . \\ . & . & . & . & -\{1-\frac{1}{2n-2}\} & 2 & -\{1+\frac{1}{2n-2}\} \\ . & . & . & . & -2 & 2 & 2\delta r\{1+\frac{\delta r}{2}\} \end{vmatrix} \tag{VI.69}$$

It needs to be pointed out that $\mathbf{C}$ is independent of δt. The eigenvalues, λ_i, and eigenvectors, $\mathbf{v_i}$ are defined through the following two equations.

$$(\mathbf{A}^{-1}\mathbf{B} - \lambda_i \mathbf{I})\mathbf{v}_i = 0 \tag{VI.70}$$

$$(\mathbf{B} - \lambda_i \mathbf{A})\mathbf{v}_i = 0 \tag{VI.71}$$

When taking advantage of the equations VI.68, one obtains

$$\left\{\mathbf{C} - \frac{2b(1-\lambda_i)}{(1+\lambda_i)} \cdot \mathbf{I}\right\}\mathbf{v}_i = 0 \tag{VI.72}$$

This shows that vectors $\mathbf{v}_i$ are eigenvectors of $\mathbf{C}$ and the eigenvalues λ_i are related to the eigenvalues, μ_i of $\mathbf{C}$ through the following equations.

$$\mu_i = \frac{2b(1-\lambda_i)}{(1+\lambda_i)} \tag{VI.73}$$

$$\lambda_i = \frac{2b-\mu_i}{2b+\mu_i} \tag{VI.73 a}$$

The time dependence of the solution is realized through equations VI.73 since the value of the group b depends on δt. As the stability criterion, Albasiny[24] gives the following set of requirements.

$$|\lambda_i| < 0 \qquad \text{and} \qquad |\lambda_0| > |\lambda_n|$$

This leads to the restriction on the choice of values of δt for any assumed values of n.

$$b > \frac{\sqrt{\mu_0 \mu_n}}{2} \tag{VI.74}$$

$$\delta t < \frac{2Z}{n^2\sqrt{\mu_0 \mu_n}} \tag{VI.74 a}$$

When applying the difference correction, equation VI.64 must be replaced with the following formulation

$$(\mathbf{A} + \mathbf{D})\theta(t+\delta t) = (\mathbf{B} - \mathbf{D})\theta(t) \tag{VI.75}$$

where **D** is a matrix from the difference corrections. It is assumed that the corrections of order higher than fourth may be easily neglected. To compute the correction $C_i(\theta_i)$ for $i = 0, 1, n-1$, and n, it is necessary to know the values of $\theta_{-2}, \theta_{-1}, \theta_{n+1}$, and θ_{n+2}, it is the values outside of the normal course of calculations. From the symmetry criterion it follows that $\theta_{-2} = \theta_2$ and $\theta_{-1} = \theta_1$. The remaining values may be obtained from the extrapolation formula:

$$\theta_{i+1} = 6\theta_i - 15\theta_{i-1} + 20\theta_{i-2} - 15\theta_{i-3} + 5\theta_{i-4} - \theta_{i-5} \tag{VI.76}$$

for $i = n, n+1$. In all the equations from VI.64 to VI.73, the matrix **C** needs to be replaced with **C** − **D**, if the corrections are to be applied.

Naturally, other ways of solving the problem of heat transfer within a fiber may also be used, as will be shown below. Nonetheless, the combined method of Andrews,[20] - Wilhelm[23] - Albasiny[24] proves to be very reliable, relatively simple and easily handled by desk computers. The size of δt or δl, as the case may be, resulting from the stability criteria may well be reduced. Much improved results may be obtained if the Z-value is constantly updated to the actual temperature, and numerical calculations lend themselves easily to such an operation. However, correct results may only be obtained with application of the heat of crystallization generated during the process.

If a "crystallization history" (as given in section IV.5) is obtained it may easily be synchronized with the temperature being calculated. The amount of polymer crystallized may be calculated for each radial position. From the heat of crystallization and specific heat, as appropriate due to the temperature at any given point, the temperature increase may be calculated. Such a correction must be added to every appropriate temperature before moving further by the next increment in time. An example of results of such calculations may be seen in figures VI.12, VI.13, and VI.14, VI.15.

The calculations described by figures VI.12 and VI.13 were performed on the basis of measured fiber diameter and surface temperature. Results for a number of processes carried out on different machines and under different conditions were used to determine heat transfer coefficient due to convection. Heat losses due to radiation were calculated separately according to Stefan-Boltzmann law, which in adaptation to the fiber shape gives the following equation.

$$H_{rad}(l) = 2\varepsilon\sigma\sqrt{\pi Q} \times \left(\frac{T_s^4 - T_a^4}{T_s - T_a}\right) \tag{VI.77}$$

where ε is emissivity, σ represents the Stefan- Boltzmann constant $= 5.6687 \cdot 10_{-12} J/(cm^2 s^{2\circ} K^4)$, T_s and T_a, temperatures of fiber surface and surrounding, respectively in $^\circ K$.

Nusselt number was calculated on the basis of the experimental data. The processes studied were fast and the fast moving threadline had considerable pumping action. The pumping action in conjunction with a cross flow quench calls for the consideration of the use of two separate air velocities. An exception is several centimeters below the spinnerette, where the cross flow component is practically

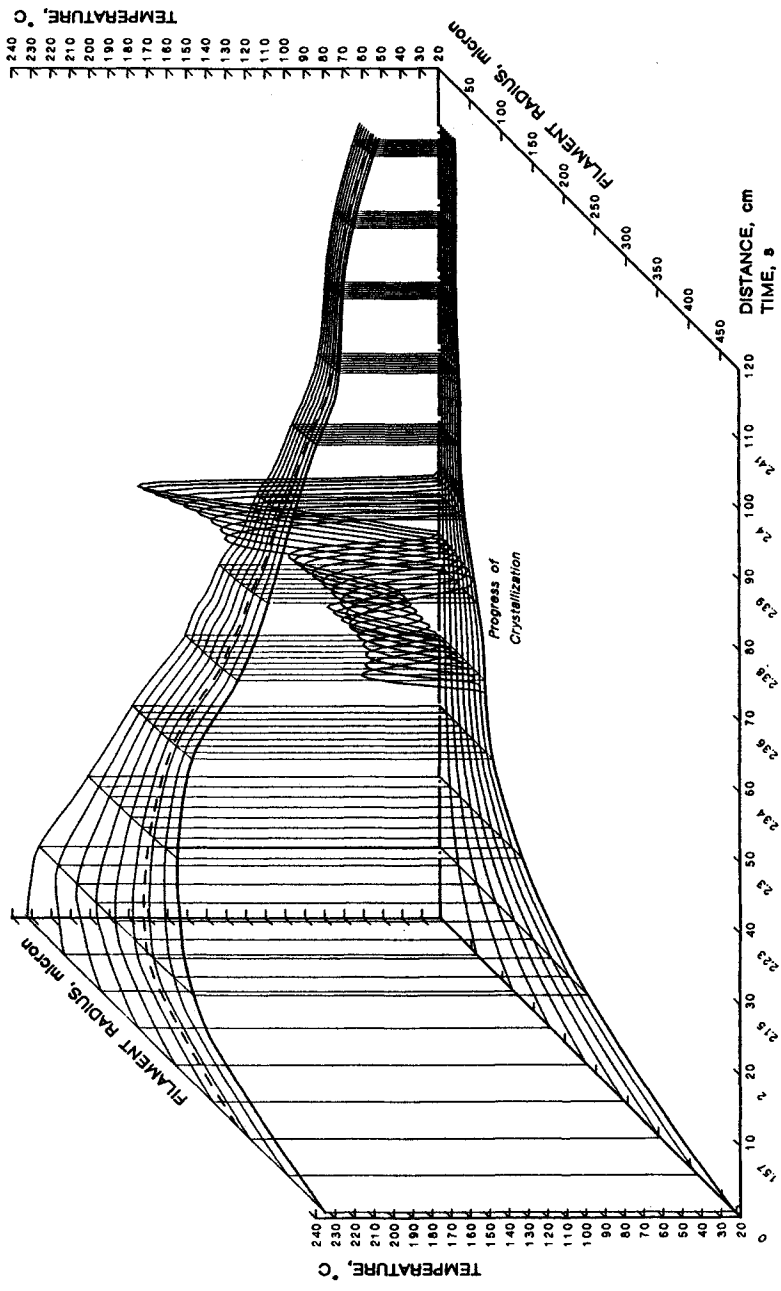

Figure VI.12: *Mapping of temperature, diameter, and crystallization rate changes against distance in formation of fibers from polypropylene, medium fast process.*

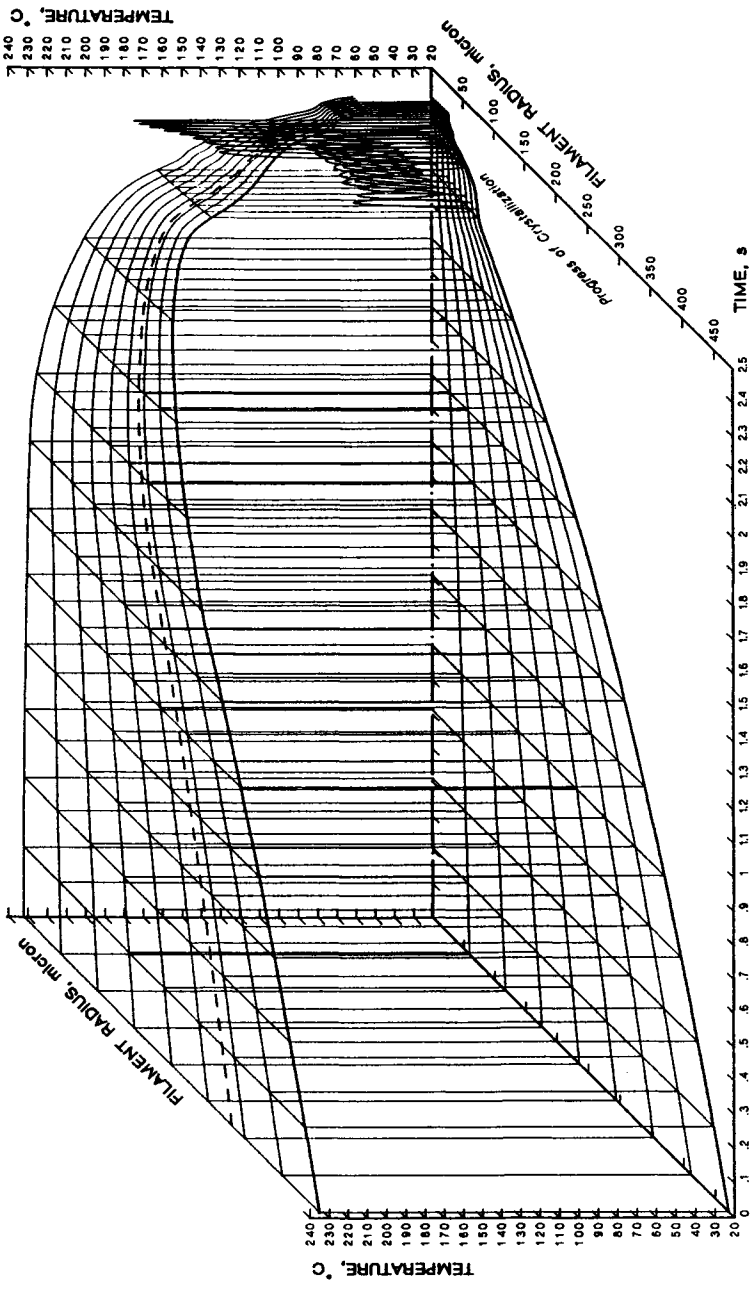

Figure VI.13: *The same process as in figure VI.12, except the mapping is against time.*

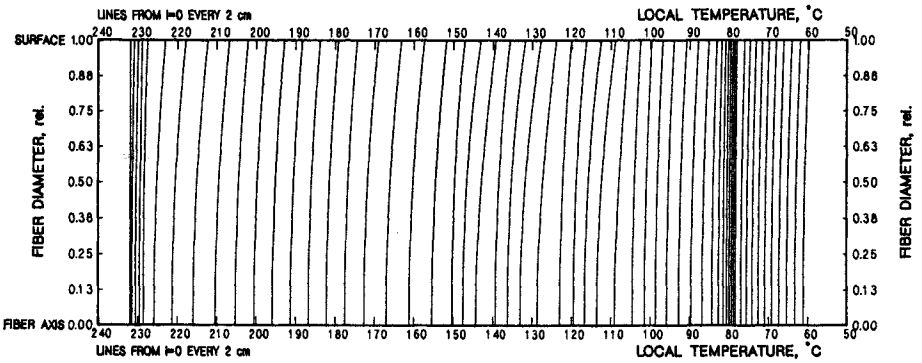

Figure VI.14: *Plot of temperature against fiber radius with 2cm intervals along the formation path. The same process as in figures VI.12 and VI.13.*

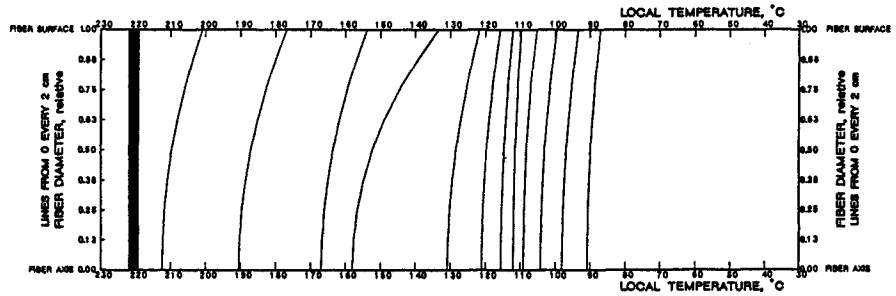

Figure VI.15: *Plot of temperature against fiber radius with 2cm intervals along the formation path. Polypropylene fiber formation with extremely intensive quench, medium fast process.*

equal zero. And so, one Reynolds number, Re_l, was calculated on the basis of the length from spinnerette, as in Sakiadis's calculations. The other Reynolds number, Re_d, was calculated on the fiber diameter and the cross flow air component. The air velocities and air temperature were mapped in the vicinity of the threadline and gave basis for the calculations.

The definition of Nusselt number is:

$$Nu = \frac{\alpha d}{\lambda_a} \tag{VI.78}$$

α is coefficient of heat transfer, λ_a is heat conductivity of air, v_f is fiber velocity, d is fiber diameter, c_{pa} is heat capacity of air at constant pressure, η_a is dynamic viscosity of air.

For $Re_l < 20$

$$Nu = 0.3298 + .015893 Re_l \tag{VI.79}$$

For $Re_d < 5.0$ and $Re_l \times Re_d < 150$

$$Nu = 0.2151 Re_l^{0.3003} \exp(0.5612 Re_d) \qquad (VI.79\,a)$$

For $Re_d < 5.0$ and $150 \leq Re_l \times Re_d \leq 6000$

$$Nu = 0.5110 Re_l^{0.1837} \exp(0.1258 Re_d) \qquad (VI.79\,b)$$

For $Re_d < 5.0$ and $Re_l \times Re_d \leq 10000$

$$Nu = 3.2745 Re_l^{-0.03844} Re_d^{0.2365} \qquad (VI.79\,c)$$

For $Re_l \times Re_d > 10000$

$$Nu \approx 3.55 \text{ to } 3.75 \qquad (VI.79\,d)$$

One must allow a suspicion that in the experiments which permitted calculation of equations VI.79, the changes of Reynolds numbers formed some kind of a pattern of mutual interrelationships. For this reason equation VI.79 is not to be taken as an "iron" rule, it is rather an indication of a dependence of the boundary layer on the actual geometry of flow, and, in consequence, on the character of heat exchange. The problem of air flow as it interacts with the motion of filaments requires a broad and systematic investigation. It is acutely necessary for calculation of heat transfer, as well as for the design of flow patterns for the quench air.

The heat transfer equation (VI.46) may be solved with the help of Bessel functions.[20,23,24] After grouping of the "constants" into Z (equation VI.36), further substitution is made:[20]

$$\theta(l,r) \equiv S(l,r)\tau(l) \qquad (VI.80)$$

As a result equation VI.46 becomes

$$\frac{Z}{\tau}\frac{\partial \tau}{\partial l} = \frac{1}{S}\left(\frac{1}{r}\frac{\partial S}{\partial r} - Z\frac{\partial S}{\partial l} + \frac{\partial^2 S}{\partial r^2}\right) \qquad (VI.81)$$

Both sides of this equation have been taken to be equal to $-p^2$, which is a function of l only.

$$\frac{Z}{r}\frac{\partial \tau}{\partial l} = -p^2(l) \qquad (VI.82)$$

$$\tau(l) = a \exp\left(-\int_0^1 \frac{p^2}{Z} dl\right) \qquad (VI.83)$$

And in effect

$$\frac{\partial^2 S}{\partial r^2} + \frac{1}{r}\frac{\partial S}{\partial r} + S\left(p^2 - \frac{Z}{S}\frac{partial S}{\partial l}\right) = 0 \qquad (VI.84)$$

Further, Andrews assumes that

$$\frac{Z}{S}\frac{\partial S}{\partial l} \ll p^2 \qquad (VI.85)$$

and in this way equation VI.84 becomes Bessel's equation of zero order with the general approximate solution

$$\theta(l,p,r) = B(l)J_0(p,r) \times \exp\left(-\int_0^1 \frac{p^2}{Z}dl\right) \tag{VI.86}$$

where $B(l)$ is an integration constant depending on the boundary conditions, $J_0(p,r)$ is Bessel's function of zero order of the form

$$J_0(p,r) = 1 - \frac{(pr/2)^2}{(1!)^2} + \frac{(pr/2)^4}{(2!)^2 3} - frac(pr/2)^6(3!)^2 4 + \ldots - \ldots \tag{VI.87}$$

By combining equation VI.87 with the radial boundary conditions given by equation VI.51a we have

$$\frac{1}{m} = \frac{F(l)}{2\pi\lambda_p} = p\frac{J_1(p)}{J_0(p)} \tag{VI.88}$$

where J_1 is Bessel's function of first order of the form

$$J_1(p,r) = \frac{pr}{2}\left[1 - \frac{(pr/2)^2}{(1!)^2} + \frac{(pr/2)^4}{(2!)^2 3} - \frac{(pr/2)^6}{(3!)^2 4} + \ldots - \ldots\right] \tag{VI.89}$$

Equation VI.88 has an infinite number of solutions p'_j for each value of $F(l)$. Andrews applies a correction for the p'_j values.

$$p_j^2 = p_j'^2 - \psi \tag{VI.90}$$

where the correction coefficient equals

$$\psi = \frac{Z}{BJ_0}\frac{\Delta BJ_0}{\Delta l} \tag{VI.91}$$

This correction is the result of the approximation defined by equation VI.85. The differences are calculated from the values for the beginning and the end of the considered section of the threadline.

The boundary conditions that $\theta = \theta_0$ for all values of r at $l = 0$ (equation VI.52) give

$$B_j = \frac{2\theta_0}{p_j}\frac{J_1(p_j)}{J_0^2(p_j) + J_1^2(p_j)} \tag{VI.92}$$

Finally for the cooling of a filament one obtains

$$\theta(l,r) = 2\theta_0 \times \sum_{j=0}^{\infty} \frac{J_1(p_j)J_0(p_j r)}{p_j[J_0^2(p_j)J_1^2(p_j)]} \times \exp\left\{-\int_0^1 \frac{p_j^3}{Z}dl\right\} \tag{VI.93}$$

Shimizu and co-workers[26] have studied heat transfer in formation of polypropylene filaments. Among others, the authors published very instructive results of measurements of the air temperature around the filament. These results are

given in figure VI.16. The thickness of the envelope increases with increasing intensity of polymer flow, and it decreases with the flow intensity of cooling air, as it is easy to predict. The relatively large diameter of the envelope of hot air must be vulnerable to distortion by both laminar flow of the cooling air, as well as, or even more so, to a turbulent flow and vorticity. This appears to be a good explanation of the fact that there were so many and so different correlations of Nusselt number published, and that the results are so widely scattered, even for relatively similar flow conditions.[55] It is to be expected that for more drastic conditions, typical of commercial operations, the discrepancies for the Nusselt number may be even larger.

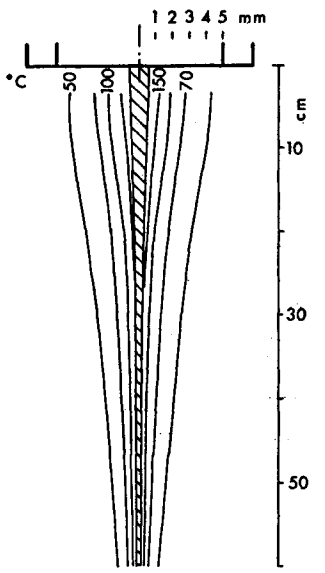

Figure VI.16: *Air temperature distribution around a melt spun filament. Melt temperature of 258 °C, take-up velocity 0.56m/s. Reproduced after J. Shimizu & al.*[26]

It is for these reasons why experience dictates that for the serious work of defining the formation conditions, it is substantially more accurate to measure the filament surface temperature rather than calculate it from the air flow data. Air flow and temperature measurements in the vicinity of a running filament are much less accurate than filament surface measurements. In addition, the calculated heat transfer coefficient may be also less certain.

Because of similar reasons, use of the numerical calculations is preferred over the method based on use of Bessel's function. The numerical calculations, besides having a little edge on the accuracy, seem to alow more flexibility, particularly if complex calculations of the entire process description are conducted. A much more accurate method has been suggested by T. Matsui and S. Kase.[27,28] These authors suggest calculation of temperature distribution across the plane of a fiber cross section, not just across a radius. There are no experimental techniques

available for exact corroboration of the results of such calculations; nevertheless, the method is of importance for research purposes, especially with cross flow, or otherwise asymmetrical, quench.

Matsui and Kase[27,28] assume an equivalence between the steady state heat conduction within a filament being formed and a stationary circular disk of fixed diameter. The asymmetry was introduced into the computations by use of non-symmetric data on Nusselt number which are the result of the air flow around a circular cylinder (see section VI.1.b and figure VI.4) and calculated by Eckert and Soehungen.[29]

The authors assume:

- steady state formation
- constant polymer density, ρ
- axisymmetric and purely extensional flow of polymer
- negligible viscous heat formation and dissipation
- negligible heat conduction in the axial direction.

As a result of the assumptions Matsuo and Kase begin with the following equations for continuity and energy, respectively. The equations are formulated in the cylindrical coordinate system, as shown in figure VI.17.

$$\frac{1}{r}\frac{\partial}{\partial r}(rv_r) + \frac{\partial v}{\partial x} = 0 \tag{VI.94}$$

$$\rho C_p \left(v_r \frac{\partial T}{\partial r} + v\frac{\partial T}{\partial x}\right) = \lambda \left[\frac{1}{r}\frac{\partial}{\partial r}\left(r\frac{\partial T}{\partial r}\right) + \frac{1}{r^2}\frac{\partial^2 T}{\partial \beta^2}\right] \tag{VI.95}$$

where T is temperature, v is velocity in the x direction, C_p is specific heat of polymer, and λ is heat conductivity of polymer.

The profile of change of filament radius is input into the calculations; the authors used a computed profile, but an experimental profile may be used as well.

In a purely extensional flow, axial velocity is independent of the radius and therefore equation VI.94 may be written as

$$v_r = -\frac{r}{2}\frac{dv}{dx} \tag{VI.96}$$

and this shows that radial velocity, v_r, is directly proportional to the radial coordinate r. The streamline in figure VI.18 may be described by

$$\frac{dr}{dx} = \frac{v_r}{v} = -\frac{r}{2v}\frac{dv}{dx} \tag{VI.97}$$

On integration, equation VI.97 yields $\pi r^2 v = const.$ = volume flow rate within radius r, and further for the filament radius R it follows that $\pi R^2 v = const. = Q$,

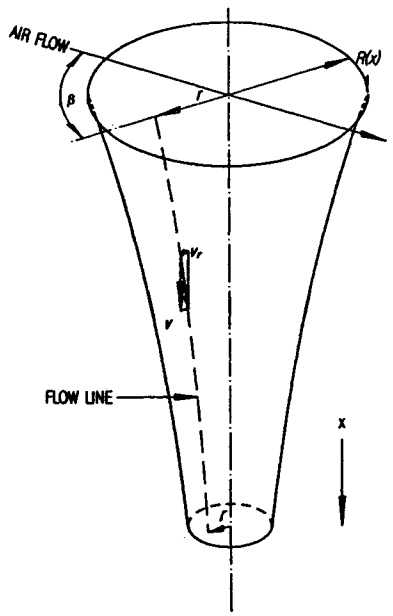

Figure VI.17: *Schematic representation of the heat conduction by T. Matsuo and S. Kase.*[27,28]

i.e. total flow rate. In view of the above, a streamline is uniquely identified by p and β, where

$$p = \frac{r}{R(x)} \tag{VI.98}$$

and β is the angle, in this case the angle with the direction of air flow.

If one assumes a filament (figure VI.18) as a stack of infinitely thin discs, than a point on a disc may be identified by its corresponding streamline and time, τ, or by three parameters p, β, and τ. In this way, in equation VI.95 the variable of length x is converted into time, τ, and

$$\tau = \int_0^x \frac{dx}{v(x)} \tag{VI.99}$$

Differentiation of temperature with respect to time along a streamline, with $p = const.$ gives

$$\left(\frac{\partial T}{\partial \tau}\right)_{p=const} = \frac{\partial T}{\partial x}\frac{dx}{d\tau} + \frac{\partial T}{\partial r}\left(\frac{\partial r}{\partial \tau}\right)_{p=const.} = \frac{\partial T}{\partial x}v + \frac{\partial T}{\partial r}v_r \tag{VI.100}$$

If we substitute equation VI.100 into the left hand side of equation VI.95, and equation VI.98 into the right hand side, we have

$$\frac{R^2 \rho C_p}{\lambda}\left(\frac{\partial T}{\partial \tau}\right)_{p=const.} = \frac{1}{p}\frac{\partial}{\partial p}\left(p\frac{\partial T}{\partial p}\right) + \frac{1}{p^2}\frac{\partial^2}{\partial \beta^2} \tag{VI.101}$$

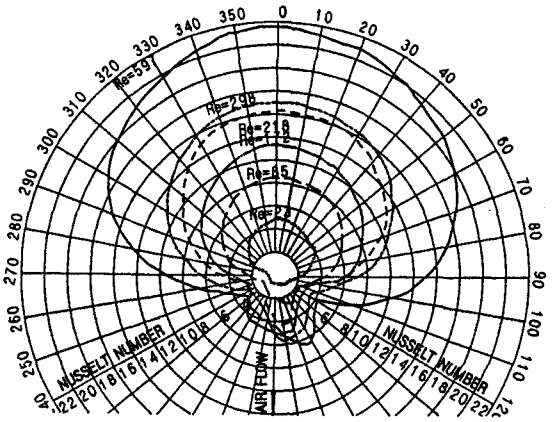

Figure VI.18: *Nusselt number around a stationary cylinder cooled by air flowing perpendicularly. After E. R. G. Eckert and E. Soehungen*[29]

Substitution of equation VI.99 onto VI.101 yields

$$\frac{R^2\rho C_p}{\lambda}\frac{\partial T}{\partial \tau} = \frac{R^2\rho C_p}{\lambda} v \frac{\partial T}{\partial x} \tag{VI.102}$$

Here the restriction of $p = const.$ for $\partial T/\partial x$ is implied.

Since $R^2 v = const.$, a new variable, X is created

$$X = \frac{\lambda x}{\rho C_p v R^2} = \frac{\pi\lambda}{Q_m C_p} \tag{VI.103}$$

where Q_m is polymer mass flow. With the new variable, X, equation VI.101 becomes

$$\frac{\partial T}{\partial X} = \frac{1}{p}\frac{\partial T}{\partial p} + \frac{\partial^2 T}{\partial p^2} + \frac{1}{p^2}\frac{\partial^2 T}{\partial \beta^2} \tag{VI.104}$$

Equation VI.104 represents unsteady two dimensional heat conduction with a ficticious time variable X. In this way, this is a two dimensional transient heat conduction within a disc of radius p.

The boundary conditions for Matsuo and Kase's solution have been set as follows:

At the filament surface

$$\lambda\frac{\partial T}{\partial r} = (T^* - T)\alpha \qquad \text{at} r = R \tag{VI.105}$$

where α is heat transfer coefficient at the filament surface. If we replace r with p in equation VI.105 then

$$\frac{\partial T}{\partial p} = (T^* - T)\frac{R\alpha}{\lambda} = (T^* - T)Nu \tag{VI.106}$$

where Nu is Nusselt number. Also, at the time zero the temperature of all the elements is equal the temperature of extrusion. The average value of the heat transfer coefficient for perpendicular flow of cooling air denoted here as $\bar{\alpha}$, Kase and Matsuo[30] defined as

$$\bar{\alpha} = 0.473 \cdot 10^{-4} A^{-0.667} Q_m^{0.334} \rho^{-0.334} \left[1 + \left(\frac{8\rho A}{Q_m} v_y\right)^2\right]^{0.167} \tag{VI.107}$$

where A is cross sectional area of the filaments, v_y is velocity of air perpendicular to the filament. The value of $\bar{\alpha}(x)$ may be calculated using equation VI.107.

As the Nusselt number varies around the periphery of a cylinder, Matsuo and Kase adjusted their average Nusselt number calculated according to equation VI.107, and calculated the angular dependence using the determinations, reproduced here in figure VI.18, of Eckert and Soehungen[29] for a stationary cylinder. A so calculated Nusselt number was expressed as a ratio $\alpha/\bar{\alpha}$. Naturally, it is a major simplification, but a more correct determination of the Nusselt number is not known even today, leave alone then, in the year 1975 or so.

To solve the equation, Matsuo and Kase considered one half of the filament cross section and divided it as shown in figure VI.19. In devising the solutions, the following assumptions were made:

- Each of the 81 segments considered is assumed to have a uniform temperature.
- The overall heat transfer coefficient at the filament surface is equal to

$$\left(\frac{R\bar{\alpha}}{\lambda}\right)\left(\frac{\alpha}{\bar{\alpha}}\right) = \frac{R\alpha}{\lambda}$$

  with the values used as functions of X and β.
- The air flow direction coinciding with the diameter line 0° - 180° is the symmetry line, and as such is non-conducting.
- The heat transfer between two adjacent elements was determined to be $\lambda/distance$ between centers of the two adjacent elements.

The difference equation resulting from the above derivations was given the following form[28]

$$\frac{T^*_{i,j} - T_{i,j}}{\Delta X} = \frac{T_{i+1,j} - T_{i-1,j}}{2p_i \Delta p} +$$
$$\frac{T_{i+1,j} - 2T_{i,j} + T_{i-1,j}}{\Delta p^2} + \frac{T_{i,j+j} - 2T_{i,j} + T_{i,j-j}}{p^2 \Delta \beta^2} \tag{VI.108}$$

If we replace the arc length $p\Delta\beta$ by Δq, equation VI.108 receives a form

$$(\Delta p \Delta q)\frac{T^*_{i,j} - T_{i,j}}{\Delta X} = \Delta q \left(1 + \frac{\Delta p}{2p_i}\right) \frac{T_{i+1,j} - T_{i-1,j}}{\Delta p} +$$

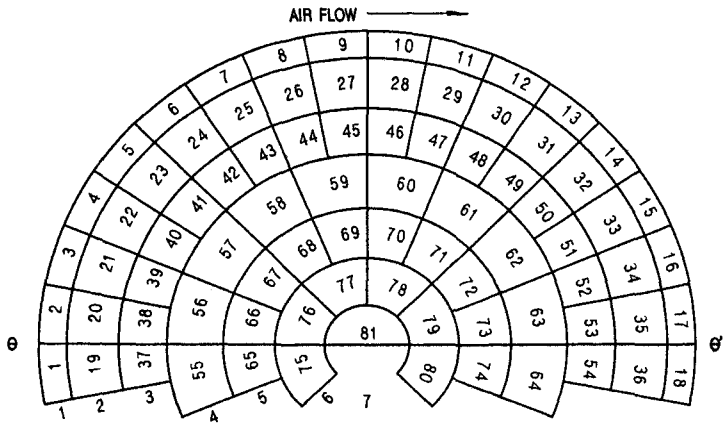

Figure VI.19: *Division of a filament cross section into elements. After R. Matsuo and S. Kase.*[27,28]

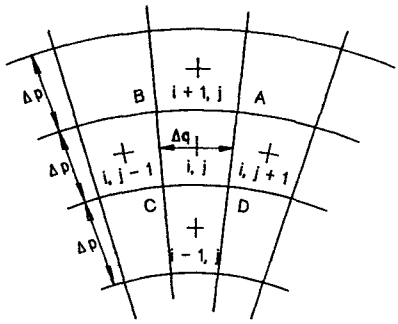

Figure VI.20: *Scheme of differencing in the cylindrical coordinates. After S. Kase.*[28]

$$+\Delta q\left(1-\frac{\Delta p}{2p_i}\right)\frac{T_{i-1,j}-T_{i,j}}{\Delta p}+\Delta p\frac{T_{i,j+1}-T_{i,j}}{\Delta q}+\Delta p\frac{T_{i,j-1}-T_{i,j}}{\Delta q} \qquad \text{(VI.109)}$$

Figure VI.20 serves as a visual aid to equations VI.108 and VI.109. The designations here are: $T^*_{i,j}$ is temperature of the cooling air, ΔX is the difference increment in X, the dimensionless distance from spinnerette. Here $\Delta p \Delta q$ gives the volume of the center element i, j assuming the thickness of the "disk" is unity, $\Delta q(1 + \Delta p/2p_i)$ is the arc length AB, Δp is the wall length $DA = BC$, and $\Delta q(1 - \Delta p/2p_i)$ is the arc length CD. The heat transfer coefficient at walls AB and CD is equal to the inverse of Δp and for walls DA and BC it is the inverse of Δq.

Examples of the computational results by T. Matsu and S. Kase are given in figure VI.21. These results were corroborated semiquantitatively by a dying test; the shape of the dyed segments coincided with the calculated results. However, there is no positive test available yet to determine such nuances with a full quantitative certainty.

The method of calculations may serve well for theoretical considerations of many problems. Naturally, better ways of determination of the heat transfer

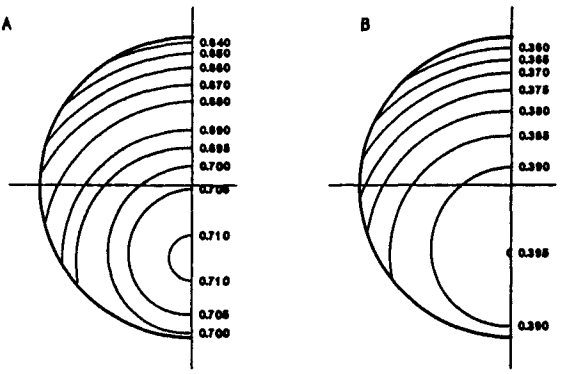

Figure VI.21: *Cross flow quench: mapping of isotherms in non-dimensional temperature in a fiber cross section, A. 2 cm from spinnerette, B. 12 cm from spinnerette. Melt temperature 260°C. After T. Matsuo and S. Kase.*[27,28]

coefficient are badly needed to allow more faith to be put into results calculated by any method.

VI.2.b Equipment

Quenching

Some comments on quench equipment have been made in the subsection on quench systems and all along the chapter on Engineering Physics. By now we are able to conclude that there is a fair amount of important design data which may be calculated. The point is: where are the pitfalls?

The difficult problems lacking adequate solution are connected to multi-filament operations, particularly the aerodynamic problems and the related estimation of heat transfer coefficients. Specifically, attention is to be paid to the pumping action, that is, to the boundary layers around a multi-filament spinline of variable filament-to-filament distance. Since with multifilament operations the most often used quench system is a cross flow of air, the mutual influence of the pumping action (i.e. the flow parallel to the spinline, and the cross flow) is of paramount importance. Thus far, these areas require heavy and expensive experimental support and careful observation of the aerodynamic and heat exchange phenomena from the initial experiments all the way through the scaling up. Szaniawski and Zachara[56] developed a quantitative solution for the entrenchment problem in wet formation. The principles of the solution are treated in section VII.3. It appears that the solution may be adapted to air systems.

In work with rapidly crystallizing polymers, or when aiming at very high modulus fibers, it may be advisable to use liquid (water) quench. Understandably, this is connected to small housekeeping problems, but sometimes it is worth the effort.

As it results from the polymer habits in fiber attenuation, location of the liquid surface very closely to the spinnerette face is rather an ill advised idea. If

the crystallization process is to be retarded, then the maximum of the attenuation work ought to be spent at a temperature where relaxation time is shorter and the temperature is also too high for the crystallization to begin, even with a work input. At the moment of the first contact between a filament and the water surface, the amount of stored work should be as small as possible. To achieve such conditions, a *delayed quench* may be recommended as a good solution. After the attenuation is done under proper conditions, rapid water quench may achieve the desired goal.

In the case of water, due to higher density and higher viscosity, the problems related to the fluid dynamics are substantially aggravated. The frictional drag on filaments is much greater, and this requires special care in the management of synchronization of the stress and temperature profiles along the spinline. Due to the very large pumping action, high filament speeds are rather impossible. If a process needs to be intensified, it is to be achieved through an increase of the number of filaments. The theoretical solution of Szaniawski and Zachara[56] may be very helpful in the design work of liquid quench.

It should also be observed that certain liquids may influence the crystallization process in some polymers. Usually such influences have negative results, sometimes so much as to prohibit the application of a particular liquid.

Neck Drawing and Annealing.

For good control of fiber properties and for good reproducibility of any process of fiber formation, it is quite essential to have as good control of the neck drawing temperature as possible. This is automatically connected with the control of the neck localization.

In the past, the neck was localized with the use of a *pin* over which the fibers were drawn. Initially, when a relatively relatively small number of filament were produced in one position, the filaments coming either from bobbins or directly from formation, were wound around *the pin*, a thin metal bar, and drawn by a set of rollers rotating faster than the fibers were fed. In this way the neck was localized within only a few millimeters of the filament travel. Nonetheless, this solution had serious drawbacks. The large friction, with its additional force requirement, caused excessive filament breaks. Equally detrimental was the heat generated by friction, in addition to the heat generated by the drawing itself.

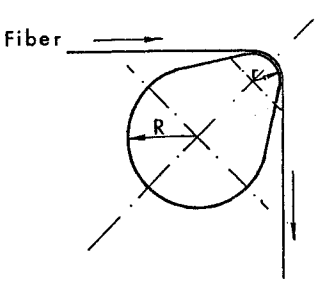

Figure VI.22: *Pin for neck drawing of multifilament threadlines.*

With time, the pins have changed to larger bars, as in figure VI.22, often with a cross section reminiscent of a pear, with cooling channels inside to remove the excess heat generated by the operation. In terms of fiber properties, such a system worked well, but the breaks, a serious problem of the process economy, still showed to be too high. With the passing of time, localization of the neck zone came to be realized only through temperature control.

The most frequently used heaters are contact heaters with a somewhat curved contact surface, as it is shown schematically in figure VI.23. The fiber guides located under the heater are often regulated by the threadline tension. In this way, an increase in tension moves a guide so to increase the length of contact between the fibers and the hot surface. The contact surfaces are plated either with chrome or with aluminum oxide; various degrees of smoothness (or grain) of the surfaces are used to adjust the heat transfer and the friction.

The convective heat transfer from the air is usually higher than the direct heat transfer between the fiber and metal surface, aside from the small area of contact between the flat metal surface and a fiber cylinder of tiny diameter. Because of this, the contact surfaces are often ribbed or grooved to enhance the heat exchange.

Such surface heaters usually have a vapor-condensation system for heating with maximum uniformity of temperature distribution. Nevertheless, such heaters heat the fibers from one side only and introduce an element of asymmetry, which sometimes may be undesirable.

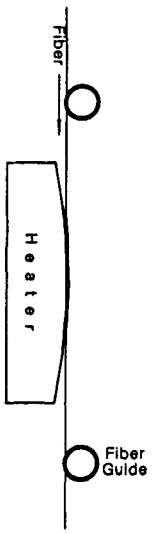

Figure VI.23: *Contact plate heater for neck drawing of fibers, schematic representation of a cross section.*

The asymmetry in heating, as well as undesirable friction, may be avoided by using heaters which utilize air. A schematic drawing of two such gadgets are reproduced in figures VI.24 and VI.25. Utilization of such solutions is particularly well suited when drawing is conducted in more than one stage, as the second (and

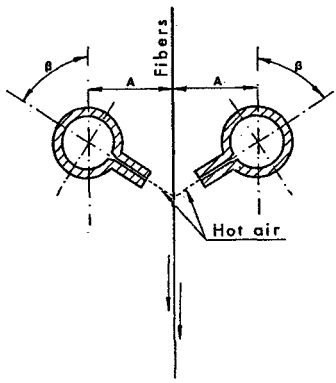

Figure VI.24: *Schematic representation of a gadget for localization of fiber drawing in jets of hot air.*

possibly third) stage drawing is usually conducted in *tunnel heaters* which are non-contacting – air is the heat transferring medium.

There are drawing operations utilizing heated rollers, the same rollers which are used to transport the threadline. Occasionally they work adequately, though it is not a solution worthy of recommendation. The drawing operation often starts before the fibers leave the roller. In effect there is a slip-stick vibration on the last ninety or so degrees of the wrap angle. This cannot be considered as an enhancement of the fiber quality.

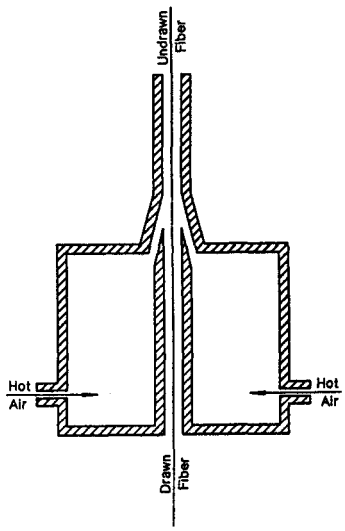

Figure VI.25: *Schematic representation of drawing in a stream of hot air.*[31]

If a neck drawing operation is conducted in more than one stage, the operations must be separated by rollers which appropriately control the tension in the zones. The journey from drawing heater through the rollers causes a change of fiber

temperature, and this must be taken in the consideration.

Immediately after neck drawing, fibers may be subjected to a heat treatment with the purpose of annealing of the fiber structure, or controlled post draw relaxation to avoid the crushing of the bobbins on which the fibers are ultimately wound up. Such an heater, depending whether the operation is to be isometric or not, may be preceded with rollers in analogy to multistage drawing steps. All the heaters, whatever their purpose, located after the first stage and localization of the neck consist of some kind of tunnel heater, as mentioned above.

As the contemporary fiber formation operations are very fast, residence time in such in-line heaters is usually very short. To go around this problem a *shock heating*[32] is often used: an exposure of fibers to a temperature higher than the fiber melting point. Such a high temperature helps the heat transfer, the fibers never reach their melting point in the available time. However, provisions for effects of possible fiber breaks ought to be here in place.

VI.3 Mass Transport

VI.3.a Polymer Transport

Practically all the fiber formation equipment now uses extruders for melting and transporting the polymer being fed into the system. Also, in cases where the formation operation is supplied directly from continuous polymerization units, extruders of one type or another are used for transporting the melt. The theory of extrusion and the design of the equipment have been described extensively elsewhere.[33–36] Similarly, design of metering pumps will not be described here, as it is a specialty of several manufacturers and the reader is referred to their literature.

The feeding of polymer to the formation machines, aside from melting it in the extruders, requires heated piping to deliver the polymer to the *spinning block* or *spinning beam.* (The nomenclature in the field varies substantially.) The difficult question of maintaining uniform temperature across the larger diameter pipes was treated by Saltuk et al.[37] The authors treated a power law non-Newtonian fluid moving through a circular duct. It was found that the viscous heat dissipation is a function of the Graetz number, and for values larger than seven the heat generated by flow may constitute a problem.

Filtration of polymer melt represents an important part of the formation process. Despite this importance, the subject has found little treatment in literature. The only significant review was published by J. G. Savins[38] for polymer solutions.

In the engineering of a fiber formation process, one of the essential questions is the drop of pressure on the filtering medium. For filtration, different media may be used: sand, sintered metal, steel balls, or metal screens. The final construction of a filtering system is usually a result of a compromise between the need for polymer homogenization, the quantity and type of impurities which like to clog the filters, and the pressure requirement to force the polymer through the filter. The

pressure requirement is important for the cost of equipment, the clogging has a bearing on the process economy through increase of the down-time. Quite often, however, the gains of reduced filtering efficiency are illusory since the poorer filtration usually leads to increased filament breaks. The two technologically important arguments which may limit the tightness (or shear) of the filter are: not to exceed the threshold of the degrading shear; and not to reach too high a pressure, which may be connected with problems of building high pressure equipment and with the high costs connected with it. The degrading shear rate is a polymer property depending on molecular mass (see chapter on rheology).

Some filtering materials may be tested experimentally in slightly modified capillary rheometers. Otherwise, calculations are a possibility. Generally, the most convenient way is to start from the general equations of Poisseuille (capillary) flow:

$$F(\tau_w) = \frac{v}{r} = \frac{1}{\tau_w^3} \int_0^{\tau_w} \tau^2 \dot{\gamma}(\tau) d\tau \tag{VI.110}$$

$$\eta = \frac{\tau_w}{4F(\tau_w)} \tag{VI.111}$$

where $F(\tau_w)$ represents the function of shear stress at the tube (capillary) wall, v is average velocity, r is tube radius, shear stress at the tube wall $\tau_w = r\Delta P/2L$, ΔP is pressure difference needed to force the fluid through the tube, L is tube length, $\dot{\gamma}$ stands for shear rate, and η means fluid viscosity. For filtering materials, the tube radius may be substituted with the *hydraulic radius* r_h, which in this case is defined as

$$r_h = \frac{d_p \epsilon}{6(1-\epsilon)} \tag{VI.112}$$

where d_p stands for particle diameter (e.g. in case of sand), and ϵ is porosity or void fraction. Some further relations are

$$r_h = \frac{\epsilon}{S} \tag{VI.113}$$

$$\frac{S}{S_0} = 1 - \epsilon \tag{VI.114}$$

$$d_p = \frac{6}{S_0} \tag{VI.115}$$

Here S is wetted surface per unit volume of the porous material, and S_0 is total surface of particles in unit volume of the porous material.

Usually the channels present in a porous material are not straight, and it is necessary to correct for this fact by introducing a coefficient c' to multiply the tube length L.[39] After applying the correction, one may rewrite equation VI.110 in the following form.

$$F(\tau_w) = \frac{3(1-\epsilon)v_0}{d_p \epsilon^2} = \frac{1}{\tau_w^3} \int_0^{\tau_w} \tau^2 \dot{\gamma}(\tau) d\tau \tag{VI.116}$$

where *superficial viscosity*, $v_0 = \epsilon\langle v\rangle$, and $\langle v\rangle$ is pore velocity.

$$\tau_\epsilon = \frac{\omega \Delta P}{6c' L} \tag{VI.117}$$

$$\omega = \frac{d_p \epsilon}{1-\epsilon} \tag{VI.118}$$

The *Darcy viscosity*[38] is

$$\eta_\epsilon = \frac{\tau_\epsilon}{4F(\tau_\epsilon} = \frac{\omega^2 \epsilon}{72c'} \frac{\Delta P}{v_0 L} \tag{VI.119}$$

When comparing the flow curves obtained for capillary flow with those for the porous layers, the latter ones are shifted by a factor of c'. It is assumed that neither the flow conditions nor the flow character changes.[38]

Essentially the same solutions, though in somewhat different form, have been published by other authors.[39,44]

In general, the agreement between experiment and calculations conducted according to the above given method are within $\pm 10\%$,[38,43] however larger deviations are observable. Such larger deviations are interpreted as resulting from a strongly elastic character of the polymer, or adsorption of the polymer on the surface of the filter material, or on simple clogging of the channels by impurities of different nature.[44,47] In some cases, it is referred to as a formation of gel on the porous surfaces,[47] though collection of gel has been proved experimentally,[48] and so it appears more likely a collection rather than a formation.

The pressure drop accompanying the passage of a viscoelastic liquid through a porous layer may be obtained by performing the calculations as for a Newtonian fluid, then the result is to be corrected as follows.[44,49]

$$\Delta P_{viscoel} = \Delta P_{viscous} \left[1 + A\left(\frac{\theta v + 0}{\epsilon d_p}\right)^2\right] \tag{VI.120}$$

where A is a constant between 5 and 10, θ is relaxation time.[50]

Since there is some uncertainty of whether a given polymer obeys the rule allowing the recalculation or not, it may be highly recommended to make an experimental check whether equation VI.116 holds. If the filtration medium has a propensity for adsorption of polymer in use, then the filtering material is unsuitable for the process. Complete chemical and physicochemical inertness of a filtering material is the primary criterion for its application.

Immediately below the bottom surface of the filter, a certain free space should be left as a flow equalizer before the polymer enters the spinnerette.

VI.3.b Spinnerette Design

A successful design of a spinnerette requires a good knowledge of the melt flow characteristics of the polymer to be used. The most informative in this case

appear to be the oscillatory experiments, though capillary experiments should also be considered for the sake of determination of die swell. Die swell is always somewhat enigmatic and changeable, calculations do not seem to suffice for good design. It is true that the small entrance angles are preferred, but an experimental check on the effects of the entrance cone angle may be worth the little extra effort.

From the rheological measurements in capillaries one may select the smallest aspect ratio which will still permit operation on the flatter portion of the curve representing the swell-aspect ratio relationship. Flow in short capillaries is normally connected with steeper dependence of the die swell on the aspect ratio, therefore slight inaccuracies in the length of different capillaries in a spinnerette may cause excessive variations between the diameters of different filaments.

The level of shear rate during extrusion through a capillary also affects the fiber quality. Generally, a higher level of shear rate leads to tougher fibers with more stable structure, therefore it is technologically advisable to use the highest shear, though staying within some reasonable limits. The limitations on the shear rate are here the same as in the case of filters.

Further, the flow considerations must be based on the simple balance of the material flow throughout the entire process of formation.

$$Q\rho_0 = \frac{\pi d_0^2 v_0 \rho_0}{4} = \frac{pid_1^2 v_1 \rho_1}{4} = \frac{\pi D_S^2 v_S \rho_s}{4} = \frac{\pi d_f^2 v_f \rho_f}{4} \tag{VI.121}$$

where Q is volumetric polymer flow rate, ρ represents polymer density, v is velocity of the polymer stream, and d is diameter of the polymer stream. The subscripts denote: 0 – in capillary, 1 – in the die swell at maximum diameter B, s – in undrawn fibers, and f – in drawn fibers. And as a reminder, *spin stretch*, $SS = v_s/v_1$, draw ratio, $DR = v_f/v_s$. Draw ratio must be corrected for the amount of post draw relaxation to assure arriving at the desired final fiber thickness. One may also use the material balance so as to arrive at the weight titer of the fibers, denier or decitex:[‡]

$$Q\rho_0 = Q_w = \frac{(dpf)_f}{9000} = \frac{(dTx)_f}{10000} \tag{VI.122}$$

After simple arithmetic, one may arrive at a useful formulation like

$$Q\rho_0 = 1.389 \cdot 10^{-3} \frac{d_0\dot{\gamma}}{B}(dpf)_f)(SS)(DR) \tag{VI.123}$$

The rest of the flow calculations are identical to those described for the flow in capillaries in the chapter on rheology. The strength of the spinnerette plate itself, as well as the mounting, are matters for mechanical engineers.

A point of much discussion is the distribution of holes in multifilament spinnerettes. The only theoretical guidelines are those that result from the aerodynamics. Naturally, the larger the distance between the capillaries the better, however,

[‡]Denier = dpf = weight in gram per 9000 m fiber; Decitex = dTx = weight in gram per 10000 m fiber.

this leads to a large size of spinnerette plate, and this requires thicker spinnerettes for the sake of strength and resistance to buckling.

In co-current axial air flow, the filament-to-filament differences are relatively small, though nothing concrete is known about a flow around converging filaments. At least the general direction of flow is the same for fibers as it is for the cooling air. Much more complicated are the matters for cross flow quench. The first row of fibers in the air path has higher flow velocity and cooler air. For each of the following rows of fibers the cross flow velocity is smaller due to the pressure drag and the pumping action, and at the same time each following row experiences higher temperature of the cooling air. In result, the fiber-to-fiber differences are large. The best distribution of holes is such which diminishes the adverse effects to the bare minimum, whatever this means.

For really large spinnerettes, a helpful way to decrease the nonuniformities may be to change from the traditional round spinnerettes to rectangular plates. In this way, there may be fewer rows of filaments, and this means fewer obstacles for the air to overcome. Additionally, the rectangular spinnerette may be helpful in reducing the plate thickness and increase the circumference to area ratio which is of importance in the strength of the spinnerette mounting.

VI.3.c Filament Transport

The term filament transport here means not only transport. In a common downward formation system, gravity would be sufficient to move the fibers. The transport must also have some muscle, it must provide force for diameter attenuation and force for neck drawing in integrated processes. The most frequent way of satisfying the strong transport needs is by way of rollers or *godets*. (Again, the nomenclature varies from place to place.) The other means — air jets are used almost exclusively for *spunbond processes*. Jets have been discussed in the section on aerodynamics.

Before the fibers solidify they are guided contactless through the air. The first contact is possible only after solidification, or glassification. The oldest and the most popular way is to wrap the threadline several times around a pair of rollers driven in the same direction. To prevent the threadline from jamming together or falling off the axes of the two rollers in one pair must be canted some five to twenty degrees. Often, particularly for smaller threadlines, like those for continuous filaments, the second roller is not driven – it is just a free wheeling *separator* roller. The nonparallel alignment of the roller axes causes the threadline to follow a spiral-like path. Such system, is often referred to as a *multiple wrap system* and is a convenient way of threadline transport. The multiple wrap is advantageous for threadlines under high tension because the higher the tension, the stronger the threadline clamps around the pair of rollers. Multiple wraps may give 1440°, or more, wrap angle. Theoretically, for constant filament diameter and fiber- roller coefficient of friction, the frictional force depends only on the wrap angle.

If there is a large number of filaments produced on one position, then application of the multiple wrap is difficult. Starting from about two hundred filaments and up, though the limit may depend also on the local filament diameter, the multiple wrap system requires excessively long rollers. Very long rollers pose problems for the designers, and, more importantly, they may also represent a safety hazard for the operators. Additionally, the really large threadlines on multiple wrap have an increased tendency to form uncontrolled fiber entanglements. A parallel alignment of the filaments during the transport is very important, overlapping fibers lead to an reduction of frictional force. If the spinline is meant to be intertwined, then it is made under controlled conditions, in the proper place in the process; it concerns usually smaller threadlines, anyhow. The matter of fiber uniformity is of constant concern, however, uncontrolled entanglements at improper points of the process may represent a threat to the fiber uniformity and to the filament break levels. The multiple wrap system always bears the danger of disobeying all the above interdictions, and with larger tows, the dangerous possibilities quickly become certainties.

The majority of vices inherent in the transport with multiple wraps around two rollers may be avoided when using the so called S-wrap system. Figure VI.26 presents the principle of the S-wrap geometry. Rollers are arranged in pairs, as in the multiple wrap system, however, their axes are exactly parallel and the rollers rotate in opposite directions. Both of the rollers must be driven. The threadline is guided through the roller surface in an S-like pattern. Although this way of guiding fiber tow is free of the vices characteristic for the multiple wrap irrespective of the size of the tow, it is connected with a problem of its own. There is a limit to the wrap angle. One pair of rollers may give a maximum wrap angle of only some 440°.

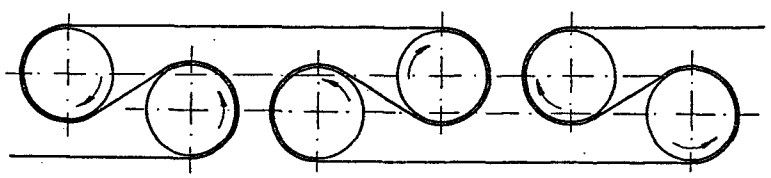

Figure VI.26: *Schematic representation of the S-wrap system for fiber transport.*

Figure VI.27 shows the details of the geometry of an S-wrap. The wrap angle around one roller, δ, may be formulates as

$$\delta = 270^\circ - (\lambda + \alpha) \tag{VI.124}$$

where

$$\alpha = \beta - \delta \tag{VI.125}$$

and β is the roller alignment angle. The other relationships of importance are

$$\sin\lambda = \frac{b}{2a} = \frac{b}{(2r + c)} \tag{VI.126}$$

and

$$\cos\alpha = \frac{r}{a} = \frac{2r}{(2r+c)} \tag{VI.127}$$

where b represents distance between the roller surface and the bypassing threadline, $a = r + 0.5c$, c stands for distance between the roller surfaces.

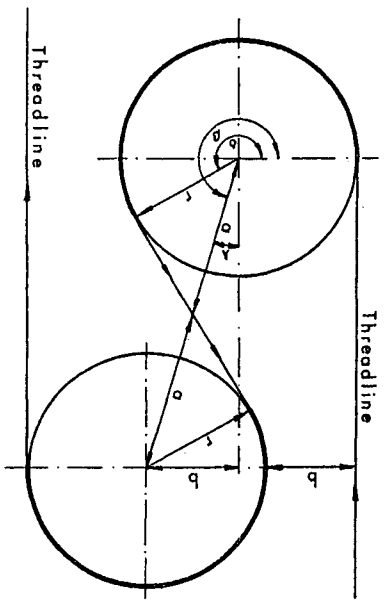

Figure VI.27: *Geometry of the S-wrap rollers. Different relative positions of the roller axes permit variations of the wrap angle δ.*

For the fibers to be laced up, it is necessary for b and c to be at some minimum size, usually the distances cannot be smaller than about 5 *cm*, though for heavier tows or for longer rollers it may be necessary to have the b and c larger than 5 *cm*. Usually, the dimensions of b and c are kept equal, and in such case the condition to obtain the maximum wrap angle of $\approx 440°$ is $b = c = 0.55\ r$.

When a reasonable increase of the roller diameter does not suffice and the wrap angle still must be increased, then wrapping may be realized only by using multiple pairs of rollers, and this may become an expensive proposition. It is self-evident that maximum utilization of any given wrap angles requires that the roller surfaces be made of a material with as great as possible coefficient of friction with the fibers in question.

The coefficient of friction varies substantially for different pairs of materials, and it is often not easily predictable. It varies even for certain variables other than just the surface quality. G. W. Schael[51] described the static coefficient of friction between surfaces of polypropylene film. These results are reproduced in figure VI.28: coefficient of friction f_s is given as a function of the degree of crystallinity expressed as density. Naturally, the friction coefficient depends also on the degree of gloss of the surface, *e.g.* line A in figure VI.28 represents film with a higher

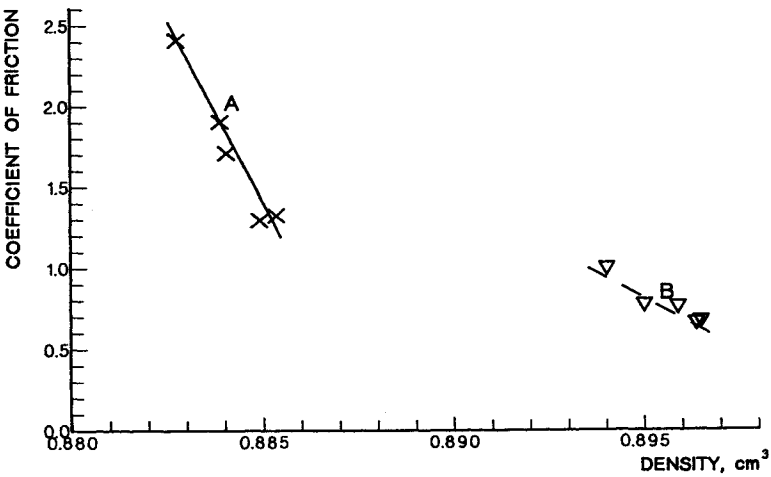

Figure VI.28: *Influence of crystallinity, expressed as density, on the coefficient of friction between the polypropylene film surfaces. A: a film of higher gloss than in case B. After G. W. Schael.*[51]

gloss than that represented by line B. The quantitative data published on the subject are rather scarce. Nonetheless, the differences of the coefficient of friction in relation to the degree of crystallinity or fiber elasticity, or fiber softness, are well realized in industry and in theory.[52,53]

A relatively extensive study of friction of polyamide yarn has been conducted by G. A. Gol'ubyev and co-workers.[54] Their results are quoted here in figures VI.29 and VI.30. Figure VI.29 presents the relationship the authors have found between the friction coefficient, diameter of a roller, and threadline tension. The influence of roller diameter on the coefficient of friction is rather difficult to explain theoretically; on a rough surface the influence of diameter is significant only at low tension (plane A in figure VI.29), while on a glossy surface, a lesser degree of influence was noticed over the entire investigated range of tensions (plane B in figure VI.29). The technological importance of the influence of tension on the coefficient of friction does not require particular stressing.

The influence of velocity on the coefficient of friction of polyamide fibers on a matted surface is shown in figure VI.30. The influence of velocity goes through a maximum at 350 to $400 m/min$ and overpowers the influence of fiber tension. The importance of these results does not require any additional emphasis.

The parameters investigated by Gol'ubyev and co-workers do not represent all the parameters which influence friction. The material of the roller surface represents a very strong factor. The most often used surfaces are chrome and aluminum oxide, both with a wide range of gloss, or grain. In special cases, roller surfaces made of various ceramic materials or rubber may be the most appropriate.

Since the degree of crystallinity and the majority of fiber properties change along the fiber path, in some cases it may be necessary to use different kinds of surfaces at different points of a machine.

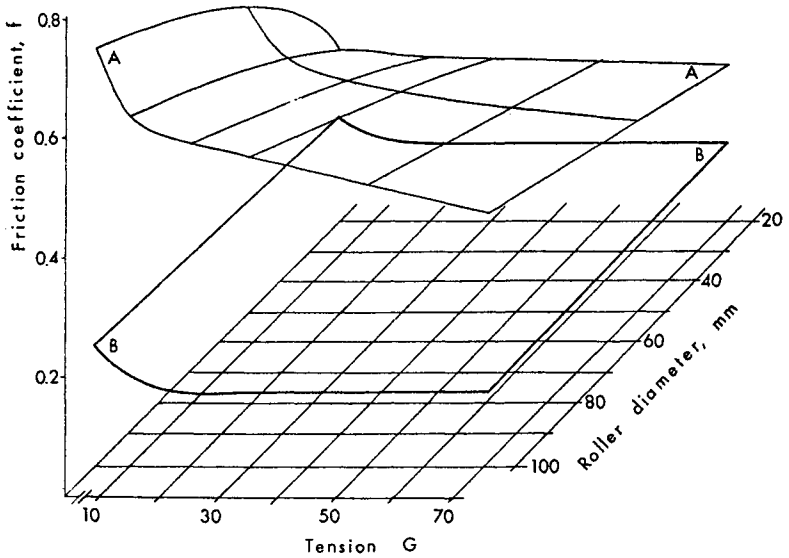

Figure VI.29: *Influence of fiber tension and roller diameter on the coefficient of friction with polyamide fibers. Plane A – glossy roller surface, plane B – rough roller surface. After G. A. Gol'ubyev and co-workers.*[54]

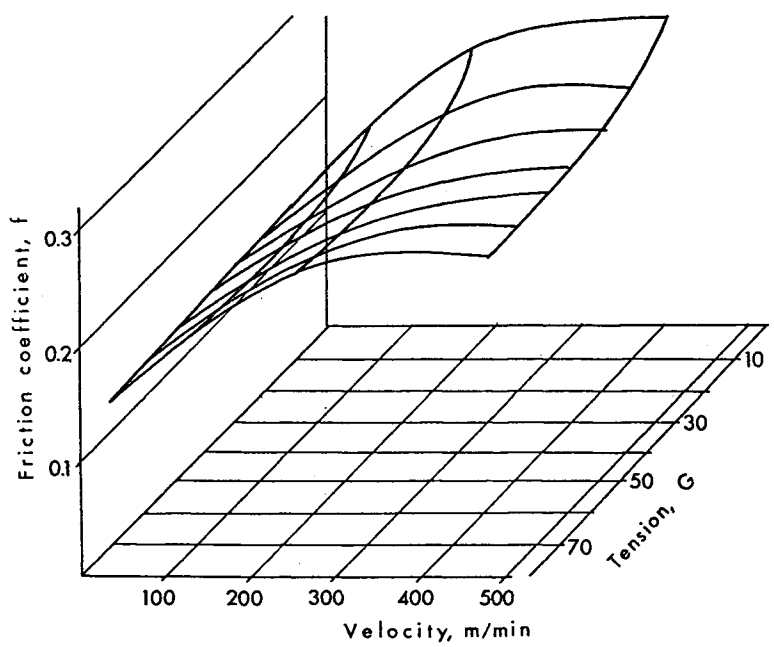

Figure VI.30: *Influence of polyamide fiber velocity and tension on the coefficient of friction with a matted chrome surface. After G. A. Gol'ubyev and co-workers.*[54]

It is quite obvious that the rollers of the drawing zone represent much more critical demands since they have to overcome much higher threadline tensions.

The hardware for transport of fibers does not consist only of driven rollers: various types of threadline guides form another separate group.

- Guides which serve to change the direction of threadline.
- Guides which spread fibers in a monofilament layer.
- Non-rotating guides.

The rotating guides may be divided according to their geometry:

The guides of the first group represent usually undriven *cylindrical* rollers of rather small diameter on the order of 25 to $100mm$. If they do not have their own mechanical drive, then they are driven by the moving threadline, and in such cases should pose a minimal resistance, thus low mass and good ball or roller bearings.

The second group consists almost exclusively of undriven rollers of still smaller diameter, ranging from some 20 to $max.$ $75mm$. Their characteristic attribute is the not quite cylindrical, but rather *barrel-like surface*. This barrel-like surface spreads a tow in a layer of single filaments, almost like a ribbon, without overlapping. Exaggerated bellowing of the guide surface may lead to excessive spreading, all the way to leading the filaments off the transporting rollers. The guides usually work in the immediate vicinity of the driven rollers.

The non-rotating guides, usually in the form of "pig-tails", rings and eyelets, are made either of steel, or ceramic surfaces on metal support. They are useful on small threadlines. On large tows they are to be avoided. Use of them in the contact with undrawn fibers is "prohibited".

The last segment of the transport arsenal are winding machines which are manufactured by companies specializing in such equipment. The winders work either with constant fiber velocity or with constant fiber tension. The manufacturers' literature is to be consulted for details of this equipment.

VI.3.d Machine Geometry

The term *machine geometry* used here represents the notions which pertain to the description of the relative positions of the technologically important elements of a fiber forming machine, spinnerette, take-up rollers (or jets), draw rollers, relaxing rollers, winding, guides, *etc.* This notion is essential to the process of formation, not only because of a space requirement.

One of the most important aspects of machine geometry is the fact that the distances together with fiber velocity profile determine time, and residence time. Fiber formation is a process, and as a process it runs in time. The availability of time determines then *how* and *how far* the physical processes involved in fiber formation may go. A change of the time scale automatically changes the whole process. For this reason, for a given process the time scale, also the machine

geometry, cannot be changed, or scaled up or down. If the geometry is changed, the process is changed, and the product properties will change.

In the machine geometry there is a delineation of different zones. The following criteria may be adapted as the definitions of the different zones.

• **Quench zone** encompasses the distance from that point below the spinnerette where the extruded filament reaches maximum diameter (die swell), which is usually one half of the fiber diameter. The end of a quench zone is at the point where the process of polymer crystallization is completed. It is a gross misconception that the quench zone stretches all the way to take-up rollers (or jets). The distance between the end of crystallization and the take-up rollers is simply a "no man's land", it represents certain length of time where the fiber is left under tension and out of control. The take-up rollers represent a border, a transition point, a necessary evil; if they are heated and prepare the fibers for drawing – then it is a draw zone. When quenching and drawing are performed in separate operations, paradoxical as it may sound, the storage of undrawn fibers belongs to the process, to the "no man's land" and out of control.

• **Drawing zone** stretches from the point where the fiber is subjected to a drawing tension, and this usually coincides with heating to a drawing temperature. The zone ends at a point where the tension exerted on the fiber is smaller than the drawing tension, be it for relaxation, for winding or for cutting. Sometimes a drawing zone may be divided into several stages; in such case only the first stage may have localized neck. Some of the ultradrawing processes may require multiple zones with gradually increasing temperature.

• **Annealing** or **stabilization zone** is the space where the fiber becomes subjected to an elevated temperature while under constant length, or when the extension is very small. This last possibility becomes similar to an additional stage of drawing, the main difference being that in drawing, fibers are exposed to heat over limited areas, while annealing uses the longest possible residence time. During drawing, some heat is generated within the fiber; in annealing no heat is generated in the process and the fiber temperatures may be significantly higher than drawing temperatures for a given fiber.

• **Relaxation zone** stretches from the end of the drawing zone, sometimes it encompasses also annealing, and it ends just before the winding of the fibers, or before any other point of removing the fibers from the process. Neck drawing is rather a brutal operation, after which the fibers, even after annealing or stabilization, have a tendency to relax and shrink. The exception may represent processes with very modest draw ratios. Normally, relaxing fibers shrink some five per cent. In extreme cases, the shrinkage might be as high as ten per cent. The purpose of the relaxation zone is to alow the fibers to shrink either to a predetermined degree or to a desired tension. Occasionally, relaxation may be divided into several zones. Fibers produced for cutting into staple are rarely subject to a relaxation under controlled conditions.

The "no man's land" may not be limited just to quench zones. It may be found in all other places as well. A "no man's land" in the quench zone is usually the

most harmful, besides being equally, or even more, costly as in all other points.

Another question, though sometimes controversial, is whether the threadline should be transported vertically or horizontally. From the point of view of economy, the vertical configurations are much more desirable. Land in industrial parks is getting more and more expensive. Technologically, the verdict ought to be the same since the threadline moves in the natural direction following the force of gravity. In horizontal configurations, the threadline is subject to the gravitational forces acting at a normal to the direction of fiber motion; this causes snag or bellowing of the filaments, which usually aids vibrations and threadline fluttering. The harm of a horizontal configuration grows with the growing distances between rollers or other points of support. Operational convenience may sometimes require horizontal configurations, but there are not many processes which would require such particular kinds of machine geometry, naturally, aside from the wet formation from solution.

A mixed configuration, with the drawing segment below take-up rollers arranged horizontally are more frequent. The horizontal position does not pose as many harms to fibers under higher tension.

Machine vibrations, were mentioned earlier at several points. Their main sources are the rotating elements of the machine, particularly those rotating at high rates of speed, and those involving powerful motors. Inaccuracies in balancing rollers or motors cause the vibrations, which may be easily transmitted to the threadline. Though somewhat less dangerous, but still worth taking into account, are building vibrations. The latter are usually of low frequency and are caused by heavy equipment like extruders, climatization, air compressors, *etc.*

VI.4 References

1. J. Łukasiewicz, Jr., *private consultations.*
2. S. F. Hoerner: *Fluid - Dynamic Drag*, published by the author, Washington, D. C., 1958, Chapter 3.
3. B. C. Sakiadis, *A. I. Ch. E. Journal*, **7 (1961)**, 26, 221, 467.
4. Y. Sano and K. Orii, *Sen-i-Gakkaishi*, **24 (1968)**, 212.
5. L. R. Glicksman, *Trans. A. S. M. E.*, **paper No 68-FE-19.**
6. M. Matsui, *Trans. Soc. Rheol.*, **20 (1976)**, 465. 56.
7. Y. D. Kwon and D. C. Prevorsek, *Trans. A. S. M. E.*, **paper No 76-TEX-7.**
8. J. Gould and F. H. Smith, *J. Text. Inst.*, **(1980), No. 1**, 38.
9. S. Middleman and G. Vasuvedan, *A. I. Ch. E. Journal*, **16 (1970)**, 614.
10. F. M. White: *Viscous Fluid Flow*, McGraw-Hill Publ., New York, 1974.
11. E. M. Sparrow, H. Quack, and C. J. Boerner, *A. I. A. A. Journal*, **8 (1970)**, 1936.
12. R. E. Sayles, *A. I. Ch. E. Journal*, **36 (1990)**, 1917. 12.
13. E. H. Andrews and D. L. M. Cansfield, in *Fibre Structure*, ed. by J. W. S. Haerle and R. H. Peters, Butterworth Publ., London, 1963, p. 487.
14. A. Selwood, *J. Text. Inst.*, **53 (1962)**, T573.

15. Z. K. Walczak, *previously unpublished*
16. A. Dutta, *Polymer Eng. Sci.*, **27 (1987)**, 1050.
17. A. Dutta, *Text. Res. J.*, **57 (1987)**, 13.
18. J. Łukasiewicz, Jr., *Aircraft Eng.*, **(1947)**, 55, 86.
19. L. Prandtl: *Essentials of Fluid Dynamics*, Blackie & Son Publ., London, 1952.
20. E. H. Andrews, *Brit. J. Appl. Phys.*, **10 (1959)**, 39.
21. J. Hennig, W. Knappe, and F. Lohe, *Kolloid Z.*, **189 (1963)**, 114.
22. T. R. Fuller and A. L. Fricke, *J. Appl. Polymer Sci.*, **15 (1971)**, 1729.
23. G. Wilhelm, *Kolloid Z., Z. Polymere*, **208 (1966)**, 97.
24. E. L. Albasiny, *Quart. J. Mech., Appl. Math.*, **13 (1960)**, 374.
25. J. Crank and P. Nicolson, *Proc. Camb. Phil. Soc.*, **43 (1947)**, 50.
26. J. Shimizu, K. Shimazaki, K. Toriumi, and T. Mitsui, *J. Text. Mach. Japan*, **18 (1972)**, 125.
27. T. Matsuo and S. Kase, *J. Appl, Polymer Sci.*, **20 (1976)**, 367.
28. S. Kase, *J. Appl. Polymer Sci.*, **27 (1982)**, 2729. 28.
29. E. R. G. Eckert and E. Soehungen, *Trans. Amer. Soc. Mech. Eng.*, **74 (1952)**, 343.
30. S. Kase and T. Matsuo, *J. Appl. Polymer Sci.*, **11 (1967)**, 251.
31. *Jap. Pat.* No. 21,566 (1966), to Sekisui Chem. Ind.
32. P. H. Geil: *Polymer Single Crystals*, Interscience Publ., New York, 1963, p. 424.
33. J. R. A. Pearson: *Mechanical Principles of Polymer Melt Processing*, Pergamon Press, Oxford, 1966.
34. R. T. Fenner: *Extruder Screw Design*, Iliffe, London, 1970. 34
35. R. T. Fenner: *Principles of Polymer Processing*, Macmillan, London, 1979.
36. Z. Tadmor and I. Klein: *Engineering Principles of Plasticizing Extrusion*, Van Nostrand Reinhold Co., New York, 1970.
37. I. Saltuk, N. Siskovic, and R. G. Griskey, *Polymer Eng. Sci.*, **12 (1972)**, 397, 402.
38. J. G. Savins, *Ind. Eng. Chem.*, **31 (1969)**, 18.
39. R. H. Christopher and S. Middleman, *Ind. Eng. Chem., Fundam.*, **4 (1965)**, 422.
40. R. B. Birds, W. E. Stewart, and E. N. Lightfoot: *Transport Phenomena*, John Wiley & Sons, New York, 1964.
41. R. M. McKinley, H. O. Jalus, W. W. Harris, and R. A. Greenhorn, *A. I. Ch. E., J.*, **12 (1966)**, 17.
42. W. B. Bogarty, Trans. Soc. Petr. Eng., **240 (1967)**, 151. 42
43. D. R. Gregory and R. G. Griskey, *A. I. CH. E., J.*, **13 (1967)**, 122.
44. R. J. Marshall and A. B. Metzner, *Ind. Eng. Chem., Fundam.*, **6 (1967)**, 393.
45. D. L. Dauben and D. E. Manzie, *Trans. Soc. Petr. Eng.*, **240 (1967)**, 1065.
46. E. Burcik, *Earth Mineral Sci.*, **37 (1968)**, 57.
47. W. Kozicki, C. J. Hsu, and C. Tiu, *Chem. Eng. Sci.*, **37 (1968)**, 487.
48. Z. K. Walczak, *unpublished results*, 1964-68.
49. E. H. Wissler, *Ind. Eng. Chem., Fundam.*, **10 (1971)**, 411.

50. J. C. Maxwell, *Phil. Trans. Royal Soc. (London)*, **157 (1867)**, 49.

51. G. W. Schael, *J. Appl. Polymer Sci.*, **10 (1966)**, 653. 51.

52. J. F. Archard, *Proc. Royal Soc. (London)*, **243 (1958)**, 190.

53. R. F. King and D. Tabor, *Proc. Phys. Soc., (London)*, **B65 (1953)**, 728.

54. G. A. Gol'ubyev, L. A. Balyasnikov, and KH. Z. Regelman, *Khim Vol'okna*, **(1968)**, 60.

55. M. M. Denn, *Ind. Rng. Chem. Res.*, **35 (1996)**, 2842. 55

56. A. Szaniawski and A. Zachara, *Polimery* (in Polish), **19 (1974)**, 143; **20 (1975)**, 87.

VII FORMATION FROM SOLUTION

VII.1 Principles

The first method used for the formation of fibers utilized polymer solutions. The first patent for fiber formation was for wet formation and was issued in 1885.[1] Historically, the second was dry formation, introduced around 1904.[2] Both of the methods using polymer solutions continue to be used today, with a large volume of fibers being manufactured commercially using the solution techniques. Moreover, the newest *high performance* fibers are produced mainly in wet processes. In the future, wet processes may be even more important, though formation from the melt is the choice technique today.

In essence, there is only one significant difference between formation from solution and from melt: the presence of a solvent in the polymer stream. Nevertheless, the solvent has a dramatic influence on many of the "unit" processes of fiber formation.[3–9] The crystallization rate increases with increasing concentration of the solution, even at the same degree of undercooling.[6–9] The process of crystallization from solution takes a much different course than the crystallization from melt. There is no maximum in the rate of crystallization from solution *versus* temperature, or the maximum is shifted toward much higher degrees of undercooling. Strain, or mechanical stretching of dissolved polymer molecules, initiates crystallization as it does in the melts. Relaxation and retardation times of polymers in solution are substantially shorter and this has great significance for the processing. The polymer habits in crystallization from solution show why it is practically impossible to obtain a low degree of crystallinity in spun fibers, unless the particular polymer crystallizes slowly and poorly by its nature.

Another factor needs to be stressed: we shall discuss only a system consisting of a polymer and a given solvent. Change of solvent changes everything else, at least to some degree. System properties depend on the both components alike, on polymer type and on solvent type.

The viscosity of solutions is lower than the viscosity of melts. The viscosity dependence on the molecular mass is of the same significance, as is the influence of abnormalities of any kind in the polymer architecture. Shear affects solutions in the same way, but the effects are shorter lasting due to the short relaxation times. Similar differences are in molecule entanglements and their persistence. The effective temperature of crystallization is equally important as in formation from the melt. All that concerns neck drawing retains its importance and its influence has similar power.

The concentration of a polymer solution changes during processing, and this must be respected in the material balance. The equation describing strain must include the local concentration, the volume of polymer solution decreases with

increasing distance from the spinnerette, $Q_{n-1} > Q_n$ and thus $Q_n/Q_{n-1} < 1$

$$\delta = \frac{v_n}{v_{n-1}} = \frac{Q_n d_{n-1}^2}{Q_{n-1} d_n^2} \tag{VII.1}$$

In effect, then, the true extension ratio in formation from solution is always smaller than it would appear just from the measurement of filament diameter.

Very few processes of fiber formation from solution permit us to obtain the spun fibers completely free of solvents. The residual solvents swell the fiber structure to some extent If the crystallization is not complete, then the residual solvent may cause it to proceed further as a kind of secondary crystallization. In practice, however, low crystallinity in fibers formed from solution is extremely rare. A low degree of crystallinity in spun fibers may be obtained if the polymer crystallizes badly. For these reasons, conventional extensive neck drawing may be difficult. If there is a need for a high degree of neck drawing, more drastic drawing conditions must applied, for example several stages of high temperature to allow "recrystallization" through a chain translation.

The above considerations indicate that the selection of a proper solvent presents a task as difficult as it is important. Unfortunately, there are no ready-made recipes to help. At this point one may suggest only a certain number of general criteria which a solvent must satisfy.[2] As such criteria one may quote:

- ability to form concentrated solutions
- convenient boiling point
- good heat stability
- ease of recovery
- low heat of evaporation
- physiological inactivity
- chemical inertness to the dissolved polymer, e.g. no cross linking.

The last point, naturally, does not concern processes which are built on a chemical modification of the polymer to achieve solubility, like in the cases of processing cellulose. When such a reactivity is needed, this becomes an additional strict requirement. For commercial operations, the price of the solvent is a matter of great significance. Conventional formation of common fibers from solution is thus far satisfied by only a few solvents: acetone, carbon disulfide, dimethylformamide, sodium thiocyanate in water, and tetrahydrofuran. The "ideal" solvent would have the ability to form relatively highly concentrated solutions of high molecular mass polymers at relatively low viscosities. Although there is a contradiction in these criteria, there is a matter of extent. Some solvents perform better than others, are closer to the "ideal". Safety of operations benefits when the solvent does not have too low an electrical conductivity. These criteria are essential from the point of

view of the ease of processing, of fiber quality, and process economy, as well as for the safety of the operating crew and equipment. Formation from solution present additional hazards, but modern technologies are able to cope with the hazards easily.

If one considers the technological aspects, the formation of fibers from solution differs from the formation from the melt by one more important point. In formation from melt the main parameters of fiber solidification are filament temperature and diameter profiles, with the other process variables playing a somewhat auxiliary role. If the velocity of take-up and rate of extrusion are constant, then the rheological properties govern the attenuation of the filament diameter. The diameter profile is a result of the temperature profile and its influence on the rheological properties of the polymer. Constant cooling conditions, with the other parameters constant, determine the actual temperature profile. And in this way the magic circle is closed. In fiber formation from solution, an additional member has to be added to this ring – diffusion. The removal of solvent, in a dry process or wet, is governed by the rate of diffusion and on the filament diameter. The diffusivity depends on the temperature and polymer concentration.[10–13] For those processes where besides diffusion osmosis also appears, the question becomes more complicated.[14] When the solvent removal from the fiber is rapid in relation to the velocity of the solvent diffusion from the fiber core towards its surface, a sheath of solid or almost solid polymer may be formed around a relatively low concentrated solution core. When this takes place, further solvent removal is additionally complicated by the necessity of solvent osmosis through a layer of solid, or almost solid, polymer. Such a course of events is also behind the mechanism which causes the fibers to have nonround cross sections. The almost solid sheath is usually formed in the beginning of solidification when the volume and diameter of the fiber are still large. The subsequent loss of solvent through the sheath is governed by osmosis and can cause a decrease of volume of about the same size as the solid sheath. The vacuum created inside causes the oversized skin to collapse and form wrinkles on the surface, or forms cavities in the fiber core, or both. In such a way microvoids or microcracks dispersed across the whole filament are formed.[15–17] The degree of the process dependence on osmosis and the degree of collapse of the cylindrical fiber are strongly interrelated.

VII.2 Diffusion in Fiber Formation

Several papers describing diffusion in fiber formation from solution have been published,[12,18–20] they pertain mainly to the wet process. The important approaches are quoted here.

Griffin and Coghanowr[21] have considered diffusion of copper ions into fibers beginning with the following equation of diffusion:

$$\frac{\partial c_t}{\partial t} = D\frac{\partial^2 c_t}{\partial r^2} + \frac{1}{r} \cdot \frac{\partial c_t}{\partial r} \qquad \text{(VII.2)}$$

$$R(T) \leq r \leq R_0 \tag{VII.3}$$

where c_t is molar concentration of the diffusing matter, t is time, r represents radial position inside the fiber, R_0 stands for fiber radius, and $R_t = R(t)$ is the radial position of the diffusion surface, where $c(R,t) = 0$.

The material balance at the diffusion surface is presented as

$$D\frac{\partial c}{\partial r}(R,t) = -\frac{1}{2}bR \tag{VII.4}$$

Griffin and Coghanowr assume diffusivity, as well as concentration of the diffusing agent at the fiber surface [$c(R_0,t) = c_0 = const.$] to be constant. They assume also absence of convection in the filament. As a result the authors arrive at the following solution to the problem:

$$\frac{c_t}{c} = 1 - 2\left(\frac{b}{2c}\right)\int_{n=1}^{\infty} \frac{J_0(\lambda_n r/R_0)}{\lambda_n J_1(\lambda_n)} \times \exp\left(-\frac{\lambda_n^2 Dt}{R_0^2}\right) +$$

$$+\frac{b}{c_0}\sum_{n=1}^{\infty} \frac{J_0(\lambda_n r/R_)}{\lambda_n J_1(\lambda_n)} \frac{R}{R_0} \frac{J_1(\lambda_n R/R_0)}{J_1(\lambda_n)} -$$

$$-\frac{\lambda_n^2 D}{R_0^2}\int_0^t \frac{R'}{R_0} \frac{J_1(\lambda_n R'/R_0)}{J_1(\lambda_n)} \times \exp\left[-\frac{\lambda_m^2 D(t-t')}{R_0^2}\right] dt \tag{VII.5}$$

where c_0 is molar concentration of the diluent around the filament, b is molar concentration of the polymer in the fiber, J_0 and J_1 are solutions of Bessel functions of zero and first order, respectively, and λ_n is an eigenvalue, $0 < \lambda_1 < \lambda_2 ...$ which are roots of $J_0(\lambda) = 0$.

From equation VII.5 describing concentration and from the condition $c(R,t) = 0$, result the two following equations which describe the moving boundary.

$$1 = 2\left(\frac{b}{2c_0}\right)\sum_{n=1}^{\infty} \frac{J_0(\lambda_n R/R_0)}{\lambda_n J_1(\lambda_n)} \times \exp\left(-\frac{\lambda_n^2 Dt}{R_0^2}\right) +$$

$$+\frac{b}{c_0}\sum_{n=1}^{\infty} \frac{J_0(\lambda_n R/R_0)}{\lambda_n J_1(\lambda_n)} \times \phi_n \tag{VII.6}$$

and

$$\frac{bR_0}{2c_0 D}\frac{dR}{dt} = -2\left(\frac{b}{2c_0}\right)\sum_{n=1}^{\infty} \frac{J_1(\lambda_n R/R_0)}{J_1(\lambda_n)} \times \exp\left(-\frac{\lambda_n^2 Dt}{R_0^2}\right) -$$

$$+\frac{b}{c_0}\sum_{n=1}^{\infty} \frac{J_1(\lambda_n R/R_0)}{J_1(\lambda_n)} \times \phi_n \tag{VII.7}$$

where

$$\phi_n(R, R_0, D, t, \lambda_n) = \frac{\lambda_n^2 D}{R_0^2}\int_0^t \frac{R'}{R_0} \frac{J_1(\lambda_n R'/R_0)}{J_1(\lambda_n)} \times$$

$$\times \exp\left[-\frac{\lambda_n^2 D(t-t')}{R_0^2}\right] dt - \frac{R}{R_0}\frac{J_1(\lambda_n R/R_0)}{J_1\lambda_n} \qquad \text{(VII.8)}$$

For long diffusion times, the first term in the solution of equations VII.6 and VII.7 has been given as

$$\frac{R_0 b}{2c_0 D}\frac{dR}{dt} = -\frac{\lambda_1 J_1(\lambda_1 R/R_0)}{J_0(\lambda_1 R/R_0)} \qquad \text{(VII.9)}$$

The equations are fit to be solved with use of a computer. If solving the problem *versus* time, it is possible to introduce corrections for changes of those parameters which were assumed constant at the derivation.

Equation VII.2 may be solved graphically,[23] if the accuracy of a graphic solution is sufficient. The relationship between the dimensionless parameters r/R and c_t/c_0 is presented in figure VII.1. The different lines in figure VII.1 correspond to another dimensionless parameter, Dt/R^2, values of which are given as parameter in the figure.

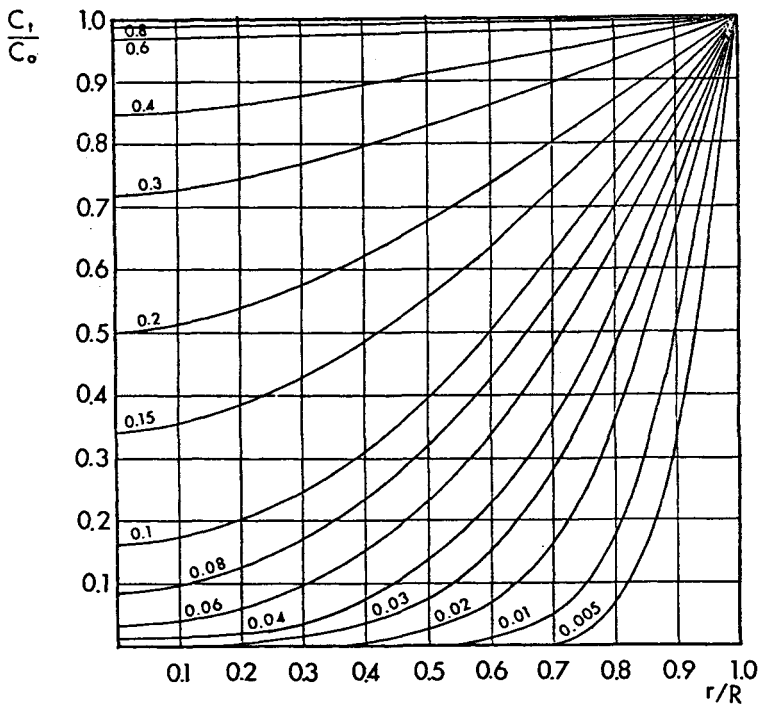

Figure VII.1: *Graphical solution of the equation for diffusion in a cylinder.*[23] *Explanation in text.*

If the values of c_0, c_t, t, and R are known from experiment, then from the graph in figure VII.1 one may read the values of the parameter Dt/R^2 corresponding to each r/R. For each value of r/R one may construct a separate plot between c_t/c_0

and the values of Dt/R^2, as read off the graph. From these graphs one may obtain the diffusivities, D.

In cases where the experimental data are available only for the average concentration across the diameter, solution is also possible, but is a little more laborious. One may assume that the whole area of the graph in figure VII.1 is equal to the amount diffused, c_0, until an equilibrium is established, that is, when $c_t = c_0$. In such a case, the amount which will diffuse in the given time, Dt/R^2, will be equal to the area under the corresponding curve and to the right of it, z_t. Then it is necessary to construct a plot of the ratio of the integrated areas, z_t over the total area z, as c_t'/c_0 against Dt/r^2. Here c is the average concentration of diffusant in a fiber cross section at time t. The further steps until obtaining the diffusivities are self evident.

Considering the diffusion in a wet process, A. Rende[22] assumed a different, somewhat more methodic approach. Namely, he considered two simultaneous diffusion processes: the diffusion of solvent out of the fiber, and the diffusion of the coagulant (nonsolvent) into the fiber. When the concentrations of polymer, solvent and nonsolvent overcome the phase equilibrium, coagulation takes place. This proceeds gradually from the filament surface toward the fiber axis, which results in a moving interface between the coagulated polymer in the outer layer and the uncoagulated dope inside.

At the first contact between the extruded filament and coagulation bath, a sudden desolvatation on the surface and the formation of a *skin* of coagulated polymer take place. This skin has different properties from the remainder of the fiber, even after the entire coagulation and drying process has been completed. The skin acts as a semipermeable membrane, such that no polymer passes through it but the low molecular mass solvent and non solvent diffuse. The volume ratio of the polymer, v_p, is considered constant during the entire process. It is also assumed that the filament is isotropic to the z-axis (along the fiber axis) and to θ – the angle in cylindrical coordinates.

Considering the above, the diffusion of solvent and coagulant are regarded as obeying Fick's law

$$\frac{dw_1}{dt} = -D_1\Omega_1\frac{dc_1}{da} \tag{VII.10}$$

$$\frac{dw_2}{dt} = -D_2\Omega_2\frac{dc_2}{da} \tag{VII.10 a}$$

where w_j is the weight of the j^{th} species that entered the system, t is time, D_j coefficient of diffusion, Ω_j is diffusion surface area, and c_j stands for concentration of the j^{th} species in the filament at the radial distance a. The diffusion process is schematically presented in figure VII.2.

After a given time, t_1, the coagulant penetrates over a distance a_t radially from the skin. The concentrations c_1 and c_2 will reach their equilibrium values c_1* and c_2* at a distance a_1; in this way a_1 determines the position of the interface between the uncoagulated dope and coagulated polymer. Across the distance a_1, forms a gradient between the external c_{e1} and c_{e2} on one side, and c_1* and c_2* on

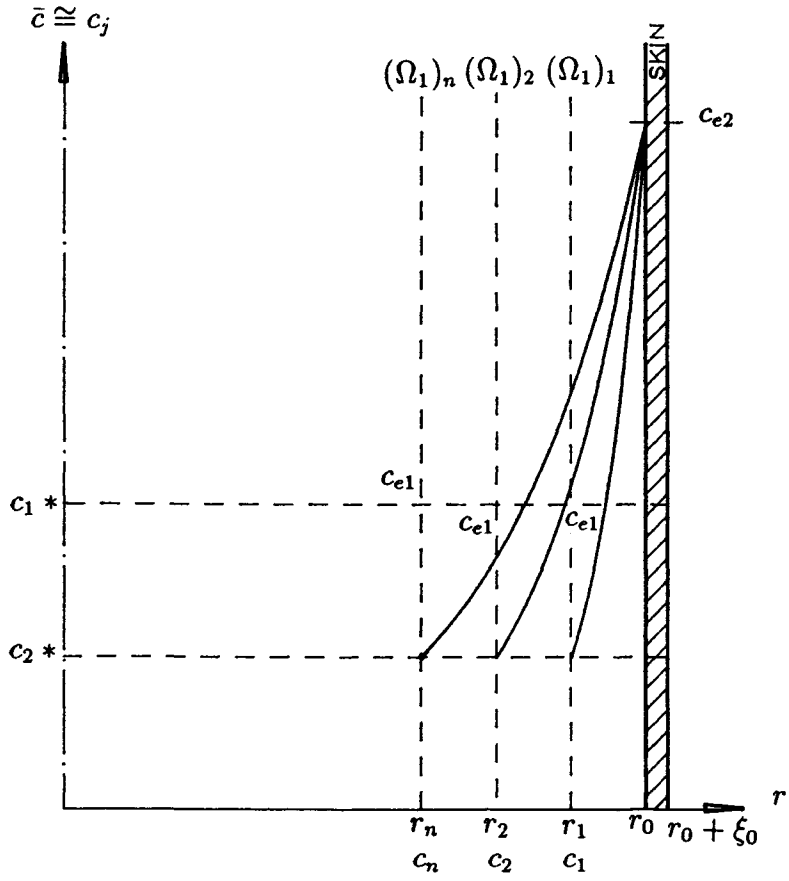

Figure VII.2: *Schematic representation of the diffusion process in a fiber.*

the other. After a time $t_2 > t_1$, the same process will be repeated on the radial distance $a_2 > a_1$.

As a consequence of this process, the diffusion surface, Ω_1, for the solvent will decrease as the process progresses.

$$\Omega_1 = 2\pi a z \tag{VII.11}$$

where, in agreement with Fick's law, a really means $a(t)$. The weight of the solvent passing through this surface is determined by the difference of the concentrations between the inner face and the external face of Ω_1, as well as by the time involved.

$$w_1 = \Delta c_1 \cdot \pi z (a_0^2 - a^2) \tag{VII.12}$$

where $a = a(t)$ and $\Delta c_1 = c_{e1} - c_1*$. And further

$$\frac{dw_1}{dt} = -2\pi z \Delta c_1 a \frac{da}{dt} \tag{VII.13}$$

For the coagulant Ω_2 is always the same and is the inner surface of the diffusion plane toward the interior of the filament.

$$\Omega_2 = 2\pi a_0 z \tag{VII.14}$$

where w_2 stands for the weight of the nonsolvent passing through the skin inside the filament, and it is determined as

$$w_2 = \Delta c_2 \pi z (a_0^2 - a^2) \tag{VII.15}$$

where $a = a(t)$ and $\Delta c_2 = c_{e2} - c_2*$, and further

$$\frac{dw_2}{dt} = -2\pi z \Delta c_2 a \frac{da}{dt} \tag{VII.16}$$

After substituting equations VII.12, VII.13, VII.14 and VII.16 into VII.10, one obtains

$$\Delta c_1 \frac{da}{dt} = -D_1 \; grad \; c_1 \tag{VII.17}$$

$$\Delta c_2 a \frac{da}{dt} = -D_2 a_0 \; grad \; c_2 \tag{VII.17 a}$$

Since the term da/dt, the *velocity of progress*, is the same for VII.17 and VII.17a, one may write

$$\frac{D_1}{\Delta c_1} \; grad \; c_1 = \frac{D_2}{\Delta c_2} \frac{a_0}{a} \; grad \; c_2 \tag{VII.18}$$

The analytical form of $grad \; c_2$ can be determined when $d \; w_2/dt = 0$. Physically, it determines $grad \; c_2$ across the uncoagulated filament at steady state. If one rewrites equation VII.15 using $\Delta c_2 = c_{e2} - c_2$, it results

$$\frac{dw_2}{dt} = 0 = \pi z \left[(c_{e2} - c_2) \frac{d}{dt}(a_0^2 - a^2) + (a_0^2 - a^2) \frac{d}{dt}(c_{e2} = c_2) \right] \tag{VII.19}$$

which on integration gives

$$\int_a^{\bar{a}} \frac{d(a_0^2 - a^2)}{(a_0^2 - a_2)} = - \int_{c_2}^{c_{i2}} \frac{d(c_{e2} - c_2)}{(c_{e2} - c_2)} \tag{VII.20}$$

In equation VII.20 we encounter for the first time $c_2 = c_{i2}$. The value of $\bar{a}$ in the integration limits means that a is the inner concentration of nonsolvent, After integration of VII.20 with the limit $\bar{a} \to 0$ one obtains

$$c_2 = c_{e2} - \Delta' c_2 \frac{a_0^2}{a_0^2 - a^2} \tag{VII.21}$$

In connection with equation VII.18, the concentration gradients may be calculated as

$$grad \; c_1 = -\frac{D_2}{D_1} \cdot \frac{\Delta c_1}{\Delta c_2} \cdot \frac{a_0^2}{a^2} \Delta' c_2 \frac{d}{da} \left(\frac{1}{a_0^2 - a^2} \right) \tag{VII.22}$$

$$grad\ c_2 = -a_o^2 \Delta' c_2 \frac{d}{da}\left(\frac{1}{a_0^2 - a^2}\right) \qquad (VII.22\,a)$$

where $\Delta c_j = c_{ej} - c_j*$ and $\Delta' c_j = c_{ej} - c_{ij}$ when c_{ij} stands for the inner concentration of the j^{th} species.

Equation VII.22 may be integrated with respect to a with limits as for equation VII.20 to yield c_1 as a function of c_{e1}, similarly as for c_2 in equation VII.21.

The velocity of coagulation (the *velocity of interface progression*), u, may be calculated from equations VII.22a and VII.17.

$$u = \frac{da}{dt} = -a_0^2 D_2 \frac{\Delta' c_2}{\Delta c_2} \cdot \frac{1}{a} \cdot \frac{d}{da}\left(\frac{1}{a_0^2 - a^2}\right) \qquad (VII.23)$$

The integral time required for complete coagulation is

$$t_c = \int u dt = \frac{a_0^2}{2} \cdot \frac{1}{D_2} \cdot \frac{\Delta c_s}{\Delta' c_2} \qquad (VII.24)$$

To solve equation VII.24, one needs the value of c_1*. To satisfy this, Rende[22] conducts the following considerations.

In view of the counterdiffusion of solvent and nonsolvent, a volume V_1 of solvent will leave the filament and a volume V_2 of nonsolvent will enter it. It is assumed that the total (original) volume of dope (filament) V_{tot} will remain constant, only a change of concentration takes place. When phase equilibrium point is reached, a phase separation into two phases with volumes $d \cdot V_{tot}$ and $c \cdot V_{tot}$, diluted and concentrated phases, respectively takes place. Naturally, $d + c = 1$. The volume fractions of the j^{th} species, v_j* in the total volume V_{tot} are related to the values of c_j* by $v_j* = c_j*/\rho_j$, where ρ_j is the density, and may further be given by the following equations.

$$\begin{aligned} dv_1 + (1-d)v_1' &= v_1* \\ dv_2 + (1-d)v_2' &= v_2* \\ dv_p + (1-d)v_p' &= v_p* \\ v_1* + v_2* + v_p* &= 1 \end{aligned} \qquad (VII.25)$$

where v_j and v_j' represent the volume fractions on the j^{th} species in the diluted and concentrated fractions at the thermodynamic equilibrium, respectively.

It is assumed that at equilibrium the chemical potential μ of each species must be equal in both phases, that is

$$\mu_j = \mu_j' \qquad (VII.26)$$

where the subscript refers to the most concentrated phase.

According to Flory[32] these equations may be written as

$$\ln v_1 + (1 - v_1) - v_2 \frac{x_1}{x_2} - v_p \frac{x_1}{x_p} +$$

$$
\begin{aligned}
&+ \quad (\chi_{12}v_2 + \chi_{1p}v_p)(v_2 + v_p) - \chi_{2p}\frac{x_1}{x_2}v_2 v = \\
&= \quad \ln v_1' + (1 - v_1') - v_2'\frac{x_1}{x_2} - v_p'\frac{x_1}{x_p} + \\
&+ \quad (\chi_{12}v_2' + \chi_{1p}v_p')(v_2' + v_p') - \chi_{2p}\frac{x_1}{x_2}v_2'v_p'
\end{aligned}
$$

$$
\begin{aligned}
&\ln v_2 + (1 - v_2) - v_1\frac{x_2}{x_1} - v_p\frac{x_2}{x_p} + \\
&+ \quad (\chi_{21}v_1 + \chi_{2p}v_p)(v_1 + v_p) - \chi_{1p}\frac{x_2}{x_1}v_1 v_p = \\
&= \quad \ln v_2' + (1 - v_2') - v_1'\frac{x_2}{x_1} - v_p'\frac{x_2}{x_p} + \\
&+ \quad (\chi_{21}v_1' + \chi_{2p}v_p')(v_1' + v_p') - \chi_{1p}\frac{x_2}{x_1}v_1'v_p'
\end{aligned}
\qquad \text{(VII.27)}
$$

$$
\begin{aligned}
&\ln v_p + (1 - v_p) - v_2\frac{x_p}{x_2} - v_1\frac{x_p}{x_1} + \\
&+ \quad (\chi_{p2}v_2 + \chi_{p1}v_1)(v_2 + v_1) - \chi_{12}\frac{x_p}{x_2}v_2 v_1 = \\
&= \quad \ln v_p' + (1 - v_p') - v_2'\frac{x_p}{x_2} - v_1'\frac{x_p}{x_1} + \\
&+ \quad (\chi_{p2}v_2' + \chi_{p1}v_1')(v_2' + v_1') - \chi_{12}\frac{x_p}{x_2}v_2'v_1'
\end{aligned}
$$

where χ_{ij} is a pair interaction parameter, $\chi_{ij} = f(kT)^{-1}$; x_j describes the number of segments of the j^{th} species molecule.

The system is rather complicated, but may be simplified by the following assumptions: Both solvent and nonsolvent are monomeric compounds, so $x_1/x_2 = 1$. Further, $\chi_{ij} = \chi_{ji}(v_i/v_j)$, where V_i and V_j are molar volumes. Additionally, for polyacrylonitrile additional simplifications are valid:[22] for dimethyl formamide - water system $V_2 \cong 4V_1$, so $\chi_{12} = 0.25\chi_{21}$. Furthermore, $V_p \cong 10^4 V_2$ (or V_1), and in effect $x_1/x_p \cong x_2/x_p \cong 0$ and $\chi_{2p} = \chi_{p2} \cdot 10^{-4} \cong 0$. Lastly, $\chi_{1p} = 0$, therefore also $\chi_{p1} = 0$. For other solvent-nonsolvent systems similar simplifications may be possible.

Even with all the simplifications, the system of equations cannot be solved analytically; only numerical solutions are possible, but in the era of easily available fast desktop computers such tasks belong to accessible methods. Nevertheless, Rende[22] introduces still further simplifications.

One may admit that the more diluted phase does not contain any polymer, and the more concentrated phase consists only of the precipitated polymer. As a result $v_p = 0$; $v_p' = 1$; and $v_1' = v_2' = 0$. Consequently one may rewrite equations

VII.25 and VII.27, in a version for polyacrylonitrile, as

$$\begin{aligned} dv_1 &= v_1 * \\ dv_2 &= v_2 * \\ (1-d) &= v_p" \end{aligned} \tag{VII.28}$$

and

$$\begin{aligned} \ln v_1 + 0.25\chi_{21} v_2^2 &= \ln v_1' + 1 \\ \ln v_2 + \chi_{21} v_1^2 &= \ln v_2' + 1 \\ v_1 + v_2 &= 1 \end{aligned} \tag{VII.29}$$

Due to the approximately constant V_{tot}. it results that $v_p = c_p/\rho_p$. Rende solved equations VII.29 by using the approximate series expansion of logarithms: $\ln(1+x) = x - x^2/2$. In this way the solution is

$$\frac{v_2}{1-v_2} = \frac{1 - sqrt1 - (1.5 - \chi_{21})(\chi_{12} + 0.5)}{\chi_{12} + 0.5} \tag{VII.30}$$

Rende[22] claims that the solution offered by equation VII.30 is "quite reliable", however, the values of χ_{21} must be determined experimentally, together with D_j, in the diffusion equations.

VII.3 Wet Process

In the wet process. we resort to the extraction of solvent by another liquid which is freely miscible with the solvent used, but it does not dissolve the polymer. The second liquid is usually called a *nonsolvent.* The depravation of the system of a sufficient amount of solvent leads to the coagulation of polymer. In another type of wet process, a polymer insoluble in any acceptable solvent is transformed chemically into a derivative which is soluble. Such a solution is extruded into a reactant, or a *nonsolvent* containing a reactant, which transforms the polymer chemically back to its original, insoluble form. The chemical reactions taking place in the coagulation bath may be taken as far as extruding a liquid *prepolymer*, which after extrusion is further polymerized to a high molecular mass solid polymer. Polyurethanes may serve here as an example.[24] Attempts have also been made to form fibers from emulsions instead of solutions.[24] Emulsions usually have much higher concentration of solids than solutions do. Viscosity of emulsions may be too low for good "spinnability", and increasing it to some necessary minimum level may be difficult without the use of auxiliaries adversely affecting important polymer properties.[14]

The concentrations of polymer solutions (*dopes*) used for fiber formation range rather widely, starting from about 3% all the way to 20% or possibly 30%. Processes are known which use much higher concentrations, all the way to a plasticized melt or semi-melt formation systems (40 to 60%) or so called *gel spinning.*[25–27] Concentration of the polymer solution used for fiber formation represents a major point in the economy of the process, thus the low concentrations may be applicable mainly for *high performance fibers* the customers of which may be willing to bear the extra high costs.

One may encounter opinions that the upper limit of concentration is limited by the high viscosity of solution and with the resulting difficulties to handle the high viscosity solutions. On the other hand, the physical properties of the resulting fibers improve with increasing solution concentration.[2] It seems, however, to be only partly true that high viscosity is the main obstacle here; melts of much higher viscosities are used with great success, fibers are formed from gels, so viscosity is not an unsurmountable problem. Use of low concentrations appears to be partially rooted in the tradition of formation from solution and partially in the difficulty of finding a solvent which would dissolve more polymer or fit all the other important requirements. The main reason for using solutions for fiber formation is the decomposition of a polymer at elevated temperature. The nature of wet processes is such that at higher temperatures, the high vapor pressure of the solvent may increase health and/or fire hazard beyond any acceptable level. The problem lies then in finding a solvent which gives sufficiently highly concentrated solutions at low temperature which is non-toxic and possibly easy to handle. Last, though not least for wet formation, a nonsolvent which is miscible and that also fulfills the other criteria valid for solvents must be available.

Theoretically speaking, mixed solvents can be used, but in practice it is very difficult to find such a mixture of solvents where the components would have similar diffusivities, and or evaporation rates. Azeotropes might be the best such possibility, but to find a suitable one may be even more difficult.

For design of spinnerettes the same general principles may be used as in case of melt spinning except that the pressures involved are most often correspondingly lower, so the plate thickness is smaller. In the majority of wet operations, the spinnerette is submerged in the coagulating bath and is connected by a transfer tube to the block containing the metering pump and filter assembly (see figure VII.3). The spacing between the spinnerette capillaries may be substantially smaller, as the easy access of the coagulating fluid provides sufficient antisticking protection.

Serkov and co-workers[11] have published an interesting study of fiber formation from polyacrylonitrile in dimethyl formamide as the solvent. The results of their investigations are presented in figures VII.4 and VII.5. The problems of diffusion were solved with the use of the graphic method[23] described in the preceeding section. The results are quoted here not because of the exactitude of the solution but because of the general idea of the time and distance scales of diffusion in the process.

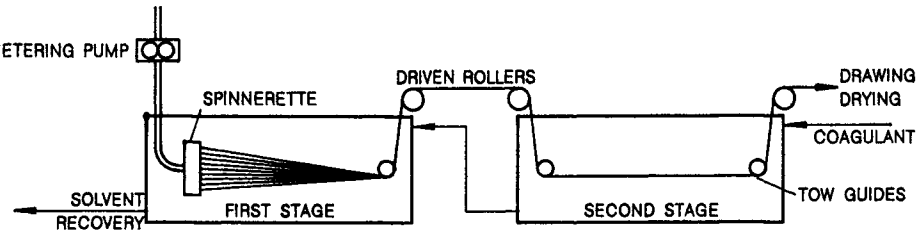

Figure VII.3: *Schematic representation of a wet process of fiber formation.*

In another publication Serkov and co-workers[47] determine diffusivity experimentally by placing a drop of solution between two glass Couette cylinders (or glass plates) and observe the flattened drop as it gradually precipitates (becomes hazy) upon introduction of nonsolvent between the glass surfaces. The necessary critical concentration for precipitation must be determined for a range of polymer concentrations, as there was found a strong dependence between the two parameters. The work was done with polyacrylonitrile dissolved in an aqueous solution of sodium thiocyanate.

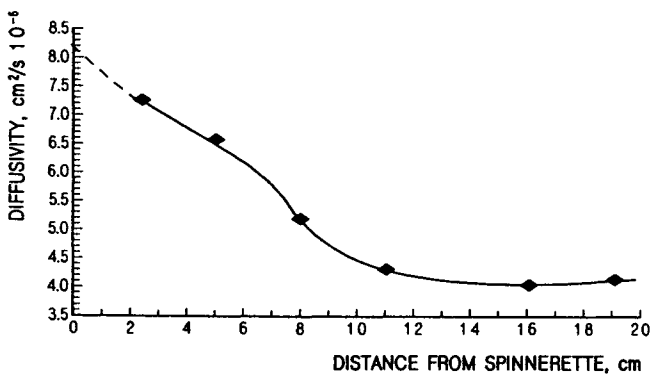

Figure VII.4: *Changes of diffusion coefficient for dimethyl formamide if polyacrylonitrile with distance from spinnerette. After Serkov et al.*[11]

As may be seen from figure VII.4, diffusivity is by no means constant, and in the quoted case it changes approximately by a factor of 2. This variability of diffusion coefficient casts serious doubts about the "wholesale solutions" suggested by some authors. A method to predict how diffusivity might change with increasing polymer concentration has been published by D. Machin and C. E. Rogers.[28] Their theory is based on comparison, analysis, and extension of free volume theories which were found mathematically equivalent. From this the authors have developed a method of determining diffusivity from the data on glass transition temperature.

Fujita and co-workers[33] have assumed that a penetrant requires a certain critical value, B_d, of free volume to promote diffusion and that the fraction of free

volume, f, increases linearly with the volume fraction of the penetrant, Φ_1.

$$f = f_0 + \beta\Phi_1 \tag{VII.31}$$

where f_0 is the mean fractional free volume of pure polymer at a given temper-

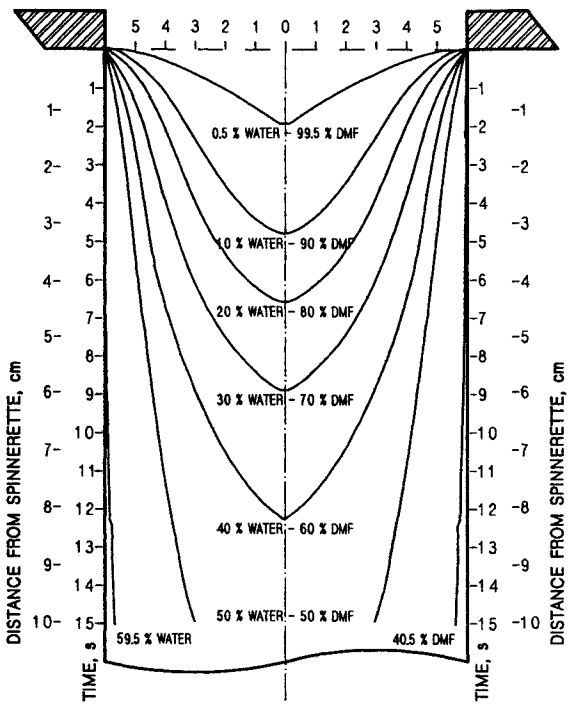

Figure VII.5: *Distribution of dimethyl formamide and water concentrations in a polyacrylonitrile fiber in relation to the distance from spinnerette and residence time in the coagulation bath. Extrusion velocity: 4m/min. After Serkov et al.*[11]

ature, $\beta = \gamma - f_0$ where γ is the corresponding fractional free volume of pure solvent. As generally $\gamma \gg f_0$ the diffusion coefficient D increases with Φ_1.

Further, the authors consider the theory by R. M. Vasenin[34] according to which a disturbance in a material is needed for the diffusing molecule to pass and this disturbance requires an energy ε. Further, Vasenin assumes that ε varies smoothly from ε_2^0 in pure polymer to ε_1^0 in a pure solvent according to a semiempirical relation.

$$\frac{-d\varepsilon}{d\Phi_1} = \frac{\beta'}{(1-\Phi_1)^2} \cdot (\varepsilon - \varepsilon_1^0) \tag{VII.32}$$

Another of Vasenin's relationships is:

$$\ln D = \ln D_0 + (\ln D_1 - \ln D_0)\left[1 - \exp\left(\frac{-\beta'\Phi_1}{1-\Phi_1}\right)\right] \tag{VII.33}$$

where D_1 is the diffusion coefficient in pure solvent. In the original work the physical meaning of β' was unclear; it was related to the plasticizing ability of the solvent.

The plots of $\ln D$ *versus* Φ_1 for solvents in glassy polymers show regions of changing curvature; these regions correspond the passage through the glass transition temperature. The calculations predict that such transitions should occur at Φ_1 lower than those observed experimentally. Under the assumptions that the energy ε varies smoothly with the composition below and above glass transition, equations analogous to equations VII.32 and VII.33 have been written.

$$\frac{d\varepsilon}{d\Phi_1} = -\frac{\beta_1'}{(1-\Phi_1)^2} \cdot (\varepsilon - \varepsilon_1^0) \tag{VII.34}$$

$$\frac{d\varepsilon}{d\Phi_1} = -\frac{\beta_1'}{(1-\Phi_1)^2} \cdot (\varepsilon - \varepsilon_1^0) \tag{$VII.34\,a$}$$

$$\ln D = \ln D_0 + (\ln D_1 - \ln D_0)\left[1 - \exp\left(\frac{-\beta_1'\Phi_1}{1-\Phi_1}\right)\right] \tag{VII.35}$$

$$\ln D = \ln D_g + (\ln D_1 - \ln D_g)\left[1 - \exp\left(\frac{-\beta_2'(\Phi_1 - \Phi_g)}{(1-\Phi_1)(1-\Phi_g)}\right)\right] \tag{$VII.35\,a$}$$

Equations VII.34 and VII.35 refer to the conditions below the glass transition and the versions "a" to conditions above glass transition. The equations open the possibility of a complete characterization of the diffusivities at $\Phi_1 = 0, \Phi_1 = 1$, at the transition, where are Φ_g and D_g, provided that the parameters β_1' and β_2' can be determined.

The measurements of the diffusivity below glass transition should be made in the steady state of diffusion to avoid the effects of slow polymer relaxation processes.

Fujita's theory has been expanded to cover a whole range of concentrations, not only the diluted ones, and to replace the linear dependence of free volume, f, on the volume fraction of the penetrant, Φ_1, with a more realistic function.

$$f = f_0 + F(\Phi_1, T) \tag{VII.36}$$

where $F(1,T) = \gamma - f_0$.

Further, Machin and Rogers[28] take into account the equations relating glass transition temperature from the volume of the penetrant in four versions by four different authors, and so the equation by Fox:[35]

$$T_g = \frac{R_g^0 T_g^s}{\Phi_1(T_g^0 - T_g^s) + T_g^s} \tag{VII.37}$$

by Kelly and Bueche:[36]

$$T_g = \frac{T_g^0 + \Phi_1 \cdot \left(\frac{\alpha_f^s}{\alpha_f^0} \cdot T_g^s - T_g^0\right)}{1 + \Phi_1 \cdot \left(\frac{\alpha_f^s}{\alpha_f^0} - 1\right)} \tag{VII.38}$$

by Jenckel and Heusch:[37]

$$T_g = T_g^0 - \Phi_1(T_g^0 - T_g^s - K) - K\Phi_1^2 \tag{VII.39}$$

by Kanig:[38]

$$T_g = \frac{T_g^0 k\frac{(1-\Phi_1)}{\Phi_1} + T_g^s K - \frac{K_1}{1+\frac{\Phi_1}{k(1-\Phi_1)}}}{K + \frac{k(1-\Phi_1)}{\Phi_1}} \tag{VII.40}$$

In the above equations T_g^0 refers to the glass transition of a dry polymer, T_g^s is the glass transition of the solvent, α_f^0 and α_f^s are the differences in the thermal expansion coefficients above and below the glass temperature for the polymer and the solvent, respectively, $k = \alpha_f^s/\alpha_f^0$, K and K_1 are constants for the system, respectively.

The function $F(\Phi_1, T)$ from equation VII.36 has been derived as

$$f(\Phi_1, t) = \Phi_1\left(\frac{A' + B'\Phi_1 + C'\Phi_1^2}{D' + E'\Phi_1 + F'\Phi_1^2}\right) \tag{VII.41}$$

The coefficients A', B', C', D', E', and F', and their dependence on the equation used for the calculation of glass transition temperature are given in table VII.1.

With the help of equation VII.41 one may calculate f from equation VII.36 and further estimate the relation

$$\frac{1}{\ln(D/D_0)} = \frac{f_0}{B_d} + \frac{f_0^2}{B_d}\cdot\left(\frac{D' + E'\Phi_1 + F'{\Phi_1}^2}{A' + B'\Phi_1 + C'{\Phi_1}^2}\right)\frac{1}{\Phi_1} \tag{VII.42}$$

The calculated functions

$$Y\left[\frac{1}{\ln(D/D_0)} - \frac{f\_0}{Bd}\right] \tag{VII.43}$$

and

$$Y\cdot\frac{\Phi_1}{\ln(D/D_0)} \tag{VII.44}$$

may be plotted *versus* Φ_1^{-1} and $Y\Phi_1$, respectively, where

$$f(\Phi_1, t) = \left(\frac{A' + B'\Phi_1 + C'\Phi_1^2}{D' + E'\Phi_1 + F'\Phi_1^2}\right)$$

If the obtained plots are linear, then it is an indication that the dependence between the diffusion and glass temperature is consistent. The value of f_0/B_d may be taken as the slope of $\Phi_1/[\ln(D/D_0)]$ *versus* Φ_1^{-1} for small Φ_1. In practice, it may be more convenient to evaluate graphically the relationship $F(\Phi_1, T)$ *versus* Φ_1 first, and then the D *versus* Φ_1. A high degree of accuracy may be obtained by this method.

Figure VII.5 presents the distribution of solvent and nonsolvent in a wet formed polyacrylonitrile fiber from the spinnerette on. The figure is drawn against time,

Table VII.1
Expression for constants in equation VII.41
and their dependence on source of T_g.[28]

Constant	Fox eqn. VII.37	Kelly & Bueche eqn. VII.38
A'	$\alpha_f^0(T_g^{0\,2} - TT_g^s)$ $+\alpha_f^s T_g^s(T - T_g^0)$	$\alpha_f^s(T - T_g^s)$ $+\alpha_f^0(T_g^0 - T)$
B'	$T(T_g^0 - T_g^s)$ $(\alpha_f^s - \alpha_f^0)$	$\alpha_f^s(\alpha_f^s - \alpha_f^0)/\alpha_f^0$ $\times(T - T_g^s)$ $+(T_g^0 - T)(\alpha_f^s - \alpha_f^0)$
C'	0	0
D'	T_g^s	1
E'	$T_g^0 - T_g^s$	$\frac{\alpha_f^s}{\alpha_f^0} - 1$
F'	0	0

Constant	Jenckel & Keusch eqn. VII.39	Kanig eqn. VII.40
A'	$\alpha_f^0(2T_g^0 - T - T_g^0 - K)$ $+\alpha_f^s(T - T_g^0)$	$\alpha_f^0(KT_g^0 - KT_g^s - K_1)$ $+\alpha_f^s/\alpha_f^0$
B'	$\alpha_f^0(2K - T_g^0 + T_g^s)+$ $+\alpha_f^s(T_g^0 - T_g^s - K)$	$\alpha_f^0[2K_1 + K(T_g^0 - T_g^s)$ $\times(\alpha_f^0/\alpha_f^s - 2)]$ $+\alpha_f^s[K(T_g^0 - T_g^s)$ $-K_1 - \alpha_f^s/\alpha_f^0] + [1 + K]$
C'	$K(\alpha_f^s - \alpha_f^0)$	$k\left(\frac{\alpha_f^0}{\alpha_f^s} - 1\right) + \left(\frac{\alpha_f^s}{\alpha_f^0} - 1\right)$ $-K(T_g^0 - T_g^s)(\alpha_f^s - \alpha_f^0)^2/\alpha_f^s$
D'	1	α_f^s/α_f^0
E'	0	$1 + K - \frac{2\alpha_f^s}{\alpha_f^0}$
F'	0	$K\left(\frac{\alpha_f^0}{\alpha_f^s} - 1\right) + \left(\frac{\alpha_f^s}{\alpha_f^0} - 1\right)$

and distance scale is also given. The slowness of the diffusion process may be here well appreciated; the consequences of the low rate of fiber formation in a wet process do not need any more emphasis.

When ions are present in the dope and/or the coagulating bath, like in processes involving water type solvents, *e. g.* rayon processes, cuprammonium, or sodium thiocyanate, the diffusion may be additionally complicated by the interphase potential.[63] The diffusion potential, $\Delta\phi$, between two phases, a and b, may be described by the Henderson equation.

$$\Delta\phi = \phi_a - \phi_b = \frac{RT}{F}\frac{\sum z_i\omega_i[c_i(b) - c_i(a)]}{\sum z_i^2\omega_i[c_i(b) - c_i(a)]} \times \ln\left[\frac{\sum z_i^2\omega_i c_i(a)}{\sum z_i^2\omega_i c_i(b)}\right] \qquad \text{(VII.45)}$$

where ω_i is molar mobility of the species i, z_i is charge of the species i, c_i is

concentration of the species, and A is the interphase area. The equation gives a fair agreement with the majority of ions involved in formation of the cellulosic fibers.

In the presence of electrical potential between phases, the flux of the ion species, J_i, is described by the Nernst-Planck equation.

$$J_i = -\omega_i RT \times \left(\frac{dc_i}{dx}\right) - z_i F \omega_i c_i \times \left(\frac{d\phi}{dx}\right) \qquad \text{(VII.46)}$$

The ion flux, as given by equation VII.46, depends on the interphase potential. In processes of wet fiber formation involving ions, the rate of coagulation would, certainly, depend on the ion flux.

From the point of view of fiber properties, it is beneficial to have the diffusion process less drastic, slower. The different nonsolvents have different precipitation powers, so for the full precipitation of certain volume of polymer solution, different volumes of nonsolvent may be needed, depending on the physico-chemical nature of the nonsolvent. For this reason it is customary to have a lower precipitating power close to the spinnerette, and to increase it gradually along the moving tow. Usually this is achieved by using a mixture of solvent and nonsolvent as the precipitating bath. The concentration of nonsolvent should increase as the degree of fiber coagulation increases.

Additionally, to provide for some concentration gradient in the coagulation process along the path of the fiber travel, the coagulation bath is pumped either counter- or co-current to the movement of fibers, To facilitate the transport of coagulation medium, the fibers are often led through several baths of increasing precipitant concentration. This, however, does not solve, nor describe the whole problem. The strength of a nonsolvent may sometimes be changed by some additives or by change of pH. For example, pH of the mixture of water and dimethyl formamide (DMF) used to precipitate poly(acrylonitrile) from DMF solution has a strong influence on the precipitating power at the same solvent-nonsolvent concentration. The effect of pH on the cross section of poly(acrylonitrile) fibers coagulated in a water - dimethyl formamide mixture may be seen in figure VII.6.[15] The stronger the deformation of the circular cross section of the fiber, the more drastic is the precipitation.

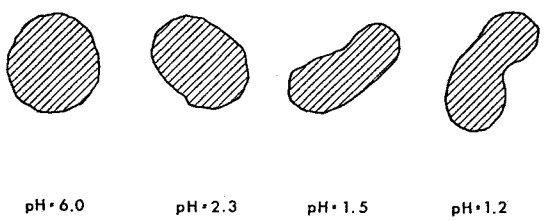

Figure VII.6: *Cross sections of fibers obtained in a wet processes with coagulants of different strength; the strength increased with decreasing pH. After Gröbe and Gieske.*[15]

The filament surface, as it moves through the coagulation bath, does have some

boundary layer across which is a gradient of solvent - nonsolvent concentration. Griffith[29] has developed an approximate analytical solution to the changes of concentration, or temperature, in the radial direction from the inside of the filament out into the fluid. The approximation is based on the following assumptions: constant filament diameter, the filament moves at an uniform (constant) velocity, and the fluid in which the fiber moves is homogeneous. The final solution for the concentration changes is suggested as

$$c* = \frac{c_t - c_0}{c_{f0} - c_0} = \int_0^\infty \exp\left[-\left(\frac{lD}{Rv_f}\right)u^2\right] J_0(u,r)J_1(u)du \qquad \text{(VII.47)}$$

where $c*$ is concentration, c_t is bath concentration, c_0 is initial bath concentration, c_f stands for initial concentration in the fiber at the distance from spinnerette of l expressed in the units of R, where R is filament radius, D represents mass diffusivity, v_f is filament velocity, u stands for medium velocity divided in v_f. J_0 and J_1 are Bessel functions of zero and first order, respectively.

An analogous equation for temperature changes in the radial direction r is

$$T* = \frac{T_t - T_0}{T_{f0} - T_0} = \int_0^\infty \exp\left[-\left(\frac{l\alpha}{Rv_f}\right)u^2\right] J_0(u,r)J_1(u)du \qquad (VII.47\,a)$$

In analogy to the equation for concentration, T_t means the medium temperature, T_0 is the initial medium temperature, T_{f0} is initial filament temperature, and α is thermal diffusivity.

The solution of equation VII.47 and VII.47a is given in the form of a graph in figure VII.7. The different curves given in the graph represent the radial distance from the filament axis in units of filament radius, R, as indicated in the figure. For an average wet spinning operation, the graph given in figure VII.6 covers some 15 to 20 cm distance from the spinnerette before the different curves join together. Velocity profile in the fluid may be estimated from the boundary layer theory suggested by Sakiadis and described in section VI.1.b, or by using any of the experimental relationships.

In today's era of the computer, numerical solutions are preferred and easily available, though the approximate graphical solution of figure VII.7 may be used for quick rough estimates if the proper computer programs are not available.

It is intuitively quite obvious that in the nearest vicinity of a wet formed filament, throughout the boundary layer, the concentrations of solvent and nonsolvent are not constant; there are gradients, and the gradients are not necessarily constant. The motion of the filament also must be expected to affect those concentration gradients. G. A. Danilin[40] has devoted some attention to the problem and in effect he published a group of equations to calculate those effects.

Danilin uses the following definition of the used symbols: x and y are the cylindrical coordinates for the system, the first one coinciding with the fiber axis; u and v are projections of the precipitating bath velocities in the boundary layer on the x and y axes, respectively; u_s and v_s are the values of u and v on the filament surface; u_e is the value of u at the outer edge of the boundary layer, it is

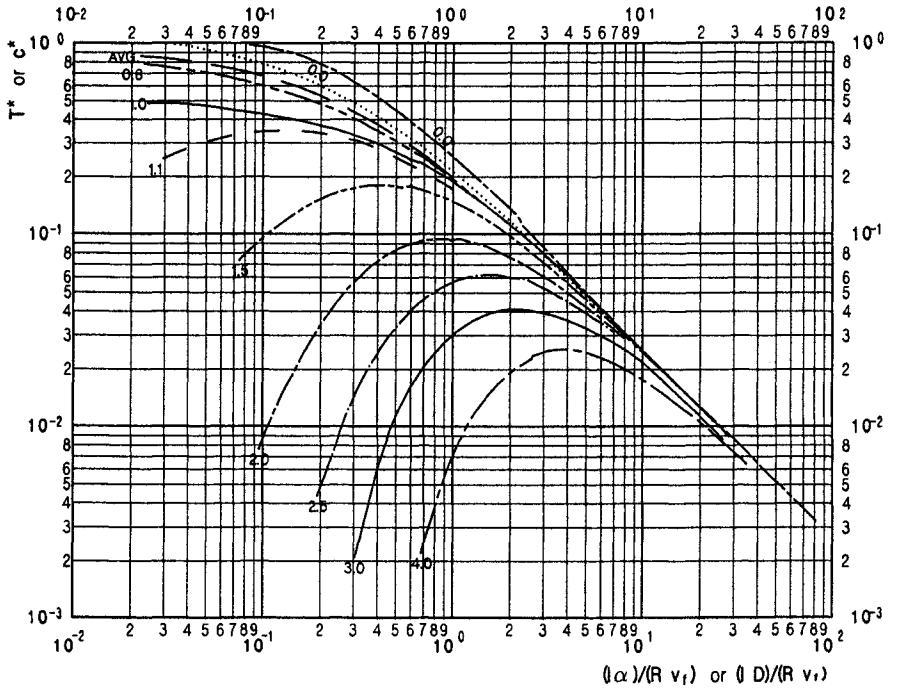

Figure VII.7: *Temperature, or concentration, inside and outside of a filament during the wet formation, as calculated according to equation VII.45 or VII.45a. After R. M. Griffith.*[29]

the lengthwise velocity of the coagulation bath; ν is the kinematic viscosity of the coagulation bath; c and c_1 are the concentrations of solvent in the bath and the initial concentration in the fiber (dope); c_e is the initial concentration of solvent in the coagulation bath; D and D_1 are the diffusion coefficients of the solvent in the precipitating bath and in filament and usually $D \neq D_1$; K is distribution coefficient; ρ_1 is the density of the solvent exiting the filament; α represents the angle between the tangent to the generatrix of the filament surface and x-axis, it describes the local rate of diameter reduction; V_p^* is the projection of the velocity of the liquid exiting the filament onto the normal to the fiber surface; Q is the volumetric flow rate of the polymer solution at a distance from spinnerette. The relationships describing the problem, as well as the boundary conditions are given as follows:

$$\frac{\partial yu}{\partial x} + \frac{\partial yv}{\partial y} = 0 \tag{VII.48}$$

$$u\frac{\partial u}{\partial x} + v\frac{\partial u}{\partial y} = u_e\frac{\partial u_e}{\partial x} + \frac{v}{y}\cdot\frac{\partial}{\partial y}\left(y\frac{\partial u}{\partial y}\right) \tag{VII.49}$$

$$u\frac{\partial c}{\partial x} + v\frac{\partial c}{\partial y} = \frac{D}{y}\cdot\frac{\partial}{\partial y}\left(y\frac{\partial c}{\partial y}\right) \tag{VII.50}$$

$$u_1 \frac{\partial c_1}{\partial c} \partial x - \frac{y}{2} \cdot \frac{\partial u_1}{\partial x} \cdot \frac{\partial c_1}{\partial y} = \frac{D_1}{y} \cdot \frac{\partial}{\partial y} \left(y \frac{\partial c_1}{\partial y} \right) \tag{VII.51}$$

$$u = u_s = u_1 + \frac{V_p}{\cos \alpha} \left(1 - \frac{\rho_1}{\rho} \right) \cos \alpha \cdot \sin \alpha \tag{VII.52}$$

$$v = v_s = u_s \tan \alpha + \frac{\rho_1 V_p}{\cos \alpha} \tag{VII.53}$$

if $c = Kc_1$ and for $y = R$ and $x \geq 0$ then

$$\rho_1 D_1 \frac{\partial c_1}{\partial y} = \rho D \frac{\partial c}{\partial y} + \frac{\rho_1 V_p}{\cos \alpha} \cdot (c_1 - c) \tag{VII.54}$$

$u = u_e$ and $c = c_e$ if $R < y < \infty$ and $x = 0$
$c_1 = c_1^0$ if $0 \leq y < R$ and $x = 0$
$u \to u_e$ and $c \to c_e$ when $y \to \infty$ and $x > 0$
when $y = 0$ and $x > 0$ then $\frac{\partial c_1}{\partial y} = 0$

And further definitions are:

$$\tan \alpha = \frac{dR}{dx} \tag{VII.55}$$

$$\frac{\rho_1 V_p}{\cos \alpha} = -\frac{1}{2\pi R} \cdot \frac{d}{dx} \tag{VII.56}$$

when $q = \rho_1 Q$ and $Q = \pi R^2 u_1$.

To solve the equations VII.48 through VII.56, one needs to have the information on the change of fiber velocity in the bath (u_1) and the volumetric flow rate of the spinning dope, Q, as a function of the process parameters.

The author[40] indicates, however, that in the real processes, the equality of the velocity components of the bath and filament does not occur, $u_s \neq u_1$. The last inequality would hold true if the densities of bath and fiber surface were equal, $\rho_1 = \rho$, or if there were no mass flow on the filament surface, $V_p = 0$. Nevertheless, the author claims that in real processes, despite the fact that $\rho_1 \neq \rho$ and $V_p \neq 0$, the values of the component velocities are very close, so in the first approximation they may be taken as equal, $U_s = u_1$.

With a more complete process analysis the equations given by Danilin may be solved, though the task is not exactly easy. However, no simpler method is available.

In commercial operations of wet formation of fibers, the number of filaments extruded from one spinnerette is very large, reaching several tens of thousands. The dense bundle of filaments presents an obstacle for the coagulation bath to penetrate inside the tow. An attempt to describe the problem has been published by Szaniawski and Zachara.[30,31] As the problem is quite complex, the authors make the following simplifying assumptions: The interior of the fiber bundle is taken as uniformly anisotropic porous medium in which the fluid flows according to the Darcy's law. The coagulating fluid is taken as homogeneous, viscous, and with constant density. The fibers are taken as rigid cylindrical rods. The mass

exchange and the influence of gravity are neglected. Flat and cylindrical geometries of the tow are considered.

When we designate as A the cross section of the tow, as N the number of filaments in the tow, as d filament diameter, and as s cross section of a filament, then one may define the ratio of the volume of fibers to the volume of the tow as

$$\varphi = \frac{\pi d^2}{4s} \tag{VII.57}$$

where $s = A/N$. In typical cases $\varphi < 0.05$, or generally $\varphi \ll 1$. Considering the slow flow of fluid one may apply Darcy's law in the form

$$w_{||} = -\frac{s}{\eta} \cdot F_{||}(\varphi) \cdot grad_{||} p \tag{VII.58}$$

$$w_{\perp} = -\frac{s}{\eta} \cdot F_{\perp}(\varphi) \cdot grad_{\perp} p \tag{VII.58 a}$$

where $w_{||}$ and $w\perp$ are the components of filtration velocity in parallel and in perpendicular directions, respectively, and correspondingly parallel and perpendicular to the fiber axis: p – pressure, η – dynamic viscosity of fluid, $F_{||}$ and $F_{\perp}$ – coefficients of filtration resistance.

As the velocity of filtration, $\vec{w}$, we define the output of fluid which flows through a unit of porous surface in relation to this surface. Generally, the linear Darcy's law is applicable up to the Reynolds number $Re < 10$, though the limit is not well defined and for Reynolds numbers somewhat over 10 it may still give acceptable results. For this case, the Reynolds number is defined as

$$Re_d = \frac{|w|d}{\mu} \tag{VII.59}$$

Here $|w|$ denoted the modulus of the filtration velocity, μ is kinematic viscosity.

The coefficients of filtration resistance, $F_{||}$ and $F_{\perp}$, basically depend on φ and on the configuration of fibers in the considered space. However, since φ is very small, one may take advantage of the simplified relationship which does not depend on the configuration.

$$F_{||} = 2F_{\perp} = \frac{1}{4\pi} \cdot \left[\ln\left(\frac{1}{\varphi}\right) - 1.5\right] \tag{VII.60}$$

In the case of a flat tow, the problem is considered in the Cartesian coordinates, with cylindrical tow, cylindrical coordinates are to be used. The axis $x - o$ is on the surface of the spinnerette, while the axis $o - z$ is parallel to the fiber axis. In such coordinates, Darcy's law has the form

$$u_z - v \cdot (1 - \varphi) - \frac{s}{\eta} \cdot F_{||} \frac{\partial p}{\partial z} \tag{VII.61}$$

$$u_x = w_x = -\frac{s}{\eta} \cdot F_{\perp} \frac{\partial p}{\partial x} \tag{VII.61 a}$$

Here $w_x = w_\perp$ and $w_z = w_\parallel$ are the components of the fluid velocity in relation to the tow; u_x and u_z are the components of the velocity of fluid in the static system connected with the spinnerette.

In view of the assumed constant fluid density and neglected mass exchange, the continuity equation may be written as

$$\frac{\partial w_z}{\partial z} + \frac{\partial w_z}{\partial x} + k\frac{w_x}{x} = 0 \tag{VII.62}$$

where $k = 0$ for flat tow, and $k = 1$ for cylindrical tow with axial symmetry.

When we substitute into equation VII.62 the values for w_x and w_z as obtained from equation VII.61, and take into account that $\eta, s, F_\parallel, F_\perp$ do not depend on x or z, we obtain the equation for the pressure

$$\frac{F_\parallel}{F_\perp} \cdot \frac{\partial^2 p}{\partial z^2} + \frac{\partial^2 p}{\partial x^2} + \frac{k}{x} \cdot \frac{\partial p}{\partial x} = 0 \tag{VII.63}$$

The boundary conditions for equation VII.63 are as follows: On the axis of symmetry $x = 0$, the transverse velocities are equal zero, $u_x = w_x = 0$. At the spinnerette ($z = 0$) $u_z = 0$ and at a large distance from the spinnerette ($z \longrightarrow \infty$) the fluid velocity reaches the velocity of fibers ($w_z = 0$). Considering all these and equation VII.63, one obtains the following relationships

$$\frac{\partial p(0,z)}{\partial x} = 0 \tag{VII.64}$$

$$\frac{\partial p(x,0)}{\partial z} = \frac{v\eta(1-\varphi)}{sF} \tag{VII.64 a}$$

$$\lim_{z\to\infty} p(x,z) = const. \tag{VII.64 b}$$

On the surface of the tow ($x = \pm a$), one needs to take into account the mutual interaction of both areas of flow. Under the assumption that outside the tow the flow resistance is relatively small, one may use Bernoulli's equation

$$p + \frac{\rho}{2} \cdot (u_x^2 + u_z^2) = p_0 \tag{VII.65}$$

where ρ is fluid density and p_0 is the pressure of stagnation. This condition the authors consider in two versions:

$$p(a,z) - p_0 = 0 \qquad \text{version 1} \tag{VII.66}$$

$$p(a,z) - p_0 = \frac{\rho u_x^2}{2} \qquad \text{version 2} \tag{VII.66 a}$$

In version VII.66, the influence of dynamic pressure has been neglected, while in version VII.66a only the main part of the dynamic pressure, $\rho u_x^2/2$, has been taken into account and the segment $\rho u_z^2/2$ has been omitted.

Upon introduction of dimensionless variables

$$\xi = \frac{x}{a} \tag{VII.67}$$

$$\zeta = \sqrt{\frac{F_\perp}{F_\parallel}} \cdot \frac{z}{a} \tag{VII.67 a}$$

$$\Pi = \frac{s}{\eta}\sqrt{F_{parallel} \cdot F_{perp}} \cdot \frac{p - p_0}{v(1-\varphi)a} \tag{VII.67 b}$$

the problem is reduced to the finding of a function which would fulfill Laplace's equation

$$\frac{\partial^2 \Pi}{\partial \zeta^2} + \frac{\partial^2 \Pi}{\partial \xi^2} + \frac{k}{\xi} \cdot \frac{\partial \Pi}{\partial \xi} = 0 \tag{VII.68}$$

and the boundary conditions

$$\frac{\partial \Pi(0,\zeta)}{\partial \xi} = 0 \tag{VII.69}$$

$$\frac{\partial \Pi(\xi,0)}{\partial \zeta} = 1 \tag{VII.69 a}$$

$$\lim_{\zeta \to \infty} \Pi(\xi,\zeta) = 0 \tag{VII.69 b}$$

$$\Pi(1,\zeta) = 0 \qquad \text{version 1} \tag{VII.69 c1}$$

$$\Pi(1,\zeta) = -\varepsilon \left[\frac{\partial \Pi(1,\zeta)}{\partial \xi}\right]^2 \qquad \text{version 2} \tag{VII.69 c2}$$

In the last equation, the authors introduced a nondimensional parameter ε, which is defined as

$$\varepsilon = \frac{Re}{N}(1-\varphi)F_\perp \sqrt{\frac{F_\perp}{F_\parallel}} \tag{VII.70}$$

where

$$Re = \frac{vA}{2a\mu} \tag{VII.70 a}$$

The Reynolds number defined with the equation VII.70a is related to the whole tow and is different from that defined with the equation VII.59, Re_d, which pertains to a filament and depends on the location in space.

Upon finding the function $\Pi(\xi,\zeta)$ and using equations VII.63 and VII.59, one may describe the flow conditions by calculating the field of flow parameters $p(x,z), u_x(x,z), u_z(x,z)$, as well as calculate the streamlines in relation to the system moving with the tow, or in relation to the spinnerette. Using nondimensional variables, the equations of the streamlines for both systems have the form

$$\tilde{q} = \int (k+1)\xi^k \left(\frac{\partial \Pi}{\partial \xi} d\zeta - \frac{\partial \Pi}{\partial \zeta} d\xi\right) = const. \tag{VII.71}$$

$$q = \xi^{k+1} + \tilde{q} = const. \qquad (VII.71\,a)$$

where the nondimensional functions q and $\tilde{q}$ are proportional to the flow intensity of the fluid as it flows between the surfaces located symmetrically to the axis.

Analytical solution of equation VII.68 for cylindrical tow (version VII.66a) has been found unsatisfactory, thus the equation must be solved numerically. The calculated results give good insight into the studied problem and are reproduced in figures VII.8 and VII.9.

A satisfactory analytical solution has been found by Szaniawski and Zachara[31] for a flat tow with a pressure differential on both sides of the tow. The nondimensional pressure drop is

$$\Pi(\xi,\zeta) = \frac{8}{\pi^2}\sum_{n=1}^{\infty}\frac{(-1)^n}{(2n-1)^2}\cdot\exp\left[-\frac{(2n-1)\pi\zeta}{2}\right]\cdot\cos\left[\frac{(2n-1)\pi\xi}{2}\right] \qquad (VII.72)$$

Pressure distribution is presented as

$$\tilde{\Pi}(\xi,\zeta) = \frac{\left(p - \frac{p_- + p_+}{2}\right)}{p_0} = \bar{\Pi}\cdot\xi + \Pi(\xi,\zeta) \qquad (VII.73)$$

where

$$\bar{\Pi} = \tilde{\Pi}(1,\zeta) = \frac{(p_+ - p_-)}{2p_0} \qquad (VII.73\,a)$$

For $\bar{\Pi} = 0$ is $\tilde{\Pi} = \Pi$.

The knowledge of the pressure field allows us to calculate from equation VII.61 the field of filtration velocity u_x, u_z. After integration of the equation of streamline $dx/u_x = dz/u_z$ one obtains the nondimensional function of stream

$$q(\xi,\zeta) = \frac{Q}{v(1-\varphi)a} = \xi + \bar{\Pi}\cdot\zeta + \tilde{q}(\xi,\zeta) \qquad (VII.74)$$

where function $\tilde{q}$ has the form

$$\tilde{q}(\xi,\zeta) = \frac{8}{\pi^2}\sum_{n=1}^{\infty}\frac{(-1)^n}{(2n-1)^2}\cdot\exp\left[-\frac{(2n-1)\pi\zeta}{2}\right]\cdot\sin\left[\frac{(2n-1)\pi\xi}{2}\right] \qquad (VII.75)$$

Q represents the volume of fluid flowing in the area between the spinnerette and a given streamline $q = const.$

Some additional equations connected to the problem are: Pressure on the surface of the spinnerette at the point $\xi = \zeta = 0$

$$\tilde{\Pi}(0,0) = \Pi(0,0) = -\frac{8\cdot G}{\pi^2} = -0.7424... \qquad (VII.76)$$

where G represents the constant of Catalan.

The coordinate ξ on the spinnerette where the pressure is at a minimum $\tilde{\Pi}(\xi_2, 0) = \tilde{\Pi}_{min.}$ and the streamline $q = 0$ looses contact with the spinnerette surface is defined as

$$\xi = \frac{4}{\pi} \arctan\left[\exp\left(-\bar{\Pi}\frac{\pi}{2}\right)\right] - 1 \qquad \text{(VII.77)}$$

The coordinate of the point where the border streamline would be tangent to the surface of the tow and the stream function reaches a minimum $q(-1, \zeta_1) = q_{min.} < 0$ is given as

$$\zeta_1 = \frac{2}{\pi} \cdot \ln\left[\frac{\exp\left(\frac{\pi}{2}\bar{\Pi}\right) + 1}{\exp\left(\frac{\pi}{2}\bar{\Pi}\right) - 1}\right] = \frac{2}{\pi} \ln\left[\coth\left(\pi\bar{\Pi}\right)\right] \qquad \text{(VII.78)}$$

The results of the pressure and streamline calculations are presented in figure VII.10 and VII.11.

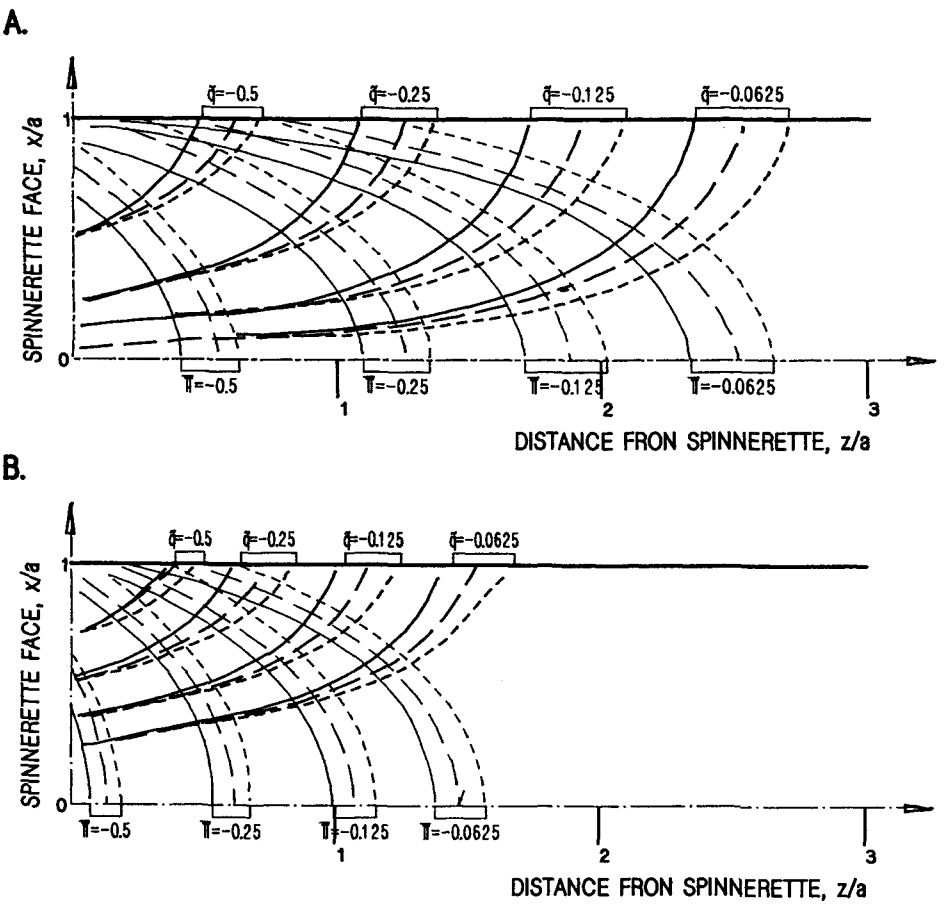

Figure VII.8: *Cylindrical tow. Isobars (Π = const.) and streamlines ($\tilde{q}$ = const.); A – flat tow, B – cylindrical tow. Full drawn line $\varepsilon = 0$, dashed line $\varepsilon = 0.1$, short dashed line $\varepsilon = 0.2$. After A. Szaniawski and A. Zachara.*[30]

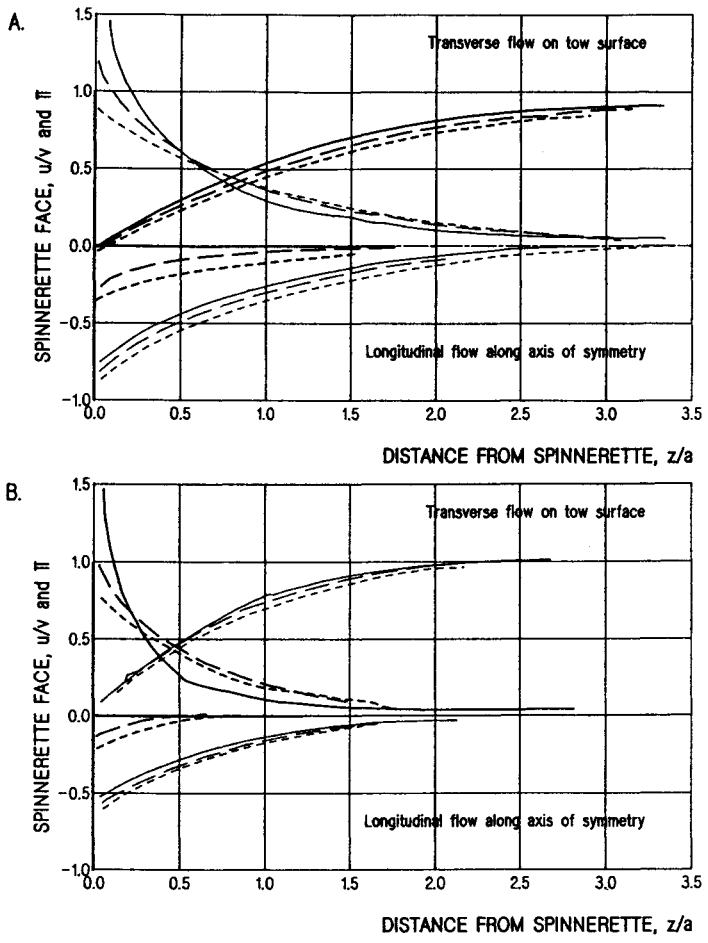

Figure VII.9: *Cylindrical tow. Fluid velocities in tow: Top of graph: transverse flow, (u_x/v), on the surface, $(x = a)$, and longitudinal flow, (u_z/v), on the axis of symmetry, $(x = 0)$. Bottom of graph: pressure drop on the surface and on the axis of symmetry. Full drawn line $\varepsilon = 0$, dashed line $\varepsilon = 0.1$, dotted line $\varepsilon = 0.2$. A – flat tow, B – cylindrical tow. After A. Szaniawski and A. Zachara.*[30]

The derivations proposed by Szaniawski and Zachara[30,31] and quoted above may be useful also for solution of similar problems encountered with the flow of quench air in the fiber formation from melt or in the dry formation from solution.

The extrusion temperature has a strong and multilateral influence on the process performance and on the resulting product. It, together with concentration, determines the solution viscosity, coefficient of diffusivity, and interaction with the nonsolvent used. Often, fiber density increases with the increasing temperature of the processing.[39] High density with strong skin effect, also depending on temperature and diffusivity, may cause difficulties with subsequent drying of the fibers.

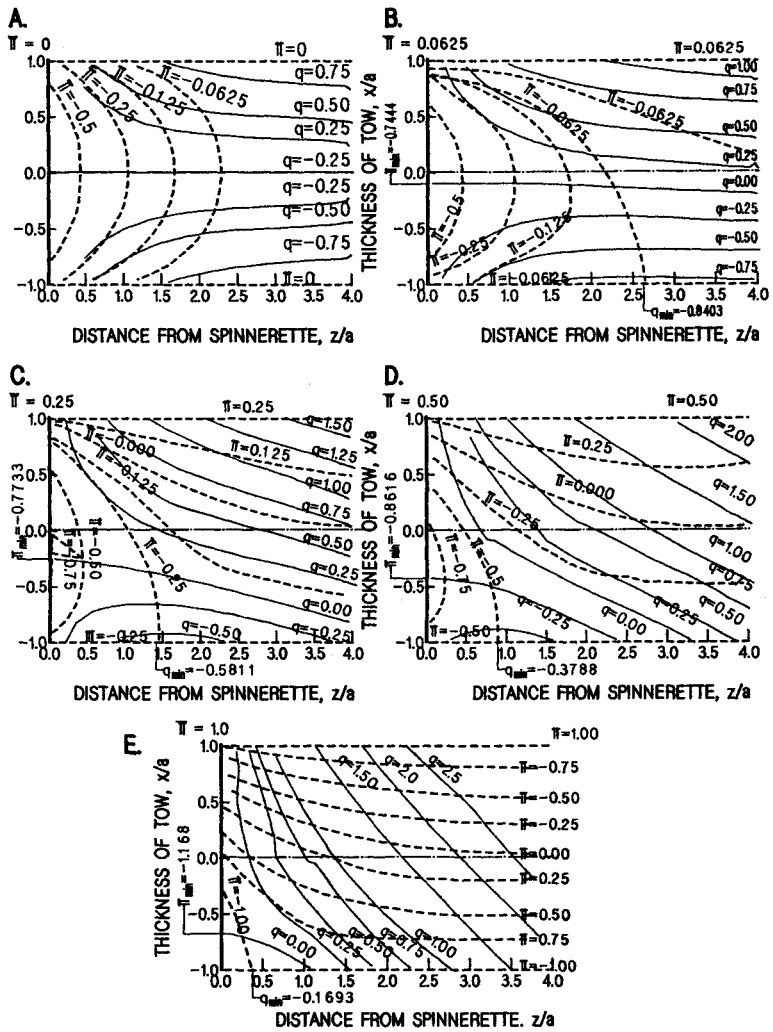

Figure VII.10: *Flat tow. Isobars, ($\tilde{\Pi}$ = const.), dashed lines, and streamlines (q = const.) full drawn lines at different values of pressure differential* Π. *After A. Szaniawski and A. Zachara.*[31]

Thus, a certain balance and compromise must be established between all of the advantages and disadvantages of high temperature extrusion.

Quite naturally, temperature of the coagulation bath cannot deviate much from the extrusion temperature, and since lacing up of the fiber tow is, more or less, a hand operation, it may be difficult to hold the bath temperature higher than what is possible for hand immersion and gloved manipulation (up to $60°C$).[14]

Both for the environment's and economy's sake, the solvent used in the formation must be regenerated. The same is true for the nonsolvent if it happens to be other than water. If it is water, it must be purified prior to discharge back into environment. The expenses connected with the recovery are often held against the

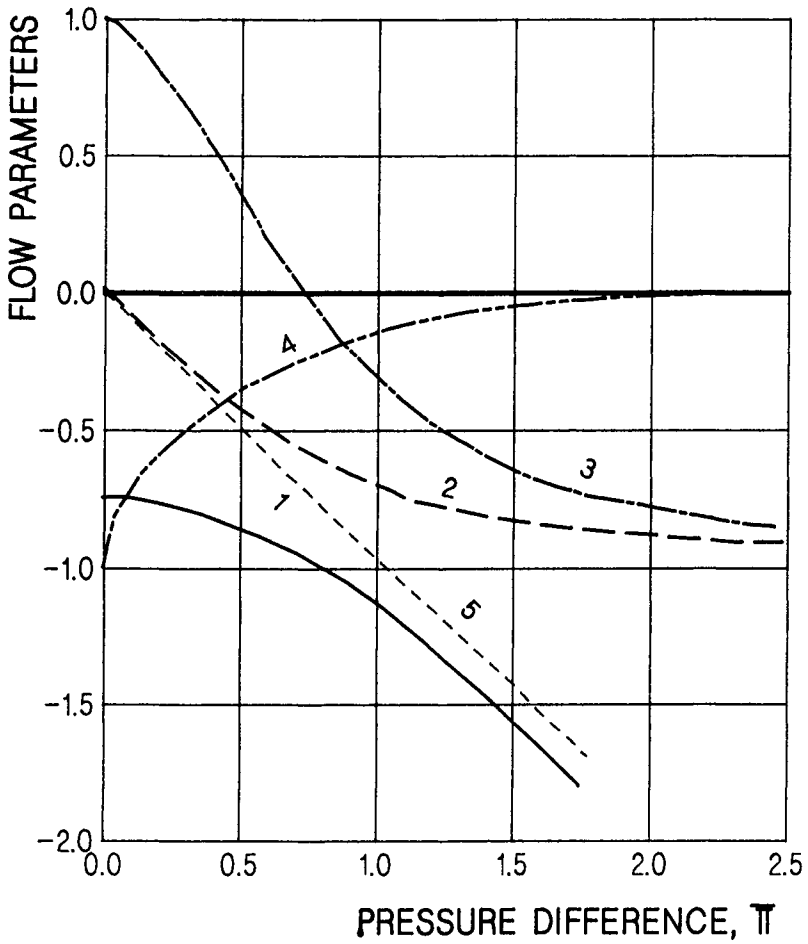

Figure VII.11: *Influence of the pressure differential on two sides of a flat tow on flow parameters. 1.* $\tilde{\Pi}_{min.} = \tilde{\Pi}(\xi_0, 0)$, *2.* $\xi_2, \tilde{\Pi}(\xi_2, 0) = \tilde{\Pi}_{min.}$; *3.* $\xi_1, \tilde{\Pi}(\xi_1, 0) = \tilde{\Pi}_{min.}$; *4.* $q_{min.} = q(-1, \xi_1)$; *5.* $-\tilde{\Pi}$. *After A. Szaniawski and A. Zachara.*[31]

viability of wet formation. In reality this notion may be or may be not true; it depends on the compounds.

If water is the nonsolvent and if the boiling point of the solvent is higher than water then water must be distilled off. This is energetically expensive, as water has a very high heat of evaporation. If the solvent is more volatile than water then the distillation expenses may be reasonable, and the rest depends on the expenses of water purification. The bulk of recovery is concentrated around distillations. Adsorption methods may be necessary to a small extent for the purification of the plant atmosphere.

Different approaches are necessary in the majority of processes involving chemical reactions during formation. Recovery of the solvent and chemicals must be treated on a case by case basis, as required by the chemistry involved.

VII.4 Dry Formation

Dry formation of fiber resembles formation from the melt much more than the wet formation does. The concentration of solutions (dopes) used ranges from some three per cent to a gel or plasticized melt. The processes involving the highest concentrations are referred to as gel spinning or plasticized melt spinning rather than a formation from solution. In the case of gel spinning, the molecular mass is usually very high ($M \geq 1000000$), so in such cases the dope concentrations are not necessarily exceedingly high; they may be within some forty to sixty percent range, or even less.[25–27]

The concentration of spinning solution is, as always, an issue of the process economy. In the technical sense, however, the fiber properties obtained from dopes of higher concentration are better.[2] Better fiber properties are also obtained from a polymer of higher molecular mass, which leads to a higher solution viscosity too. It has been found[41] that tenacity of fibers decreases if the extrusion is conducted above the point of fracture, which in some cases may occur at relatively low shear rates, occasionally as low as $100s^{-1}$; an increase of temperature does not always help. This is a good reason to keep the concentration low. The same authors[41] claim that at substantially higher shear rates fracturing may cease and fiber tenacity goes up again. Similar effects have been found also in the case of melts of block copolymers.[42] Nevertheless, there is also a voice claiming that extrusion with fracturing may lead to higher fiber tenacities, provided that the fibers are extensively drawn at high temperature.[46]

There is no doubt that in some cases the low concentration of dopes used is a matter of tradition, and in dry formation the tradition is quite old, reaching the time when the knowledge of physical chemistry of solutions and their rheology was much more limited than it is today. On other occasions, it may be a compromise between the most convenient solvent, viscosity of solution, and feasible temperature of extrusion.

All of the polymers currently processed from solution, except for the high performance polymers, have low thermal resistance, and this is the main reason for solution processing. In dry formation, contrary to the wet processes, the extruded filament enters into the air atmosphere, which may aggravate the tendency to decomposition. Even if the drying process is carried out in the atmosphere of an inert gas, it is rather difficult to keep the air completely out if the cost of equipment is not to be excessively high.

Mixed solvents may be considered and their application in dry processes may be easier than in wet ones. Again, tradition seems to be responsible for the fact that we do not see them applied yet. Improper differences in the rate of evaporation of the various components of the mixture may have some adverse effects on the resulting fiber properties or on their appearance, e.g. matted surface, etc.

Formation of fibers from solutions undergoing phase separation may be considered as a border case with formation from the melt. According to Zwick[43], solutions of three to twenty percent concentration may be spinnable at velocities

of 100 to $1000 m/min$. The polymer-solvent system must be chosen so that after leaving the spinnerette, the solution undergoes a phase separation into a pure polymer or its highly concentrated gel and a pure solvent phase. The expelled solvent may be dried or eventually washed away before the fiber reaches the take-up device. Solvents useful for such a method of formation must satisfy one of the following conditions:

- The temperature of extrusion must be closely above the theta- temperature, but the temperature in the drying cell is lower than theta-temperature.
- The polymer is soluble only in the liquid solvent but the solvent solidifies at temperatures a little below the temperature of extrusion.
- The solvent consists of more than one component, while none of the components alone is able to dissolve the polymer. At the same time either miscibility of the solvent components must be highly temperature dependent or one component is highly volatile and evaporates quickly after leaving the spinnerette.

Preparation of solutions for dry formation is usually carried out in conventional equipment used for the purpose in polymer processing. Dissolution of polymers is slow, often it takes around three hours. Consequently it is performed in batches, with several groups of equipment in parallel put in-line with the entire operation. Additionally, the phenomena of *aging* or *ripening* of polymer solutions need to be taken into account. Depending on the polymer-solvent system in question, on concentration, and on temperature used, it may be good to subject the solution to a longer *ripening*, but a really long storage may be difficult to incorporate into a continuous, in- line operation. When concentrated solutions are used, continuous dissolution and transport may be easier to achieve, *e.g.* by coupling a mixer and screw extruder in line.[44]

The polymer solution for dry formation must be filtered. Commonly, there are two stages of filtration. The first stage is placed immediately after dissolution to remove accidental mechanical impurities and particles of undissolved polymer (gel), etc.; the second stage filter is located just before the solution enters the spinnerette, as in melt formation. The filtering assemblies are similar to the one used for melt processes. The first stage is solely for the purification of the solution, the second stage serves mainly for the rheological and morphological purposes.

The spinnerettes for dry formation are designed according to the same principles as for the other processes. Naturally, the lower viscosity in many cases requires thinner plates due to lower extrusion pressures. The lower viscosity of solutions allows for the formation of very fine fibers, without applying excessively large extrusion pressures. After drying, the filaments become even thinner due to the loss of solvent.

Extrusion is commonly carried in a downwards configuration into a vertical drying chamber (*cell*). Upwards extrusion is used only occasionally due to a potential of dripping of low viscosity solutions. Similar problems may be associated with large diameter of filaments.

As a drying medium, the most often used is air, in rare cases an inert gas. The equipment for drying the fibers is similar to an air quench with a counter-current air flow, except that the air (or other gas) containing solvent vapors must be carefully and quantitatively withdrawn and led to the solvent recovery system. The air stream in formation from the melt serves only for cooling and is, if not blown across the fiber bundle, usually led co-currently with the filaments. In dry formation, the air is primarily a drying medium. In some processes, the solution is also cooled, but the heat balance between the solution cooling and supplying the necessary heat of evaporation usually leads to the need of heated air. According to the material and heat balance, the air is blown either in co- or counter-current.[2] There are processes known with a combination of co- and counter-current air flow.[45] In such "mixed" flow cases, the portion of filaments close to the spinnerette receives counter-current flow, while the filament portion close to the receiving is in co-current configuration. The mixed configuration requires that there is one point of air injection point and two points of air withdrawal. Depending on the heat balance, the walls of the drying chamber may need to be heated, though in all cases the wall temperature should be carefully controlled.

The volume of air and its temperature must be chosen so as to assure the fullest possible removal of the solvent. The evaporation of solvent may not be permitted to proceed too rapidly for the sake of fiber structure. Concentration of the solvent vapors in the withdrawn air must be kept below explosivity limits, which often amounts to less than 2 or 3% by volume.[2] The aerodynamic drag forces acting on filaments are also to be carefully observed; the rules are here the same as in the formation from melt.

The profile of filament temperature during drying changes in a characteristic pattern, which is similar in most of the dry processes. Shortly after leaving the spinnerette, the filament temperature drops, and this drop may be large. This is a consequence of rapid solvent evaporation. The temperature drop takes place despite the fact that the temperature of the drying air is at this point usually substantially higher than the extrusion temperature. The magnitude of the temperature drop is, as signaled earlier, related to the magnitude of heat of evaporation of the solvent used, of the local heating intensity, and of the resulting rate of evaporation. In the subsequent segments of the drying cell, the temperature of filaments rises and the changes take place at a more moderate rates. The temperature of the filaments should not be allowed to drop too low, as water from the air may condense, or even freeze. Entirely water-free air is difficult and expensive to maintain in the process.

A rapid loss of solvent takes place primarily on the fiber surface, which may cause an increase in the skin-core effect in the fiber structure, and this effect is rarely wanted, though in some cases it may be considered a "special effect". For this reason, the drying process should be carried out possibly gently. To provide for gentle drying conditions, the filaments are given a long drying time by being provided long drying chimneys (cells), on the order of three to six meters. The take-up velocities generally range between $100m/min$ and $900m/min$.[2,24]

The spin stretch in dry formation is normally very low, only of the order of two to four times. The low strength of the extruded polymer solution rarely permits higher extensions. Higher fiber velocities cause the obtaining of a higher stretch to be more difficult.

There were not many attempts to solve the problems of dry formation theoretically, at least not many appeared in publications. One of the earlier attempts was by R. G. Griskey and S. Y. Fok.[48–50] These authors attempted to calculate the changes of the solvent contents during a dry formation starting with the equation

$$\frac{\partial^2 c}{\partial \phi^2} + \frac{1}{\phi}\frac{\partial c}{\partial \phi} - \frac{Q}{\pi D \rho}\frac{\partial c_z}{\partial z} \tag{VII.79}$$

with the designations: c is concentration of solvent in the radial direction, c_z is concentration of solvent along the fiber axis (z), ϕ is the nondimensional radial position r/R, with R being the filament radius at any given z, Q is volumetric solution flow rate, $Q = R^2 v_z \pi \rho$, v_z is velocity component in the z direction; velocity components in the radial v_r, and angular, v_θ, directions are assumed equal zero; D is diffusivity, and ρ is density of the solution.

As boundary conditions were taken: at $z = 0$ $c = c_0$ at all r; c is finite at all $r = 0$ and all z; $c_z = f(z)$ at $z = z$ and $r = R$.

Equation VII.77 can be solved only numerically. For the solution Griskey and Fok used the Gregory-Newton formula[51]

$$\begin{aligned}(c_z)^n_{m+1}\left[\frac{1}{(\Delta\phi)^2} + \frac{1}{m(\Delta\phi)^2}\right] \quad &+ \quad (c_z)^n_m\left[-\frac{2}{\Delta\phi} - \frac{1}{m(\Delta\phi)^2} + \frac{Q}{\pi\rho D \Delta z}\right] + \\ +(c_z)^n_{m-1}\left[\frac{1}{(\Delta\phi)^2}\right] \quad &- \quad (c_z)^{n+1}_m\left[\frac{1}{\Delta Z}\frac{Q}{\pi\rho D}\right] = 0\end{aligned} \tag{VII.80}$$

where $(c_z)^n_m = c_z(\phi_0 = m\phi, z_0 + nz)$ is concentration of the solvent at the n^{th} position along z-axis and m^{th} position along the radius. The flow rate Q was determined experimentally as a function of z alongside of the average concentrations. The diffusivity was takes as constant. At $z = 0$, the concentrations inside of the filament are known and equal, however, the concentrations at the two points outside the filament need to be known too. The authors computed them from equation VII.79 and from the following equation.

$$(c_c)^n_0\left[\frac{q}{\pi\rho\Delta z} - \frac{4}{(\Delta\phi)^2}\right] + \frac{4}{(\Delta\Phi)^2}\cdot(c_z)^n_1 - \frac{Q}{\pi\rho D\Delta z}\cdot(c_z)^{n+1}_0 = 0 \tag{VII.81}$$

Equation VII.81 holds at $\phi = 0$, it is $m = 0$ and $\partial c/\partial r = 0$ and gives only (c_z) at $m + 1$ position. The value of the concentration at position $m + 2$ was calculated from the average concentration using Simpson's rule.

The results, experimental average and the concentrations calculated for $R/2$, by Griskey and Fok are reproduced in figure VII.12.

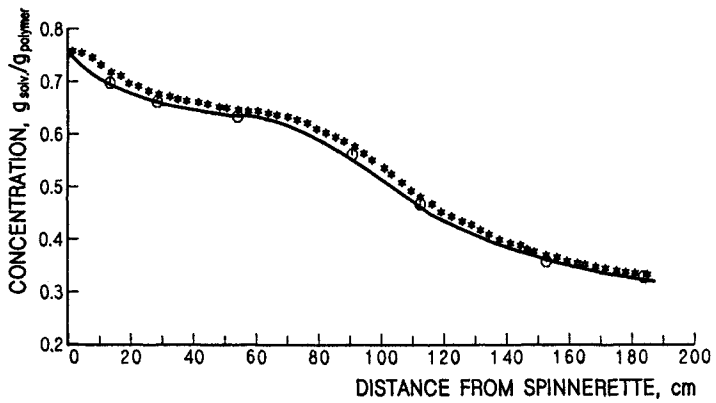

Figure VII.12: *Concentration of solvent in polymer during a dry fiber formation from poly(methyl methacrylate) in benzene. Line and circles give the experimental data average per radius, star points give the results calculated for the half of the radius. After Fok and Griskey*[49]

The experimental line presented in figure VII.12 goes though a *quasi* plateau after the initial rapid drop of solvent concentration and before a second rapid concentration decrease. Such behavior is rather usual in commercial dry formation operations and does not have any plausible explanation as of yet. The agreement between the calculated and empirical results is relatively good, and it is likely that the results might be substantially improved by more dense calculation, more points along the radius and more points along the fiber axis. It needs to be taken into account that the data for half radius do not represent the average.

A somewhat more refined solution is offered by Barzinsky and co- workers.[52] These authors consider a set of five equations. The first of these equations represents the diffusion of a solvent in the filament.

$$v\frac{\partial c}{\partial z} = D\left(\frac{1}{r}\frac{\partial c}{\partial r} + \frac{\partial^2 c}{\partial r^2}\right) + \left(\frac{\partial c}{\partial r} \times \frac{\partial D}{\partial r}\right) \qquad \text{(VII.82)}$$

Here v stands for axial filament velocity, c stands for solvent concentration in the filament, z is position along the filament axis in relation to the maximum in the die swell, r is position along the fiber radius, and D stands for diffusivity. It is worth stressing that this solution considers changes of diffusivity.

The differential energy balance is described as

$$\rho C_p v\frac{\partial T}{\partial z} = \lambda\left(\frac{1}{r}\frac{\partial T}{\partial r} + \frac{\partial^2}{\partial r^2}\right) + \left(\frac{\partial T}{\partial r} \times \frac{\partial \lambda}{\partial r}\right) \qquad \text{(VII.83)}$$

where ρ is density of the filament, T is temperature in the filament, λ is thermal conductivity, and C_p represents specific heat. The second bracketed term in equation VII.83 describes the variation of thermal conductivity.

The total material balance is given as

$$\frac{dQ}{dz} = 2\pi R M_s \alpha_m (c^* - c_a) \qquad \text{(VII.84)}$$

and the symbols here mean: Q is flow rate, R is filament radius, M_s is molecular mass of solvent, α_m is coefficient of mass transfer between the filament interface and air, c^* is the concentration of solvent in the vapor phase and in equilibrium with the liquid at the filament interface, and c_a describes the solvent concentration in the air.

The filament momentum balance is represented by

$$dF = d(\rho A v^2) + F_D dz - F_g dz - dF_{surf} \tag{VII.85}$$

where F is tension acting on the fiber, F_D is aerodynamic drag force, F_g is force of gravity, F_{surf} is surface tension force, A is the cross sectional area of the filament, and $\rho A v^2$ represents the rate of transport of momentum.

The constitutive equation was taken to be the same as for a Newtonian fluid

$$\sigma = \zeta_T \frac{dv}{dz} \tag{VII.86}$$

with the designation of σ as stress, and ζ_T as elongational viscosity. From equation VII.86 results that

$$F = \bar{\eta_z} A \frac{dv}{dz} \tag{VII.87}$$

where $\bar{\eta_T}$ represents the integrated average elongational viscosity across the filament.

The boundary conditions are taken as:

- At $z = 0$ the values of r, c, T, and Q are assumed as equal to the values of the solution being extruded.
- At the take up point, the filament velocity is assumed to be equal to the circumferential velocity of the roller.
- At $r = 0$, and all z is assumed axisymmetric nature and circular cross section of the filament what means that $\partial c/\partial r = \partial T/\partial r = 0$.
- At $r = R$ at any z: $-\rho D \partial c/\partial r = \alpha_m M_s (c^* - c_a)$, and $-\alpha \partial T/\partial r = \alpha(T_s - T_a) + H M_s \alpha_m (c^* - c_a)$; and α is the heat transfer coefficient between the filament interface and the surrounding gas, H is the enthalpy of solvent evaporation, and α_m is mass transfer coefficient.

The set of equations needs to be solved numerically. Tension at the take-up point can rarely be measured, and thus may need to be assumed. Calculations according to this system show that the most dramatic changes in the process take place during the first ten millimeters from the spinnerette face. This applies to filament radius, temperature, and velocity. The filament velocity becomes constant (plug flow), while the diameter changes only due to the solvent losses taking place. The drastic changes taking place during the first instant after leaving the spinnerette are attributed to the rapid increase of viscosity due to quick solvent evaporation and the accompanying temperature drop.

The confrontation of the calculated values with the experimental data has been moderately successful. Filament radius decreased even more abruptly than predicted. Incidentally, a similar deviation is seen in the calculations by Griskey and Fok. Velocity, naturally, changes in line with the diameter changes. The deviations of the theory from the experimental data seem to be smaller here than in the corresponding theoretical solutions for fiber formation from the melt published thus far. One may speculate that the smaller deviations result from the lower viscosities and consequently smaller discrepancies between the use of the constitutional rheology equation rather than creep, which gives substantially better results for formation from the melt.

It may be important to mention that there is an analogy between the heat transfer coefficient, α, and the mass transfer coefficient in diffusion, α_m.[53] Based on this analogy, it is possible to calculate the mass transfer coefficient, α_m, from the heat transfer coefficient, which may be easier to determine.[54,55] An apparatus for the measurements has been described by T. Mitzushina and M. Nakajima.[54]

$$\ln\left(1+\frac{c_{s,0}-c_{s,\infty}}{1-c_{s,0}}\right)=\frac{\alpha}{\alpha_m C_{ps}}\left[1+\frac{\xi C_{ps}(T_\infty-T_0)}{H_{sT}}\right] \tag{VII.88}$$

where $c_{s,0}$ and $c_{s,\infty}$ are the mole fractions of the solvent in the air before and after the solvent contact, respectively; α is heat transfer coefficient; α_m is mass transfer coefficient; T_∞ and T_0 are wet bulb and dry bulb temperature, respectively, C_{ps} is heat capacity of the solvent vapor; H_{sT} is heat of evaporation of the solvent at the dry bulb temperature; ξ is a correction coefficient which depends on the apparatus used and usually amounts to little more than one.[54]

The heat transfer coefficient may be calculated from the equations developed by Ohzawa and Nagano.[56] For the heat transfer related to a situation where the entrained convection is superimposed on the forced parallel convection, the proposed equation is

$$\alpha=\frac{0.886\lambda^*}{\sqrt{A}}\left[0.35+0.146\left(\frac{1.129\sqrt{A}U_p}{\nu}+R\right)^{0.5}\right] \tag{VII.89}$$

where

$$R=\left[1.076\left(\frac{\sqrt{A}v_z}{\nu}\right)^{0.36}-0.685\right]^2 \tag{VII.89 a}$$

where α is heat transfer coefficient, λ^* is heat conductivity at the interface, A is filament cross section area, U_p is the velocity of forced air (gas) parallel to the filament, ν is kinematic viscosity in the interface, v_z filament velocity in the axial direction.

For the case of the entrained convection and superimposed perpendicular convection the equation is

$$\alpha=\frac{0.886\lambda^*}{\sqrt{A}}\left[0.35+0.50\left(\frac{1.129\sqrt{A}U_c}{\nu}+R\right)^{0.5}\right] \tag{VII.90}$$

where

$$R = \left[0.313 \left(\frac{\sqrt{A} v_z}{\nu} \right)^{0.36} - 0.20 \right]^2 \qquad (VII.90\,a)$$

Here U_c means air velocity in cross flow.*

The spun fibers in the dry processes are mostly highly crystalline and of low crystalline orientation.[2] Normally, it is difficult to remove the solvent completely from the spun fibers. When fibers are subjected to a neck drawing, it is performed in a separate operation. For this reason, a substantial secondary crystallization, enhanced by the presence of the residual solvent, takes place after the extrusion and drying and before drawing. These processes depend, naturally, on the crystallization propensity of the polymer in question; on the other hand, there are few polymers which crystallize poorly in the presence of solvent, if they crystallize at all.

When fibers have a strong skin-core structure, which may be considered as a structural inhomogeneity, highly inhomogeneous drawn fibers, with a large volume of cracks and voids may be formed. If there is any stronger orientation in spun fibers, then most probably it is limited to the skin, which has coagulated earlier and was exposed to the tension longer.[53] Such a structural inhomogeneity may cause further deepening of this effect in the subsequent drawing operation. To remove residual solvent from spun fibers, washing – extraction may be used,[2] though this is usually done when the fibers are not subjected to neck drawing operation.

The large amounts of solvents used in the dry fiber formation must be recovered to prevent pollution of the environment. Also, the solvent must be removed from the air not to create an explosion or fire hazards. At the same time the recovery is needed to enhance the process economy. The content of solvent in the drying gas is normally very low, condensation alone is normally entirely insufficient or outright inappropriate and therfore it is rarely used. To remove the solvent from gas (air), the mixture is separated through adsorption of the solvent on activated carbon, or sometimes on silica gel. It is rather expensive process, both in investment and maintenance of the carbon beds.

By subjecting the spun fibers to neck drawing, their tensile properties may be improved. However, the high degree of crystallinity present in dry formed fibers, the voids in the internal structure, as well as the non-uniformities of the fiber cross sections due to the skin roughness make it difficult to perform a drawing operation, particularly a more extensive drawing and at commercially interesting speeds. Naturally, the drawing operations, if performed, are carried out at elevated temperatures, similar to the analogous treatment of fibers formed from melt. If a high degree of porosity, is present in the solution formed fibers, the drawing operations become additionally troublesome. In very difficult cases, one may resort to swelling of the fibers just prior to, or during, neck drawing. Hot water,[54] or glycerol bath,[55,56] or water steam[57,58] may be used as the swelling medium.

*Data on some of the physical properties and their functions of temperature are given in the Appendix.

The liquids or vapors used must be able to swell the polymer, but any stronger dissolving power is to be avoided. The most ideal are liquids or vapors then which are not able to swell crystalline and oriented polymer structures. Preferably, they should affect only amorphous portions of the structure. In such ideal cases, a large portion of the swelling agent is expelled from the fiber structure in the necking. If the swelling agent is strong, then it must be removed immediately after drawing; otherwise the fibers would shrink back to *undo* the gains obtained in drawing.

Like in the other methods of formation, dry formed fibers may be subjected to post treatments. Sometimes a post treatment is simply necessary. The most frequently applied means are: washing and annealing. The purpose of washing is mainly to remove residues of solvents and/or processing finishes remaining in the fibers, and sometimes quite stubbornly. Annealing is used primarily for general stabilization of the fiber structure, though it may also help in removal of the unnecessary residuals. A successful structure stabilization through annealing is possible only when all solvents or swelling agents are removed from the fiber.

Heat treatment of some polymers may result in some degree of cross linking, even without the use of cross linking agents. In some fibers, a small amount of cross linking introduced into already formed fibers may have a highly beneficial influence on the fiber properties. Such fiber modifications are occasionally taken advantage of.[2]

VII.5 References

1. *Ger. Pat.* No. 38,368 (1885).
2. W. Frey and A. Sippel in *Fasern aus synthetischen Polymeren*, ed. by R. Hill, Berliner Union Verlag, Stuttgart, 1956, pp. 407 - 426.
3. P. H. Geil: *Polymer Single Crystals*, Interscience Publ., New York, 1963, pp. 86, 382.
4. D. C. Basset, A. Keller, and S. Nitsuhashi, *J. Polymer Sci.*, **A1 (1963)**, 763.
5. H. D. Keith and E. J. Padden, Jr., *J. Appl. Phys.*, **34 (1963)**, 2409.
6. H. A. Lanceley and A. Sharples, *Makromol. Chem.*, **94 (1966)**, 30.
7. L. Mandelkern: *Growth and Perfection of Crystals*, John Wiley and Sons, New York, 1958, p. 490.
8. J. G. Fatou, E. Riande, and R. Garcia Valdecasas, *J. Polymer Sci., (Phys.)*, **13 (1975)**, 2103.
9. A. B. Dessai and G. L. Wilkes, *J. Polymer Sci., Symposia*, **No. 46 (1974)**, 291.
10. R. M. Secor, *A. I. Ch. E., J.*, **11 (1965)**, 482.
11. A. T. Serkov, G. J. Kudryavcev, V. S. Klimenkov, L. A. Serkova, and Yu. P. Kozhevnikov, *Faserforsch. Textitech.*, **20 (1969)**, 125.
12. J. J. Hermans, *J. Colloid Sci.*, **2 (1947)**, 387.
13. J. R. Booth, *A. C. S. Polymer Preprints*, **7 (1966)**, 759.
14. J. M. Preston in *Fasern aus synthetischen Polymeren*, e. by R. Hill, Berline Union Verlag, Stuttgart, 1956, pp. 389 - 405.

15. V. Gröbe and R. Gieske, *Faserforsch. Textitech.*, **20 (1969)**, 30.
16. V. Gröbe and H. J. Gensrich, *Faserforsch. Textiltech.*, **20 (1969)**, 118, 425.
17. M. C. Botty, C. D. Felton, and R. E. Anderson, *Text. Res. J.*, **30 (1960)**, 959.
18. P. H. Hermans: *Physics and Chemistry of Cellulose Fibers*, Elsevier Publ., New York, 1949.
19. H. Fujita, *J. Chem. Phys.*, **21 (1953)**, 700.
20. Sin Yuen Fok and R. G. Griskey, *J. Appl. Polymer Sci.*, **11 (1967)**, 2417.
21. J. R. Griffin and D. R. Coghanowr, *A. I. Ch. E., J.*, **11 (1965)**, 133, 1521, 246.
22. A. Rende, *J. Appl. Polymer Sci.*, **16 (1972)**, 585.
23. H. Gröber, S, Erk, and V. Girgull: *Die Gruntgesetze der Wärme- übertragung*, Springer Verlag, Berlin - Göttingen - Heidelberg, 1955.
24. T. Rosner and H. Wójcikiewicz: *Włókna syntetyczne* (Synthetic Fibers), Wydawnictwo Naukowo-Techniczne, Warszawa, 1969.
25. Swiss Pat. No. 314,609.
26. Brit. Pat. No. 1,021,972.
27. U. S. Pat. No. 2,822,237.
28. D. Machin and C. E. Rogers, *Makromol. Chem.*, **155 (1972**, 269.
29. R. M. Griffith, *Ind. Eng. Chem.*, **3 (1964)**, 245.
30. A. Szaniawski and A. Zachara, *Polimery* (in Polish), **19 (1974)**, 143.
31. A. Szaniawski and A. Zachara, *Polimery* (in Polish), **20 (1975)**, 87.
32. P. J. Flory: *Principles of Polymer Chemistry*, Cornell University Press, Ithaca, 1967, p. 548 ff.
33. H. Fujita, *Fortschr. Hochpolymer. - Forsch.*, **3 (1961)**, 1.
34. R. M. Vasenin, *Vysokomol. Soyedin.*, **2 (1960)**, 851. 34
35. T. G. Fox, *Bull. Am. Phys. Soc.*, **1 (1956)**, 121.
36. F. N. Kelly and F. Bueche, *J. Polymer Sci.*, **50 (1961)**, 549.
37. E. Jenckel and R. Heusch, *Kolloid-Z.*, **13 (1953)**, 89. 37
38. G. Kanig, *Kolloid-Z.*, **190 (1963)**, 1.
39. U. S. Pat. No. 2,451,420.
40. G. A. Danilin, *Khim. Vol'okna*, **(1981)**, 22.
41. J. H. Southern and R. L. Ballman, *Text. Res. J.*, **53 (1983)**,230.
42. Z. K. Walczak, *previously unpublished results*, 1982.
43. M. M. Zwick, *A.C.S. Polymer Preprints*, **7 (1966)**, 814; *Appl. Polymer Symp.)*, **No. 6 (1967)**, 109.
44. E. Masłowski, *Polimery*, (in Polish) **9 (1966)**, 429.
45. *Netherl. Pat.* No.66,15,961.
46. S. Gogolewski, A. J. Pennings, *J. Appl. Polymer Sci.*, **28 (1983)**, 1045.
47. Ye. Alyeva, Yu. P. Kozhevnikov, V. A. Medvedev, and A. T. Serkov, *Khim. Vol'okna*, **(1990)**, 6.
48. S. Y. Fok and R. G. Griskey, *Appl. Sci. Res.*, **16 (1966)**, 141.
49. S. Y. Fok and R. G. Griskey, *J. Appl. Polymer Sci.*, **11 (1967)**, 2417.

50. R. G. Griskey and S. Y. Fok, *Fundamental Consideration of Dry Spinning*, paper presented at A. I. Ch. E. Meeting, Atlanta, February, 1970.

51. K. S. Kunz: *Numerical Analysis*, McGraw - Hill, New York, 1957, p. 275.

52. I. Barzinsky, A. G. Williams, and H. L. LaNieve, *Polymer Eng. Sci.*, **15 (1975)**, 834.

53. R. B. Bird, W. E. Stewart, and E. N. Lightfoot: *Transport Phenomena*, John Wiley and Sons, New York, 1960, p. 667.

54. T. Mitzushina and M. Nakajima, *Kagaku Kikai*, **15 (1951)**, 30.

55. Y. Ohzawa, Y. Nagano, and Y. Matsuo, *J. Appl. Polymer Sci.*, **13 (1969)**, 257.

56. Y. Ohzawa, and Y. Nagano, *J. Appl. Polymer Sci.*, **14 (1970)**, 1879.

57. V. Elsasser, *Kolloid-Z.*, **113 (1949)**, 37.

58. *French Pat.* No. 913,927.

59. H. Rein, *Angew. Chem.*, **60A (1948)**, 159.

60. P. A. Koch, *Textil Rundschau*, **5 (1950)**, 414.

61. *U. S. Pat.*, No. 2,418,507.

62. *U. S. Pat.*, No. 2,420,565.

63. F. Fushimi, T. Watanabe, T. Hiyoshi, Y. Yamashita, and T. Osakai, *J. Appl. Polymer Sci.*, **59 (1996)**, 15.

VIII PROCESS VARIABLES

In fiber formation processes, the variables responsible for process control are not as obvious as is the case of many of chemical processes. On the other hand, the large number and the complicated character of variables is responsible for the complexity of the entire process.

Normally, in chemical technologies we have to deal with three different types of variables:[1]

- Theoretical variables
- Technological variables
- Operational variables

Theoretical variables deal with the most important properties of the raw material and the necessary changes the material must undergo to be transformed into a fiber.

Technological variables take into account the theoretical variables and the requirements imposed by the particular process used. The *"what we are doing"* is more than often influenced by the *"how we are doing it"*. Polymer processing may be bound by this principle to more than an average degree.

Operational variables result from the superposition and interaction of the technological variables with the equipment used. Since there is almost an infinite number of solutions in the equipment design, a limitless pattern of knobs and switches, operational variables cannot be generalized, and in consequence, they will not be discussed further here.

The quantitative justifications, if available, were given for the most part in the previous chapters. The discussion of the process variables contained in this chapter is intended to introduce some organizational and systemic gradation of the different elements of the process. The large number of variables involved in fiber formation and their strong interrelationships seem to justify this kind of synthetic recapitulation.

The variables discussed here are related primarily to the "basic process", to fiber formation from the melt, as is the entire book. The small differences necessary to apply the system to the processes from solution are given in addition to the main concept. The possibility of such an organization of variables dictates that fiber formation ought to be considered as one process. Melt, dry, or wet processes are only variants of the "basic formation". In a similar way, the other, newer processes, like gel spinning and semi-melt spinning, may be considered as only variants of the basic principles.

VIII.1 Theoretical Variables

The process variable may be considered only with the understanding that the type of polymer, and possibly polymer-solvent, or polymer-solvent-nonsolvent system, as the case may be, is constant. With such an assumption, one may list the theoretical process variables as they are given below in table VIII.1.[1] The list of variables is followed by a list of the most important effects the variables have on the fiber structure, which in turn determines the fiber properties.

Table VIII.1
THEORETICAL VARIABLES IN FIBER FORMATION.
POLYMER, EXTRUSION, SOLIDIFICATION

- MOLECULAR MASS (DISTRIBUTION FUNCTION)
- CHAIN STRUCTURE IMPERFECTIONS
- CHAIN ENTANGLEMENTS (shear history)
- TEMPERATURE PROFILE *versus* TIME
- STRESS PROFILE *versus* TIME and TEMPERATURE
- PHASE COMPOSITION *versus* TIME and TEMPERATURE
- RATE OF SOLIDIFICATION *versus* TEMPERATURE

PLASTIC DEFORMATION - NECK DRAWING

- DRAW RATIO
- DRAWING RATE
- DRAWING TEMPERATURE

EFFECT ON FIBER STRUCTURE

EXTRUSION AND SOLIDIFICATION	*PLASTIC DEFORMATION*
CRYSTALLINE STRUCTURE	FIBER MORPHOLOGY
DEGREE OF CRYSTALLINITY	FIBRIL DIAMETER
SIZE OF "MOSAIC" BLOCKS (a -, b - axes)	FIBRIL LENGTH
LATTICE DISTORTIONS (g - factor)	NUMBER OF TIE MOLECULES
FOLD LENGTH (long period)	NUMBER OF LINK MOLECULES
NUMBER OF TIE MOLECULES	FROZEN STRESSES

Molecular mass, understood as the entire distribution of the molecular masses, describes all polymer properties. Viscosity function, relaxation and retardation functions, and the entire rheological behavior depend on the molecular mass and its distribution. The same is true of all the other properties related to phase transitions, solubility, etc., etc.

If we know the polymer, we know everything else that there is to know. However, there is one question to be asked: is the polymer really what we believe it should be?

Chain structure of polymers is not always what it is supposed to be; the sequence of monomer units in the chain is not always, and not in all individual molecules, reflected by the chemical structural formulas we write. Organic reactions are known to have incomplete yields, byproducts are formed. In the case of polymers, there can be no purification to remove the byproducts, as they are built in into the chains. The amount and distribution of the chain imperfections has an influence on polymer properties; sometimes the influences are small, outright negligible, sometimes they mean very much. Colloquially we speak of polymer quality, which often translates to the difference between one vendor and another.

Characterization of chain imperfections is difficult, laborious, and costly in the majority of cases. For this reason, in industrial practice the presence, or rather change, in the frequency or distribution of chain imperfections is only first noticed when "something goes wrong". It is this "something" which may be so difficult to determine but is always threatening.

It is obvious that deviation from a regular chain structure changes the material properties, behavior in processing, and thus the results of the process. The quantities of the imperfections involved are extremely small, a minute fraction of one per cent. The effects of those small quantities on product, and particularly on the process performance are usually disproportionately large. An effort invested in the determination of the structural purity is often time and money well spent.

Chain entanglements, may vary quantitatively for the same chains, depending on the temperature and deformation history. On the other side they introduce changes in polymer properties and behavior, and these changes are not necessarily subtle. There is no method known to "dial" the entanglement density, we may just try to maintain constant history of the material, on top of the constant purity. The structural deviations have a very strong effect on the chain rigidity, and this is related to the propensity for development of entanglements.

Temperature profile *versus* **time** belongs to the most obvious variables, it determines rheological properties of the polymer and the phase transition(s) involved in the structure development.

Stress profile *versus* **time and temperature** determines how the fiber diameter attenuates. The attenuation, in turn, is the main determinant of stress; force applied is constant and it changes relatively little along the way. Stress together with the temperature-time profile influences phase transitions.

Phase composition *versus* **time and temperature** has a particularly strong effect in solution processes, as it also determines rheological properties. In all

processes it determines solidification and the resulting change of polymer behavior.

Rate of solidification *versus* **temperature** has a great responsibility for the quality and quantity of structural elements in the fiber. This variable is strongly related to the phase composition - time - temperature relationship; it may be outright derived from it. Despite the fact that this variable does not always have a simple relation to the profile of phase composition, the rate of solidification must be treated as a separate variable. Also, in cases of polymers which do not crystallize eagerly, the solidification may extend to the time outside of the formation machine.

The list of theoretical variables seems to describe everything important in the raw material and its transformation to obtain fibers of a desired structure; it describes the variables down to the most basic, most fundamental, elementary core. The fact that the number of technological variables is about three times as large speaks of the enormous complexity of the process.

VIII.2 Technological Variables

In a real process we have to create a situation which assures that the theoretical variables related to the raw material will be satisfied by the raw material used, and that the physical conditions and mechanical processes will create an environment which will satisfy the variables related to the processing. This is a rule in the general technology. By the time we determine all the variables needed to be under control for a process, the number of technological variables will be about threefold the number of theoretical variables. To facilitate the discussion we shall divide the variables into four groups: polymer system, extrusion, quench or coagulation, and drawing.

The subject is further complicated by a not entirely usual fact: not all of the variables can be changed at will. Thus we have two types of variables: *independent* and *dependent*. The independent variables may be changed at will within a technologically sensible range, for instance molecular mass of a polymer or extrusion temperature. There are, however, such properties, conditions or states which do have an influence on the course or the result of the process but cannot be regulated independently, like shear rate or profile of the filament temperature – these are the dependent variables.

A change of every independent variable causes alteration of at least one dependent variable, though it is usually more than one. The dependent variables, on the other hand, are usually affected by changes of more than one of the independent variables. Yes, initially it may appear confusing. Nonetheless, there is a logical system in this, almost like in a Cretan labyrinth. Table VIII.2[1] presents the technological variables and a sketchy, not very perfect scheme of the variable interdependence. Despite its imperfections, the table visualizes the far reaching effects of some of the independent variables; the higher up they are in the table the further down effects of their change reach.

Table VIII.2
TECHNOLOGICAL VARIABLES AND THEIR INTERRELATIONSHIPS

POLYMER SYSTEM																
MOLECULAR MASS FUNCTION	Δ															
STRUCTURAL IMPERFECTIONS		Δ														
PHASE COMPOSITION (CONC.)*			Δ													
RELAXATION/RETARDATION FUNCTIONS	↑	↑↓	↑													
SHEAR VISCOSITY FUNCTTION	↑	↑↓	↑													
EXTENSIONAL VISCOSITY FUNCTION	↑	↑↓	↑													
SOLIDIFICATION KINETICS	↑	↓	↑													
EXTRUSION																
SHEARING HISTORY				Δ												
EXTRUSION TEMPERATURE					Δ											
CAPILLARY DIAMETER						Δ										
CAPILLARY LENGTH							Δ									
CAPILLARY ENTRANCE ANGLE								Δ								
POLYMER FLOW RATE									Δ							
SHEAR RATE						↓			↑							
SHEAR STRESS	↑	↑↓	↑	↑↓	↓	↓	↑	↑↓	↑							
DIE SWELL	↑	↑↓	↑	↑↓	↓	↓	↓	↑	↑							
CHAIN ENTANGLEMENTS	↑	↑↓	↑	↑	↓	↓	↓	?	↑							
QUENCH or SOLVENT REMOVAL																
LENGTH OF THE ZONE									Δ							
TAKE-UP VELOCITY or FORCE										Δ						
HEAT/MASS TRANSF. AGENT — FLOW VELOCITY											Δ					
HEAT/MASS TRANSF. AGENT — TEMPERATURE PROFILE												Δ				
HEAT/MASS TRANSF. AGENT — CONCENTRATION PROFILE*													Δ			
FIBER TEMPERATURE PROFILE	↑↓	?	↑↓	↑↓	↑	↑	↑↓	↑	↑	↑↓	↑↓	↓	↑	↑↓		
SOLVENT CONTENT PROFILE*	↓	?	↑	?	↓	↑	?	?	?	↓	↓	↓	↑↓	↑		
FIBER DIAMETER PROFILE	↑↓	↑↓	↑↓	↑	↓	↑	↑↓	↑↓	↑	↑↓	↓	↑↓	↑↓	↑		
EXTENSIONAL STRESS PROFILE	↑↓	↑↓	↑↓	↑	↓	↓	↑↓	↑↓	↓	↑↓	↑	↑↓	↑↓	↑↓		
UNRELAXED STRESS PROFILE	↑↓	↑↓	↑↓	↑↓	↓	↓	↑↓	↑↓	↓	↑↓	↑	↑↓	↑↓	↑↓		
SOLIDIFICATION PROFILE	↑↓	↑↓	↑↓	↑↓	↑↓	↑↓	↑↓	↑↓	↑↓	↑↓	↑	↑↓	↑↓	↑↓		
COLD DRAWING (PLASTIC DEFORMATION)																
DRAW RATIO														Δ		
RATE OF DRAWING															Δ	
TEMPERATURE OF DRAWING																Δ
NATURAL DRAW RATIO	↑	↑↓	↑↓	↑↓	↑↓	↑↓	↑↓	↑↓	↑↓	↑↓	↑↓	↑↓	↑↓	↑↓	↑	↓
MAXIMUM DRAW RATIO	↑	↑↓	↑↓	↑↓	↑↓	↑↓	↑↓	↑↓	↑↓	↑↓	↑↓	↑↓	↑↓	↑↓	↓	↑
MAXIMUM DRAWING TEMPERATURE	↑↓	↑↓	↑↓	↑↓	↑↓	↑↓	↑↓	↑↓	↑↓	↑↓	↑↓	↑↓	↑↓	↑↓	↓	
DRAWING TENSION PROFILE	↑	↑↓	↑	↑↓	↑↓	↑↓	↑↓	↑↓	↑↓	↑↓	↑↓	↑↓	↑↓	↑↓	↑	↓

Δ Intentional increase; ↑ Resulting increase; ↓ Resulting decrease; ↑↓ Result depends also on other variables. ? Effect unknown. * Concerns only solution or gel processes.

VIII.2.a Polymer Related Variables

The **Molecular mass function** and its importance have been discussed in many places throughout this book. Its importance from the technological point of view remains the same as from the theoretical one. The full function is best described by the whole curve of the amount of species of different molar mass. In practice it is given mostly by the averages of different kinds and their ratios describing the *distribution of molar masses.* The "shorthand representations" are derivable from the whole curve; on some occasions they are convenient as different polymer properties depend on the averages of different type.

Should all the other independent variables be held constant, then all of the dependent variables would be affected by a change in the molecular mass function. In table VIII.2, such an interdependence is demonstrated. A triangle in the row of an independent variable denotes an intentional increase of this variable, or shift upwards of the entire function with all other independent variables held constant. In the corresponding column, arrows indicate an increase or decrease of value of the dependent variables. A double, up and down, arrows indicates a complicated relationship where the direction of the change may depend on the setting of other variables.

Imperfections of polymer structure are almost equally important as the polymer itself, since they modify the polymer properties. This variable must be classified as independent, although in practice the imperfections are very difficult, often impossible, to control; they *just happen.* Taken from a different side, a change of vendor may mean a change of manufacturing process resulting in a different set of chain distortions, perhaps with less damaging consequences.

Phase composition here means concentrations of the chosen polymer in the chosen solvent. This is undoubtedly an independent variable of high importance, though absent in processes of formation from the melt. This variable affects practically all dependent variables, just as the molecular mass does.

Relaxation and retardation functions depend strongly on the molecular mass and, naturally, on the polymer and its character. Naturally, the relaxation processes are influenced by the presence and quality of solvent. They cannot be changed independently, though often it would be convenient to have such a possibility. Dependence of retardation/relaxation function on applied stresses is stipulated.

Shear and extensional viscosities are equally dependent on molecular mass, solvent (if present), structural perfection, and on other variables located further down on the list.

Solidification kinetics is an inherent property of a polymer, of its molecular mass and other variables. It cannot be changed independently. Imperfections of polymer chain usually slow the kinetics down, however, depending on the nature of the polymer and of the structural distortions, other directions in the changes of kinetics are not out of question.

VIII.2.b Variables in Fiber Extrusion

Shearing history is, to a large extent, a dependent variable since every polymer accumulates some history since its synthesis. Nonetheless, the same variable may be viewed as independent as the accumulated effects of history may be affected by the subsequent shearing and relaxation (temperature effects). The possibilities of modifying the history have been taken as the ground to recognize the history as independent variable, or rather as a variable of qualified independence. It is primarily a matter of chain entanglements but, one may also include here effects of possible shear and/or thermal degradation.

Extrusion temperature is an independent variable of far reaching and strong consequences.

Capillary diameter and capillary length represent two independent variables which may be limited only by technological reasons. The variables have strong effects on other variables, as well as an influence on the phase change kinetics and on the polymer morphology.

The **Capillary entrance angle** represents an independent variable, though preferably it ought to be small in practically all cases.

Polymer flow rate is an independent variable with very strong and far reaching effects on many variables in the process. Those far reaching indirect effects are often underrated. On the other hand, this variable may be the subject of severe technological limitations.

Shear rate depends on the capillary diameter and on the polymer flow rate. This variable is dependent, but it has the smallest number of determinants. Shear rate influences many other variables, mainly those related to rheology.

Shear stress is a typical dependent variable with many independent variables controlling its magnitude.

Die swell results from a number of factors and determines the starting point of the diameter attenuation. Its nature and significance still require research.

Chain entanglements are affected by the shearing history. Repeated consideration of this may appear redundant but it is to reflect the changing nature of the polymer chain morphology. Under the heading of "shearing history" above we understand the state of the polymer as it is coming into the extrusion. Here we consider how the extrusion process changes it, what kind of polymer is going out of the extrusion section, and further, what is entering into the processes of quench zone after relaxation in the die swell.

VIII.2.c Variables in Quench or Solvent Removal

The **length of the quench or coagulation zone** is without any doubt an independent variable from the point of view of hardware. In the technological sense, it is a dependent variable. Depending on the cooling intensity, a filament may be solidified after passing only a fraction of the physical length of the zone.

If such a thing happens, then over the rest of the distance other processes take place, though they should take place in another segment of the line under much better control. Physically the length of the zone may not be shorter than some minimum necessary for cooling. It should not be longer than necessary, as this would be detrimental to the proper process control.

Take-up velocity or force – one of these two is independent, the other is dependent. Which one is which depends on the choice of fiber transport. Roller transport is a constant velocity device and force is whatever results from the velocity, the rheological properties, etc. Pneumatic transport, for example, is essentially a constant force device (provided the filament diameter is constant) and velocity is whatever results from the force and rheology, temperature, etc.

Flow velocity profile regards the velocity of cooling air or of the mass exchange medium. This independent variable "cooperates" with several other independent variables.

Temperature profile regards the temperature of the cooling and/or mass exchange medium. It also has highly cooperative significance, similar to the previous variable.

Concentration profile regards only processes involving solvents and describes the concentration of the mass exchange medium along the filament path.

Fiber temperature profile represents an enormously important variable which cannot be changed independently. There are many independent variables which affect the temperature profile which makes the variable difficult to control positively.

Solvent content profile is valid only for solution or gel processes. It is a result of many independent and dependent variables, similar to the temperature profile.

Fiber diameter profile, like the other variables of the quench zone, is highly dependent on many other dependent variables. The diameter profile itself has strong influence on temperature, solvent content. The fiber diameter profile determines the *time scale* of the process, and further, it determines the residence time of the polymer at any point of the linear distance from the spinnerette.

Extensional stress profile is again highly dependent on many variables and controls other processes, mainly the diameter attenuation profile and phase changes.

Unrelaxed stress profile depends on many variables in a rather complex way, primarily on the level of strain and stress retardation, which themselves depend on other variables. Unrelaxed stress is decisive in acceleration of the crystallization process and in the final fiber morphology.

Solidification profile is equally important in melt as it is in solution processes. It determines the melting profile of a crystalline fiber. In solution processes it determines additionally the structural uniformity along the fiber radius.

VIII.2.d Variables of Cold Drawing

The **Draw ratio**, or as otherwise called plastic deformation, is the main variable responsible for imparting a structural and property orientation along the fiber axis. It is an independent variable within technological limits, provided the drawing is done with positive (roller) transport. When fibers are transported by pneumatic jets, that is with *quasi constant force*, the variable is not exactly independent; the drag force depends on the fiber diameter and on the resultant fiber velocity. In effect, it is constant only with a very stable process.

Rate of drawing may be an independent variable if the drawing process is executed separately from the previous stages of fiber formation. In cases where the drawing operation is performed in-line with the entire process, the rate of drawing may need to be subordinated to the take-up velocity and draw ratio. In the case of pneumatic transport it becomes vulnerable to the changes resulting from the potential variations of draw ratio.

Temperature of drawing is similarly an independent variable with qualification. The process of plastic deformation is exothermic, and this introduces certain dependence on the control of drawing temperature. Any instability of draw ratio and/or drawing rate is bound to be reflected in the amount and rate of heat generation. The variable heat generation, in turn, will interfere with the temperature control system.

Natural draw ratio depends on the structural features of the undrawn fibers, on total crystallinity, and on a "preorientation" which often may be present. The dependences go all the way back to the molecular mass of the polymer.

Maximum draw ratio has qualitatively similar dependencies as natural draw ratio but the quantitative influence of different factors is different.

Maximum drawing temperature (before the necking disappears) depends on the amount and the type of crystallinity in the undrawn fibers, including melting temperature of the crystals. As the drawing progresses, the maximum drawing temperature usually increases.

Drawing tension profile pertains primarily to cases of multistage drawing. In a single stage drawing the drawing tension is more or less constant.

VIII.3 Process Analyses

Analyses of technological processes are usually performed for one or more of the following three reasons:

- Control of raw materials for agreement with specifications and/or suitability for the process.
- Control of the proper functioning of the process.
- Control of product properties and their agreement with specifications.

Such an analytical routine should be introduced already during process development. This facilitates process start-up and provides the best tools for so called *trouble shooting.* It is certainly much better to have the tools, and an "exemplary" data bank, prepared in time, before any bad events begin to be pressing.

Analyses of fiber formation processes ought to be divided in agreement with the technology requirements, that is, according to the four groups of technological variables.

All of the analytical work on polymers is related to the following three areas:

- Physico-chemical characterization of polymers: molecular mass, structural purity, as well as solvents and solubility if needed.
- Rheological analysis, mainly in oscillatory mode, in some cases reinforced by a rotational mode, and/or capillary measurements.
- Crystallization kinetics and thermal properties.

The depth of these analyses should depend on the type and character of the polymer used. Some polymers may require more detailed rheological analysis, which is *per se* very sensitive and may serve as an indicator that something is different in the chain structure. Other polymers, including some polycondensation products, may require more physico-chemical determinations, while still others may need to be analyzed for cross linked material.

Economic sensitivity obviously calls for a minimum of analytical work. On the other hand, poor results in manufacturing may cost substantially more than the systematic analyses would. Capabilities of more detailed determinations should be accessible in case more serious problems should develop.

The segment of extrusion represents no problems as far as analyses are concerned. The spinnerette design is fixed for a given process, extrusion conditions are usually controlled and recorded automatically. Metering pumps are normally reliable, with automatically controlled velocities and recorded polymer pressure.

The only variable of concern may be the die swell, and how constant it is for a given process. The potential die swell variability may be also connected with changes of chain entanglements. None of the two variables may be controlled independently, but any change of them would indicate changes of polymer, either its chemical nature or its physical state. Warnings of such changes and their magnitude should be obtained from the polymer characterization.

Control of the quench or coagulation zone represents an entirely different, infinitely more complex task. The independent variables may be controlled fairly easily. They are either constant for the process, like the physical length of the quench (coagulation zone), or readily controlled, like flow, distribution and temperature of the heat and/or mass transfer agents. The dependent variables may represent serious difficulties and therefore characterization of the quench zone processes is treated in a separate section.

In a cold drawing operation, the independent variables must be qualified, as elaborated above. Assuming a positive transport system and independently con-

trolled draw ratio and drawing rate, the temperature of drawing may be controlled only indirectly through the heating/cooling device. Direct control of the filament temperature would require infrared devices, and so far this is not done on a standard, operational basis.

The dependent variables of the drawing zone are immaterial in a well established process, provided that there are sufficient *safety margins, e.g.* for the maximum draw ratio and maximum drawing temperature.

VIII.4 Description of Quench and Coagulation

The group of dependent variables in quench and/or coagulation processes forms a closed circle of *causes and effects.* All of the dependent variables have nonlinear relationships and are mutually interdependent. The relatively large number of them, five or six, places the system into danger of the *butterfly effect.* It is not exactly to a degree comparable to the famous butterfly in China triggering a hurricane in the Atlantic, but it is sufficient to affect the stability of a process to a degree clearly detectable in the quality of the manufactured product. An attempt of a "visual" presentation of the complexity of the interdependencies is presented in figure VIII.1.

It is necessary to stress that all the variables given in figure VIII.1 represent nonlinear functions of either distance or time lapsed from the spinnerette, or rather from the maximum of die swell. For the process of formation from a melt, Nusselt number is used, which *per se* is not a variable. Nevertheless, it was used here to stress the complexity of the influences on temperature. A similar situation exists in the wet process, where the heat exchange is not so dramatically affected unless there is a large difference between the temperature of extrusion and the temperature of the coagulation bath. In the case of dry processes the influence of the concentration function on temperature is indicated. This is meant to stress the influence of rapidly evaporating solvent on temperature through the heat of evaporation. The obvious influence of temperature on the *modus* of crystallization is omitted to avoid more complications on the already busy diagrams.

The unusual complexity of the dependencies represents a very good reason why it is so difficult to develop a satisfactory quantitative description of the processes. At the same time, the diagrams of figure VIII.1 explain why an consideration of a part of the problem offers little hope for real success – to make progress all the necessary influences must be considered. Also, particular care should be taken with the simplifications of any mathematical solutions. One has to bear in mind that we speak of products with diameters in the range of microns and processes where every degree of temperature is meaningful. All this causes the demand for a high degree of accuracy and a very low tolerance for errors.

To describe a fiber formation process, a certain number of experimental characterizations are unavoidable. The relationship between the unrelaxed stress and temperature for the onset of the process of crystallization is described in section IV.5. However, the diameter attenuation and unrelaxed stress may be pre-

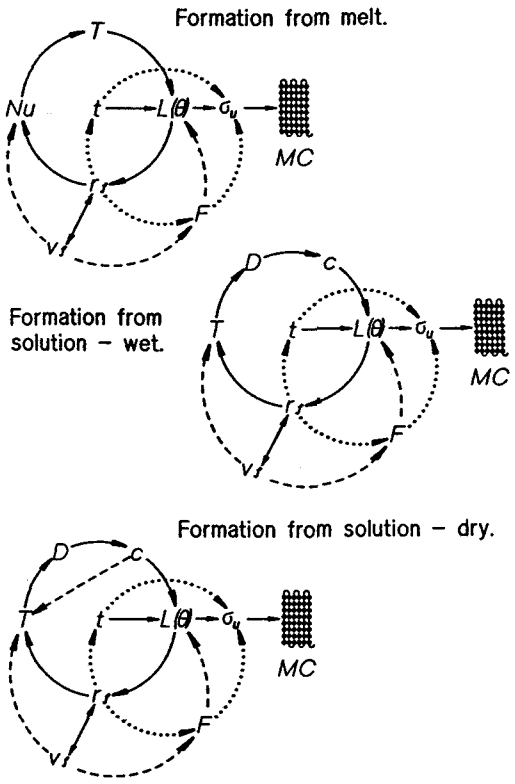

Figure VIII.1: *Schematic representation of the interdependencies of variables in quench and coagulation zone. Symbols: T is filament temperature, Nu is Nusselt number, t is time, r_f is radius of filament, v_f is velocity of filament, F is extensional force, $L(\theta)$ is creep retardation function, σ_u is unrelaxed stress, D is diffusivity, c is concentration; all the values represent functions versus distance from spinnerette or time.*

dicted with some qualifications, and the initiation of crystallization can be predicted in a way similar to figures IV.28 through IV.30. The process of crystal growth is still unpredictable. For this reason laboratory determination of polymer crystallization and of *crystallization history* (CH) is highly recommended. The crystallization profile is necessary to calculate the filament temperature profile with a sufficient accuracy. In reverse, the temperature profile must also be determined to define the "location" of the crystallization profile.

From experience, as reported in the previous chapters, we know that the most accurate description of diameter attenuation is obtainable when the process is considered in terms of creep relaxation. On the other hand, it has been demonstrated that the creep retardation function is not universally constant: it depends also on the magnitude of the applied initial stress. These relationships are known to allow neither an *a priori* prediction of the retardation function, nor limits of its validity. In effect, the function must be determined experimentally and it may be used only for cases where the initial stresses do not deviate significantly. The

specific conditions of any formation process, particularly its velocity, are difficult to simulate in any laboratory instrumental characterization. All this leads to the necessity of experimental determination of filament diameter and/or velocity profile together with the temperature profile. Shortly, a whole characterization of the whole quench zone is necessary to describe the process.

In the case of wet formation from solution, the concentration profile may be calculated with fair accuracy. In dry formation, the sensitivity of the process to the temperature profile makes it rather necessary to determine experimentally both the temperature and the concentration profiles.

Since different events are taking place simultaneously in the discussed segment of the process, the evaluation of many of the experimentally gathered data should be performed simultaneously, in one computational run. This means that, for example, the solution of the differential equations for the heat transfer and for the diffusion of solvent should be done in parallel, step by step; the results from each of the strings of calculations should be fed into the other strings as the computation progresses. Parameters, which in many publications are taken as constants, like density, heat conductivity, and others, should be step by step corrected for actual temperature, concentration, etc. All of the calculations here are based on differential equations, and error propagation in such cases is exceptionally large. Results of such calculations are given in figure IV.4.

To obtain reasonably accurate results, the number of points calculated over radius should not be smaller than eight, but more than sixteen points might call for accuracies of experimental data which are unattainable. Many methods of solution of differential equations require the number of points in the axial direction to match the number of points in the radial direction, and if so, this is an important point.

Another important point to be made is that the experimental data need to be of high precision, naturally, with points taken as densely as practical. As the number of points calculated in the axial direction will always be larger than the number of experimental points, an interpolation technique must be used. It is advisable not to smooth the data, or many important features may be lost. One needs an open mind about unexpected events. A case in point may be seen in figure VIII.2, which presents extension rate plotted against distance from spinnerette, filament temperature and time.

A closer look at figure VIII.2 shows that the extension rate goes initially through a maximum, which has been denied by some authors. Yet all the examples quoted here show this behavior, as do all of the many cases studied, irrespectively of the polymer. Certain segments of the curves are drawn in thick lines to indicate where crystallization was taking place. From these it is evident that crystallization starts in the vicinity of the first minimum of the curves. After the first peak in the curves follow two or three peaks, much steeper and larger then the first one. The process of crystallization coincides with the first large peak, sometimes the whole peak, sometimes one half of it, or so. The next large peak indicates onset of neck drawing. Presence of such peak indicates too long a quench zone.

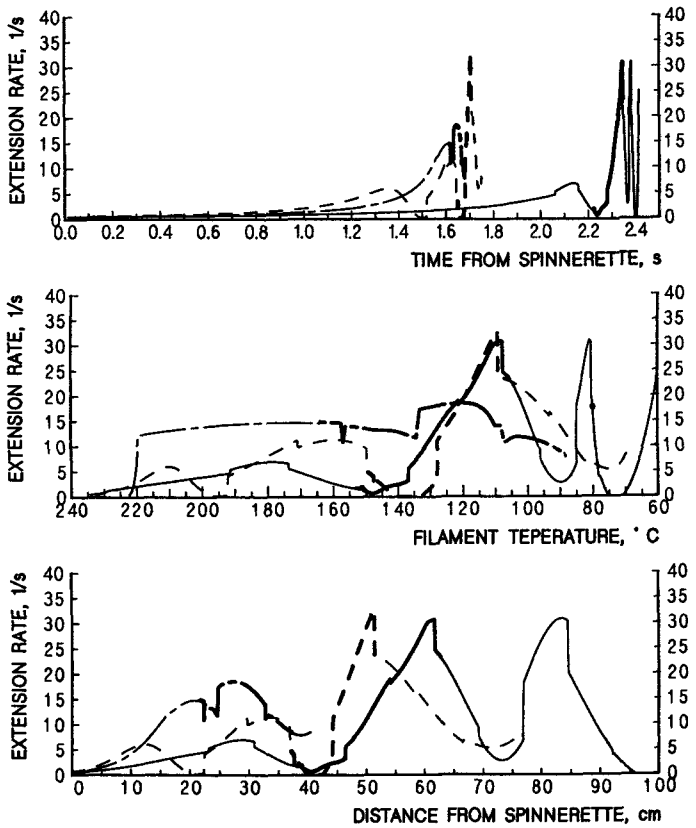

Figure VIII.2: *Dependence of extension rate on time, temperature, and distance from spinnerette. Different line patterns represent processes with different effective lengths of quench zones. Heavy line segment indicates crystallization.*

It is important to note that in the area where crystallization takes place and in the area of necking, the curves are bumpy. Such bumps are always present in the area of crystallization and indicate some instabilities. In the area of necking the instabilities appear often in fast "one step" processes without separation into formation and drawing zones. Such instabilities indicate that the drawing is out of control. Smoothing out of the input data might remove the bumps and show the process as fully stable when it really is not.

Calculations of the forces acting on filaments cannot be performed in the same group as above; a second group must be formed. Force of gravity, inertia, fluid dynamic drag force, force of momentum all must be integrated from the point of fiber take-up upwards to the spinnerette. These calculations must go then in the opposite direction as those of the first group. The outcome of such force calculations is presented in figure IV.3.

After the second group of calculations has been done, one may use the results

on the available force and the results obtained in the first group of calculations to obtain the creep retardation function, as given in figure IV.23.

Subsequently, calculations may be performed involving various correlations, such as heat transfer coefficient (provided the cooling medium data have been collected.

It is quite clear that such a characterization represents a fairly large task, and as such cannot be performed routinely. Such work, however, should be performed during development of a process and from time to time in manufacturing to prevent the "drifting" of a process.

VIII.5 Prediction of Quench and Coagulation

It is the goal of every technology to predict the process, to be able to calculate everything *a priori*, and use experiment just for the confirmation of the accuracy of calculations. The technology of fiber formation, despite its age and commercial importance, clearly is not developed to this point yet.

The main points which currently are developed insufficiently for full predictability are

- Calculation, or recalculation, of the creep retardation functions *a priori*, theoretically.

- Description of the kinetics of polymer crystallization, particularly crystallization under strain.

It is possible to perform a number of process characterizations, as described above, during the development stage of a process. Correlations may be obtained for a polymer and a process, and based on this it may be possible to construct systems of calculations which would predict, *e.g.* operating conditions for machines to offset small variations of raw material, or similar. Investment of time and effort in such partial, semiempirical correlations is highly recommended as worthwhile and economically highly justified. Naturally, such correlations must be done with full respect for the process complexity and with the proper separation of variables. Otherwise, the outcome may be misleading.

As for knowledge of the missing links, this is a task for further research in rheology to discover exactly what affects the creep retardation functions and how they are affected. Such information represents a necessary minimum for full predictability of the rheological behavior of polymer, filament attenuation and interaction with the process of crystallization initiation and crystal growth.

Another area needing effort involves cooperation between kinetics of crystal growth in conjunction with rheology. Special attention to the morphology of polymer melts would be very helpful. Morphology of the melts is of high importance to rheology. Rheology provides an indirect measure of basically unknown conformational states, and those conformations are most likely the quantities contributing

to the crystal growth. The "interdisciplinary" character of the task adds to the difficulty.

VIII.6 References

1. Z. K. Walczak: *Formation of Synthetic Fibers*, Gordon and Breach, London - New York, 1977, Chapter 6.

IX SCALE CHANGE OF A PROCESS

In all of the experimental disciplines, experimentation is done on as small a scale as is practical for the sake of both convenience and economy. If a process is to be developed to a commercial scale, the scale enlargement practically always poses problems. The problems of scaling are related to the physical and engineering aspects of a process. Since fiber formation processes are almost always entirely physical, and very complex at that, the scaling often poses great difficulties. The most general advice based on long experience teaches that the more time spent in a library, the less time is needed in the laboratory, the more time spent in the laboratory the less time is needed to scale the process, the more time spent on scaling the better the machine design and the smoother its start up.

After the experiments on a small scale are completed, the product which possesses the same properties must be obtained in larger volumes. Manufacturing equipment must be enlarged, in comparison with the experimental machines, in such a way as to assure that the theoretically essential variables will remain unchanged. In chemical engineering, some more complicated cases are divided into several steps of scaling-up, which may be advantageous. It may happen that a perfect reproducibility of the product properties in not attainable, thus it is the task of engineering to limit these bad cases to a minimum.

Generally, in the fiber producing industry, scaling of the fiber formation processes is considered to be exceedingly difficult. It appears that this is to a large extent due to the fact that scaling of fiber formation may well be one of the most misunderstood tasks of its kind. The problem of scaling fiber formation processes in any broader general sense has been treated earlier only by this author.[1] In contrast to the majority of other processes utilized by chemical industry, fiber formation does not involve chemical changes, with those few exceptions involving wet processes. A chemical process may be accelerated, or slowed down by change of temperature or pressure; the product remains essentially the same. Perhaps some of the impurities resulting from side reactions may change. In chemistry of low molecular mass compounds the impurities may be removed. In processes involving macromolecules, such a purification is practically impossible.

In the majority of physical processes, especially in those involving macromolecules, time scale cannot be changed, and this is also the case with the temperature of a process. Crystallization is a physical process whose rate depends on temperature, but along with the changes of temperature follow qualitative changes in the crystal structure, most conspicuously changes of the melting point. Similar considerations are also valid in regard to the rheological properties; time is important to relaxation and retardation processes, and the relaxation times depend on temperature.

In summary, if we want to reproduce a process in a different scale, the time and temperature profiles cannot be changed. At this point we meet another limitation: the time scale in fiber formation depends on filament diameter. Thus, for a process to be unchanged, the profile of diameter attenuation also must remain

unchanged to prevent alteration of the time scale. If these conditions are not met then everything else, like velocity of extrusion, temperature, etc., must be changed to reach an equivalency in the rates of the unit processes involved. The problems become difficult indeed.

Parenthetically, one may consider the necessary degree of constancy or the sensitivity, or tolerance of the process. This certainly varies with polymers and by no means least importantly, with the demand on the quality and reproducibility of the properties for any given product. However, such decisions to a large extent reach beyond the boundaries of technology.

To begin with, one must realize that the enlarging of the scale of a fiber making operation may be achieved truly only in one way: by enlarging the number of filaments produced in one position of a machine with identical geometry. All other ways seek some equivalency which is not a true scale-up. There is more than one way in seeking an equivalency for the processes, some of the ways may be easier than others.

The task of changing the fiber titer while all other properties remain unchanged, may also be treated as changing of scale.

IX.1 Changing the Number of Filaments

If the operation of changing the number of filaments is to be a true change of scale with all fiber properties unchanged, the machine geometry must be the same and all the technological variables, except flow of cooling media, must remain unchanged. Similarly unchanged must remain the technological variables of the drawing operation.

The only change introduced in the process is an increase of the number of filaments per position, and the resulting increased volume of polymer flow per position. A larger volume of polymer carries a larger amount of heat to be removed from the tow, but the heat removed from an individual filament should remain unchanged along the entire profile. The magnitude of the problem depends on the magnitude of the scaling factor, but after consulting the section on heat transfer the task will not be found easy.

The task may be approached by increasing the velocity (volume) of the cooling medium used, or by decreasing the medium temperature, or both. The limitations on the medium flow intensity are related primarily to the drag forces exerted on the filaments, and this is particularly unpleasant in case of cross flow. Excessive bellowing of the spinline does change somewhat the profile of forces acting on the filament. An angle between medium flow and filament other than ninety degrees causes the formation of an axial force component. In the lower segment, the component is directed against the drawing force, and in the top segment it is increases the drawing force. At higher gas velocities, there is also a threat of filament vibrations which might lead to fiber nonuniformities.

Lowering of the medium temperature is a much more appealing proposition. When the scaling factor is large, the lowering of the temperature may be limited by

economy since cooling energy is expensive. Very cold air also causes troublesome water condensation. Thus, this remedy also has its limitations. Some advice: when developing a process in small scale do not use very cold air, leave yourself a safety margin for the future scale up.

The number of capillaries is increased mostly in proportion to the surface of the spinnerette plate. In cases of circular spinnerettes, this is proportionally to the square of the spinnerette diameter. The access of quenching air to the filaments, irrespective of the type of quench or coagulation medium, is proportional to the spinnerette diameter. Consequently, to provide a comparable cooling effect, the air flow must be largely redesigned taking all the above features into account. An enlarged spinnerette may be designed in such a way that the diameter will be scaled up rather than the surface area. Such a possibility represents a relatively convenient solution in respect to the scaling of quench or drying. Nevertheless, such a convenience may be expensive in terms of other consequences, the acuteness of which increases with the increase of the scaling modulus.

When the scaling modulus of the spinnerette diameter is chosen, then the force acting on the spinnerette plate during extrusion grows in quadratic proportion to the modulus by which the diameter has been increased. In operations of multifilament formation, the force acting on the spinnerette surface may reach a magnitude that is difficult to cope with. Another consequence of such scaling would be an increase in fiber-to-fiber nonuniformity between the first and last rows of filaments in the path of the air. In such a situation a remedy may be changing the spinnerette plate from circular to rectangular. The latter may offer the possibility of retaining a reasonably similar number of filament rows and expanding the length of the plate in proportion to the increased number of filaments. Such a solution has the additional benefit that the ratio of the circumference to the area is larger for rectangles than for circles. This is certainly helpful in designing a sufficiently strong, buckling resistant mounting of the spinnerette plate. Rectangular spinnerettes certainly represent a much superior solution over large circular spinnerettes with quench air introduced into the center of the filament bundle.

Rectangular spinnerettes may be equally well suited for cross flow as for cocurrent air flow. Switching from circular to rectangular spinnerettes may also be understood as a measure to limit the excessively high air velocities which would be needed for circular spinnerettes while simultaneously maintaining the fiber-to-fiber differences within technologically reasonable limits.

In the drawing zone, large amounts of heat are developed within a small space. The degree of spatial limitation depends on how well the necking is localized. Assuming a drawing system with the necking localized within very narrow limits, the problem may be described in the following comparative way: For 1 to about 100 filament lines, the zone of drawing must be heated. The amount of heat needed decreases with an increasing number of filaments. Also, when a smaller number of filaments are drawn, it is highly advisable to heat the fibers beyond the necking point. When the number of filaments reaches some 200 to 300, depending on the draw ratio, polymer, fiber titer, and method of drawing, the threadline may

require gentle cooling. In some operations where the number of filaments reaches over 1000 per position, the filaments may display a tendency to fuse.

In the case of very heavy threadlines, temperature control becomes a difficult task indeed. Here we have a conflict of interest: for the sake of high quality, the necking ought to be well localized with a good temperature control. For a very large number of filaments satisfying the two conditions is difficult. The way out of the conflict may be to spread the threadline into a wide band for easier temperature control. Not without significance is here the choice of the type of drawing device.

Although the scaling method just described may seem to be relatively uncomplicated, it should not be assumed a perfect way of achieving the goal. In performing such a scaling up, certain changes are unavoidable in the extrusion area. In reality, the increased size of the polymer delivery equipment, such as the screw melter or autoclave, longer transfer lines, etc., increases the residence time of polymer at elevated temperature and under shear. For many polymers, this may lead to changes of the fiber properties. For some polymers this may mean increased degradation or other structural changes. When changes of molecular mass are involved, corrections may be possible, but when branching or cross linking results from the prolonged heat exposure, then there exists no corrective remedy.

The necessary changes of size, and frequently of geometry, of the polymer supply system may have an influence on the shear history of the polymer with further consequences reflected in the fiber properties or in the processing characteristics.

Another unavoidable effect of scale increase is an increase of the thickness of the spinnerette plate for the sake of its mechanical strength. This leads to the necessary alterations in the geometry of the capillary entry, which in turn may have an influence on the total shear history. The outcome of so many adjustments in the flow conditions is impossible to predict *a priori* unless a very extensive examination of the polymer rheology has been performed.

IX.2 "Scaling by Equivalence"

A change of the machine geometry or any of the technological variables would not be considered a scaling-up, but rather a seeking of an *equivalent process* that will preserve a majority of the critical fiber properties. If the machine geometry is altered so that the length of the quench zone is different, then automatically a score of technological variables will change. To bring the operation back to the point where the fiber properties will be the same is practically impossible. One may adjust the independent variables so as to create a new formation environment leading to fiber properties more or less similar to those obtained in a smaller scale. There exist situations when this is the only way available to solve the scaling operation problem. Such situations are always painful, time and money consuming, and they often lead to a frustrating repetition of a majority of the original work of the original process development.

Let us consider some possibilities of changes of the process parameters. If the

polymer flow is changed by a scaling factor of m, then to preserve the same shear rate in the capillary we have

$$\dot{\gamma} = \frac{4Q}{\pi r^3} = \frac{4mQ}{\pi r_1^3} \tag{IX.1}$$

This leads to the requirement that the new capillary diameter be

$$r_1 = m^{1/3} r \tag{IX.1 a}$$

If the original capillary aspect ratio, l/d, is preserved, along with the original shear rate, then the die swell will remain unchanged. This means that the maximum diameter of the extrudate will be $2B \cdot m^{1/3} r$ and the polymer stream velocity in the die swell will increase by the same factor of $m^{1/3}$.

If we preserve the same timing, then with identical machine geometry and appropriately scaled cooling, the filament velocity at the end of quench should increase by the same factor of $m^{1/3}$. As a result of the changes of polymer flow by the factor of m, and velocity by the factor of $m^{1/3}$, the fiber titer will increase by a factor of

$$9 \cdot 10^5 \frac{mQ\rho}{m^{1/3} v} = 9 \cdot m^{2/3} \frac{Q\rho}{v}$$

Then we have a factor of $m^{2/3}$, not m. The polymer flow problems connected with the scale changing from one segment of the process to another have been noticed earlier by W. E. Fitzgerald and J. P. Craig[2].

In view of the different filament velocities, the timing and the strain profiles may be preserved only when the quench zone is expanded by a factor of $m^{1/3}$. Here it is necessary to stress that equivalent cooling means that the temperature profile must be reproduced against distance multiplied by $m^{1/3}$ if the timing is to be preserved accurately. The net drawing force, that is, the rheology force available for extension without the losses due to other forces, must be increased by a factor of $m^{2/3}$.

Thus, we have just presented a nice scaling operation to increase fiber titer. However, there are certain questions remaining: How much can the titer be increased in this way? If we have the possibility of extending the quench zone by 14.47 per cent, then we may increase titer by 31 per cent. If, for example, the titer increase is from 10 dTx to 13.1 dTx, this is significant. If, however, there is a question of changing titer by the same percentage but for finer fibers, say from 2 dTx to 2.62 dTx, it is not very significant. If a greater increase is needed, then another question arises: How big a flexibility in expanding the quench zone should a machine have? Usually, increased flexibility means increased investment costs.

Occasionally one may find in the literature papers describing the attempts to intensify extrusion with preservation of the spun fiber diameter. To evaluate such a situation, one may conduct considerations similar to those described above. In this case, the filament velocity at the end of quench zone would have to be larger by the scaling factor m. In such a case, however, the extension would increase $\lambda = m/m^{1/3} = m^{2/3}$. If the length of the quench zone were increased by $m^{2/3}$,

then the original temperature profile *versus* distance may possibly be reproduced. The problems begin when we consider the attenuation profile and the connected time scale.

The present knowledge in the area of creep (extension) is insufficient to solve the problem theoretically. To successfully accomplish the task, one needs to find some way to manipulate the stress - temperature - time profiles in order to obtain a similar structure formation. This kind of work is no longer a scaling, but a clear reworking of the most difficult segment of the process *"from scratch"*.

Another way of solving such a problem may be through redesigning extrusion to the point that the minimum filament velocity (in the die swell) will be increased by the factor of m, and thus final fiber velocity, $v_{f_1} = m \cdot v_f$, will be increased by the same factor. The cooling must be redesigned to preserve the original temperature profile over the quench length, scaled also by m to preserve both the timing and the degree of extension, λ.

The remaining problem is how to increase the minimum velocity of the filament. Velocity is in direct proportion to the volume of the polymer flowing with an unchanged diameter, but shear rate increases also by the same factor m. The latter results in an increase of die swell. The solution of this will depend on the polymer in question. Sometimes extended capillary length may help to lower again the increased die swell, provided there is room to increase the resulting higher extrusion pressure. Decrease of the capillary diameter is in such cases counterproductive as the velocity is affected by the square of the diameter and shear rate by the diameter to the third power, thus the die swell may be even larger. Increase of the extrusion temperature may help in reducing the die swell, other factors permitting. On the other hand, an increase of temperature would aggravate the effort to redesign the cooling to preserve the temperature profile.

In each of the cases presented in this section, the length of the quench zone had to be changed, as had some profiles of the quench zone. One change had to be traded for another, not to mention the additional difficulties which may appear, such as a higher force of the higher air velocity acting on a longer filament, and others. Flexibility of the forming machines to meet the demands represents another question. For all these reasons, this section has been named *"Scaling by Equivalence"* (in quotation marks) to indicate that these methods of scaling are not exactly a scaling as it is understood in the area of chemical engineering.[3]

IX.3 Experimental Formation Machines

Successes in research and development depend to a large extent on the availability of proper equipment. The same is true of scaling operations. The notion "proper equipment" is not necessarily equivalent to "expensive equipment". In many fiber research laboratories, one may find an impressive number of experimental machines designed specifically for the performance of different tasks, for work with different polymers, and so on.

In reality, a laboratory for research on fiber formation from melt needs one

experimental machine per fifteen to twenty persons of independently working technical personnel (engineers). In fact, two to three days of well planned experiments by an engineer with the help of an operating crew of technicians (two to three) is able to produce enough data for the investigator to work on processing the data for two to three months, and sometimes longer.

A both technically and economically efficient machine ought to be built from individual elements, something like the laboratory glassware, or Lego^R blocks. Within such a system, all kinds of experiments are possible, all types of endeavors, from basic, fundamental research to fairly far reaching scaling operations.

The heaviest section of a formation machine, in the physical sense, is the extrusion section. For this reason, this section should be planned to have a fixed location on top of the area to be occupied by the machine. The section should consist of two extruders, one smaller and one larger, connected to one block containing two metering pumps, filters, and spinnerette. The two extruders offer a possibility of forming fibers from one or several filaments to some 300 or even 500 filaments. The actual size of the extruders may be adjusted to the prevailing type of work expected in the laboratory. In case a large range of filament numbers is needed, a third little extruder for the smallest number of filaments may be "wheeled in" and connected to the block when needed.

Beside the wide range of total polymer flow, such an extrusion section offers also the possibility of working with two different polymers for bicomponent fibers or some other nonstandard combinations. Naturally, the bicomponent work requires melt distribution plates for the spinnerettes and the block must be so designed to be able to accommodate them.

Underneath of the extrusion section should be located a metal frame, just like in a laboratory for organic synthesis, but it must have strength appropriate for the size and weight of the equipment. All elements needed for the experimentation and for characterization of the process may be fastened on the railing. For the purpose of fastening the various elements on the railing, a set of clamps standardized for the machine is necessary.

The quench system ought to consist of modules of possibly variable length to allow for greater flexibility in assembling any length within small increments. All types of quench may be used here, coaxial, with the easiest subdivision into modules; cross flow or cross flow with recirculated air. The last variation is highly recommended, particularly for experimental work, but also for commercial machines since it offers a better air pattern in flow through the fiber line and reduces fiber-to- fiber variability. Increased ecological friendliness of the recirculating system is not without great significance.

The quench modules of all types should have provisions for use of characterization equipment, i.e. see-through window strips on two opposing sides with a possibility to open small sections of the windows for those techniques which cannot tolerate glass obstruction.

Another provision of importance are heaters delaying quenching. These must be built in small modules, but a total length of some 75 cm might be found useful.

Such heaters must also be equipped with transparent windows.

Work with a small number of filaments requires careful regulation of quench. Extrusion into stagnant ambient air (room temperature) results in as rapid cooling as may not be easily attainable with five hundred filaments. For this reason, the same heaters may be used also to slow down the cooling, not only for a total delay. For the same purpose, all of the quench systems with air temperature higher than ambient may be used. For this kind of experimentation, the cross flow quench with air recirculation is the most suited, the most convenient, and interferes the least with the general working ambiance.

Fume removal usually needs to be separate for each quench system and quench delay, as these pieces of hardware need to cooperate. A careful design that obtains a good match is to be recommended.

The choice of transporting rollers may be a little difficult. The question is whether to use the multiple wrap system or the S-wrap system. Another question is whether to build the moduli of single rollers and set them appropriately, or to combine two rollers in one package. The single rollers represent more flexible, but also a slightly more expensive, solution – each roller has a separate motor which needs precise velocity synchronization. The roller pair packages are heavier and more difficult to realign. The single rollers, with a good mounting bracket design may be easier to use both for multiple and S-wrap. One must remember that for the S-wrap, the rollers within a pair rotate in opposite directions.

Generally, a minimum of three pairs of rollers are needed: take-up, drawing, and relaxing. If drawing is to be done in more than one step, then each additional step requires an additional pair of rollers. The number of rollers may need to be increased if there is the necessity of covering a very extensive range of velocities. Generally, velocity regulation spans a range of 1 to 10.

Depending on the aims of the experimental work, drawing, or lay- down, jets may be considered in addition to, or instead of, the rollers.

As the preferred configuration of the machine from extrusion to take-up is vertical, the drawing section may be arranged horizontally. A decision on this point may depend on the availability of sufficiently high space. The operation of such a machine requires an vertically movable platform because of the variability of quench zone length, as well as possible changes of the configuration.

It is quite obvious that depending on the expected application of the fibers, different types of devices to receive the drawn fibers may be required – a bobbin winder, staple cutter, or others.

For successful research, the process characterization possibilities are equally important as the machine itself. Basic equipment for the purpose includes:

- Infrared equipment for measurement of the fiber surface temperature (and other surfaces).
- Photographic equipment with a *telemicroscope* or a high class, very long focal length objective, which allows photography on a close distance.
- Laser Doppler anemometer (LDA) for measurements of filament and air ve-

locities (not mandatory but necessary). In absence of an LDA, a set of good anemometers.

- X-ray diffraction and low angle scattering equipment (not mandatory but very important).
- High precision fiber tension meter.

There are necessary provisions for mounting of the characterization equipment on the frame with the possibilities of the vertical movement along the threadline, and also with the access to the spinline (i. e. the windows as indicated above).

A machine for dry formation from solution may be built very much like one for the formation from melt. The extrusion section is likely to be replaced with a nitrogen pressure feeding of the metering pumps directly from the dissolution equipment. An appropriate solvent recovery system (adsorption on active carbon) is a must. The rest of the machine is almost identical to that for the formation from melt.

The wet formation from solution has the smallest possibilities for variations. The extrusion section should be substituted like in dry formation. It is important to have the coagulation baths of different (variable) lengths. The method of just moving the spinnerette closer to the take-up roller to shorten the bath does not solve the problem adequately. Control of the flow of the coagulating bath becomes difficult. Also, use of LDA may be problematic in this case. Solvent and nonsolvent recovery needs to be done according to the solvent system used.

Experiments with a new polymer start from the absolute minimum of polymer usage. Normally new polymers are in short supply. Formation experiments start from the smallest number of filaments. Quenching must be designed appropriately to increase the number of filaments while maintaining unchanged technological variables. In the case of other development work, it is equally important to experiment with the future in mind and always asking the question: Will it be possible to duplicate the results on an appropriately large scale? A good experimental machine allows far reaching increase of scale and almost automatically forces the question: How will it be when we make more filaments?

IX.4 References

1. Z. K. Walczak: *Formation of Synthetic Fibers*, Gordon and Breach, London – New York, 1977, chapter 9.
2. W. E. Fitzgerald and J. P. Craig, *A. C. S., Polymer Preprints*, **7 (1966)**, 742.
3. R. E. Johnstone and M. W. Thring: *Pilot Plants, Models and Scale-up Methods in Chemical Engineering*, McGraw - Hill, New York, 1957.

X FIBER PROPERTIES

Properties of polymers are not as constant as properties of low molecular weight compounds. The large size of the molecules and the resulting state of not necessarily full thermodynamic equilibrium lead to a range of properties. Fibers are not an exception from such behavior.[1,2] Thus, polymer properties depend not only on the type of polymer, but also on the physical perturbations of the material during processing. For any given polymer one may define only a range of properties which may be obtained. The processing determines finally where within the range a property may fall. The physical changes taking place in processing may proceed in various ways, and depending on the specific perturbations, different types of properties may change in different directions and to relatively different degrees. A set of those physical perturbations a material undergoes during processing is commonly referred to as the material history. This character of *"one material with many possible properties"* makes polymers so interesting and valuable, despite that a certain degree of difficulty is involved in processing them.

This chapter summarizes the directions of changes various fiber properties may undergo depending on the changes in the polymer properties and on the changes of different "unit processes" in fiber formation. For general descriptions of fiber properties the reader is referred to the monographs in that field.

X.1 Properties Dependent on the Polymer

X.1.a Polymer Chain Structure

As stated above, the polymer determines the range of properties which may be imparted to fibers. The definition of the possibilities a polymer offers is for some properties known better than for others. Which of the properties are better defined in terms of processing seems to depend on the importance of the property; those of primary importance were researched first, knowledge of others may still lag behind.

Modulus of elasticity is usually considered as one of the more important properties, therefore it seems to be better described. The limits of modulus for polymer, and fibers, have been quite well established theoretically from calculations based on the deformation of polymer chains,[3–7] and from the velocity of propagation of deformation impulses.[8] Experimentally, the moduli were determined from the relationship between stress and the deformation of crystalline lattice as detected by x-ray diffraction.[9–12] The values of calculated and experimental moduli of elasticity for polymer crystals of fiber forming polymers are collected in table X.1. Figure X.1 shows the stress - strain relationships for the single chains of different kinds of polymers, but these relationships do not coincide with the stress - strain curves characteristic for fibers. The moduli of elasticity determined in the direction perpendicular to the polymer chains axis amount only to some 0.8 to 5.5 per cent of the modulus determined parallel to the chain axis. On the other hand, he mod-

uli of amorphous polymers have been estimated to range only between $0.29 \cdot 10^{10}$ and $2.45 \cdot 10^{10}$ Pa. The maximum value represents cellulose,[8,9,15] though this is without consideration of the high performance polymers.[87,88] The anisotropy of modulus is very large indeed. And so is the disparity between the crystalline and amorphous properties.

Table X.1
Moduli of Elasticity of Polymer Crystals.

Polymer	Modulus of elasticity, $Pa \times 10^{-10}$			
	Parallel to polymer chain axis			Normal to chain axis
	Calculated		Experimental	
	from chain deformation mation	from impulse propa-gation[8,14]	from x-ray dif-fraction	
Nylon 66	15.7[4]	21	13.7[9]	
Poly(ethylene terephthalate)	18.2[7]		7.45[10]	
Poly(ethylene terephthalate)	14.6[4]	21.6	13.7[9]	
Poly(ethylene)	34.0[5]	19.4	23.5[10]	0.196[13]
syn-Poly(vinyl chloride)	16 to 20[6]	12.45		
Poly(isobutylene)	7.0 to 8.0[6]			
iso-Poly (propylene)	4.9[6]	8.74	4.11[10]	0.226[13]
Poly(vinyl alcohol)		16.8	24.5[10]	0.706[13]
Poly(vinylidene chloride)	9.8[8]	9.35	4.07[10]	
Cellulose	18.0[4]	13.8		
Cellulose	7.75 to 12.1[3]			
Cellulose	5.7 [14]			
Cellulose triacetate	5.89 to 8.83[8]	8.24		
Poly(acrylonitrile)	14.7[8]	13.25		

The moduli of elasticity of conventional fibers normally amount to some 3.75 to 22 per cent of the X-ray determined modulus of any given polymer. This is an obvious reflection of the dual nature of fiber structure, the crystalline - non-crystalline relations, both quantitatively and qualitatively. Qualitatively means, of course, the morphology. In high performance fibers the moduli may reach up

to about 30 per cent of the X-ray determined moduli of a crystal of the respective polymer. The moduli fibers from the same polymer may span from 2 to 20 times higher than the moduli estimated for the amorphous segment of the fiber structure.[15]

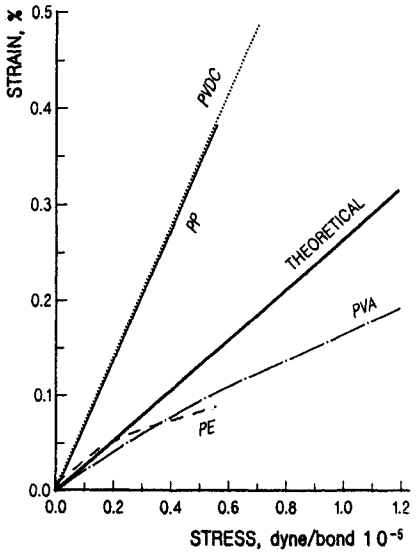

Figure X.1: *Stress - strain relationship for polymer molecules: the flat zigzag chain is indicated by the line named "theoretical"; poly(vinylidene chloride) (PVDC); polypropylene (PP); poly(vinyl alcohol) (PVA); polyethylene (PE). After Perepyol'kin*[8]

Investigations of the elasticity of polymer chains conducted by Sakurada and Kaji[12] indicate that the modulus of elasticity depends primarily on the chain conformation. Data supporting this conclusion are quoted in Table X.2 which gives the relationships of the mechanical chain properties in relation to the chain conformation. Figures X.2 and X.3 provide a communication reference regarding chain conformations. Those polymers which have fully extended chains, *trans*-configuration, have the largest force requirement for an extention of one per cent, which ranges from 4 to 5 *dyn/chain*. The force needed for extension of one per cent decreases with the extent to which the conformation deviates from that of a fully extended backbone. The force requirement reaches a minimum for the loose conformation of the type *trans' - trans' - gauche' - gauche'*. Conformations with regular helices have intermediate force requirement.

As one may conclude from the work of Sakurada and Kaji,[12] the modulus determined for amorphous polymers represents moduli based on the uncoiling of the amorphous molecules and not on the chain stretching. This is compatible with the views expressed in chapter V; the data reported by Sakurada and Kaji are for only one per cent of strain. At larger strains the situation may certainly look differently.

Sakurada and Kaji[12] report also another important observation: the level of forces acting in the direction normal to the chain axis, like in highly polar polymers,

Table X.2

Chain Conformations and Moduli[12]

Polymer	Chain conformation	Modulus of Elasticity $Pa \cdot 10^{10}$	Chain cross section area $m^2 \cdot 10^{20}$	Force for 1% chain strain *dyn*
Polyethylene	T (*zigzag*)	23.5	18.2	4.28
iso-Poly-(propylene)	TG (3/1 helix)	3.4	34.4	1.18
Poly(vinyl alcohol)	T (*zigzag*)	25.0	21.6	5.4
Poly(vinylidene chloride), α form	TG'TG'	4.1	35.1	1.43
Poly(pivalolactone), α form	T'T'G'G' (2/1 helix)	0.65*	44.8	029
Poly(ethylene oxybenzoate), α form	—	0.59	49.8	0.29
Poly(ethylene terephthalate)	TT' (near *zigzag*)	10.1	20.4	2.24
Nylon 6	TT'T'TT'T' (near *zigzag*)	16.5	18.0	2.97
Nylon 66	TT'T'TT'T' (near *zigzag*)	17.3	17.9	3.1
Nylon 610	TT'T'TT'T' (near *zigzag*)	19.6	18.0	3.52

does not have an influence on the modulus in the direction parallel to the chain axis.

There were many attempts to relate the fiber moduli to the degree of crystallinity present in the fiber.[15,18] Those considerations were based on different models of distribution of the crystalline and amorphous areas. Successes of these efforts were limited; the obtained results better fit experimental data for bulk, unoriented materials rather than oriented fibers or films.

The *high performance* polymers, like poly(p- phenylene phthalamid) ($Kevlar^R$), poly(p–phenylene-benzo-bis-oxazole), poly(aryl- ether-ether-ketone), and others have very high moduli as one of the main properties qualifying them for the *high performance* group. What they have in common is the high degree of chain rigidity which results primarily from the chains built of cyclic monomers. Because of the high chain rigidity, even in solution the molecules do not coil but assume rod-like conformation. Consequently, these polymers crystallize predominantly in the extended chain conformation. Lack of the folded type crystallization leads to structures which are closer to the extended chain crystals rather than to conventional fibers. The noncrystalline fraction present in those polymers is mostly due

to imperfections in polymer chain structure or due to some steric hindrances during crystallization process. In general, crystallinity of such polymers is very high. Quite naturally, the structure - property relationship for such polymers deviates significantly from that for the polymers with flexible chains. For example, the rigid chain polymers show modulus in the direction parallel to the chain axis comparable to steel or glass.[19] Some of the commercial fibers have moduli exceeding 1000 g/den, while theoretically it is possible to reach around 2500 g/den.[20]

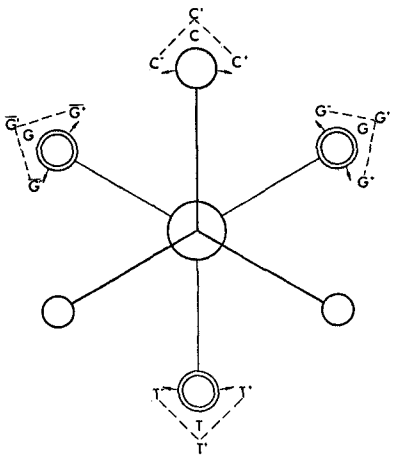

Figure X.2: *Diagram of various chain configurations: C for cis, G for gauche, T for trans.* The superscripts indicate a deviation: positive, negative, or general (apostrophe). *After Sakurada and Kaji*[12]

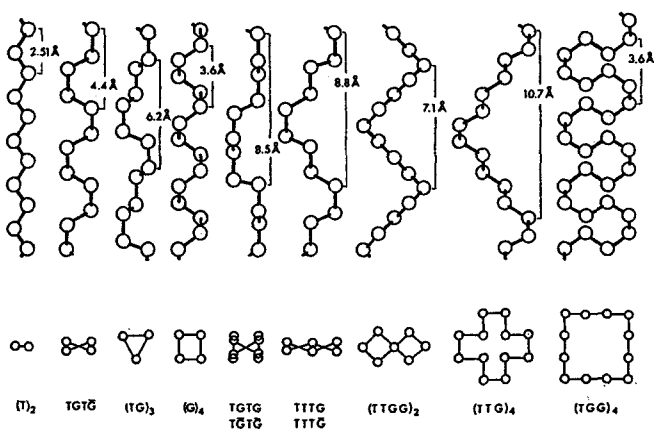

Figure X.3: *Basic chain conformations for linear polymers. After Bunn*[16] *and Mizushima et. al.*[17]

Another group of high performance fibers may be obtained from polymers with flexible chains *via* very extensive drawing (ultradrawing). The spun fibers which

perform best in ultradrawing are made from polymers with a low level of chain entanglements, *e. g.* in gel spinning. The drawing is performed in several stages, so to assure chain propagation within the crystal. Ultimately, this leads to fiber structures approaching straight chain conformations. Similar results are obtained with solid state extrusion.[91&ref]

The basic properties of polymers, as usually quoted in the literature, may be greatly affected by irregularities in polymer structure or by impurities. Impurities are understood here as the fractions of polymer with molecules of greatly deformed structure or a larger amount of additives. Inclusion of abnormal monomer addition, as for example of syndiotactic - isotactic, or head-to-head nature, may strongly affect crystallinity and the crystallization process by affecting chain conformation, mostly by making the chains more flexible. Similar effects may result from low molecular mass impurities, but if not present in larger quantities, they may be somewhat less harmful as it is possible for them to undergo some kind of fractionation during the processing. During a crystallization process the low molecular mass impurities are usually pushed into the amorphous phase, though the crystallizability and crystallization kinetics will, most likely, be affected.

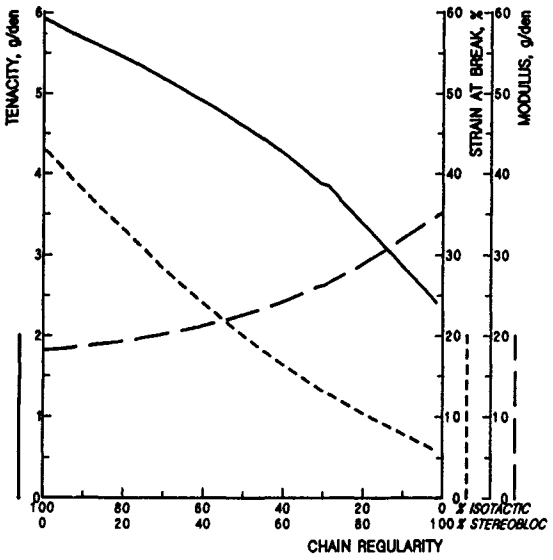

Figure X.4: *Tensile properties of polypropylene fibers in relation to the regularity of polymer structure. After G. Natta*[21]

Chain imperfections mostly can not be expelled or fractionated, and therefore may cause either a decrease of crystallizability, or a change of crystallization rate, or both. The influence of imperfect polymer structure is exemplified in figure X.4 where there are given tensile properties of polypropylene fibers in relation to the stereoregularity of polymer. The magnitude of the effect requires no additional comments.

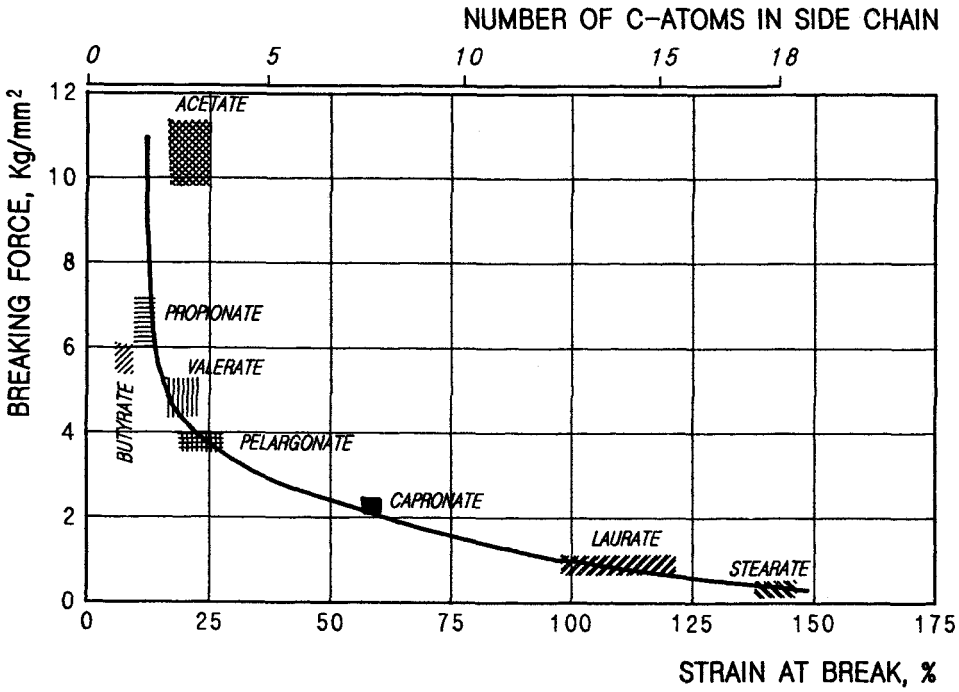

Figure X.5: *Tensile properties of fibers made from cellulose esters with different lengths of side chains. After Hagedorn and Mőller.*[22]

Chain branching, an additional kind of structural irregularity, may have an effect similar to other chain imperfections; a decrease of crystallinity and crystal perfection are mainly observed. In general, short branches in large numbers are more detrimental than a few very long ones. The influence of the side chain length on fiber tensile properties is exemplified in figure X.5 which presents data for the series of cellulose esters of different length of the acid chain.[22] This is an excellent example showing the influence of the side groups with increasing uniform length. Full analogy should be expected between the cases of side chains resulting as a reaction byproduct and the effect of the side chain introduced on purpose; the effect on polymer properties must be expected to be equivalent. This principle is the basis for the development of the linear low density polyethylene (LLDP). The difference is that in the case of the abnormalities arising in synthesis, the side chains are usually of variable length so no such nice graph could be produced.

One must take seriously the possibility of cross linking of polymer chains. Often the fraction of cross linked polymer is encountered in small quantities, about 0.0001%. If the quantities are so small, they may have an influence on the resulting fiber modulus. However, processing of such polymers is proportionately more difficult. A gel content higher than some 0.0005% normally causes major problems with formation, primarily with the process continuity, with filament breaks. Filters become clogged easily, which also leads to process discontinuity. If the cross links

are generated after the fiber formation, then this represents an entirely different, usually more positive situation.

X.1.b Effect of Molecular Mass

A strong influence of molecular mass on the mechanical properties of fibers was realized already in the very early days of fiber formation history, primarily in connection with cellulose fibers.[2] With progressing development, the originally proposed relationships were confirmed for other polymers.[23,24] H. F. Mark published the dependence of fiber tensile strength on molecular mass already in 1932.[25] Mark's relationship, although entirely general in nature, is shown in Figure X.6 for the case of nylon 66.[26] The relationship was presented in the following mathematical form.

$$\Theta = \Theta_\infty - \frac{B}{M_n} \tag{X.1}$$

where Θ is fiber tenacity originally expressed in the weight titer (denier), Θ_∞ is a constant equal to the fiber tenacity at infinite molecular mass, B s a constant depending on the polymer, and M_n is number average molecular mass.

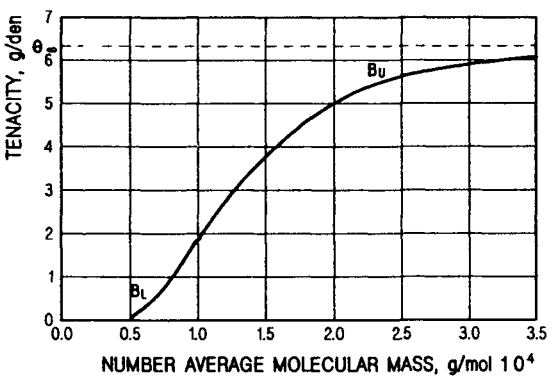

Figure X.6: *Dependence of fiber tenacity on number average molecular mass for nylon 66. After H. F. Mark*[26]

Mark's relationship was confirmed by Sookne and Harris[23] and elaborated on by P. J. Flory,[27] who found it more convenient to plot the data against the reciprocal number average molecular mass, or even better, the reciprocal degree of polymerization.

The curve reproduced in figure X.6 has two transition points indicated as B_U and B_L. If the molecular mass is smaller than that corresponding to B_L, no fiber with useful properties may be obtained. If the molecular mass is increased beyond the point B_U, no significant gains of tenacity is observed, the extra effort to produce and process higher molecular mass polymer is wasted. The part of the curve contained between the two transition points, B_L and B_U, is steep and, in industrial practice, operation on such a steep slope is not advisable, small variations in the molecular mass of a commercial polymer may cause large changes

in fiber properties resulting in nonuniform product quality. Ideally the molecular mass of the polymer should be slightly higher than the upper transition point, B_U. For some polymers, mainly for those obtained in polycondensation reactions, use of high molecular mass polymer may be unfeasible due to the high costs of the appropriate polycondensation reaction. The transition points for different polymers are quoted after H. F. Mark in Table X.3.[26]

Table X.3

Transition Points in the Influence of Molecular Mass on Fiber Tenacity.

Polymer	B_L		B_U	
	Number average		Number average	
	molecular mass g/mol	molecule length $\mathring{A}$	molecular mass g/mol	molecule length $\mathring{A}$
Nylon 66	6000	425	24000	1800
Nylon 6	6000	452	24000	1810
Poly(ethylene terephthalate)	8000	440	30000	1300
Poly(acrylonitrile)	15000	705	45000	2110
Poly(vinyl alcohol)	15000	870	45000	2600
Cellulose	20000	575	75000	2160
Poly(vinylidene chloride)	25000	515	75000	1920
Polystyrene	60000	1440	300000	7230

Although the molecular masses of the transition points vary substantially for polymers of different kind, the lengths of the stretched molecules are similar within relatively narrow limits. The data of table X.3 indicate that the strong polarity of a polymer tends to decrease the length of the molecule corresponding to the B_U transition. The trend is reverse for polymers with poor crystallizability. It is necessary to underline the apparent contradiction of this finding and the statement made in the previous section that the polar forces do not influence the polymer modulus. The only way the discrepancy may be explained is that here it concerns the fibers, their crystalline and amorphous phase, while in the previous section the questions were related to the crystalline phase only.

The relationship between tenacity and molecular mass was the object of many re-examinations by different authors. In cases when Mark's results were challenged, the experimental evidence invariably was in doubt.

The fact that the potential fiber strength depends on number average molecular mass has important practical implications. With the increasing broadness of molecular mass distribution and constant number average, the weight average, naturally, must increase. Since rheological properties are proportional to the

weight, or to z- average, or to a combination of both, the increased breadth of the molecular mass spectrum requires more mechanical work without any gains in fiber strength. Since relaxation time changes in a way similar to the other rheological properties, widening of the molecular mass distribution must change the whole processing characteristics at potentially unchanged maximum of the obtainable fiber strength.

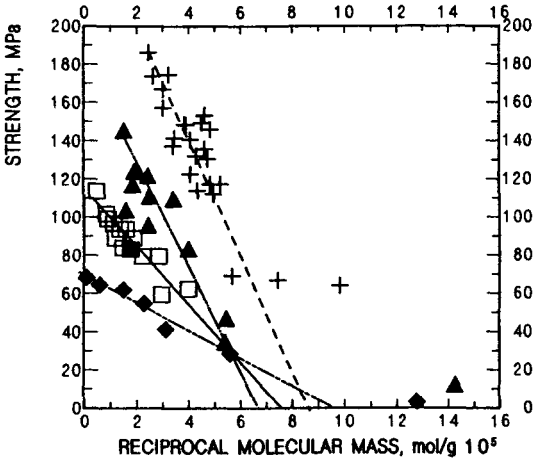

Figure X.7: *Strength versus reciprocal number average molecular mass. Open symbols denote monodisperse (fractionated) samples, filled points denote polydisperse samples, crosses denote bending strength at $-196°C$. Squares – cellulose acetate,*[23] *crosses – poly(ethylene),*[32] *triangles – aromatic polyimide,*[33] *diamonds – poly(methyl mathacrylate).*[36]

The strength of polymers depends also on the number of chain entanglements or *enchainments* present in the polymer.[6,28--30] Figure X.7 presents the relationships between the reciprocal number average molecular mass and the breaking strength for a number of polymers. The good correlation, considering the matter and the experimental problems involved, of the data is quite well visible. The values of M_t, it is of the molar mass where the polymer strength reaches zero, are close to the values of B_L quoted in table X.3. It has been suggested[31] that there is a relationship between M_t and molar mass critical for formation of entanglements $M_t = 2M_e$.

In brittle materials, the tensile strength is assumed to result from the simultaneous fracture of all the load bearing bonds in the cross section where the fracture takes place.

$$\Theta = n\, f \tag{X.2}$$

Here Θ is strength (tenacity), n is number of load bearing bonds per unit of cross section area, and f is the strength of an individual bond.

F. Bueche[34] proposed the following formula to calculate the maximum strength.

$$\Theta_\infty = n\, f = \left(\frac{\rho N}{3M_e}\right)^{2/3} f \qquad \text{at } M = \infty \tag{X.3}$$

The notation here is: Θ_∞ - maximum attainable strength, ρ - density of polymer, N - Avogadro's number, M_e - Molecular mass critical in respect to the entanglements.

To equation X.3 D. T. Turner[30] applied Flory's end correction factor[35] to obtain the following equation for strength.

$$\Theta = n\, f = \left(\frac{\rho N}{3M_e}\right)^{2/3} f\left(1 - \frac{2M_e}{M}\right) \tag{X.4}$$

Further, by combining equations X.3 and X.4, Turner obtained an equation very similar in form to the Mark-Flory equation X.1.

$$\Theta = \Theta_\infty - 6.8 \cdot 10^{15} \rho^{2/3} M_e^{1/3} f\left(\frac{1}{M}\right) \tag{X.5}$$

Thus, it appears that the number average molecular mass is really the determinant of of the obtainable fiber tenacity, however, there is still no certainty. Intuitively, one might expect that molecular mass distribution ought to play some, though not a necessarily large, role. More research is needed for full clarification of the issue. There seems to be no doubt, though, about the role of entanglements in the strength of polymers.

A role similar to the molecular entanglements are played by those *hard blocks* in the block copolymers which work on the basis of high glass transition temperature. A functionally similar role is played by those hard segments which are based on strong intermolecular forces, though there is some difference between the two.

X.1.c Thermal Properties

The equilibrium melting points are constant in polymers, but they rarely may be reached in practice. One may treat them as a theoretical limit. How much of this potential will be reached in any given fiber depends on the processing; melting point of crystals depends on the temperature of their growth.

Since normally polymers are not all crystalline, one needs also to take note of the amorphous material. Its basic properties, like chain flexibility and relaxation character (to a large extent, but not completely) belong to the material character. The whole rest, in terms of its behavior, depends on the processing.

Presence of a solvent causes differences in the polymer crystallization and melting, it also influences the behavior of the noncrystalline fractions, particularly in terms of accumulating stresses and in their relaxation. Presence and absence of solvent is a processing feature and as such is discussed in section X.2.b and in chapter VII.

X.2 Influence of Processing on Properties

The effects of *history* of the mechanical and thermal perturbations on polymers are discussed over large portions of this book. Mostly the discussion is of the *shear*

history and, to a lesser degree, the *not so near history*. Technologically speaking, the *near*, and *not so near*, history is nothing else but the effects of a processing of the raw material, as well as sum of relaxation processes which took place at different stages. The term *history* in this case is a kind of "shorthand" convention to describe the influence of a processing on the fiber properties. Naturally, it is an indirect influence *via* the the influence on fiber structure.

X.2.a Tensile Properties

Cold drawing (or neck drawing) is the principal mean of building up the tensile properties of fibers. The potential effect of neck drawing depends on the structure of undrawn (or spun) fibers.[83,89] There are some authors[84--86] who claim the opposite, in disregard of what has been found over the years of fiber industry existence. The structure of undrawn fibers depends on the type of the formation process, as well as on the details of the process conditions, and the last relationship is of a high sensitivity. Naturally, as discussed in the preceeding section, everything takes place within a framework offered by the polymer in question. All of these truisms were realized for a long time,[37-39] though not described in easily accessible way.

An interesting opinion about the relationship between molecular mass and type of process has been expressed by the team of P. Smith, P. J. Lemstra, and J. P. L. Pijpers;[40] their opinion is represented in figure X.8.

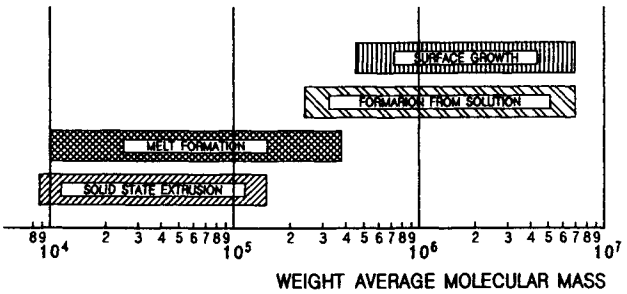

Figure X.8: *Approximate match between the type of process and molecular mass for polyethylene. After P. Smith, P. J. Lemstra, and J. P. L. Pijpers*[40]

The scheme of figure X.8 is somewhat idealized since, depending on the polymer and its chemistry, there are limitations on the attainable molecular mass or solubility. Nonetheless, the same authors published interesting data on the property buildup in fibers formed from polyethylene, depending on the molecular mass and on the type of process. Some of their results are presented in figures X.9 and X.10. The first of the figures presents the relationship between the initial modulus and tensile strength if a fiber formed from the melt is cold drawn to various degrees. The three different curves represent molecular masses: $M_n = 13 \cdot 10^3$ and $M_w = 100 \cdot 10^3$; $M_n = 28 \cdot 10^3$ and $M_w = 115 \cdot 10^3$; $M_n = 110 \cdot 10^3$ and $M_w = 120 \cdot 10^3$. Thus, the weight average molecular masses are close to each

other and the number averages vary widely. Figure X.10 presents similar data but on fibers formed from a solution and cold drawn, as the previous set. The molecular masses were: $M_n = 120 \cdot 10^3$ and $M_w = 800 \cdot 10^3$; $M_n = 150 \cdot 10^3$ and $M_w = 1.1 \cdot 10^6$; $M_n = > 300 \cdot 10^3$ and $M_w = 4 \cdot 10^6$.

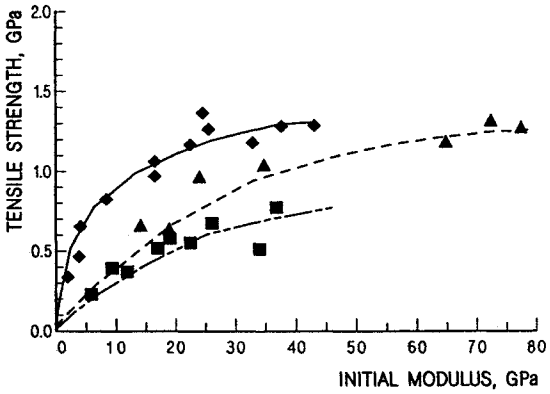

Figure X.9: *Tensile strength-modulus relationship for fibers formed from melt and neck drawn to various draw ratios. Squares – $M_n = 13 \cdot 10^3$ and $M_w = 100 \cdot 10^3$; triangles – $M_n = 28 \cdot 10^3$ and $M_w = 115 \cdot 10^3$; diamonds – $M_n = 110 \cdot 10^3$ and $M_w = 120 \cdot 10^3$. After P. Smith, P. J. Lemstra, and J. P. L. Pijpers*[40]

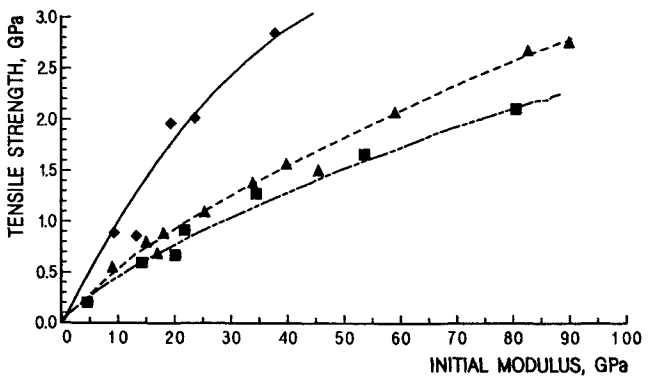

Figure X.10: *Tensile strength-modulus relationship for polyethylene fibers formed from a solution and neck drawn to various draw ratios. Squares – $M_n = 120 \cdot 10^3$ and $M_w = 800 \cdot 10^3$; triangles – $M_n = 150 \cdot 10^3$ and $M_w = 1.1 \cdot 10^6$; diamonds – $M_n = > 300 \cdot 10^3$ and $M_w = 4 \cdot 10^6$. After P. Smith, P. J. Lemstra, and J. P. L. Pijpers*[40]

In both of these figures, the maximum obtainable tenacities appear to fit the equation X.1, with the data scatter not larger than any other sets. What is important here is the good depiction of matching the method of formation with molecular mass. The second point is that the initial modulus of a fiber is not in a linear relationship with the strength of the same fiber; and the slope of tenacity *versus* initial modulus invariably increases with the increase of molecular mass.

Very similar results to those by Smith, Lemstra, and Pijpers were reported by

M. Kanamoto and co-workers.[41–43] From all of the reports quoted here transpires that the factors controlling the drawability are limited to the density of entanglements and to the number of tie molecules in the undrawn material. Also, in case of semicrystalline polymers the results of the drawing operation depend on the same factors. The latter of the factors is usually related to the prior one anyway. Kanamoto and co-workers[41–43] report also that in the case of two stage drawing, the drawing performance and the results depend on the same factors: the chain morphology, as well as on the crystalline morphology, of the undrawn material, in poly(ethylene terephthalate) in this case.

The amount of crystallinity in the predrawn material is equally important.[89] Not in all polymers is it as easy to obtain a low, or even practically non-crystalline material as in case of poly(ethylene terephthalate). Low crystalline material is easier to draw, more extensive draw ratios are possible and higher strength may be obtained. Also, the degree of crystallinity in such cases increases. Contrary to this, if the initial degree of crystallinity is high, upon drawing it often decreases. These results represent a confirmation of what was determined earlier by R. Bonart,[44] as is evident from figure X.11.

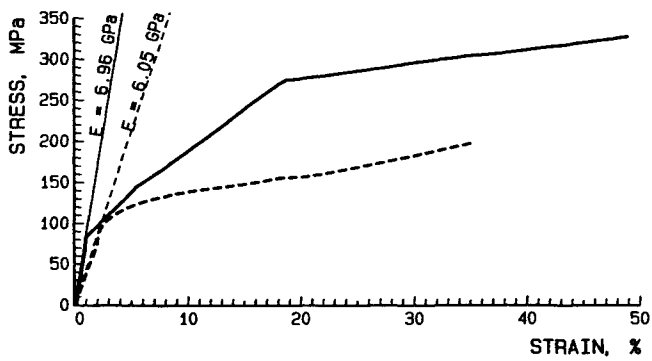

Figure X.11: *Stress - strain curves for poly(ethylene terephthalate) fibers: full drawn line: paracrystalline, room temperature drawn, low crystallinity, high modulus; dashed line: drawn at 125°C, higher crystallinity with relaxed amorphous regions, lower modulus. Quoted after R. Bonart.*[44]

In addition to the importance of the degree of crystallinity, or may be even more important, is the size of the crystalline blocks (along the a and b crystallographic axes).[44] The size of the paracrystalline blocks determines, to a large extent, how many *link molecules* will be formed. The link molecules are formed mostly from the polymer chains on the peripheries of the crystalline blocks, and for the smaller blocks, the ratio of the circumference to the volume of the block increases. Besides, clearly mechanically, the smaller units are easier to relocate, also, they lead to a better distribution of tensile force. With increasing number of link molecules, the strength, and possibly modulus, increase.

How can the important features of morphology in undrawn fibers be regulated? Degree of enchainment depends on the molecular mass, and therefore tenacity potentially increases with molecular mass. However, the degree of enchainment may

be influenced by a balance of shearing - relaxation processes, and therefore so much space is devoted in this book to this and related topics. The size of crystallites is found to depend on the crystallization rate during fiber formation.[49] The shorter the total time of crystallization, the larger the sizes along the a and b crystalline axes. The slower the process of crystallization, the smaller crystalline blocks are formed. This has been known for long time; a slow formation process produced material which was easier to draw and better properties could be obtained.

It is necessary to remember that there are no miracles; increase of axial modulus is invariably connected with corresponding decrease of the modulus in the direction normal to the fiber axis. This principle is very well depicted on the diagram of the macroscopic modulus of fiber elasticity in relation to cold draw ratio published by Rauman and Saunders.[50] This diagram is reproduced in figure X.12. The diagram is a result of studies of unidirectionally stretched film of polyethylene. The authors stress that the result of drawing depends on orientation of both the crystalline and the amorphous phase; the properties of both phases are oriented likewise. The relatively very small values of the modulus in the direction of 45° to the direction of drawing are worthy of being remembered.

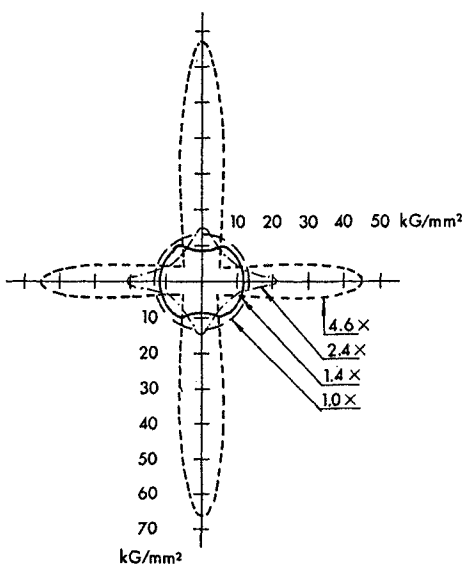

Figure X.12: *Macroscopic modulus of elasticity in relation to the ratio of cold drawing as obtained for polyethylene film. A polar diagram after G. Rauman and D. W. Saunders.*[50]

Another aspect of tensile properties is the mechanical stability of the fibers, or otherwise its succeptibility to creep. The creep in fibers is mostly considered as a negative property, and something to keep at the lowest level possible. High crystallinity, low modulus, and low orientation favor creep resistance, particularly the unrecoverable creep deformation.[38,44,51] Other factors diminishing creep are a higher molecular mass and polar character of the polymer chains. Darlington

and co-workers concluded that essentially every aspect of fiber structure has an influence on creep.[53]

Higher modulus leads to higher creep. Higher modulus may be easier obtained when the fiber is drawn with neck at a lower temperature, closer to the glass transition, though not below it. And also the lower the temperature of the plastic deformation, the higher the succeptibility to creep.[45,53] And all this is in agreement with what was said before. Namely, lower crystallinity in drawn fibers favors high modulus[44,90], but stability (creep resistance) is favored by a high degree of crystallinity, provided that all other elements of structure are equal. As Darlington and co-workers found,[53] one should not even attempt to compare fibers of the same draw ratio, if drawn at different temperatures. In effect, one needs a compromise. Among two fibers with the same modulus, the one drawn at higher temperature will have lower creep. If possible, it is better to regulate the modulus not with temperature but rather with other means.

At this point it is necessary to mention another preference, if the fiber quality is of high interest. The closer a fiber is drawn to its maximum draw ratio the more stable is its structure, including a low creep. If a fiber is *incompletely drawn* then it may be more or less easily deformed additionally, despite the structure stabilization by the time factor, otherwise called aging.[52] Ideally then, a fiber ought to be drawn to its practical maximum, without incurring excessive breaks in the neck drawing. If a fiber of lower modulus is required, *e.g.* for soft and pliable apparels, the maximum draw ratio ought to be reduced by adjusting the formation process so to develop an appropriate structure in the undrawn fiber.

It is necessary to underscore that an increase of elongational strength and modulus is accompanied by a decrease of transverse strength. The better the fibrils are defined, the more stretched are the link molecules, the smaller is the cohesive force between the stretched molecules and between the fibrils.[89] The first and most obvious casualty of a low transverse strength is low abrasion resistance and peeling. By nature of polymers both high axial and high transverse properties cannot be had. High performance fibers are an example for this. Thus there are choices that must be made.

X.2.b Thermal Properties

As repeated many times earlier, the melting point of polymer crystals is not a material constant, it depends on the temperature of crystallization and solvent, if present. The prevailing mode of crystallization taking place during fiber formation is crystallization under strain, where the same rules are valid.[54] Additionally, it must be taken into account that crystallization during fiber formation, with the exception of some wet formation processes, does not proceed isothermally. Subsequent cold drawing is most often performed at more or less elevated temperatures rather than cold. In effect, fibers contain crystals of a wide range of long periods and the corresponding broad melting points.

The range of different melting points depends on the crystallization profile

which results from the interrelation of the temperature profile and the profile of accumulation of unrelaxed work. The latter profile depends on the elastic character of the polymer melt or solution, it is on the polymer succeptibility for the acceleration of crystallization by strain. If a polymer crystallizes "sluggishly", then the spun fibers have low crystallinity and some fraction of the polymer may crystallize during the neck drawing. If the fibers are drawn in a step separate from the formation, a secondary crystallization may take place during storage, and this means crystallization at more or less room temperature, which indicates low melting. In such cases the subsequent neck drawing may determine the final melting profile to a much greater degree than it would otherwise.

During cold drawing, the entropy of the noncrystalline fraction is reduced, which may be observed in small changes of melting point (equation IV.75). As a result of annealing, the stretched noncrystalline chains may retract to some degree. The degree depends on the temperature of annealing, and also on the temperature of the cold drawing. Relaxation during annealing is specially strong when the temperature of drawing was lower than the temperature of annealing. The last phenomenon does not have a full and plausible theoretical explanation, though encountered experimentally many times.

Fibers in use are often exposed to elevated temperatures, apparels are laundered, technical fabrics often work at elevated temperatures too. Elevated temperature causes the same effects as annealing, and mostly it is annealing without any, or little, dimensional restrain. Fibers must have some dimensional stability and the stability may be regulated by the thermal history, the crystallization profile, and by the drawing history. As it was sketched here, the ways to produce thermally stable fibers are rather complex, but regulation is possible. Naturally, post-production improvement is possible through annealing under dimensional restrain. This does have the advantage that it may not only increase the thermal stability but also pre-shrinks the material, which may be welcomed by the user.

X.2.c Sorption Related Properties

Besides the tensile and thermal properties, there are other important attributes: dyeability, water absorption, swelling. Despite the fact that all these properties are strongly related to the nature of the polymer molecules, they may be influenced by altering the super-molecular structure in the solid state.[55–60] Naturally, when a polymer, *e.g.* polyolefin, is incapable of absorbing water in quantities which may have a practical significance, any changes of the supermolecular structure cannot increase the absorptivity. When a polymer has a potential for sorption, then the changes of fiber morphology will influence the degree and kinetics of sorption.

Fluids or dyes may be adsorbed on the surface, but they may also diffuse deep inside the fibers. Adsorption on the surface is limited by the size of the surface, and diffusion inside is normally the slowest of all processes involved. As the slowest process, diffusion determines the overall rate of a complex process, like swelling or dyeing.[61] Since all fiber structures are anisotropic, it is natural that the diffusion rates are different in different directions, which is described by the

following equation.[62]

$$\frac{\partial C_A}{\partial t} + \frac{\partial C_B}{\partial t} + \frac{\partial C_C}{\partial t} = D_A \frac{\partial^2 C_A}{\partial x^2} + D_B \frac{\partial^2 C_B}{\partial x^2} + D_C \frac{\partial^2 C_C}{\partial x^2} \qquad \text{(X.6)}$$

where C_A, C_B, C_C are numbers of molecules of diffusant per volume of the media which are present in the crystalline phase, amorphous phase, and vacuoles, respectively, and D_A, D_B, D_C are effective diffusion coefficients in the crystalline phase, amorphous phase, and in the vacuoles, respectively. Crystalline lamellae are basically impermeable[60], which means that $D_A = 0$. Consequently, diffusion in a fiber depends chiefly on the diffusivity in the amorphous phase and in the vacuoles. But there is one additional factor to be considered: κ, the influence of the tortuosity of the diffusion paths. The diffusing molecules must execute a "slalom" between the crystalline segments of the fiber structure. The coefficient of tortuosity may be determined from

$$\kappa = \frac{\bar{D}}{D_B} \qquad \text{(X.7)}$$

where $\bar{D}$ is average diffusion coefficient in fiber. In practice, κ may be found from a plot of $\bar{D}/D_B$ *versus* the volume fraction of the crystalline phase in the fiber. Attempts to describe the structure factor quantitatively in relation to the measurable structural characteristics have not led to success yet.[62]

Another way of determining the diffusivity is based on the measurements of the glass transition temperature changes in relation to a solvent content.[63] More details on this topic are to be found in section VII.2.

Dyeing of fibers is one of the areas heavily dependent on diffusivity. Nonetheless, the diffusion of dyes depends on the polymer and its morphology as well as on the affinity of the dye molecules to the polymer chains. The stronger the dye adsorbtion on the surface of a polymer chains, the more permanent the molecule location within the fiber, the more difficult it is for the dye molecules to move around. The diffusion of dyes depends also on the size of the dye molecules or on the size of the molecule agglomerates in cases of disperse dyes. The size of the dye molecules is often larger than the available interchain distances in the amorphous phase, particularly if the fiber was highly drawn. In such cases, dying technology resorts to widening of passages through swelling of the fiber structure. Since the majority of fibers do not swell in water, or they swell insignificantly, *carriers* are used to swell the fibers gently, to help the dyeing process.[61,64] The carriers are removed from the fiber, the swelling recedes and the dye molecules remain clenched and trapped within the fiber structure.

Aside from the nature of the polymer chains and any physico-chemical interaction between the polymer and the diffusant, sorption depends strongly on the level of crystallinity and on the morphology. The diffusivity along the fiber radius initially increases with the draw ratio to reach a maximum at the draw ratio of about two. With the draw ratio increasing further, diffusion decreases again. The diffusivity along the fiber axis decreases steadily with increasing draw ratio,

without any maximum, and always is smaller than the diffusivity in the radial direction.[65–67] Thus, the orientation effect, rather the density increase connected to it, has a very strong influence on the diffusivity, even with the unchanged level of crystallinity.

Annealing initially causes a decrease of diffusion of dyes; after the diffusivity reaches a minimum, it increases again. Conditions of the annealing determine the location of the minimum of adsorption.[68] Diffusion of solvents, and its ultimate stage – solubility, changes in an analogous way.[69]

Dyeing is a two way process, the fiber morphology influences absorption of a dye, and presence of a dye in the fiber influences the fiber properties. The latter influence is small since the relative amounts of dyes are normally very small. When there is a necessity for the polymer molecules to undergo some realignment to accommodate the dye or other molecules, then this is connected with some change, usually an increase, of entropy.[70] Should the amount of dye or other material absorbed be larger, then the chain mobility may be restricted by the absorbed molecules. Whatever the dye uptake, degree of swelling, etc., presence of the " foreign" molecules finds a reflection in some change of the glass transition temperature.[71]

If the nature of the polymer allows adsorption of water or other solvents, then the adsorption proceeds according to the same rules as in the case of dyeing. There may be, however, quantitative differences related to the size of molecules; dye molecules are usually fairly large, while water and solvents have small molecules. The small molecules may be easier, or in larger quantities accommodated within the fiber structure.

X.2.d Fiber Uniformity

Uniformity of fiber diameter almost always belongs to the crucial parameters determining the product usefulness and quality. The uniformity of fiber diameter is related to the uniformity of the fiber morphology along the fiber axis. Uniformity, as a strong determinant of the fiber quality, represents an important economic factor. Thus, fiber uniformity is a matter of constant concern in the fiber manufacturing. The importance of securing uniformity in commercially produced fibers, along with the complexity of the problem, may well be the reason for the scarcity of publications in the field. General experience teaches that fiber nonuniformity may originate from many sources and reasons which may disturb the stability of the process. The analysis of fiber formation processes presented here gives sufficient indication of the extremely fragile nature of the process. The teachings of experience are in agreement with this. That is, probably, why fiber formation is still called an art. This section presents only the more important points concerning uniformity, the subject is mentioned often in other chapters.

One of the more common sources of nonuniformities in fibers is inhomogeneity of polymer.[72] Accidental mechanical impurities, lumps of cross linked (gelled) polymer, lumps of degraded polymer[73] belong in this category.[74] The character

of the polymer determines, to a large extent, the character of the impurities, *e.g.* its thermal stability, tendency toward cross linking, general efficiency of the polymerization catalyst as reflected in the chain abnormalities, etc. Poorly designed transfer lines, *e.g.* dead spots, constitute good conditions for generation of degraded polymer. It is self understood that the best remedy here are good, efficient filters. In some polymers, presence of gel is unavoidable. High shear rate in the filters, though still below the shear degradation of the matrix polymer, may be able to degrade, at least partially, gelled polymer as its molecular mass is high so its degrading shear rate may be well below the applied conditions.

It is self understood that extrusion from the spinnerette cannot result in a fractured flow. Narrow entry cones and relatively long capillaries are to be recommended here (see sections III.6 and III.7). Generally, it is not good to operate on steep slopes of die swell *versus* capillary length; small inaccuracies in the the capillary dimensions may increase fiber-to-fiber nonuniformities, and further they may cause differences in the degree of extension of the melt. Inaccuracies in the capillary drilling, minor changes in diameter, influence shear rate to the third power, and this may create conditions where some of the filaments will be closer to the critical shear rate than the other.[75]

The most sensitive area of the process is, without any doubt, the quench (or coagulation) zone. One of the most obvious reasons for nonuniformities is the presence here of an excessive drawing force (or speed, or initial stress on die swell). If the extension rate reaches a critical level, the extrudate becomes nonuniform.[76] If the extension is close to the critical value, any fluctuation in quench intensity may cause the flow to fracture intermittently, all this leads to uneven diameter.

As mentioned earlier, the segment of filament path where the polymer crystallizes almost always shows some signs of instability. The true reason for this is not known, though one may consider that a phase transition is by its nature a kind of instability. However, the question "why?" and "when?" about that instability cannot be answered yet.

Even greater potential danger of instabilities exists when at the end of the crystallization process the filament is still physically in the quench zone; when under the influence of high forces the cold drawing begins. In some commercial processes exist such, or similar, situations. Invariably there is a danger of diameter nonuniformities, at least intermittently. This danger increases with the increasing drawing force, which is often typical in formation of fibers for spunbond fabrics. (See chapter 11.)

Vibrations of the machine are easy to transfer to the filaments; contemporary high velocity transporting rollers may be quite capable of causing such vibrations. Turbulent flow of the cooling medium may cause similar effects.[80] All sorts of vibrations, or filament fluttering, cause periodically variable tension and this may be the cause of periodic uneven diameter attenuation of the formed fibers. This, in turn,may lead to small fluctuations in the development of structure, leading to uneven drawing, which results in diameter variations. The cycle of cause and effect becomes closed. The variable diameter, and especially the structural variations,

may lead to the formation of excessive differences in the local drawing ratios and to relatively large fiber unevenness in the cold drawing step.[46,81]

Uneven diameter may cause uneven heat exchange in the point of neck down. If so, then this would result in local variations of the draw ratio. Nonuniformity of quench may have very similar symptoms as vibrations,[72] and this may complicate the diagnosis of a case.

If the rollers are incorrectly designed, the filaments may slip on the surface of the drawing rollers, and this is another very obvious cause for generation of nonuniformities of fiber structure and diameter.

One has to take note that practically all conditions leading to filament nonuniformities result in a variable spinline tension[77] and velocity, so the tension, and/or the corresponding filament velocity measurements represent a primary diagnostic tool. Comparison of the tension in drawing zone with the tension in quench zone may help localize the point where the nonuniformities arise. Experience permits one to distinguish between some of the nonuniformities from the character of the tension and velocity fluctuations.

Depending on the structure of the undrawn fibers, there appears to be an optimum range of drawing temperature which is most favorable also for fiber uniformity.[77–79] Periodic stress oscillations and the resulting diameter changes have been noticed during drawing operations.[79] The conditions for such oscillations to take place appear to depend on the rate of deformation and on temperature inside the neck, as well as on the compliance of the sample. In this case the compliance has been defined in a somewhat unusual way: it is the change in the length of the sample divided in the stress causing the change.[79] Although in the original work, the experiments were carried out in the vicinity of glass transition temperature, the conclusions may very well be valid under other temperature conditions too. The conclusion that follows here immediately is that the length of the drawing zone must be adjusted so as to operate at low values of compliance, as defined here. Especially dangerous is the high range of possible temperature, as filaments may occasionally stick to the hardware.

The nonuniformities created in various stages of the process will be transmitted down the threadline. Therefore, the higher up in the process line the instability occurs, the more dangerous it is. But, contrary to the intuitive expectations and to some opinions,[82], neck drawing may sometimes improve the fiber evenness over that present in the undrawn fibers. When the fibers are cold drawn under proper conditions, some types of the nonuniformities generated in quench (or coagulation) zone may be diminished or outright eliminated. As an example: small temperature variations would lead to changes of rheological properties; the hotter segments may be extended more and at higher rate, which may eventually lead to an increased crystallization rate at higher temperature. As a result the thinner segment may be cold drawn less than the neighboring segment, initially thicker but possessing a crystalline structure more apt to the plastic deformation. Nevertheless, such a "self-improvement" of uniformity is not a rule to depend on; if it happens, it is rather a "patch up" by way of a good luck. It is highly unlikely to obtain perfectly

drawn fibers from poor quality undrawn fibers.

X.2.e A Summary

Simultaneously as a summary and as a quick reference, the trends in changes of the neck drawing performance and of the resulting fiber properties are given in table X.4.

Table X.4.
DRAWING PERFORMANCE IN RELATION TO FIBER PROPERTIES

PROPERTIES OF UNDRAWN FIBERS	DRAWING PERFORMANCE				PROPERTIES OF DRAWN FIBERS				
		MAXIMUM							
	DRAWING TENSION	DRAW RATIO	TEMPERATURE	DRAWING RATE	CRYSTALLINITY	ORIENTATION	MODULUS	CREEP	THERMAL STABILITY
LOW CRYSTALLINITY	L	H	L	H	↑	H	H	H	L
HIGH CRYSTALLINITY	H	L	H	L	↓	↓	L	L	H
HIGH PRE-ORIENTATION	H	L	↑	L	↑↓	H	L	L	H
SMALL CRYSTALLITES	L	H	L	H	↑	H	H	H	L
LARGE CRYSTALLITES	H	L	H	L	↑↓	L	L	↑↓	↑↓

H Higher or high; L Lower or low; ↑ Tendency to be higher;
↓ Tendency to be lower; ↑↓ Illdefined result, complex relationships.

The conditions of a cold drawing process influence the properties of the resulting fibers. However, the range of applicable drawing conditions depends on the structure of the fiber entering the drawing stage. The information summarized in table X.4 underscores the obvious fact that in effect all fiber properties depend on the fiber structure. Any change of the fiber properties, if it is to be achieved,

must be realized through alteration of the fiber structure, and the structural alterations must start from the development of the morphology of undrawn fibers and continue all the way through the end of the neck drawing. It is necessary to remember that drawing of a fiber to an extent much smaller than the practical maximum is, with few exceptional cases, ill advised.

And what makes the fiber formation processes so difficult and so interesting is the large number of different process variables. All of the variables must be carefully controlled throughout the process; this is needed to have a command over the development of fiber structure, which determines the fiber properties. The full understanding of the relationships is the main key to success.

X.3 References

1. H. Kast, in *Die Physik der Hochpolymeren*, Ed. by H. A. Stuart, Springer Verlag, Berlin – Heidelberg – Wien, 1956, Vol. 4, p. 427.
2. H. Berg, *Kolloid Z.*, **210 (1966)**, 64.
3. H. Mark and W. Lothmar, *Helv. Chim. Acta*, **19 (1936)**, 68.
4. W. J. Lyons, *J. Appl. Phys.*, **29 (1958)**, 1429.
5. T. Shimanouchi, M. Asakina, and S. Enomoto, *J. Polymer Sci.*, **59 (1962)**, 93.
6. M. Asahina and S. Enomoto, *J. Polymer Sci.*, **59 (1962)**, 101.
7. S. Enomoto and M. Asahina, *J. Polymer Sci.*, **59 (1962)**, 113.
8. K. E. Perepyol'kin, *Mekhanika Polimerov*, **1 (1966)**, 34.
9. W. L. Dulmage and L. E. Cantois, *J. Polymer Sci.*, **28 (1958)**, 275.
10. I. Sakurada, H. Nukushina, and I. Ito, *J. Polymer Sci.*, **57 (1962)**, 651.
11. I. Sakurada and K. Nahamae, *Makromol. Chem.*, **78 (1964)**, 1.
12. I. Sakurada and K. Kaji, *J. Polymer Sci., Pt. C*, **No. 31 (1970)**, 57.
13. I. Sakurada, *quoted in ref. 8*
14. L. R. G. Treloar, *Polymer*, **1 (1960)**, 95, 279, 290. 14
15. K. E. Perepyol'kin, *Mekhanika Polimerov*, **3 (1968)**, 3.
16. C. W. Bunn, *Proc. Royal Soc. (London)*, **A180 (1942)**, 40.
17. S. Mizushima and T. Shimanouchi, *J. Am. Chem. Soc.*, **86 (1964)**, 3521
18. R. H. Boyd, *J. Polymer Sci., Polymer Phys. Ed.*, **21 (1983)**, 493 and ref.
19. J. Preston, *Polymer Eng. Sci.*, **15 (1975)**, 199.
20. A. Cifferi, *Polymer Eng. Sci.*, **15 (1975)**, 191.
21. G. Natta, *Ősterr. Chem. Ztg.*, **62 (1961)**, 205.
22. M. Hagedorn and P. Mőller, *Cellulose Chemie*, **12 (1931)**, 29.
23. A. M. Sookne and M. Harris, *Ind. Eng. Chem.*, **37 (1945)**, 478.
24. N. Mikhayl'ov, *Khim. Vol'okna*, **1 (1964)**, 7.
25. H. F. Mark, *cit. in ref. 2.*
26. H. F. Mark in *Die Physik der Hochpolymeren*, Ed. by H. A. Stuart, Springer Verlag, Berlin – Heidelberg – Wien, 1956, Vol. 4, p. 629.

27. P. J. Flory, *J. Am. Chem. Soc.*, **67 (1945)**, 2048.
28. H. D. Keith, F. J. Padden, Jr., and R. G. Vadimsky, *J. Appl. Polymer Sci., Pt. A-2*, **4 (1966)**, 267.
29. R, B, Williamson and W. F. Busse, *J. Appl. Phys.*, **38 (1967)**, 4187.
30. D. T. Turner, *Polymer*, **23 (1982)**, 626 and *references cited.*
31. A. N. Gent and A. G. Thomas, *J. Polymer Sci., Pt. A-2*, **10 (1972)**, 751.
32. P. I. Vincent, *Polymer*, **1 (1960)**, 425.
33. M. L. Wallach, *J. Polymer Sci., Pt. A-2*, **6 (1968)**, 953.
34. F. Bueche: *Properties of Polymers*, Interscience Publ., New York, 1962, p. 237.
35. P. J. Flory: *Principles of Polymer Chemistry*, Cornell Univ. Press, Ithaca, 1953, p. 458.
36. Bopp and Sisman, *cited in ref. 28.*
37. W. H. Carothers and J. W. Hill, *J. Am. Chem. Soc.*, **54 (1932)**, 1579.
38. A. Nowakowski, *Technology of Plastics and Sybthetic Fibers*, lectures at Polytechnic of Łódź, 1953.
39. I. Marshall and A. B. Thompson, *Proc. Roy. Soc. (London), Pt. A*, **221 (1954)**, 541.
40. P. Smith, P. J. Lemstra, and J. P. L. Pijpers, *J. Polymer Sci., Polymer Phys. Ed.*, **20 (1982)**, 2229.
41. T. Kanamoto, A. Tsuruta, K. Tanaka, A. Takeda, and R. S. Porter, *Polymer J.*, **15 (1983)**, 327.
42. T. Kanamoto, A. Tsuruta, K. Tanaka, A. Takeda, and R. S. Porter, *Polymer J.*, **16 (1984)**, 87.
43. M. Ito, K. Tanaka, and T. Kanamoto, *J. Polymer Sci., Pt. B, Polymer Phys.*, **25 (1987)**, 2127.
44. R. Bonart, *Kolloid Z.*, **210 (1966)**, 16.
45. *U. S. Pat. Appl.* Ser. No. 81,834 (1970) (to Phillips Petroleum Co.)
46. H. Ludewig: *Polyesterfasern*, Akademie Verlag, Berlin, 1965, p. 214 ff; *Polyester Fibers*, John Wiley and Sons, New York, 1971.
47. V. Capuccio, A. Coen, F. Bertinotti, and V. Conti, *Chim. e Ind. (Milano)*, **44 (1962)**, 463.
48. I. Gigli and E. Del Nauro, *Austral. Pat.*, No. 275,863.
49. Z. K. Walczak, *previously unpublished results.*
50. G. Rauman and D. W. Saunders, *Proc. Phys. Soc.*, **77 (1961)**, 1028.
51. T. Komatsu and A. Aoshima, *J. Polymer Sci., Pt. B, Polymer Phys.*, **33 (1995)**, 179.
52. L. C. E. Struik, Polymer, **30 (1989)**, 799, 815 and references cited.
53. M. W. Darlington, B. H. McConkey, and D. W. Saunders, *J. Mater. Sci,*, **6 (1971)**, 1447.
54. A. Peterlin, *Kolloid Z,*, **216-217 (1967)**, 129.
55. G. J. van Amerongen, *J. Polymer Sci.*, **2 (1947)**, 381. 55
56. L. Valentine, *J. Polymer Sci,*, **27 (1958)**, 313.
57. D. Jeschke and H. A. Stuart, *Z. Naturforsch.*, **16 (1961)**, 37.

58. W. O. Statton, *J. Polymer Sci.*, **58 (1962)**, 205.
59. D. F. Dismore and W. O. Statton, *J. Polymer Sci, Polymer Letters*, **2 (1964)**, 1113.
60. A. S. Michaelis, H. J. Bixler, and H. L. Fein, *J. Appl. Phys.*, **35 (1964)**, 3165.
61. R. H. Peters, in *Diffusion in Polymers*, Ed. by J. Crank and G. S. Park, Academic Press, London – New York, 1968.
62. R. M. Barrer, in *Diffusion in Polymers*, Ed. by J. Crank and G. S. Park, Academic Press, London – New York, 1968.
63. D. Machin and C. F. Rogers, *Makromol, Chem.*, **155 (1972)**, 269.
64. T. Vickerstaff: *The Physical Chemistry of Dyeing*, Oliver and Boyd Publ., London and Interscience Publ., New York, 1954.
65. Y. Tabbagi and H. Hattori, *J. Appl. Polymer Sci.*, **9 (1965)**, 2167.
66. Y. Tabbagi, *J. Appl. Polymer Sci.*, **9 (1965)**, 3887. 66
67. G. T. Davis and H. S. Taylor, *Textil Res. J.*, **35 (1965)**, 439.
68. D. N. Marvin, *J. Soc. Dyers and Col.*, **70 (1954)**, 16. 68
69. K. Selivertassek, cit. in ref. 46, p. 250.
70. D. Patterson and R. P. Sheldon, *Trans. Faraday Soc.*, **55 (1959)**, 1254.
71. S. Rosenbaum, *J. Appl. Polymer Sci.*, **7 (1963)**, 1225. 71
72. H. I. Freeman and M. J. Coplan, *J. Appl. Polymer Sci.*, **8 (1964)**, 2389.
73. R. M. Lodge, in *Fasern aus synthetischen Polymeren*, Ed. by R. Hill, Berliner Union Verlag, Stuttgart, 1956, p.376 ff.
74. A. Ziabicki: Fizyka procesöw formowania włókien, Wydawnictwa Naukowo - Techniczne, Warszawa, 1970, pp. 132, 275.
75. A. Ziabicki in *Man Made Fibers*, Ed. By Mark, Atlas, and Cernia, Interscience Publ., New York, 1967, Vol. 1.
76. H. Nitschmann and J. Schrade, *Helv. Chim. Acta*, **31 (1948)**, 297.
77. see ref. 46, p. 194 ff.
78. S. Ya. Mezhirova, D. V. Filbert, A. B. Pakshver, and R. G. Lebyedyeva, *Khim. Volokna*, **5 (1967)**, 51.
79. G. P. Adryanova, A. S. Kechekyan, and V. A. Kargin, *J. Polymer Sci, Pt. A-2*, **9 (1971)**, 1919.
80. O. Einsporn, *Melliand Textiber.*, **40 (1959)**, 28.
81. A. Peterlin and G. Meinel, *J. Polymer Sci., Pt. C*, **No. 12 (1966)**, 85.
82. A. Ziabicki: *Physics of Fiber Formation Processes*, Interscience Publ., New York, 1976.
83. M. F. Butler, A. M. Donald, and A. J. Ryan, *Polymer*, **39 (1998)**, 39.
84. R. Popli and L. Mandelkern, *J. Polymer Sci., Polymer Physics*, **25 (1987)**, 441.
85. M. A. Kennedy, A. J. Peacock, and L. Mandelkern, *Macromolecules*, **27 (1994)**, 5297; 7941.
86. B. K. Annis, J. Strizak, G. D. Wignall, E. G. Alamo, and L. Mandelkern, *Polymer*, **37 (1996)**, 137.
87. K. Tashiro and M. Kobayashi, *Polymer*, **37 (1996)**, 1775.
88. A. Bruggeman and J. A. H. M. Buijs, *Polymer*, **39 (1998)**, 4883.
89. N. S. Murthy, D. T. Grubb, K. Zero, C. J. Nelson, and G. Chen, *J. Appl. Polymer Sci.*, **70 (1998)**, 2527.
90. D. T. Grubb and L. W. Jelinski, *Macromolecules*, **30 (1997)**, 2860.
91. W. G. Hu and K. Schmidt - Rohr, *Acta Polym.*, **50 (1999)**, 271.

XI PROCESSES OF "SPUNBOND"

The textile operations of spinning yarn and weaving are relatively time consuming – *ergo* – they are expensive. This was a good reason to search for a better solution, for a way to make flat textile products faster and thus less expensive. Two basic ways of accomplishing the goal are: glueing or welding the fibers together, or entangling the fibers in a permanent way while avoiding yarn twisting and weaving or knitting operations. These materials bear a common name, *nonwovens,* to express their origin in a nontraditional manufacturing process. Papers, where short cellulose fibers are held together primarily by polar forces, and felts made of wool where the fibers are enchained and hooked together by the natural scales on the fiber surface are the oldest nonwoven materials. The second half of the nineteenth century witnessed the development of felts from fibers other than wool by the way of entangling the individual fibers through a *needling* operation. The twentieth century came up with the invention of the name *nonwoven* for such materials, and with newer processes to make them.

The ultimate step, thus far, in reducing the costs of production of the textile flat structures was the development of the *spunbond* process. Some of the commercial processes produce material up to five meters wide at linear velocities exceeding five hundred meters per minute. The fiber formation and bonding are in one uninterrupted line which runs with velocities up to five hundred meters per minute, or even higher. The majority of spunbond processes, as taken by volume, uses fiber formation from the melt and fibers are bonded by thermal methods, utilizing thermoplastic properties of the polymers involved. The more important of the spunbond processes are described in the following pages since they involve fiber formation. Depending on the bonding methods, there are some requirements and/or limitations on the fiber properties, so these are discussed also.

From the point of view of mechanics, twisted yarn is a unique structure, The individual filaments have a helical conformation and are held together with the other filaments by frictional forces. Upon application of strain the helices become tighter, the normal forces acting on the individual fibers grow with increasing strain, the frictional forces increase appropriately. Without strain the yarn is soft and pliable, under strain it becomes tougher and stronger.[1,2]

Irrespective of the method of bonding the fibers together, the nonwoven web morphology resembles a rigid lattice, such as on a miniature iron bridge or high voltage power line. In consequence, the nonwovens are by nature stiff and papery; their morphology is somewhat similar to that of a paper. There are various ways to diminish some of the often unwanted properties, but it should not be expected that a nonwoven will duplicate the character of woven materials, as was the idea driving the developers of nonwovens. In effect, nonwovens are used primarily for inexpensive disposable products and for technical applications, and these applications have a bearing on the directions of the nonwoven development.

As it is difficult to put the different spunbond processes in any systematic framework, they are discussed here in accordance to the type of fiber formation,

whatever the bonding technique may be. The bonding techniques and their requirements are discussed in places of their relevance.

XI.1 Spunbond Formation from Melt

The first spunbond process was developed more or less simultaneously by Imperial Chemical Industries and by Du Pont De Nemours. The processes used essentially standard fiber formation from the melt, if there is such a thing as a standard process. In this case, we mean that the fibers are extruded, attenuated, and drawn by means of drawing rollers. Fibers are received from the drawing rollers by lay-down jets, which blow the fibers down on a moving belt which transports the fleece to the bonding section of the process.

Newer processes rely primarily on drawing jets. These are mostly *one step* processes, where the filament attenuation and the neck drawing are driven by one drawing jet, which serves at the same time as a lay-down jet. Drawing rollers are used when higher draw ratios are needed to obtain fibers with higher tenacities, but there are not many such demanding applications.

In some cases, a corona charge is put on the fibers just prior to the entry to the lay-down jets. The purpose of this is to prevent the fibers from clinging together, and at the same time to help them cling to the transporting wire belt, which must be grounded. The jets are operated with quite a large volume of air which is removed by suction applied under the transporter wire. Nonetheless, some portion of the air may bounce off the wire and adversely affect the uniformity of fiber deposition. The corona charge, or an electrostatic charge may prevent or reduce the effects of adverse air currents.

In spunbond formation from the melt, the fibers are bonded practically exclusively by utilizing their thermoplastic character. There are processes that rely on swelling of the fibers to make them tacky, but these processes are of lesser importance.[3] For thermal bonding, there are basically two systems of fiber formation with a number of subgroups or modifications.

Firstly, two different polymers with greatly different melting character may be used. Separate strands of fibers are formed from the two polymers, and the fibers blended before the deposition jets. This method offers many possible variations of hardware for blending and depositing the fibers. More frequently, however, side-by-side bicomponent fibers are made where one side (bonding side) of the fiber melts at a lower temperature, so the properties of the "matrix" part of the fiber deteriorate due to the heat exposure less than it would be the case for single component fibers.

Secondly, only one polymer may be used. Fibers are formed so that different melting characteristics are obtained. There may be separate strands with differing melting ranges. There may be segmented fibers, where the different segments melt differently.[4] The majority of spunbond processes, again judged by the production volume, are based on forming one strand of uniform fibers and bonding is performed by "welding" the fibers in discrete areas, by so called *point bonding.*

Whichever way the fibers are made, all the principles of fiber formation, as given in other chapters, must be obeyed. However, as is evident from the description given above, there are many different configurations a spunbond process may be given. Each of these configurations has more than one solution as the arrangement of the hardware is concerned. The bicomponent formation is usually a standard solution for such types of process, as described in section XII.3. Formation from two polymers in parallel means essentially two separate positions located side by side; the only difference is whether the threadline is lead through common rollers or if the whole machine must be duplicated.

In cases where one polymer is used with a differentiation of the melting characteristics, the number of possible solutions is much larger.[5,6] More often than not, the extrusion section is common both for matrix and binder filaments. In such cases a portion of fibers extruded from a spinnerette is diverted to a different formation for binder fibers. Another, more frequent design, feeds the polymer from a common extruder to separate spinning blocks for the binder formation. In the last named cases, one binder threadline usually cooperates with two neighboring threadlines of matrix fibers.

Segmented fibers are normally made in one threadline, one formation, and one drawing. The fibers entering the drawing zone pass through a take-up or feed roller which has hot and cold segments. Due to the difference in temperature, the draw ratio, as well as the thermal history, is different in the different segments. The obtainable difference in the onset of melting amounts to some two, to a maximum of seven degrees.

The processes which differentiate the matrix from binder fibers operate, as a rule, with positive (roller) transport. The majority of processes which do not differentiate the fibers operate with constant force (pneumatic jet) drawing systems.

If two polymers are used, then usually the binding fibers are made from the same polymer as the matrix fibers, but copolymerized with other monomers to change the melting characteristics. To change the melting characteristics of fibers made of the same polymer one must use the principle of melting temperature dependence on the crystallization temperature. Development of the appropriate conditions for the formation sector is rather involved. Drawing of the binder fiber must be performed also at a low temperature, and preferably to a lower draw ratio.

At this point it may be said that if the formation and drawing of the binder and matrix fibers are separate, there is a danger that the velocities for the two tows entering the lay-down jet will not be equal. Unequal velocities at this point of the process create frequent cobwebbing and jamming of the depositing jets, which causes expensive discontinuities of the process and is highly aggravating to the operators. When the two streams are separate for the whole path, inciuding the lay- down, obtaining proper distribution of the binder fibers may be difficult indeed.

Such are the often used possibilities with their good sides and pitfalls. Which of these ways may be more suitable for the conditions considered may be decided only in accordance with the choice of both the desired fabric properties and of the

boding method.

XI.1.a Meltblown

The original authorship of the meltblown process is difficult to establish with full certainty. It appears that first the process of meltblowing fine fibers for production of filter cartridges was developed by F. W. Manning[7] in 1946. Later, in 1954 a process for producing meltblown fibers was described by V. A. Wente of the U. S. Naval Research Laboratory.[8] Since that time, patents regarding meltblown are multiplying, but with little, if any, real innovation.

The principle of the process is given in figure XI.1. A polymer melt, preferably of low viscosity, is extruded from a capillary. On both sides of the capillary are located channels through which high velocity air is led as close, and as parallel to the extrudate as possible. The high velocity air simultaneously provides cooling and force to attenuate the filaments. There are many different variants for the design of such a meltblowing head. Low viscosity (low molecular mass) polymers are often used, despite the fact that this is counter productive from the point of view of fiber strength. However, the polymer pressure requirement is given special consideration in view of the unavoidable inherent mechanical weakness of the extrusion tip geometry. Some of the heads have capillary exits flush with the bottom line of the head, some put the capillary exit in a recess. Usually the capillaries are short, also because of the desire for low extrusion pressure.

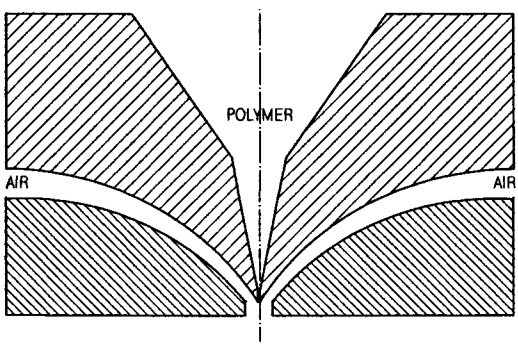

Figure XI.1: *Schematic drawing of a meltblowing head.*

From the theoretical point of view, the process must obey all the rules of fiber formation from the melt. One may say that this is a formation from the melt with pneumatic transport, where the air jet is to provide a pushing rather than a drawing force, while simultaneously providing for the quenching.

R. L. Shambough and co-workers have published attempts at a theoretical solution of the meltblown process at relatively low air velocities.[9–12] The efforts were concentrated on adopting the solutions published for fiber formation from the melt, in particular the works by Ziabicki, Petrie, Phan Thien, Kase and Matsuo. The experimental results agree with the theoretical calculations to a somewhat lesser degree than the similar solutions for the "classic" process of fiber formation from

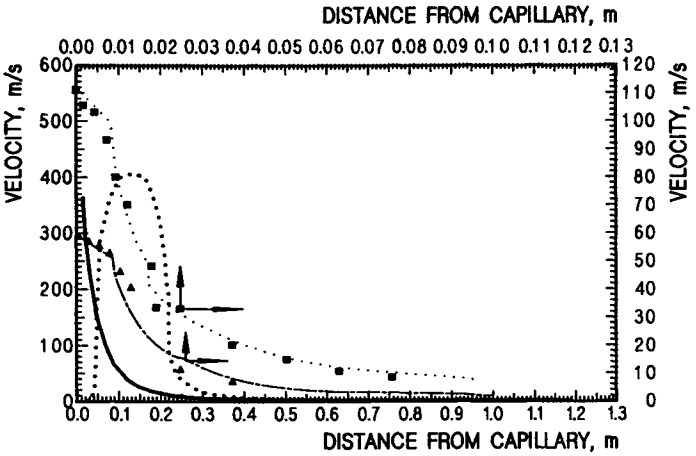

Figure XI.2: *Air velocity versus distance in meltblown processes: dashed and dot-dashed lines – low air velocity data after Uyttendaele and Shambough,*[12] *full drawn line air velocity close to sonic, heavy dotted line fiber velocity after H. Bodaghi.*[13]

the melt. In particular, the discrepancy between the calculated and experimental fiber diameter appears to be different by a factor of up to fifty.

Some portion of the problems preventing closer agreement between the theory and experiment may well constitute the treatment of rheology. A much larger problem, however, seems to be the treatment of aerodynamics. If to judge from the published sketches, the air flow up to the exit from the slot next to the exit of the capillary is not necessarily an accelerated one. This does not provide a guarantee of vortex free flow. The high velocity air discharged from the orifices looses its velocity very rapidly, as indicated by Shambough[10,11] and Bodaghi,[13] and shown in figure XI.2. Moreover, at some 40 *mm* to 50 *mm* from the exit of the capillary, the filament velocity exceeds the velocity of the drawing air, which indicates that the first impetus of air provides an appreciable momentum to the fiber to slow it down later.

One of the most common characteristics of aerodynamics is that vortices are practically always formed in a decelerating flow (see also section VI.1). As a consequence, the fibers start loosing momentum. Fast photography shows that the fibers form loops, which represents direct evidence of the air vorticity and allows us to infer that the fiber velocity is higher than air velocity. The last inferences have been confirmed experimentally by Bodaghi, [13] as shown in figure XI.2.

In summary, one may state that fiber formation in the meltblown process must obey the general principles ruling fiber formation from a melt, however, first the aerodynamics of the process need thorough scrutiny and definition. To apply the general principles of fiber formation from melt, some modifications must be introduced in respect to the decelerating forces of air drag over a large segment of the threadline.

There have been attempts to enclose the meltblown formation from the blowing head down. So far, such solutions have shown to be impractical, however. If the enclosure is close to the fibers, then major operational problems with the fibers sticking to the enclosing walls appear. If the enclosure is more spacious, then maintaining the air velocity requires so large a volume of high pressure air that the process begins to have problems with economy, not to speak of the removal of large volumes of spent air. Nevertheless, there seems to be a large room for inventiveness here.

The high acceleration of the extrudate immediately after leaving the capillary leads to the formation of very fine fibers; in commercial products the fibers range generally from $1\mu m$ to $10\mu m$, though submicron fibers are also obtainable. Additionally, rather small capillary diameters are in use. The decrease of the forces acting on the fibers and the deceleration of fibers exclude any possibility of cold drawing. This, naturally, leads to very low tensile strength of the obtained fibers. At the moment, the only potential improvement of this aspect of the product would be bidirectional drawing of a bonded fabric. Nonetheless, so far the applications of meltblown fibers have not required higher tenacities. The fibers are used primarily for application as filters of one sort or another, and there the materials work mostly in a compression mode, that is, transverse to the fiber axis. Where a higher strength is needed, the meltblown fibers are laminated with stronger spunbonded materials, which represents an entirely natural marriage.

Commercial meltblown products often have a wide distribution of fiber diameters, or outright, small clumps of polymer. Generally, this originates from the very low quality of polymers used for meltblowing. The most frequently used polymer – polypropylene – often is highly degraded with the help of peroxides to achieve low viscosity. However, the peroxides produce a lot of cross linking, gel. On the other hand, good quality polymer, free from cross linked (gel like) material, permits us to obtain very fine products with narrow distributions of fiber diameters, but there is a matter of price. Thermoplastic elastomers of a different nature are also used for meltblowing; some of them, those with very high molecular mass, may be diluted with parafine or similar materials. This is proof enough that slightly higher melt viscosity is not the problem reducing the quality of the meltblown fabrics.

The meltblown materials have some integrity of their own, without bonding, however, to improve their usefulness they are subjected almost exclusively to thermal bonding.

Despite its age, the meltblown process enjoys a modest commercial success. Additional developments, or perhaps modifications of the process, might boost the product applicability. Manufacturing of very fine diameter fibers is difficult and always expensive. Meltblowing has some potential in this respect.

XI.2 Thermal Bonding

Thermal bonding is executed with two different types of equipment: *through-air bonders* and calenders of several types. A schematic representation of the

principle of action of a through-air bonder is given in figure XI.3.[14] The fiber fleece is introduced between the surface of a large perforated drum and a wire belt which presses the fleece against the drum surface. Hot air is introduced into the chamber containing the drum and removed from the center of the drum. The direction of the hot air may well be reversed. In this way the hot air is forced to pass through the wire belt, through the fleece and drum perforation thereby providing the necessary energy to heat the fibers of the fleece. The pressure of the wire belt compacts the fleece and forces the fibers to more numerous and more intimate contacts.

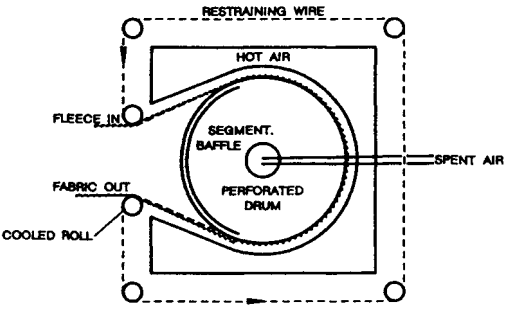

Figure XI.3: *Schematic description of the action principles of the through-air bonding. After T. A. Zack et al.*[12]

Zack and co-workers[14] devised a way to calculate heat transfer in a through-air bonder. The equations are not quoted here since they seem to contain more simplifications than necessary.

Generally, through-air bonding is well suitable for thick materials. Since the number of fiber-to-fiber contacts is large, this method of bonding gives better results with matrix and binder fibers, otherwise the number of bond points may be too large, leading to a stiff fabric. By the nature of the method, compacting of the fleece is moderate, so the resulting fabrics have a tendency to be thick, low density.

The most frequently used method of bonding appears to be by the way of calenders. The rollers used may have plain surfaces or may have pins arranged in some pattern. In the past, rollers with rubber surfaces were also used to increase the area of the nip, that is, to increase the residence time of the fabric in the roller nip.

It has been shown that heat transfer directly from a metal surface to the fibers is very small, thanks to limited contact due to the curvature of fiber surface and due to the generally unfavorable heat transfer coefficients on metal-polymer interfaces.[15] Much more efficient is the heat transfer *via* convection with air as the carrier.[14,15] S. B. Warner[16] stressed the importance of the adiabatic heat generation due to compression.

Considering the heat transfer possibilities, one may conclude that the through-air system is a good one, if the relatively low compaction pressure and not very high maximally obtainable speed are acceptable from the other standpoints. The most

favorable thermal bonding system is discrete point bonding with calender rollers equipped with bonding pins. Since essentially the entire load in the calender nip is concentrated on the bonding pins, pressure there is very high and such is the adiabatic heat generation. The material which finds itself between the pins is exposed to much lower temperature and pressure, thus the majority of the fibers suffer much less damage. The degree of bonding may be regulated by the size, distribution and the total area of the bonding pins in relation to the entire surface, a separate binding fiber is not needed.

A comprehensive analysis of the heat transfer to a fleece in a calender nip has been done, considering all aspects of the process. No shortcuts were taken *a priori*, relatively few simplifications were used, the results of the calculations were used to decide the significance of different aspects of the process.[17] The results are applicable to calenders with plain rolls, to point bonding, and to spiral rollers.

For these considerations, the calender nip was defined as the angle (or the corresponding length of the roller circumference) between the center point of the contact of the two rollers and the point where the rollers' separation is equal to the thickness of the uncompressed fleece. This means that at the moment the compaction of the fleece begins, the fleece enters the nip. From this assumption it results that the size of the nip increases with the increasing "fluffiness" of the heated material and with its surface weight. More justifications for such a definition will become apparent as the consideration progresses. A schematic picture of a nip is given in figure XI.4.

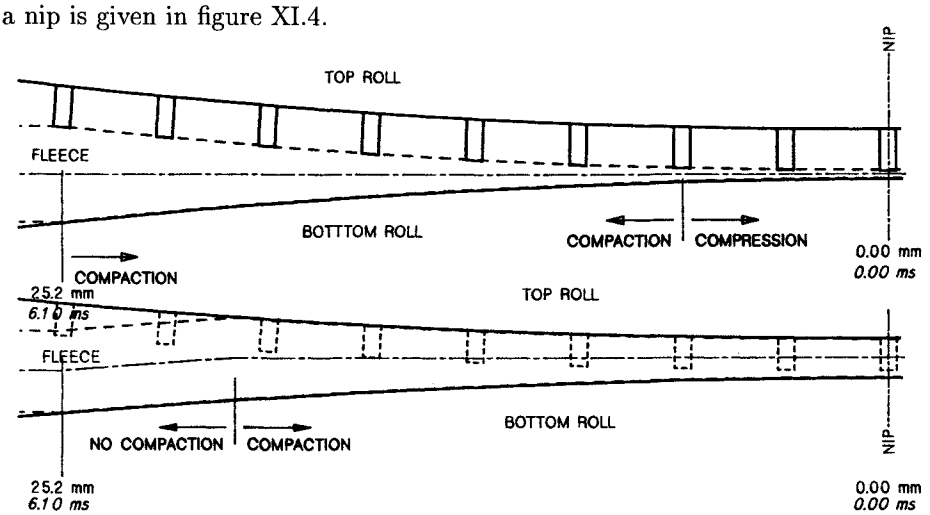

Figure XI.4: *Schematic depiction of the calender nip: top – for bonding pins, bottom – areas between the pins. After Z. K. Walczak.*[17]

For rollers with a pattern, the first point of contact is the contact with the pins. Of course, the areas between the pins enjoy more freedom of space. For the case of point bonded materials, the gap between the rollers is determined to be the thickness of a solid film of the fiber polymer minus a certain amount of material which is squeezed out of the bond point area. The squeezed amount depends on

the temperature and pressure of the operation and on the polymer viscosity at the existing conditions.

The calculation of heat transfer consists here of two segments. One segment treats the fibers individually before compression, and with respect to their location in the nip (the distance from the top and bottom rollers); these calculations may be done according to those for quenching fibers (see section VI.2). The second segment considers the individual fibers being compressed in groups of various numbers of fibers, and of fibers originating from the different locations in the cross section of the fleece. In this way, the results depict the inhomogeneities in the bond point formation. The second segment of the calculations considers only the "vertical" heat transfer. In the "horizontal" direction there is both mass and heat transfer, which so far has not been defined. Full description of this process would require a very large number of assumptions, many difficult to verify. Considering this and the unavoidable inhomogeneities existing during the bond formation, more detailed calculations may not be worth the effort needed.

For the first segment the heat balance is as follows.

$$q_r - q_d = q_c \tag{XI.1}$$

where

$$q_d = v\ da\ T_d\ \rho\ C_p \tag{XI.2}$$

$$q_r = v\ da\ T_r\ \rho\ C_p \tag{XI.3}$$

Here q is heat flow, v is fiber velocity, a is cross sectional area of the fiber, T is temperature, ρ is polymer density, C_p is the specific heat of the polymer of the fiber. The subscripts d and r mean delivered and removed, respectively.

The conductive heat transfer is according to the Fourier's equation:

$$q_c = -\lambda_p\ \nabla^2\ T\ da\ dl \tag{XI.4}$$

Here λ_p stands for heat conductivity of the polymer of the fiber, ∇ is the Laplacian, and l is the length of fiber along its axis.

After substitution of equations XI.2 and XI.3 into XI.1, and after substituting $v = dl/dt$ (where t is time) we have

$$\frac{dl\ da}{dt} dT = \frac{\lambda_p}{C_p\ \rho} \nabla^2\ T\ dl\ da \tag{XI.5}$$

and in a developed form it becomes

$$\frac{dT}{dt} = \frac{\lambda_p}{C_p\ \rho} \left(\frac{\partial^2 T}{\partial r^2} + \frac{1}{r} \cdot \frac{\partial T}{\partial r} + \frac{\partial^2 T}{\partial l^2} \right) \tag{XI.5 a}$$

where r is the radial distance from the fiber axis. Time may be eliminated from equation XI.5a by taking advantage of the equation for fiber velocity.

$$v = \frac{dl}{dt} = \frac{V_f}{\pi R^2} \tag{XI.6}$$

Here V_f stands for the volume of a single fiber of d_t weight titer moving through the calender per second. In the case of d_t in denier this leads to

$$V_f = d_t \cdot \frac{v}{900000\ \rho\ \pi\ R^2} \tag{XI.7}$$

In view of the above, and introducing normalized variables, θ for temperature and u for radius equation XI.5 obtains the form:

$$Z \cdot \frac{\partial \theta}{\partial l} = \frac{1}{u} \cdot \frac{\partial}{\partial u} \cdot u \frac{\partial \Theta}{\partial u} + R^2 \cdot \frac{\partial^2 \theta}{\partial l^2} \tag{XI.8}$$

where

$$Z = \frac{d_t\ v\ C_p}{900000\ \pi\ \lambda_p} \tag{XI.8 a}$$

The second term in the right hand side of equation XI.8 is dropped as very small. The boundary conditions are set as $T = T_a$ for all $l = 0$ and T_a is the ambient temperature. Next one may define

$$dq = \alpha\ T\ ds \tag{XI.9}$$

where α is heat transfer coefficient, $ds = 2\pi\ R\ dl =$ *surface of a fiber segment.*

From Fourier's equation (equation XI.4) results

$$dq = \lambda_p \cdot \frac{\partial T}{R\ du}\ ds \Big|_{-u=1} \tag{XI.10}$$

Equations XI.9 and XI.10 determine the spatial boundary condition:

$$\frac{\alpha R}{\lambda_p} = \frac{1}{T} \cdot \frac{\partial T}{\partial u} \Big|_{u=1} \tag{XI.11}$$

The dependence of heat conductivity on temperature for polypropylene, the polymer most frequently used for spunbonded fabrics, one may determine from the Weber formula[18]

$$\lambda_p = \lambda_p^0\ C_p\ M_w^{0.333} \rho_p^{1.333} \tag{XI.12}$$

where M_w is weight average molecular mass, λ_p^0 is heat conductivity at $0°C$. The last value for polypropylene[19] is $3.0871 \cdot 10^{-5}$. Heat capacity for polypropylene may be calculated from the weighed average of heat capacities calculated for solid (about 50 % crystalline) and noncrystalline fractions. For the solid: $C_p = 0.00136T°C + 0.4120\ cal/g$ For the molten: $C_p = 0.001223T°C + 0.3809\ cal/g$.

The left hand side of equation XI.11 may be written using Nusselt number ($Nu = \alpha\ D/\lambda_a$)

$$\frac{\alpha\ R}{\lambda_p} = \frac{Nu\ \lambda_a\ \Delta T}{2\ \lambda_p} \tag{XI.13}$$

In addition to the heat transferred through the air, heat is also transfered *via* radiation. This may be calculated using Stefan-Boltzmann law

$$E_r = \epsilon\ \sigma\ T^4 \tag{XI.14}$$

where E_r stands for radiation energy, σ is the Stefan- Boltzmann constant [$\sigma = 5.7686 \cdot 10^{-8} j/(m^2\ s^\circ K^4)$], and ϵ represents the material emissivity. For polypropylene, the emissivity has been determined to be $\epsilon = 0.92$ to 0.93, while for oxidized metal surfaces (roll surface) it is $\epsilon = 0.7$.

The rate of heat exchange between two surfaces of areas F_1 and F_2, with temperature T_1 and T_2, respectively, is

$$\dot{q} = \sigma(T_1^4 - T_2^4)F_1\ \psi_{12} = \sigma(T_1^4 - T_2^4)F_2\ \psi_{21} \tag{XI.15}$$

Here ψ is shape-emission coefficient equal

$$\psi_{12} = \left[\frac{1}{\psi_\rho} + \left(\frac{1}{\epsilon_1} - 1\right) + \frac{F_1}{F_2} \cdot \left(\frac{1}{\epsilon_2} - 1\right)\right]^{-1} \tag{XI.16}$$

Here ψ_ρ represents the shape-refractive coefficient which for the case of a fiber and a relatively large plane may be assumed to be around 0.9,, as for very long rectangles. In spunbonded materials, the fibers are usually at an angle, ranging from 30° to 45°, to the surfaces. For this reason, the value of ψ_ρ amounts to between 0.67 and 0.83 (1 is for 90°). In the considered case, one half of the fiber faces one roll surface, the other half faces the other roll surface.

Equations XI.15 and XI.16 may give a more convenient formulation of the heat transfer coefficient in radiation.

$$\alpha_r = \sigma\ \psi_{12}\left(T_1^4 - T_2^4\right) \tag{XI.17}$$

In consequence of the consideration of heat transfer through radiation, another term representing radiation must be added to equation XI.13

$$\frac{\alpha\ R}{\lambda_p} = \frac{Nu\ \lambda_a\ \Delta T}{2\ \lambda_p} + \frac{(\lambda_{r1} + \lambda_{r2})\ R}{2\ \lambda_p} \tag{XI.18}$$

The heat transfer coefficient, λ_r, ought to be calculated for both the top roll and bottom roll temperature differences in case they are not equal.

The contribution of radiation to the overall heat transfer is not very large, but it is by no means negligible. Practical calculations show that the radiation contribution results in some three to ten degrees temperature increase, depending on the other conditions. In terms of crystal melting, such a temperature difference may be equivalent to the additional melting of ten to even twenty per cent of crystals.

Obtaining of the heat transfer coefficient between the fibers and the surrounding air requires additional considerations. When fleece moves gradually into the calender nip, the available volume decreases. The volume of fibers remains constant, naturally, and the air entrained between the fibers is gradually expelled. In aerodynamics, any formal studies of such a case are not available. To cope with the problem, the following speculation is offered with the help of figure XI.5.

If one considers the fleece element with volume V_5 moving forward to replace the element V_4, the volume of air flowing through the cross section of the elements

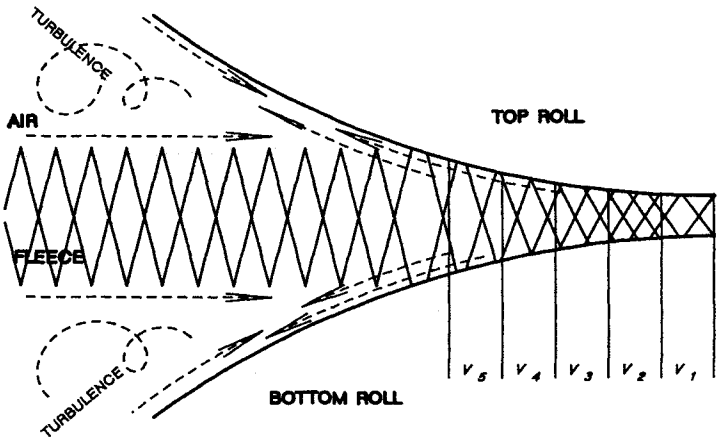

Figure XI.5: *Schematic depiction of the air flow in the nip of a calender. The dashed lines depict the expected paths of air. After Z. K. Walczak*[17]

5 equals V_5. Such a decrease of the volume continues all the way to the minimum of the nip cross section. At the minimum there is either practically no air left, like in the bond points, or there is some minimum volume in the areas outside of the bond points. In this way, there is a constant stream of air "backing up" toward the entry to the nip. One may well expect that the warmer air from elements V_1, V_2 mixes with the colder air of the earlier elements V_5, V_6, moving in with the fresh portions of the cold fleece.

The multitude of fibers inside of the fleece represents strong resistance to the air flow. The squeezed air must then seek a path with a lower flow resistance, and this will be closer to the roll surface, particularly in the area of the first contact between the roll and the fleece. As a result, one may assume that there is a gradient of air flow, the lowest velocity being in the center of the fleece and the highest at the roller surface. Such an gradient of air flow will lead to a temperature gradient across the fiber assembly, from its surface to the center.

It is doubtful whether such a situation exists over the entire extent of the nip, however, it may be in the areas between the bond points. In the areas of bonding pins ultimately there is no air left, so in the final segments there is probably a much smaller air velocity.

The roll surfaces outside of the nip area are in contact with air of approximately ambient temperature. The rolls must certainly have some pumping action, and so does the moving fleece. The "fuzzy" surface of the fleece may cause its pumping action to be even stronger than that of the rolls. In consequence, there are two air streams heading toward the nip and colliding at the entry. It would be difficult to admit that the colliding air displaces the air entrained in the fleece. While the air brought by the fleece has ambient temperature, the air pumped in by the roll must be substantially warmer.

The aerodynamic situation in the nip, as ill defined as it is, does not allow

us to calculate the temperature distribution accurately. As a consequence, the heat transfer in the calender nip cannot be calculated with full accuracy, certain approximations are needed.

The approach adapted here was:

1. Neglecting the "back flow" of air, the air temperature distribution was calculated using conventional engineering methods.
2. Using the obtained temperature distribution, numerical methods were used to perform a "mixing" operation. The hotter air flowing back has been given a parabolic velocity distribution across the nip thickness.
3. The mixing procedure has been iterated several times, but the results stopped "being reasonable" after the third iteration. To remain on the safer side, only two iterations have been accepted.
4. The resulting air temperature distribution has been described in general terms in a simplified way.

The (maximum) air temperature near the top roll for the $i-th$ volume (or cross section element) is

$$T_{mt} = T_{rt} - 2T_{amb}\frac{N_i - i}{n_i} \tag{XI.19}$$

For the bottom half of the fleece, it is

$$T_{mb} = T_{rb} - 2T_{amb}\frac{N_i - i}{n_i} \tag{XI.20}$$

Here T_{mt} and T_{mb} is maximum air temperature near top and bottom roll, respectively; T_{rt} and T_{rb} is roll temperature top and bottom, respectively; N_i is the total number of elements considered in the calculation, and i is the sequential number of the element. At the point of roll-to-roll contact $i = N_i$ (contrary to figure XI.5).

The distribution of temperature across the fleece, the thickness of which is defined as the number of single fiber layers in the fleece, N_y, for the case when the upper roll is the hottest, is for the upper half:

$$T(i,j) = T_{mt} \cdot \left[\frac{(j - 0.5\ N_y)}{(0.5 \cdot N_y)}\right]^p \tag{XI.21}$$

and for the bottom half:

$$T(i,j) = T_{mb} \cdot \left[\frac{(0.5\ N_y + 1 - j)}{(0.5 \cdot N_y)}\right]^p \tag{XI.22}$$

When the top and bottom roller temperatures are the same, or when the bottom roll temperature is lower, the equation may be written as follows.

$$T(i,j) = T_{mt} \cdot \left[\frac{1}{(0.5 \cdot N_y)}\right]^p + T_{mb} \cdot \left[\frac{(0.5 \cdot N_y + 1 - j)}{(0.5 \cdot N_y)}\right]^p \tag{XI.23}$$

where j is the consecutive number of the fiber layer, counted from the bottom of the fleece; and $p = 2L_i$, when L_i is the gap between the rolls for the considered element.

Using a so assumed air temperature distribution one may calculate the Nusselt number as given in section VI.2.a. At this point, all the needed input data are secured and one may solve equation XI.8 for the different locations in the fleece. The method of solution is essentially the same as in section VI.2.a.

When a fiber reaches a temperature in the melting range, then the heat effect may by no means be taken as negligible. Using the actual integral melting curve, it is necessary to determine the slope of crystal melting *versus* temperature, $d\alpha/dT$, for a given segment of the fiber cross section. Based on the melting crystals, one may calculate the heat effect, or rather, the temperature decrease caused by the heat loss due to melting.

$$T_d = \frac{d\alpha \ \alpha \ H_m \ \Delta T_r}{dT \ w \ \Delta x \ C_p} = \Upsilon \ \Delta T_r \tag{XI.24}$$

Here w is the fiber weight titer adjusted to the used system, Δx is the length of the fiber interval used in the calculations, C_p is specific heat of the polymer, α is degree of crystallinity, ΔT_r is the actual temperature increase from the previous segment, H_m is the heat of crystal melting. The last quantity is not exactly constant and ought to be calculated separately for crystals grown at different temperatures. The net effect of the fiber temperature change may be conveniently obtained from the following equation.

$$\Delta T_r = \Delta T_i - T_d = \frac{\Delta T_i}{(1 + \Upsilon)} \tag{XI.25}$$

Here ΔT_i is increase of the temperature over the previous segment due to the heat transfer.

All of the temperatures are taken as relative values, usually divided by the maximum roll temperature.

Figures XI.6 and XI.7 present results of the calculations for two cases of bonding: at approximately correct temperature, and with somewhat excessive heat, respectively. At the top of each of the figures are calculations of temperature between the bonding pins and at the bottom of the graphs what happens under the bonding pins is shown. In the latter case, the final bond compression stage is shown separately; temperatures are given across the fiber radius for the surface and for the center of the fabric. For the more correctly heated material, the fibers between the pins never reach the temperature where the melting of crystals begins; this threshold is crossed only in the bond sites. In the second example, figure XI.7, the surface layer of the fibers between bonds do reach initial melting point. In the data presented in both of the figures, heating due to the impact compression has not been included.

The calculations of heat generation due to impact compression require some additional comments. The fiber distribution in a fleece, irrespective of the opinions based on macroscopic estimates, are never ideal in a microscopic sense. In view of

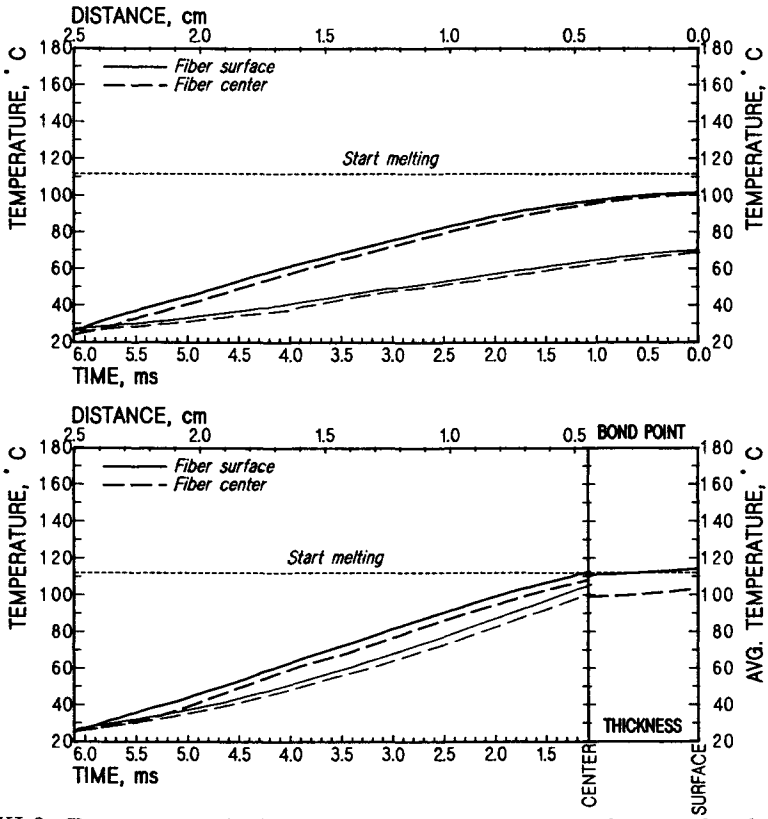

Figure XI.6: *Temperature of a fabric in the calender nip. Top – between bonds, bottom – under bonding pins. Correct heating, low pressure. Heavy lines - - surface of the fleece, fine lines – center of the fleece. No impact heat included.*

the small dimensions of the bond points, and even much smaller dimensions of the fiber diameter, the fiber distribution is never even and this in consequence leads to the formation of inhomogeneous bonds. A typical case, especially important for light weight fabrics, is presented by the photomicrograph of figure XI.8.

If the fibers are parallel to each other, there is a danger that under the pressure of a small bonding pin, room permitting, the fibers may spread into a monofiber layer. Fibers crossing each other have a smaller chance for such an escape. In addition, there is a question as to how many fibers may find themselves in one fiber cross section, their thickness, and from which location in the fleece cross section they originate. As it may be seen from figures XI.6 and XI.7, the fiber temperature is not uniform. As usual in similar situations, the uniformity of fiber distribution increases with the number of filaments, that is, with the surface weight of the fabric.

Calculations of the effect of impact compression lead to a number of possibilities. In figures XI.9 and XI.10 results of just such calculations are presented. Figure XI.9 – top corresponds to the heating conditions of figure XI.6, and the results given in figure XI.9 – bottom correspond to the case from figure XI.7. The

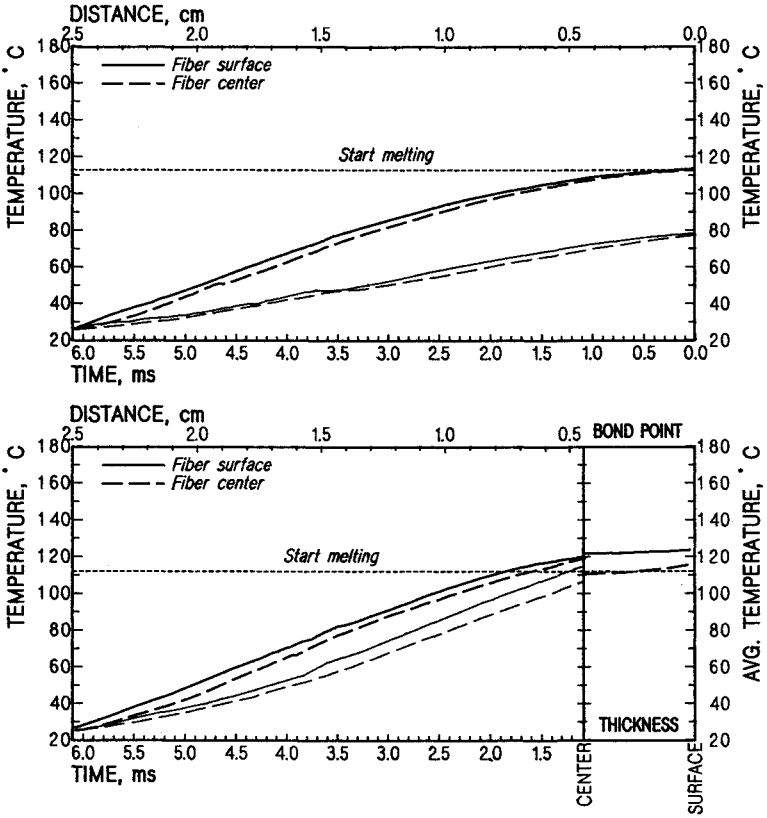

Figure XI.7: *Temperature of a fabric in the calender nip. Top – between bonds, bottom – under bonding pins. Too high heating, low pressure. Heavy lines – surface of the fleece, fine lines – center of the fleece. No impact heat included.*

same is true of figure XI.10 which shows the extent of the crystal melting *versus* bond thickness, where zero represents the bottom surface. Each of the figures presents the calculations of four different possibilities:

1. Four fibers *per* crossing, all from or near the top surface of the fleece – full drawn line.

2. Two fibers *per* crossing, both from the center of the fleece – dashed line.

3. Two fibers *per* crossing, both from the bottom surface of the fleece – dot - dash line.

4. Four fibers *per* crossing, two from the top and two from the bottom surfaces – dot - dot - dash line.

As the figures show, the different cases lead to markedly different results. As may be seen in figure XI.11, in real fabrics such situations really do exist. The figure presents photomicrographs of a 1 μm thick cross section of a bond point, cut perpendicularly to the fabric surface. The fabric is middle weight, too lightly

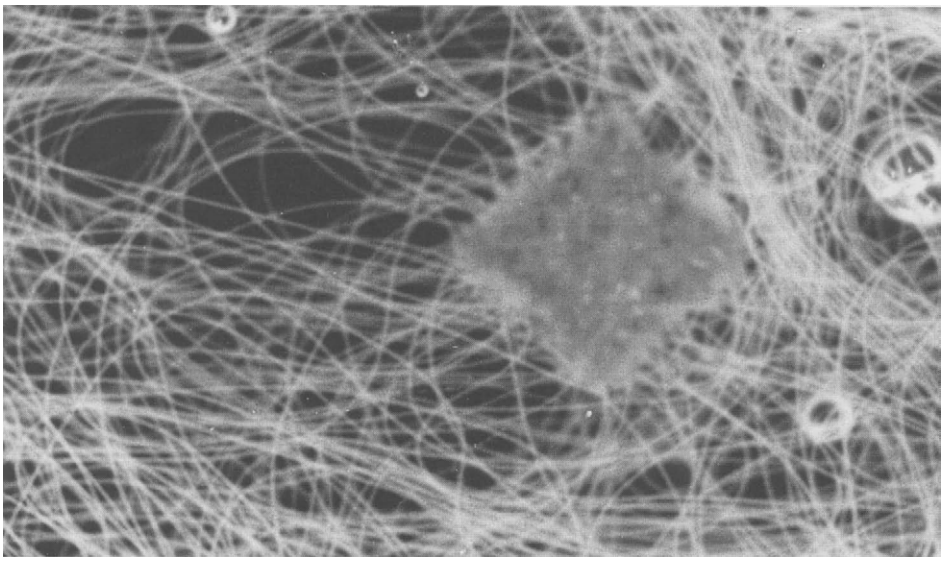

Figure XI.8: *Photomicrograph of a bond point in a lightweight fabric with not very uniform fiber distribution. Despite the high degree of fusion, nonuniformities of the bond point are visible.*

bonded, so the bond shows a tendency to disintegrate. One may see that the fibers adhere lightly, only a thin surface layer must have melted. The fiber cross sections, particularly those in the center of the fabric, are almost unaffected. Some fiber fusion did take place on the top surface of the fabric.

From the comparison of the figures, it is quite clearly evident how great a role the impact compression force plays in bonding. It is mostly a very positive role. As an optimum bonding situation one may define such a set of conditions which leads to the formation of strong bond points, while simultaneously the segments of fibers connecting the bond points are not permitted to lose their strength due to excessive heat exposure. The demands are high and perhaps difficult. To rephrase them, the fiber must be melted in a limited area of bond point and the rest of its length must stay as "cold" as possible. Reality does not permit full realization of this ideal, but closeness to the ideal condition may certainly be accepted as a determinant of the quality of the operation.

As difficult it may be to attain the ideal conditions in point bonding, it is still substantially easier than in any other operation of thermal bonding, as no other thermal bonding process known today offers the possibility of impact compression heating in discrete areas under largely controlled conditions. And this is the only thermal bonding operation known today which is able to provide well delineated, localized heating areas. To demonstrate the advantage more clearly, figure XI.12 shows also the temperature of a bond point of material with the more intense heating, as in figure XI.7, but the top graph shows a case with the generation of heat due to impact bonding omitted. This corresponds fairly closely to the

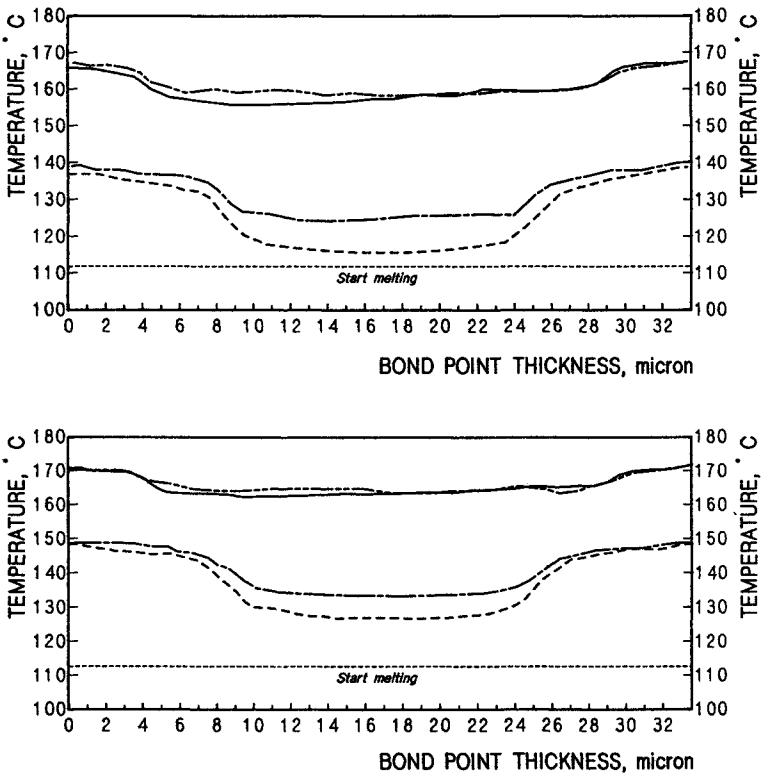

Figure XI.9: *Temperature of the cross sections of a bond point. Heat effect of the impact compression included. Top – heating from figure XI.6; bottom – heating from figure XI.7. Detailed explanation in text.*

condition obtainable in a plain roll calender or even through-air bonder. The bottom graph of figure XI.12 shows the same conditions with application of a higher bonding pressure, that is, with stronger generation of adiabatic heat. Figure XI.13 gives the melting of crystals in a bond point produced under the conditions of figure XI.12 – bottom. The bonding is, no doubt, excessive.

Due to the different bonding pressure in figure XI.12 – bottom and in figure XI.13, there is a somewhat different "fiber mix" than in figures XI.9 and XI.10. Here the combinations are as follows:

1. Five fibers *per* crossing, all from or near the top surface of the fleece – full drawn line.

2. Three fibers *per* crossing, all from the center of the fleece - - dashed line.

3. Four fibers *per* crossing, all from the bottom surface of the fleece – dot - dash line.

4. Five fibers *per* crossing, three from the top and two from the bottom surfaces – dot

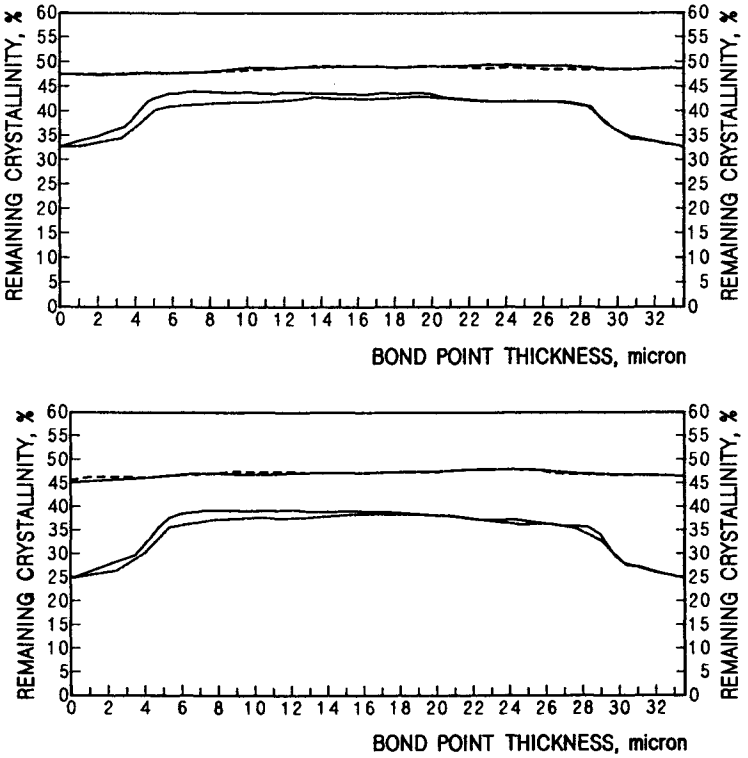

Figure XI.10: *Melting of the crystals in a bond point. The figure corresponds to figure XI.9. Detailed explanation in text.*

Figure XI.13 shows that the combinations 1 and 4 give the same result, fully superimposed lines, with crystallinity over a great majority of the bond point equal zero. Combination three gives results very close to those of combinations one and four. Only combination number two, all fibers from the center, has some 17 to 21 per cent of crystallinity left of the 50% determined for the fibers before bonding. The case without application of adiabatic heat generation, not shown in the figure, yields crystallinity of about 48 to 49% throughout the bond thickness; this means barely a surface softening.

Closer examination of the fiber cross sections in the bond sites shown in figures XI.8, XI.14, and XI.16 leads to the conclusion that the majority of fibers, even after being severely deformed, do not lose their identity totally. Even when the fibers are fused to form a block, the individual fibers, or their remnants, may be recognized; the optical properties of the oriented structures survive. Measurements of birefringence on bonded fiber cross sections indicate that the fibers, or better what were fibers, are still birefringent; the birefringence is highest along the fiber axis and decreases toward the surface.

The behavior of fibers in bonding, naturally, depends on the viscosity of the polymer melt under the bonding conditions. The portion of fibers which melts

completely and is heated to the point of relatively low viscosity is to a large extent

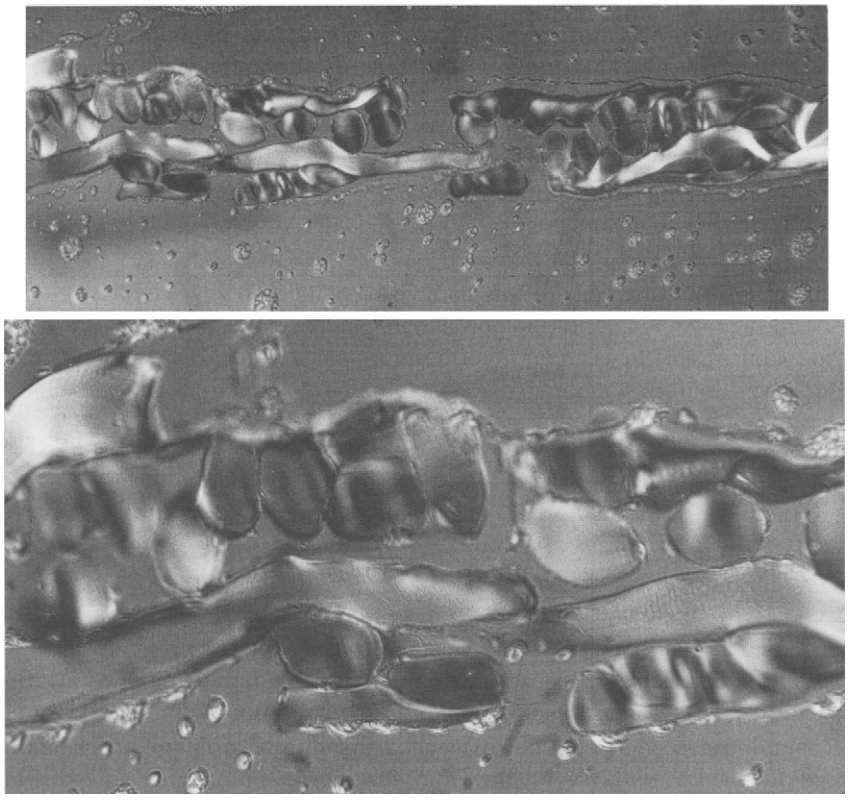

Figure XI.11: *Photomicrograph of a cross section of a bond point showing uneven, incomplete bonding and a tendency to disintegrate. Bottom – same at a higher magnification.*

expelled from the bond point to its perimeter. Some portion of the melt may fill the voids between the individual filaments, and all of it serves as a heat transfer agent delivering the heat to the unmelted fiber segments.

The calculations quoted above do not take into consideration the lateral heat flow, which for fibers and polymer melts is quite small and may be neglected. When the polymer if forced to flow, however, this represents a different story. There seem not to be enough justifiable assumptions to start contemplating the direction, intensity, extent of the flow and the connected heat transfer or conduction.

The effect of the point bonding process on overall crystallinity is presented in table XI.1, which presents experimental data on polypropylene fibers bonded in close to optimum conditions. Interpretation of the data given in the table XI.1 is not completely clear. An increase of the degree of crystallinity between the bond points may easily be ascribed to an annealing-like effect caused by the heat. The decrease of crystallinity in the bond points may be explained by a far reaching

melting and extremely short residence time in the nip. Past the nip exists a

Table XI.1
Crystalline properties in polypropylene fibers before and after point bonding.

Specimen	Crystal-linity %	Begin melting °C	Peak melting °C	End melting °C
Unbonded fiber	50.4	112	170	195
Bond points	42.3	119	167	192
Between bonds	54.5	138	166	187

Data from differential scanning calorimetry.

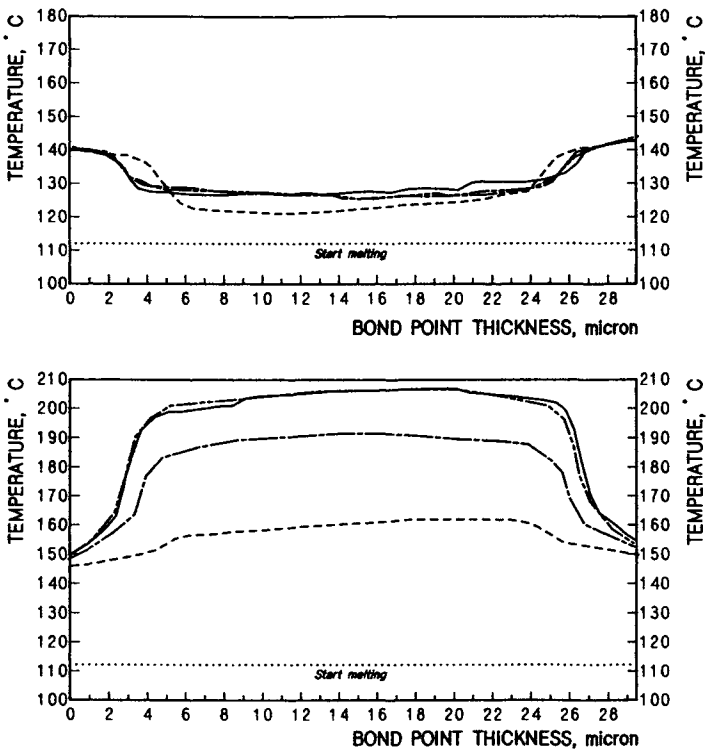

Figure XI.12: *Temperature distribution in a bond point. Case similar to that in figure XI.10. Here the top graph is without adiabatic heat generation, and the bottom shows a case with higher bonding pressure and somewhat different fiber combinations. Details in text.*

situation reverse to that before the nip; the fabric recovers to some extent from the compaction and admits air, but the air at this location is much cooler. In effect, at a lower temperature and without strain, the polymer may crystallize to a smaller extent. The shift in the temperature of the beginning of melting may

also be explained by an annealing effect. However, there is no good explanation

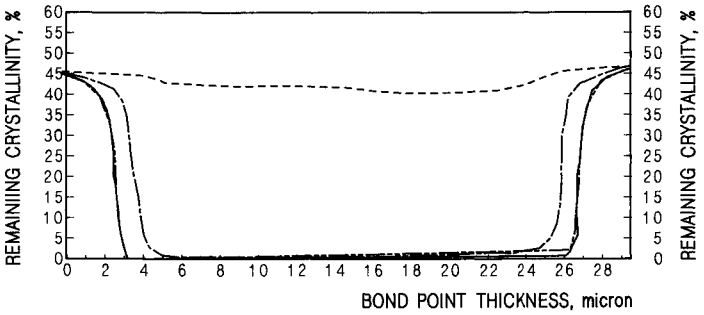

Figure XI.13: *Crystal melting in a bond point. Case from figure XI.12 – bottom, strongly overbonded. Details in text.*

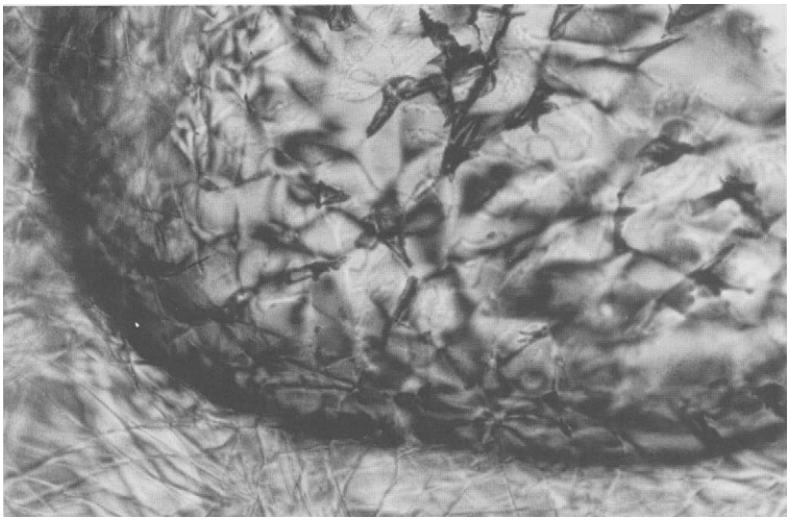

Figure XI.14: *Photomicrograph of an overbonded bond point, top view, showing some portion of the polymer expelled to the perimeter. Similar to the case given in figure XI.13.*

for the decrease of the peak and final melting temperatures. The $3°C$ to $4°C$ decrease is too large to be explained by the entropy changes, particularly since the fibers were drawn only to a modest degree. The only tentative explanation may be that these are the results of a recrystallization in the presence of some surviving crystal embryos; fibers retain their identity past the bonding process. However, why the highest melting elements were to suffer more remains unclear.

The methods of thermal bonding, other than point boning, may be treated in the same way as the heat transfer considered here. Naturally, for through-air

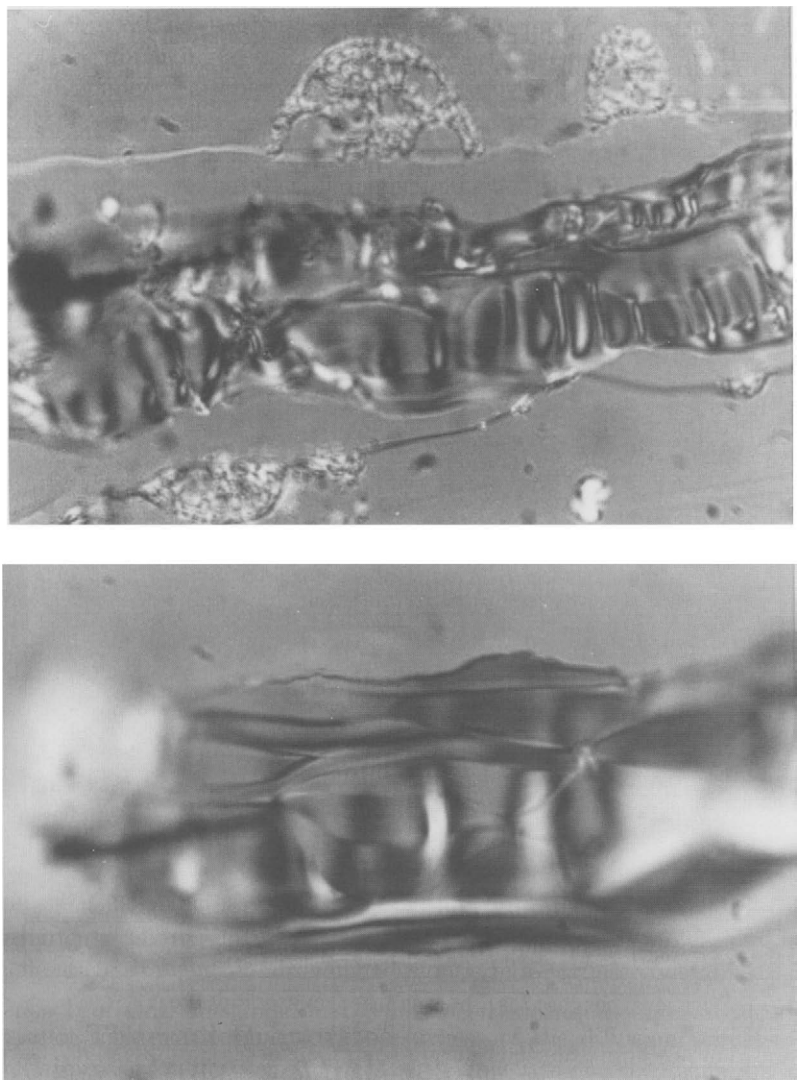

Figure XI.15: *Cross section of a bond point, similar to the overbonded case given in figure XI.13, medium weight fabric. Bottom, same specimen at higher magnification. Cross section 1μm, differential interference contrast.*

bonding it is necessary to omit the adiabatic heat generation due to the impact compression. In the case of plain roller calender bonding, there is some impact force to be considered on every fiber crossing which stands above the nip gap setting. It is usually many crossings and the load is distributed on all of those crossings, what results in a low adiabatic affect and a large number of bonds with

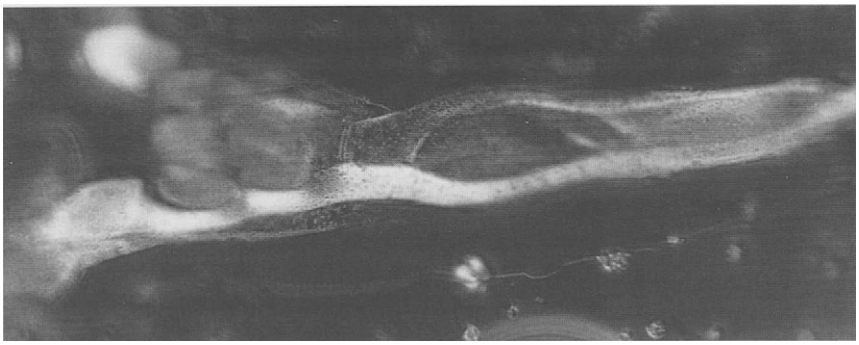

Figure XI.16: *Edge of a bond point in a light fabric, overbonded, fibers escaping to the perimeter. Cross section 1μm, differential interference contrast.*

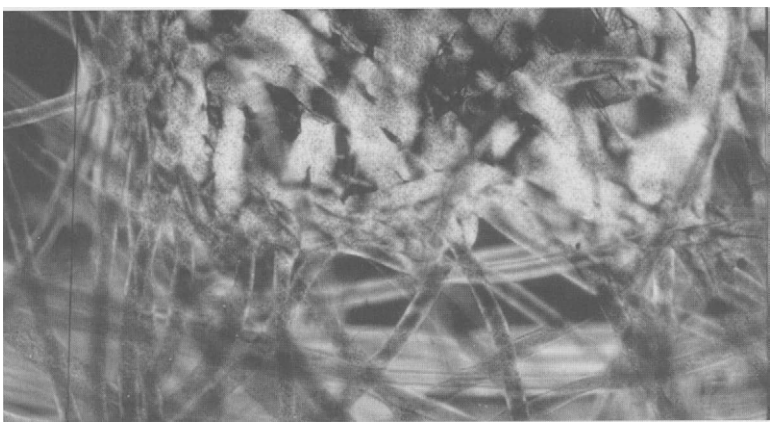

Figure XI.17: *Top view of a close to the optimum bond point quality, medium weight fabric. Differential interference contrast.*

short distances between them.

XI.3 Properties of Fabrics

The fabric properties depend on the properties of the individual fibers and on the strength of the fiber bonds. Morphology of the fibers is of a great significance. Theoretical calculations of the mechanical properties of nonwovens were conducted by Haerle and Newton,[18], Żurek[19] using analytical approaches, and Walczak[15] applying numerical methods to the discrete point bonded fabrics. In an effort not to cross over the boundaries of the subject matter of this book, only a summary of the spunbond properties are covered here.

The fabric morphology has the overpowering influence on the fabric strength, mainly the fiber directionality and strength of the individual fibers. The fiber directionality depends on the methods and equipment used to deposit the fibers

on the conveying wire. The fiber bending modulus has a very small, practically negligible influence. As for the fiber strength, the matters are not quite as straight forward. Thermal bonding, as any other heat treatment, does have an influence on the entire stress-strain curve of fibers.

The numerical calculations[15] permitted us to use the entire stress strain curve, rather than just a constant value of the modulus or any other simplification. It has been found that the stress-strain curve of fibers removed from bonded fabrics could be described by the general model as given in the equation XI.26[19].

$$\sigma = A\varepsilon + B[1 - \exp(-k\varepsilon)] \tag{XI.26}$$

Here σ is extensional stress, ε is extensional strain, A, B, and k are constants. The majority of stress-strain curves of the unbonded fibers could be described very successfully with the following formula.

$$\sigma = A\varepsilon^b \exp(-k\varepsilon) \tag{XI.27}$$

In the last equation A and b are constants.

The difference in the equations describing the stress-strain curves indicates the great depth of the changes suffered by the fibers as a result of heat exposure. This explains also why in the previous section so much emphasis was put on the protection from excessive heat exposure of those segments of fibers which do not form bond points.

Somewhat surprisingly, the initial modulus has a very strong influence on fabric strength. For example, an increase of the initial fiber modulus by a factor of 8.3 in an anisotropic fabric gives an insignificant increase of strength in the 0° (machine) - direction at break elongation smaller by about 25%. In the 90° (transverse) - direction, the strength is 15% higher and break elongation 15% lower.

The area occupied by the bond points has little influence on the fabric strength when more than some five per cent of the fabric surface is covered by bond points; strength increases slightly up to six or seven per cent of bond area. Below five per cent area, however, the decrease of fabric strength with the decreasing bond area is quite dramatic.

When the fiber morphology is highly anisotropic, bond point area has a somewhat larger effect on the tensile strength in the directions transverse to the machine direction. The pattern of bond point distribution, as well as the size of the individual points have very little influence on tensile properties.

Tear strength of nonwoven fabrics shows very similar dependencies as the tensile strength; bond point pattern and bond point area have even a little smaller influence on tear than on tensile strength.

Bending modulus is a very important property. It governs such subjective fabric properties as "drape" and "pliability", those properties in which nonwovens are by their nature deficient. But here we have a surprise: boding pattern has a very significant influence on bending modulus. The earlier attempts at calculation of bending[20,21] gave results showing large discrepancies with experimental data.

Żurek[22] suggested that the discrepancies may be the result of the fact that buckling of the fibers was not taken into account.

Microscopic investigations[15] of fabric bending show that, contrary to the normal treatment of bending bars or plates, the neutral plain is not located in the middle of the specimen thickness, but rather on the surface which bends over the largest radius. This results from the fact that the force needed to extend a fiber is many times greater than the force needed to buckle it. Even in case of nonwovens made of elastic polyurethanes, the neutral plane, depending on the type of polymer, is either on the surface with the largest radius or closely under this surface, never in the center.

If the above is taken into consideration, the results are easy to predict. Such morphologies show low bending modulus which have long fiber segments between bonds. The length facilitates buckling. Often the length of fibers between bond points in a fabric is uneven; in such cases, the larger the fraction of long segments, the lower the bending modulus. Also, space is needed for the fibers to buckle, so for lower bending force the fabric density ought to be low.

Naturally, where bending modulus of a nonwoven fabric is of particular importance, elastomeric fibers or crimped fibers would be the obvious choice of fibers. Unfortunately, so far no spunbond process resulting in crimped fibers is known.

Abrasion resistance belongs to the group of more important textile properties. In the case of nonwovens, the mechanism of abrasion is somewhat complicated. If the abrading force acts parallel to the fibers, then the fiber resistance is higher. If the force acts perpendicular to the fibers, their resistance depends on the fiber length between the bonds. When the force acts perpendicularly, then the fibers behave similarly to a sling, and in this case the fiber resistance depends primarily on its ability to recover from deformation.[22] In pure abrasion, such as that under forces acting parallel, the resistance of fibers is inversely proportional to their tenacity.

XI.4 Spunbonded from Solution

Dry fiber formation from solution has an important advantage. If the fibers are collected on the transporting wire with an impact, and if at the moment of impact the fibers are still tacky, incompletely dry, then the process is *self bonding.* This means that the bonding is accomplished in one operation with the fiber formation.

The self bonding process is advantageous not only from the point of view of economy: there may be little differentiation in the bond strength across the fabric thickness. With other bonding techniques providing for uniform bonding across the fabric thickness is difficult; a tendency to delamination is observed, and the tendency grows with the increasing fabric thickness.

Theoretically, wet formation may yield selfbonded spunbonded materials; the inherent slowness of the wet processes, however, collides with the commercial interests. There are known spunbond processes utilizing dry formation from solution, but they employ nonconventional formation methods: electrostatic[24] or centrifu-

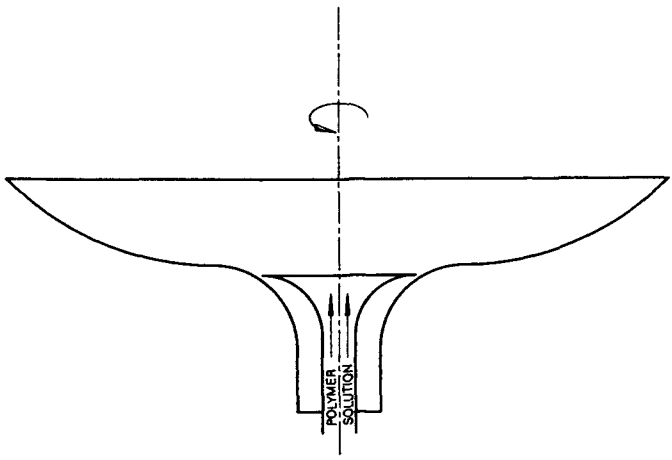

Figure XI.18: *Schematic sketch of the rotating cup used for centrifugal- electrostatic fiber formation. According to J. Fine and S. de Tora.*[25]

gal - electrostatic.[25] None of the processes has achieved great commercial success. However, the centrifugal-electrostatic process is capable of yielding very interesting products, and therefore it is given some attention here.

A filtered and metered polymer solution is introduced axially to a rotating cup, as in the schematic sketch in figure XI.18. Centrifugal force spreads the solution over the surface of the cup, with the increasing radius the solution layer becomes correspondingly thinner. In a properly running process, the viscosity of solution and velocity of rotation (the centrifugal force) must be so adjusted that the thin film of polymer solution splits into filaments on leaving the rim of the rotating cup. The splitting may actually take place on the rim itself or some five to six millimeters outward.

The centrifugal force throws the filaments out in a radial direction. To attract the fibers to the collecting wire an electriostatic field, of strength usually between some 50 and 120 KV,is applied between the rotating cup and the collecting wire. The distance between the cups and the collecting wire is so selected that the fibers adhere to each other on impact since they are not completely dry. The original patent suggests the spraying operation to be upwards, but with a little change in the design of the solution entry to the cup, the configuration may be reversed to a downward spraying.

Solvents of low electrical conductivity must be used to avoid discharges in the electric field. All the machinery must be in an enclosure which serves as a drying chamber, and this is one of the points which makes the process somewhat cumbersome.

To provide for high basis weight uniformity, the rotating bells are made to oscillate in the direction perpendicular to the wire motion. The natural pattern from one bell is a ring with fiber lay down density of approximately normal distribution in the radial direction.

The original process was capable of producing exceptionally uniform fabrics of a wide range of surface weights. Fibers of ten micron or less are easily obtainable. Polyurethane solutions gave very delicate fabrics of very interesting properties. If the individual fibers are around ten microns or less, then elastomeric fibers do not have any rubbery appearance, they are rather soft and velvety. Fine fibers of some elastomeric polymers other than polyurethanes may be obtained also in the meltblown process. Nevertheless, meltblown fabrics must be bonded and in this operation the exceptional properties of fabrics are lost. The electrostatic - centrifugal process is also well suited for laminations.

Many other polymers may be used in the process, however, the fibers cannot be cold drawn, so only such polymers which do not require drawing are really suitable.

XI.5 References

1. W. Żurek: *Struktura przędzy* (Structure of yarn), Wydawnictwa Naukowo - Techniczne, 2^{nd} Ed., Warszawa, 1971.
2. W. Żurek and A. Kopias: *Struktura płaskich wyrobó włókien-niczych* (Structure of flat textile products), Wydawnictwa Naukowo – Techniczne, 2^{nd} Ed., Warszawa, 1983.
3. *U. S. Pat.* **No. 3,352,734 (1967)**, to Imperial Chemical Industries.
4. *U. S. Pat.* **No. 3,341,394 (1967)**, to E. I. Du Pont De Nemours.
5. *U. S. Pat.* **No. 3,117,055 (1964)**, to E. I. Du Pont De Nemours.
6. *U. S. Pat.* **No. 3,368,934 (1968)**, to E. I. Du Pont De Nemours.
7. F. W. Manning, *U. S. Pat.* **2,411,660**.
8. V. A. Wente, *Tech. Report No. PB111437, Naval Research Lab.*, **NRL - 4364, 4/15/1954.**
9. R. L. Shambough, *Ind. Eng. Chem. Res.*, **27 (1988)**, 2363.
10. M. A. J. Uyttendaele and R. L. Shambough, *AIChE., J.*, **36 (1990)**, 175.
11. T. T. Wu and R. L. Shambough, *Ind. Eng. Chem. Res.*, **31 (1992)**, 379.
12. R. S. Rao and R. L. Shambough, *Ind. Eng. Chem. Res.*, **32 (1993)**, 3100.
13. H. Bodaghi, *INDA JNR*, **1, No. 1**, 14.
14. T. A. Zack, A. S. Curro, K. R. Randall: *New Developments in Through - Air Bonding*, paper presented at *Index 84* Congress, 1984.
15. A. A. Buykis and Ya. Ya. Tehts, *Primen. Modif. Polim. Mater. Konstr. Melior. Sist.*, **(1983)**, 54.
16. S. B. Warner, *Text. Res. J.*, **59 (1989)**, 151.
17. Z. K. Walczak: *Thermal Bonding of Fibers*, Kimberly - Clark Corp., Dalla – Atlanta – Neenah, 1992.
18. C. L. Choy, *Polymer*, **18 (1977)**, 984.
19. D. Hands, K. Lane, and R. P. Sheldon, *J. Polymer Sci., Symposia*, **No. 42 (1973)**, 717.
20. J. W. S. Haerle and A. Newton, *Text. Res. J.*, **37 (1967)**, 778.

21. it ref. 2, pp. 294 ff.
22. W. D. Freeston, Jr. and M. M. Platt, *Text. Res. J.*, **35 (1965)**, 48.
23. S. M. Lee and S. Argon, *Text. Res. J.*, **74 (1983)**, 1; 12.
24. *ref. 15*, p. 226.
25. *ref. 15*, p. 253.
26. *Ca. Pat.* **No. 937,827 (1973)**, to Farbenfabriken Bayer 26
27. J. Fine and S. A. De Tora, *U. S. Pat.*, **No. 4,223,101 (1980)**, to Inmont Corp.

XII SPECIAL TECHNIQUES

XII.1 Fibers with Noncircular Cross Sections

Generally, natural fibers do not have plain surfaces: wool has tiny scales, cellulosic fibers have other kinds of surface roughnesses. Fibers are produced with variegate surfaces not only to imitate nature, but also because certain fiber properties are affected by the surface structure. They are:

- Fiber-to-fiber friction , which affects the way fibers are processed and influences the resulting fiber and yarn properties.
- Fiber appearance is highly dependent on the surface. The more pleasing appearance is obtained with fiber cross sections of lower symmetry, *e.g.* cross sections with an odd number of lobes give a more eye-pleasing effect than do those with an even number of lobes.
- The bulk density of fiber changes somewhat. This is also a matter of bending rigidity and its dependence on the cross section. The bending rigidity and the density of fiber-to-fiber packing are responsible for the bulkiness and *hand*, that is the sensual perception to touch.
- Increase of the fiber surface area affects the sorptional properties, water retention, and dyeability.

Figure XII.1 presents some of the more common fiber cross section and the cross sections of the capillaries from which they were extruded (top row). The figure must be treated as an approximation only; the deformation from the capillary cross section to the fiber cross section is related to the die swell. The die swell depends on the nature of the polymer in question, and on the particular processing conditions; the larger the die swell the larger the deformation. Not without significance is time. The longer the filament remains hot after leaving the spinnerette, the larger the

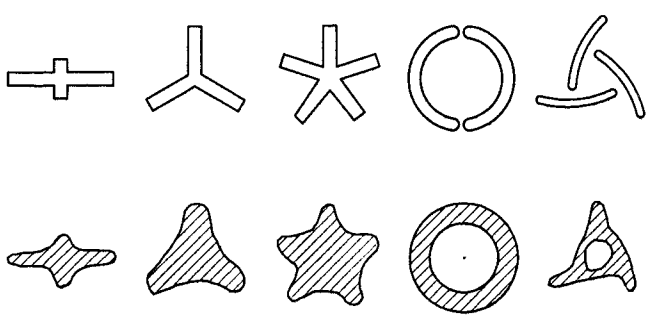

Figure XII.1: *Cross section of capillaries (top) and the approximate cross sections of resulting fibers (bottom).*

deformation of its cross section by the normal forces remaining after the capillary flow.[1] If the fiber stays hot for a prolonged time, the surface tension may also contribute to the deformation of the cross section, though the surface tension forces are much weaker.

Han and co-workers have studied the effect of diameter attenuation on the shape of the cross sections.[2,3] The authors have found that in wet formation, increasing extension decreases the changes of the cross section. In formation of polypropylene fibers from the melt, the cross sections were insensitive to the extention ratio.

The generalizations of flow in noncircular ducts are mathematically involved,[4–9] therefore for capillary design purposes, a simplified method developed by Miller[10] is more often used. According to Miller's view, for non- Newtonian fluids the relationship between the average wall shear stress and the apparent wall shear rate, to a good approximation, do not depend on the duct geometry. The average shear stress at the wall for noncircular cross section ducts is described as follows.

$$\tau = \frac{\Delta P \; D_h}{4 \; L} \tag{XII.1}$$

Here ΔP stands for extrusion driving pressure, L is length of the duct (capillary), and D_h represents the hydraulic diameter.

$$D_h = \frac{4 \; q}{S} \tag{XII.2}$$

where q is cross sectional area of the channel, and S is the wetted perimeter. For the circular ducts the hydraulic diameter equals the actual diameter.

The apparent shear rate at the wall is

$$\dot{\gamma} = \frac{Q \; \lambda}{2 \; q \; D_h} \tag{XII.3}$$

where Q is volumetric flow rate, and λ is the shape factor, which depends only on the geometry of the cross section, it is a product of Reynolds number, based on average velocity and hydraulic diameter, and friction factor for a given channel. Values of the shape factors for some shapes are given in table XII.1

The relationship between the fiber cross section and the capillary cross section is largely proportional to the die swell, which may be estimated from laboratory measurements and recalculated using the above given equations. Agreement between the recalculated predictions and experiment is not necessarily good.

Depending on the degree of sophistication of the capillary maker, some problems with the junction between the conical entry to the capillary and beginning of the capillary itself can be expected. The practical results are sensitive to this element of spinnerette construction. This is the reason why many noncircular capillaries are made with flat entries.

Generally, one hears just complains about die swell. For once, there is an advantage being taken of the die swell in the case of some types of cross sections,

Table XII.1
Values of shape factor for various cross sections.
After C. Miller[10]

Shape of cross section	Shape factor λ
Three-pointed star	6.50
Four-pointed star	6.61
Five-pointed star	6.63
Square	14.3

as may be seen in figure XII.1. This is particularly true in the case of hollow fibers, which may be produced also from capillaries having a solid core, although these are much more expensive to produce and much less durable.

Cross sections with sharp points, for example, certain stars, may cause problems with local fracturing. This is often the reason that noncircular fibers are not much extended from the melt and even less neck drawn. The majority of this type of fibers is produced for the sake of their appearance and for their textile properties, there are no great demands put on their strength. Hollow, particularly circular hollow, fibers represent an exception. Their main application is for *reverse osmosis*: for desalination and purification of water, for dialysis, and the likes. The applications for reverse osmosis are demanding in terms of fiber quality.

With applications of hollow fibers other than reverse osmosis, particular care must be taken since various bacteria immensely enjoy the long "tunnels", and there is no good way to get them out of there.

XII.2 Crimping - Bulking - Interlacing

Beside the changes in the cross section of fibers, there is another way to make man-made fibers more like natural fibers – *crimping* or *bulking* or *texturing*. This means making the fibers wavy or spiral rather than straight. One needs to add that making the fibers more like natural fibers is not just a matter of empty copying, it is changing the fibers to fulfill the demands of textile structures and processing.

The techniques used for texturing fibers may be divided into two groups:

- Processes which take advantage of the thermoplastic properties of fibers to change the fiber axis into a curvilinear.
- Strictly mechanical processes to rearrange the positions of the fibers in a bundle so that the fiber axes will no longer be parallel.

Among the first group the most common are:

Gear crimping, which is based on heating a tow of continuous fibers to a temperature close to the onset of melting and passing it between a set of hot gears.

The gears force a wave shape on the hot fibers, and the new form is set by the subsequent cooling.

Stuffer box is a hot chamber into which a tow of continuous filaments is overfed and removed at a lesser velocity. The hard packing of the fibers forces the fibers to change their axes into an irregular three dimensional arrangement, which is fixed by cooling upon removal of the fiber from the chamber.

Bulked continuous filament, (BCF), process may be considered a modernization of the stuffer box process. High pressure hot air, or steam, instead of a mechanical device is used to pack the filament tow into a chamber and exert pressure. The changes imposed on the fibers are similar to those produced by the stuffer box. The quality of the three dimensional crimp is regulated by the design of the chamber, pressure, temperature, and speed of removing the tow. This method of crimping is used particularly often to produce yarn for the carpet industry.

False twisting is an operation where a tow of yarn is twisted, heat set, and untwisted in one line. The speeds of operation are reaching $1200 m/min$ with rotational yarn speed reaching $7,200,000 rev/min$. The spiral type of twist is responsible for high stretch of the yarn, and it is not suitable for every textile application; nonetheless, almost three quarters of crimped fibers are made by this technique.

"Knit - de-knit" texturing is similar in principle to the false twisting, the fibers have looping rather than spiral configuration. This technique is not very frequently used.

All the texturizing processes utilizing heat impose some damage to the fiber properties. The high temperature, close to the crystalline melting point, affects the fiber morphology; the high pressure treatment may also result in mechanical damage to the fibers, particularly in combination with high temperature.

Air jet texturing[11,12] is the only process which uses cold air and therefore the damage to the fibers is small. The device for the jet texturing is a nozzle which generates a supersonic, turbulent and non-uniform flow. When the filaments are overfed into the nozzle they are transported by the air flow and discharged from the texturing end. The supersonic turbulent air forces the individual filaments into all kinds of loops which are trapped in the tow (yarn) structure. The fibers are usually wetted before entering the nozzle. The entry and discharge of the yarn is, as a rule, perpendicular to the nozzle axis, while the compressed air is introduced into the nozzle on an angle of some 45° to the nozzle axis. There are, naturally, a great variety of different nozzle designs.[12]

The character of air jet textured yarn is different from the yarn textured by the processes of the first group. They remind one of yarn spun from staple fibers, both by their properties and appearance. Due to the entangled yarn morphology and due to the loops being locked between the neighboring fibers; the flat bundle of fibers has stable shape under normal use forces, contrary to false twisted yarn and other, the bulk of which decreases with imposed strain.

There is another group of crimping operations known which involve fiber formation processes like asymmetric quench and neck drawing over a sharp edge.

These processes yield a rather mild crimp, more like wavy fibers. Asymmetric quench is difficult to control well enough to assure sufficient reproducibility of the results. Drawing over a sharp edge cannot be done sufficiently fast, or break level is too high. In effect, these historical processes do not have a practical significance today.

The texturing operations are often done by the textile industry rather than by the fiber producers, and this is dictated by reasons such as adjusting the texturing to the demands of a given fabric, and that texturing velocities are closer to the velocities of textile processes rather than to the velocities common in a modern fiber production. The fiber industry textures mainly staple fibers. Because texturing is mostly connected to textile problems, the mechanical properties due to crimp are not quoted here and the interested reader is referred to the specialistic literature.[16,17]

Continuous filament yarn, consisting of straight fibers with flat surface, have neither high friction nor forces normal to the fiber axis which would hold the bundles together. Bulked yarn, say false twisted, also does not have the normal forces to hold the yarn together. This creates problems with winding and processing as the yarn may snatch between the overlapping layers, which leads to tension irregularities and breaks. To alleviate these problems the yarn might be sized or twisted, or both, but these operations are expensive. The situation was helped greatly when the process of *interlacing* (or *intermingling*) was developed.[13,14] The relative costs of the operations are *sizing : twisting : interlacing = 100 : 72 : 11*.[15]

Interlacing is an in-line process whereby the yarn is led through a tube to which a cold air jet is introduced mostly perpendicularly to the yarn. In the place where the yarn and the air jet meet the channel is slightly widened. However, there is a great variety of designs of the interlacing nozzles.[12,13] The turbulent air jet locally opens up the bundle of fibers and causes the fibers of the neighboring segments, up and down the line, to intermingle with each other to form a compact segments (so called *nips*). If an intermingled section moves in from up- stream, then the jet cannot open it. This leads to the situation where the interlacing works in segments.

The interlacing operations are done mostly by the fiber industry on the continuous straight filament yarn. The nozzle is placed usually after neck drawing and relaxing, just before winding. For intermingling are mostly used low pressure nozzles which produce continuous intermingling, without forming "nips",[14] tiny fiber bundles, which could be disturbing in the further textile processing or bulking of the yarn.

XII.3 Biconstituent Fibers

Utilization of two polymers for fiber making has been tempting fiber developers for a very long time and a substantial effort has been invested in this field. The main obstacle here is the small number of compatible polymer pairs.

The problems of polymer compatibility are being investigated from many dif-

ferent angles, primarily from the point of view of thermodynamics. [18–25] This field has not been developed to the point of applicability for the needs of technology. More suitable are the gains made in the field of rheology,[26–30] and particularly those efforts coupled to the investigations of the interfacial tension and glass transition temperatures.[30,31]

Helfand and co-workers[32–34] stressed the connection between the Flory-Huggins polymer - polymer interaction parameter, χ, and interfacial tension, $\gamma_{1,2}$.

$$\gamma_{1,2} = \sqrt{\frac{\chi_{1,2}}{6}} \cdot \rho_0 \; b \; k_B \; T \tag{XII.4}$$

In equation XII.4, ρ_0 is the number density of repeat units in pure polymer, b is the effective length per repeat unit, k_B is the Boltzmann constant, and T is absolute temperature. The interaction (or compatibility) parameter is related also to the solubility parameter, δ.

$$\chi_{1,2} = \frac{(\delta_1 - \delta_2)^2}{\rho_0 \; k_B \; T} \tag{XII.5}$$

Determination of the interaction parameter is almost as difficult experimentally as is the determination of the solubility parameters. On the other hand, determination of the interfacial tension in polymers also is rather difficult. A convenient way for these determinations has been suggested by Gramespacher and Meissner.[30] While analyzing rheological behavior of a series of polymer blends of different compatibilities, the authors have found that in oscillatory tests, the loss moduli of the blends are between the loss moduli of the components, and this is the case over the entire frequency range of four and a half decades. The storage modulus, however shows a dependence on the composition of the blend. The composition dependence is almost nonexistent above the frequency of about $\omega = 0.5 \; rad/s$, but becomes progressively larger with decreasing frequency.

In analyzing the frequency dependence of the complex moduli, the authors take into account the contributions of the viscoelastic properties of the components and of the interfacial tension. Thus, for the complex modulus we have:

$$G^*_{1,2} = G^*_{components} + G^*_{interface} \tag{XII.6}$$

The value of the modulus of the component the authors obtain from a simple additivity of the components.

$$G^*_{1,2} = \phi \; G^*_2 + (1 - \phi) \; G^*_1 + G^*_{interface} \tag{XII.7}$$

In equation XII.7, subscript 2 denotes the dispersed phase, subscript 1 is for the continuous phase, and ϕ stands for the volume fraction of the dispersed phase. To describe the influence of the interfacial tension on the moduli, Gramespacher and Meissner[30] take advantage of the theory of mixtures of Newtonian fluids developed by Choi and Schowalter.[35] The theory presents a constitutive equation for the rheological behavior of concentrated emulsion of two Newtonian liquids. Scholz

and co-workers[36] simplified the equation by neglecting the nonlinear terms and derived the storage and loss moduli as follows.

$$G'(\omega) = \eta \frac{\omega^2(\theta_1 - \theta_2)}{1 + \omega^2\ \theta_1^2} = \frac{\eta}{\theta_1}\left(1 - \frac{\theta_2}{\theta_1}\right)\frac{\omega^2\ \theta_1^2}{1 + \omega^2\ \theta_1^2} \tag{XII.8}$$

$$G''(\omega) = \eta \frac{\omega^3\ \theta_1\ \theta_2 - \omega}{1 + \omega^2\ \theta_1^2} = \frac{\eta}{\theta_1}\left(1 - \frac{\theta_2}{\theta_1}\right)\frac{\omega\ \theta_1}{1 + \omega^2\ \theta_1^2} + \omega\ \eta \frac{\theta_2}{\theta_1} \tag{XII.9}$$

Here θ is relaxation time, η represents the Newtonian viscosities of the two components; in both cases the subscripts determine as above, 2 for the dispersed phase. If we designate

$$k = \frac{\eta_2}{\eta_1} \tag{XII.10}$$

then viscosity may be further defined as follows.

$$\eta = \eta_1 \left[1 + \phi \cdot \frac{(5k + 2)}{2\ (k + 1)} + \phi^2 \cdot \frac{5\ (5k + 2)^2}{8\ (k + 1)^2}\right] \tag{XII.11}$$

$$\theta_1 = \theta_0 \left[1 + \phi \cdot \frac{5\ (19\ k + 16)}{4\ (k + 1)(2\ k + 3)}\right] \tag{XII.12}$$

$$\theta_2 = \theta_0 \left[1 + \phi \cdot \frac{3\ (19\ k + 16)}{4\ (k + 1)(2\ k + 3)}\right] \tag{XII.13}$$

$$\theta_0 = \frac{\eta_1\ R}{\gamma_{1,2}} \times \frac{(19\ k + 16)(2\ k + 3)}{4\ (k + 1)} \tag{XII.14}$$

In equation XII.14 R stands for the radius of the monodisperse inclusions.

The emulsion has elastic properties as described by the storage modulus (equation XII.8) despite the Newtonian character of both its components. The reason for this is the interfacial energy on the boundary of the two phases. In equation XII.9, the last term on the right hand side does not depend on the interfacial tension but results from the viscosities of the Newtonian fluids. In equation XII.8 the interfacial tension comes only in the first term on the right side.

The reason for the greater influence of interfacial tension on the storage modulus at low frequencies is this: this region of the viscoelastic behavior is dominated by viscous effects. Therefore to describe the complex modulus at the interface Gramespacher and Meissner[30] take advantage of equation XII.8 and only the first term of equation XII.9. In equation XII.10 the viscosities η_1 and η_2 are taken as zero-shear viscosities of the matrix and dispersed phase, respectively. Thus the final equations will have the form as follows.

$$G'_{1,2} = \phi\ G'_2 + (1 - \phi)\ G'_1 + \frac{\eta}{\theta_1}\left(1 - \frac{\theta_2}{\theta_1}\right)\frac{\omega^2\ \theta_1^2}{1 + \omega^2\ \theta_1^2} \tag{XII.15}$$

$$G''_{1,2} = \phi\ G''_2 + (1 - \phi)\ G''_1 + \frac{\eta}{\theta_1}\left(1 - \frac{\theta_2}{\theta_1}\right)\frac{\omega^2\ \theta_1^2}{1 + \omega^2\ \theta_1^2} \tag{XII.16}$$

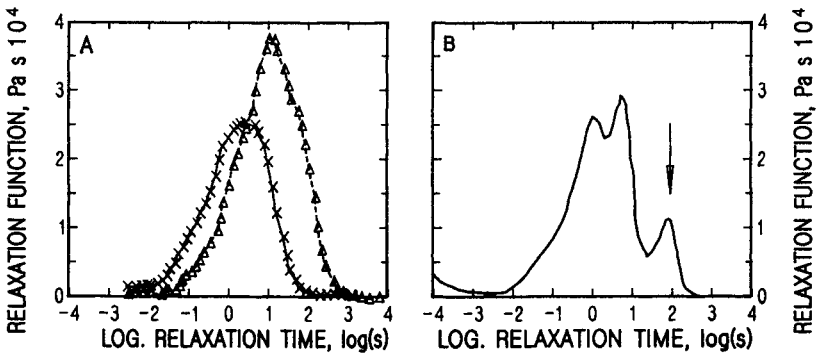

Figure XII.2: *Weighted relaxation spectra, $\theta\, H(\theta)$. A. For poly(methyl methacrylate) and polystyrene, B. for a blend of the two polymers (8% PS). The arrow indicates the relaxation time θ_1. After Gramespacher and Meissner.*[30]

The term $(\eta/\theta_1)(1-\theta_2/\theta_1)$ represents the spring modulus of a simple Maxwell model with relaxation time of θ_1.

Equations XII.15 and XII.16 describe the dynamic behavior of the polymer blends, if the interfacial tension is known. Gramespacher and Meissner[30] have shown that the reverse is also true, that interfacial tension can be determined from the oscillatory experiments. If one obtains the relaxation spectra of the pure components and of the blend, and if the weighted spectra are plotted *versus* the logarithm of the relaxation time, as it is reproduced in figure XII.2, than one may notice that in the spectrum of the blend appear three peaks. Two peaks correspond to the relaxation times of the two components of the blend, matrix and dispersed phases. The third peak (marked with an arrow) increases with increasing content of the dispersed phase. The relaxation time corresponding to the third peak is related to the interfacial tension. The value of the third relaxation time, equal to θ_1, may be converted to the interfacial tension using equations XII.12 and XII.14.

A comparison of the values of interfacial tension determined by other methods and by the described above "rheology" method is very good, though perhaps the rheology method is more accurate. The rheology method is particularly convenient, since it may be obtained as a "byproduct" of the rheology measurements, which are necessary also for other reasons. Any more serious work with biconstituent systems is hard to imagine without rheological determinations, methods of obtaining viscoelastic spectra are many and well described,[37–42] while other methods of determination of interfacial tension would have to be made *ad hoc.*

Another, theoretically fairly easily determinable property which may detect compatibility is glass transition temperature. Incompatible polymers show two transition points as for pure components, while the compatible ones, molecular solutions give one transition point. Nonetheless, in practice it is not so convenient; glass transition is a range rather than a sharp point and the spread of the glass transitions for the interesting pair of polymers may be not a large one. This may often lead to situations of an insufficient resolution, or outright indeterminabil-

ity. Interfacial tension, as a competitive method, has a certain range, a scale of gradation permitting to judge changes, to observe trends.

Knowledge of the interfacial tension or of the interaction parameter does not solve the whole problem at once. If interfacial tension is equal zero then we have a solution, a molecular dispersion. How high a value of the interfacial tension may be accepted to be still deemed as compatible one cannot say. In this respect compatibility is similar to the solubility, equality of solubility parameters does not give a guarantee of solubility. Similarity to van der Wals forces and hydrogen bonding must be considered in addition.[43] The unpleasant point here is that compatibility depends on the ratio of polymers and on temperature. Experimental determination of the materials of interest is unavoidable. The methods of rheology allow for rather convenient experimentation within wide range of conditions. One may expect that oscillatory measurements performed on solids should give equally good results.

XII.3.a Bicomponent Fibers

Originally, bicomponent fibers were developed to impart a crimp to the fibers, a crimp which would be "built-in" without the need for additional operations. To have such properties, the fiber was to be made of two different polymers formed side-by-side. The fiber cross section consisted of two approximately equal parts, each made of a different polymer. The polymers must have sufficient compatibility to assure adhesion between the two halves of one fiber.

During the formation process, both polymers experience the same conditions but their behavior and/or response to these conditions almost certainly is different. The differences become most strongly evident after neck drawing. At this point the difference in the post draw relaxation of the two halves of the fiber leads to the formation of, mostly helical, crimp.

Only about fifteen per cent of the polymer pairs investigated thus far have been found compatible, and majority of these pairs is unsuitable for fiber formation. Unfortunately, this good idea may find only a limited realization.

The majority of those bicomponent fibers which enjoy commercial success are of the type *side-by-side*, that is, the type which mainly serves as crimped fibers with a fair amount of elasticity. The largest field of application is women's hosiery. A simplified sketch of the spinnerette and polymer distribution plate is given in figure XII.3.[44] Each of the two polymers is guided between two rows of entry channels to the capillaries. A partition passes through the middle of the capillary entrance and prevents the two polymers from contact before they enter the delivery channels leading to the capillaries.

There have been many patents issued for the design of the distribution plates. The design may be sometimes complicated, specially if the plates are to cooperate with round hole patterns of large spinnerettes. For rectangular spinnerettes the design is simpler. More complications may arise if the two polymers have largely different viscosities or elastic behavior. Longer capillaries are advantageous, recov-

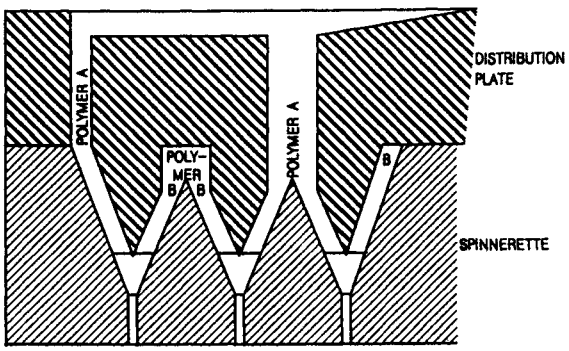

Figure XII.3: *Simple sketch of an assembly of a spinnerette and a polymer distribution plate for formation of side-by-side bicomponent fibers.*

ery in die swell may represent difficulties if the compatibility of the two polymers is marginal at the extrusion conditions.

The "imbalance" of the melt viscosity of the two polymers used for side-by-side formation may influence cross section of the fiber, it is the distribution of the two polymers (see figure XII.4.). The symmetric cross section is obtainable when both polymers, A and B, have practically the same melt viscosity. If viscosity of polymer B increases than the fiber cross section changes from I to II, and to III. Cross sections like the case III in figure XII.4 may be obtained when fibers are made of the same polymer but of much different molecular mass, what is sometimes practiced.

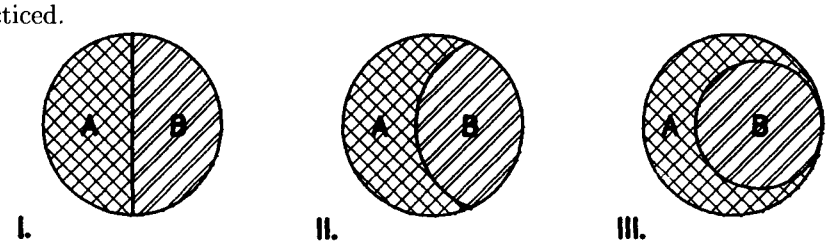

Figure XII.4: *Cross section of side-by-side bicomponent fibers with various melt viscosities of the components: I.* $\eta_A = \eta_B$*; II.* $\eta_A < \eta_B$*; III.* $\eta_A \ll \eta_B$.

Naturally, side-by-side fibers may have a ratio of polymer volumes other than 50 : 50. The ratio of the two polymers may have an influence on the type of crimp. Development of bulk in the fiber is by no means the only effect on fiber properties. Nevertheless, other properties like moisture regain, different *hand*, dyeability and other optical effects may be affected and they may very well serve as a good reason for development of such fibers. Naturally, the properties may change equally well for the better as for the worse. One of the more sensitive is dyeability, which may lead to very interesting effects as well as to disastrous difficulties.

Another type of bicomponent fiber is the *sheath and core* variety. The main reason for production of such fibers is to change the character of the fiber surface, and in such cases a very thin sheath may suffice to assure dyeability, change the *hand*, or perhaps affect the moisture regain or electrostatic properties. The core

is usually the main element providing the strength; nevertheless, the difference between the properties of the sheath and the core cannot be too large for the sake of the fiber integrity under load. Polymers with any degree of compatibility do not have such large difference in their properties anyhow. In order for the fiber to keep its integrity, for the sheath not to turn loose from the core, the degree of polymer compatibility must be higher than for the side-by- side fibers.

The sheath - core bicomponent fibers represent also a good raw material for nonwovens; they are used mainly for the "classic" processes, rather than for spunbonded. The sheath serves as the binder for thermal bonding. *e.g.* through air bonding. Side-by-side types of bicomponents sometimes are also used for the same purpose, particularly when a bulkiness of the fabric is important.

In general, the principles of fiber formation are valid for bicomponent fibers as in every other case; there are only additional complications: two polymers instead of one and matching them all the way from the raw polymer to the fiber properties.

Since the bicomponent fibers are produced primarily for creation of the crimping effect, it seems appropriate to quote the work of M. J. Denton[45] on the crimp curvature of such fibers. The general equation for the crimp curvature is given as:

$$R\,\Delta = \frac{I_0}{A_1\,u_1} + \frac{m-1}{A_0\,u_1}\left(I_{1P} - \frac{A_2}{m\,A_1}I_{2P} - \frac{m-1}{m}A_1\,u_1^2\right) \qquad \text{(XII.17)}$$

In equation XII.17 the meaning of the symbols is as follows. R is radius of the crimp curvature (of the fiber axis), Δ is the fractional differential shrinkage between the components of the fiber, and is expressed as

$$\Delta = \delta_2 - \delta_1 = F\left(\frac{1}{E_1\,A_1} + \frac{1}{a_2}\right) + \frac{1}{R}\,(u_1 + u_2) \qquad \text{(XII.18)}$$

δ is fractional shrinking potential of the respective components, F is compressive force owing to the higher shrinkage potential of the other component and this forms two bending moments M of the appropriate components.

$$M_1 + M_2 = F\,(U_1 + u_2) \qquad \text{(XII.19)}$$

where u are the distances from the geometric centers of the two component cross section from the geometric center of the entire cross section, P. A are cross sectional areas of the respective components, E are moduli of the components, I_1 and I_2 are second moments of the respective component cross sections about the axis connecting the geometric centers of these cross sections, and the second moment of area of the whole cross section is I_0 (about the axis over the geometric center of the whole fiber and approximately parallel to the line dividing the different polymer sections).

$$I_0 = I_{1P} + I_{2P} \qquad \text{(XII.20)}$$

I_{1P} and I_{2P} are the moments of the cross section segments about the axis of the whole cross section. $m = E_2/E_1$ is the ratio of the moduli.

If the cross section is symmetrical around its axis, then equation XII.17 simplifies to

$$R\,\Delta = \frac{2\,I_0}{A_0\,u_1} + \frac{(m-1)^2}{2\,m\,A_0\,u_1}\left(I_0 - A_0\,u_1^2\right) \qquad \text{(XII.21)}$$

It is important to note that crimp depends on m, on the ratio of the moduli, not on the absolute values of the moduli. On the other hand, when m is either very small or very large then R becomes large, which means that the crimp is small or none. Denton[45] suggests therefore that, except of the fibers consisting of a hard polymer and an elastomeric polymer, m may be taken as unity. This leads to another simplification of equation XII.17.

$$R\,\Delta = \frac{I_0}{a_1\,u_1} \qquad \text{(XII.22)}$$

Equation XII.22 may be expressed in a verbal form:

$$\frac{1^{st}\ moment\ of\ area\ of\ one\ component\ cross\ sect. \times differ.\ shrink.}{2^{nd}\ moment\ of\ area\ of\ the\ whole\ fiber\ cross\ section} \qquad (XII.22\,a)$$

The above calculations are to be taken, to some extent, as an approximations. For details of the derivation and some additional elaborations the reader is referred to the original source.[45]

XII.3.b Fibers from Blended Polymers

Blending of polymers has been initiated in the plastics industry. One of the earliest products, ABS (acrylonitrile - butadiene - styrene) or high impact polystyrene, has long been very successful. The idea of blending was transplanted also to the

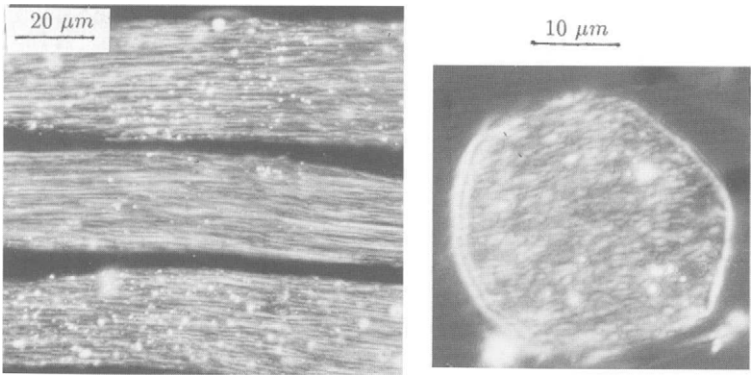

Figure XII.5: *Dark field photomicrographs of a longitudinal, 1 μm thick, cross section (left) and transverse, also 1 μm thick, cross section (right) of a fiber from blended polymers. The protofibrillar nature of the inclusions is well visible.*

fiber industry, but it may be difficult to name a very successful product in this

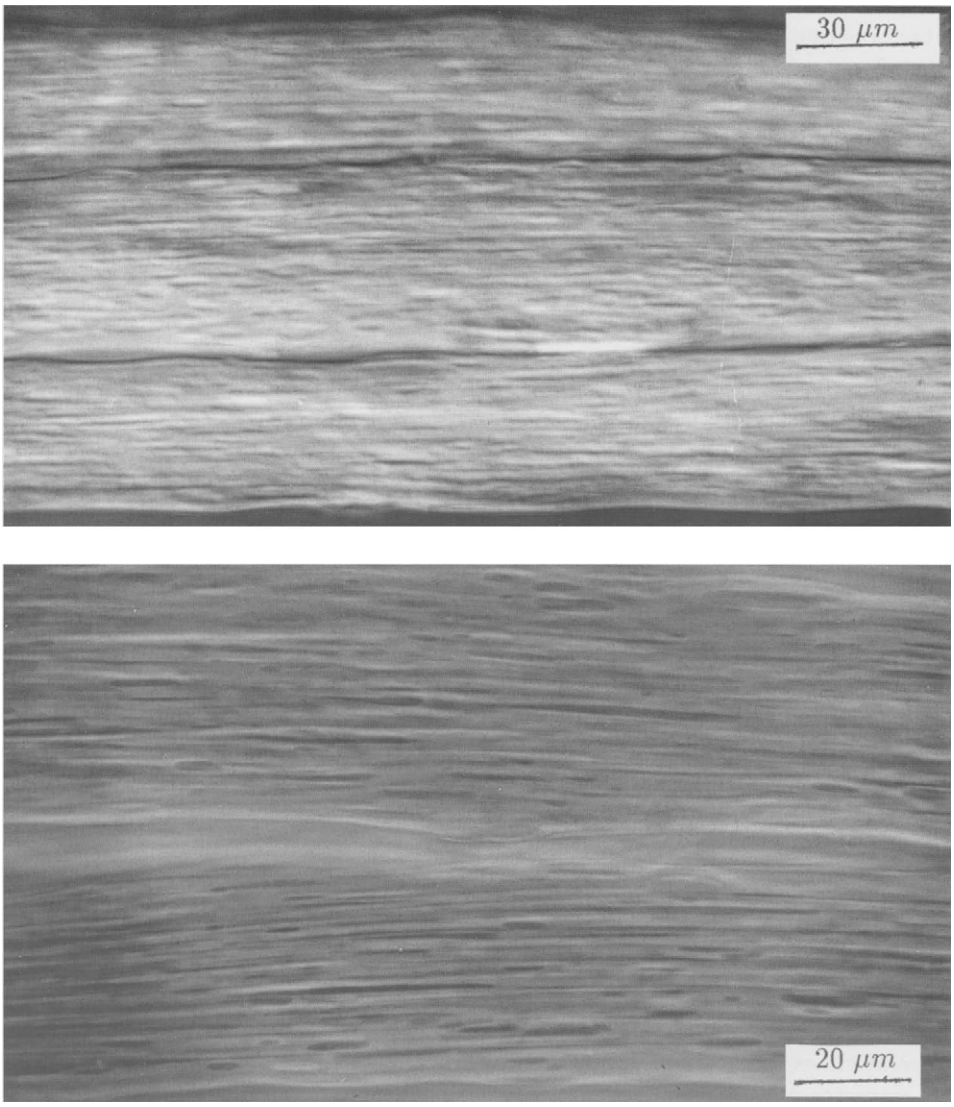

Figure XII.6: *Photomicrographs of a fiber from blended polymers, similar to those in figure XII.5, 1 μm axial cross sections. Top: differential interference contrast by Nomarski. Bottom: phase contrast in polarized light. The lateral sizes of the structures range from 3000 Å to 7700 Å.*

group. It appears that the big difference between the two types of industries, plastics and fibers, is created by the the very small size of fiber diameters.

As mentioned above, if a blend is to have reasonable mechanical properties, there must be a good compatibility between the two components, a good adhesion between the phases. Generally, crystallinity does not help adhesion and fiber forming polymers are predominantly crystalline for now. The neck drawing of

fibers creates additional obstacles. As it may be seen in figures XII.5 and XII.6, neck drawing transforms the inclusions of the dispersed phase into elongated shapes of *protofibrils* or fibrils. The dimensions of the structures in figures XII.5 and XII.6 range from about 3000 Å to about 7700 Å, they are relatively large and the size justifies the term *protofibrils*. The fibers in figures XII.5 and XII.6 were not extensively drawn, but fibers from blended polymers can rarely be drawn more anyway. In plastics, the inclusions retain mostly spherical shape, unless subjected to high shearing forces at not too high a temperature. The fibrillar structure of fibers is responsible for the relatively low lateral strength and the fibrils of dispersed phase may only decrease the transverse properties even further.

The structure of fibers prepared from polymer blends, as well as of the bicomponent fibers, requires a substantial research effort. Investigation of the bicomponent structures using classical methods is very difficult, and next to nothing has been published in the field. Availability of the electron microscopes with spectroscopic imaging appears to be ideal for the purpose; distribution of the dispersed phase and of the interphases may be well visible. Nevertheless, judging from the scarcity and the character of the published information, there appears to be quite a sizeable effort being spent on the development of all sorts of biconstituent fibers, however, the effort appears to be an exercise in the "Edisonian approach", if to use the common euphemism.

True, blending of polymers expands the possibility of varying fiber properties and the technique is relatively simple, if not simplistic. Much more promise, however, is carried by the application of block copolymers. This possibility requires much more effort, mainly intellectual, to realize; but the potential gains are many times larger since one may obtain whole groups of polymers leading to "tailor made" properties.

XII.4 Microfibers

Very thin fibers of fractional decitex, usually referred to as *microfibers* have been found to offer unusual and interesting textile properties. It was mentioned several times above that obtaining very thin fibers with the standard processes of diameter attenuation and neck drawing becomes difficult and expensive once the barrier of three or two decitex is crossed. The incompatibility of polymers, so bothersome in case of polymer blends and bicomponent fibers, has been utilized as one way of solving the problem of microfibers.

The first commercial microfibers were obtained by way of coextrusion of polyesters or polyamides with another polymer, mostly polystyrene. Due to the lack of compatibility the sections of different components usually separate during neck drawing. The relatively easily soluble polystyrene may be dissolved away while the wanted fine fibers remain intact. The need of dissolution makes such processes exceptionally cumbersome and expensive.

Using the similar principle of coextrusion, high molecular mass polystyrene, or similar, may be substituted with either low molecular mass compounds or water

soluble polymer in as small ratios as possible. In this way the burdensome process of dissolving relatively large quantities of polymer in organic solvents may be simplified, becoming more like a wash.

The essential part of the method – coextrusion – imposes limitations on the shape of the cross sections of the microfibers. The simplest way is to divide the round cross section of the capillary into sectors of a circle which have a cross section close to a triangle – a cross section well acceptable for the textile purposes.

Another variation on the theme is the use of two incompatible polymers which split in cold drawing but both of them remain in the fiber blend. A high molecular mass fiber finish, which has a surfactant like nature, may be used as a "separator" for the coextruded sectors. This area presents a really large room for inventiveness.

"Felix qui potuit rerum
*cognoscere causas."**

XII.5 References

1. V. Gröbe and H. Versäumer, *Faserforsch. Textitech.*, **14 (1963)**, 249.
2. C. D. Han, *J. Appl. Polymer Sci.*, **17 (1973)**, 187.
3. C. D. Han, R. Lamonte, and L. H. Drexler, *J. Appl. Polymer Sci.*, **17 (1973)**, 1165.
4. R. S. Schechter, *AIChE J.*, **7 (1961)**, 445.
5. J. A. Wheeler and E. H. Wissler, *AIChE J.*, **11 (1965)**, 207.
6. T. Mizushima, N. Mitsuishi, and R. Nakamura, *Kagaku Kogaku*, **28 (1965)**, 648. 6
7. W. Kozicki, C. H. Chou, and C. Tiu, *Chem. Eng. Sci.*, **21 (1966)**, 665.
8. W. Kozicki and C. Tiu, *Can. J. Chem. Eng.*, **45 (1967)**, 127.
9. N. Mitsuishi, Y. Litayama, and A. Oyagi, *Int. Chem. Eng.*, **8 (1968)**,
10. C. Miller, *Ind. Chem. Eng., Fundam.*, **11 (1972)**, 187. 10
11. *Brit. Pat.* **No. 762,630 (1954)** to Du Pont de Nemours. 11
12. G. R. Wray and M. Acar, *Proc. Instn. Mech. Engrs.*, **204 (1990)**, Preprint No. 6.
13. A. Demir, *Chemiefasern/Textilin.*, **40/92 (1990)**, 614. 13
14. *U. S. Pat.* **No. 2,985,995 (1961)** to E. I. Du Pont De Nemours.
15. H. Weinsdörfer, *Chemiefasern/Textilin.*, **36/88 (1986)**, E41.
16. D. K. Gupta and A. El-Shiekh, *Textile Res. J.*, **52 (1982)**, 621.
17. D. K. Gupta and A. El-Shiekh, *Textile Res. J.*, **53 (1983)**, 313.
18. G. Beaucage, R. S. Stein, and R. Koningsveld, *Macromolecules*, **26 (1993)**, 1603.
19. G. Beaucage and R. S. Stein, *Macromolecules*, **26 (1993)**, 1609, 1917.

*Happy are those who possessed the cognition of the nature of matter. *Publius Vergilius Maro*: Georgica, **2**, 490.

20. K. S. Schweizer, *Macromolecules*, **26 (1993)**, 6033, 6050.

21. F. S. Bates and G. H. Fredrickson, *Macromolecules*, **27 (1994)**, 1065.

22. G. H. Fredrickson, A. J. Liu, and F. S. Bates, *Macromolecules*, **27 (1994)**, 2503.

23. G. H. Fredrickson, *Macromolecules*, **27 (1994)**, 7382. 23

24. R. Krishnamoorti, W. G. Grwassley, N. P. Balsara, and D. J. Lohse, *Macromolecules*, **27 (1994)**, 3073.

25. C. M. Kuo and S. J. Clarson, *Eur. Polymer J.*, **29 (1993)**, 661.

26. E. Martuscelli, *Makromol. Chem., Rapid Commun.*, **5 (1984)**, 261.

27. R. Steller and D. Żuchowska, *J. Appl. Polymer Sci.*, **43 (1990)**, 1595.

28. D. Żuchowska and R. Steller, *Angew. Makromol. Chem.*, **175 (1990)**, 69.

29. R. Steller and D. Żuchowska, *J. Appl. Polymer Sci.*, **43 (1991)**, 1411.

30. H. Gramespacher and J. Meissner, *J. Rheol.*, **36 (1992)**, 1127.

31. R. L. Sammler, R. P. Dion, C. J. Carriere, and A. Cohen, *Rheol. Acta*, **31 (1992)**, 554.

32. E. Helfand and Y. Tagami, *J. Polymer Sci., Pt. B*, **9 (1971)**, 741.

33. E. Helfand and Y. Tagami, *J. Chem. Phys.*, **56 (1971)**, 3592.

34. D. Broseta, G. H. Fredrickson, E. Helfand, and L. Leibler, *Macromolecules*, **23 (1990)**, 132.

35. S. J. Choi and W. R. Schowalter, *Phys. Fluids*, **18 (1975)**, 420.

36. P. Scholz, D. Froelich, and R. Müller, *J. Rheol.*, **33 (1989)**, 481.

37. N. W. Tschoegl: *Phenomenological Theory of Linear Viscoeastic Behavior*, Springer Verlag, Berlin-Heidelberg-New York, 1989.

38. J. D. Ferry: *Viscoelestic Properties of Polymers*, John Wiley & Sons Publ., New York, 1980.

39. I. Emri, N. W. Tschoegl, *Rheol. Acta*, **32 (1993)**, 311, 327.

40. N. W. Tschoegl, *Seminar for Kimberly-Clark Corp.*, Roswell, Ga., Sept. 24, 1993.

41. V. M. Kamath, M. R. Mackley, *J. Non-Newton. Fluid Mech.*, **32 (1989)**, 119.

42. M. Baumgartel, H. H. Winter, *Rheol. Acta*, **28 (1989)**, 511.

43. H. - G. Elias: *Macromolecules*, Plenum Press, New York – London, 1984, Chaper 6. 43

44. Z. K. Walczal, *U. S. Pat.* **No. 3,659,988 (1972)** to Phillips Petroleum Co.

45. M. J. Denton, *J. Text. Res.*, **73 (1982)**, 253.

Appendix A NUMERIC DATA

A.1 Data on Air

Table A.1
Flow Parameters *versus* Mach Number for Subsonic Flow.
Values from National Advisory Commitee for Aeronautics TN 1428.
After L. Prandtl: *Essentials of Fluid Dynamics*, Blackie & Son, London, 1952.

M	$\frac{p}{p_0}$	$\frac{\rho}{\rho_0}$	$\frac{T}{T_0}$	$\frac{a}{a_0}$	$\frac{A^*}{A}$
0.00	1.0000	1.0000	1.0000	1.0000	0.00000
0.01	0.9999	1.0000	1.0000	1.0000	0.01728
0.02	0.9997	0.9998	0.9999	1.0000	0.03455
0.03	0.9994	0.9996	0.9998	0.9999	0.05181
0.04	0.9989	0.9992	0.9997	0.9998	0.06905
0.05	0.9983	0.9988	0.9995	0.9998	0.08627
0.06	0.9975	0.9982	0.9993	0.9996	0.10350
0.07	0.9966	0.9976	0.9990	0.9995	0.12060
0.08	0.9955	0.9968	0.9987	0.9994	0.13770
0.09	0.9944	0.9960	0.9984	0.9992	0.15480
0.10	0.9930	0.9950	0.9980	0.9990	0.1718
0.11	0.9916	0.9940	0.9976	0.9988	0.1887
0.12	0.9900	0.9928	0.9971	0.9986	0.2056
0.13	0.9883	0.9916	0.9966	0.9983	0.2224
0.14	0.9864	0.9903	0.9961	0.9980	0.2391
0.15	0.9844	0.9888	0.9955	0.9978	0.2557
0.16	0.9823	0.9873	0.9949	0.9974	0.2723
0.17	0.9800	0.9857	0.9943	0.9971	0.2887
0.18	0.9776	0.9840	0.9936	0.9968	0.3051
0.19	0.9751	0.9822	0.9928	0.9964	0.3213
0.20	0.9725	0.9803	0.9021	0.9960	0.3374
0.21	0.9697	0.9783	0.9913	0.9956	0.3534
0.22	0.9668	0.9762	0.9904	0.9952	0.3693
0.23	0.9638	0.9740	0.9895	0.9948	0.3851
0.24	0.9607	0.9718	0.9886	0.9943	0.4007
0.25	0.9875	0.9694	0.9877	0.9938	0.4162
0.26	0.9541	0.9670	0.9867	0.9933	0.4315
0.27	0.9506	0.9645	0.9856	0.9928	0.4467
0.28	0.9470	0.9619	0.9846	0.9923	0.4618
0.29	0.9433	0.9592	0.9835	0.9917	0.4767

Continued on next page

Table A.1
Continuation
Flow Parameters *versus* Mach Number for Subsonic Flow.

M	$\frac{p}{p_0}$	$\frac{\rho}{\rho_0}$	$\frac{T}{T_0}$	$\frac{a}{a_0}$	$\frac{A^*}{A}$
0.30	0.9395	0.9564	0.9823	0.9911	0.4914
0.31	0.9355	0.9535	0.9811	0.9905	0.5059
0.32	0.9315	0.9506	0.9799	0.9899	0.5203
0.33	0.9274	0.9476	0.9787	0.9893	0.5345
0.34	0.9231	0.9445	0.9774	0.9886	0.5486
0.35	0.9188	0.9413	0.9761	0.9880	0.5624
0.36	0.9143	0.9380	0.9747	0.9873	0.5761
0.37	0.9098	0.9347	0.9733	0.9866	0.5896
0.38	0.9052	0.9313	0.9719	0.9859	0.6029
0.39	0.9004	0.9278	0.9705	0.9851	0.6160
0.40	0.8956	0.9243	0.9690	0.9844	0.6289
0.41	0.8907	0.9207	0.9675	0.9836	0.6416
0.42	0.8857	0.9170	0.9659	0.9828	0.6541
0.43	0.8807	0.9132	0.9643	0.9820	0.6663
0.44	0.8755	0.9094	0.9627	0.9812	0.6784
0.45	0.8703	0.9055	0.9611	0.9803	0.6903
0.46	0.8650	0.9016	0.9594	0.9795	0.7019
0.47	0.8596	0.8976	0.9577	0.9786	0.7134
0.48	0.8541	0.8935	0.9560	0.9777	0.7246
0.49	0.8486	0.8894	0.9542	0.9768	0.7356
0.50	0.8430	0.8852	0.9524	0.9759	0.7464
0.51	0.8374	0.8809	0.9506	0.9750	0.7569
0.52	0.8317	0.8766	0.9487	0.9740	0.7672
0.53	0.8259	0.8723	0.9468	0.9730	0.7773
0.54	0.8201	0.8679	0.9449	0.9721	0.7872
0.55	0.8142	0.8634	0.9430	0.9711	0.7968
0.56	0.8082	0.8580	0.9410	0.9701	0.8063
0.57	0.8022	0.8544	0.9390	0.9690	0.8155
0.58	0.7962	0.8498	0.9370	0.9680	0.8244
0.59	0.7901	0.8451	0.9349	0.9669	0.8331
0.60	0.7840	0.8405	0.9328	0.9658	0.8416
0.61	0.7778	0.8357	0.9307	0.9647	0.8499
0.62	0.7716	0.8310	0.9286	0.9636	0.8579
0.63	0.7654	0.8262	0.9265	0.9625	0.8657
0.64	0.7591	0.8213	0.9243	0.9614	0.8732
0.65	0.7528	0.8164	0.9221	0.9603	0.8806
0.66	0.7464	0.8115	0.9199	0.9591	0.8877
0.67	0.7401	0.8066	0.9176	0.9579	0.8945
0.68	0.7338	0.8016	0.9153	0.9567	0.9012
0.69	0.7274	0.7966	0.9131	0.9555	0.9076
0.70	0.7200	0.7916	0.9107	0.9543	0.9138
0.71	0.7145	0.7865	0.9084	0.9531	0.9197
0.72	0.7080	0.7814	0.9061	0.9519	0.9254
0.73	0.7016	0.7763	0.9037	0.9506	0.9309
0.74	0.6951	0.7712	0.9013	0.9494	0.9362

Continued on next page

Table A.1
Continuation
Flow Parameters *versus* Mach Number for Subsonic Flow.

M	$\frac{p}{p_0}$	$\frac{\rho}{\rho_0}$	$\frac{T}{T_0}$	$\frac{a}{a_0}$	$\frac{A^*}{A}$
0.75	0.6886	0.7660	0.8989	0.9481	0.9412
0.76	0.6821	0.7609	0.8964	0.9468	0.9461
0.77	0.6756	0.7557	0.8940	0.9455	0.9507
0.78	0.6690	0.7505	0.8915	0.9442	0.9551
0.79	0.6625	0.7452	0.8890	0.9429	0.9592
0.80	0.6560	0.7400	0.8865	0.9416	0.9632
0.81	0.6495	0.7347	0.8840	0.9502	0.9669
0.82	0.6430	0.7295	0.8815	0.9389	0.9704
0.83	0.6365	0.7242	0.8789	0.9375	0.9737
0.84	0.6300	0.7189	0.8763	0.9361	0.9769
0.85	0.6235	0.7136	0.8737	0.9347	0.9797
0.86	0.6170	0.7083	0.8711	0.9333	0.9824
0.87	0.6106	0.7030	0.8685	0.9319	0.9849
0.88	0.6041	0.6977	0.8659	0.9305	0.9872
0.89	0.5977	0.6924	0.8632	0.9291	0.9893
0.90	0.5913	0.3870	0.8606	0.9277	0.9912
0.91	0.5849	0.6817	0.8579	0.9262	0.9929
0.92	0.5785	0.6764	0.8552	0.9248	0.9944
0.93	0.5721	0.6711	0.8525	0.9233	0.9958
0.94	0.5658	0.6658	0.8498	0.9218	0.9969
0.95	0.5595	0.6604	0.8471	0.9204	0.9979
0.96	0.5532	0.6551	0.8444	0.9189	0.9986
0.97	0.5469	0.6498	0.8416	0.9174	0.9992
0.98	0.5407	0.6445	0.8389	0.9159	0.9997
0.99	0.5345	0.6392	0.8361	0.9144	0.9999
1.00	0.5283	0.6339	0.8333	0.9129	1.0000

Dynamic viscosity of air may be calculated from Sutherland's equation with the Suntherland's constant of 114:

$$\eta_a = 1.709 \cdot 10^{-5} \frac{387.15}{T + 114} \left(\frac{T}{273.15} \right)^{1.5} = 1.4656 \cdot 10^{-6} \frac{T^{1.5}}{T + 114} \tag{A.1}$$

where T is in $^\circ K$ and viscosity in $Pa \cdot s$.

Density of air may be calculated as

$$\rho_a = \frac{378.99725}{T} \tag{A.2}$$

where T is in $^\circ K$ and density in Kg/m^3.

Heat conductivity of air may be calculated from Sutherland's equation with the Sutherland's constant of 114:

$$\lambda_a = 0.0243067\frac{387.15}{T+114}\left(\frac{T}{273.15}\right)^{1.5} = 2.0845 \cdot 10 * -3\frac{T^{1.5}}{T+114} \tag{A.3}$$

where T is in $°K$ and heat conductivity in $J/(m \cdot °C \cdot s)$.

Heat capacity of air:

$0°C - 1297.91 J/m^3$ $100°C - 1302.09 J/m^3$ $200°C - 1318.84 J/m^3$

$$c_p = 935.44 + 3.1956(T - 273.15)(J/Kg) \tag{A.4}$$

A.2 Data on Mass Transfer

Table A.2
Coefficients of Diffusion of Air - Solvent. *After* Y. Ohzawa, Y. Nagano, J. Appl. Polymer Sci., **14 (1970)**, 1879.

Solvent	D^0_{as} at $0°C$ cm^2/s	m in eq. 5
Methanol	0.1325	2.0
Ethanol	0.1016	2.0
Water	0.220	1.75
Toluene	0.0709	2.0

$$D_{as} = D^0_{as}\left(\frac{T}{T_{(0)}}\right)^m \tag{A.5}$$

A.3 Data on Heat of Evaporation

Table A.3
Spacific Heat, Heat of Evaporation and Data for Eqn. 6. *After* Y. Ohzawa, Y. Nagano, J. Appl. Polymer Sci., **14 (1970)**, 1879.

Solvent	C_{ps} at $0°C$ $cal/(mole°C)$	H_s $cal/mole$	T_b $°C$	T_c $°C$	α/k $cal/(mole°C)$
Methanol	15	8450	64.7	240.0	8,1
Ethanol	21	9410	78.5	243.0	9.6
Water	8.6	9717	100	374.2	6.5
Toluene	45	8000	110.6	320.8	11.1
Acetone	20	6950	56.5	235	
DMF	26	8480	153	373	

$$H_s(T) = H_s(0)\left(\frac{T_c - T}{T_c - T_b}\right)^{0,38} \tag{A.6}$$

where T_b = boiling point; T_c = critical temperature.

A.4 Data on Polymers

Density

Nylon 6

(J. Brandrup, E. H. Immergut, and W. McDowell, *Polymer Handbook*, John Wiley & Sons, New York, 2nd edition, 1975, pp, III-25.)

Amorphous $\rho_a = 1110 \ kg/m^3$

Crystalline $\rho_c = 1230$ to $1250 \ kg/m^3$

Nylon 66

(J. Brandrup, E. H. Immergut, and W. McDowell, *Polymer Handbook*, John Wiley & Sons, New York, 2nd edition, 1975, pp, III-28.)

Amorphous $\rho_a = 1090 \ kg/m^3$

Crystalline $\rho_c = 1240 \ kg/m^3$

Poly(ethylene terephthalate)

(H. W. Starkweather, Jr., P. Zoller, and G. A. Jones, *J. Polymer Sci., Polymer Phys. Ed.*, **21 (1983)**, 295.)

Amorphous $\rho_a = 1185.96 \ kg/m^3$ at $261.8°C$

Crystalline $\rho_c = 1385.6 \ kg/m^3$ at $261.8°C$

$\rho_c = 1474.9 \ kg/m^3$ at room temp.

Polypropylene

Amorphous $\rho_a = 1028.5 - 0.639 \ T$ in kg/m^3

T in $°K$

Crystalline $\rho_c = 946 \ kg/m^3$ at $22°C$

Equilibrium Melting Point

Nylon 6

(J. Brandrup, E. H. Immergut, and W. McDowell, *Polymer Handbook*, John Wiley & Sons, New York, 2nd edition, 1975, pp, III-25.)

$T_m^0 = 223$ to $250 \ °C$

Nylon 66

(J. Brandrup, E. H. Immergut, and W. McDowell, *Polymer Handbook*, John Wiley & Sons, New York, 2nd edition, 1975, pp, III-28.)

$T_m^0 = 265$ to $270 \ °C$

Poly(ethylene terephthalate)

(H. W. Starkweather, Jr., P. Zoller, and G. A. Jones, *J. Polymer Sci., Polymer Phys. Ed.*, **21 (1983)**, 295.)

$T_m^0 = 261.8 \pm 0.5 \ °C$

Polypropylene

Equilibrium melting point is strongly dependent on the stereoregularity and other chain imperfections, therefore it must be determined for any given polymer. Usually T_m^0 ranges from 195 *to* 212 $°C$.

Heat of Fusion

Heat of fusion depends on temperature at which the polymer specimen crystallized, it is on the size of the long period. Values at any given temperature of crystallization may be determined from

$$\Delta H_m = \Delta H_m^0 \left(1 - \frac{T_m^0 - T_m}{T_m^0}\right) \quad kJ/kg \tag{A.7}$$

where temperatures in $^\circ K$.

Nylon 6

(J. Brandrup, E. H. Immergut, and W. McDowell, *Polymer Handbook*, John Wiley & Sons, New York, 2nd edition, 1975, pp, III-25.)$\Delta H_f^0 = 212.98 \quad kJ/kg$

Nylon 66

(J. Brandrup, E. H. Immergut, and W. McDowell, *Polymer Handbook*, John Wiley & Sons, New York, 2nd edition, 1975, pp, III-28.) $\Delta H_f^0 = 205.45 \quad kJ/kg$

Poly(ethylene terephthalate)

(H. W. Starkweather, Jr., P. Zoller, and G. A. Jones, *J. Polymer Sci., Polymer Phys. Ed.*, **21 (1983)**, 295.)

$\Delta H_f = 129.79 \quad kJ/kg \qquad \Delta S_f = 0.2512 \quad kJl/(kg^\circ C)$

Other values for heat of fusion are quoted between 128.53 and 143.2 kJ/kg.

Polypropylene

Heat of fusion of polypropylene depends on the chain perfection and may be estimated from the equilibrium melting point. The equation has been derived on the basis of this author's work and using the published (J. Brandrup, E. H. Immergut, and W. McDowell, *Polymer Handbook*, John Wiley & Sons, New York, 2nd edition, 1975, pp, III-217, V-25.) .

$\Delta H_f^0 = 0.1320 \cdot T_m^0 + 164.245 \quad kJ/kg$

T in $^\circ C$

Specific Heat

Poly(ethylene terephthalate)

(C. W. Smith and M. Oda, *J. Polymer Sci.*, **20 (1956)**, 37.)

Amorphous $C_p = 1.143 \quad kJ/kg$

Crystalline $C_p = 1.1011 \quad kJ/kg$

Polypropylene

Amorphous $C_p = 0.005694 \cdot T + 1.725 \quad kJ/kg$

Semicrystalline $C_p = 0.00512 \cdot T + 1.5948 \quad kJ/kg$

T in $^\circ C$

Thermal Expansion

Poly(ethylene terephthalate)

P. Zoller and P. Bolli, *J. Macromol. Sci., Phys.*, **B18 (1980)**, 555.

Melt $\beta = 6.55 \cdot 10^{-4} \quad 1/^\circ C$

Thermal Conductivity

Polypropylene

D. Hands, K. Lane, and R. P. Sheldon, *J. Polymer Sci., Symp.*, **No 42 (1973)**, 717; C. L. Choy, *Polymer*, **18 (1977)**, 984.

On introduction into Weber's formula one obtains the temperature dependence of thermal conductivity:

$$\lambda = 1.2925 \cdot 10^{-5} \cdot C_p \cdot M_w^{1/3} \cdot \rho^{4/3} \quad \frac{kJ}{ms^\circ C} \tag{A.8}$$

SUBJECT INDEX